

AEROACOUSTICS

Marvin E. Goldstein

Research Engineer, Lewis Research Center

McGRAW-HILL International Book Company

New York St Louis San Francisco Auckland Bogotá Düsseldorf
Johannesburg Madrid London Mexico Montreal New Delhi Panama
Paris São Paulo Singapore Sydney Tokyo Toronto

Library of Congress Cataloging in Publication Data

Goldstein, Marvin E.
Aeroacoustics.

Includes bibliographical references and index.

1. Aerodynamic noise. I. Title.

TL574.N6G64 1976 629.132'3 76-44521
ISBN 0-07-023685-2

Copyright © 1976 by McGraw-Hill, Inc. All rights reserved. Printed in the United States of America. No part of this publication may be reproduced, stored in a retrieval system, or transmitted, in any form or by any means, electronic, mechanical, photocopying, recording, or otherwise, without the prior written permission of the publisher.

PRINTED AND BOUND IN THE UNITED STATES OF AMERICA

For Evelyn, Priscilla, Deborah, and Judith

CONTENTS

	<i>Page</i>
Preface	xi
Commonly Used Notation and Special Terminology	xv
1 Review of Acoustics of Moving Media	1
1.1 Introduction	1
1.2 Derivation of Basic Equations	2
1.3 Wave-like Solutions of Acoustic Equations	10
1.4 Solutions of Acoustic Equations by Superposition of Elementary Sources	22
1.5 Source Distribution in Unbounded Regions.....	32
1.6 Radiation Field	37
1.7 Energy Relations	39
1.8 Moving Sound Sources	45
1.9 Concluding Remarks	53
Appendix 1.A—Fourier Representation of Functions.....	54
Appendix 1.B—Derivation of Generalized Green's Formula	59
Appendix 1.C—Calculation of Green's Functions	61
References	66
	vii

	<i>Page</i>
2 Aerodynamic Sound	67
2.1 Introduction	67
2.2 Lighthill's Acoustic Analogy	68
2.3 Solution to Lighthill's Equation when no Solid Boundaries are Present	72
2.4 Application of Lighthill's Theory to Turbulent Flows	74
2.5 Physics of Jet Noise	83
2.6 Concluding Remarks	109
Appendix—Transformation of Source Correlation Function ..	110
References	111
 3 Effect of Solid Boundaries	113
3.1 Introduction	113
3.2 Derivation of Fundamental Equation	114
3.3 Ffowcs Williams-Hawkings Equation	116
3.4 Calculation of Aerodynamic Forces	127
3.5 Applications of the Ffowcs Williams-Hawkings Equation	139
3.6 Flows with Sound Field Determined by Green's Function Equations Tailored to the Geometry	171
3.7 Concluding Remarks	182
Appendix 3.A—Reduction of Volume Displacement Term to Dipole and Quadrupole Terms	183
Appendix 3.B—Lift Spectra	184
References	185
 4 Effect of Uniform Flow	189
4.1 Introduction	189
4.2 Derivation of Basic Equation	189
4.3 Application to Fan and Compressor Noise	192
4.4 Concluding Remarks	215
References	216
 5 Theories Based on Solution of Linearized Vorticity— Acoustic Field Equations	219
5.1 Introduction	219
5.2 Decomposition of Linearized Solutions into Acoustical and Vortical Modes: Splitting Theorem	220
5.3 Sound Generated by a Blade Row	222
5.4 Concluding Remarks	240
Appendix 5.A—Solution to Cascade Problem	240
Appendix 5.B—Evaluation of Single-Airfoil Integral	244
Appendix 5.C—Evaluation of Terms in Duct Coordinates ..	245
References	248

	<i>Page</i>
6 Effects of Nonuniform Mean Flow on Generation of Sound	249
6.1 Introduction	249
6.2 Derivation of Phillips' Equation	250
6.3 Derivation of Lilley's Equation	253
6.4 Interpretation of Equations	253
6.5 Simplification of Phillips' and Lilley's Equations	254
6.6 Equations for Transversely Sheared Mean Flows	255
6.7 Applications of Acoustic Equations to Round Jets ..	259
6.8 Flows of Finite Extent	278
6.9 Concluding Remarks	280
Appendix 6.A—Derivation of Equation (6.26)	281
Appendix 6.B—Construction of One-Dimensional Green's Function	281
Appendix 6.C—Asymptotic Solutions to Sturm–Liouville Equation	282
References	285
Index	287

PREFACE

Aeroacoustics is concerned with sound generated by aerodynamic forces or motions originating in a flow rather than by the externally applied forces or motions of classical acoustics. Thus, the sounds generated by vibrating violin strings and loudspeakers fall into the category of classical acoustics, whereas sounds generated by the unsteady aerodynamic forces on propellers or by turbulent flows fall into the domain of aeroacoustics. The term "aerodynamic sound" introduced by Lighthill (who developed the foundations of this field) is also frequently used.

Although there has undoubtedly been much interest in the field of aerodynamically generated sound, up to now no systematic text has been devoted specifically to this subject. However, a few aspects of aeroacoustics are discussed briefly in Morse and Ingard's book *Theoretical Acoustics* (McGraw-Hill (1968)).

After teaching the subject of aeroacoustics to a group of engineers and scientists working on aircraft noise at Lewis Research Center, I concluded that there was a definite need for both a text and reference work in this field. I felt that the book should be moderately advanced and aimed at the reader

with a knowledge of fluid mechanics and applied mathematics at the master's degree level. Moreover, I tried to make it complete enough to serve as a reference work not only for researchers just starting out in the field but also for those with considerable experience. In fact, by limiting the scope of the work specifically to aeroacoustics and by developing related subjects (such as acoustic propagation in ducts, unsteady aerodynamics, etc.) only as much as needed for this topic, I was able to include most of the important ideas which have been developed in this field.

The emphasis is on imparting basic understanding of the physical mechanisms involved in aerodynamic sound generation. Experimental results are presented to verify the basic theory and to augment it whenever it is incomplete. Thus, the book has a fairly mathematical flavor. However, certain applications of the theory to important engineering devices such as fans and compressors are definitely not neglected.

There is sometimes a tendency in the literature to try to separate aeroacoustic problems into an acoustic part and an aerodynamic part and to treat each one separately. In this book, I have not attempted to make this distinction and have combined all the acoustics and aerodynamics needed to relate the sound field to the basic parameters of the problem.

The first chapter is concerned with certain aspects of the acoustics of moving media which are required in the remaining chapters. It also serves to familiarize the reader with some basic concepts of classical acoustics and to develop some mathematical techniques that are needed in the remaining chapters. The second chapter introduces Lighthill's acoustic analogy and applies it to the case where the solid boundaries do not directly influence the sound field. This is the situation in jet noise. A detailed analysis of subsonic jet noise and a qualitative discussion of supersonic jet noise are given. The third chapter develops the acoustic analogy to include the effect of solid boundaries. The results are applied to the discussion of the sound generated by struts, splitters, propellers, helicopter rotors, and so forth. The effects of a uniform mean flow are included in the fourth chapter, and the concepts are used to obtain detailed analyses of the various fan and compressor noise mechanisms. In Chapter 5 the acoustic analogy approach is abandoned, and a direct calculation procedure is developed. It is applied to the prediction of compressibility and cascade effects on the sound generated by a blade row. Finally, in the last chapter the effects of a nonuniform mean flow are included, and equations are developed which are intermediate between Lighthill's acoustic analogy and the direct calculational approach. These results are used to predict the effects of the mean flow field on jet noise.

Credit is given to the original source of an idea whenever possible. Although some of the analyses and formulations developed are somewhat original or extensions of analyses in the literature, the omission of a reference is not meant to imply originality on my part. In fact, I wish to apologize in advance if I have inadvertently not given credit to the originators of any of the ideas which appear in this text.

There are a number of people who have helped with the text. I am especially grateful to Sir James Lighthill (Cambridge University) for his encouragement as well as for his extremely helpful suggestions. Sincere thanks are due to Professors J. E. Ffowcs Williams (Cambridge University), H. S. Ribner (University of Toronto), C. K. W. Tam (Florida State University), and H. Atassi (University of Notre Dame) for suggesting improvements in the manuscript. I am also indebted to several of my co-workers at Lewis Research Center: W. A. Olsen, C. E. Feiler, A. M. Karchmer, W. L. Howes, and W. H. Braun; for supplying experimental data and/or taking the time to read and comment on the typescript. Dr. Thomas Balsa (General Electric Research and Development Center) provided particularly valuable assistance by reading the manuscript and making detailed comments. Last, but certainly not least, my thanks are also extended to the members of Margaret Appleby's editorial branch and Ruth Bert's report typing section who helped in preparing the manuscript—especially to Florence Sprosty for being so conscientious in her typing.

COMMONLY USED NOTATION AND SPECIAL TERMINOLOGY

B	number of propeller or fan blades
C^{\dagger}	convective amplification factor, $1 - M \cos \theta$
c	chord length; local speed of sound
c_0	speed of sound at steady background state
e_{ij}	viscous stress tensor
\mathbf{F}	total force exerted on solid boundaries
f	frequency; $ \mathbf{f} $; arbitrary function
\mathbf{f}	force per unit area exerted by solid boundaries on fluid
\mathcal{f}	force per unit volume of fluid
G	fundamental solution of wave equation
G^0	free-space Green's function
G_{ω}	fundamental solution of Fourier transformed wave equation
I_{ω}	Fourier transform of \bar{I}
\bar{I}	magnitude of $\bar{\mathbf{I}}$
\mathbf{I}	acoustic energy flux
$\bar{\mathbf{I}}$	intensity vector
$\hat{\mathbf{i}}$	unit vector in x_1 - or y_1 -direction

\hat{j}	unit vector in x_2 - or y_2 -direction
k_0	ω/c_0
k	wave number
\mathbf{k}	wave number vector
\hat{k}	unit vector in x_3 - or y_3 -direction
M	Mach number, U/c_0
\hat{n}	unit normal vector to solid surface (drawn outward from region containing the fluid); unit vector
\mathcal{P}	acoustic power
p	pressure
p_0	pressure of steady background flow; or constant reference pressure
R	$ \mathbf{x} - \mathbf{y} $
\mathbf{R}	$\mathbf{x} - \mathbf{y}$ vector between observation point and source point
R_e	$ \mathbf{R}_e $
\mathbf{R}_e	vector between observation point and center of moving source point or region
r	radial coordinate of observation point in cylindrical coordinate system
r', r_0	radial coordinate of source point in cylindrical coordinate system
S	entropy; Sears' function; fixed surface
$S(\tau)$	moving surface
T	large time interval (eventually put equal to infinity)
T_{ij}	Lighthill's stress tensor
T_p	period, f^{-1}
T'_{ij}	Lighthill's stress based on relative velocity \mathbf{v}'
t	time associated with the arrival of sound wave at observation point
U, U_∞	mean flow velocity
\mathbf{u}	unsteady velocity
V	number of stator vanes
\mathbf{V}_s	surface velocity
\mathbf{v}	complete fluid velocity
\mathbf{v}'	velocity of fluid in moving frame, $v'_i = v_i - \delta_{1i}U$
\mathbf{x}	coordinates associated with observation point
\mathbf{y}	coordinates associated with source point
Γ	normalized pressure autocorrelation function, $\overline{p(t)p(t+\tau)}/\rho_0 c_0$; Fourier transform of γ
γ	source term
$\delta(\mathbf{x})$	Dirac delta function
δ_{ij}	Kronecker delta (1 if $i = j$; 0 if $i \neq j$)
ζ	moving coordinates attached to source
Θ	temperature
θ	polar coordinate (polar angle) or direction between line connecting source and observation points and direction of motion of source
$\kappa_{m,n}$	eigenvalue
λ	wavelength

$v(\tau)$	volume of fluid exterior or interior to solid surfaces
ρ	density
ρ_0	density of steady background flow; or constant reference density
ρ'	fluctuating density, $\rho - \rho_0$
σ	reduced frequency; interblade phase angle in Chapter 5
τ	time associated with emission of sound wave; time delay
Φ	phase; velocity potential
φ	polar coordinate (azimuthal angle)
Ω	angular velocity
Ω	$ \Omega $; or source frequency $= \omega(1 - M_c \cos \theta)$
ω	angular frequency $= 2\pi f$

Subscripts:

D	drag component
T	thrust component
0	constant reference value; or value of quantity in steady background flow

We write $f(x) = O(g(x))$ as $x \rightarrow x_0$ to indicate that the ratio $f(x)/g(x)$ remains finite as $x \rightarrow x_0$. It shows that $f(x)$ approaches its limiting value at x_0 at least as fast as $g(x)$ does. If $\lim f(x)/g(x) = 1$ as $x \rightarrow x_0$, we write $f(x) \sim g(x)$.

PRESENTATION OF DATA

Experimental data are presented as pressure or power levels in decibels, dB. This means that the ordinate of the plot is either $20 \log_{10} (\bar{p}/p_r)$, where p_r is some reference pressure (usually 2×10^{-4} dynes/cm²), or $10 \log_{10} (\mathcal{P}/\mathcal{P}_r)$, where \mathcal{P}_r is some reference power (usually 10^{-13} W).

The unit of frequency is the hertz (1 Hz = 1 cycle/s). Sound pressure or power measurements will either include signals of all frequencies and be referred to as "overall" measurements or they will include only the signals in a certain band of frequencies. The widths of these bands are usually taken to be either independent of frequency—in which case the bands are usually quite narrow—or to be proportional to the center frequency of the band. The former are called *narrow bands*, while the latter are called *proportional bands*. The most commonly used proportional band is known as the one-third-octave band. A plot of narrow or proportional band sound pressure (power) as a function of frequency is known as a sound pressure (power) spectrum.

1 REVIEW OF ACOUSTICS OF MOVING MEDIA

1.1 INTRODUCTION

Many of the concepts and techniques used in aeroacoustics have been taken directly from classical acoustics or, more recently, from the acoustics of moving media. Therefore, in order to make the material in this book available to as broad an audience as possible, portions of the first chapter are devoted to a review of those aspects of these subjects that are necessary for understanding the theory of aerodynamic sound. The remainder of the chapter is used to develop certain more or less mathematical ideas that are needed in the succeeding chapters on aerodynamic sound theory. It is assumed that the reader is already familiar with basic fluid mechanics.

Boldface type (**A**) is used to denote a vector while the same letter (*A*) in italic type is used to denote its magnitude. Its components, A_i with i equal to 1, 2, or 3, are denoted by placing subscripts on this letter. An asterisk (*) is used to denote the conjugate of a complex quantity and, whenever possible, the capital and lowercase of the same letter are used to denote Fourier transform pairs with respect to the time variable. Overbars ($\bar{}$) denote time

averages, and brackets $\langle \rangle$ denote space averages. The letter T (without subscripts) denotes a large time interval. Other commonly used symbols are defined in the notation list.

1.2 DERIVATION OF BASIC EQUATIONS

All real fluids possess both elasticity and inertia. Elasticity causes the fluid to resist compression while inertia causes it to “overshoot” whenever it is displaced. Because of these two properties, pressure (or density) fluctuations occurring anywhere in a fluid are communicated to the surrounding medium and propagate outward from their source. When such disturbances travel through the air and arrive at the ear, they cause vibrations of the eardrum that are transmitted via the auditory nerve to the brain. At this point they are recognized as sound.

Aeroacoustics is almost exclusively concerned with sound propagation through fluids such as air and water that have only very small viscosity and thermal conductivity; while in this book we are for the most part interested in disturbances which are so weak that their spatial gradients are never much larger than the disturbances themselves—as, for example, they would be in shock waves. Then as long as the disturbances are not allowed to propagate over excessively large distances the effects of viscosity and heat conduction can be neglected and the fluid motion can be determined by solving Euler’s equation (i.e., the momentum equation for an inviscid flow)

$$\rho \left(\frac{\partial \mathbf{v}}{\partial \tau} + \mathbf{v} \cdot \nabla \mathbf{v} \right) = -\nabla p + \mathcal{F} \quad (1.1)$$

the continuity equation

$$\frac{\partial \rho}{\partial \tau} + \mathbf{v} \cdot \nabla \rho + \rho \nabla \cdot \mathbf{v} = \rho q \quad (1.2)$$

and the entropy (or energy) equation

$$\frac{\partial S}{\partial \tau} + \mathbf{v} \cdot \nabla S = 0 \quad (1.3)$$

where ∇ is the vector operator

$$\mathbf{i} \frac{\partial}{\partial y_1} + \mathbf{j} \frac{\partial}{\partial y_2} + \mathbf{k} \frac{\partial}{\partial y_3}$$

$\mathbf{v} = \{v_1, v_2, v_3\}$ is the velocity of the fluid, ρ is its density, p is its pressure, and S is its entropy. The time is denoted by τ , $\{y_1, y_2, y_3\}$ are Cartesian spatial coordinates, q denotes an external volume flow source within the fluid, and \mathcal{F} denotes an externally applied volume force. It is assumed that these source terms cause no entropy production.

We shall assume that the fluid is homocompositional and that it maintains itself in a state of local thermodynamic equilibrium (i.e., that relaxation effects can be neglected). Then, since any thermodynamic property can be expressed as a function of any two others, we can always suppose that

$$\rho = \rho(p, S)$$

and, as a result, that

$$d\rho = \frac{1}{c^2} dp + \left(\frac{\partial \rho}{\partial S} \right)_p dS \quad (1.4)$$

where we have put

$$c^2 \equiv \frac{1}{\left(\frac{\partial \rho}{\partial p} \right)_S} = \left(\frac{\partial p}{\partial \rho} \right)_S \quad (1.5)$$

since it can be shown that $(\partial p / \partial \rho)_S$ is always positive. Hence it follows from Eq. (1.3) that

$$\frac{\partial \rho}{\partial \tau} + \mathbf{v} \cdot \nabla \rho = \frac{1}{c^2} \left(\frac{\partial p}{\partial \tau} + \mathbf{v} \cdot \nabla p \right) \quad (1.6)$$

For a steady flow with velocity \mathbf{v}_0 , pressure p_0 , density ρ_0 , entropy $S_0 \equiv S(p_0, \rho_0)$, and $c_0 \equiv c(p_0, \rho_0)$, Eqs. (1.1) to (1.3) and (1.6) become

$$\left. \begin{aligned} \rho_0 \mathbf{v}_0 \cdot \nabla \mathbf{v}_0 &= -\nabla p_0 \\ \nabla \cdot \rho_0 \mathbf{v}_0 &= 0 \\ \mathbf{v}_0 \cdot \nabla S_0 &= 0 \\ \mathbf{v}_0 \cdot \nabla p_0 &= c_0^2 \mathbf{v}_0 \cdot \nabla \rho_0 \end{aligned} \right\} \quad (1.7)$$

provided there are no external forces or mass addition.

Since, as we have indicated, sound is simply our perception of pressure disturbances passing through the atmosphere, it is appropriate to consider an unsteady disturbance with characteristic length λ traveling at a propagation speed whose typical value is \tilde{C} through a fluid in which the velocity, pressure, and density are otherwise determined by Eqs. (1.7). Such a disturbance, shown schematically in Fig. 1.1, will introduce changes in velocity, pressure, density, entropy, and c^2 ($\mathbf{u} \equiv \mathbf{v} - \mathbf{v}_0$, $p' \equiv p - p_0$, $\rho' \equiv \rho - \rho_0$, $S' \equiv S - S_0$, $c'^2 \equiv c^2 - c_0^2$, respectively) as it passes by a fixed observer.† These changes will all occur on the time scale $T_p = 1/f$, where $f = \tilde{C}/\lambda$ is the characteristic frequency of the disturbance.

The amplitude of the disturbance is measured by the magnitude of the

† The flow velocity \mathbf{u} induced by the passage of the disturbance is called the *acoustic particle velocity*. It is entirely distinct from the propagation speed \tilde{C} of the disturbance.

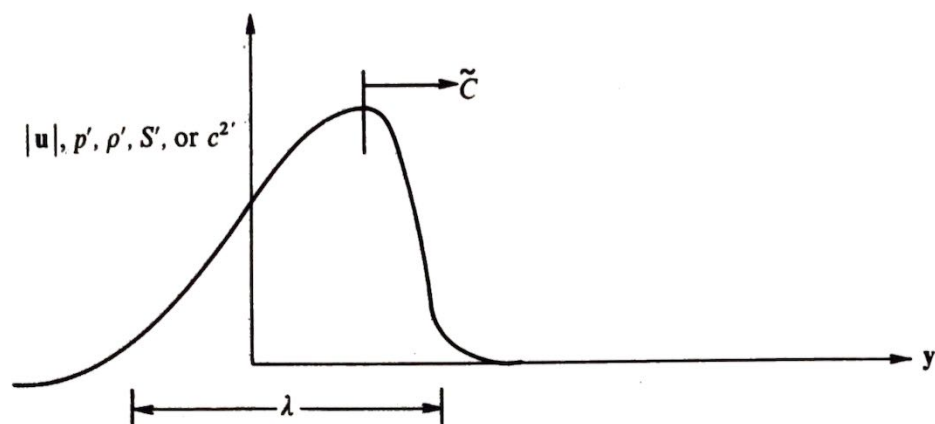


Fig. 1.1 Propagating disturbance.

fluctuations u , p' , ρ' , S' , and $c^{2'}$. But these fluctuations are usually so weak, even for the loudest sounds, that we need only consider those flows which not only satisfy the inequality

$$|u| \ll \tilde{C} = \lambda/T_p \quad (1.8)$$

but also† the inequalities $p' \ll \langle p_0 \rangle$, $\rho' \ll \langle \rho_0 \rangle$, $S' \ll \langle S_0 \rangle$, and $c^{2'} \ll \langle c_0^2 \rangle$. Then the amplitude of the disturbance can be characterized by a dimensionless variable ε such that

$$0 < \varepsilon \ll 1 \quad (1.9)$$

and

$$\left. \begin{aligned} |u|/\tilde{C} &= O(\varepsilon) \\ p'/\langle p_0 \rangle &= O(\varepsilon) \\ \rho'/\langle \rho_0 \rangle &= O(\varepsilon) \\ S'/\langle S_0 \rangle &= O(\varepsilon) \\ c^{2'}/\langle c_0^2 \rangle &= O(\varepsilon) \end{aligned} \right\} \quad (1.10)$$

Inequality (1.8) rests on the assumption (to be verified subsequently for specific cases) that the propagation speed \tilde{C} of a sufficiently small disturbance is independent of its amplitude, so that \tilde{C} will not approach zero as $\varepsilon \rightarrow 0$.

We allow $|v_0|$ to be of the same order as \tilde{C} and suppose that f and q are of order ε . Then since the time and length scales associated with the disturbance are T_p and λ , respectively, while for most common fluids $\langle p_0 \rangle \leq \langle \rho_0 \rangle \langle c_0^2 \rangle$, it is reasonable to introduce the nondimensional variables

† The first inequality requires that the velocity induced by the disturbance be small compared with its propagation speed. The remaining inequalities ensure that the fluctuations in thermodynamic properties are small relative to their mean background values.

$$\begin{aligned}
\tilde{\tau} &= \tau/T_p = f\tau & \tilde{\rho}_0 &= \rho_0/\langle\rho_0\rangle \\
\tilde{y}_i &= y_i/\lambda & \tilde{S}_0 &= S_0/\langle S_0\rangle \\
\tilde{\mathbf{v}}_0 &= \mathbf{v}_0/\tilde{C} & \tilde{c}_0^2 &= c_0^2/\langle c_0^2\rangle \\
\tilde{p}_0 &= (p_0 - \langle p_0 \rangle)/(\langle \rho_0 \rangle \langle c_0^2 \rangle) & \tilde{\mathbf{u}} &= \mathbf{u}/\tilde{C}\varepsilon \\
\tilde{p}' &= p'/\langle \rho_0 \rangle \langle c_0^2 \rangle \varepsilon & \tilde{S}' &= S'/\langle S_0 \rangle \varepsilon \\
\tilde{\rho}' &= \rho'/\langle \rho_0 \rangle \varepsilon & \tilde{c}^{2'} &= c^{2'}/\langle c_0^2 \rangle \varepsilon
\end{aligned}$$

Substituting these quantities into Eqs. (1.1) to (1.3) and (1.6), and subtracting out Eqs. (1.7) yields

$$\begin{aligned}
(\tilde{\rho}_0 + \varepsilon\tilde{\rho}') \left[\frac{\partial \tilde{\mathbf{u}}}{\partial \tilde{\tau}} + \tilde{\mathbf{v}}_0 \cdot \tilde{\nabla} \tilde{\mathbf{u}} + \tilde{\mathbf{u}} \cdot \tilde{\nabla} (\tilde{\mathbf{v}}_0 + \varepsilon \tilde{\mathbf{u}}) \right] + \tilde{\rho}' \tilde{\mathbf{v}}_0 \cdot \tilde{\nabla} \tilde{\mathbf{v}}_0 \\
= - \frac{\langle c_0^2 \rangle}{\tilde{C}^2} \tilde{\nabla} \tilde{p}' + \frac{f}{\varepsilon f \langle \rho_0 \rangle \tilde{C}} \\
\frac{\partial \tilde{\rho}'}{\partial \tilde{\tau}} + \tilde{\nabla} \cdot [(\tilde{\rho}_0 + \varepsilon\tilde{\rho}') \tilde{\mathbf{u}} + \tilde{\rho}' \tilde{\mathbf{v}}_0] = \frac{(\tilde{\rho}_0 + \varepsilon\tilde{\rho}') q}{\varepsilon f} \\
\frac{\partial \tilde{S}'}{\partial \tilde{\tau}} + \tilde{\mathbf{v}}_0 \cdot \tilde{\nabla} \tilde{S}' + \tilde{\mathbf{u}} \cdot \tilde{\nabla} \tilde{S}_0 + \varepsilon \tilde{\mathbf{u}} \cdot \tilde{\nabla} \tilde{S}' = 0 \\
(\tilde{c}_0^2 + \varepsilon \tilde{c}^{2'}) \left[\frac{\partial \tilde{\rho}'}{\partial \tilde{\tau}} + \tilde{\mathbf{v}}_0 \cdot \tilde{\nabla} \tilde{\rho}' + \tilde{\mathbf{u}} \cdot \tilde{\nabla} (\tilde{\rho}_0 + \varepsilon\tilde{\rho}') \right] + \tilde{c}^{2'} \tilde{\mathbf{v}}_0 \cdot \tilde{\nabla} \tilde{\rho}_0 \\
= \left[\frac{\partial \tilde{p}'}{\partial \tilde{\tau}} + \tilde{\mathbf{v}}_0 \cdot \tilde{\nabla} \tilde{p}' + \tilde{\mathbf{u}} \cdot \tilde{\nabla} (\tilde{p}_0 + \varepsilon\tilde{p}') \right]
\end{aligned}$$

Then since the nondimensionalization has been specifically chosen to insure that the dimensionless variables are all of order 1, the inequality (1.9) shows that we can neglect the terms multiplied by ε to obtain, upon reverting to dimensional quantities,

$$\left. \begin{aligned}
\rho_0 \left(\frac{\partial \mathbf{u}}{\partial \tau} + \mathbf{v}_0 \cdot \nabla \mathbf{u} + \mathbf{u} \cdot \nabla \mathbf{v}_0 \right) + \rho' \mathbf{v}_0 \cdot \nabla \mathbf{v}_0 &= -\nabla p' + f \\
\frac{\partial \rho'}{\partial \tau} + \nabla \cdot (\rho_0 \mathbf{u} + \rho' \mathbf{v}_0) &= \rho_0 q \\
\frac{\partial S'}{\partial \tau} + \mathbf{v}_0 \cdot \nabla S' + \mathbf{u} \cdot \nabla S_0 &= 0 \\
c_0^2 \left(\frac{\partial \rho'}{\partial \tau} + \mathbf{v}_0 \cdot \nabla \rho' + \mathbf{u} \cdot \nabla \rho_0 \right) + c^{2'} \mathbf{v}_0 \cdot \nabla \rho_0 &= \frac{\partial p'}{\partial \tau} + \mathbf{v}_0 \cdot \nabla p' + \mathbf{u} \cdot \nabla p_0
\end{aligned} \right\} (1.11)$$

These results are frequently referred to as linearized gas-dynamic equations. We have shown that they govern the propagation of small disturbances

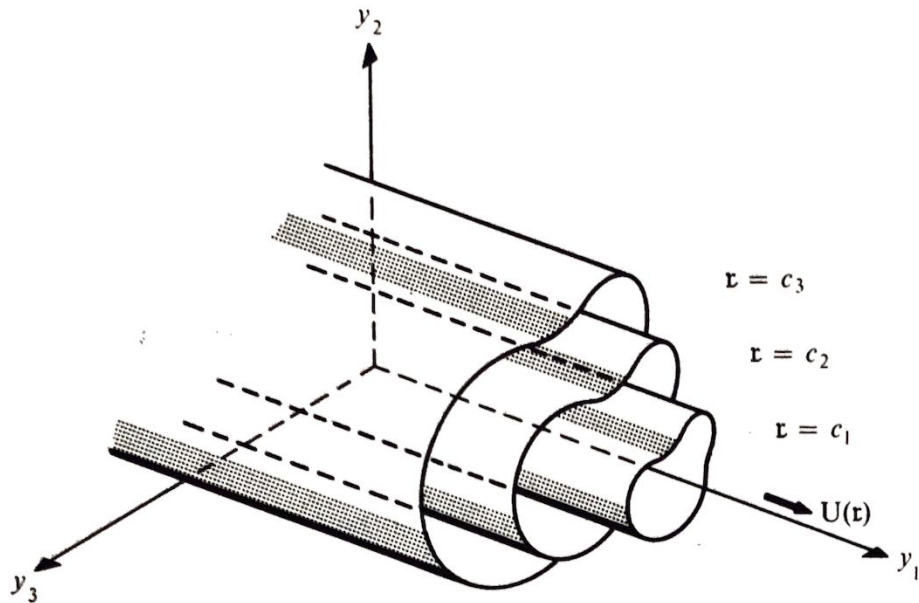


Fig. 1.2 Cylindrical coordinate surfaces.

through a steady flow. They will not apply to any region of the flow where the disturbances and their gradients do not remain small.

Perhaps the simplest nontrivial solution to Eqs. (1.7) is provided by a *unidirectional, transversely sheared mean flow* wherein

$$\mathbf{v}_0 = \hat{\mathbf{i}}U(\mathbf{r}(y_2, y_3)), \quad \rho_0 = \text{constant}, \quad p_0 = \text{constant}, \quad S_0 = \text{constant} \quad (1.12)$$

$\hat{\mathbf{i}}$ denotes the unit vector in the y_1 -direction, and the transverse coordinate variable $\mathbf{r}(y_2, y_3)$ is an arbitrary function of the rectangular coordinates y_2 and y_3 in the crossflow direction. The surfaces on which \mathbf{r} , and as a consequence the mean velocity U , remain constant can be thought of as coordinate surfaces in a cylindrical coordinate system, such as the one depicted in Fig. 1.2. Changes in U occur only in the direction $\nabla \mathbf{r}$ normal to these surfaces. Thus, when

$$\mathbf{r} = r_0 \equiv \sqrt{y_2^2 + y_3^2} \quad (1.13)$$

the coordinate surfaces become circular cylinders and, as a result, $\mathbf{r} = r_0$ becomes the radial coordinate in a standard cylindrical coordinate system with polar axis in the y_1 -direction. In this case the velocity profiles are purely radial. On the other hand, when

$$\mathbf{r} = y_2 \quad (1.14)$$

the coordinate surfaces become parallel planes and the corresponding mean flow a parallel shear flow such as the one illustrated in Fig. 1.3.

For several reasons the main emphasis in this book will be on cases where the background flows are of the type (1.12).[†] The first is the relative

[†] A treatment of the acoustics of moving media from an entirely different point of view can be found in Blokhintsev.¹

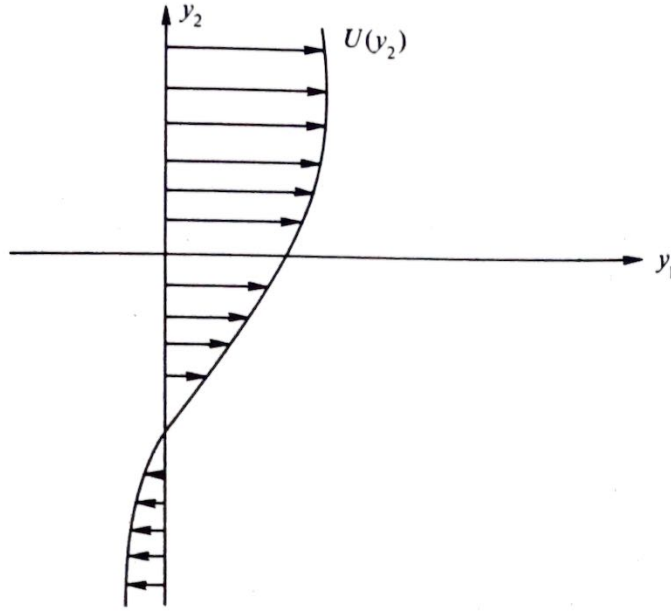


Fig. 1.3 Parallel sheared, mean flow.

simplicity of such flows. Since the equations governing the propagation of sound in a moving medium are, in general, quite complex, it is helpful to consider one of the simplest cases. The second reason results from the fact that in the following chapters it is mainly the effects of velocity gradients on aerodynamic sound generation that are considered and not the effects of gradients in thermodynamic variables. Since the flow field given by Eq. (1.12) has only velocity gradients and no pressure or density gradients, it is particularly suitable for illustrating the effect of the former. Finally, it turns out that many of the flows that are of interest in aeroacoustics are actually fairly well described by Eq. (1.12).

Inserting Eq. (1.12) into Eqs. (1.11) and eliminating ρ' between the second and last equations yields

$$\left. \begin{aligned} \rho_0 \left(\frac{D_0 \mathbf{u}}{D\tau} + \mathbf{i} \frac{dU}{dr} u_r g \right) &= -\nabla p + \mathcal{F} \\ \frac{1}{\rho_0 c_0^2} \frac{D_0 p}{D\tau} + \nabla \cdot \mathbf{u} &= q \\ \frac{D_0 S}{D\tau} &= 0 \end{aligned} \right\} \quad (1.15)$$

where

$$\frac{D_0}{D\tau} \equiv \frac{\partial}{\partial \tau} + U \frac{\partial}{\partial y_1}$$

$$g(y_2, y_3) = |\nabla \mathbf{r}|$$

and since $\nabla \mathbf{r} / |\nabla \mathbf{r}|$ is the unit normal to the $r = \text{Constant}$ coordinate surfaces,

$$u_r \equiv \mathbf{u} \cdot \frac{\nabla \mathbf{r}}{|\nabla \mathbf{r}|}$$

is the disturbance velocity in the direction perpendicular to these surfaces. When r is determined by Eq. (1.13), u_r becomes the radial velocity. The geometric weighting factor g is equal to unity in both of the transverse coordinate systems introduced above. Finally it should be noted that we have dropped the prime on the p so that this symbol now denotes the fluctuating pressure. This will be done whenever no confusion is likely to result.

The operator $D_0/D\tau$ represents the time rate of change seen by an observer moving along with the mean flow. The third Eq. (1.15) therefore states that the entropy does not change with time for such an observer. Thus, the entropy will be constant everywhere in the flow whenever it is uniform and steady far upstream. Equation (1.4) then shows that

$$d\rho = \frac{1}{c^2} dp$$

while the fifth Eq. (1.10) implies

$$c^2 = c_0^2 + O(\varepsilon)$$

But, since, c_0^2 is constant, integrating the previous equation from the background state yields

$$\frac{p}{\rho_0 c_0^2} = \frac{\rho - \rho_0}{\rho_0} \equiv \frac{\rho'}{\rho_0} \quad \text{for } S = \text{Constant} \quad (1.16)$$

The quantity on the right is called the *condensation*.

Since

$$\nabla \cdot \frac{D_0 \mathbf{u}}{D\tau} = \frac{D_0}{D\tau} \nabla \cdot \mathbf{u} + \frac{dU}{dx} g \frac{\partial u_r}{\partial y_1}$$

taking the divergence of the first Eq. (1.15), operating with $D_0/D\tau$ on the second, and subtracting the result yields

$$\nabla^2 p - \frac{1}{c_0^2} \frac{D_0^2}{D\tau^2} p + 2\rho_0 \frac{dU}{dx} g \frac{\partial u_r}{\partial y_1} = \nabla \cdot \mathcal{F} - \rho_0 \frac{D_0 q}{D\tau} \quad (1.17)$$

Because this equation has two dependent variables, it cannot by itself be solved to determine the disturbance field. However, in the special case where the mean velocity U is constant, the last term on the left side drops out and the equation becomes

$$\nabla^2 p - \frac{1}{c_0^2} \frac{D_0^2}{D\tau^2} p = \nabla \cdot \mathcal{F} - \rho_0 \frac{D_0 q}{D\tau} \equiv -\gamma \quad (1.18)$$

which (together with suitable initial and boundary conditions) can be solved to uniquely determine the fluctuating pressure p . Once this quantity is found, the acoustic particle velocity \mathbf{u} can be determined from the first Eq. (1.15). Equation (1.18) is an inhomogeneous wave equation for a uniformly moving medium. The reason for this terminology will be clear subsequently.

Equations (1.16) and (1.18) show that, if the entropy is everywhere constant, the density fluctuation also satisfies an inhomogeneous wave equation

$$\nabla^2 \rho' - \frac{1}{c_0^2} \frac{D_0^2}{D\tau^2} \rho' = \frac{1}{c_0^2} \left(\nabla \cdot \mathcal{J} - \rho_0 \frac{D_0 q}{D\tau} \right) \quad \text{for } S = \text{Constant} \quad (1.19)$$

Finally, when $U = 0$, Eq. (1.18) reduces to the inhomogeneous wave equation for a stationary medium or simply the inhomogeneous wave equation

$$\nabla^2 p - \frac{1}{c_0^2} \frac{\partial^2 p}{\partial \tau^2} = \nabla \cdot \mathcal{J} - \rho_0 \frac{\partial q}{\partial \tau} \equiv -\gamma \quad (1.20)$$

which forms the basis of the field of classical acoustics.

We now return to the general Eq. (1.17). This result closely resembles the wave Eq. (1.18) but the additional term on the left side involves the velocity and must be eliminated in order to obtain a single differential equation for the pressure. To this end, we form the dot product of the momentum Eq. (1.15) with the unit vector $\nabla \mathbf{r}/|\nabla \mathbf{r}|$ and differentiate the result with respect to y_1 to obtain

$$\rho_0 \frac{D_0}{D\tau} \frac{\partial u_r}{\partial y_1} = -g \frac{\partial^2 p}{\partial \mathbf{r} \partial y_1} + \frac{\partial \mathcal{J}_r}{\partial y_1} \quad (1.21)$$

where \mathcal{J}_r , of course, denotes the component, $\mathcal{J} \cdot \nabla \mathbf{r}/|\nabla \mathbf{r}|$, of \mathcal{J} in the direction perpendicular to the constant \mathbf{r} coordinate surfaces and

$$\frac{\partial}{\partial \mathbf{r}} \equiv \frac{\nabla \mathbf{r}}{|\nabla \mathbf{r}|^2} \cdot \nabla$$

denotes a derivative in this direction.[†] Then operating on Eq. (1.17) with $D_0/D\tau$ and substituting Eq. (1.21) into the result yields

$$\begin{aligned} \frac{D_0}{D\tau} \left(\nabla^2 p - \frac{1}{c_0^2} \frac{D_0^2}{D\tau^2} p \right) - 2 \frac{dU}{d\mathbf{r}} g^2 \frac{\partial^2 p}{\partial \mathbf{r} \partial y_1} \\ = \frac{D_0}{D\tau} \nabla \cdot \mathcal{J} - 2 \frac{dU}{d\mathbf{r}} g \frac{\partial \mathcal{J}_r}{\partial y_1} - \rho_0 \frac{D_0^2}{D\tau^2} q \equiv -\gamma \end{aligned} \quad (1.22)$$

[†] Suppose that $s(y_2, y_3) = \text{constant}$ defines a family of coordinate surfaces which are orthogonal to the surfaces $\mathbf{r}(y_2, y_3) = \text{constant}$. Then $\partial/\partial \mathbf{r}$ will be the partial derivatives with respect to \mathbf{r} with s held constant. Notice that the coordinates s and \mathbf{r} can always be used as independent variables in place of y_2 and y_3 . The function g will then in general depend on both these quantities.

Thus, in the general case of a transversely sheared unidirectional mean flow the wave equation is of higher order (in two of the variables) than it is for a uniformly moving medium. We shall show subsequently that the terms on the right will, in certain cases, behave like sound sources. The first two of these can then be associated with the sound generation by the volume force \mathcal{f} while the last term can be associated with the sound generated by the volume flow of fluid q .

The solution (1.12) to the steady-flow Eqs. (1.7) can be generalized to include the effects of transverse density and entropy gradients. Thus, it is easy to verify that

$$\mathbf{u}_0 = \mathbf{i}U(\mathbf{r}(y_2, y_3)), \quad \rho_0 = \rho_0(\mathbf{r}(y_2, y_3)), \quad S_0 = S_0(\mathbf{r}(y_2, y_3)), \quad p_0 = \text{Constant} \quad (1.23)$$

is indeed a solution to Eqs. (1.7). A procedure almost identical to that used in deriving Eq. (1.22) now shows that the generalization of that equation to include transverse density and entropy gradients is

$$\begin{aligned} \frac{D_0}{D\tau} \left(\rho_0 \nabla \cdot \frac{1}{\rho_0} \nabla p - \frac{1}{c_0^2} \frac{D_0^2}{D\tau^2} p \right) - 2 \frac{dU}{d\mathbf{r}} g^2 \frac{\partial^2 p}{\partial \mathbf{r} \partial y_1} \\ = \frac{D_0}{D\tau} \left(\rho_0 \nabla \cdot \frac{\mathcal{f}}{\rho_0} \right) - 2 \frac{dU}{d\mathbf{r}} g \frac{\partial \mathcal{f}_\tau}{\partial y_1} - \rho_0 \frac{D_0^2}{D\tau^2} q \equiv -\gamma \end{aligned} \quad (1.24)$$

Notice, however, that this result does not actually depend on the mean entropy $S_0(\mathbf{r})$.

Since p_0 is constant, c_0 can be expressed in terms of ρ_0 (or vice versa) once an equation of state for the fluid is given. Thus, the pressure and density in an ideal gas are related (through a gas constant \mathcal{R}) to the absolute temperature Θ by $p = \rho \mathcal{R} \Theta$, and, whenever the entropy is held constant, are related to each other by $dp/p = \kappa d\rho/\rho$, where κ is the specific heat ratio. Hence, it follows from Eq. (1.5) that

$$c_0 = \sqrt{\kappa \frac{p_0}{\rho_0}} = \sqrt{\kappa \mathcal{R} \Theta_0} \quad (1.25)$$

This relation can be used to eliminate the density in the first term in parentheses on the left side of Eq. (1.24) to obtain

$$\frac{D_0}{D\tau} \left(\nabla \cdot c_0^2 \nabla p - \frac{D_0^2 p}{D\tau^2} \right) - 2c_0^2 \frac{dU}{d\mathbf{r}} g^2 \frac{\partial^2 p}{\partial \mathbf{r} \partial y_1} = -c_0^2 \gamma$$

1.3 WAVE-LIKE SOLUTIONS OF ACOUSTIC EQUATIONS

In principle, all acoustic phenomena that occur in a transversely sheared flow can be analyzed simply by solving the wave equation (1.24). In this

section we study some of the wave-like solutions that are pertinent to the aerodynamic sound generation process. We shall, for simplicity, restrict our attention to the case where both the mean gradients in thermodynamic properties and the source distributions that comprise the right side of Eqs. (1.22) and (1.24) are zero.

First suppose that p is either stationary in time or vanishes as $\tau \rightarrow \pm \infty$. Then taking the Fourier transform of Eq. (1.22) and using the first entry in Table 1.1 of Appendix 1.A.2 yields

$$-i\left(k_0 + iM \frac{\partial}{\partial y_1}\right) \left[\nabla^2 P + \left(k_0 + iM \frac{\partial}{\partial y_1}\right)^2 P \right] - 2 \frac{dM}{d\tau} g^2 \frac{\partial^2 P}{\partial \tau \partial y_1} = 0 \quad (1.26)$$

where $M = U/c_0$ is the mean-flow Mach number, $k_0 \equiv \omega/c_0$, and P denotes the Fourier transform of p . This result also applies when p is periodic in time provided, of course, that P is interpreted as its n th Fourier coefficient and ω as the n th harmonic of its fundamental frequency. We shall henceforth refer to quantities such as P , which can represent either Fourier coefficients or Fourier transforms, simply as *Fourier components*.

Solutions to Eq. (1.22) (with zero right-hand side) are obtained by inserting the solutions to Eq. (1.26) into the appropriate Fourier inversion formula. (See Appendix 1.A.) Of course, when p is a simple harmonic function of time the solutions to these two equations are related by

$$p = P e^{-i\omega\tau}$$

1.3.1 Simple Waves in a Stationary Medium

Many of the wave-like properties of the solutions to Eq. (1.22) are exhibited even in the case of a stationary medium, and such properties are probably most easily understood in this context. Thus, when the Mach number M of the medium is zero, Eq. (1.26) reduces to the *Helmholtz* equation

$$(\nabla^2 + k_0^2)P = 0 \quad (1.27)$$

which, of course, could also have been obtained simply by taking the Fourier transform of Eq. (1.20). Suppose, for simplicity, that $\omega \geq 0$. Then Eq. (1.27) possesses a solution of the form

$$P = A e^{ik_0 \cdot y}$$

where

$$|\mathbf{k}_0| = k_0 \equiv \frac{\omega}{c_0}$$

and A is a constant. Hence, whenever its source term γ is zero, Eq. (1.20) possesses a solution of the form†

† When solutions to the wave equation are given in complex form, the solution to the physical problem is generally understood to be the real part.

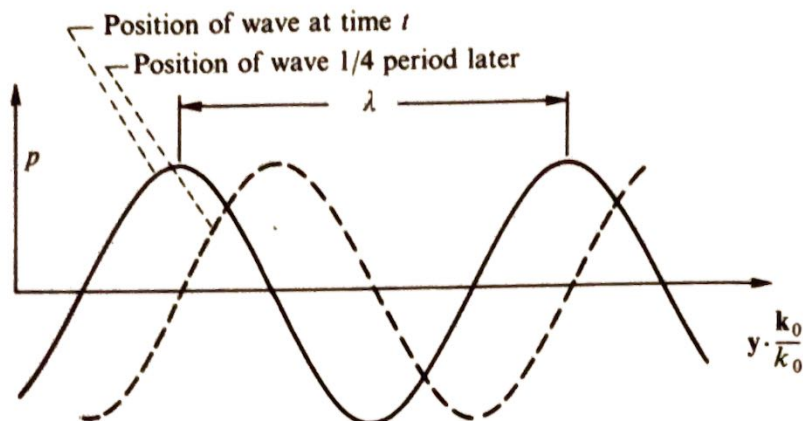


Fig. 1.4 Plane wave propagation $\frac{1}{4}$ period after time t .

$$p = A e^{i(\mathbf{k}_0 \cdot \mathbf{y} - \omega \tau)}, \quad |\mathbf{k}_0| = \frac{\omega}{c_0} \quad (1.28)$$

called a *plane wave*. The constant A is called the complex *amplitude* of the wave, $\Phi_0 \equiv \arg A \equiv \tan^{-1} (\mathcal{I}m A / \mathcal{R}e A)$ is called the phase constant, and

$$\Phi = \mathbf{k}_0 \cdot \mathbf{y} - \omega \tau + \Phi_0 \quad (1.29)$$

is called the *instantaneous phase* or simply the *phase*.

When the solution is given by this relation, the pressure must be a simple harmonic function of time at each fixed point \mathbf{y} . The *angular frequency* of this motion is ω ; its *frequency* f is $\omega/2\pi$ and its period T_p is $1/f$. The vector \mathbf{k}_0 is called the *wave number vector*.

Although the pressure oscillations have the same frequency and the same amplitude $|A|$ at every point, the oscillations at different points will usually not be in phase. In fact, the difference in phase between any two points, say \mathbf{y}_1 and \mathbf{y}_2 , is given by $\mathbf{k}_0 \cdot (\mathbf{y}_1 - \mathbf{y}_2)$ and as a result remains constant in time. This also shows that the phase is constant on any plane perpendicular to the \mathbf{k}_0 -direction. Since the trigonometric functions are periodic, with period 2π , the pressure fluctuations at any two points will be in phase whenever $(\mathbf{k}_0/k_0) \cdot (\mathbf{y}_1 - \mathbf{y}_2)$, the component in the \mathbf{k}_0 -direction of the distance between these points, is equal to

$$\frac{2\pi}{k_0} = \frac{2\pi c_0}{\omega} = \frac{c_0}{f} = T_p c_0$$

This length, which we denote by λ , is called the *wavelength*. Thus, at any time $t = t_0$, the pressure will vary along the \mathbf{k}_0 -direction in the manner shown by the solid curve in Fig. 1.4 and will remain constant along any plane perpendicular to this direction. At a time $\frac{1}{4}$ period later, the wave will be in the position indicated by the dotted curve. Hence, the pressure oscillations at each point are passed on to adjacent points with a phase relation that causes them to propagate as a wave with unchanging shape. Every surface of constant phase Φ (given by Eq. (1.29)), called a *phase surface*,

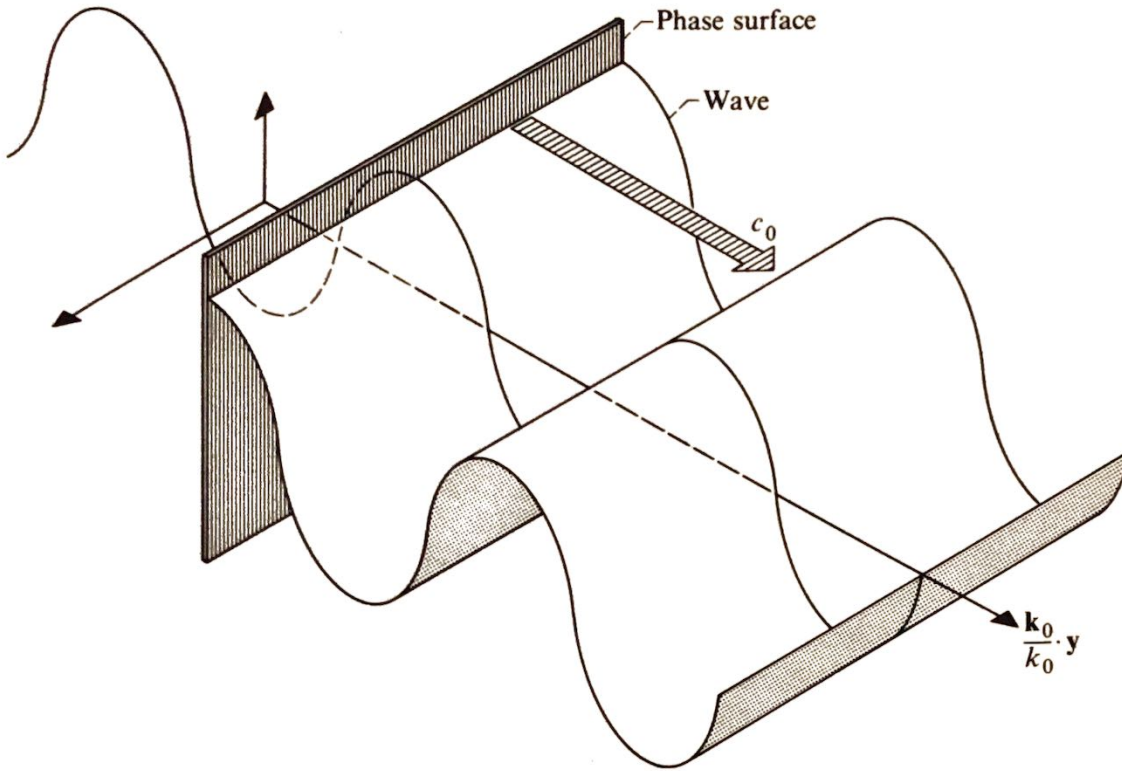


Fig. 1.5 Motion of phase surfaces for plane wave.

must be perpendicular to the \mathbf{k}_0 -direction and move along with the wave as shown schematically in Fig. 1.5. Similar behavior will occur when ω is less than zero but $|\mathbf{k}_0|$ will then equal minus ω/c_0 , and the wave will propagate in the minus \mathbf{k}_0 direction.

It can be seen from Eq. (1.29) that the common velocity of the phase surface and the disturbance is equal to c_0 —which is usually called the *speed of sound*.[†] Thus, we have shown that, at least in this special case, the initial assumption used in deriving the basic wave equations (i.e., that the propagation speed of a small disturbance is independent of the amplitude of that disturbance) is indeed justified. This will not be the case for disturbances that are too large to be governed by linearized equations. Moreover, such nonlinear behavior will even occur for weak disturbances when they are allowed to propagate over sufficiently long distances.

Since Eq. (1.20) is linear, it is easy to see that, when $\gamma = 0$, any linear combination of the plane wave solutions (Eq. (1.28)) must also be a solution. Hence, this equation possesses a solution of the form

$$p = \iint A(\mathbf{k}_0) e^{i(\mathbf{k}_0 \cdot \mathbf{y} - \omega\tau)} d\hat{\mathbf{k}}_0 d\omega \quad (1.30)$$

[†] For an ideal gas, it is given by Eq. (1.25) and is equal to about 335 m/s (1100 ft/s) in air at standard conditions.

where

$$\omega = c_0 k_0$$

and $\hat{\mathbf{k}}_0$ denotes the unit vector $\mathbf{k}_0/|\mathbf{k}_0|$. If the regions under consideration were all of space, this would, in fact, be the most general solution to this equation. However, solid boundaries usually play a role in most physically interesting problems that do not involve source distributions.

1.3.2 Waves in a Moving Medium

Properties of wave-like solutions in the general case. The plane wave solution (1.30) only satisfies the stationary medium wave Eq. (1.20) (with $\gamma = 0$) and even for that equation does not apply to the usual case where the sound field has external boundaries. Indeed, the general solution to Eq. (1.22) (with $\gamma = 0$) will not be a superposition of plane waves but rather a superposition of a number of "eigenfunctions", say P_α , which are determined by Eq. (1.26) as well as by the region under consideration and are usually called *modes* (see Sec. 1.C.2 of Appendix 1.C). Thus, the solution to Eq. (1.22) will usually be represented by a sum or integral (or perhaps both) of a number of simple harmonic solutions $P_\alpha(\mathbf{y}) e^{-i\omega\tau}$ which, upon expressing P_α in complex polar form, can be written as

$$A(\mathbf{y}) e^{i[k_0 S(\mathbf{y}) - \omega\tau]}$$

where $k_0 \equiv \omega/c_0$ and S and A are real.

We may regard the quantity $\Phi = k_0[S(\mathbf{y}) - c_0\tau]$ as the analogue of the instantaneous phase that appears in the plane wave solutions discussed in the previous section. At any given instant of time, Φ will be constant on any surface where $S(\mathbf{y}) = \text{Constant}$. These surfaces of constant phase are called *wave fronts* or *wave surfaces*, and the function $S(\mathbf{y})$ is called the *eikonal*. But, the amplitude of the wave $A(\mathbf{y})$ is not necessarily constant on the wave fronts as it is for plane waves. More importantly, however, A can decay with distance in such a way that the solutions need not even represent propagating waves or indeed propagating disturbances of any type.

Now the wave surface

$$k_0[S(\mathbf{y}) - c_0\tau] = \Phi = \text{Constant} = C_1$$

will, in general, move with time. Thus, a point \mathbf{y} on $\Phi = C_1$ at time τ will move to a point $\mathbf{y} + \delta\mathbf{y}$ at time $\tau + \delta\tau$ so that

$$\begin{aligned} k_0[S(\mathbf{y}) - c_0\tau] &= k_0[S(\mathbf{y} + \delta\mathbf{y}) - c_0(\tau + \delta\tau)] \\ &= k_0[S(\mathbf{y}) + \nabla S \cdot \delta\mathbf{y} - c_0(\tau + \delta\tau)] + O(|\delta\mathbf{y}|^2) \end{aligned}$$

This shows that, to first order in $\delta\tau$,

$$\nabla S \cdot \delta \mathbf{y} = c_0 \delta \tau$$

Hence, in the limit as $\delta\tau \rightarrow 0$,

$$\nabla S \cdot \left(\frac{d\mathbf{y}}{d\tau} \right)_{\Phi = \text{Constant}} = c_0 \quad (1.31)$$

Since $\nabla S/|\nabla S|$ is a unit normal to the wave front $\Phi = C_1$ (see Fig. 1.6) and $(d\mathbf{y}/d\tau)_{\Phi = \text{Constant}}$ is the time rate of change of position of a point that moves with this surface,

$$V_p \equiv \frac{\nabla S}{|\nabla S|} \cdot \left(\frac{d\mathbf{y}}{d\tau} \right)_{\Phi = C_1}$$

is the normal velocity of this wave front. It is called the *phase speed*, and since Eq. (1.31) shows that it is related to $|\nabla S|$ by

$$V_p = \frac{c_0}{|\nabla S|} > 0 \quad (1.32)$$

the phase surface will always move in the positive ∇S -direction.

Uniformly moving media. Now suppose that the velocity U of the medium is constant so that the wave motion is governed by Eq. (1.18). This formula closely resembles the stationary-medium wave Eq. (1.20). In fact, suppose the analysis is carried out in a reference frame that moves with the velocity U . Then the medium ought to appear at rest, and the sound propagation ought to be governed by the stationary-medium wave Eq. (1.20).

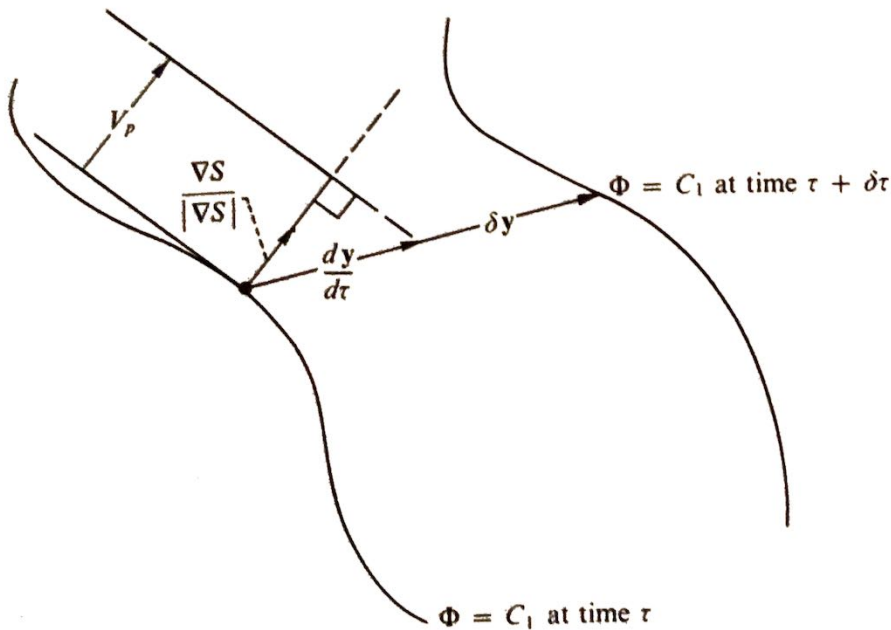


Fig. 1.6 Wave fronts.

Indeed, it is easy to see that the change in variable

$$\mathbf{y}' = \mathbf{y} - \hat{\mathbf{i}}U\tau, \quad \tau' = \tau \quad (1.33)$$

transforms Eq. (1.18) into the stationary-medium wave equation

$$\left(\nabla'^2 - \frac{1}{c_0^2} \frac{\partial^2}{\partial \tau'^2} \right) p = \nabla' \cdot \mathcal{F} - \rho_0 \frac{\partial q}{\partial \tau'} \quad (1.34)$$

where ∇' denotes the operator

$$\hat{\mathbf{i}} \frac{\partial}{\partial y'_1} + \hat{\mathbf{j}} \frac{\partial}{\partial y'_2} + \hat{\mathbf{k}} \frac{\partial}{\partial y'_3}$$

Solutions to the moving-medium wave Eq. (1.18) can therefore frequently be obtained simply by transforming solutions to the stationary-medium wave Eq. (1.34) back to the laboratory frame. Thus, transforming the plane wave solution

$$p = e^{i(\mathbf{k} \cdot \mathbf{y}' - \omega' \tau')} \quad \text{for } k = |\mathbf{k}| = \frac{\omega'}{c_0} \geq 0$$

to the wave Eq. (1.34) (with the source term omitted) back into the fixed frame by means of Eq. (1.33), we obtain

$$p = e^{i[\mathbf{k} \cdot \mathbf{y} - (\omega' + \mathbf{k} \cdot \mathbf{U})\tau]}$$

where $\mathbf{U} = U\hat{\mathbf{i}}$. This result represents a plane wave in the fixed (or laboratory) frame with frequency

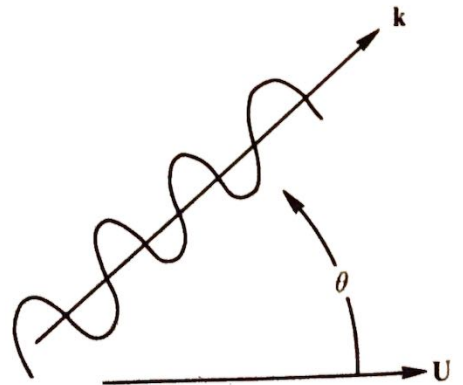
$$\omega \equiv \omega' + \mathbf{k} \cdot \mathbf{U} = \omega'(1 + M \cos \theta)$$

where $M = U/c_0$ is the mean-flow Mach number and, when $M \cos \theta \geq -1$, θ is the angle between the propagation direction \mathbf{k}/k and the mean flow direction $\hat{\mathbf{i}}$ (see Fig. 1.7). (When $M \cos \theta < -1$ the wave will actually propagate in the minus \mathbf{k}/k direction relative to the laboratory frame. Notice that this can only occur when $M > 1$, i.e., at supersonic flow speeds.)

The phase speed of the signal is

$$V_p = \frac{|\omega|}{k} = |1 + M \cos \theta| c_0 = |c_0 + U \cos \theta|$$

Fig. 1.7 Plane wave propagation in a constant-velocity medium.



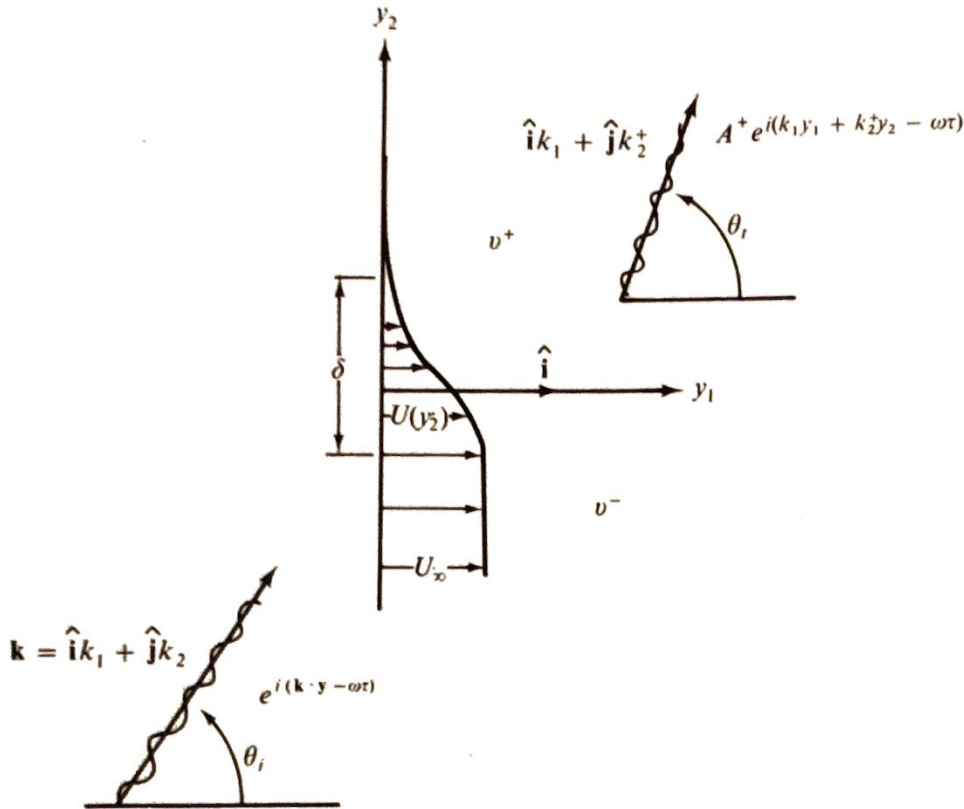


Fig. 1.8 Plane wave incident on velocity-adjustment interface.

This shows that the wave travels with a speed that is equal to the sum of its propagation speed c_0 relative to the medium and the velocity $U \cos \theta$ of the medium in its direction of propagation (or minus its direction of propagation if $-U \cos \theta > c_0$). At subsonic flow speeds, the frequency in the laboratory frame is increased if the medium has a component of its velocity in the direction of wave motion and is decreased if it has a component in the opposite direction. However, the wave has the same wavelength, $\lambda = 2\pi/k$, in both reference frames. This is simply a consequence of the fact that the moving wave pattern must appear the same to both stationary and moving observers.

Propagation of waves across a region of velocity adjustment. Consider a plane wave

$$e^{i(\mathbf{k} \cdot \mathbf{y} - \omega\tau)}, \quad \omega > 0$$

propagating through a region v^- of uniform subsonic velocity $\hat{\mathbf{i}}U_\infty$ and impinging on an interface across which the velocity $\hat{\mathbf{i}}U(y_2)$ goes to zero (see Fig. 1.8). The results of the previous section show that the frequency ω and wave number $k = |\mathbf{k}|$ of this wave must be related by

$$k_0 \equiv \frac{\omega}{c_0} = k(1 + M_\infty \cos \theta_i) \quad (1.35)$$

where $M_\infty = U_\infty/c_0 \leq 1$ is the Mach number of the mean flow in v^- and

$$\theta_i = \cos^{-1} \frac{k_1}{k} \quad (1.36)$$

is the angle between the propagation direction and the y_1 -axis. The amplitude

$$P = p e^{i\omega t} \quad (1.37)$$

of the acoustic pressure is determined by Eq. (1.26) with $r = y_2$ and $g = 1$. Inspection of this result reveals that the solution to the present problem must be of the form

$$P = e^{ik_1 y_1} F(y_2) \quad (1.38)$$

Part of the incident wave will be transmitted through the interface, and once it has traveled a sufficiently large distance will again behave like a plane wave. Consequently

$$F(y_2) \sim A^+ e^{ik_2^+ y_2} \quad \text{as } y_2 \rightarrow \infty \quad (1.39)$$

where, in order to ensure that this satisfies the stationary-medium wave equation, we must take

$$k^+ \equiv \sqrt{k_1^2 + (k_2^+)^2} = \frac{\omega}{c_0} \equiv k_0$$

Hence, it follows from Eqs. (1.35) and (1.36) that the angle θ_t which the transmitted wave propagation direction makes with the mean flow is determined by

$$\cos \theta_t = \frac{k_1}{k^+} = \frac{k_1}{k(1 + M_\infty \cos \theta_i)} = \frac{\cos \theta_i}{1 + M_\infty \cos \theta_i} \quad (1.40)$$

This angle is plotted against θ_i in Fig. 1.9. Since this plot shows that θ_t is always greater than the incident angle we can conclude that the incident wave will be turned outward upon passing through the interface whenever it initially has a component of its motion in the mean flow direction; while the transmitted wave will always be bent toward the interface whenever the incident wave opposes the mean flow. This behavior is called *refraction*.

Notice that there is a smallest angle θ_t which the transmitted wave can make with the y_1 -axis. It occurs when the incident wave is just tangent to the interface and is called the *critical angle* θ_c . Since $\cos \theta_i$ is then equal to unity, it follows from Eq. (1.40) that

$$\theta_c = \cos^{-1} \frac{1}{1 + M_\infty} \quad (1.41)$$

The region $0 \leq \theta_t \leq \theta_c$ (shown in Fig. 1.10) is inaccessible to plane waves originating in v^- and can be thought of as an acoustic "shadow region", often called the "zone of silence".

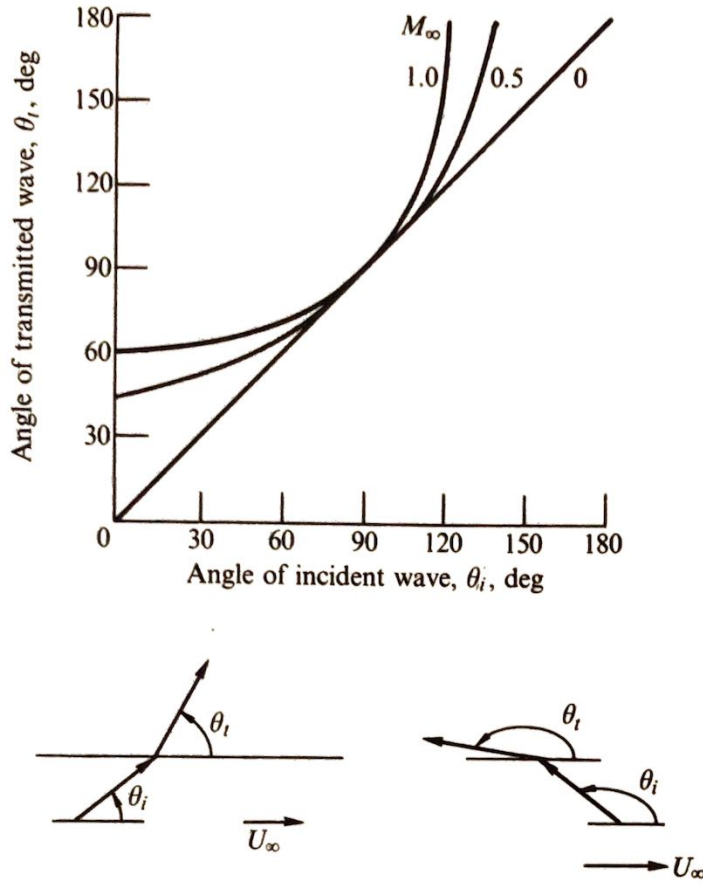


Fig. 1.9 Angle of transmitted wave for Mach numbers at infinity M_∞ of 0, 0.5, and 1.0.

The results obtained so far are purely kinematic. In order to acquire more information, it is necessary to return to the differential Eq. (1.26). Thus, inserting Eq. (1.38) into Eq. (1.26) with $g = 1$ and $r = y_2$ shows that F is determined by the equation

$$(1 - M\kappa)^2 \left[\frac{1}{(1 - M\kappa)^2} F' \right]' + k_0^2 [(1 - M\kappa)^2 - \kappa^2] F = 0 \quad (1.42)$$

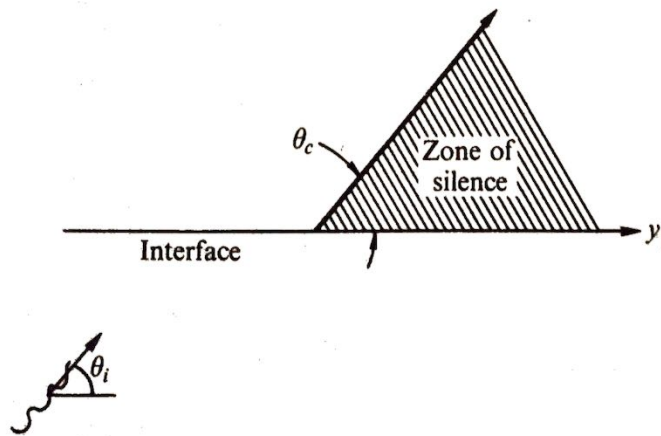


Fig. 1.10 Zone of silence.

where the primes denote differentiation with respect to y_2 and, in view of Eqs. (1.35) and (1.40), $\kappa \equiv k_1/k_0 = \cos \theta_t$. While it is usually necessary to solve this equation numerically, it is still possible to obtain a certain amount of useful information analytically by considering the case where the distance δ over which the change in mean velocity occurs is very much less than the wavelength $2\pi/k$ of the incident wave. But in view of Eq. (1.35), this implies that

$$k_0\delta \ll 1 \quad (1.43)$$

The first term in Eq. (1.42) will have order of magnitude $|F|/\delta^2$ in the vicinity of the interface, while the second term will have order of magnitude $k_0^2|F|$. The inequality (1.43) therefore shows that the contribution of the latter term can be neglected in this region and as a result that

$$\left[\frac{1}{(1 - M\kappa)^2} F' \right]' = 0.$$

This equation can be integrated immediately to show that

$$\frac{F'}{(1 - M\kappa)^2} = \text{Constant} = O(1) \quad (1.44)$$

while a second integration yields

$$F\left(\frac{\delta}{2}, \tau\right) - F\left(-\frac{\delta}{2}, \tau\right) = \text{Constant} \int_{-\delta/2}^{\delta/2} (1 - M\kappa)^2 dy_2$$

Hence it follows from the mean value theorem that the change in F across the interface is of the order of δ and is, as a consequence, negligible on the scale of wavelength. Equations (1.37) and (1.38) therefore show that $p(y_1, \delta/2, \tau) = p(y_1, -\delta/2, \tau)$. Or since the pressure outside the interface changes on the scale of a wavelength, we can neglect the difference between $y_2 = \pm\delta/2$ and $y_2 = 0$ to write

$$p_+ = p_- \quad (1.45)$$

where p_+ is the limiting value of $p(y_1, y_2, \tau)$ as y_2 goes to zero through positive values and a similar definition holds for p_- . Moreover, since $M = 0$ above the interface and $M = M_\infty$ below, Eqs. (1.37), (1.38), and (1.44) imply that

$$(1 - M_\infty\kappa)^2 \frac{\partial p_+}{\partial y_2} = \frac{\partial p_-}{\partial y_2}$$

which, in view of the functional dependence of p on τ and y_1 exhibited by Eqs. (1.37) and (1.38), can also be written as

$$\left(\frac{\partial}{\partial \tau} + U_\infty \frac{\partial}{\partial y_1} \right)^2 \frac{\partial p_+}{\partial y_2} = \frac{\partial^2}{\partial \tau^2} \frac{\partial p_-}{\partial y_2} \quad (1.46)$$

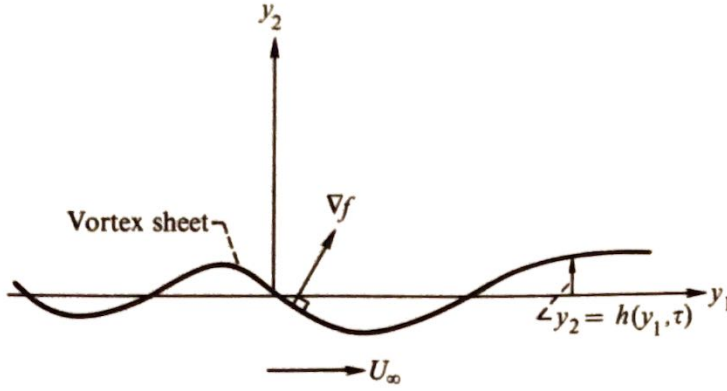


Fig. 1.11 Equivalent vortex sheet for mean velocity interface.

Equations (1.45) and (1.46) provide a set of “jump” conditions that must be satisfied by the acoustic pressure across any region where the velocity changes very rapidly on the scale of a wavelength. Although they have been derived for plane waves, they apply to any acoustic signal incident on such a region. When combined with the results already obtained, they are just sufficient to determine the amplitude A^+ of the transmitted wave (1.39) and, as a consequence, the complete solution in the region v^+ . In order to understand the significance of these conditions, consider an undulating surface separating two fluid regions, in the manner indicated in Fig. 1.11. We suppose that the mean velocity is equal to U_∞ below this surface and equal to zero above it. The equation of this interface can be written as

$$f(y_1, y_2, \tau) \equiv y_2 - h(y_1, \tau) = 0$$

so that the chain rule implies

$$\frac{\partial f}{\partial \tau} + \frac{dy}{d\tau} \cdot \nabla f = 0$$

whenever y is on the interface. But, since (see page 15) $dy/d\tau \cdot \nabla f / |\nabla f|$ represents the velocity of the surface normal to itself, we must, in order to insure that no holes will open up in the fluid, set this equal to the component of the fluid velocity \mathbf{v} normal to the interface. The preceding two equations therefore imply that

$$\frac{\partial h}{\partial \tau} + v_1 \frac{\partial h}{\partial y_1} = v_2 \quad (1.47)$$

where \mathbf{v} now represents the fluid velocity either immediately above or immediately below the interface.

We shall only consider the case where the unsteady motions are small. Then if we write $\mathbf{v} = \mathbf{u}^+$ above the interface and $\mathbf{v} = \hat{\mathbf{i}}U_\infty + \mathbf{u}^-$ below, we can suppose that \mathbf{u}^+ , \mathbf{u}^- as well as the vertical displacement h of the surface all represent small quantities. Inserting these results into Eq. (1.47) and

neglecting the squares of small quantities therefore yields

$$\frac{\partial h}{\partial \tau} = u_2^+$$

immediately above the surface and

$$\left(\frac{\partial}{\partial \tau} + U_\infty \frac{\partial}{\partial y_1} \right) h = u_2^-$$

immediately below the surface. Since the displacement of the surface must be the same on either side, h can be eliminated between these two equations to obtain

$$\left(\frac{\partial}{\partial \tau} + U_\infty \frac{\partial}{\partial y_1} \right) u_2^+ = \frac{\partial u_2^-}{\partial \tau}$$

But using the y_2 -component of the first Eq. (1.15) (with $\rho, dU/dx = 0$) to eliminate u_2^+ yields an equation that is identical to Eq. (1.46). On the other hand, it is clear that we can recover Eq. (1.45) merely by requiring that the pressure be continuous across the surface $y_2 = h(y_1, \tau)$. These results imply that the region of velocity adjustment shown in Fig. 1.8 can, in so far as its acoustics are concerned, be replaced by a fictitious velocity discontinuity or "*vortex sheet*" which (1) sustains no transverse force and (2) follows the local fluid motions.

1.4 SOLUTIONS OF ACOUSTIC EQUATIONS BY SUPERPOSITION OF ELEMENTARY SOURCES

In Sec. 1.3.1 we showed how arbitrary solutions to the homogeneous moving-medium wave equation could be constructed by superposing a number of its elementary wave-like solutions. In this section we show how general solutions to the corresponding inhomogeneous equation can be constructed by superposing the acoustic fields due to certain types of elementary concentrated sources. In doing this, we shall arrive at a certain integral formula which will, in subsequent chapters, allow us to develop a unified approach to the aerodynamic noise problem. In order to obtain this result, which is a generalization of Green's formula for the classical wave equation, it is necessary to extend the usual Green's function methods beyond what is usually done in classical acoustics. The development will therefore be somewhat more complicated.

Before proceeding, however, it is necessary first to understand the acoustics of certain simple types of concentrated sound sources.

1.4.1 Radiation from a Small Pulsating Sphere

Consider a small uniformly pulsating sphere of radius $a(\tau)$ centred at a point \mathbf{x} in a stationary medium. We suppose, as indicated in Fig. 1.12, that

$$a(\tau) \ll T_p c_0 \quad (1.48a)$$

where T_p is a characteristic period of the pulsation, and that the amplitude $\delta a(\tau)$ of the oscillation is so small compared with $a(\tau)$ that

$$\frac{\delta a}{a} \ll 1 \quad (1.48b)$$

Then the pressure disturbances induced by the oscillations will be small enough so that they can be determined from the classical wave Eq. (1.20) (with $\gamma = 0$). The solution to the present problem is most easily obtained by expressing this equation in terms of a spherical polar coordinate system with its origin at the source point \mathbf{x} . Then because of the symmetry in the boundary conditions the acoustic field will depend only on the radial coordinate $R = |\mathbf{y} - \mathbf{x}|$ and the time τ so that Eq. (1.20) becomes

$$\frac{1}{R^2} \frac{\partial}{\partial R} \left(R^2 \frac{\partial p}{\partial R} \right) - \frac{1}{c_0^2} \frac{\partial^2 p}{\partial \tau^2} = 0$$

The general solution to this equation can be written as

$$p = p_+ + p_- \quad (1.49)$$

where

$$p_{\pm} = \frac{1}{R} f_{\pm} \left(\tau \mp \frac{R}{c_0} \right) \quad (1.50)$$

and f_{\pm} denote arbitrary functions of their arguments. In order to interpret this result, notice that Rp_{\pm} is constant everywhere along each line

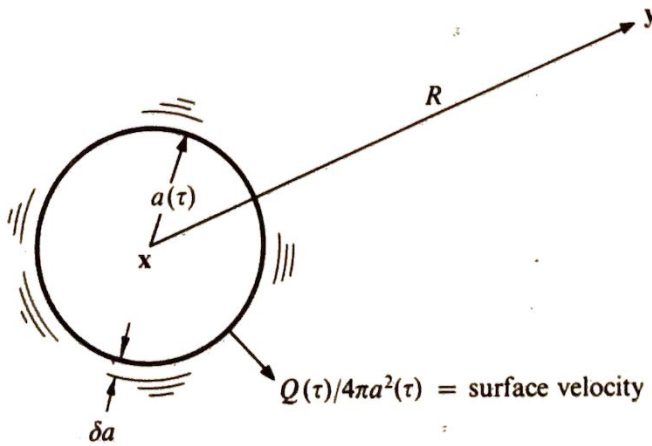


Fig. 1.12 Pulsating sphere.

$c_0\tau - R = \text{Constant}$ in the R - τ plane shown in Fig. 1.13. It therefore represents an arbitrary pulse propagating outward in the radial direction with no change in shape. The propagation speed is again equal to the speed of sound c_0 . Hence, p_+ represents an outward propagating pressure pulse whose amplitude is diminished by the factor $1/R$ while its shape remains unchanged. Similarly, p_- represents an inward-traveling wave. Since it is assumed that there are no solid surfaces to reflect the sound generated by the sphere and that there are no other acoustic sources, all the waves should ultimately travel outward toward infinity. Consequently, we must put $f_- \equiv 0$. This amounts to imposing a boundary condition at $R = \infty$ called a *radiation condition*. We could alternatively solve the problem by imposing the initial condition that the sound field be identically zero before some prescribed instant when the sphere begins to oscillate. But this would again lead to the requirement that $f_- \equiv 0$. On the other hand, we could impose the more general restriction that the sound field be confined to some finite region of space at the instant when the sphere begins to pulsate. Then the effects of this initial condition will eventually die out and, provided that the sphere continues to oscillate, the acoustic field will again contain only the outgoing wave f_+ .

The functional form of f_+ is determined by conditions at the boundary of the sphere. Thus the first Eq. (1.15) (with $U = \dot{r} = 0$) shows that the pressure is related to the radial fluid particle velocity u_R by

$$\rho_0 \frac{\partial u_R}{\partial \tau} = - \frac{\partial p}{\partial R} \quad (1.51)$$

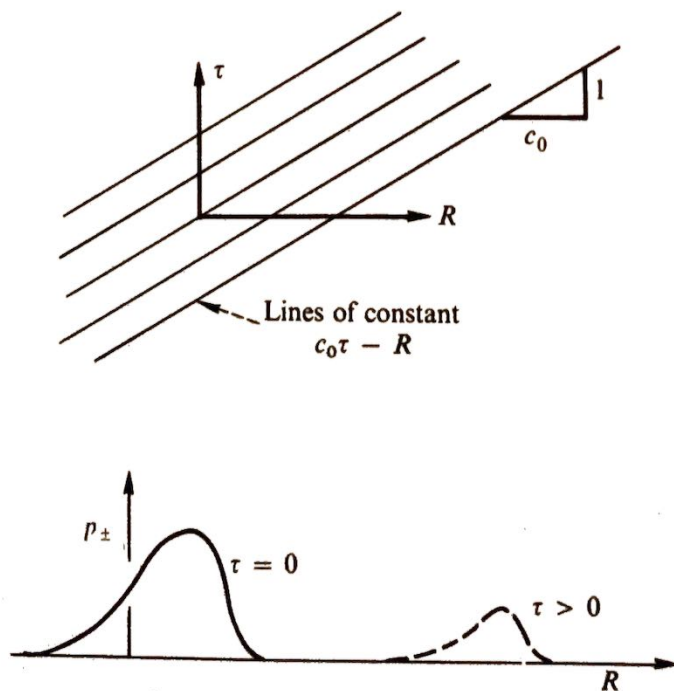


Fig. 1.13 Propagation of spherical waves.

But at the surface of the sphere where $R = a(\tau)$, u_R must be equal to the velocity of the surface which in turn is equal to $Q(\tau)/4\pi a^2(\tau)$ where Q denotes the net volume flow crossing any small spherical surface of fixed radius that surrounds the sphere. Hence, inserting Eqs. (1.49) and (1.50) into Eq. (1.51) (with $p_- = 0$) yields

$$\frac{\rho_0}{4\pi a^2} \left(\frac{dQ}{d\tau} - 2 \frac{da}{d\tau} \frac{1}{a} Q \right) = \frac{1}{a^2} f_+ \left(\tau - \frac{a}{c_0} \right) + \frac{1}{c_0 a} \frac{\partial f_+}{\partial \tau} \left(\tau - \frac{a}{c_0} \right)$$

Now, the inequality (1.48b) shows that the second of the two terms on the left side of this equation is negligible compared to the first while, since changes in time are of the order of T_p , the inequality (1.48a) shows that the second of the two terms on the right side is likewise small compared to the first. Then, since inequality (1.48a) also insures that the argument of f_+ will not differ appreciably from τ , we find that it is sufficient to put

$$f_+(\tau) = \frac{\rho_0}{4\pi} \frac{dQ(\tau)}{d\tau} \quad (1.52)$$

in order to satisfy the boundary condition on the surface of the sphere.

We have therefore shown that the acoustic pressure at a distance R from a small pulsating sphere is related to the associated volume flow $Q(\tau)$ by

$$p(R, \tau) = \frac{\rho_0}{4\pi R} \frac{\partial}{\partial \tau} Q \left(\tau - \frac{R}{c_0} \right) \quad (1.53)$$

Since the radius $a(\tau)$ is small the sphere is, in effect, concentrated at a single point. It can therefore be thought of as a "point source" of sound. On the other hand, we also used the word source in connection with the inhomogeneous terms that appear on the right-hand sides of the acoustic wave equations. In order to understand the relations between these two entities, notice that Eq. (1.49) (with p_{\pm} given by Eq. (1.50)) satisfies the acoustic wave Eq. (1.20) with the source term γ equal to zero at every point except $\mathbf{y} = \mathbf{x}$, where it becomes infinite and is therefore undefined in the usual sense. Its behavior at this point can be interpreted with the aid of the divergence theorem which states that

$$\int_v \nabla \cdot \mathbf{A} \, dy = \int_S \hat{\mathbf{n}} \cdot \mathbf{A} \, dS \quad (1.54)$$

for any vector \mathbf{A} defined on an arbitrary volume v bounded by the surface S with outward-drawn normal $\hat{\mathbf{n}}$. Thus, if v is taken to be a sphere of fixed radius R_0 centered about the point $\mathbf{y} = \mathbf{x}$ and if $d\Omega$ denotes an element of solid angle (so that $dS = R_0^2 d\Omega$), this result shows that

$$\int_v \gamma_{\pm} \, dy = R_0^2 \int_{4\pi} \left(\frac{\partial p_{\pm}}{\partial R} \right)_{R=R_0} d\Omega - \frac{1}{c_0^2} \frac{\partial^2}{\partial \tau^2} \int_{4\pi} \int_0^{R_0} p_{\pm} R^2 \, dR \, d\Omega$$

where

$$\gamma_{\pm} \equiv \nabla^2 p_{\pm} - \frac{1}{c_0^2} \frac{\partial^2 p_{\pm}}{\partial \tau^2}$$

But since Eq. (1.50) implies that

$$\frac{\partial}{\partial \tau} R p_{\pm} = \mp c_0 \frac{\partial}{\partial R} R p_{\pm}$$

the second term can be integrated by parts and combined with the first to obtain

$$\int_v \gamma_{\pm} d\mathbf{y} = -4\pi \lim_{R \rightarrow 0} R p_{\pm} = -4\pi f_{\pm}(\tau)$$

Consequently, $\gamma_{\pm} = 0$ whenever $\mathbf{y} \neq \mathbf{x}$, while its integral over any region containing \mathbf{x} is $4\pi f_{\pm}(\tau)$. However, the Dirac delta function $\delta(\mathbf{x} - \mathbf{y})$ is also zero when $\mathbf{x} \neq \mathbf{y}$, while its integral over any region containing \mathbf{x} is equal to unity. Hence, p_{\pm} actually satisfies the inhomogeneous wave equation

$$\nabla^2 p_{\pm} - \frac{1}{c_0^2} \frac{\partial^2 p_{\pm}}{\partial \tau^2} \equiv \gamma_{\pm} = -4\pi f_{\pm}(\tau) \delta(\mathbf{x} - \mathbf{y}) \quad (1.55)$$

whose source term is concentrated at the point $\mathbf{x} = \mathbf{y}$. It therefore follows from Eq. (1.52) that the solution (1.53) actually satisfies

$$\nabla^2 p - \frac{1}{c_0^2} \frac{\partial^2 p}{\partial \tau^2} = -\rho_0 \frac{\partial}{\partial \tau} Q(\tau) \delta(\mathbf{x} - \mathbf{y})$$

Upon comparing this result with Eq. (1.20) we find that the pulsating sphere has precisely the same effect acoustically as a source of volume flow q that has become concentrated at the point $\mathbf{y} = \mathbf{x}$ in such a way that its total volume flow $Q(\tau) = \int q(\mathbf{y}, \tau) d\mathbf{y}$ remains finite (Fig. 1.14). This justifies our use of the term source to refer to the inhomogeneous terms on the right sides of the acoustic equations.

More generally, we can think of the solution p_+ , given by Eq. (1.50), as an outward traveling pulse emitted from an acoustic source located at the point \mathbf{x} . Since this pulse traverses the distances R in the time R/c_0 , the altered time variable $\tau - (R/c_0)$ that appears in Eq. (1.50) must represent the time at which the signal arriving at the point \mathbf{y} was emitted from the point \mathbf{x} ; it is called the *retarded time*.

The solution p_- is somewhat less susceptible to physical interpretation. Nevertheless, it is, at least for two special choices of the arbitrary function f_- , even more useful than p_+ . The first of these is the delta function $(1/4\pi)\delta(\tau - t)$ and the second is the harmonic function $(1/4\pi)e^{i\omega\tau}$. For reasons that will become clear subsequently, the resulting expressions for p_- are

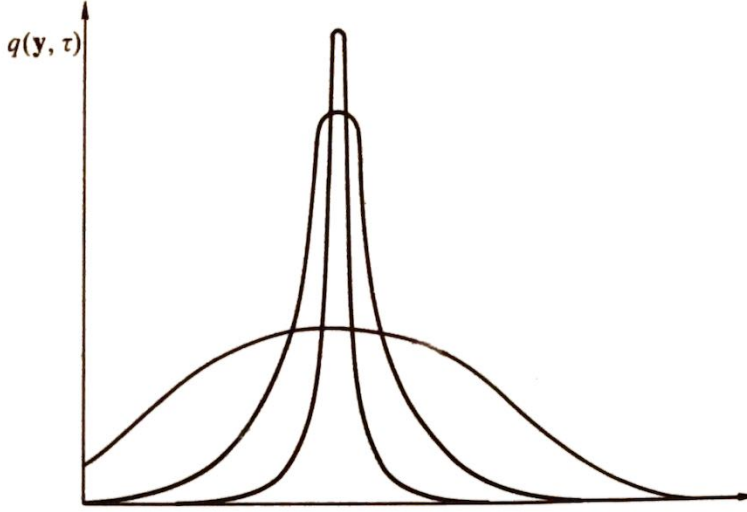


Fig. 1.14 Limiting process for concentrated source. $Q(\tau)$ is the total volume flow emitted by the source and equals the area under the curve.

called free-space Green's functions[†] and because of their importance in the remainder of the text, we assign them the special notations G^0 and $G_\omega^0 e^{-i\omega\tau}$. Thus,

$$G^0(\mathbf{y}, \tau | \mathbf{x}, t) = \frac{1}{4\pi R} \delta\left(\tau - t + \frac{R}{c_0}\right) \quad (1.56)$$

$$G_\omega^0(\mathbf{y} | \mathbf{x}) \equiv \frac{1}{4\pi R} e^{i\omega R/c_0} \quad (1.57)$$

and Eq. (1.55) shows that G^0 is determined by

$$\left(\nabla^2 - \frac{1}{c_0^2} \frac{\partial^2}{\partial \tau^2}\right) G^0 = -\delta(\tau - t) \delta(\mathbf{y} - \mathbf{x}) \quad (1.58)$$

These quantities are nearly Fourier transform pairs. In fact, it is easy to see that they are related by

$$G^0 = \frac{1}{2\pi} \int_{-\infty}^{\infty} e^{-i\omega(t-\tau)} G_\omega^0 d\omega \quad (1.59)$$

Moreover, since G^0 possesses the symmetry

$$G^0(\mathbf{x}, -t | \mathbf{y}, -\tau) = G^0(\mathbf{y}, \tau | \mathbf{x}, t) \quad (1.60)$$

it must also satisfy an equation of the form (1.58) with \mathbf{y} replaced by \mathbf{x} and t by τ . But in these variables it represents an outgoing wave. Finally, notice that since R is always positive, G^0 (and all its derivatives) will vanish identically whenever $t < \tau$.

[†] In order to distinguish them, the latter is sometimes referred to as the *reduced* free-space Green's function.

1.4.2 The Generalized Green's Formula

We now show how certain generalizations of the point-source solutions developed in the preceding section can be superposed to obtain a general formula that relates the solution to the inhomogeneous, uniformly moving medium wave equation

$$\nabla^2 p - \frac{1}{c_0^2} \frac{D_0^2}{D\tau^2} p = -\gamma(\mathbf{y}, \tau) \quad (1.61)$$

to the source distribution γ and the boundary values of p . This result is a generalization of the usual Green's formula used in classical acoustics.

Thus, let $G(\mathbf{y}, \tau | \mathbf{x}, t)$ be a solution to the inhomogeneous uniformly moving medium-wave equation

$$\nabla^2 G - \frac{1}{c_0^2} \frac{D_0^2}{D\tau^2} G = -\delta(t - \tau)\delta(\mathbf{x} - \mathbf{y}) \quad (1.62)$$

in some region of space $v(\tau)$ that is bounded (internally or externally) by the surface $S(\tau)$ (which is generally moving). The function G is called a *fundamental* solution to the wave equation. We further require that G satisfy the causality condition

$$G = \frac{D_0}{D\tau} G = 0 \quad \text{for } t < \tau \quad (1.63)$$

This quantity is clearly a generalization of the incoming-wave, free-space Green's function defined by Eq. (1.56). If the region $v(\tau)$ is not all of space, there are many functions which satisfy these conditions. However, if the region v is all of space there is only one such function, which in the case of a stationary medium is determined by Eq. (1.56).

In aerodynamic sound problems we are, for the most part, interested only in time-stationary processes (Appendix 1.A, Sec. 1.A.3). We therefore restrict the discussion in this case. Thus, let T be some very large but finite interval of time, \mathbf{V}_s and $\hat{\mathbf{n}}$ be the velocity and unit normal (drawn outward from v) of the surface $S(\tau)$ surrounding the region $v(\tau)$, and

$$V'_n = (\mathbf{V}_s - \hat{\mathbf{i}}U) \cdot \hat{\mathbf{n}} \quad (1.64)$$

the velocity of this surface normal to itself relative to a reference frame moving with the velocity $\hat{\mathbf{i}}U$. Then it is shown in Appendix 1.B that the acoustic pressure at an arbitrary point \mathbf{x} and time t is related to the distribution γ of sources within v and the distribution of the pressure and its derivatives on the boundary of v by the *generalized Green's formula*

$$\int_{-T}^T d\tau \int_{v(\tau)} \gamma(\mathbf{y}, \tau) G(\mathbf{y}, \tau | \mathbf{x}, t) d\mathbf{y} + \int_{-T}^T d\tau \int_{S(\tau)} \left[G(\mathbf{y}, \tau | \mathbf{x}, t) \left(\frac{\partial}{\partial n} + \frac{V'_n}{c_0^2} \frac{D_0}{D\tau} \right) p(\mathbf{y}, \tau) - p(\mathbf{y}, \tau) \left(\frac{\partial}{\partial n} + \frac{V'_n}{c_0^2} \frac{D_0}{D\tau} \right) G(\mathbf{y}, \tau | \mathbf{x}, t) \right] dS(\mathbf{y}) = \begin{cases} p(\mathbf{x}, t) & \text{if } \mathbf{x} \text{ is in } v(t) \\ 0 & \text{if } \mathbf{x} \text{ is not in } v(t) \end{cases} \quad (1.65)$$

The region $v(\tau)$ in this equation can be either interior or exterior to the closed surface (or surfaces) $S(\tau)$. However, in the latter case we must require that the surface integral vanish when carried out over a large sphere whose boundary moves out to infinity. This will occur whenever $p(\mathbf{y}, \tau)$ behaves like an outgoing wave at large distances from the source. When applying Eq. (1.65), it is necessary to be sure that the direction of the outward-drawn normal $\hat{\mathbf{n}}$ to S is always taken to be from the region v to the region on the opposite side of S .

The argument used to derive this result applies even when the surface $S(\tau)$ is absent. Hence, Eq. (1.65), with the surface integral omitted, will apply whenever the region v is all of space. However, as indicated above, there is then only one possible solution to Eq. (1.62) that satisfies condition (1.63) and vanishes at infinity. When $U = 0$, it is the function G^0 defined by Eq. (1.56). Equation (1.65) therefore becomes

$$p(\mathbf{x}, t) = \int_{-T}^T \int \gamma(\mathbf{y}, \tau) G^0(\mathbf{y}, \tau | \mathbf{x}, t) d\mathbf{y} d\tau \quad (1.66)$$

This formula can be used to compute the acoustic pressure due to any localized source distribution γ whose radiation field is uninfluenced by solid boundaries.

On the other hand, suppose that the bounding surface S is stationary and the velocity U of the medium is zero or tangent to this surface (so that $\hat{\mathbf{n}} \cdot \hat{\mathbf{i}} = 0$). Then the normal relative surface velocity V'_n becomes the normal surface velocity

$$V'_n = \mathbf{V}_s \cdot \hat{\mathbf{n}} \quad (1.67)$$

and Eq. (1.65) reduces to the classical Green's formula

$$\int_{-T}^T d\tau \int_v \gamma G d\mathbf{y} + \int_{-T}^T d\tau \int_S \left(G \frac{\partial p}{\partial n} - p \frac{\partial G}{\partial n} \right) dS = \begin{cases} p(\mathbf{x}, t) & \text{if } \mathbf{x} \text{ is in } v \\ 0 & \text{if } \mathbf{x} \text{ is not in } v \end{cases} \quad (1.68)$$

Of course, when $U = 0$, p and G must satisfy the inhomogeneous stationary-medium wave equations

$$\nabla^2 p - \frac{1}{c_0^2} \frac{\partial^2 p}{\partial \tau^2} = -\gamma(\mathbf{y}, \tau) \quad (1.69)$$

$$\nabla^2 G - \frac{1}{c_0^2} \frac{\partial^2 G}{\partial \tau^2} = -\delta(t - \tau) \delta(\mathbf{x} - \mathbf{y}) \quad (1.70)$$

1.4.3 Boundary Conditions: Green's Function

Up to this point we have not explicitly taken into account the effects of solid boundaries which, in practice, impose certain restrictions (that is boundary conditions) on the allowable solutions to the wave equation.

For the small amplitude motions consistent with the acoustic approximation the boundary conditions are usually linear; that is, they consist of linear relations between p and its derivatives (or perhaps integrals) which are specified on the boundary of the region wherein the solution is being sought. Such conditions will arise, for example, from the requirement that when $U = 0$ the normal acoustic velocity $\mathbf{u} \cdot \hat{\mathbf{n}}$ must vanish at any stationary surface that is impermeable to the flow, in which case it follows from the first Eq. (1.15) (with $\mathcal{F} = 0$) that

$$\frac{\partial p}{\partial n} = \hat{\mathbf{n}} \cdot \nabla p = 0 \quad \text{for } \mathbf{y} \text{ on a fixed surface}$$

This provides a condition that the solution p to the wave equation must satisfy on the boundary.

Since the pressure and its normal derivative cannot be independently specified in the surface integral of Eq. (1.65) and since the correct relation between them is not known *a priori*, this result cannot be used by itself to compute solutions of the inhomogeneous wave Eq. (1.61). However, whenever the solutions of Eq. (1.61) satisfy linear boundary conditions, this difficulty can, in principle, be eliminated by imposing additional restrictions on the fundamental solution G . The resulting function is then called a *Green's function*.

We shall restrict our attention to the case where the boundary surfaces are stationary† and the mean flow, if it exists, is nearly tangent to these surfaces. Then Eq. (1.65) reduces to Eq. (1.68). A Green's function for a region v is defined to be a solution $G(\mathbf{y}, \tau | \mathbf{x}, t)$ to the inhomogeneous, uniformly moving medium, wave Eq. (1.62) that satisfies linear homogeneous time-independent boundary conditions on the surface of S as well as the causality condition (1.63). If the region v is exterior to S , we require, in addition, that G vanish like y^{-1} as $y \rightarrow \infty$. Then the function G^0 defined by Eq. (1.56) is the Green's function for the case where the region v is all of space and the mean flow is zero—which justifies calling it the *free-space Green's function*.

When the mean flow is zero, the Green's function satisfies the *reciprocity relation*‡

$$G(\mathbf{y}, \tau | \mathbf{x}, t) = G(\mathbf{x}, -t | \mathbf{y}, -\tau)$$

† We can treat a surface undergoing small amplitude motion as if it were stationary and take account of its movement through boundary conditions imposed at its mean position.

‡ We omit the proof of this important result. The interested reader is referred to Ref. 2, Sec. 7.3.

which generalizes the result (1.60). Inserting this into Eq. (1.70), we find

$$\nabla_{\mathbf{x}}^2 G(\mathbf{y}, \tau | \mathbf{x}, t) - \frac{1}{c_0^2} \frac{\partial^2 G(\mathbf{y}, \tau | \mathbf{x}, t)}{\partial t^2} = -\delta(t - \tau) \delta(\mathbf{x} - \mathbf{y})$$

where

$$\nabla_{\mathbf{x}}^2 \equiv \frac{\partial^2}{\partial x_1^2} + \frac{\partial^2}{\partial x_2^2} + \frac{\partial^2}{\partial x_3^2}$$

Thus, $G(\mathbf{y}, \tau | \mathbf{x}, t)$ also satisfies the wave equation in the variables \mathbf{x} and t . But since condition (1.63) shows that G vanishes for $t < \tau$, we can now think of this entity as representing the pressure at the point \mathbf{x} and the time t caused by an impulsive source located at the point \mathbf{y} and triggered at the time τ . The causality condition (1.63) then ensures that events will propagate forward in time. The moving-medium Green's function can be interpreted in a similar fashion.

Suppose that it is desired to find a solution to the inhomogeneous wave Eq. (1.61) subject to either of the linear boundary conditions

$$\left. \begin{array}{l} \text{Case A:} \quad \frac{\partial p}{\partial n} + b(\mathbf{y})p = a(\mathbf{y}, \tau) \\ \text{or} \\ \text{Case B:} \quad p = a(\mathbf{y}, \tau) \end{array} \right\} \quad \text{for } \mathbf{y} \text{ on } S \quad (1.71)$$

where b can be any function of \mathbf{y} and a can be any function of \mathbf{y} and τ . And suppose that we can find a Green's function that satisfies the homogeneous boundary conditions

$$\left. \begin{array}{l} \text{Case A:} \quad \frac{\partial G(\mathbf{y}, \tau | \mathbf{x}, t)}{\partial n} + b(\mathbf{y})G(\mathbf{y}, \tau | \mathbf{x}, t) = 0 \\ \text{Case B:} \quad G(\mathbf{y}, \tau | \mathbf{x}, t) = 0 \end{array} \right\} \quad \text{for } \mathbf{y} \text{ on } S \quad (1.72)$$

Then inserting the corresponding pairs of boundary conditions from Eqs. (1.71) and (1.72) into the surface integral in Eq. (1.68) shows that for \mathbf{x} in v

$$\left. \begin{array}{l} \text{Case A:} \quad p(\mathbf{x}, t) = \int_{-T}^T d\tau \int_v G(\mathbf{y}, \tau | \mathbf{x}, t) \gamma(\mathbf{y}, \tau) d\mathbf{y} \\ \quad \quad \quad + \int_{-T}^T d\tau \int_S G(\mathbf{y}, \tau | \mathbf{x}, t) a(\mathbf{y}, \tau) dS(\mathbf{y}) \\ \text{Case B:} \quad p(\mathbf{x}, t) = \int_{-T}^T d\tau \int_v G(\mathbf{y}, \tau | \mathbf{x}, t) \gamma(\mathbf{y}, \tau) d\mathbf{y} \\ \quad \quad \quad - \int_{-T}^T d\tau \int_S \frac{\partial G(\mathbf{y}, \tau | \mathbf{x}, t)}{\partial n} a(\mathbf{y}, \tau) dS(\mathbf{y}) \end{array} \right\} \quad (1.73)$$

Thus, once the appropriate Green's function has been found, any solution to the wave Eq. (1.61) satisfying one of the linear boundary conditions (1.71) can be calculated from its volume source distribution γ and its prescribed boundary values $a(y, \tau)$ by using Eqs. (1.73). When no solid boundaries are present, this can be accomplished by using Eq. (1.66).

Since a Green's function represents the sound field due to an impulsive point source located at the point y at the time τ , Eq. (1.73) shows that any acoustic field can be thought of as the superposition of the fields due to a distribution $\gamma(y, \tau)$ of volume sources and a distribution $a(y, \tau)$ of boundary sources.

There are two fairly general methods for finding Green's functions called the *method of images* and the *method of eigenfunctions*. They are described in Appendix 1.C, where the general procedures are illustrated by working out certain examples—the results of which are used in Chaps. 3 and 4.

1.5 SOURCE DISTRIBUTION IN UNBOUNDED REGIONS

1.5.1 Interpretation of Solution: Kirchhoff's Theorem

The results of the preceding section are especially simple when the mean flow is zero and no solid boundaries are present. The sound field due to a localized source distribution γ is then given by Eq. (1.66). But inserting the expression (1.56) for the free-space Green's function into this result and carrying out the integration with respect to τ yields

$$p(\mathbf{x}, t) = \frac{1}{4\pi} \int \frac{\gamma(\mathbf{y}, t - R/c_0)}{R} d\mathbf{y} \quad (1.74)$$

where as usual

$$R \equiv |\mathbf{x} - \mathbf{y}|$$

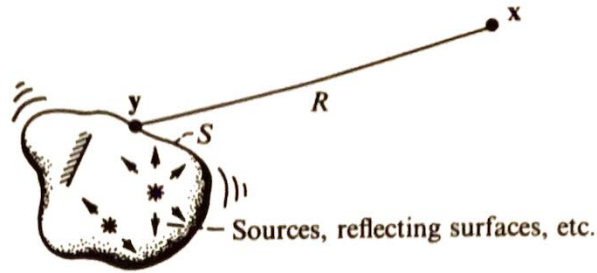
We, of course, assume that γ vanishes fast enough as $|\mathbf{y}| \rightarrow \infty$ to insure that the integral converges. Comparing Eq. (1.74) with Eqs. (1.50) and (1.55) shows that the volume element $d\mathbf{y}$ emits an elementary wave

$$\frac{1}{4\pi} \frac{\gamma(\mathbf{y}, t - R/c_0)}{R} \quad (1.75)$$

which is exactly the same as that emitted from an acoustic point source of strength γ and that the resultant acoustic pressure field is just the superposition of these waves.

In the more general case where there are, in addition to the acoustic sources, solid boundaries which reflect, absorb, or even emit sound, it is

Fig. 1.15 Emission from bounded source region.



still possible to represent the resulting acoustic pressure field by a distribution of sources of this type. Thus, consider that case where all the sources producing the sound field and all solid boundaries that interact with the sound are confined to a finite region of space, as indicated in Fig. 1.15, and let S be an imaginary surface enclosing these sources and surfaces. Then upon choosing G to be the free-space Green's function G^0 , Eq. (1.68) shows that

$$p(\mathbf{x}, t) = \int_{-T}^T d\tau \int_S \left(G^0 \frac{\partial p}{\partial n} - p \frac{\partial G^0}{\partial n} \right) dS$$

whenever the observation point \mathbf{x} is exterior to S .

Now let p_0 denote a solution to the homogeneous wave equation

$$\left(\nabla^2 - \frac{1}{c_0^2} \frac{\partial^2}{\partial \tau^2} \right) p_0 = 0$$

in the region v_0 interior to S which takes on the same values on the surface S as the exterior solution p . This fictitious pressure can be calculated mathematically by solving the boundary value problem described previously; but since there are solid surfaces and sources within S , it need not coincide with the actual pressure in this region. Setting G equal to G^0 in Eq. (1.68) and applying the result to this solution yields

$$\int_{-T}^T d\tau \int_S \left(G^0 \frac{\partial p_0}{\partial n} - p_0 \frac{\partial G^0}{\partial n} \right) dS = 0$$

whenever the observation point \mathbf{x} is exterior to S (i.e., outside v_0).

We must realize that the direction of the normal in the first formula is opposite to that in the second and, as a result, that the normal derivative $\partial/\partial n$ in the former expression corresponds to the negative of $\partial/\partial n$ in the latter. Subtracting these two equations therefore shows that

$$p(\mathbf{x}, t) = \int_{-T}^T d\tau \int_S G^0 \gamma(\mathbf{y}, \tau) dS(\mathbf{y})$$

where

$$\gamma(\mathbf{y}, \tau) \equiv \frac{\partial p}{\partial n} - \frac{\partial p_0}{\partial n} \quad \text{for } \mathbf{y} \text{ on } S$$

Inserting Eq. (1.56) into this result and carrying out the integration with respect to τ now yields

$$p(\mathbf{x}, t) = \frac{1}{4\pi} \int_S \frac{1}{R} \gamma\left(\mathbf{y}, t - \frac{R}{c_0}\right) dS(\mathbf{y}) \quad (1.76)$$

This result, which is known as *Kirchhoff's theorem*, shows that whenever the initial conditions can be neglected the acoustic pressure due to any system of sources and interacting surfaces can be represented by a suitable distribution of surface sources of the type (1.75). However, unlike the previous case where only prescribed sources are present, the strength of the surface sources will generally be unknown and will have to be found by solving the appropriate acoustic problem. Equation (1.76) is therefore mainly important because of its implication about the qualitative behavior of sound fields. Thus, since it shows that the external pressure field produced by any system of sources and interacting surfaces can be duplicated by suitable distribution of fictitious surface sources, it enables us to conclude that *it is impossible to deduce from information obtained from the acoustic field outside of the source region the precise nature of the source distribution that actually produced the sound.*

1.5.2 Multipole Expansion

Expanding the integrand of Eq. (1.74) in a Taylor series (with respect to the variable $\mathbf{R} = \mathbf{x} - \mathbf{y}$) about the point $\mathbf{R} = \mathbf{x}$, while treating the variable \mathbf{y} as a constant, yields

$$\begin{aligned} \frac{\gamma(\mathbf{y}, t - R/c_0)}{4\pi R} &= \sum_{j,k,l=0}^{\infty} \frac{(R_1 - x_1)^j (R_2 - x_2)^k (R_3 - x_3)^l}{j! k! l!} \\ &\quad \times \left[\frac{\partial^{j+k+l}}{\partial R_1^j \partial R_2^k \partial R_3^l} \frac{\gamma(\mathbf{y}, t - R/c_0)}{4\pi R} \right]_{\mathbf{R}=\mathbf{x}} \\ &= \sum_{j,k,l=0}^{\infty} \frac{\partial^{j+k+l}}{\partial x_1^j \partial x_2^k \partial x_3^l} \frac{(-y_1)^j (-y_2)^k (-y_3)^l}{j! k! l!} \frac{\gamma(\mathbf{y}, t - x/c_0)}{4\pi x} \end{aligned}$$

Hence Eq. (1.74) becomes

$$p(\mathbf{x}, t) = \sum_{j,k,l=0}^{\infty} \frac{\partial^{j+k+l}}{\partial x_1^j \partial x_2^k \partial x_3^l} \frac{(-1)^{j+k+l}}{4\pi x} m_{j,k,l} \left(t - \frac{x}{c_0} \right) \quad (1.77)$$

where

$$m_{j,k,l}(t) \equiv \int \frac{y_1^j y_2^k y_3^l}{j! k! l!} \gamma(\mathbf{y}, t) d\mathbf{y}$$

is called the *instantaneous multipole moment* and the j, k, l th term of the expansion (1.77) is called a *multipole of order* 2^{j+k+l} . Of course, it is assumed

that the source distribution vanishes rapidly enough at infinity to ensure convergence. Since, as shown in Sec. 1.4.1, each term

$$\frac{1}{4\pi x} m_{j,k,l} \left(t - \frac{x}{c_0} \right)$$

is a solution to the homogeneous wave equation whenever x is nonzero and since, as can be easily verified, the derivative of a solution is also a solution, each member of the multipole expansion (1.77) must itself be a solution of this equation.

It is easy to show† by partial integration that

$$m_{j,k,l}(t) \equiv 0 \quad \text{for all } j + k + l < N$$

whenever there exist 3^N functions $\psi_{i_1, i_2, \dots, i_N}$ which satisfy the relation

$$\gamma(\mathbf{y}, \tau) = \sum_{i_1, i_2, \dots, i_N=1}^3 \frac{\partial^N \psi_{i_1, i_2, \dots, i_N}}{\partial y_{i_1} \partial y_{i_2} \dots \partial y_{i_N}} \quad (1.78)$$

and which, together with their first N partial derivatives, vanish sufficiently fast as $y \rightarrow \infty$. The lowest order pole that appears in the multipole expansion will then be of order 2^N . Thus, we have seen, for example, that the source term due to an applied volume force \mathcal{F} will always be of the form (see Eq. (1.20))

$$\nabla \cdot \mathcal{F} = \sum_{i=1}^3 \frac{\partial \mathcal{F}_i}{\partial y_i}$$

The lowest order poles appearing in its multipole expansion of the solution will therefore be of order 2.

The multipole source structure exhibited by Eq. (1.77) becomes particularly simple for small source regions that are located at large distances from the observation point. Thus, since

$$\frac{\partial}{\partial x_i} \frac{1}{x} = O(x^{-2}) \quad \text{as } x \rightarrow \infty$$

and

$$\frac{\partial}{\partial x_i} f \left(t - \frac{x}{c_0} \right) = - \frac{x_i}{c_0 x} \frac{\partial}{\partial t} f \left(t - \frac{x}{c_0} \right)$$

for any function f of $(t - x/c_0)$, expanding Eq. (1.77) for large values of x yields

$$p(\mathbf{x}, t) \sim \sum_{j,k,l=0}^{\infty} \frac{(x_1/x)^j (x_2/x)^k (x_3/x)^l}{4\pi x} \left(\frac{1}{c_0} \frac{\partial}{\partial t} \right)^{j+k+l} m_{j,k,l} \left(t - \frac{x}{c_0} \right) \quad \text{as } x \rightarrow \infty \quad (1.79)$$

† An example of how this assertion can be proved for the case where $N = 2$ is given in Sec. 2.3.

Now suppose that the source distribution γ is essentially confined to a region whose size is of order L . Then

$$m_{j,k,l} = O(\langle \gamma \rangle L^{j+k+l+3})$$

where $\langle \gamma \rangle$ denotes the average value of γ over the source region. The j, k, l th term in Eq. (1.79) will therefore be of the order of

$$L^3 \frac{\langle \gamma \rangle}{x} \left(\frac{L}{T_p c_0} \right)^{j+k+l} = \frac{\langle \gamma \rangle}{x} \left(\frac{L}{\bar{\lambda}} \right)^{j+k+l} L^3$$

where T_p is a typical period of oscillation of the source (so that $\bar{\lambda} = c_0 T_p$ is a typical wavelength of the sound field).

This result shows that only the lowest order poles in the multipole expansion will contribute to the distant sound field emanating from a source region that is very small relative to its wavelength. A source distribution satisfying this condition is said to be *compact*. Only poles of order 2^N , where N is the largest integer for which a compact source distribution γ can be expressed in the form (1.78), will contribute to the distant sound field. Consequently, any source region that can be expressed in the form (1.78) is called a *multipole source* of order 2^N . Nevertheless it is only when the source is compact that its multipole order is of any real significance. The entity comprised of the 3^N functions $\psi_{i_1, i_2, \dots, i_N}$ which enter Eq. (1.78) is often referred to as the *source strength*. It is important to bear in mind that the lower order multipole moments will not vanish or, for that matter, may not even exist unless the $\psi_{i_1, i_2, \dots, i_N}$ vanish sufficiently fast as $y \rightarrow \infty$.

Compact, higher order multipole sources are clearly much less efficient emitters of sound than those of lower order. However, Eq. (1.77) shows that the amount of energy contained in the region near the source (often called the *near field*) will be roughly the same for all equal strength sources, regardless of their order. Consequently, some sort of "phase cancellation" must occur at large distances from the higher order sources in order to prevent this energy from being radiated away as sound.

If $N = 0$ (i.e., if γ cannot be expressed as a derivative which vanishes at infinity or on the boundary of the source region), the source is called a *monopole*, or a *simple source*. When $N = 1$ the source is called a dipole, and when $N = 2$ it is called a quadrupole. Notice that each multipole source has its own characteristic radiation pattern.

Equations (1.50) and (1.55) show that the monopole term $m_{0,0,0}(t - x/c_0)/4\pi x$ in Eq. (1.79) produces the same sound field as a concentrated point source with strength $m_{0,0,0}(\tau) = \int \gamma(y, \tau) dy$. Thus a compact source of monopole order acts as if its entire strength were concentrated at a single point (which we have for convenience taken to be the origin). This result could also have been obtained by neglecting retarded time variations over the source region in the far field (large x) expansion of Eq. (1.76) (see Sec. 1.6 below). If, however, the monopole moment $\int \gamma(y, \tau) dy$ were to vanish,

such a procedure would lead to a gross overestimate of the sound field and an incorrect picture of its radiation pattern unless the vanishing of this term were explicitly accounted for. Notice that it should nevertheless be possible to neglect the source region retarded time variations in Eq. (1.74) whenever $T_p \gg L/c_0$, i.e., whenever the source is compact. However, the preceding remarks show that it is essential to first represent the solution in a form that will allow its true multipole structure to be exhibited once retarded times variations are neglected.

Since the mean value theorem implies that

$$\gamma(\mathbf{y} + \boldsymbol{\delta}, \tau) - \gamma(\mathbf{y}, \tau) = \sum_{i=1}^3 \frac{\partial \psi_i}{\partial y_i} + O(|\boldsymbol{\delta}|^2 \gamma) \quad \text{as } |\boldsymbol{\delta}| \rightarrow 0$$

where $\psi_i \equiv \gamma \delta_i$, we can always think of a dipole source as being composed of two equal-strength monopoles that have been brought together while holding the product $\gamma \delta_i$ of their strengths times the distance between them constant. Similarly, we can always think of a quadrupole source as composed of two dipoles that are of equal strength but have opposite sign.

Now we have seen that an unsteady volume force behaves acoustically like a dipole sound source. Consequently, an unsteady stress, which can be synthesized by bringing together two equal and opposite volume forces, ought to act like a quadrupole source.

1.6 RADIATION FIELD

Since the coefficients of $m_{j,k,l}/x$ in Eq. (1.79) depend only on the orientation of the vector \mathbf{x} and not on its magnitude and since this orientation can be characterized by the two polar coordinates θ and φ shown in Fig. 1.16, it is

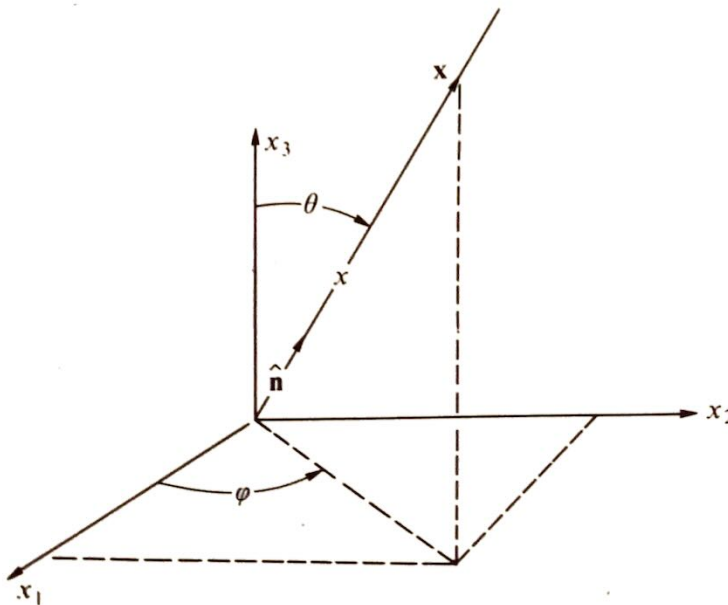


Fig. 1.16 Polar coordinates of observation point.

easy to see that the pressure fluctuations occurring at large distances from any distribution of volume sources must behave like

$$p(\mathbf{x}, t) \sim \frac{1}{4\pi x} g\left(t - \frac{x}{c_0}, \theta, \varphi\right) \quad (1.80)$$

It is not especially surprising (in view of the resemblance between Eqs. (1.74) and (1.76)) that this behavior is also exhibited at large distances from any region containing both sources and interacting solid surfaces. In fact, when $|\mathbf{x}|$ is much larger than the largest dimension of the surface S ,

$$R = \sqrt{x^2 - 2\mathbf{x} \cdot \mathbf{y} + |\mathbf{y}|^2} = x \sqrt{1 - \frac{2\mathbf{x} \cdot \mathbf{y}}{x^2} + \frac{|\mathbf{y}|^2}{x^2}} = x - \frac{\mathbf{x} \cdot \mathbf{y}}{x} + O\left(\frac{|\mathbf{y}|^2}{x}\right) \quad \text{as } x \rightarrow \infty$$

whenever \mathbf{y} is confined to S . But since $\mathbf{x} \cdot \mathbf{y}/x$ depends only on the orientation of \mathbf{x} and not on its magnitude, we can insert this expansion into Eqs. (1.76) to show, upon neglecting higher order terms in x^{-1} , that the fluctuating pressure at large distances from any region containing both sources and interacting surfaces is indeed a function of the form (1.80).

The *radiation field*, or *far field*, is defined to be that region of space which is far enough away from the sources and interacting objects (in terms of both wavelength and the size of the source) to insure that the pressure fluctuations will be characterized by Eq. (1.80).

Ideally, a source system can have a radiation field only when it is embedded in a uniform medium of infinite extent. In practice, especially in aeronautical applications, there is usually a region at some distance from the source system in which there is no appreciable radiation from reflecting objects lying even further from the source system and hence in which radiation field behavior is approximately achieved.

Let $\nabla_{\mathbf{x}}$ denote the gradient operator $\hat{\mathbf{i}}(\partial/\partial x_1) + \hat{\mathbf{j}}(\partial/\partial x_2) + \hat{\mathbf{k}}(\partial/\partial x_3)$ in the variable \mathbf{x} . Then since $\varphi = \tan^{-1} x_2/x_1$ and $\theta = \cos^{-1} x_3/x$, it is easy to see that $\nabla_{\mathbf{x}}\theta$ and $\nabla_{\mathbf{x}}\varphi$ go to zero like x^{-1} as $x \rightarrow \infty$. Hence, it follows from Eq. (1.80) that

$$\nabla_{\mathbf{x}}p \sim \frac{\hat{\mathbf{n}}}{4\pi x} \frac{\partial g}{\partial x}\left(t - \frac{x}{c_0}, \theta, \varphi\right) \quad \text{as } x \rightarrow \infty$$

where $\hat{\mathbf{n}} \equiv \nabla_{\mathbf{x}}x$ is the unit vector in the \mathbf{x} -direction shown in Fig. 1.16. Inserting this result into the momentum Eq. (1.15) (written in terms of the variables \mathbf{x} and t in place of \mathbf{y} and τ) and using the fact that $\partial g/\partial x = -(\partial g/\partial t)/c_0$ yields

$$\frac{\partial}{\partial t}\left(\mathbf{u} - \frac{1}{\rho_0 c_0} \frac{\hat{\mathbf{n}}}{x} p\right) \sim 0$$

which implies that

$$\mathbf{u}(\mathbf{x}, t) \sim \frac{1}{\rho_0 c_0} \hat{\mathbf{n}} p(\mathbf{x}, t) \quad (1.81)$$

This equation shows that the velocity $\mathbf{u} = \hat{\mathbf{n}} u_R$ is purely radial, and that its magnitude u_R is related to the pressure by

$$u_R = \frac{p}{\rho_0 c_0} \quad (1.82)$$

The highest pressures in the radiation field will therefore be found in those regions where the fluid is moving its fastest. In fact, the far field pressure and velocity will always be in phase when the sound field has harmonic time dependence.

The ratio $\rho_0 c_0$ of pressure to velocity in the radiation field is called the *characteristic acoustic impedance* of the medium. It is equal to 429 newton-seconds per cubic meter for air at 0° C and 1-atmosphere pressure.

1.7 ENERGY RELATIONS

1.7.1 Basic Definitions

In this section we shall define an acoustic energy density E and a corresponding acoustic energy flux vector \mathbf{I} for certain types of flows that are governed by the linearized gas-dynamic Eqs. (1.11). Perhaps the most obvious procedure that comes to mind when attempting to introduce suitable definitions for these quantities is to simply subtract out the energy density and energy flux vectors for the mean background flow from the corresponding total quantities for the actual flow. However, this approach has certain failings. Thus we are, for the most part, concerned with the time average acoustic energy flux $\bar{\mathbf{I}}$ (or *acoustic intensity*) rather than \mathbf{I} itself. But when the energy flux associated with the steady background flow is subtracted from this quantity the remaining terms will generally be of second order.† Moreover, some of these will not simply be products of two first-order terms and consequently will not be calculable from the solutions to the linear gas-dynamic Eqs. (1.11). In order to obtain useful definitions for E and $\bar{\mathbf{I}}$, we must require that these quantities be completely determined by the solutions to Eqs. (1.11).

† The process used in the derivation of the Eqs. (1.11) can be thought of as the first step in obtaining an asymptotic expansion of the flow variables in powers of the (small) amplitude ε of the acoustic disturbance. Since the variables which satisfy Eqs. (1.11) are of the same order as this amplitude, they can be termed first-order quantities. The next smallest terms in the expansion will be of the order of the amplitude squared and can be called second-order terms. Clearly, the product of two first-order terms is also a second-order term.

On the other hand, once we abandon this procedure the acoustic intensity will generally not be a true measure of the mean energy flux carried by the acoustic disturbance. Nevertheless (for reasons which we shall indicate subsequently) the concept of acoustic energy still retains its utility in flows where it is conserved, i.e., in flows where the net flux of acoustic energy across any surface S enclosing a source-free region v is equal to the time rate of change of energy within v . We will therefore insist that

$$-\frac{d}{d\tau} \int_v E dy = \int_S \mathbf{I} \cdot \hat{\mathbf{n}} dS \quad (1.83)$$

However, after using the divergence theorem (1.54) to eliminate the surface integral we can conclude from the fact that this relation must hold in any source-free volume v that E and \mathbf{I} must also satisfy the conservation law (or energy equation)

$$\frac{\partial E}{\partial \tau} + \nabla \cdot \mathbf{I} = 0 \quad (1.84)$$

in any such region.

Consequently, any acceptable definitions for acoustic energy and acoustic energy flux must at least satisfy the following conditions:

(1) They must be consistent with the conservation law (1.84) in any source-free region of space.

(2) They must be expressible as sums of terms each of which is the product of at most two first-order quantities with a quantity which depends only on the mean flow.

(3) They must reduce to the corresponding classical acoustics definitions whenever the steady flow is zero and the mean thermodynamic properties are constant. Such entities, if they can be found, will certainly satisfy Eq. (1.83) in any source-free region v . But averaging this equation over the time interval $T_2 - T_1$ yields

$$\frac{\mathcal{E}(T_2) - \mathcal{E}(T_1)}{T_2 - T_1} = \int_S \bar{\mathbf{I}} \cdot \hat{\mathbf{n}} dS \quad (1.85)$$

where, in view of condition (2),

$$\mathcal{E}(\tau) \equiv \int_v E(\mathbf{y}, \tau) dy$$

must be a sum of terms each of which involves a product of at most two acoustic quantities. This function will therefore be periodic in time whenever the unsteady flow is periodic. Consequently, setting the time interval in Eq. (1.85) equal to the corresponding period yields

$$\int_S \bar{\mathbf{I}} \cdot \hat{\mathbf{n}} dS = 0 \quad (1.86)$$

for any surface S enclosing a source-free region of space.

Since, on the other hand, $\mathcal{E}(\tau)$ remains bounded as $\tau \rightarrow \infty$ when the acoustic quantities are stationary random functions of time, we can, in this case, let the interval $T_2 - T_1$ become infinite so that the left side of Eq. (1.85) will again vanish and Eq. (1.86) will again hold.

The acoustic power crossing a surface S (closed or opened) is defined as

$$\mathcal{P} = \int_S \bar{\mathbf{I}} \cdot \hat{\mathbf{n}} dS$$

Hence the total acoustic power crossing any surface that completely encloses the acoustic sources will be equal to the total acoustic power crossing any other such surface. Then when the source region is localized in space we can always assume that one of these surfaces is in the radiation field. Consequently, the total acoustic power radiated by the sources can, in this case, be deduced solely from measurements taken in the far field. It is these properties from which the concepts of acoustic power and acoustic intensity derive their utility.

1.7.2 Construction of Acoustic Intensity for Isentropic Irrotational Flows

We now show how the quantities E and \mathbf{I} can be constructed. Thus, taking the dot product of the first Eq. (1.11) with $\mathbf{J} \equiv \mathbf{u} + (\rho'/\rho_0)\mathbf{v}_0$, multiplying the second by $\mathcal{H}' \equiv (p'/\rho_0) + \mathbf{u} \cdot \mathbf{v}_0$, adding the results, and finally using the vector identity $\mathbf{U} \cdot \nabla \mathbf{V} + \mathbf{V} \cdot \nabla \mathbf{U} + \mathbf{U} \times \nabla \times \mathbf{V} + \mathbf{V} \times \nabla \times \mathbf{U} = \nabla(\mathbf{U} \cdot \mathbf{V})$ (which holds for any two vectors \mathbf{U} and \mathbf{V}) in conjunction with the first Eq. (1.7) to simplify the result yields

$$\begin{aligned} \frac{\partial E}{\partial \tau} + \nabla \cdot \mathbf{I} = & \left[\frac{\mathbf{J}}{\rho_0} \cdot (\rho' \nabla p_0 - p' \nabla \rho_0) + \frac{1}{2\rho_0} \left(\rho' \frac{\partial p'}{\partial \tau} - p' \frac{\partial \rho'}{\partial \tau} \right) \right] \\ & + \mathbf{u} \cdot [\mathbf{v}_0 \times (\rho_0 \boldsymbol{\omega}' - \rho' \boldsymbol{\omega}_0)] + (\mathbf{J} \cdot \boldsymbol{\mathcal{F}} + \rho_0 \mathcal{H}' q) \end{aligned} \quad (1.87)$$

where we have put

$$E \equiv \frac{p' \rho'}{2\rho_0} + \left(\frac{\rho_0 u^2}{2} + \rho' \mathbf{u} \cdot \mathbf{v}_0 \right) \quad (1.88)$$

$$\mathbf{I} \equiv \left(\frac{p'}{\rho_0} + \mathbf{u} \cdot \mathbf{v}_0 \right) (\rho_0 \mathbf{u} + \rho' \mathbf{v}_0) \quad (1.89)$$

and $\boldsymbol{\omega}' \equiv \nabla \times \mathbf{u}$ and $\boldsymbol{\omega}_0 \equiv \nabla \times \mathbf{v}_0$ denote the perturbation and steady-state vorticity vectors.

When $\boldsymbol{\omega}' = \boldsymbol{\omega}_0 = 0$, the flow is said to be *irrotational*. The second term on the right side of Eq. (1.87) clearly vanishes for such flows. On the other

hand, Eq. (1.4) shows that $\nabla \rho_0 = \nabla p_0 / c_0^2$ in any isentropic flow and as a result Eq. (1.16) shows that the first term in brackets on the right side of Eq. (1.87) vanishes for flows of this type. Consequently, the definitions (1.88) and (1.89) satisfy the conservation law (1.84) in any source-free region of an isentropic irrotational flow. It is also easy to see that they satisfy condition (2) and that whenever $\mathbf{v}_0 = 0$, they reduce to

$$\mathbf{I} = p' \mathbf{u} \quad (1.90)$$

$$E = \frac{p'^2}{2\rho_0 c_0^2} + \frac{\rho_0 u^2}{2} \quad (1.91)$$

which are the definitions of \mathbf{I} and E that are used in classical acoustics. We have therefore shown that Eqs. (1.88) and (1.89) will provide acceptable definitions of E and \mathbf{I} for any isentropic irrotational flow. These relations were first applied to such flows by Chernov.⁶ However, Blokhintsev¹ had previously shown that a special case of definition (1.89) will lead to an appropriate average energy equation whenever the acoustic wavelength is short compared with the scale on which the mean velocity changes.

In order to interpret the first term in Eq. (1.88), notice that, in an isentropic flow, the work per unit mass done against the surroundings by the acoustic pressure p' is

$$\int_{\rho_0^{-1}}^{\rho^{-1}} p' d \frac{1}{\rho} = - \int_0^{p'} \frac{p'}{\rho^2 c_0^2} dp' = - \frac{p'^2}{2\rho_0^2 c_0^2} + \text{Third-order terms}$$

Hence, the work done per unit volume is

$$- \frac{p'^2}{2\rho_0 c_0^2} + \text{Third-order terms}$$

The first term, $p' \rho' / 2\rho_0 = p'^2 / 2\rho_0 c_0^2$, in E can therefore be interpreted as the potential energy per unit volume associated with the acoustic field.

On the other hand, the kinetic energy per unit volume is one-half the absolute value of the momentum density squared divided by the density. Then since the momentum density in the acoustic wave is

$$\rho \mathbf{v} - \rho_0 \mathbf{v}_0 = \rho_0 \mathbf{u} + \rho' \mathbf{v}_0 + \text{Second-order terms}$$

the kinetic energy per unit volume is

$$\frac{|\rho_0 \mathbf{u} + \rho' \mathbf{v}_0|^2}{2\rho} = \frac{\rho_0 u^2}{2} + \rho' \mathbf{u} \cdot \mathbf{v}_0 + \frac{\rho'^2 v_0^2}{2\rho_0} + \text{Third-order terms}$$

Consequently, the second term in Eq. (1.88) represents a portion of the kinetic energy per unit volume carried by the wave.

1.7.3 Relations for the Radiation Field

It is generally possible to assume that Eqs. (1.90) and (1.91) will hold in the radiation field. Then since the velocity and pressure are related by Eq. (1.81) in this region, it follows from Eq. (1.90) that the energy flux is in the radial direction $\hat{\mathbf{n}}$ and is given by

$$\mathbf{I} = \hat{\mathbf{n}}I$$

where

$$I = \frac{p^2}{\rho_0 c_0}$$

Taking the appropriate time average yields

$$\bar{I} = \frac{\overline{p^2}}{\rho_0 c_0} \quad (1.92)$$

Thus, the acoustic intensity in the radiation field is proportional to the mean square acoustic pressure. Now most microphones in most cases measure root-mean-square (rms) sound pressure, while the rms fluctuating pressure at the ear is believed to be the quantity most closely related to the sensation of loudness. But since Eq. (1.92) only holds under special circumstances, the acoustic intensity does not always provide a measure of the signal sensed by the ear or a microphone. Moreover, an ear, and usually a microphone, which is basically a diaphragm encased on a reflecting object (head or microphone housing) will not sense the pressure that would exist if it were not present unless its housing is small compared with the wavelength—primarily because of the pressure increase caused by the reflected sound.

Equations (1.80) and (1.92) imply that

$$\bar{I} = \frac{1}{16\pi^2 x^2 \rho_0 c_0} \overline{g^2\left(t - \frac{x}{c_0}, \theta, \varphi\right)}$$

Then, since the results of Appendix 1.A show that the average is independent of time translations for both periodic or time-stationary processes, this becomes

$$\bar{I} = \frac{1}{16\pi^2 \rho_0 c_0 x^2} \overline{g^2(t, \theta, \varphi)}$$

which shows that the average intensity is proportional to x^{-2} in the radiation field.

When the sound field is periodic so that

$$p(\mathbf{x}, t) = \sum_{n=-\infty}^{\infty} P_n(\mathbf{x}) e^{-i\omega n t}$$

Eqs. (1.92) and (1.A.7) imply that

$$\bar{I} = \frac{1}{\rho_0 c_0} \sum_{n=-\infty}^{\infty} |P_n|^2$$

The quantity

$$\bar{I}_n \equiv \frac{|P_n|^2}{\rho_0 c_0}$$

can therefore be interpreted as the average acoustic energy flux carried by the n th harmonic of the sound field and is accordingly called the *intensity spectrum*. Equation (1.A.6) shows that it is related to the normalized pressure autocorrelation function $\Gamma(\tau)$ by

$$\Gamma(\tau) \equiv \frac{\overline{p(t)p(t+\tau)}}{\rho_0 c_0} = \sum_{n=-\infty}^{\infty} \bar{I}_n e^{-i\omega_n \tau} \quad (1.93)$$

When the sound field is time *stationary*, Eqs. (1.92) and (1.A.22) imply that

$$\bar{I} = \frac{1}{\rho_0 c_0} \int_{-\infty}^{\infty} S_{11}(\omega) d\omega$$

where $S_{11}(\omega)$ is the Fourier transform of the pressure autocorrelation function $\overline{p(t)p(t+\tau)}$. Hence, the quantity $\bar{I}_\omega \equiv S_{11}(\omega)/\rho_0 c_0$ can be interpreted as the average acoustic energy flux per unit frequency and is therefore called the *intensity spectrum*. Equation (1.A.21) shows that it is related to the normalized pressure autocorrelation function $\Gamma(\tau)$ by

$$\Gamma(\tau) \equiv \frac{\overline{p(t)p(t+\tau)}}{\rho_0 c_0} = \int_{-\infty}^{\infty} \bar{I}_\omega e^{-i\omega \tau} d\omega \quad (1.94)$$

These relations have only been shown to hold in the radiation field and will not, in general, apply at points near the source region.

1.7.4 Definitions of Intensity and Energy in General Inviscid Non-heat-conducting Flows

It is impossible to find expressions for E and \mathbf{I} that satisfy the requirements given in Sec. 1.7.1 and at the same time depend only on the physical variables u , p , ρ' , etc., if the flow is not isentropic and irrotational. However, Möhring⁴ has shown that such quantities can always be constructed by introducing an auxiliary set of variables called Clebsch potentials. The resulting expressions for the energy and intensity reduce to those given previously when the flow is irrotational and isentropic and in the general case contain additional terms

that account for the energy associated with the angular momentum of the flow and entropy fluxes. However, these results are quite complicated and will not be pursued further. For our purposes it is enough to note that the resulting expression for E depends on both the entropy and vortical motions which, as we shall see in Chap. 5, are generally not considered to be part of the acoustic field.

1.8 MOVING SOUND SOURCES

The sound emission from any real moving source is generally complicated by such effects as the interaction of the acoustic field with the (usually turbulent) flow about the body or even a back reaction of the flow on the sound source. Nevertheless it is possible to illustrate the essential features of this process, by considering the acoustic radiation from an ideal point source moving through a stationary medium in which no such flow reactions are possible. We shall also limit the discussion to the case where the source is moving uniformly. (Acceleration effects will be discussed in Chap. 2.)

1.8.1 Solutions to Equations

Consider a point volume flow source moving with velocity \mathbf{V}_0 through an infinite medium that is otherwise at rest.[†] The volume source density is then given by $q(\mathbf{y}, \tau) = q_0(\tau)\delta(\mathbf{y} - \mathbf{V}_0\tau)$ and the wave Eq. (1.20) for the sound pressure therefore becomes

$$\nabla^2 p - \frac{1}{c_0^2} \frac{\partial^2 p}{\partial \tau^2} = -\rho_0 \frac{\partial}{\partial \tau} [q_0(\tau)\delta(\mathbf{y} - \mathbf{V}_0\tau)]$$

It is convenient to introduce a *velocity potential* ψ by

$$p = \frac{\partial \psi}{\partial \tau} \quad (1.95)$$

Then

$$\nabla^2 \psi - \frac{1}{c_0^2} \frac{\partial^2 \psi}{\partial \tau^2} = -\rho_0 q_0(\tau)\delta(\mathbf{y} - \mathbf{V}_0\tau)$$

[†] A source of this type could result, for example, from the heating and subsequent expansion caused by a modulated beam of radiation focused on a point moving through the fluid but not (as in Sec. 1.4.1) from a pulsating sphere.

so that, upon comparing this result with Eq. (1.69), we can conclude from Eqs. (1.56) and (1.66) that

$$\begin{aligned}\psi(\mathbf{x}, t) &= \frac{\rho_0}{4\pi} \int_{-\infty}^{\infty} \int \frac{q_0(\tau)}{R} \delta\left(t - \tau - \frac{R}{c_0}\right) \delta(\mathbf{y} - \mathbf{V}_0\tau) d\mathbf{y} d\tau \\ &= \frac{\rho_0}{4\pi} \int_{-\infty}^{\infty} \frac{q_0(\tau)}{|\mathbf{x} - \mathbf{V}_0\tau|} \delta\left(t - \tau - \frac{|\mathbf{x} - \mathbf{V}_0\tau|}{c_0}\right) d\tau\end{aligned}\quad (1.96)$$

The last integral can be evaluated by using the identity (which holds for any function f of τ and any function g of τ which has at most simple zeros)

$$\int_{-\infty}^{\infty} f(\tau) \delta[g(\tau)] d\tau = \sum_i \frac{f(\tau_e^i)}{\left| \frac{dg(\tau_e^i)}{d\tau_e} \right|} \quad (1.97)$$

where τ_e^i is the i th real root of

$$g(\tau_e^i) = 0 \quad (1.98)$$

Thus since

$$\frac{dg}{d\tau} = \frac{V_0^2\tau - \mathbf{V}_0 \cdot \mathbf{x}}{c_0|\mathbf{x} - \mathbf{V}_0\tau|} + 1$$

when

$$g = \frac{|\mathbf{x} - \mathbf{V}_0\tau|}{c_0} + \tau - t,$$

Eq. (1.97) implies that Eq. (1.96) can be written as

$$\psi(\mathbf{x}, t) = \frac{\rho_0}{4\pi} \sum_i \frac{q_0(\tau_e^i)}{\left| \frac{V_0^2\tau_e^i - \mathbf{V}_0 \cdot \mathbf{x}}{c_0} + |\mathbf{x} - \mathbf{V}_0\tau_e^i| \right|} \quad (1.99)$$

where τ_e^i is the i th real solution of

$$\frac{|\mathbf{x} - \mathbf{V}_0\tau_e|}{c_0} + \tau_e - t = 0 \quad (1.100)$$

The latter equation being quadratic in τ_e , will have at most two roots which we shall denote by τ_e^{\pm} . Correspondingly, there will be two terms in the solution (1.99), which we shall denote by ψ^{\pm} . Then, the source Mach number

$$\mathbf{M}_0 = \frac{\mathbf{V}_0}{c_0} \quad (1.101)$$

and the separation vector

$$\mathbf{R}_e^{\pm} = \mathbf{x} - \mathbf{V}_0\tau_e^{\pm} \quad (1.102)$$

can be introduced into Eq. (1.99) to obtain

$$\psi^\pm(\mathbf{x}, t) = \frac{1}{4\pi} \frac{\rho_0 q_0(\tau_e^\pm)}{R_e^\pm |1 - M_0 \cos \theta^\pm|} \quad (1.103)$$

where

$$\cos \theta^\pm \equiv \frac{\mathbf{M}_0 \cdot \mathbf{R}_e^\pm}{M_0 R_e^\pm} \quad (1.104)$$

is the cosine of the angle between the vectors \mathbf{R}_e^\pm and \mathbf{M}_0 . Moreover, Eq. (1.100), which determines τ_e , can be written as

$$\tau_e^\pm = t - \frac{R_e^\pm}{c_0} \quad (1.105)$$

1.8.2 Interpretation of Solution

Equation (1.102) shows that \mathbf{R}_e is simply the vector between the observation point \mathbf{x} and the position of the source at the time τ_e (see Fig. 1.17). But Eq. (1.105) implies that the length R_e of this vector is exactly equal to the distance $c_0(t - \tau_e)$ that a sound wave must travel in the time interval $t - \tau_e$ in order to reach the point \mathbf{x} at the time t . A sound pulse emitted by the source at time τ_e will therefore just reach the observation point \mathbf{x} at time t . Hence, R_e is the distance between the observation point and the source point at the time of emission of the sound wave, and τ_e is the time at which the sound wave reaching the point \mathbf{x} at time t was emitted—i.e., the *retarded time*.

Inserting Eq. (1.105) into Eq. (1.102) and squaring the result yields

$$-\frac{|\mathbf{x} - \mathbf{V}_0 t|^2}{c_0^2} - 2 \frac{\mathbf{V}_0}{c_0^2} \cdot (\mathbf{x} - \mathbf{V}_0 t)(t - \tau_e^\pm) + \left(1 - \frac{V_0^2}{c_0^2}\right)(t - \tau_e^\pm)^2 = 0$$

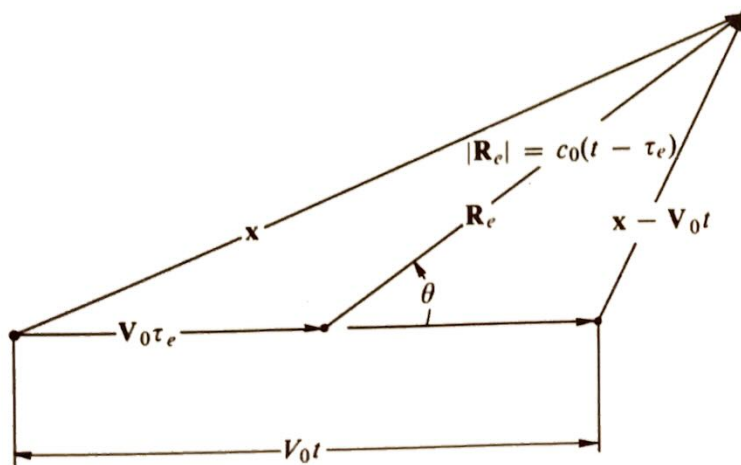


Fig. 1.17 Orientation of source and observer.

which can readily be solved to obtain

$$R_e^\pm \equiv c_0(t - \tau_e^\pm) = \frac{\mathbf{M}_0 \cdot (\mathbf{x} - \mathbf{V}_0 t) \pm \sqrt{[\mathbf{M}_0 \cdot (\mathbf{x} - \mathbf{V}_0 t)]^2 + (1 - M_0^2) |\mathbf{x} - \mathbf{V}_0 t|^2}}{1 - M_0^2} \quad (1.106)$$

When M_0 is less than unity the radical will always be greater than the remaining term in the numerator of this equation and only the + sign can be used if R_e is to remain positive. There will therefore be a unique emission point for the acoustic pulse reaching any fixed point of space at any given instant of time.

On the other hand, R_e^+ and R_e^- will both be positive when M_0 is greater than unity. But the radical will then be imaginary (i.e., no solutions for R_e will exist) unless

$$\frac{\sqrt{(M_0^2 - 1)}}{M_0} \frac{|\mathbf{x} - \mathbf{V}_0 t|}{|\mathbf{M}_0 / M_0 \cdot (\mathbf{x} - \mathbf{V}_0 t)|} < 1$$

This condition is equivalent to requiring that the *Mach angle*

$$\alpha = \cos^{-1} \frac{\sqrt{M_0^2 - 1}}{M_0} = \sin^{-1} \frac{1}{M_0} < \frac{\pi}{2}$$

be greater than the angle

$$\delta \equiv \cos^{-1} \frac{\mathbf{M}_0 / M_0 \cdot (\mathbf{x} - \mathbf{V}_0 t)}{|\mathbf{x} - \mathbf{V}_0 t|}$$

shown in Fig. 1.18. Thus no solutions will exist unless the observation point lies within a cone having its vertex at the source and a semivertex angle equal to the Mach angle. It is called the *Mach cone*.

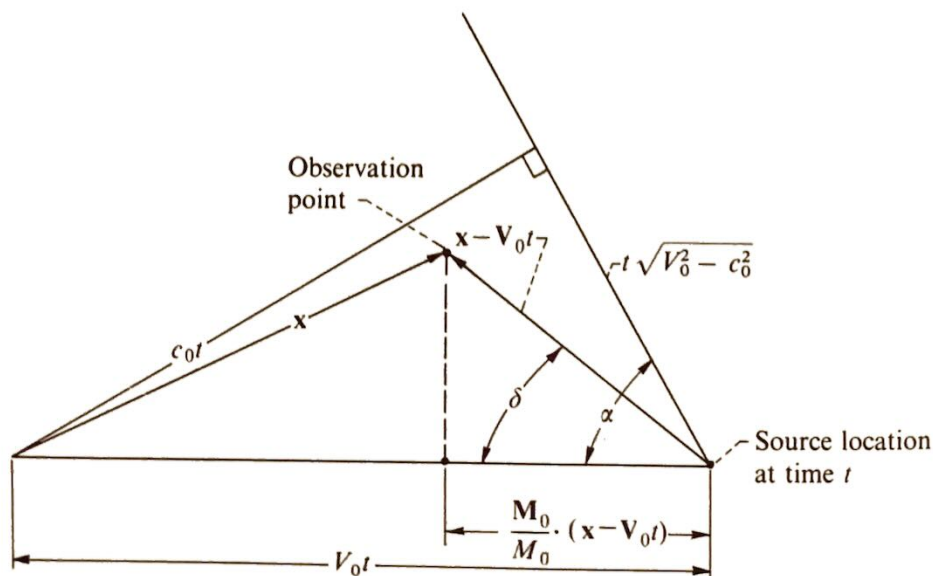


Fig. 1.18 Orientation of observation point relative to Mach cone.

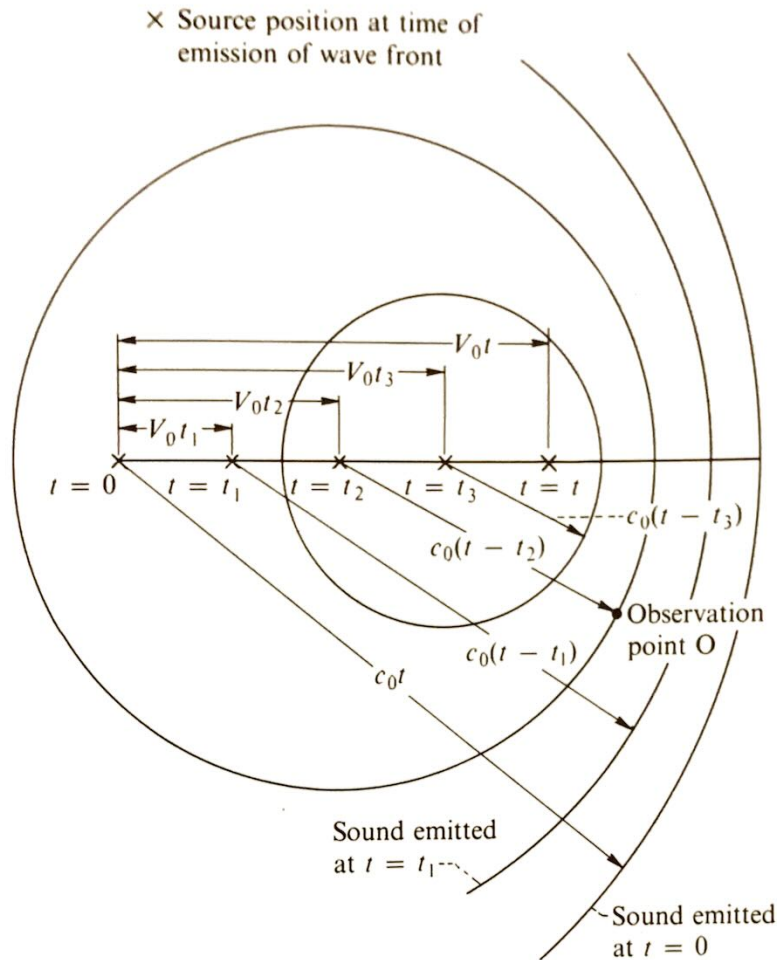


Fig. 1.19 Subsonic source motion (at time t). Source Mach number, $M_0, \frac{2}{3}$.

In order to interpret these results, consider the circles shown in Figs. 1.19 and 1.20. They correspond to the surfaces which “contain” the sound emitted by the source at certain fixed instants of time, say $t = 0, t_1, t_2$, and so forth. Figure 1.19 represents the case where source speed is less than the speed of sound. It shows that only one of these surfaces can pass through any given observation point. Thus, for example, the sound on the surface passing through the point O was emitted by the source at the time $t = t_2$ when it was located at $\mathbf{x}_s = \mathbf{V}_s t_2$.

Notice that the surfaces are closer together in the forward direction (and farther apart in the backward direction) than they would be if the source were stationary. Thus, in any given interval of time, more of these surfaces will pass an observer who is in front of the source than will pass one who is behind the source. Since all the energy emitted during this time is carried between the first and last of these surfaces, we anticipate that the intensity of the sound (energy flow per unit time) received by the forward observer will be larger than the intensity received by the trailing observer.

The situation is quite different when the source is moving faster than the speed of sound (i.e., supersonic source motion). In this case the source overtakes the sound it emits, and the surfaces “containing” the sound take

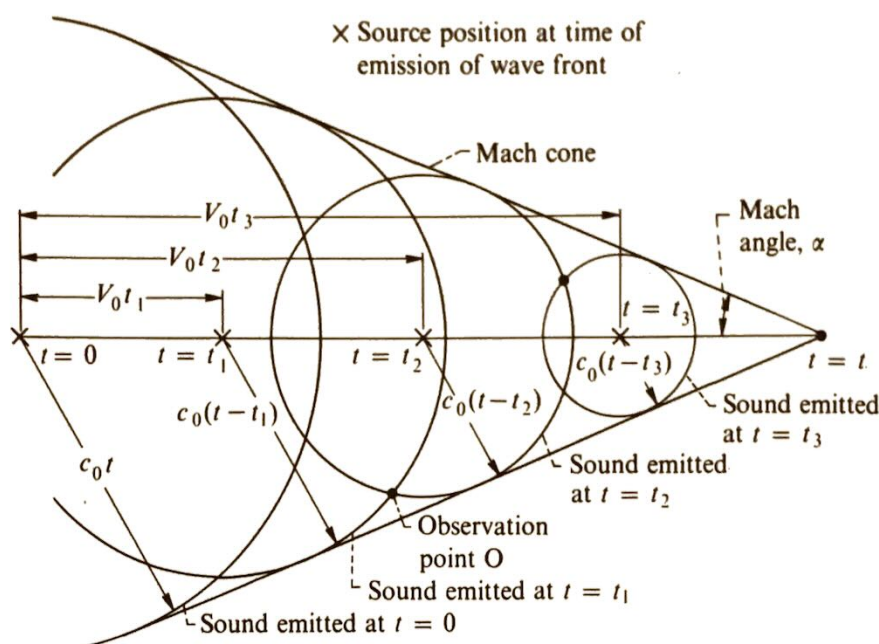


Fig. 1.20 Supersonic source motion (at time t).

on a configuration such as that shown in Fig. 1.20. They are now all tangent to the Mach cone and there will be at any time t two such surfaces passing any fixed observation point O that lies within the Mach cone. The sound reaching these surfaces will have been emitted by the source when it was at two different positions. (In this figure the sound was emitted at the times t_1 and t_2 when the source was at the positions $\mathbf{x}_s^+ = \mathbf{V}_0 t_1$ and $\mathbf{x}_s^- = \mathbf{V}_0 t_2$, respectively.) An observer located outside the Mach cone will hear no sound at the time t . Thus, a stationary observer will not hear any sound until the Mach cone passes. After that he will hear, at any instant of time, the sound coming from two different points. The acoustic field will be particularly intense at the instant when the Mach cone passes since all the spheres coalesce along this surface.

1.8.3 Explicit Expression for Pressure Field

In order to obtain an explicit expression for the pressure fluctuations, notice that Eqs. (1.101), (1.102), (1.104), and (1.105) imply

$$-R_e^\pm (1 - M_0 \cos \theta^\pm) = (\mathbf{x} - \mathbf{V}_0 t) \cdot \mathbf{M}_0 - (1 - M_0^2) R_e^\pm \quad (1.107)$$

which can be differentiated to show with the aid of Eq. (1.106) that

$$\frac{1}{c_0} \frac{d}{dt} [R_e^\pm (1 - M_0 \cos \theta^\pm)] = \frac{M_0 (M_0 - \cos \theta^\pm)}{1 - M_0 \cos \theta^\pm} \quad (1.108)$$

and hence that

$$\frac{1}{c_0} \frac{dR_e^\pm}{dt} = - \frac{M_0 \cos \theta^\pm}{1 - M_0 \cos \theta^\pm} \quad (1.109)$$

Equation (1.103) can therefore be inserted in Eq. (1.95) to obtain

$$p^\pm = \frac{\partial \psi^\pm}{\partial t} = \pm \rho_0 \left[\frac{q'_0(t - R_e^\pm/c_0)}{4\pi R_e^\pm (1 - M_0 \cos \theta^\pm)^2} + \frac{(\cos \theta^\pm - M_0) V_0 q_0(t - R_e^\pm/c_0)}{4\pi R_e^{\pm 2} (1 - M_0 \cos \theta^\pm)^3} \right] \quad (1.110)$$

where

$$q'_0\left(t - \frac{R_e^\pm}{c_0}\right) \equiv \left(\frac{dq_0}{dt}\right)_{t=t-(R^\pm/c_0)}$$

At supersonic source speeds, this result becomes singular when $\theta^\pm = \cos^{-1}(1/M_0)$ which, as can easily be shown,[†] only occurs when the observer is on the Mach cone. If, on the other hand, the source motion is subsonic, the second term will always be negligible at large distances from the source and the equation will closely resemble the solution for a stationary point source. The principal difference is due to the convection factor $(1 - M_0 \cos \theta^\pm)^{-2}$, which appears in Eq. (1.110) and causes the pressure to be higher in the forward direction and lower in the backward direction.

1.8.4 Simple Harmonic Source

When the source has simple harmonic time dependence, $q_0(t) = A e^{-i\Omega t}$ and Eq. (1.110) becomes

$$p^\pm = \frac{\pm \rho_0 c_0 A}{4\pi R_e^\pm (1 - M_0 \cos \theta^\pm)^2} \left[-i \frac{\Omega}{c_0} + \frac{M_0 (\cos \theta^\pm - M_0)}{R_e^\pm (1 - M_0 \cos \theta^\pm)} \right] e^{-i\Omega[t - (R_e^\pm/c_0)]} \quad (1.111)$$

Due to the time dependence of θ^\pm and R_e^\pm this expression is clearly not periodic. However, these quantities will change only slightly during a period of oscillation whenever the observer is far enough away from both the source and the Mach cone. The pressure will then be approximately periodic with slowly changing amplitude and phase—in which case it still makes sense to talk about the frequency of the sound field.

In order to show this, we expand R_e^\pm and $R_I^\pm \equiv R_e^\pm (1 - M_0 \cos \theta^\pm)$ in Taylor series about some fixed time t_0 to obtain

$$R_e^\pm(t) = R_e^\pm(t_0) + \frac{dR_e^\pm(t_0)}{dt_0} (t - t_0) + \frac{1}{2} \frac{d^2 R_e^\pm(t_0)}{dt_0^2} (t - t_0)^2 + \dots$$

$$R_I^\pm(t) = R_I^\pm(t_0) + \frac{dR_I^\pm(t_0)}{dt_0} (t - t_0) + \dots$$

[†] By substituting Eq. (1.106) into Eq. (1.107) and recalling that the observer is on the Mach cone only when the radical in Eq. (1.106) vanishes.

Then substituting the relation

$$\frac{1}{c_0^2} \frac{d^2 R_e^\pm}{dt^2} = \frac{M_0^2 \sin^2 \theta^\pm}{R_e^\pm (1 - M_0 \cos \theta^\pm)^3}$$

together with Eqs. (1.108) and (1.109) into these expansions yields

$$\begin{aligned} \frac{R_e^\pm(t)}{c_0} - (t - t_0) &= \frac{R_e^\pm(t_0)}{c_0} - \frac{t - t_0}{1 - M_0 \cos \theta_0^\pm} \\ &\quad \times \left[1 - \frac{1}{2} \frac{M_0^2 \sin^2 \theta_0^\pm}{(1 - M_0 \cos \theta_0^\pm)^2} \frac{c_0(t - t_0)}{R_e^\pm(t_0)} + \dots \right] \\ R_I^\pm(t) &= R_I^\pm(t_0) \left[1 + \frac{M_0(M_0 - \cos \theta_0^\pm)}{R_e^\pm(t_0)(1 - M_0 \cos \theta_0^\pm)^2} c_0(t - t_0) + \dots \right] \end{aligned}$$

where we have put $\theta_0^\pm \equiv \theta^\pm(t_0)$. But since $t - t_0$ will change by the amount $2\pi/\Omega$ during one period, the second terms in the square brackets will be negligible during this time interval whenever

$$R_e^\pm(t_0) \gg \frac{2\pi c_0}{\Omega} \frac{M_0^2}{(1 - M_0 \cos \theta_0^\pm)^2}$$

Thus, when the observer is many wavelengths distant from the source position at the time of emission (and not too close to the Mach cone if the source velocity is supersonic), Eq. (1.111) becomes approximately

$$p^\pm \simeq - \frac{i\Omega \rho_0 A \exp\left(-\frac{i\Omega t}{1 - M_0 \cos \theta_0^\pm}\right) \exp\left\{i\Omega \left[\frac{R_e^\pm(t_0)}{c_0} + t_0 \left(\frac{M_0 \cos \theta_0^\pm}{1 - M_0 \cos \theta_0^\pm}\right)\right]\right\}}{4\pi R_e^\pm(t_0)(1 - M_0 \cos \theta_0^\pm)^2} \quad (1.112)$$

which shows that the pressure is nearly periodic. However, its frequency is now equal to

$$\omega = \frac{\Omega}{1 - M_0 \cos \theta_0^\pm}$$

and not the frequency Ω of the source. This is the well-known Doppler shift in frequency. As θ_0^\pm varies from 0 to π , the frequency ω varies from $\Omega/(1 - M_0)$ to $\Omega/(1 + M_0)$. Hence, the frequency is increased when the source is moving toward the observer at the time of emission and is reduced when it moves away from the observer.

Only the plus sign can be used when the motion is subsonic. The frequency of the sound will therefore be higher than the *source frequency* when the source approaches the observer and will progressively deepen in pitch as it moves by.

If, on the other hand, the source velocity is supersonic, the observer

will not hear any sound until after the source has passed—at which time he will hear, at any given instant of time, the sound arriving from two distinct emission points. At the point corresponding to the plus sign in Eq. (1.112) the source will be moving away from the observer at the time of emission, while at the point corresponding to the minus sign it will be moving toward the observer. It is interesting to note that the sound waves from the two different emission points can have different phases and can therefore interfere with one another.

1.8.5 Multipole Sources

The results obtained in the last section can be extended to multipole sources. Thus, it is easy to show by putting

$$p = \frac{\partial^N \psi_{i_1, i_2, \dots, i_N}}{\partial y_{i_1} \partial y_{i_2}, \dots, \partial y_{i_N}}$$

in the equation

$$\nabla^2 p - \frac{1}{c_0^2} \frac{\partial^2 p}{\partial \tau^2} = - \frac{\partial^N M_{i_1, i_2, \dots, i_N}(\tau) \delta(\mathbf{y} - \mathbf{V}_0 \tau)}{\partial y_{i_1} \partial y_{i_2}, \dots, \partial y_{i_N}}$$

for the sound pressure from a moving point multipole source of order N , and using the results obtained for a volume flow source in Sec. 1.8.1 that

$$p = \frac{1}{4\pi} \frac{\partial^N}{\partial x_{i_1} \partial x_{i_2}, \dots, \partial x_{i_N}} \frac{M_{i_1, i_2, \dots, i_N}(\tau_e)}{R_e^\pm |1 - M_0 \cos \theta^\pm|} \quad (1.113)$$

This result will also apply to monopole sources if we agree that $N = 0$ implies that no derivative will be taken. The indicated differentiations tend to increase the exponent of the “convection factor” $(1 - M_0 \cos \theta^\pm)$ that appears in the denominator. When M_0 is close to unity, this quantity is a strong function of θ^\pm and, if it is raised to a large power in the expression for the pressure, will cause the far field radiation pattern to be highly directional. Consequently, the acoustic radiation from higher order multipole sources will, at high subsonic convection speeds, be concentrated in a relatively small sector in front of the source, or in other words, the radiation will be “beamed” in the direction of source motion. The far field pressure from a quadrupole source resembles a quadrupole term in Eq. (1.79) multiplied by $(1 - M_0 \cos \theta^\pm)^{-3}$. The mean square pressure signal from such a source will therefore contain the convection factor $(1 - M_0 \cos \theta^\pm)^{-6}$.

1.9 CONCLUDING REMARKS

Two entities of relatively recent origin have been introduced in this chapter. These are the generalized Green’s formula and the acoustic equations for

unidirectional transversely sheared mean flows. However, we have, up to now, only used them to recover more or less classical results, which could have been obtained from the usual formulas of classical acoustics. Nevertheless they are essential ingredients in many of the aeroacoustic theories developed in the following chapters—especially the newer ones. And it is this fact which justifies the added complication which they incur.

APPENDIX 1.A

FOURIER REPRESENTATION OF FUNCTIONS

1.A.1 Periodic Functions

Any sufficiently smooth periodic function of time $f(t)$ with period T_p can be represented as a superposition of simple harmonic functions by the Fourier series

$$f(t) = \sum_{n=-\infty}^{\infty} C_n e^{-in\omega t} \quad (1.A.1)$$

where $\omega = 2\pi/T_p$ is called the *fundamental angular frequency*, $f = \omega/2\pi$ is the *fundamental frequency*, and the terms with $n \neq 0$ are called *harmonics*. Each *Fourier coefficient* C_n is determined by

$$C_n = \frac{1}{T_p} \int_0^{T_p} f(t) e^{in\omega t} dt \quad (1.A.2)$$

The absolute value of this coefficient $|C_n|$ is called the *amplitude* of the n th harmonic, and its argument is called the *phase*. Sometimes C_n itself is called the (complex) amplitude of the n th harmonic. When the function $f(t)$ is real, the Fourier coefficients satisfy the relation

$$C_{-n} = C_n^* \quad \text{for } n = 0, 1, 2, 3, \dots \quad (1.A.3)$$

Motion which can be represented by such a series is the basis of all musical sound. Thus, the vibrations of wind and string instruments can be approximately represented in this way, and the “tone quality” of their sounds is determined to a great extent by the relative amplitudes of the various harmonics that are present. Representing a periodic function by a Fourier series is therefore more than just a means of representing complex functions in terms of simpler functions. It somehow corresponds to the way we hear and distinguish sounds.

The periodic *cross-correlation function*

$$\overline{f_1^*(t)f_2(t+\tau)} \equiv \frac{1}{T_p} \int_0^{T_p} f_1^*(t)f_2(t+\tau) dt \quad (1.A.4)$$

of any two periodic functions

$$f_1(t) = \sum_{n=-\infty}^{\infty} A_n e^{-in\omega t}$$

$$f_2(t) = \sum_{n=-\infty}^{\infty} B_n e^{-in\omega t}$$

satisfies the relation

$$\overline{f_1^*(t)f_2(t+\tau)} = \sum_{n=-\infty}^{\infty} A_n^* B_n e^{-in\omega\tau} \quad (1.A.5)$$

which shows that $A_n^* B_n$ is the Fourier coefficient of the cross-correlation function. Hence, in particular, the autocorrelation function $\overline{f_1^*(t)f_1(t+\tau)}$ satisfies the relation

$$\overline{f_1^*(t)f_1(t+\tau)} = \sum_{n=-\infty}^{\infty} |A_n|^2 e^{-in\omega\tau} \quad (1.A.6)$$

and the mean-square value $\overline{|f_1(t)|^2}$ of $f_1(t)$ satisfies the relation

$$\overline{|f_1(t)|^2} = \sum_{n=-\infty}^{\infty} |A_n|^2 \quad (1.A.7)$$

The cross-correlation is independent of translations in time, which means that

$$\overline{f_1^*(t+t_0)f_2(t+t_0+\tau)} = \overline{f_1^*(t)f_2(t+\tau)} \quad (1.A.8)$$

for any t_0 .

1.A.2 Aperiodic Functions Which Vanish at Infinity

A periodic sound repeats itself continuously throughout all time. On the other hand, it can be shown that any sufficiently smooth function $f(t)$ which vanishes sufficiently rapidly at $t = \pm\infty$ can be represented by the Fourier integral

$$f(t) = \int_{-\infty}^{\infty} F(\omega) e^{-i\omega t} d\omega \quad (1.A.9)$$

where the Fourier transform $F(\omega)$ of $f(t)$ is determined by

$$F(\omega) = \frac{1}{2\pi} \int_{-\infty}^{\infty} f(t) e^{i\omega t} dt \quad (1.A.10)$$

This result shows that any function which vanishes sufficiently rapidly at infinity can be represented as the superposition of harmonic functions of all possible frequencies $\omega/2\pi$.

The quantity $|F(\omega)|^2$ is called the *spectral density* of $f(t)$ at the frequency $\omega/2\pi$. For small $\Delta\omega$, an electronic filter which cuts out all frequencies except those between $\omega/2\pi$ and $(\omega + \Delta\omega)/2\pi$ would deliver a measurable power proportional to $|F(\omega)|^2$ times $\Delta\omega/2\pi$, the width of the frequency band passed by the filter.

A sufficient condition for the Fourier transform of a function $f(t)$ to exist is that it be a square integrable function. This means that

$$\int_{-\infty}^{\infty} |f(t)|^2 dt < \infty \quad (1.A.11)$$

The cross-correlation function

$$\overline{f_1^*(t)f_2(t + \tau)} = \int_{-\infty}^{\infty} f_1^*(t)f_2(t + \tau) dt \quad (1.A.12)$$

of any two square integrable functions

$$f_1(t) = \int_{-\infty}^{\infty} F_1(\omega) e^{-i\omega t} d\omega$$

$$f_2(t) = \int_{-\infty}^{\infty} F_2(\omega) e^{-i\omega t} d\omega$$

exists and satisfies the relation

$$\overline{f_1^*(t)f_2(t + \tau)} = 2\pi \int_{-\infty}^{\infty} F_1^*(\omega)F_2(\omega) e^{-i\omega\tau} d\omega \quad (1.A.13)$$

which shows that the cross-power spectrum $F_1^*(\omega)F_2(\omega)$ is the Fourier transform of the cross-correlation function. Hence, the power spectrum $|F_1(\omega)|^2$ is the Fourier transform of the autocorrelation function $\overline{f_1^*(t)f_1(t + \tau)}$. Some useful properties of the Fourier transform are listed in Table 1.1.

It is also convenient to consider Fourier transforms with respect to spatial variables. In this case, however, the previous results need to be extended to three dimensions. Thus, Eq. (1.A.9) can be generalized to show that the function $f(\mathbf{y})$ can be represented by the Fourier integral

$$f(\mathbf{y}) = \int F(\mathbf{k}) e^{i\mathbf{k} \cdot \mathbf{y}} d\mathbf{k} \quad (1.A.14)$$

where the integration is now carried out over the three-dimensional (k_1, k_2, k_3) space and the Fourier transform $F(\mathbf{k})$ of $f(\mathbf{y})$ is determined by

$$F(\mathbf{k}) = \frac{1}{(2\pi)^3} \int f(\mathbf{y}) e^{-i\mathbf{k} \cdot \mathbf{y}} d\mathbf{y} \quad (1.A.15)$$

Table 1.1 SOME PROPERTIES OF FOURIER TRANSFORMS

Function, $f(t)$	Fourier transform, $F(\omega)$
$\frac{d^n f(t)}{dt^n}$; $n = 1, 2, \dots$	$(-i\omega)^n F(\omega)$
$f\left(\frac{t}{a} + b\right)$	$ a e^{-iabe\omega} F(a\omega)$
$\delta(t)$ (Dirac delta function)	$\frac{1}{2\pi}$
$\int_{-\infty}^{\infty} f(t)g(\tau - t) dt$	$F(\omega)G(\omega)$

Notice that the sign convention is the reverse of the one used for the Fourier transforms with respect to time.

1.A.3 Aperiodic Stationary Functions

We shall frequently have to deal with functions that are not periodic and do not possess Fourier transforms. Rather than satisfy the condition (1.A.11) (which would ensure the existence of the Fourier transform), these functions, called *stationary functions*, merely satisfy the requirement that the average value†

$$\overline{|f(t)|^2} \equiv \lim_{T \rightarrow \infty} \frac{1}{2T} \int_{-T}^T |f(t)|^2 dt \quad (1.A.16)$$

remains finite.

For such functions the Fourier transform $\lim_{T \rightarrow \infty} F(\omega, T)$ where

$$F(\omega, T) \equiv \frac{1}{2\pi} \int_{-T}^T f(t) e^{i\omega t} dt \quad (1.A.17)$$

will not, in general, exist. However, for any two such functions $f_1(t)$ and $f_2(t)$ the *cross-power spectral density function*

$$S_{12}(\omega) \equiv \lim_{T \rightarrow \infty} \pi \frac{F_1^*(\omega, T) F_2(\omega, T)}{T} \quad (1.A.18)$$

† According to this definition, periodic functions are always stationary.

where

$$F_j(\omega, T) \equiv \frac{1}{2\pi} \int_{-T}^T f_j(t) e^{i\omega t} dt \quad \text{for } j = 1, 2$$

does exist and in fact is equal to the Fourier transform of the cross-correlation function

$$\overline{f_1^*(t)f_2(t+\tau)} = \lim_{T \rightarrow \infty} \frac{1}{2T} \int_{-T}^T f_1^*(t)f_2(t+\tau) dt \quad (1.A.19)$$

Hence,

$$\overline{f_1^*(t)f_2(t+\tau)} = \int_{-\infty}^{\infty} S_{12}(\omega) e^{-i\omega\tau} d\omega \quad (1.A.20)$$

The autocorrelation function $\overline{f_1^*(t)f_1(t+\tau)}$ satisfies the relation

$$\overline{f_1^*(t)f_1(t+\tau)} = \int_{-\infty}^{\infty} S_{11}(\omega) e^{-i\omega\tau} d\omega \quad (1.A.21)$$

and the average value $\overline{|f_1(t)|^2}$ satisfies

$$\overline{|f_1(t)|^2} = \int_{-\infty}^{\infty} S_{11}(\omega) d\omega \quad (1.A.22)$$

where $S_{11}(\omega)$ is called the power spectral density function. Equations (1.A.18) and (1.A.20) should be compared with Eq. (1.A.13).

Equation (1.A.19) shows that $\overline{f_1^*(t+t_0)f_2(t+t_0+\tau)} = \overline{f_1^*(t)f_2(t+\tau)}$. Hence, the cross correlation of a stationary function is independent of time translations.

Since the integral (1.A.17) exists for finite T , we can use the theory of Fourier transforms to treat stationary functions by introducing the "shutoff" function

$$f(t, T) = \begin{cases} 0 & |t| > T \\ f(t) & |t| < T \end{cases}$$

Then $F(t, T)$ and $f(t, T)$ are Fourier transform pairs and can be treated by using the theory of Fourier transforms. At the end of the analysis the power spectral density function can be calculated by taking the limit as $T \rightarrow \infty$ indicated in Eq. (1.A.18).

This trick of only analyzing $f(t)$ during the interval $2T$ is related to the actual measuring process. Thus, the length of time required for the filter to separate out the components within a band $\Delta\omega/2\pi$ is longer the narrower the bandwidth. However, even though the only way we can obtain a minutely detailed representation of the spectral density is to average over an infinite time, we can never afford to wait forever.

The stationary functions encountered in practice are usually random variables. Because of the complexity of these functions the information lost by dealing only with their autocorrelation functions and power spectra is usually of little interest.

These ideas can be extended to stationary functions of a three-dimensional spatial variable \mathbf{y} . The cross-correlation function of two functions $f_1(\mathbf{y})$ and $f_2(\mathbf{y})$ is defined by

$$\langle f_1^*(\mathbf{y}) f_2(\mathbf{y} + \boldsymbol{\eta}) \rangle = \lim_{\Delta V \rightarrow \infty} \frac{1}{\Delta V} \int \int \int_{\Delta V} f_1^*(\mathbf{y}) f_2(\mathbf{y} + \boldsymbol{\eta}) d\mathbf{y}$$

where $\Delta V \rightarrow \infty$ indicates that the volume element ΔV grows to fill all space. It is related to the cross-power spectral density

$$S_{12}(\mathbf{k}) = \lim_{\Delta V \rightarrow \infty} (2\pi)^3 \frac{F_1^*(\mathbf{k}, \Delta V) F_2(\mathbf{k}, \Delta V)}{\Delta V} \quad (1.A.23)$$

where

$$F_j(\mathbf{k}, \Delta V) \equiv \frac{1}{(2\pi)^3} \int \int \int_{\Delta V} f_j(\mathbf{y}) e^{-i\mathbf{k} \cdot \mathbf{y}} d\mathbf{y} \quad \text{for } j = 1, 2 \quad (1.A.24)$$

by the Fourier integral

$$\langle f_1^*(\mathbf{y}) f_2(\mathbf{y} + \boldsymbol{\eta}) \rangle \equiv \int \int \int_{-\infty}^{\infty} S_{12}(\mathbf{k}) e^{i\mathbf{k} \cdot \boldsymbol{\eta}} d\mathbf{k} \quad (1.A.25)$$

We have again reversed the sign convention in the Fourier transform.

APPENDIX 1.B

DERIVATION OF GENERALIZED GREEN'S FORMULA

Let $v(\tau)$ denote an arbitrary region of space bounded (internally or externally) by the surface $S(\tau)$ (which is generally moving), and let \mathbf{A} be an arbitrary vector defined on $v(\tau)$. Then the divergence theorem (1.54) states that

$$\int_{S(\tau)} \mathbf{A} \cdot \hat{\mathbf{n}} dS(\mathbf{y}) = \int_{v(\tau)} \nabla \cdot \mathbf{A} d\mathbf{y} \quad (1.B.1)$$

provided the integrals exist. If $\mathbf{V}_s(\mathbf{y}, \tau)$ denotes the velocity at any point \mathbf{y} of the surface $S(\tau)$, the three-dimensional *Leibniz's rule* shows that

$$\frac{d}{d\tau} \int_{v(\tau)} \Psi d\mathbf{y} = \int_{v(\tau)} \frac{\partial \Psi}{\partial \tau} d\mathbf{y} + \int_{S(\tau)} \mathbf{V}_s \cdot \hat{\mathbf{n}} \Psi dS(\mathbf{y}) \quad (1.B.2)$$

for any function $\Psi(\mathbf{y}, \tau)$ defined on $v(\tau)$. Finally, it is a direct consequence of the divergence theorem that Green's theorem

$$\int_{S(\tau)} \left(\Psi \frac{\partial \psi}{\partial n} - \psi \frac{\partial \Psi}{\partial n} \right) dS(\mathbf{y}) = \int_{v(\tau)} (\Psi \nabla^2 \psi - \psi \nabla^2 \Psi) d\mathbf{y} \quad (1.B.3)$$

holds for any two functions Ψ and ψ defined on v . In this equation we have written $\partial \Psi / \partial n$ in place of $\hat{\mathbf{n}} \cdot \nabla \Psi$.

In this appendix, these results are used to derive an integral formula which can be used to relate any solution p of the wave Eq. (1.61) to an appropriate fundamental solution G of Eq. (1.62). To this end we apply Green's theorem to p and G and integrate the result with respect to τ from $-T$ to $+T$ (where T is some large interval of time) to show that

$$\begin{aligned} \int_{-T}^T \int_{S(\tau)} \left(G \frac{\partial p}{\partial n} - p \frac{\partial G}{\partial n} \right) dS d\tau &= \int_{-T}^T \int_{v(\tau)} (G \nabla^2 p - p \nabla^2 G) d\mathbf{y} d\tau \\ &= \frac{1}{c_0^2} \int_{-T}^T \int_{v(\tau)} \left(G \frac{D_0^2}{D\tau^2} p - p \frac{D_0^2}{D\tau^2} G \right) d\mathbf{y} d\tau \\ &\quad - \int_{-T}^T \int_{v(\tau)} \\ &\quad \times [G\gamma(\mathbf{y}, \tau) - \delta(t - \tau)\delta(\mathbf{y} - \mathbf{x})p] d\mathbf{y} d\tau \end{aligned} \quad (1.B.4)$$

But since

$$\left(G \frac{D_0^2}{D\tau^2} p - p \frac{D_0^2}{D\tau^2} G \right) = \frac{\partial}{\partial \tau} \left(G \frac{D_0 p}{D\tau} - p \frac{D_0 G}{D\tau} \right) + U \frac{\partial}{\partial y_1} \left(G \frac{D_0 p}{D\tau} - p \frac{D_0 G}{D\tau} \right)$$

applying Leibniz's rule to the first term and the divergence theorem to the second yields

$$\begin{aligned} \int_{v(\tau)} \left(G \frac{D_0^2}{D\tau^2} p - p \frac{D_0^2}{D\tau^2} G \right) d\mathbf{y} &= \frac{d}{d\tau} \int_{v(\tau)} \left(G \frac{D_0 p}{D\tau} - p \frac{D_0 G}{D\tau} \right) d\mathbf{y} \\ &\quad + \int_{S(\tau)} (U\hat{\mathbf{i}} - \mathbf{V}_s) \cdot \hat{\mathbf{n}} \left(G \frac{D_0 p}{D\tau} - p \frac{D_0 G}{D\tau} \right) dS(\mathbf{y}) \end{aligned}$$

Hence,

$$\begin{aligned} \int_{-T}^T \int_{v(\tau)} \left(G \frac{D_0^2}{D\tau^2} p - p \frac{D_0^2}{D\tau^2} G \right) d\mathbf{y} d\tau &= \int_{v(\tau)} \left(G \frac{D_0 p}{D\tau} - p \frac{D_0 G}{D\tau} \right) d\mathbf{y} \Big|_{\tau=-T}^{\tau=T} \\ &\quad - \int_{-T}^T \int_{S(\tau)} V'_n \left(G \frac{D_0 p}{D\tau} - p \frac{D_0 G}{D\tau} \right) dS(\mathbf{y}) d\tau \end{aligned} \quad (1.B.5)$$

where V'_n is defined by Eq. (1.64).

The integrated term

$$\int_{v(\tau)} \left(G \frac{D_0 p}{D\tau} - p \frac{D_0 G}{D\tau} \right) dy \bigg|_{\tau=-T}^{\tau=T} \quad (1.B.6)$$

vanishes at the upper limit ($\tau = T$) as a result of the causality condition (1.63) while at the lower limit ($\tau = -T$) it represents the effects of initial conditions in the remote past (Ref. 2, p. 837). But since we have restricted our attention to time-stationary (and not transient) sound fields, there should also be little contribution from such effects and it ought to be possible to neglect (1.B.6) entirely.[†] Then Eq. (1.B.5) becomes

$$\int_{-T}^T \int_{v(\tau)} \left(G \frac{D_0^2 p}{D\tau^2} - p \frac{D_0^2 G}{D\tau^2} \right) dy d\tau = - \int_{-T}^T \int_{S(\tau)} V_n' \left(G \frac{D_0 p}{D\tau} - p \frac{D_0 G}{D\tau} \right) dS(y) d\tau$$

And the validity of Eq. (1.65) can now be established by substituting this result into Eq. (1.B.4) and carrying out the integrals over the delta functions.

APPENDIX 1.C

CALCULATION OF GREEN'S FUNCTIONS

1.C.1 Method of Images

Since the Green's function $G(\mathbf{y}, \tau | \mathbf{x}, t)$ is only singular when $\mathbf{y} = \mathbf{x}$ and $\tau = t$, it must be of the form

$$G(\mathbf{y}, \tau | \mathbf{x}, t) = G^0(\mathbf{y}, \tau | \mathbf{x}, t) + h(\mathbf{y}, \tau | \mathbf{x}, t)$$

where G^0 is the free-space Green's function (Eq. (1.56)) and h is a solution of the homogeneous wave equation that satisfies Eq. (1.63) and has no singularities in the region v where G is defined. The details of the method are best illustrated by considering a particular example.

Thus, suppose that the mean flow is zero and let v be the region $y_2 \geq 0$ (shown in Fig. 1.21). We shall construct the Green's function whose normal derivative vanishes on the boundary $y_2 = 0$. Since

$$G^0(\mathbf{y}, \tau | \mathbf{x}, t) = \frac{1}{4\pi R} \delta\left(\tau - t + \frac{R}{c_0}\right)$$

is a solution to the homogeneous wave equation when $\mathbf{y} \neq \mathbf{x}$, and since this equation is invariant under the transformation $y_2 \rightarrow -y_2$, the function

[†] It is assumed that the boundary condition is such that the effect of any initial state will decay with time. In any event, it is always possible to require that

$$p = \frac{D_0 p}{D\tau} = 0 \quad \text{at } \tau = -T$$

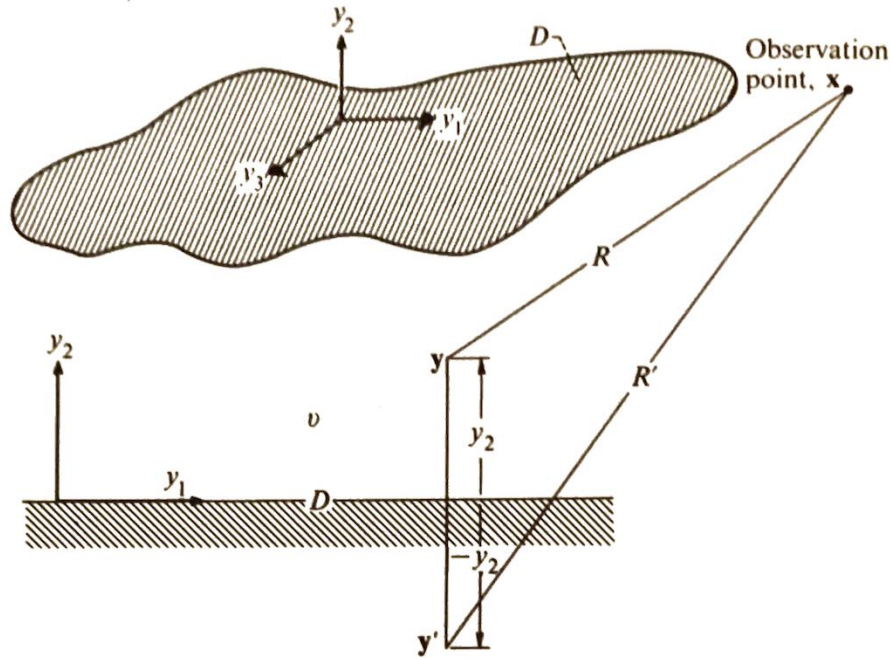


Fig. 1.21 Coordinate system for half-space Green's function.

$h_0 = (1/4\pi R')\delta(\tau - t + R'/c_0)$, where $R' = |\mathbf{x} - \mathbf{y}'|$ and $\mathbf{y}' = \hat{\mathbf{i}}y_1 - \hat{\mathbf{j}}y_2 + \hat{\mathbf{k}}y_3$, must also be a solution to this equation. Then since \mathbf{y}' is never in v , h_0 is nonsingular in this region and therefore satisfies the conditions imposed on h . Hence,

$$G(\mathbf{y}, \tau | \mathbf{x}, t) = \frac{1}{4\pi R} \delta\left(\tau - t + \frac{R}{c_0}\right) + \frac{1}{4\pi R'} \delta\left(\tau - t + \frac{R'}{c_0}\right) \quad (1.C.1)$$

satisfies the wave Eq. (1.70) in the region v . Moreover, it is now easy to verify that it also satisfies the boundary condition

$$\frac{\partial G}{\partial y_2} = 0 \quad \text{at } y_2 = 0$$

and as a result that it is the required Green's function.

1.C.2 Method of Eigenfunctions

We now turn to the method of eigenfunctions. Since Eq. (1.62) shows that G depends on τ and t only in the combination $\tau - t$, taking the τ -Fourier transform of this equation together with that of the boundary conditions (1.72) and introducing the function $G_\omega(\mathbf{y} | \mathbf{x})$, which is related to the Fourier transform $\mathcal{G}_\omega(\mathbf{y} | \mathbf{x}, t)$ of G by

$$G_\omega(\mathbf{y} | \mathbf{x}) = 2\pi e^{i\omega t} \mathcal{G}_\omega^* \quad (1.C.2)$$

yieldst[†] (after taking complex conjugates)

$$\left(\nabla^2 - M^2 \frac{\partial^2}{\partial y_1^2} - 2iMk_0 \frac{\partial}{\partial y_1} + k_0^2 \right) G_\omega(\mathbf{y}|\mathbf{x}) = -\delta(\mathbf{x} - \mathbf{y}) \quad (1.C.3)$$

and

$$\left. \begin{array}{l} \text{Case A:} \quad \frac{\partial G_\omega}{\partial n} + bG_\omega = 0 \\ \text{Case B:} \quad G_\omega = 0 \end{array} \right\} \quad \text{for } \mathbf{y} \text{ on } S \quad (1.C.4)$$

where as usual $k_0 \equiv \omega/c_0$ and $M \equiv U/c_0$ is the mean-flow Mach number. Then it follows from Eq. (1.C.2) that the time-dependent Green's function G can be determined from the solution G_ω to this boundary-value problem by

$$G = \frac{1}{2\pi} \int_{-\infty}^{\infty} e^{-i\omega(t-\tau)} G_\omega(\mathbf{y}|\mathbf{x}) d\omega \quad (1.C.5)$$

(This result is a generalization of the relation (1.59).)

It is frequently possible to solve the problem posed by Eqs. (1.C.3) and (1.C.4) by expanding its solution in terms of an appropriate set of "eigenfunctions". However, caution must be used in carrying out the inversion integral in Eq. (1.C.5) since G_ω will then usually have singularities along the ω -axis—in which case it will be necessary to deform the contour of integration in a manner dictated by the causality condition (1.63).

These ideas are again best illustrated by considering an example. Thus, suppose the region v is the interior of an infinite, straight, hard-walled duct (shown in Fig. 1.22) whose cross-sectional area is A and whose axis is in the y_1 -direction. In order to construct the Green's function G_ω that satisfies the boundary condition

$$\frac{\partial G_\omega}{\partial n} = 0 \quad \text{for } \mathbf{y} \text{ on } S \quad (1.C.6)$$

it is convenient to first consider the functions Ψ that satisfy the two-dimensional Helmholtz equation

$$\left(\frac{\partial^2}{\partial y_2^2} + \frac{\partial^2}{\partial y_3^2} \right) \Psi + \kappa^2 \Psi = 0 \quad (1.C.7)$$

in the region A together with the boundary condition

$$\frac{\partial \Psi}{\partial n} = 0 \quad \text{on the boundary } D \text{ of } A \quad (1.C.8)$$

[†] It is easy to show that causality condition (1.63) will be satisfied if the solution to this equation represents an outgoing wave at infinity.

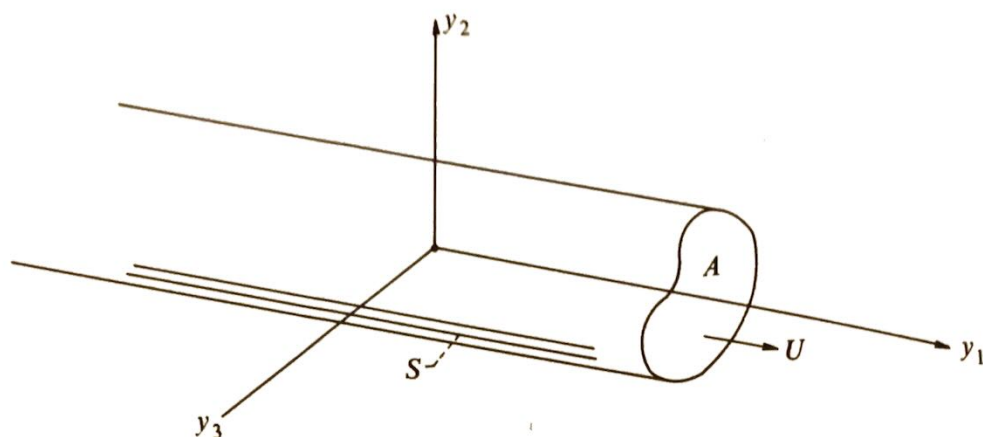


Fig. 1.22 Duct geometry for Green's function.

It can be shown† that such solutions exist only for a discrete set of real values, say κ_n for $n = 0, 1, 2, \dots$, of the constant κ , called *eigenvalues*. The corresponding solutions, Ψ_n , are called *eigenfunctions* and satisfy the orthogonality condition

$$\int_A \Psi_m \Psi_n^* dy_2 dy_3 = \begin{cases} 0 & \text{if } m \neq n \\ \Gamma_n & \text{if } m = n \end{cases} \quad (1.C.9)$$

where

$$\Gamma_n \equiv \int_A |\Psi_n|^2 dy_2 dy_3 \quad (1.C.10)$$

We attempt to expand the solution to Eq. (1.77) in terms of these functions to obtain

$$G_\omega = \sum_n f_n(y_1) \Psi_n(y_2, y_3)$$

Then the boundary condition (1.C.6) on the surface of the cylinder is automatically satisfied. We can now show by substituting this expansion into Eq. (1.C.3), multiplying the result by Ψ_m^* , integrating over the cross-sectional area A , and using Eqs. (1.C.7), (1.C.9), and (1.C.10), that the expansion coefficients f_m satisfy the equation

$$\left(\beta^2 \frac{d^2}{dy_1^2} - 2iMk_0 \frac{d}{dy_1} + k_0^2 - \kappa_m^2 \right) f_m = - \frac{\Psi_m^*(x_2, x_3)}{\Gamma_m} \delta(x_1 - y_1)$$

where

$$\beta \equiv \sqrt{1 - M^2}$$

Consequently (see Appendix 6.B),

$$f_m = \frac{i\Psi_m^*(x_2, x_3)}{2k_m\Gamma_m} \exp \left\{ \frac{i[Mk_0(y_1 - x_1) + k_m|x_1 - y_1|]}{\beta^2} \right\}$$

† See, e.g., Ref. 2, Chap. 11.

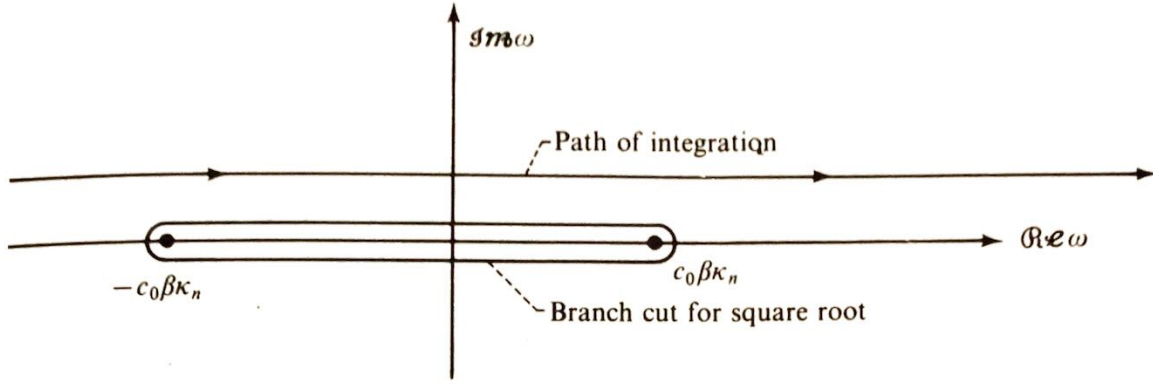


Fig. 1.23 Contour of integration for inversion of Green's function.

where

$$k_m \equiv \sqrt{k_0^2 - \beta^2 \kappa_m^2} \quad (1.C.11)$$

and in order to ensure that f_m remains bounded for large values of $|x_1 - y_1|$, we must select the branch of the square root (1.C.11) that has a positive imaginary part when $k_0^2 < \beta^2 \kappa_m^2$. Then,

$$G_\omega(\mathbf{y}|\mathbf{x}) = \frac{i}{2} \sum_n \frac{\Psi_n(y_2, y_3) \Psi_n^*(x_2, x_3)}{k_n \Gamma_n} \exp \left\{ \frac{i[Mk_0(y_1 - x_1) + k_n |y_1 - x_1|]}{\beta^2} \right\} \quad (1.C.12)$$

Finally, substituting this into the inversion formula (1.C.5) yields

$$G(\mathbf{y}, \tau | \mathbf{x}, t) = \frac{i}{4\pi} \sum_n \frac{\Psi_n(y_2, y_3) \Psi_n^*(x_2, x_3)}{\Gamma_n} \times \int_{-\infty}^{\infty} \frac{\exp \left\{ i \left[\omega(\tau - t) + \frac{Mk_0}{\beta^2} (y_1 - x_1) + \frac{k_n}{\beta^2} |y_1 - x_1| \right] \right\}}{k_n} d\omega \quad (1.C.13)$$

The contour of integration in the complex ω -plane which ensures that the causality condition (1.63) will be satisfied is shown in Fig. 1.23.

There are a number of important cases† where it is convenient to express the index n in terms of a doubly infinite set of indices, say m and n . Then the eigenvalues are denoted by $\kappa_{m,n}$, the eigenfunctions by $\Psi_{m,n}$, and Eq. (1.C.13) becomes

$$G(\mathbf{y}, \tau | \mathbf{x}, t) = \frac{i}{4\pi} \sum_{m,n} \frac{\Psi_{m,n}(y_2, y_3) \Psi_{m,n}^*(x_2, x_3)}{\Gamma_{m,n}} \times \int_{-\infty}^{\infty} \frac{\exp \left\{ i \left[\omega(\tau - t) + \frac{Mk_0}{\beta^2} (y_1 - x_1) + \frac{k_{n,m}}{\beta^2} |y_1 - x_1| \right] \right\}}{k_{n,m}} d\omega \quad (1.C.14)$$

† When the surface D is a coordinate surface in a coordinate system where Eq. (1.C.7) is separable.

Thus suppose for example that the region v is the interior of a circular duct of radius r_d . Then it is easy to show by introducing the polar coordinates

$$r' = \sqrt{y_2^2 + y_3^2}$$

$$\tilde{\varphi} = \tan^{-1} \frac{y_3}{y_2}$$

into Eq. (1.C.7), that the eigenfunctions $\Psi_{m,n}$ are given by

$$\Psi_{m,n} = J_m(\kappa_{m,n}r') e^{-im\tilde{\varphi}} \quad (1.C.15)$$

where J_m is the Bessel function of order m , $\kappa_{m,n}$ is the n th root of

$$J'_m(\kappa_{m,n}r_d) \equiv \left. \frac{dJ_m(x)}{dx} \right|_{x=\kappa_{m,n}r_d} = 0 \quad (1.C.16)$$

$$\Gamma_{m,n} = \pi \left(r_d^2 - \frac{m^2}{\kappa_{m,n}^2} \right) J_m^2(\kappa_{m,n}r_d), \quad (1.C.17)$$

and $m = 0, \pm 1, \pm 2, \dots; n = 1, 2, \dots$

REFERENCES

1. Blokhintsev, D. I., "Acoustics of a Nonhomogeneous Moving Medium," *NACA TM 1399*, 1956. (Translation.)
2. Morse, Philip M. and Herman Feshbach, *Methods of Theoretical Physics, Part 1*, McGraw-Hill, New York, 1953.
3. Doak, P. E., "An Introduction to Sound Radiation and Its Sources," in *Noise and Acoustic Fatigue in Aeronautics*, E. J. Richards and D. J. Mead (eds), pp. 1-42. John Wiley & Sons, New York, 1968.
4. Möhring, W., "Energy Flux in Duct Flow," *J. Sound Vibr.*, **18**, 1, 101-109, September 1971.
5. Keenan, Joseph H., *Thermodynamics*. John Wiley & Sons, New York, 1941.
6. Chernov, L. A. (B. W. Kuvshinoff, trans.), "Flow and Density of Acoustical Energy in a Moving Medium," *APL/JHU TG 230-T291*, Johns Hopkins University, April 1962. (*Zhurnal Tekhnicheskoi Fiziki*, USSR, **16**, 6, 733-736, 1946.)

2 AERODYNAMIC SOUND

2.1 INTRODUCTION

Pressure fluctuations occur in an unsteady flow in order to balance the fluctuations in momentum. But as indicated in Sec. 1.2 such fluctuations will propagate outward from their source and, if an observer is present, will subsequently be recognized as sound.

At fairly low Mach numbers the pressure variations in the vicinity of a more or less localized flow are substantially uninfluenced by compressibility and can be determined from the velocity field by solving a Poisson's equation

$$\nabla^2 p = \gamma$$

in which the source term γ is a known function of the instantaneous velocity. Moreover, the Biot-Savart law shows that it is possible to treat the velocity field as if it were in turn driven by a prescribed vorticity field. However, Kelvin's theorem of conservation of circulation shows that the vorticity in an inviscid fluid is simply carried along with the flow and, as a consequence,

that any initially localized region of vorticity will remain that way for some time to come. Thus, many flows can be envisioned as relatively concentrated regions of vorticity which drive not only the pressure fluctuations in their immediate vicinity but also those at large distances.

Although the localized pressure fluctuations (sometimes called *pseudo-sound*) have been extensively studied, the theory of aerodynamic sound is largely concerned with those that occur far from the source where the amplitude of the motion is small and the effects of compressibility and finite propagation speed of the disturbances are important. Thus in this region, which we shall often call the *acoustic field*, the pressure (and density) fluctuations are weak and satisfy the acoustic wave equation.[†]

The study of these flow-generated acoustic waves probably began with Gutin's theory¹ of propeller noise, which was developed in 1937. Yet, it was not until 1952, when Lighthill^{2,3} introduced his acoustic analogy to deal with the problem of jet noise, that a general theory began to emerge. Lighthill's ideas were subsequently extended by Curle,⁴ Powell,⁵ and Ffowcs Williams and Hall⁶ to include the effects of solid boundaries. These extensions include Gutin's analysis and, in fact, provide a complete theory of aerodynamically generated sound that can be used to predict blading noise as well as jet noise.

The fundamental equation which forms the basis of the acoustic analogy approach is derived in the next section. The methods of classical acoustics (developed in Chap. 1) are then used to obtain solutions that are applicable to flows without solid boundaries. (The treatment of solid boundaries is deferred to Chaps. 3 and 4.) These results are applied to high-speed subsonic jets, and fairly detailed conclusions are reached. Supersonic and low-speed subsonic jets are treated in a somewhat more qualitative fashion.

In Lighthill's analogy, certain terms associated with the propagation of sound are treated as source terms. In practice, this places certain limitations on the capacity of the theory. Alternative approaches developed to overcome these limitations are presented in Chap. 6.

2.2 LIGHTHILL'S ACOUSTIC ANALOGY

In this section we develop the acoustic analogy approach which was introduced by Lighthill^{2,3} to calculate acoustic radiation from relatively small regions of turbulent flow embedded in an infinite homogeneous fluid in which the speed of sound c_0 and the density ρ_0 are constants. Upon

[†] If the Mach number is sufficiently low, there will be an intermediate region where the pressure fluctuations have some of the properties of both the localized fluctuations and those in the sound field. Thus, in this region, the pressures are as weak as in the sound field, but the distances involved are small enough so that the effects of finite propagation speed, and hence of compressibility, can be neglected.

realizing that the density fluctuations $\rho' \equiv \rho - \rho_0$, at large distances from the turbulent region ought to behave like acoustic waves in such flows, Lighthill arranged the exact equations of continuity and momentum so that they reduce to the homogeneous acoustic wave equation†

$$\frac{1}{c_0^2} \frac{\partial^2 \rho'}{\partial \tau^2} - \nabla^2 \rho' = 0$$

at large distances from the turbulent flow.

2.2.1 Derivation of Lighthill's Equation

In order to derive Lighthill's result, notice that we can use the summation convention to write the continuity and momentum equations as

$$\frac{\partial \rho}{\partial \tau} + \frac{\partial}{\partial y_j} \rho v_j = 0 \quad (2.1)$$

$$\rho \left(\frac{\partial v_i}{\partial \tau} + v_j \frac{\partial}{\partial y_j} v_i \right) = - \frac{\partial p}{\partial y_i} + \frac{\partial e_{ij}}{\partial y_j}$$

where e_{ij} is the (i, j) th component of the viscous stress tensor. For a Stokesian gas it can be expressed in terms of the velocity gradients by

$$e_{ij} = \mu \left(\frac{\partial v_i}{\partial y_j} + \frac{\partial v_j}{\partial y_i} - \frac{2}{3} \delta_{ij} \frac{\partial v_k}{\partial y_k} \right) \quad (2.2)$$

where μ is the viscosity of the fluid.

Multiplying the continuity Eq. (2.1) by v_i , adding the result to the momentum equation, and combining terms yields

$$\frac{\partial}{\partial \tau} \rho v_i = - \frac{\partial}{\partial y_j} (\rho v_i v_j + \delta_{ij} p - e_{ij})$$

which upon adding and subtracting the term‡ $c_0^2 \partial \rho / \partial y_i$, becomes

$$\frac{\partial \rho v_i}{\partial \tau} + c_0^2 \frac{\partial \rho}{\partial y_i} = - \frac{\partial T_{ij}}{\partial y_j} \quad (2.3)$$

where

$$T_{ij} = \rho v_i v_j + \delta_{ij} [(p - p_0) - c_0^2 (\rho - \rho_0)] - e_{ij} \quad (2.4)$$

is *Lighthill's turbulence stress tensor*. We can now differentiate Eq. (2.1)

† The notation introduced at the beginning of Sec. 1.2 will be used in this section.

‡ The subscript 0 is used here to denote constant reference values, which will usually be taken to be the corresponding properties at large distances from the flow.

with respect to τ , take the divergence of Eq. (2.3), and subtract the results to obtain *Lighthill's equation*

$$\frac{\partial^2 \rho'}{\partial \tau^2} - c_0^2 \nabla^2 \rho' = \frac{\partial^2 T_{ij}}{\partial y_i \partial y_j} \quad (2.5)$$

2.2.2 Interpretation of Lighthill's Equation

Equation (2.5) clearly has the same form as the wave equation that governs the acoustic field produced by a quadrupole source $\partial^2 T_{ij} / \partial y_i \partial y_j$ in a non-moving medium (see Sec. 1.5.2). It therefore shows that there is an *exact* analogy between the density fluctuations that occur in any real flow and the small amplitude density fluctuations that would result from a quadrupole source distribution (of strength T_{ij}) in a fictitious (nonmoving) acoustic medium with sound speed c_0 . We shall show subsequently that these sources will vanish in the region outside certain types of turbulent flows so that Eq. (2.5) will indeed reduce to the homogeneous wave equation in such regions.

The crucial step in Lighthill's analysis is to regard the source term as a quantity about which we have at least some prior knowledge. However, this term involves the fluctuating density and can therefore not be completely determined until Eq. (2.5) is solved. In fact, since Lighthill's equation is an exact consequence of the laws of conservation of mass and momentum, it must be satisfied by all real flows: most of which are certainly not sound-like. Even for those flows that are sound-like, $\partial^2 T_{ij} / \partial y_i \partial y_j$ must account for all those effects which occur whenever acoustic waves interact with moving flows (convection, refraction, etc.) and which therefore can not be predicted without some knowledge of the sound field. Thus, a knowledge of T_{ij} is, in effect, equivalent to solving the complete nonlinear equations governing the flow problem, which is virtually impossible for most flows of interest. Nevertheless, the insensitivity of the ear as a detector of sound tends to obviate the need for highly accurate predictions of the acoustic field and we are usually content with approximate indications of its magnitude and suggestions about its dependence on parameters that are at the disposal of the designer. Moreover, we shall show subsequently that there are certain types of flows where it is often possible to obtain fairly good estimates of T_{ij} , and as a consequence to obtain, through Eq. (2.5), correspondingly good estimates of the sound field. When this is coupled with the fact that the acoustic analogy approach allows us to utilize the powerful tools of classical acoustics, it becomes clear why this technique serves as a foundation for most analyses of aerodynamic sound problems.

It is rather important that the quadrupole nature of the source term is explicitly exhibited in Eq. (2.5) since, as we shall see subsequently, the aero-

dynamic sound sources of practical interest are very often acoustically compact. Hence, the far-field solutions of this equation will automatically account for the extreme inefficiency of these sources (see Sec. 1.5.2) and will thereby provide reasonable estimates of the acoustic field even when T_{ij} is not very precisely known.

In this chapter we consider only the case where the sound field is substantially uninfluenced by any solid boundaries that may be present in the flow. Then the only important applications of the results will be to jet noise. (In fact, Lighthill actually developed his theory specifically to deal with this problem.) In Chap. 3 we show how solid boundaries can be included in the analysis and apply the theory to a number of special cases.

2.2.3 Approximation of Lighthill's Stress Tensor

Lighthill's equation can only serve as the starting point for the solution of aerodynamic sound problems if it is possible to regard its right side as a known source term that vanishes at large distances from the flow. We shall now show that there are at least some situations where this is a reasonable assumption.

To this end, consider a subsonic turbulent airflow (or for that matter any unsteady high-Reynolds-number subsonic flow) of relatively small spatial extent (such as the flow in a jet) embedded in a uniform stationary atmosphere. The subscript 0 will now be used to denote the constant values of the thermodynamic properties in this atmosphere. Within the flow we anticipate that the viscous stress e_{ij} , will make a much smaller contribution to T_{ij} , than the usually far larger Reynolds stress term $\rho v_i v_j$. In fact, it is well known from the study of turbulence that the ratio of these terms is of the order of magnitude of the Reynolds number $\rho UL/\mu$, which in virtually all applications of aerodynamic noise theory is quite large.

In the region outside the flow (or at least at sufficiently large distances from this flow) the acoustic approximation should apply, and hence the velocity v_i should be small. Then the quadratic Reynolds stress term $\rho v_i v_j$ will be negligible. Moreover, we expect the effects of viscosity and heat conduction to be no different in this region than they are in any other sound field. This means (as shown by Kirchhoff, see Ref. 8) that they only cause a slow damping due to the conversion of acoustic energy into heat and have a significant effect only over very large distances. Thus, it should be possible to neglect e_{ij} entirely.

Now whenever the flow emanates from a region of ambient temperature, the effects of heat conduction ought to be of the same order of magnitude as the viscous effects (provided the Prandtl number is of order 1 as it is for most fluids). Hence, heat transfer should also be relatively unimportant within the flow. Then the entropy changes will be governed by

the inviscid energy Eq. (1.3), which, in view of the assumption that the flow emanates from a region of uniform temperature, implies that the entropy should be relatively constant. But it is shown in Sec. 1.2 that

$$p - p_0 = c_0^2(\rho - \rho_0) \quad (2.6)$$

for any isentropic flow in which $(p - p_0)/p_0$ and $(\rho - \rho_0)/\rho_0$ are sufficiently small; which is usually the case in subsonic flows.[†]

We have therefore shown that T_{ij} is approximately equal to $\rho_0 v_i v_j$ inside the flow and approximately equal to zero outside this region. Hence, upon assuming that the density fluctuations are negligible within the moving fluid, we obtain the following approximation to Lighthill's stress tensor

$$T_{ij} \simeq \rho_0 v_i v_j \quad (2.7)$$

But since only a very small fraction of the energy in the flow gets radiated as sound, it is reasonable to suppose that the Reynolds stress $\rho_0 v_i v_j$ can be determined, say from measurements or estimates of the turbulence, without any prior knowledge of the sound field. Then the right side of Lighthill's Eq. (2.5) can indeed be treated as a known source term.

It is important to notice that these approximations were not introduced until after Eq. (2.5) was derived and the quadrupole nature of the sound sources established. Approximations at an early stage could introduce dipole or monopole sources which, due to their relatively higher acoustic efficiency, are able to cause significant errors in the sound field.

2.3 SOLUTION TO LIGHTHILL'S EQUATION WHEN NO SOLID BOUNDARIES ARE PRESENT

It is shown in Sec. 2.2 that the problem of predicting the sound emission from a region of unsteady flow embedded in a uniform atmosphere can be reduced to the classical problem of predicting the sound field from a known quadrupole source of limited spatial extent. If any solid boundaries which may be present do not influence the sound field to any appreciable extent, the solution to this problem can be expressed in terms of the free-space Green's function. Indeed, it is easy to see upon comparing Eqs. (2.5) and (1.69), that Eq. (1.74) implies

$$\rho(\mathbf{x}, t) - \rho_0 = \frac{1}{4\pi c_0^2} \int \frac{1}{R} \left[\frac{\partial^2 T_{ij}}{\partial y_i \partial y_j}(\mathbf{y}, \tau) \right]_{\tau=t-(R/c_0)} d\mathbf{y} \quad (2.8)$$

where, as usual,

$$R \equiv |\mathbf{x} - \mathbf{y}|$$

[†] Of course, it is assumed that no combustion occurs in the flow. This could result in large fluctuations in entropy and hence in $(p - p_0) - c_0^2(\rho - \rho_0)$. This term would then have to be included in T_{ij} .

and, as indicated in Chap. 1, the omission of the limits on a volume integral denotes an integration over all space. In order to transform this result into a more suitable form (see remarks at end of Sec. 1.5.2), it is convenient to introduce the differential operator $\delta/\delta y_i$, which denotes partial differentiation with respect to y_i with both t and R held fixed, to obtain

$$\rho(\mathbf{x}, t) - \rho_0 = \frac{1}{4\pi c_0^2} \int \frac{\delta^2}{\delta y_i \delta y_j} \frac{T_{ij}(\mathbf{y}, t - R/c_0)}{R} d\mathbf{y} \quad (2.9)$$

Now suppose that the operator $\partial/\partial y_i$ denotes partial differentiation with respect to y_i with \mathbf{x} and t held fixed. Then since $\partial/\partial x_i$ denotes partial differentiation with respect to x_i with \mathbf{y} and t held fixed, the chain rule for partial differentiation shows that

$$\frac{\delta F}{\delta y_i} = \frac{\partial F}{\partial y_i} + \frac{\partial F}{\partial x_i}$$

for any function $F(\mathbf{y}, R, t)$ and hence that

$$\frac{\delta^2 F}{\delta y_i \delta y_j} = \frac{\partial^2 F}{\partial y_i \partial y_j} + \frac{\partial^2 F}{\partial y_i \partial x_j} + \frac{\partial^2 F}{\partial y_j \partial x_i} + \frac{\partial^2 F}{\partial x_i \partial x_j}$$

Using this result in Eq. (2.9) yields

$$\begin{aligned} \rho(\mathbf{x}, t) - \rho_0 = & \frac{1}{4\pi c_0^2} \int \frac{\partial^2}{\partial y_i \partial y_j} \frac{[T_{ij}]}{R} d\mathbf{y} + \frac{1}{4\pi c_0^2} \frac{\partial}{\partial x_j} \int \frac{\partial}{\partial y_i} \frac{[T_{ij}]}{R} d\mathbf{y} \\ & + \frac{1}{4\pi c_0^2} \frac{\partial}{\partial x_i} \int \frac{\partial}{\partial y_j} \frac{[T_{ij}]}{R} d\mathbf{y} + \frac{1}{4\pi c_0^2} \frac{\partial^2}{\partial x_i \partial x_j} \int \frac{[T_{ij}]}{R} d\mathbf{y} \end{aligned} \quad (2.10)$$

provided the integrals exist. The notation $[T_{ij}]$ is used to denote $T_{ij}(\mathbf{y}, t - R/c_0)$. Notice that each of the first three integrands is the divergence of a vector while the divergence theorem (Eq. 1.54) shows that

$$\int \nabla \cdot \mathbf{A} d\mathbf{y} = \lim_{R \rightarrow \infty} \int_{S_R} \mathbf{A} \cdot d\mathbf{S}$$

where S_R denotes a sphere of radius R and \mathbf{A} denotes any vector for which the integrals exist. Hence, upon assuming[†] that T_{ij} is smooth and decays

[†] Since T_{ij} should behave like $\rho v_i v_j$ at large distances from a localized region of turbulent flow (Sec. 2.2.3) and since v_i decays at the y^{-1} rate characteristic of acoustic disturbances (Eqs. (1.80) and (1.81)), it is clear that T_{ij} will decay like y^{-2} as $y \rightarrow \infty$ —which is not fast enough to ensure that the last integral in Eq. (2.10) will converge. On the other hand, the incompressible flow velocities, which dominate in the region of turbulent flow at sufficiently low Mach numbers, will decay at least as fast as y^{-3} as $y \rightarrow \infty$. Hence, the last integral in Eq. (2.10) would certainly converge if it were possible to neglect the acoustic velocities at the outset of the analysis. And, in fact, it can be shown, by using the method of matched asymptotic expansions⁹ that this can be done whenever the wavelength of the sound is large compared with the size of the source region. In all other cases we must rely on fairly subtle phase cancellations to insure convergence (i.e., the integral will only be conditionally convergent).

faster than y^{-1} for large y , we can conclude that the first three integrals vanish and, as a consequence, that

$$\rho(\mathbf{x}, t) - \rho_0 = \frac{1}{4\pi c_0^2} \frac{\partial^2}{\partial x_i \partial x_j} \int \frac{T_{ij}}{R} \left(\mathbf{y}, t - \frac{R}{c_0} \right) d\mathbf{y} \quad (2.11)$$

We are usually concerned with the sound field at large distances from the source where, as we have seen, the expression for the density fluctuations becomes particularly simple. Thus, suppose that the observation point \mathbf{x} is many wavelengths away from any point in the source region—which need not represent a large distance relative to the overall dimensions of this region. Then (see Sec. 1.5.2)

$$\frac{\partial^2}{\partial x_i \partial x_j} \frac{T_{ij}(\mathbf{y}, t - R/c_0)}{R} = \frac{R_i R_j}{c_0^2 R^3} \frac{\partial^2 T_{ij}(\mathbf{y}, t - R/c_0)}{\partial t^2} + O(R^{-2})$$

where

$$\mathbf{R} = \mathbf{x} - \mathbf{y}$$

and Eq. (2.11) becomes

$$\rho(\mathbf{x}, t) - \rho_0 \sim \frac{1}{4\pi c_0^2} \int \frac{R_i R_j}{R^3 c_0^2} \frac{\partial^2 T_{ij}}{\partial t^2} \left(\mathbf{y}, t - \frac{R}{c_0} \right) d\mathbf{y} \quad \text{as } R \rightarrow \infty$$

If, on the other hand, the distance between the observation point and any source point is also large compared with the dimensions of the source region (i.e., if the observation point is in the radiation field), we can (upon assuming that the origin of the coordinate system is in the source region) replace $R_i R_j / R^3$ by $x_i x_j / x^3$ to obtain

$$\rho(\mathbf{x}, t) - \rho_0 \sim \frac{1}{4\pi c_0^2} \frac{x_i x_j}{x^3} \int \frac{1}{c_0^2} \frac{\partial^2 T_{ij}}{\partial t^2} \left(\mathbf{y}, t - \frac{R}{c_0} \right) d\mathbf{y} \quad (2.12)$$

provided the integral converges.† This equation allows us to calculate the density fluctuations in the radiation field once the source term is known. It has been cast into a form which correctly displays the true quadrupole structure of the sound sources (see Sec. 1.5.2, especially Eq. (1.79) and ff.).

2.4 APPLICATION OF Lighthill's THEORY TO TURBULENT FLOWS

2.4.1 Derivation of Basic Equations

Equation (2.12) is mainly useful for predicting the acoustic radiation from turbulent jets.‡ In such flows it is reasonable to suppose that T_{ij} is a stationary

† We can now only be sure that this integral will converge if T_{ij} decays faster than y^{-3} for large y .

‡ It can also be used to predict the sound from periodic jets. See Sec. 2.5.3.

random function of time. Then Eq. (2.12) shows that the density fluctuation in the radiation field must also be a function of this type. Consequently, (as shown in Sec. 1.7.3) both the average intensity and its spectrum can readily be determined from the normalized pressure autocorrelation function

$$\Gamma(\mathbf{x}, \tau) \equiv \frac{[p(\mathbf{x}, t + \tau) - p_0][p(\mathbf{x}, t) - p_0]}{\rho_0 c_0}$$

And since Eq. (2.6) must certainly hold in the radiation field, it follows from Eq. (2.12) that this function is related to the source term by

$$\Gamma(\mathbf{x}, \tau) = \frac{1}{16\pi^2 c_0^5 \rho_0} \frac{x_i x_j x_k x_l}{x^6} \int \int \frac{\partial^2 T_{ij}}{\partial t^2}(\mathbf{y}', t') \frac{\partial^2 T_{kl}}{\partial t^2}(\mathbf{y}'', t'') d\mathbf{y}' d\mathbf{y}'' \quad (2.13)$$

where

$$\left. \begin{aligned} t' &= t - \frac{|\mathbf{x} - \mathbf{y}'|}{c_0} \\ t'' &= t + \tau - \frac{|\mathbf{x} - \mathbf{y}''|}{c_0} \end{aligned} \right\} \quad (2.14)$$

Moreover, it is shown in the appendix that the integrand in Eq. (2.13) can be put in the form

$$\frac{\partial^2 T_{ij}}{\partial t^2}(\mathbf{y}', t') \frac{\partial^2 T_{kl}}{\partial t^2}(\mathbf{y}'', t'') = \frac{\partial^4}{\partial \tau^4} \overline{T_{ij}(\mathbf{y}', t') T_{kl}(\mathbf{y}'', t'')} \quad (2.15)$$

But since (as shown in Appendix 1.A.3) the cross correlation of a stationary function is independent of time translations, it follows from Eq. (2.14) that

$$\overline{T_{ij}(\mathbf{y}', t') T_{kl}(\mathbf{y}'', t'')} = \overline{T_{ij}(\mathbf{y}', t) T_{kl}\left(\mathbf{y}'', t + \tau + \frac{|\mathbf{x} - \mathbf{y}'| - |\mathbf{x} - \mathbf{y}''|}{c_0}\right)} \quad (2.16)$$

And since $|\mathbf{x} - \mathbf{y}'|$ behaves like

$$|\mathbf{x} - \mathbf{y}'| = x - \frac{\mathbf{x}}{x} \cdot \mathbf{y}' + O(x^{-1})$$

for large x it follows that

$$\frac{|\mathbf{x} - \mathbf{y}'| - |\mathbf{x} - \mathbf{y}''|}{c_0} \sim \frac{\mathbf{x}}{x} \cdot \frac{(\mathbf{y}'' - \mathbf{y}')}{c_0} \quad (2.17)$$

Inserting Eqs. (2.17) and (2.16) into Eq. (2.15) and using the result in Eq. (2.13) therefore yields

$$\Gamma(\mathbf{x}, \tau) = \frac{1}{16\pi^2 c_0^5 \rho_0} \frac{x_i x_j x_k x_l}{x^6} \frac{\partial^4}{\partial \tau^4} \int \int \overline{T_{ij}(\mathbf{y}', t) T_{kl}(\mathbf{y}'', \tau_0)} d\mathbf{y}' d\mathbf{y}'' \quad (2.18)$$

where

$$\tau_0 \equiv t + \tau + \frac{\mathbf{x}}{xc_0} \cdot (\mathbf{y}'' - \mathbf{y}')$$

It is now convenient to introduce the separation vector $\boldsymbol{\eta} \equiv \mathbf{y}'' - \mathbf{y}'$ as a new variable of integration in Eq. (2.18) and to define a two-point time-delayed fourth-order correlation tensor by

$$\mathcal{R}_{ijkl}(\mathbf{y}', \boldsymbol{\eta}, \tau) \equiv \frac{\overline{T_{ij}(\mathbf{y}', t) T_{kl}(\mathbf{y}'', t + \tau)} - \varphi_{ijkl}(\mathbf{y}', \boldsymbol{\eta})}{\rho_0^2} \quad (2.19)$$

where φ_{ijkl} is an arbitrary time-independent tensor which will eventually be chosen to simplify the equations. Then, since the Jacobian of the transform $\mathbf{y}', \mathbf{y}'' \rightarrow \mathbf{y}', \boldsymbol{\eta}$ is unity, inserting these quantities into Eq. (2.18) yields

$$\Gamma(\mathbf{x}, \tau) = \frac{\rho_0 x_i x_j x_k x_l}{16\pi^2 c_0^5 x^6} \frac{\partial^4}{\partial \tau^4} \int \int \mathcal{R}_{ijkl} \left(\mathbf{y}', \boldsymbol{\eta}, \tau + \frac{\boldsymbol{\eta}}{c_0} \cdot \frac{\mathbf{x}}{x} \right) d\mathbf{y}' d\boldsymbol{\eta} \quad (2.20)$$

This equation relates the pressure autocorrelation in the sound field to the source correlation tensor \mathcal{R}_{ijkl} . Upon taking its Fourier transform and using Eq. (1.94) and Table 1.1 in Appendix 1.A, we find that the acoustic intensity spectrum is given by

$$\bar{I}_\omega(\mathbf{x}) = \frac{\omega^4 \rho_0}{32\pi^3 c_0^5} \frac{x_i x_j x_k x_l}{x^6} \int_{-\infty}^{\infty} \int \int e^{i\omega[\tau - (\mathbf{x}/x) \cdot \boldsymbol{\eta}/c_0]} \mathcal{R}_{ijkl}(\mathbf{y}', \boldsymbol{\eta}, \tau) d\mathbf{y}' d\boldsymbol{\eta} d\tau \quad (2.21)$$

This result can, in principle, be used to calculate the spectrum of the sound field emitted from a turbulent flow whenever solid boundaries do not play a direct role in the process. However, most turbulent flows which are not in the immediate vicinity of solid boundaries (e.g., jets, wakes, etc.) have nearly parallel mean flows. In the next section we deduce certain properties of the correlation tensor which will be helpful in understanding the sound fields produced by such flows.

2.4.2 Parallel or Nearly Parallel Mean Flows

Whenever the mean flow is nearly parallel, it is of interest to consider the case where the velocity $\mathbf{v}(\mathbf{y}, t)$ is the sum of a parallel mean flow $\hat{\mathbf{i}}U(y_2)$ as shown in Fig. 2.1 and a fluctuating part $\mathbf{u}(\mathbf{y}, t)$ with zero mean so that†

$$v_i = \delta_{1i}U + u_i \quad (2.22)$$

† This type of model for the turbulence correlation tensor appears to have been introduced by Ribner^{10,11}.

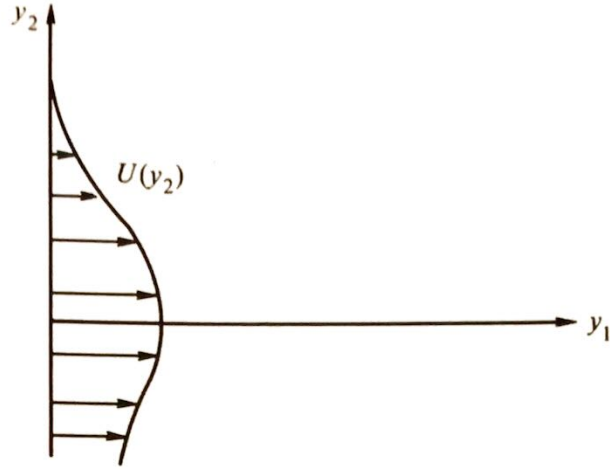


Fig. 2.1 Parallel sheared mean flow.

Special form of Reynolds stress approximation to correlation tensor. Before turning to more general considerations, we shall attempt to gain some insight into the connection between the turbulence velocity correlations and the correlation tensor \mathcal{R}_{ijkl} by approximating T_{ij} by the Reynolds stress. Thus, after substituting Eq. (2.22) into the Reynolds stress approximation (2.7) and choosing φ_{ijkl} in Eq. (2.19) to be

$$U'^2 \delta_{1i} \delta_{1j} \overline{u_k'' u_l''} + U''^2 \delta_{1k} \delta_{1l} \overline{u_i' u_j'} + U'^2 U''^2 \delta_{1i} \delta_{1j} \delta_{1k} \delta_{1l} + \overline{u_i' u_j'} \overline{u_k'' u_l''}$$

we find, after carrying out a very tedious calculation, that

$$\begin{aligned} \mathcal{R}_{ijkl}(\mathbf{y}', \boldsymbol{\eta}, \tau) \int &= (\overline{u_i' u_j' u_k'' u_l''} - \overline{u_i' u_j'} \overline{u_k'' u_l''}) + 2(U' \delta_{1i} \overline{u_j' u_k'' u_l''} + U'' \delta_{1k} \overline{u_i' u_j' u_l''}) \\ &+ 4U' U'' \delta_{1i} \delta_{1k} \overline{u_j' u_l''} \end{aligned} \quad (2.23)$$

where the double primes indicate that the quantities are to be evaluated at \mathbf{y}'' and $t + \tau$, while the primed quantities are to be evaluated at \mathbf{y}' and t . The notation $\int =$ indicates that the quantities on both sides of the equal signs are not necessarily equal but merely make equal contributions to Eqs. (2.20) and (2.21). In order to obtain this relation, we changed the names of dummy indices in the summations. The details can be found in Ref. 12.

Introduction of moving coordinates. Let l denote a typical correlation length of the turbulence. This quantity is, by definition, the smallest length for which

$$\frac{\mathcal{R}_{ijkl}(\mathbf{y}', \boldsymbol{\eta}, \tau)}{\mathcal{R}_{ijkl}(\mathbf{y}', 0, \tau)} \simeq 0 \quad \text{whenever } |\boldsymbol{\eta}| > l$$

If \mathcal{R}_{ijkl} changed so slowly with time that it was practically constant for time changes of the order of l/c_0 (the change in retarded time across a

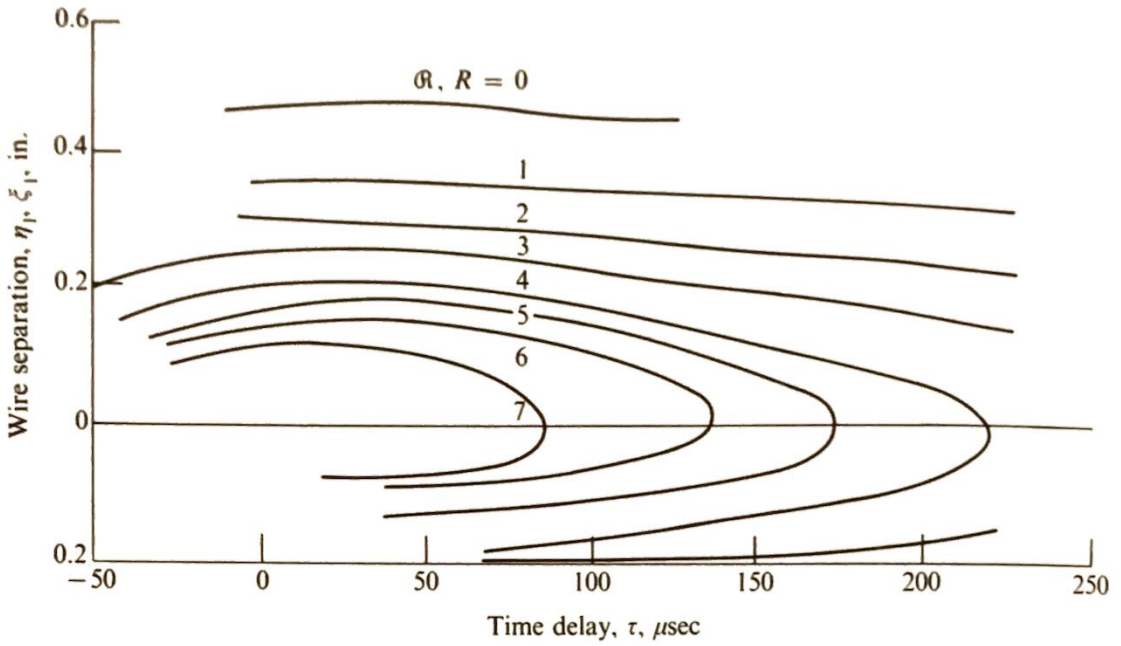


Fig. 2.2 Isocorrelation contours in moving frame (measurements in mixing region $1\frac{1}{2}$ diameters downstream). (From Reference 13.)

turbulent eddy) or, what is the same thing, if τ_η (the characteristic decay time of a turbulent eddy) satisfied the inequality

$$\tau_\eta \gg \frac{l}{c_0} \quad (2.24)$$

it would certainly be possible to replace $\mathcal{R}_{ijkl}(\mathbf{y}', \boldsymbol{\eta}', \tau + \mathbf{x} \cdot \boldsymbol{\eta}/xc_0)$ by $\mathcal{R}_{ijkl}(\mathbf{y}', \boldsymbol{\eta}, \tau)$ (since $(\boldsymbol{\eta}/c_0) \cdot \mathbf{x}/x$ is certainly $O(l/c_0)$ in the region where the integrand in Eq. (2.20) is of significant magnitude). Indeed, if it were not for the mean flow, a plot of constant correlation contours might appear as shown in Fig. 2.2 and the inequality (2.24) would then be satisfied. However, due to the convection of the random spatial pattern of the turbulence by the mean flow, moving eddies will produce very rapid fluctuations relative to a fixed observer (i.e., τ_η will be very small). The fluctuations seen by an observer moving with the flow will, on the other hand, be much slower. Hence, the eddy pattern will appear to be nearly frozen† and the constant correlation contours in any real flow should resemble those shown in Fig. 2.3. In fact, this figure is a plot of actual measurements of the second-order time-delayed correlation $u_1(\mathbf{y}', t)u_1(\mathbf{y}' + \hat{\mathbf{i}}\eta_1, t + \tau)$ carried out in the mixing region of a jet by Davies, Fisher, and Barratt.¹³

The inequality (2.24) will therefore not generally be satisfied in most real flows. However, the constant correlation contours should again resemble those shown in Fig. 2.2 when measured in a coordinate system which, roughly speaking, “moves with the eddies.” (In fact, this figure was obtained from Fig. 2.3 by introducing just such a coordinate system.) Thus, suppose

† This result is frequently referred to as *Taylor's hypothesis*.

that the correlation $\mathcal{R}_{ijkl}(\mathbf{y}', \boldsymbol{\eta}, \tau)$ is expressed in terms of the variables \mathbf{y}', τ and

$$\boldsymbol{\xi} = \boldsymbol{\eta} - \hat{\mathbf{i}} c_0 M_c \tau \quad (2.25)$$

where $\hat{\mathbf{i}}$ is a unit vector in the mean flow direction (i.e., y_1 -direction) and $c_0 M_c$ is the slope of the dashed line in Fig. 2.3. Then ξ_1 will remain constant along any line having this slope and changes in ξ_1 with τ held fixed will correspond to displacements in the direction perpendicular to these lines. The constant correlation contours in the $\xi_1 - \tau$ plane must therefore resemble those shown in Fig. 2.2. Consequently, the decay time τ_ξ of the "moving-axis correlation tensor" R_{ijkl} defined by

$$R_{ijkl}(\mathbf{y}', \boldsymbol{\xi}, \tau) = \mathcal{R}_{ijkl}(\mathbf{y}', \boldsymbol{\eta}, \tau) \quad (2.26)$$

is more likely to satisfy the inequality

$$\tau_\xi \gg \frac{l}{c_0} \quad (2.27)$$

than is the fixed-frame decay time τ_η . Suppose that an experimenter moving downstream with the convection velocity $c_0 M_c$ attempted to measure the two-point correlation tensor, \mathcal{R}_{ijkl} and that, relative to his reference frame, his two measurement points are separated by the distance $\boldsymbol{\xi}$. Then, since he will have moved downstream a distance $c_0 M_c \tau$ in the time interval τ between his first and second measurements, the distance between his two observation points will be $\boldsymbol{\eta} = \boldsymbol{\xi} + \hat{\mathbf{i}} c_0 M_c \tau$ when reckoned relative to a fixed coordinate system. Hence $R_{ijkl}(\mathbf{y}', \boldsymbol{\xi}, \tau)$ can be interpreted as the correlation tensor that

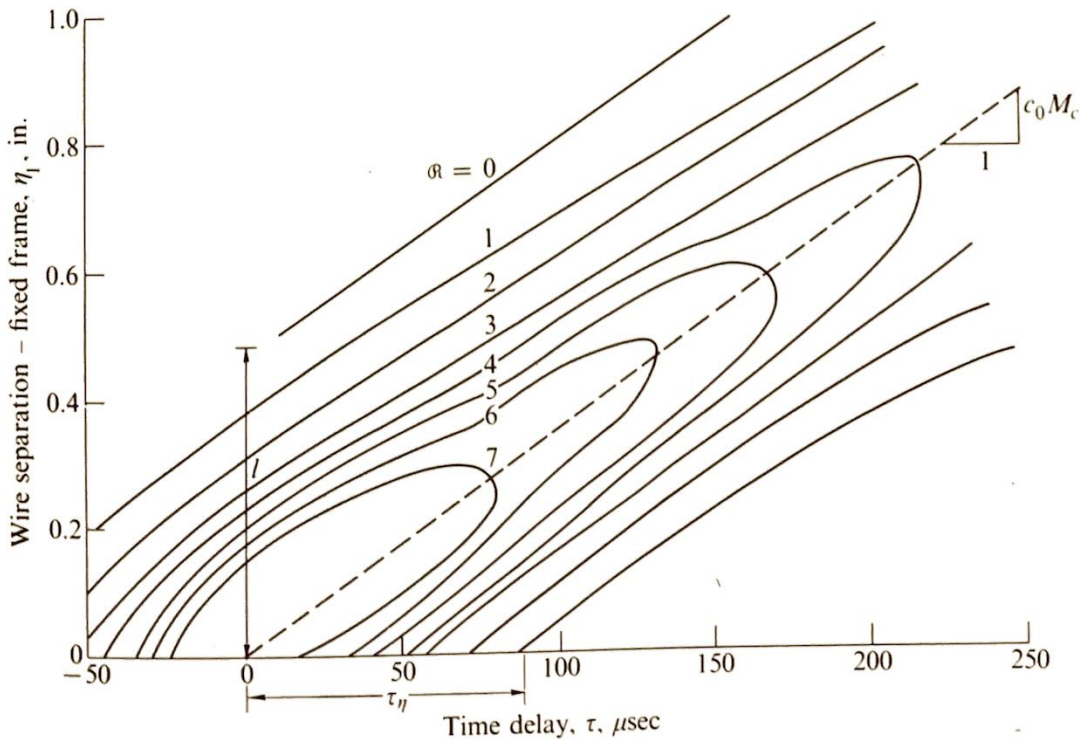


Fig. 2.3 Isocorrelation contours for fixed observer (measurements in center of mixing region $1\frac{1}{2}$ diameters downstream). (From Reference 13.)

would be seen by an observer who moves downstream with the convection velocity $c_0 M_c$ but measures the magnitudes of all velocities relative to a fixed frame.

Substituting Eq. (2.26) together with the change of variable (2.25) into Eq. (2.21) yields

$$\bar{I}_\omega(\mathbf{x}) = \frac{\omega^4 \rho_0}{32\pi^3 c_0^5} \frac{x_i x_j x_k x_l}{x^6} \iiint \left(\exp \left\{ i\omega \left[(1 - M_c \cos \theta) \tau - \frac{\mathbf{x} \cdot \boldsymbol{\xi}}{x c_0} \right] \right\} \right) \times R_{ijkl}(\mathbf{y}', \boldsymbol{\xi}, \tau) d\boldsymbol{\xi} dy' d\tau \quad (2.28)$$

where, as shown in Fig. 2.4,

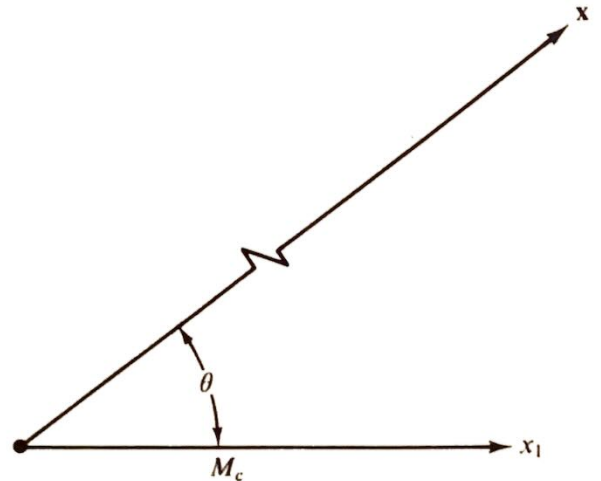
$$\cos \theta = \frac{x_1}{x}$$

is the angle between the mean flow direction and the line connecting the observation and source points. Instead of carrying out a similar operation on Eq. (2.20) for the pressure autocorrelation function, it is simpler to take the inverse transform of Eq. (2.28) to obtain

$$\begin{aligned} \Gamma(\mathbf{x}, t) &= \frac{\rho_0}{16\pi^2 c_0^5} \frac{x_i x_j x_k x_l}{x^6} \int \left(\frac{1}{1 - M_c \cos \theta} \right) \frac{\partial^4}{\partial t^4} \int R_{ijkl} \left(\mathbf{y}', \boldsymbol{\xi}, \frac{t + \frac{\mathbf{x} \cdot \boldsymbol{\xi}}{x c_0}}{1 - M_c \cos \theta} \right) d\boldsymbol{\xi} dy' \\ &= \frac{\rho_0}{16\pi^2 c_0^5} \frac{x_i x_j x_k x_l}{x^6} \int \frac{1}{(1 - M_c \cos \theta)^5} \\ &\quad \times \left\{ \frac{\partial^4}{\partial \tau^4} \int R_{ijkl} \left[\mathbf{y}', \boldsymbol{\xi}, \tau + \frac{\mathbf{x} \cdot \boldsymbol{\xi}}{x c_0 (1 - M_c \cos \theta)} \right] \right\}_{\tau = t/(1 - M_c \cos \theta)} d\boldsymbol{\xi} dy' \end{aligned} \quad (2.29)$$

Even if it were not possible to neglect variations in retarded time, this result would still be superior to Eq. (2.20) by virtue of its reduced sensitivity to any small errors that may be made in determining the correlation function.

Fig. 2.4 Orientation of observation point relative to flow direction.



In order to see this, notice that the largest time variations in the correlation function occur as a result of the convection of the frozen eddy pattern by the mean flow. Hence, the largest part of the time derivatives of \mathcal{R}_{ijkl} and therefore of the integrand in Eq. (2.20) will be due to the convection. But the steady subsonic motion of a frozen eddy pattern cannot contribute to the sound field. Hence, only a small part of this integrand will not integrate to zero. This difficulty does not occur with Eq. (2.29) since the changes with respect to time now occur on the time scale of the sound-producing turbulence fluctuations. The integrand in this equation should therefore be much less sensitive to small errors made either in the measurement or in the analytical approximation of the turbulence correlation function—an important attribute in light of our inadequate knowledge of this quantity.

The essential simplicity of Eq. (2.28) becomes especially apparent when the four-dimensional *power spectral density tensor*

$$H_{ijkl}(\mathbf{y}', \mathbf{k}, \omega) = \frac{1}{(2\pi)^4} \int_{-\infty}^{\infty} \int e^{i(\omega\tau - \mathbf{k} \cdot \boldsymbol{\xi})} R_{ijkl}(\mathbf{y}', \boldsymbol{\xi}, \tau) d\boldsymbol{\xi} d\tau$$

is introduced to obtain

$$\bar{I}_{\omega}(\mathbf{x}) = \frac{\pi\omega^4\rho_0}{2c_0^5} \frac{x_i x_j x_k x_l}{x^6} \int H_{ijkl}\left(\mathbf{y}', \frac{\omega}{c_0} \frac{\mathbf{x}}{x}, \omega(1 - M_c \cos \theta)\right) d\mathbf{y}' \quad (2.30)$$

This result clearly reveals which components of the turbulence actually participate in the sound generation process. Thus, it shows that the wave number vector of the sound field $(\mathbf{x}/x)(\omega/c_0)$ is the same as that of the turbulence which generates it, even when the latter is measured in the moving frame. However, the frequency of the turbulence is equal to the Doppler factor $(1 - M_c \cos \theta)$ times the frequency of the sound it generates. Notice that this is the same Doppler shift in frequency that takes place when an ideal point source moves with the convection velocity $c_0 M_c$ (see Sec. 1.8.4).

The region of frequency-wave number space containing significant turbulent energy is shown schematically in Fig. 2.5. It reflects the fact that the vertical dimension of this region is smaller than the horizontal dimension by a factor of the fluctuating turbulence Mach number u'/c_0 —which is a very small number indeed at subsonic speeds. Equation (2.30) implies that all the sound-emitting elements of the turbulence lie along the line shown in the figure. Only a relatively small segment of this line will pass through the region of significant turbulent energy when M_c is small and/or $|\theta|$ is near $\pi/2$. Consequently, not much of the turbulent energy gets radiated as sound under these conditions. On the other hand, the slope of the line of sound producing elements decreases with increasing subsonic convection Mach number at forward angles ($|\theta| < \pi/2$) and increases with Mach number at the rearward angles ($|\theta| > \pi/2$). More sound is therefore emitted in the forward direction than in the backward direction, and the higher the Mach number, the greater the forward emission.

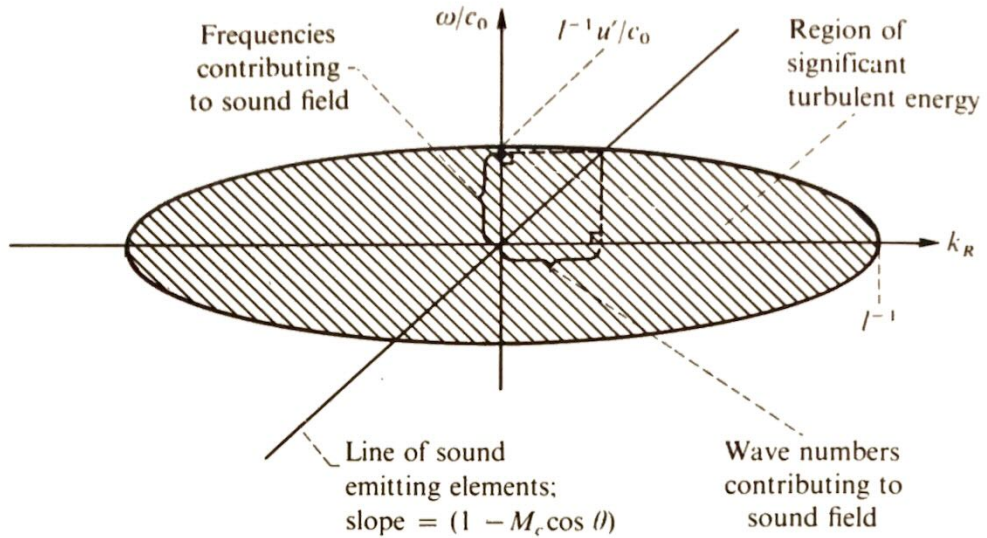


Fig. 2.5 Region of wave number space containing significant turbulent energy: measured in moving frame.

When the line of sound producing elements is close to the vertical axis, nearly all the available turbulence frequencies can participate in the sound generation process, while only a small fraction of its wave numbers will be involved. Conversely, when the slope of this line approaches zero, only a small fraction of the turbulence frequencies are effective in generating sound but nearly all the wave numbers can contribute to the process.

Neglect of retarded time in subsonic flows. Equations (2.29) and (2.30) have been put into a form wherein the omission of retarded-time variations will introduce the smallest error. It can be seen from Eq. (2.29) that these variations can be neglected whenever the decay time τ_ξ of the moving-axis correlation is long enough so that

$$\frac{l}{c_0(1 - M_c \cos \theta)} \ll \tau_\xi \quad (2.31)$$

Thus, when this inequality is satisfied, Eq. (2.29) and its Fourier transform Eq. (2.30) can be approximated by

$$\Gamma(\mathbf{x}, t)$$

$$= \frac{\rho_0}{16\pi^2 c_0^5} \frac{x_i x_j x_k x_l}{x^6} \int \frac{1}{(1 - M_c \cos \theta)^5} \left[\frac{\partial^4}{\partial \tau^4} \int R_{ijkl}(\mathbf{y}', \xi, \tau) \right]_{\tau=t(1 - M_c \cos \theta)} d\xi d\mathbf{y}' \quad (2.32)$$

and

$$I_\omega(\mathbf{x}) = \frac{\pi \omega^4 \rho_0}{2c_0^5} \frac{x_i x_j x_k x_l}{x^6} \int H_{ijkl}(\mathbf{y}', 0, \omega(1 - M_c \cos \theta)) d\mathbf{y}' \quad (2.33)$$

respectively. Equation (2.33) does not imply that the sound is emitted by the zero-wave-number components of the turbulence. In fact, these components

radiate no sound at all. The equation merely indicates that the energy in the turbulence at the small wave number $\mathbf{k} = (\omega/c_0)(\mathbf{x}/x)$ at which the sound is emitted is approximately the same as the energy in the turbulence at $\mathbf{k} = 0$.

The quantity $l/c_0(1 - M_e \cos \theta)$ that appears in the inequality (2.31) can be interpreted as the time it takes a sound wave to cross a moving eddy at an angle θ to its direction of motion. Thus, whenever l is small enough so that this time is much less than the turbulence decay time, the variation in retarded time can be neglected and the eddy can be treated as compact source. Notice that, as the convection Mach number of the eddy increases, the error created by neglecting the retarded time gets worse. Hence, this approximation is essentially limited to subsonic (or perhaps very high-Mach-number supersonic) flows.

2.5 PHYSICS OF JET NOISE

In this section the equations derived in Sec. 2.4 will be used in conjunction with experimental observations of jet flow fields to explain and, in some cases, predict certain types of jet noise.

2.5.1 High-Reynolds-Number Subsonic Cold-Air Jets

The sound emission from subsonic cold (i.e., unheated) air jets has been more extensively studied than any other type of jet noise. We shall show subsequently (on page 90) that the inequality (2.31) is reasonably well satisfied in the sound-producing region of such flows so that Eq. (2.32) can be used to predict the noise. However, this cannot be done unless the turbulence correlation tensor R_{ijkl} is known. Since our knowledge of this quantity is quite limited, we shall try to model it in some approximate fashion. This will be accomplished by making a series of progressively more restrictive assumptions—each of which leads to a formula for the sound field that requires less information about the turbulence than the preceding one.

Approximations to source term for subsonic jet flows. The parallel mean flow approximation (2.22) and the Reynolds stress approximation (2.7) should be adequate to describe the flow in a jet and are therefore adopted in this section. Then Eqs. (2.23) and (2.26) show that the moving-axis turbulence correlation tensor is a sum of three terms. However, it is shown in Ref. 12 that, if the turbulence is assumed to be locally homogeneous† and incompressible, the middle term integrates to zero and only the first and

† This simply means that R_{ijkl} is assumed to be a much stronger function of ξ than of \mathbf{y}' .

last terms contribute to Eq. (2.32). It is now convenient to change the variable of integration in Eq. (2.32) from \mathbf{y}' to

$$\mathbf{y} \equiv \left\{ y'_1, \frac{y'_2 + y''_2}{2}, \frac{y'_3 + y''_3}{2} \right\} \\ = \{ y'_1, y'_2 + \frac{1}{2}\eta_2, y'_3 + \frac{1}{2}\eta_3 \}$$

Then it follows from Eqs. (2.23) and (2.26) that Eq. (2.32) becomes

$$\Gamma(\mathbf{x}, t) = \frac{\rho_0}{16\pi^2 c_0^5} \frac{x_i x_j x_k x_l}{x^6} \int \frac{1}{(1 - M_c \cos \theta)^5} \left\{ \frac{\partial^4}{\partial \tau^4} \right. \\ \times \left[\int R_{ijkl}^0(\mathbf{y}, \xi, \tau) d\xi + 4\delta_{1i}\delta_{1k} \int U' U'' R_{jl}^0(\mathbf{y}, \xi, \tau) d\xi \right] \Bigg|_{\tau=t/(1-M_c \cos \theta)} dy \quad (2.34)$$

where

$$R_{ijkl}^0(\mathbf{y}, \xi, \tau) = \overline{u'_i u'_j u''_k u''_l} - \overline{u'_i u'_j} \overline{u''_k u''_l} \\ R_{ij}^0(\mathbf{y}, \xi, \tau) = \overline{u'_j u''_i}$$

are, respectively, the fourth- and second-order time-delayed turbulence velocity correlation tensors.

Now let $\bar{I}(\mathbf{x} | \mathbf{y})$ denote the acoustic intensity at \mathbf{x} due to a unit volume of turbulence located at the point \mathbf{y} , and let $I_\omega(\mathbf{x} | \mathbf{y})$ and $\Gamma(\mathbf{x} | \mathbf{y}, t)$ denote its associated spectra and autocorrelation function, respectively. Then

$$\bar{I}(\mathbf{x}) = \int \bar{I}(\mathbf{x} | \mathbf{y}) d\mathbf{y}, \quad I_\omega(\mathbf{x}) = \int I_\omega(\mathbf{x} | \mathbf{y}) d\mathbf{y}, \quad \Gamma(\mathbf{x}, t) = \int \Gamma(\mathbf{x} | \mathbf{y}, t) d\mathbf{y}$$

and it follows from Eq. (2.34) that

$$\Gamma(\mathbf{x} | \mathbf{y}, t) = \frac{\rho_0}{16\pi^2 c_0^5 (1 - M_c \cos \theta)^5} \frac{x_i x_j x_k x_l}{x^6} \left\{ \frac{\partial^4}{\partial \tau^4} \right. \\ \times \left[\int R_{ijkl}^0(\mathbf{y}, \xi, \tau) d\xi + 4\delta_{1i}\delta_{1k} \int U' U'' R_{jl}^0(\mathbf{y}, \xi, \tau) d\xi \right] \Bigg|_{\tau=t/(1-M_c \cos \theta)} \quad (2.35)$$

The corresponding expression for the acoustic intensity is obtained by setting $t = 0$ in this formula. This result is similar to the formula for a moving point quadrupole source (Secs. 1.5.2 and 1.8.5). Thus notice that it is multiplied by a convection factor $(1 - M_c \cos \theta)$ raised to a negative power. This factor arises because of the introduction of the moving frame correlation tensor (2.26) and is therefore again related to the motion of the sources. However, it is now raised to the power -5 rather than the power -6 that was shown to occur in the mean square pressure signal from convecting point quadrupole sources (see last paragraph in Sec. 1.8.5). The difference

can be attributed to the fact that we are now dealing with an aggregate of acoustic sources¹⁴ that fill a finite volume of space.

The two terms in curly brackets are more or less directly related to the turbulence structure of the jet.[†] The first of these is often called the *self-noise*, and the second is referred to as the *shear noise*. This terminology was introduced by Lilley¹⁵ to indicate that the former represents noise generated by turbulence–turbulence interactions while the latter represents noise generated by turbulence–mean-shear interactions. However, the actual definitions given above are somewhat different from Lilley's. Over the years, a great deal of effort (both experimental and analytical) has been directed toward evaluating these terms. The simplest approaches amount to little more than dimensional analysis; the more complex involve attempts to measure the detailed turbulence correlation tensors. However, the latter procedure is so complicated and time consuming as to be almost impractical. Thus, in order to get some idea of how these terms affect the variation in the sound field, it is necessary to make some assumptions about the relative magnitudes of the various components of the turbulence correlation tensors. Perhaps the simplest such assumptions are those used by Ribner^{10,11}. The first of these is that the joint probability distribution of the velocities at two points is approximately normal; the second is that the turbulence is incompressible; and the third is that the turbulence is isotropic. By introducing these approximations into Eq. (2.35) and carrying out a rather tedious calculation it is possible to show that^{11,12}

$$\Gamma(\mathbf{x}|\mathbf{y}, t) = \frac{\rho_0}{16\pi^2 c_0^5 (1 - M_c \cos \theta)^5 x^2} \left\{ \frac{\partial^4}{\partial \tau^4} \left[\int R_{1111}^0 d\xi + 4 \right. \right. \\ \left. \left. \times (\cos^4 \theta + \cos^2 \theta \sin^2 \theta \sin^2 \varphi) \int U' U'' R_{11}^0 d\xi \right] \right\}_{\tau=t/(1-M_c \cos \theta)} \quad (2.36)$$

where

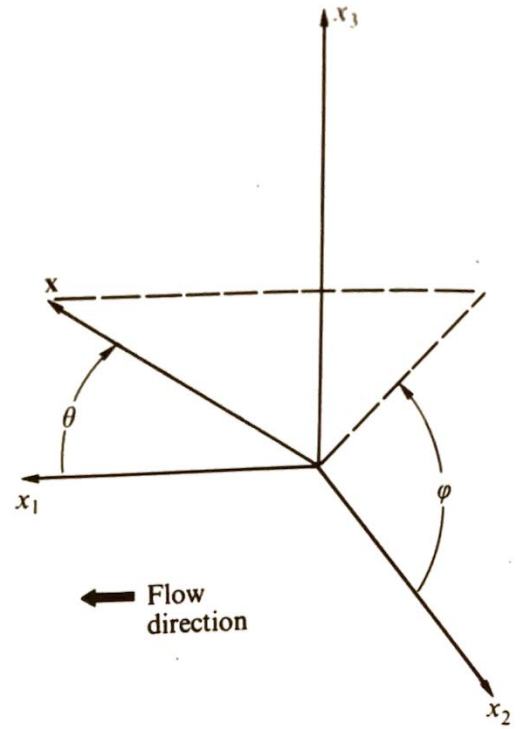
$$\cos \varphi = \frac{x_2}{\sqrt{x_2^2 + x_3^2}} \quad (2.37)$$

is the azimuthal angle shown in Fig. 2.6. For axisymmetric jets, averaging over this angle will account for the different orientations of the sound sources in any given annular slice of jet. Equation (2.36) then becomes

$$\Gamma(\mathbf{x}|\mathbf{y}, t)_{av} = \frac{\rho_0}{16\pi^2 c_0^5 (1 - M_c \cos \theta)^5 x^2} \\ \times \left\{ \frac{\partial^4}{\partial \tau^4} \left[\int R_{1111}^0 d\xi + \frac{\cos^4 \theta + \cos^2 \theta}{2} 4 \int U' U'' R_{11}^0 d\xi \right] \right\}_{\tau=t/(1-M_c \cos \theta)}$$

[†] Thus the effects of source convection are decoupled from the details of the turbulence structure.

Fig. 2.6 Coordinate system for jet flow.



Taking the Fourier transform of this result and using the relations (between the intensity, its spectra, and the autocorrelation function) given in Sec. 1.7.3 now yields

$$I_{\omega}(\mathbf{x}|\mathbf{y})_{av} = \frac{\Omega^4 \rho_0}{32\pi^3 c_0^5 (1 - M_c \cos \theta)^4 x^2} \times \left(\int e^{i\Omega\tau} \int R_{1111}^0 d\xi d\tau + \frac{\cos^4 \theta + \cos^2 \theta}{2} 4 \int e^{i\Omega\tau} \int U' U'' R_{11}^0 d\xi d\tau \right) \quad (2.38)$$

where

$$\Omega = \omega(1 - M_c \cos \theta)$$

is the source frequency (see Sec. 1.8.4) and

$$\bar{I}(\mathbf{x}|\mathbf{y})_{av} = \frac{\rho_0}{16\pi^2 c_0^5 (1 - M_c \cos \theta)^5 x^2} \times \left(\frac{\partial^4}{\partial \tau^4} \int R_{1111}^0 d\xi \right)_{\tau=0} \left(1 + \frac{\cos^4 \theta + \cos^2 \theta}{2} A \right) \quad (2.39)$$

where

$$A \equiv \frac{4 \left(\frac{\partial^4}{\partial \tau^4} \int U' U'' R_{11}^0 d\xi \right)_{\tau=0}}{\left(\frac{\partial^4}{\partial \tau^4} \int R_{1111}^0 d\xi \right)_{\tau=0}}$$

is the ratio of the maximum shear noise to the self-noise. While the simplicity of the latter formula is quite appealing, there are a number of reasons to believe that it may not be much better than the results that would have been obtained if we had simply neglected all directivity effects associated with the turbulence structure at the outset. The first is that a good estimate of the ratio A has yet to be obtained (although Ribner^{10,11} has concluded that it should be near unity). A more significant factor, however, is that the anisotropy that characterizes real jet turbulence could cause the directivity factor $[1 + A(\cos^4 \theta + \cos^2 \theta)/2]$ to be largely in error. In fact, Goldstein and Rosenbaum¹² have combined an axisymmetric turbulence model with measurements of the turbulence anisotropy to show that the self-noise term may be nearly as directional as the shear noise. Finally, as will be shown in Chap. 6, certain effects that have already been excluded in this chapter will probably have a much larger influence on the radiated sound than any alterations that may be caused by the term $[1 + A(\cos^4 \theta + \cos^2 \theta)/2]$. Fortunately, the variation of this term with angle will, in any case, be small in comparison with that of $(1 - M_c \cos \theta)^{-5}$. Therefore, any alterations in the directivity pattern that might arise from this term will simply be ignored in the remainder of this chapter—though we shall consider its influence on the acoustic spectrum.

We anticipate from similarity considerations that

$$\left(\frac{\partial^4}{\partial \tau^4} \int R_{1111}^0 d\xi \right)_{\tau=0}$$

will be of the order $(u'^4 l^3 / \tau_\xi^4) K$, where u' denotes a typical root-mean-square turbulence velocity and K is some dimensionless constant. Hence, it follows from Eq. (2.39) that

$$\bar{I}(\mathbf{x} | \mathbf{y})_{av} \simeq K \frac{\rho_0 (\tau_\xi)^{-4} u'^4 l^3}{16\pi^2 c_0^5 (1 - M_c \cos \theta)^5 x^2} \quad (2.40)$$

The total power emitted per unit volume of turbulence $\mathcal{P}(\mathbf{y})$ is obtained by integrating Eq. (2.40) over the surface of a large sphere of radius x . Thus,

$$\mathcal{P}(\mathbf{y}) \simeq \frac{K \rho_0 u'^4 l^3}{4\pi c_0^5 \tau_\xi^4} \frac{1 + M_c^2}{(1 - M_c^2)^4} \quad (2.41)$$

The factor $(1 + M_c^2)/(1 - M_c^2)^4$, which results from integrating the convection factor over all angles, is always greater than unity. Thus, source convection not only causes more power to be radiated upstream than downstream, but also increases the total amount of energy that the source actually emits.

Fluid mechanics of subsonic jets. The approximations given in the preceding section were introduced to simplify the equations and are, for the most part, not based on any specific information about the flow field

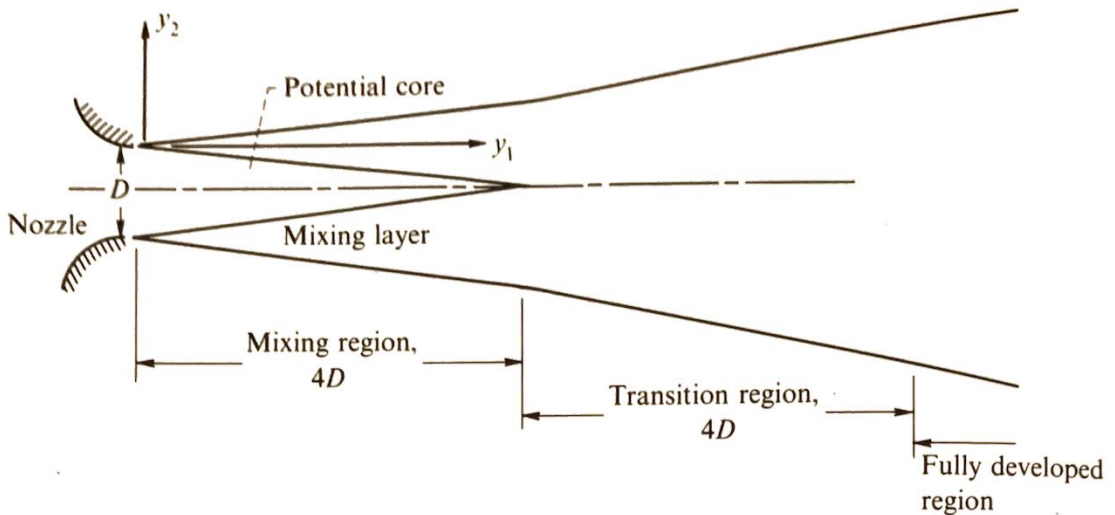


Fig. 2.7 Jet structure.

in a jet. In this section we shall summarize those aspects of the fluid mechanics of the jet that are relevant to the sound generation process. The information is based on the measurements of Laurence¹⁷; Davies, Fisher, and Barratt¹³; and Bradshaw, Ferriss, and Johnson¹⁸.

Consider a high-Reynolds-number air jet issuing from a convergent nozzle (with a fairly uniform velocity U_j) into a stationary fluid, as shown in Fig. 2.7. As the jet leaves the nozzle, an annular *mixing layer* forms between the moving fluid and its surroundings. The flow in this region becomes turbulent within about one-half of a jet diameter downstream. It then spreads linearly in both directions until it fills the entire jet at 4, or perhaps 5, diameters downstream. Hence, the thickness of the mixing layer is about $0.2 y_1$ to about $0.25 y_1$. Since the motion remains laminar within the conical domain enclosed by the turbulent flow we usually refer to this region as the *potential core*. Of course, the boundary of the mixing layer is not straight as shown in Fig. 2.7 but has more the appearance shown in Fig. 2.8.

Once the mixing layer fills the jet its uniform growth ceases and it evolves differently as it passes first through a *transition* region and finally, at about 8 diameters downstream, into a region of self-preserving flow called the *fully developed region*. The latter also grows linearly with y_1 but

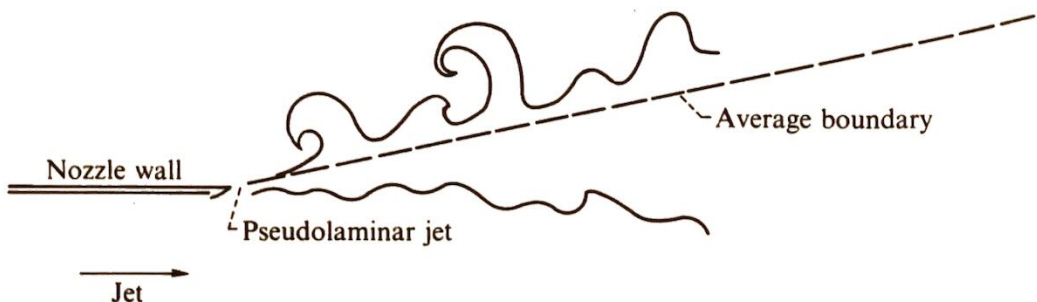


Fig. 2.8 Boundary of mixing layer.

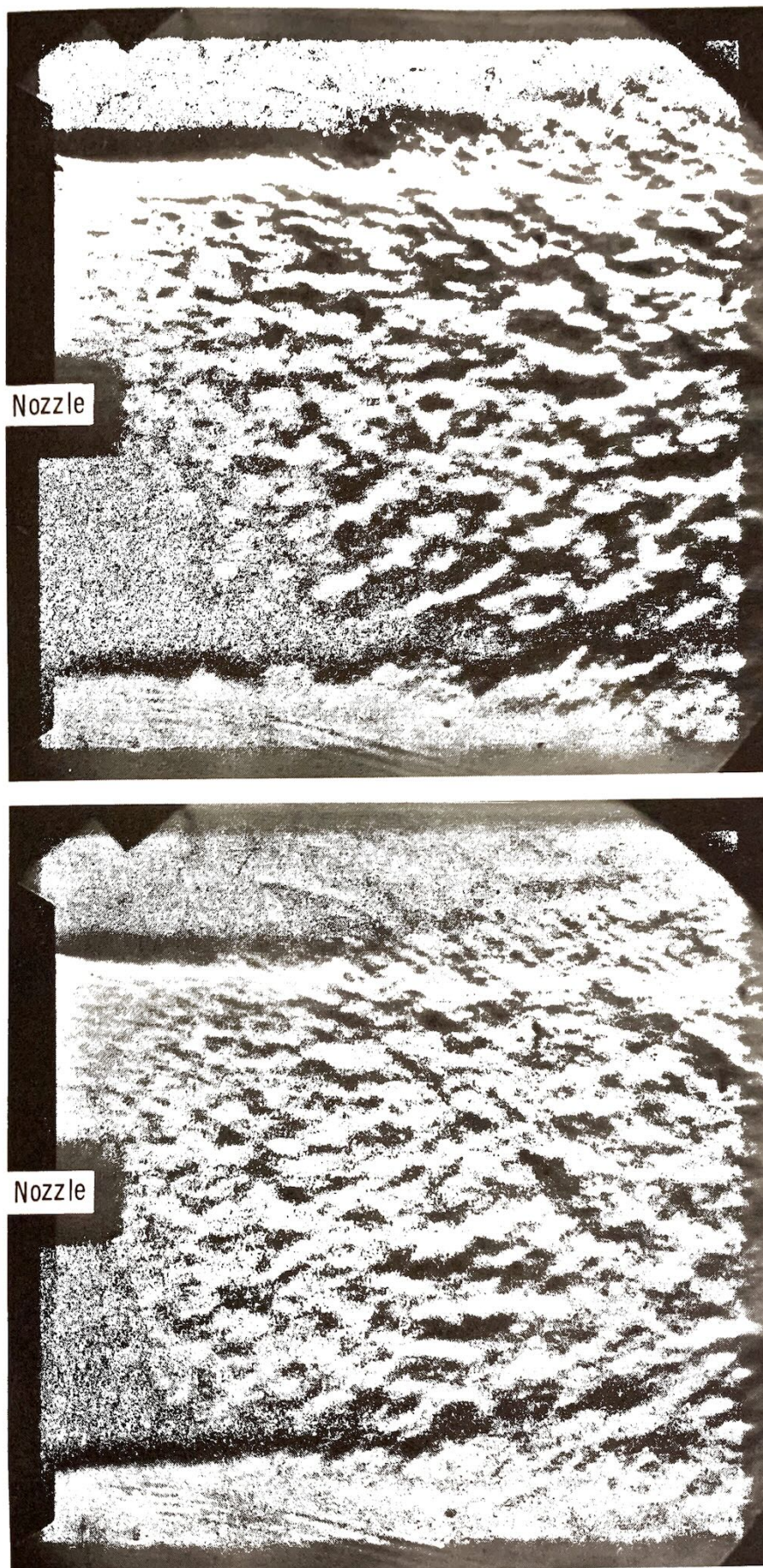


Fig. 2.9 Schlieren photographs of flow in a high-velocity subsonic jet from a 7.6 cm (3 in.) diameter nozzle (Taken by W. L. Howes at NASA Lewis Research Center.) (a) Jet exit Mach number, U_J/c_0 , 0.9. (b) Jet exit Mach number, U_J/c_0 , 0.74.

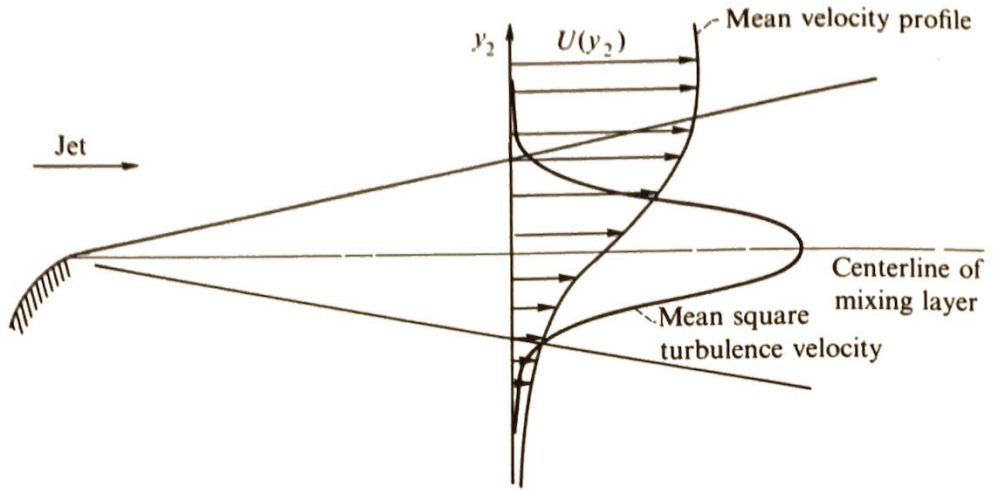


Fig. 2.10 Mixing layer profiles.

at a different rate than the mixing layer. Schlieren photographs of a typical high-velocity subsonic jet are shown in Fig. 2.9.

The mean velocity profile and the mean square turbulence velocity variation across the mixing layer are shown (roughly to scale) in Fig. 2.10. The peak turbulence intensity u'_{\max} occurs on the centerline of the mixing layer. Moreover it is fairly constant and approximately equal to

$$u'_{\max} \simeq 0.16U_J \quad (2.42)$$

until well into the transition region. It finally falls off as y_1^{-2} in the fully developed region. As indicated in the figure, most of the turbulent energy is confined to a fairly narrow region at the center of the mixing layer.

The turbulent “eddies” in the mixing region are generally believed to be elongated in the flow direction. Thus, the longitudinal correlation length l_1 in the direction of flow is about twice the longitudinal correlation† length l_2 in the radial direction. However, both of these lengths vary linearly with distance from the nozzle and, in fact,

$$l_1 \simeq 0.1y_1 \quad \text{and} \quad l_2 \simeq 0.05y_1 \quad (2.43)$$

In the fully developed region the correlation length is relatively independent of y_1 to about 20 diameters.

A suitable measure of the decay time τ_ξ is the delay time τ required for the second-order moving-frame turbulence correlation to fall to $1/e$ of its $\tau = 0$ value. Davies, Fisher, and Barratt¹³ found that this quantity satisfied the relation

$$l_1 \simeq 0.2U_J\tau_\xi \quad (2.44)$$

along the centerline of the mixing region. Hence, for $U_J < c_0$, the inequality (2.31) is fairly well satisfied. And, as a result, we are fairly well justified in

† The longitudinal correlation length in the i th-direction is here defined as the distance for the longitudinal correlation coefficient in that direction, $R_{ii}(\mathbf{y}', \mathbf{k}_i \xi_i, 0)/R_{ii}(\mathbf{y}', 0, 0)$ (no sum on i ($i = 1, 2$, or 3)), to fall to $1/e$. The quantity \mathbf{k}_i denotes the unit vector in the i th-direction.

adopting the assumption (see page 77) that the retarded time is negligible.

A number of investigators^{13,19-21} have measured the eddy convection velocity $U_c = c_0 M_c$ in the mixing region. The measurements taken by Davies, Fisher, and Barratt¹³ are shown in Fig. 2.11. These results indicate that the convection velocity varies across the mixing region but not nearly as much as the mean velocity. They also show that it is equal to the mean velocity and to about $0.62U_j$ at the center of the mixing region, where most of the turbulent energy is concentrated. This behavior is relatively independent of axial distance.

Power emitted per unit length of jet. We now use the measurements described in the previous section to estimate $\mathcal{P}'(y_1)$, the power emitted per unit length of the jet. This quantity can be approximated by multiplying the power emitted per unit volume (given by Eq. (2.41)) by the cross-sectional area of the jet $A(y_1)$ to obtain

$$\mathcal{P}'(y_1) \simeq \frac{K \rho_0 u'^4 l^3}{4\pi c_0^5 \tau_\xi^4} A(y_1) \frac{1 + M_c^2}{(1 - M_c^2)^4} \quad (2.45)$$

We first consider the mixing layer, whose cross-sectional area is

$$A(y_1) = \pi D \times (\text{Thickness of mixing region}) = \frac{\pi D y_1}{4}$$

Then approximating the factors l and u' in Eq. (2.45) by l_1 and u'_{\max} , respectively, and inserting the empirical Eqs. (2.42) to (2.44) into the results yields

$$\mathcal{P}'(y_1) \simeq 6.5 \times 10^{-7} K \frac{\rho_0 U_j^8 D}{c_0^5} \frac{1 + M_c^2}{(1 - M_c^2)^4} \quad (2.46)$$

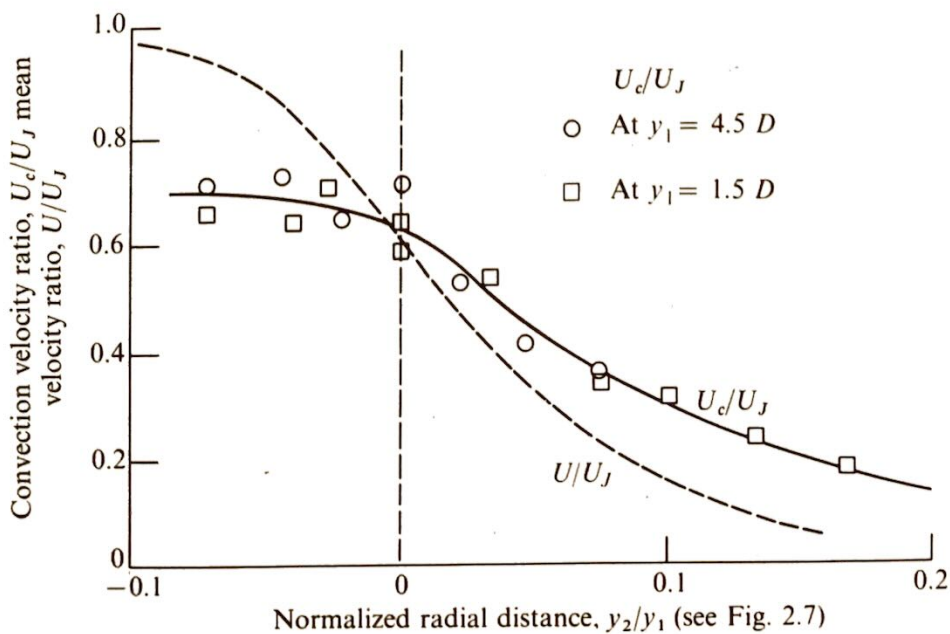


Fig. 2.11 Radial distribution of convection velocity. (From Reference 13.)

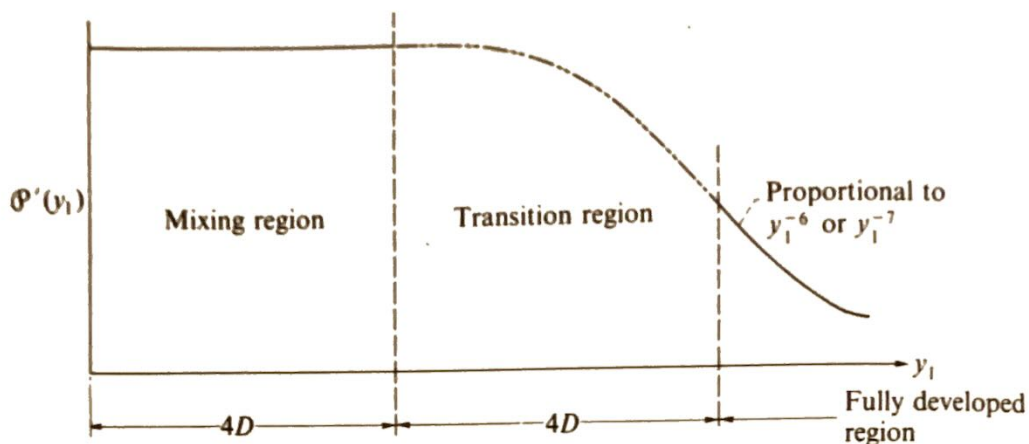


Fig. 2.12 Distribution of power emission in a jet.

This shows (since M_c is independent of y_1) that the power emitter per unit length of the mixing region is independent of axial position y_1 .

Since the local mean velocity U of the mixing layer (say along the centerline) is independent of y_1 , Eqs. (2.42) and (2.44) show that $\tau_\xi \propto l/U$ and $u' \propto U$ within this region. Although the experimental information is less complete beyond $y_1 = 4D$, it is not unreasonable to assume that this proportionality is still maintained (even though U now varies with y_1). Then Eq. (2.45) implies

$$\mathcal{P}'(y_1) \propto \frac{U^8}{l} A(y_1) \quad (2.47)$$

Now consider the fully developed region $y_1 > 8D$. Since the centerline velocity falls off as y_1^{-1} and since the cross-sectional area increases roughly as y_1^2 , it follows from Eq. (2.47) that

$$\mathcal{P}'(y_1) \propto \frac{1}{y_1^6 l} \quad (2.48)$$

which shows that the power emitted per unit length approaches zero very rapidly in this region. Although the correlation length l becomes proportional to y_1 for large values of y_1 , it appears to remain fairly constant up to a distance of about 20 diameters from the nozzle.

Equations (2.46) and (2.48) indicate that the power emitted per unit length of jet might vary in the manner shown in Fig. 2.12, although it must be admitted that there is no reason to suppose that \mathcal{P}' is a monotonically decreasing function of y_1 in the transition region. In any event this curve tends to imply that practically all the acoustic power is emitted from the first 8 to 10 jet diameters, with most of it coming from the mixing layer. However, if, as some investigators believe,[†] \mathcal{P}' actually increases in the transition region, most of the jet noise could, in fact, be generated in this region.

[†] Personal communication, J. E. Ffowcs Williams.

Comparison of predicted sound field with experiments. The total power \mathcal{P}_M emitted from the mixing layer can be approximated by multiplying Eq. (2.46) by the length $4D$ of this region to obtain

$$\mathcal{P}_M \simeq 2.5 \times 10^{-6} K \frac{\rho_0 U_J^8 D^2}{c_0^5} \frac{1 + M_c^2}{(1 - M_c^2)^4}$$

Since the factor

$$\frac{1 + M_c^2}{(1 - M_c^2)^4}$$

is a slowly varying function of U_J compared with U_J^8 , we can replace it by its value at $M_c = \frac{1}{2}$ to obtain

$$\mathcal{P}_M \simeq 10^{-5} K \frac{\rho_0 U_J^8 D^2}{c_0^5}$$

Thus, if about one-half the power is emitted from the mixing region, the total sound power emitted by the jet \mathcal{P}_T will be roughly

$$\mathcal{P}_T \simeq 2 \times 10^{-5} K \frac{\rho_0 U_J^8 D^2}{c_0^5} \quad (2.49)$$

This is the now famous U^8 law of jet noise obtained by Lighthill. The small size of the numerical factor is a consequence of the inefficiency of the quadrupole source. Measurements of the sound emission from subsonic air jets with low initial turbulence levels indicate that the "Lighthill parameter" $\mathcal{P}_T/(\rho_0 U_J^8 D^2/c_0^5)$ is actually 3×10^{-5} . Hence, considering the very approximate nature of the arguments, Eq. (2.49) is certainly in very good agreement with the observed facts. For jets with high initial turbulence,[†] the Lighthill parameter can increase by more than a factor of 30. The good agreement of the eighth-power law with the experimental data is illustrated in Fig. 2.13. This figure, taken from Reference 22, is a composite of Lewis Research Center data and data taken by Lush²³.

Equation (2.40) implies that the directional pattern of the jet noise is primarily the result of the convection factor $(1 - M_c \cos \theta)^{-5}$, which arises from the motion of the turbulent eddies relative to the observer. (Recall that we have omitted any small directivity effects that might arise from the turbulence structure itself.) Since most of the sound is probably coming from the mixing region, it is reasonable to assume that M_c is approximately equal to $0.62 U_J/c_0$. The directivity patterns predicted by $(1 - M_c \cos \theta)^{-5}$ with this value of M_c are compared with the air-jet sound field measurements of Olsen, Gutierrez, and Dorsch²² in Fig. 2.14 and with those of Lush²³ in Fig. 2.15. (The level of the theoretical curves is adjusted to go

[†] Most jets with high initial turbulence produce considerable internal noise, which is difficult to separate from the jet noise.

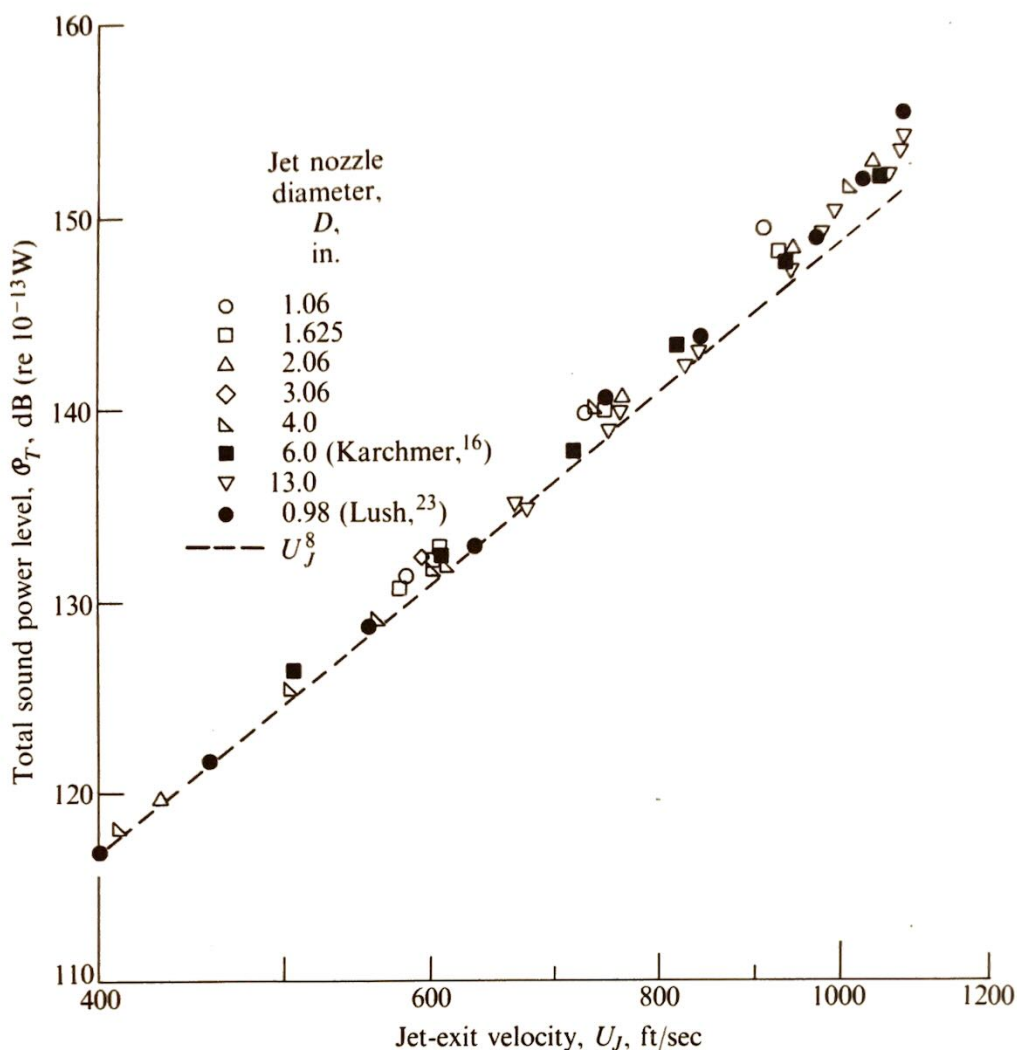


Fig. 2.13 Variation of total sound power level with jet velocity for subsonic circular nozzles. (All data scaled to an area of 1 ft² and an ambient temperature of 298 K (77° F). Free-field lossless data. From Reference 22.)

through the experimental data at 90° from the jet axis, where the convection effect is zero.) It is shown in Sec. 6.7 that the agreement improves significantly when the shielding effect of the mean jet velocity field is included in the theory.

The figures show that the measured sound intensity tends to decline at small angles (<20°) to the jet axis. It was suggested independently by Powell²⁴ and Ribner²⁵ that this dropoff is caused by refraction—an effect already implicit in the results discussed on pages 17–19 which show that sound waves emanating from a region of non-zero mean velocity will be bent away from the downstream flow direction. Such refraction effects are discussed more fully in Chap. 6 where it is shown that there are other ways in which the mean flow field of the jet can influence the sound field.

Spectra. It follows from Eq. (2.38) that the intensity spectrum at 90° from the jet axis is given by (see Fig. 2.6)

$$\bar{I}_\omega(x, \varphi, 90^\circ) = \frac{\omega^4 \rho_0}{32\pi^3 c_0^5 x^2} \int e^{i\omega\tau} \int R_{1111}^0 d\xi d\tau$$

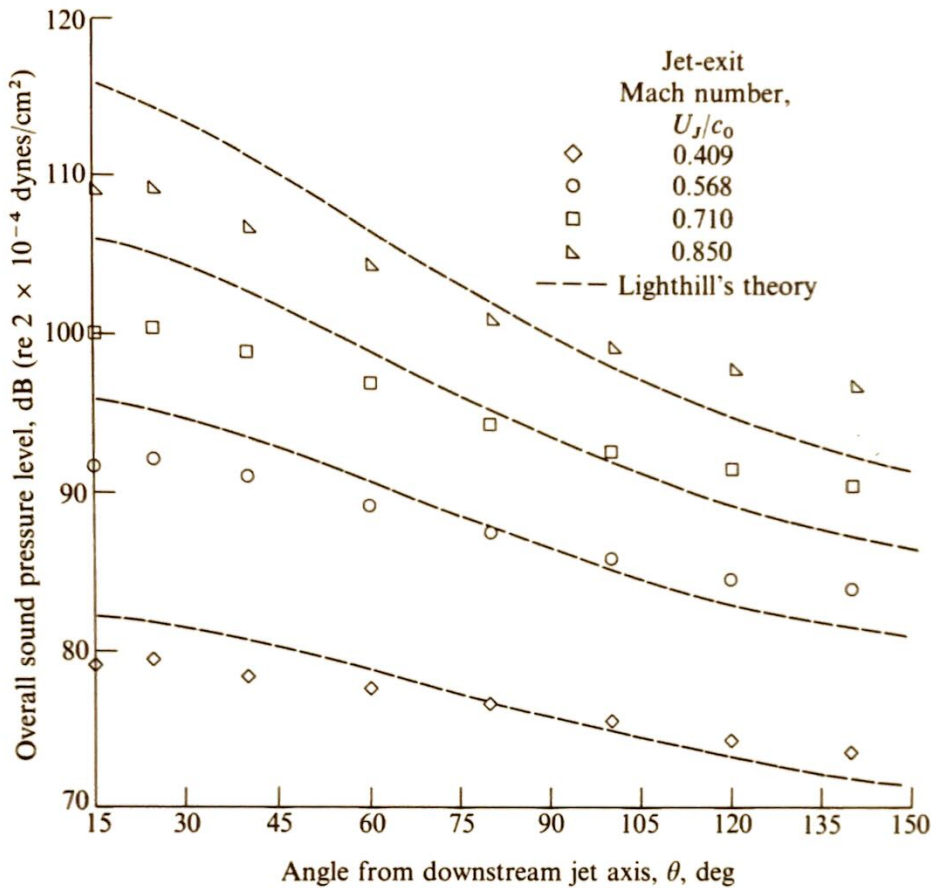


Fig. 2.14 Experimental directivity data from Reference 22. Jet nozzle diameter, D , 5.08 cm (2 in.).

while the results given on page 90 show that the times, lengths, and velocities associated with turbulence vary like D/U_J , D , and U_J , respectively. Hence, the third octave sound pressure level spectrum, which is proportional to $I_\omega \omega \times \text{jet volume}$ must, when nondimensionalized by $U_J^8 \rho_0 (D/x)^2 / c_0^5$, be a function only of the Strouhal number fD/U_J . The collection of data plotted in Fig. 2.16 shows that this is indeed the case. These results, which were compiled by Olsen and Friedman²⁶, cover a wide range of nozzle diameters and jet velocities.

If the shear noise term were neglected, Eq. (2.38) would also imply that $\mathcal{J} \equiv \text{the nondimensionalized third octave sound pressure spectrum} \times (1 - M_c \cos \theta)^5$ is a function only of the source Strouhal number $(fD/U_J)(1 - M_c \cos \theta)$. Then the peak frequency heard by an observer at the side of the jet would become progressively higher in pitch as he moved downstream. In fact, since the eddies are being convected downstream by the mean flow, the results of Sec. 1.8.4 indicate that this Doppler shift in frequency is precisely what we should expect to occur. Nevertheless the plot of peak frequency versus angle (Fig. 2.17; from Ref. 26), shows that this behavior is not at all consistent with the experimental results—especially at angles close to the jet axis. On the other hand, \mathcal{J} would not depend only on the source Strouhal number if the shear noise term were not being

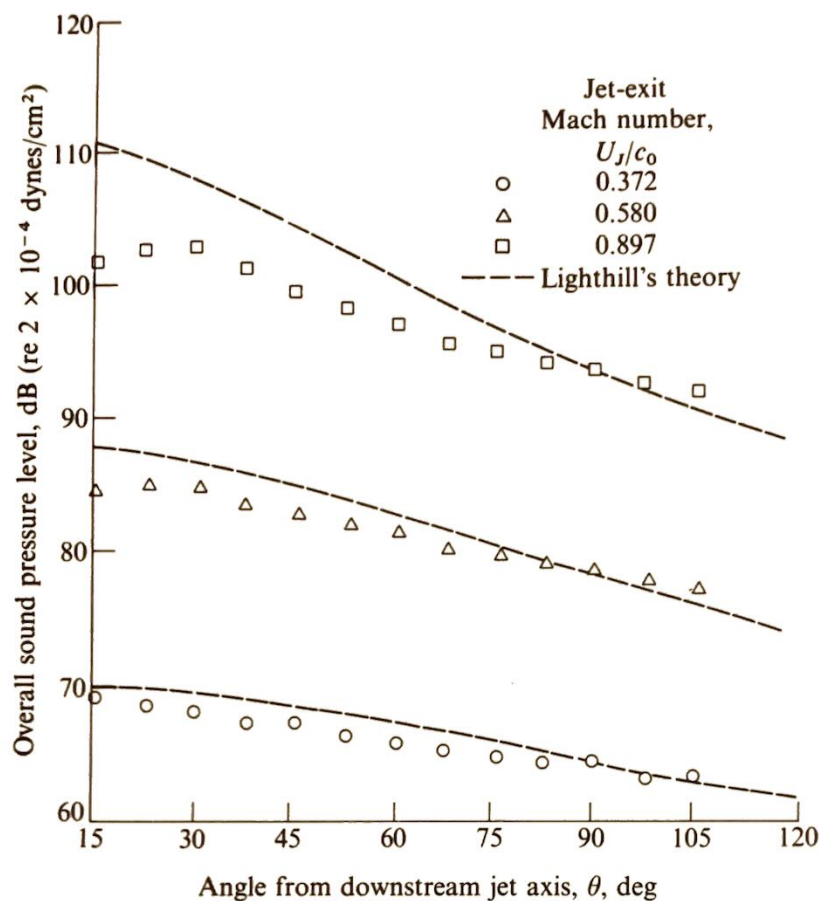


Fig. 2.15 Experimental directivity data of Reference 23. Jet nozzle diameter, D , 2.54 cm (1 in.).

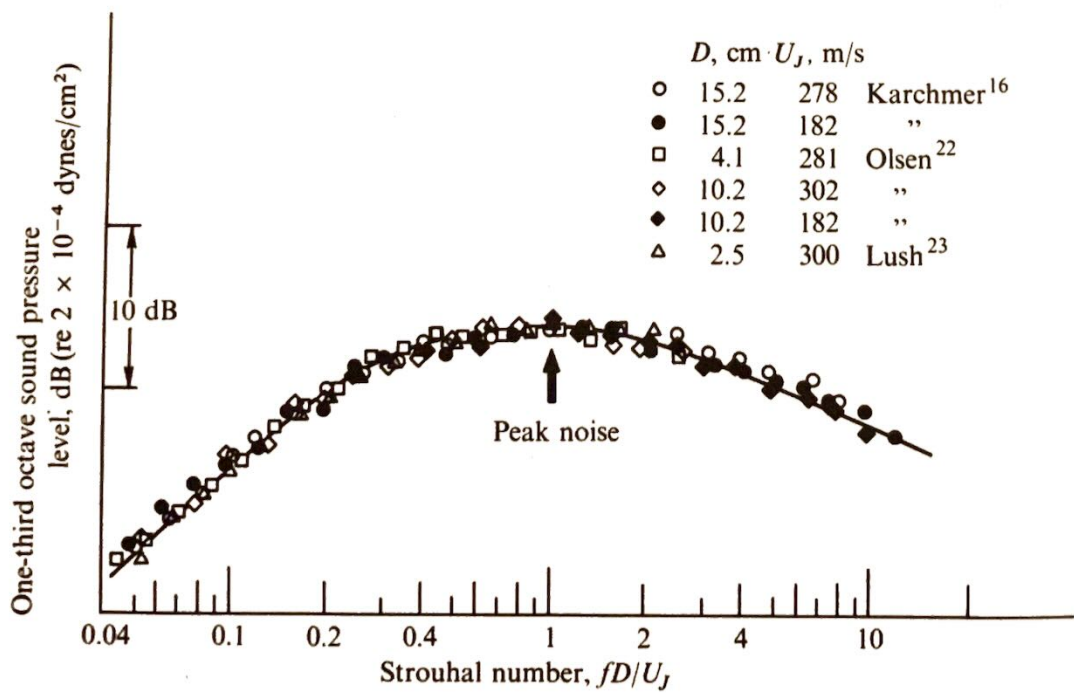


Fig. 2.16 Subsonic jet one-third-octave sound pressure level spectrum at 90° from downstream axis.²⁶

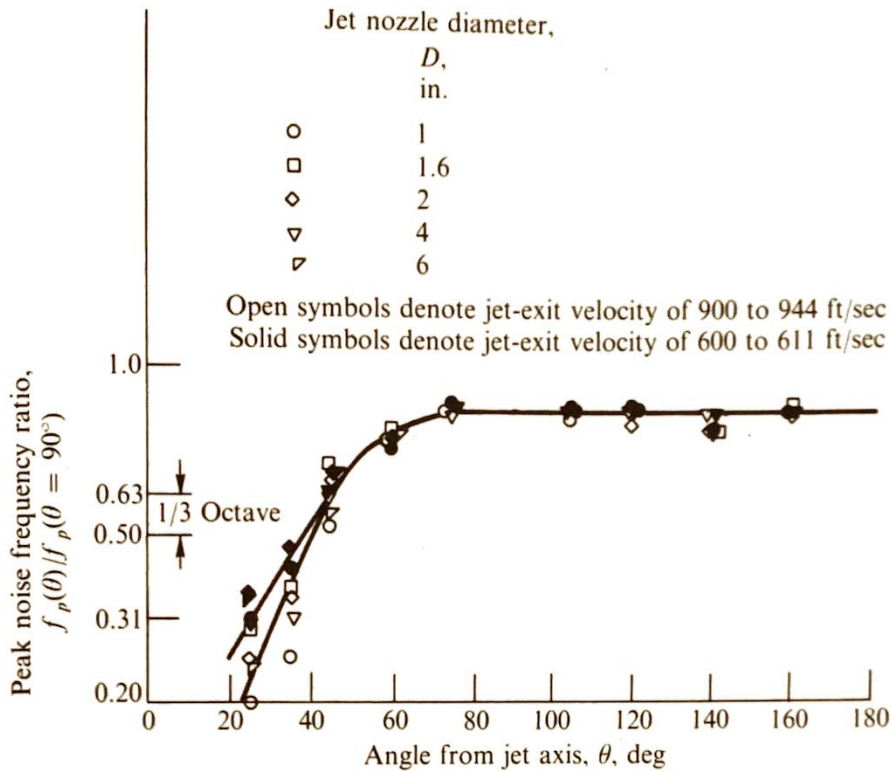


Fig. 2.17 Variation of peak noise frequency with angle. Ambient temperature, subsonic, circular nozzles; free-field, lossless data. (From Reference 26.)

neglected. Indeed, Eq. (2.38) shows that the shear noise is “beamed” downstream while the self noise is nondirectional. Consequently, if, as proposed by Ribner and MacGregor²⁷ the self noise were to be of higher frequency than the shear noise,[†] the resultant downstream beaming of low-frequency sound would tend to counteract the Doppler effect. Ribner and MacGregor further proposed that the refraction of the sound by the mean flow could also act to decrease the concentration of low-frequency sound at small angles to the jet axis. In fact, even if the shear noise term were retained, Eq. (2.38) would imply that \mathcal{J} should be a function only of the source Strouhal number at any fixed angle θ while the experimental data clearly show that this is not the case at angles near the downstream jet axis. Moreover, Eq. (2.33) shows that this discrepancy is not in any way due to the assumptions about the turbulent structure that were used to obtain Eq. (2.38). But such behavior could certainly be caused by refraction. Indeed we shall ultimately demonstrate (in Chap. 6) that much of the discrepancy between the theory and experiment can be attributed to such acoustic-mean flow interaction effects.

[†] This can be made plausible by noting that if R_{11} varied with time as $\exp[-(\omega_f \tau)^n]$ for any integer n , $R_{1111} \approx R_{11}^2$ (roughly) should vary as $\exp[-2(\omega_f \tau)^n]$ —indicating that the latter term had a higher characteristic frequency than the former.

2.5.2 Supersonic Jets

At supersonic speeds we cannot use the arguments of Sec. 2.2.3 to show that the right side of Lighthill's equation can be treated as a source term. Consequently, the acoustic analogy approach may not apply to such flows. Nevertheless, we shall suppose that it can still be used to qualitatively explain some of the observed features of supersonic jet noise.

Emission of Mach waves. The discussion in Sec. 2.5.1 is for the most part limited to subsonic flows. Indeed, the entire development of that section is based on Eq. (2.32) whose denominator vanishes at supersonic convection speeds. Consequently, $\bar{I}(\mathbf{x}) = \Gamma(\mathbf{x}, 0)$ could become infinite at the points where $1 - M_c \cos \theta$ goes to zero (i.e., at points on the Mach cone of the moving eddies). However, the inequality (2.31) will not hold at these points and Eq. (2.32) will, as a result, be invalid. On the other hand, the term

$$R_{ijkl} \left(\mathbf{y}', \xi, \tau + \frac{\mathbf{x}}{x} \cdot \frac{\xi}{c_0(1 - M_c \cos \theta)} \right)$$

in the numerator of Eq. (2.29) will also go to zero at these points (since any reasonable correlation function must certainly vanish at large times). Consequently, the integrand in Eq. (2.29) is able to remain finite at these points even when $t = 0$. This shows that the finite lifetime and the finite size of the turbulent eddies act in concert to prevent the radiation from becoming infinite in the Mach wave direction.

We have already indicated that the factor $(1 - M_c \cos \theta)^{-5}$ results from source convection effects and is related to the corresponding factors that appear in the formulas for the point quadrupole sources discussed in Sec. 1.8.5. It causes the sound intensity to increase whenever the sources move toward the observer and has a larger exponent for quadrupole sources than it does for a monopole to account for a decrease in phase cancellation between the component monopole sources that comprise the quadrupole. Thus, we have seen that this cancellation causes the quadrupole source to be very inefficient at zero velocity. However, the effect decreases as the source acquires a larger component of velocity in the direction of the observer. In fact, when $M_c \cos \theta = 1$, the source is approaching the observer at precisely the speed of sound and the sound emitted by the elements of the quadrupole further from the observer cannot overtake the sound emitted by those nearer the observer. At this condition the cancellation effect is absent and the acoustic waves behave as if they were generated by a noncompact monopole source. We therefore expect the sound field to be relatively intense in the direction

$$\theta = \cos^{-1} \frac{1}{M_c}$$

where this occurs. On the other hand, Eq. (2.30) shows that

$$\bar{I}_\omega(\mathbf{x}) \simeq \frac{\pi\omega^4\rho_0}{2c_0^5} \frac{x_i x_j x_k x_l}{x^6} \int H_{ijkl}\left(\mathbf{y}', \frac{\omega}{c_0} \frac{\mathbf{x}}{x}, 0\right) d\mathbf{y}' \quad (2.50)$$

in this direction. The wave number of the sound field is therefore the same as that of the turbulence which produced it, as it is in subsonic flow, but it is now the zero-frequency (stationary) components of the turbulence that produce the sound (see Fig. 2.5). Hence, the sound emission results from the convection of an essentially frozen pattern of turbulence by the mean flow. This behavior should be contrasted with that which occurs at low Mach numbers where the turbulent eddies behave like compact sources that radiate sound only as a consequence of their intrinsic unsteadiness. Since supersonically moving eddies behave acoustically like moving projectiles, the resulting sound emission is often called *Mach wave radiation*.

In order to obtain an expression for the sound field that remains finite in the Mach wave direction, we take the inverse Fourier transform of Eq. (2.50) to get

$$\Gamma(\mathbf{x}, t) = \frac{\rho_0}{16\pi^2 c_0} \frac{x_i x_j x_k x_l}{x^6} \int_{-\infty}^{\infty} \int \int \delta\left(t + \frac{\mathbf{x} \cdot \boldsymbol{\xi}}{xc_0}\right) \left(\frac{x_m}{x} \frac{\partial}{\partial \xi_m}\right)^4 \times R_{ijkl}(\mathbf{y}', \boldsymbol{\xi}, \tau) d\boldsymbol{\xi} d\mathbf{y}' d\tau$$

Then separating the vector $\boldsymbol{\xi}$ into its component ξ_n in the Mach wave direction \mathbf{x}/x and its component ξ_s perpendicular to this direction (as indicated in Fig. 2.18) yields

$$\Gamma(\mathbf{x}, t) = \frac{\rho_0}{16\pi^2} \frac{x_i x_j x_k x_l}{x^6} \int_{-\infty}^{\infty} \int \int \left[\frac{\partial^4}{\partial \xi_n^4} R_{ijkl}(\mathbf{y}', \xi_n + \xi_s, \tau) \right]_{\xi_n = -cot} d\xi_s d\mathbf{y}' d\tau$$

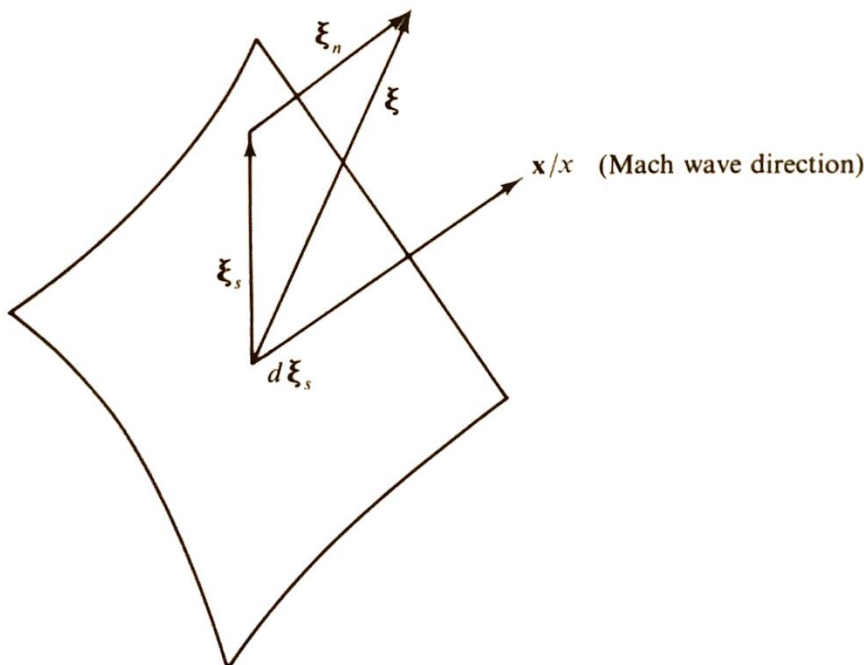


Fig. 2.18 Coordinate system for Mach wave equation.

Accordingly

$$\bar{I}(\mathbf{x}) = \Gamma(\mathbf{x}, 0) = \frac{\rho_0}{16\pi^2} \frac{x_i x_j x_k x_l}{x^6} \int \int \int \left[\frac{\partial^4}{\partial \xi_n^4} R_{ijkl}(\mathbf{y}', \xi_n + \xi_s, \tau) \right]_{\xi_n=0} d\xi_s dy' d\tau \quad (2.51)$$

This result was first obtained by Ffowcs Williams¹⁴. We might try, as we did in the subsonic case, to use experimental flow measurements to estimate the strength of its source term. But, since hot-wire measurements are unfeasible at supersonic speeds, little is known about the turbulence. Nevertheless, there is hope that this situation will be remedied by the recent development of laser-Doppler velocimeter techniques. In any event we can still attempt to determine the dominant characteristics of the sound field by performing a similarity analysis. Thus the differentiation with respect to ξ_n ought to scale with the jet diameter D , the integration with respect to time τ ought to scale with D/U_j , and R_{ijkl} ought to scale with U_j^4 . Then, dimensionally, Eq. (2.51) becomes

$$\bar{I} \sim \frac{\rho_0}{x^2} D^2 U_j^3$$

Notice that the radiated sound now varies as the jet velocity to the third power instead of the eighth. It is generally believed that this behavior actually occurs at sufficiently high supersonic Mach numbers. A typical plot of radiated power as a function of jet velocity (taken from Reference 14) is shown in Fig. 2.19.

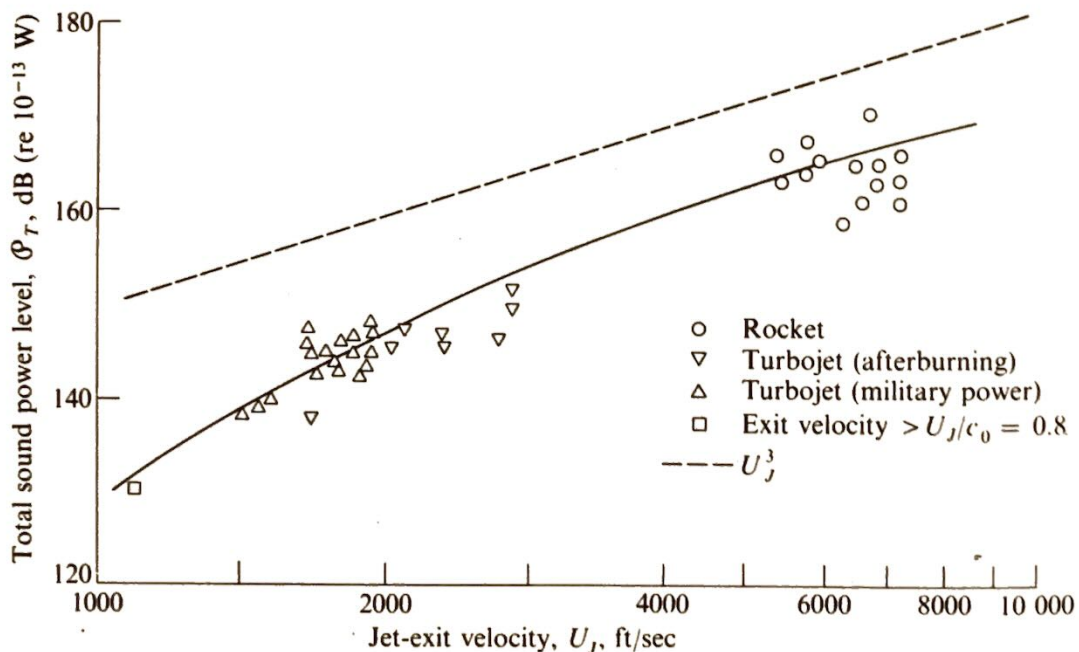
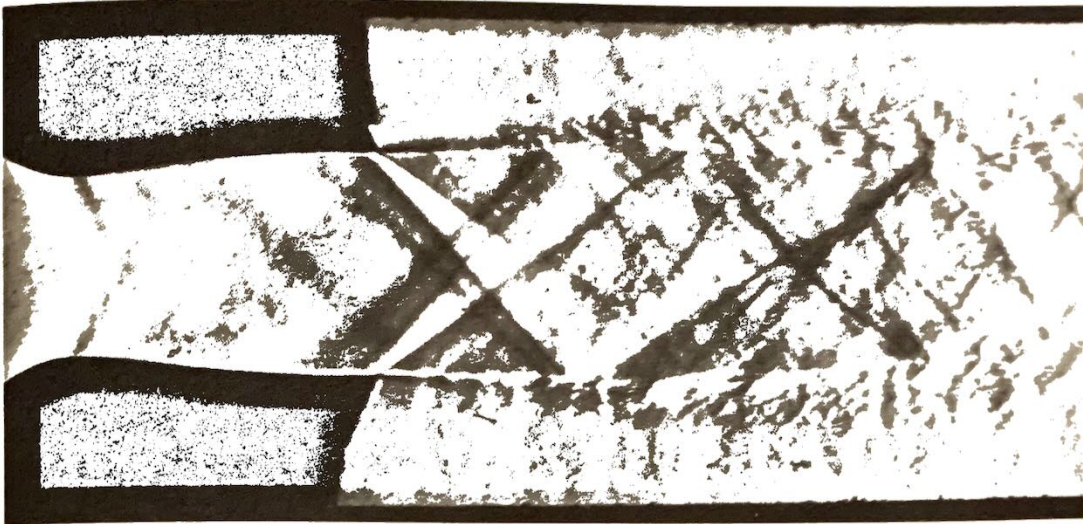


Fig. 2.19 Variation of total sound power level with jet velocity for supersonic nozzles. (From Reference 14.)



(a)



(b)

Fig. 2.20 Flow from a convergent-divergent nozzle at different back pressures. (From Reference 47.) (a) Ratio of pressure just ahead of exit to atmospheric pressure, 1.5. (b) Ratio of pressure just ahead of exit to atmospheric pressure, 0.8.

Fluid mechanics of supersonic jets. The flow characteristics of supersonic jets are different depending on whether the pressure at the nozzle exit is greater than (underexpanded), less than (overexpanded), or equal to the ambient pressure surrounding the jet (fully expanded). As shown in Fig. 2.20 the first two cases are characterized by well-defined shock bottles. Under certain operating conditions the attendant shock structure will become relatively unstable and can be easily displaced by even slight variations in pressure and velocity at the nozzle exit. The general characteristics of a fully expanded supersonic jet are illustrated in Fig. 2.21. Unlike its subsonic counterpart, the length of its potential core can change with Mach number. A number of investigators have measured this length as well as that of the supersonic mixing region. The data of Nagamatsu and Sheer²⁸ together with those of other investigators (which they collected) is shown in Fig. 2.22.

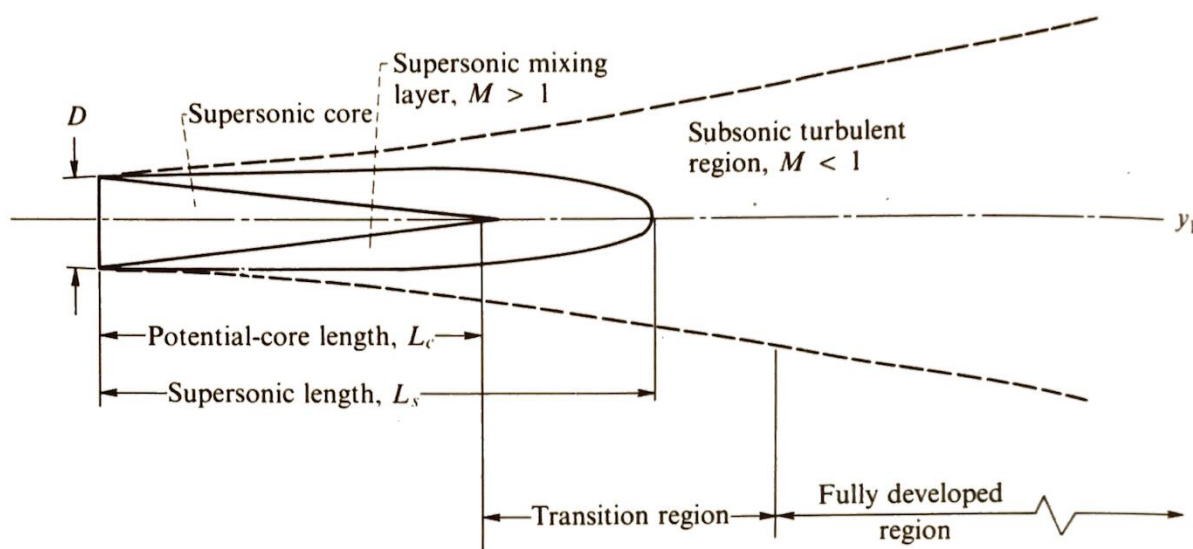


Fig. 2.21 Parallel-flow supersonic jet expanded to ambient pressure.

Location of acoustic sources. One of the most important acoustic properties of a jet is the distribution of its sound sources. There are numerous techniques that can be used to determine the location of these sources. They include the use of acoustic mirrors, operating the jet through a small hole in a large sound-absorbing screen^{29,30}, extrapolating back from the directional maxima in the sound field^{31,32}, and measuring near-field pressures along the jet boundary.³³ There are a number of objections to using each of these methods,^{14,29} and a great deal of caution should be observed in interpreting the results. Indeed, as shown in Sec. 1.5.1 it is not even possible to determine completely the nature of an acoustic source by working backward from measurements of its sound field. Nevertheless, the general indication is that the maximum noise-producing region occurs just downstream of the sonic line. The measurements of Bishop, Ffowcs Williams, and Smith,²⁹ which indicate that the principal sound sources occur well upstream of this line, are an important exception.

Experimental evidence for existence of Mach waves. A large number of optical measurements have been made to investigate the eddy Mach wave radiation emitted by jets. For example, Lowson and Ollerhead³⁴ and Dosanjh and Yu³⁵ have taken shadowgraphs, and Eggers³⁶ and Jones³⁷ have taken Schlieren photographs. It is possible to distinguish two distinct types of waves possessing characteristics of Mach waves. One of these occurs within the first few diameters of the nozzle exit and can be detected from shadowgraphs, the other, which is not prominent in the shadowgraphs but can be seen in the Schlieren photographs, has been observed to extend further downstream to perhaps 8 to 10 diameters—depending on the Mach number.

Since Mach waves must always originate in the supersonic region and since there is some experimental indication that the dominant sound is

generated downstream in this region, Mach wave radiation may not be an important source of supersonic jet noise. Moreover, as indicated by Tam³⁸, the frequencies of these waves may even be too high to contribute significantly to the dominant part of the observed acoustic spectrum.

Large-scale structure models of jet noise. A Mach wave model has been proposed by Bishop, Ffowcs Williams, and Smith²⁹ to explain certain types of supersonic jet noise. Their experiments indicate that the dominant noise sources are extremely large eddies which are coherent on a scale much larger than the width of the shear layer and are clustered around the potential core of the jet. They propose that these eddies have a relatively ordered structure and arise from an instability of the primary flow. A mechanism for calculating the relevant flow structure (analogous to the one used for laminar instability calculations) is suggested by the authors.

Tam³⁸ has also proposed a model (for a nearly fully expanded supersonic jet) in which the sound generation is related to the large-scale flow structure. In Tam's model, however, it is large-scale spiral-mode instabilities involving the entire jet that are responsible for producing the

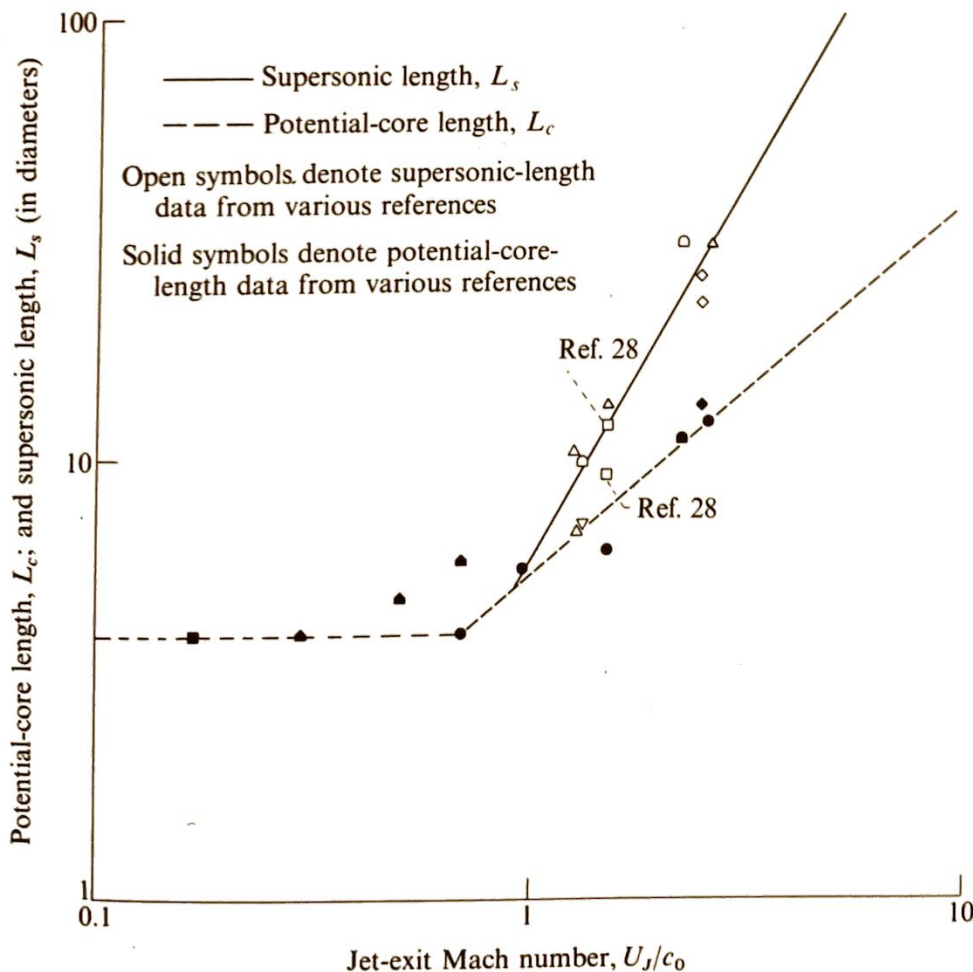


Fig. 2.22 Jet potential-core length and supersonic length as function of jet-exit Mach number. (From Reference 28.)

noise. These instabilities (it is proposed) arise as a result of a periodic resonant excitation by the shock waves of disturbances originating in the nozzle. They generate sound both by stimulating unsteady entrainment and by causing the jet to vibrate physically.

Noise generated by shock waves. In addition to the noise-generation mechanisms discussed in the last section, mechanisms involving shock-turbulence interactions and a feedback mechanism involving the shock wave structure have been proposed as important sources of supersonic jet noise. Thus, when turbulence passes through a shock wave, it causes a localized deformation of the shock, that results in the emission of a broadband but still rather strongly peaked sound field—usually called “*shock associated noise*.” Analyses of the sound produced by turbulence passing through individual shock waves have been carried out by Lighthill,³⁹ Ribner,⁴⁰ and Kerrebrock.⁴¹ This process is generally regarded as the dominant noise source in supersonic wind tunnels. However, the turbulent eddies in a jet are, as a result of their finite lifetime, able to pass through several shock waves before losing their identity. Hence the acoustic radiation may, to some extent, be controlled by interference effects between the sound fields produced at the individual waves comprising the shock system.⁴⁹

The feedback mechanism was proposed by Powell⁴² to explain the discrete tones in the spectrum of choked cold-model jets that are called “*jet screech*.” Powell’s explanation involves (like the large scale structure models discussed above) an amplification of downstream travelling disturbances. However, in Powell’s model the motion of the shock wave emits a sound wave that propagates upstream through the subsonic ambient fluid to the nozzle lip. The ensuing change in pressure that occurs at this point will, under certain conditions, initiate a new downstream propagating disturbance that continues the cycle. The process maintains itself mainly because all energy lost to radiation and viscous effects is resupplied to the propagating disturbance by an instability of the flow.

Figure 2.23 (based on measurements taken by Stone and Gutierrez⁴³) shows the acoustic spectra at 80° from the axis of a jet issuing from a convergent nozzle. Results are presented for several Mach numbers. Since the angle is close to 90° , they should be more or less uninfluenced by mean flow interaction effects. The solid curves have the same shapes and are simply translations of one another. The Strouhal number is constant along the dashed line drawn through their peaks. The figure shows that the low-frequency part of the spectrum is pretty much the same at supersonic speeds as it is at subsonic speeds. However, the supersonic spectra exhibit spikes, which can probably be attributed to the feedback tones, and additional high-frequency sound (shaded area), which is probably shock-associated noise. Indeed, Fig. 2.24 (based on the measurements of Tanna and Dean,⁴⁴) shows that the 90° spectra for correctly expanded (shock free) jets have the same shape at supersonic speeds as they do at subsonic speeds. Moreover, these

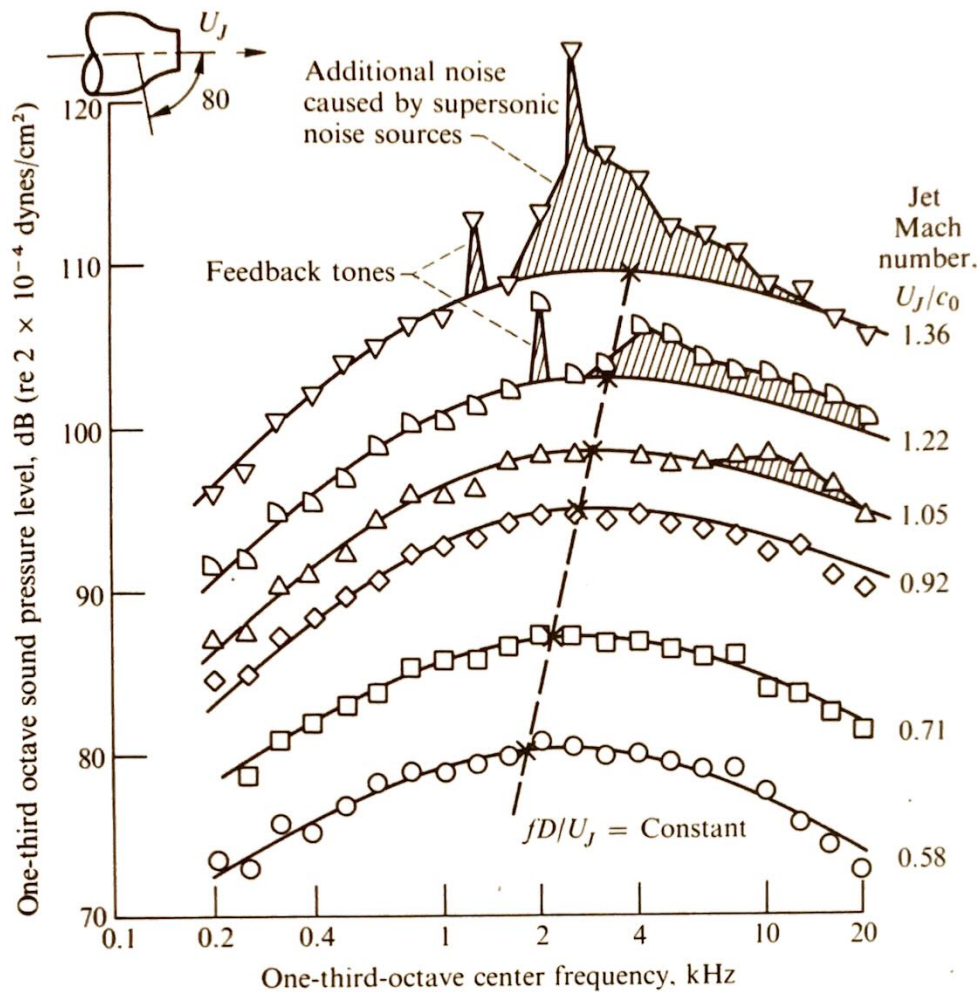


Fig. 2.23 Jet noise spectra for a convergent nozzle at subsonic and supersonic velocities; angle from downstream jet axis, 80° . Based on data presented in Reference 43, courtesy W. Olsen. (Although these data were reported as available in Reference 43, they were not actually presented.)

results show no indication of the additional noise sources that are so apparent in Fig. 2.23. The peak frequencies again scale with the Strouhal number.

Tanna and Dean's measurements also reveal that the overall sound pressure level at 90° from the jet axis varies as the velocity to the eighth power at all Mach numbers—while the corresponding quantity for the data shown in Fig. 2.23 follows a tenth power law at the highest velocities.

2.5.3 Low-Velocity Jets: Orderly Structure

At very low Reynolds numbers the flow in a jet is laminar and produces no sound. However, the jet becomes unstable to small disturbances when the Reynolds number is increased and an unsteady periodic flow is set up.

Plane jets: edge tones. First, consider a jet issuing with a velocity U_J from a long slit of width h into an unbounded quiescent fluid. When the

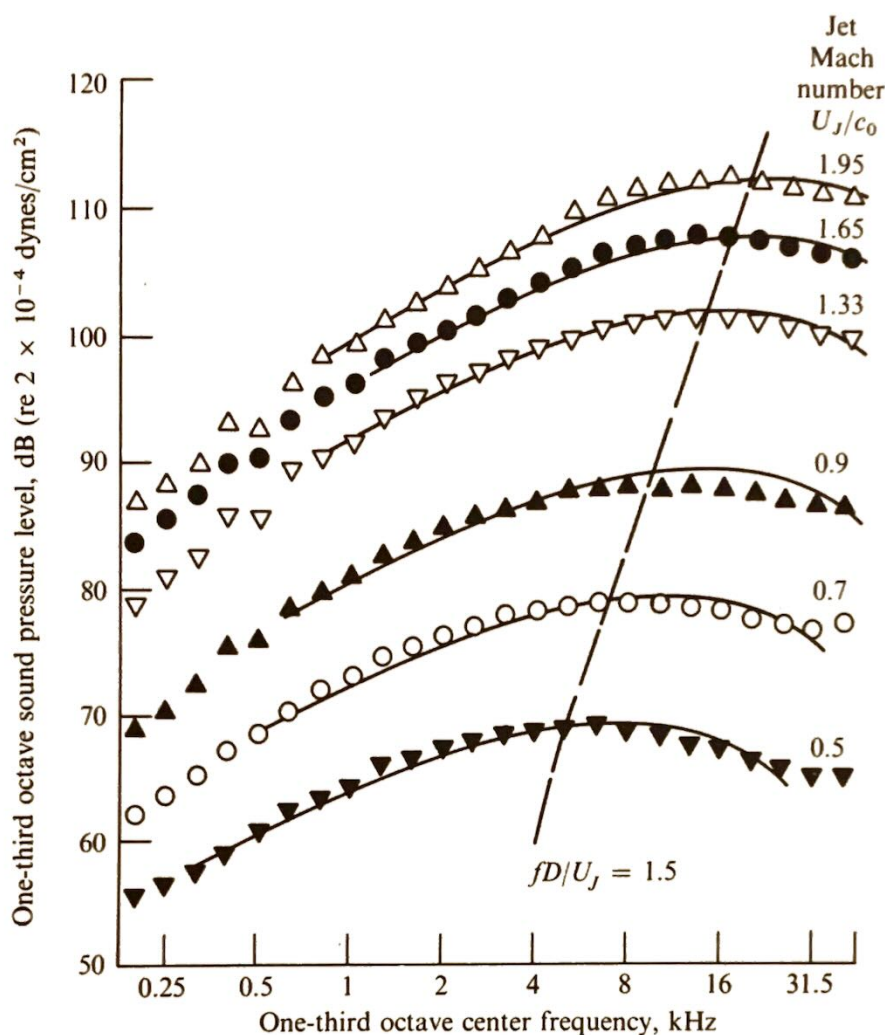


Fig. 2.24 Jet noise spectra for a correctly expanded (shock free) jet from a convergent-divergent nozzle; angle from downstream jet axis, 90°. (From Reference 44.)

Reynolds number $\rho_0 U_j h / \mu$ is greater than about 100, the flow becomes unstable to disturbances in a certain range of frequencies and begins to oscillate, taking on a sinuous appearance. This unsteadiness gives rise to a hissing noise which has a peak frequency near $f = 0.055 U_j / h$.

This sound can be converted into a distinct tone of a much greater intensity, called an “edge tone,” by placing a wedge some distance downstream from the slit, as shown in Fig. 2.25. These tones, which are involved in the sound production by flutes and organ pipes, have been thoroughly investigated both theoretically and experimentally. The experiments indicate that the jet oscillations are associated with discrete vortex centers shed alternately from the top and bottom of the wedge vertex, as shown in Fig. 2.26.

It is generally agreed that the tones can be attributed to a feedback mechanism that is very similar to the one that produces jet screech. (See page 104.) However, in this instance the emission of the acoustic wave is the result of a downstream propagating disturbance impinging on the wedge. As in the case of jet screech, the impingement of the acoustic

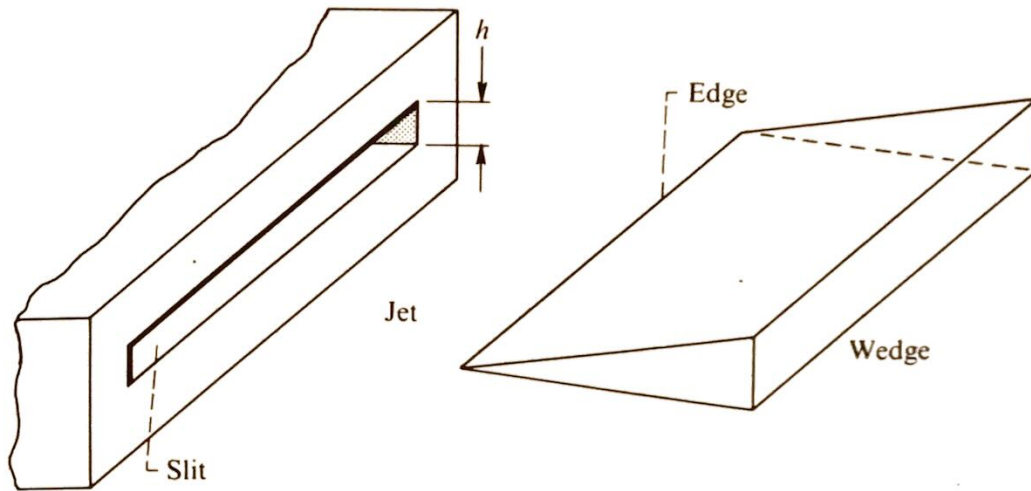


Fig. 2.25 Experimental arrangement for edge-tone production.

wave on the nozzle lip initiates a new disturbance which continues the cycle. Moreover, the process again maintains itself because an instability in the flow is able to supply energy to the propagating disturbance.

For any given jet velocity there is a minimum distance from wedge to slit below which no tone occurs. Beyond this distance the frequency of the tone increases with increasing velocity and decreases with increasing distance until a condition is reached where there is a marked irregularity in the flow. At this point there is a sudden jump in the frequency of the tone. Further increases in distance or velocity result in a continuous change in frequency until a second jump occurs and so on. When the process is reversed, the jumps in frequency will again occur—but at somewhat different values of the velocity and distance.

Circular jets: bird tones. When a round jet issuing from a round hole of diameter D becomes unstable, the vortex sheath at the edge of the orifice rolls up into a vortex ring (which is swept downstream), and the jet takes on the appearance shown in Fig. 2.27. This behavior occurs for Reynolds numbers in the range $160 < \rho_0 U_J D / \mu < 1200$. A more pronounced periodic behavior can be obtained by allowing the circular orifice to discharge into a pipe. This periodicity can produce pure tones. However, in order to produce a sharp tone which is insensitive to small changes in orifice shape, it is necessary to blow through two (suitably shaped and spaced) orifice plates. The sound produced by this arrangement is called a “bird tone.” It occurs in some brass instruments and when a human whistles.

The behavior of the flow from a circular nozzle is similar to that from an orifice with the jet instability evolving from a sinusoid to a helix and finally into a train of vortices. When the Reynolds number is increased beyond about 1200, the flow in the jet becomes turbulent and the periodic structure gradually disappears. The jet then behaves in the manner described on page 88. However, there has been some conjecture^{45,46} that the low-velocity periodic structure persists (even at these high Reynolds numbers)

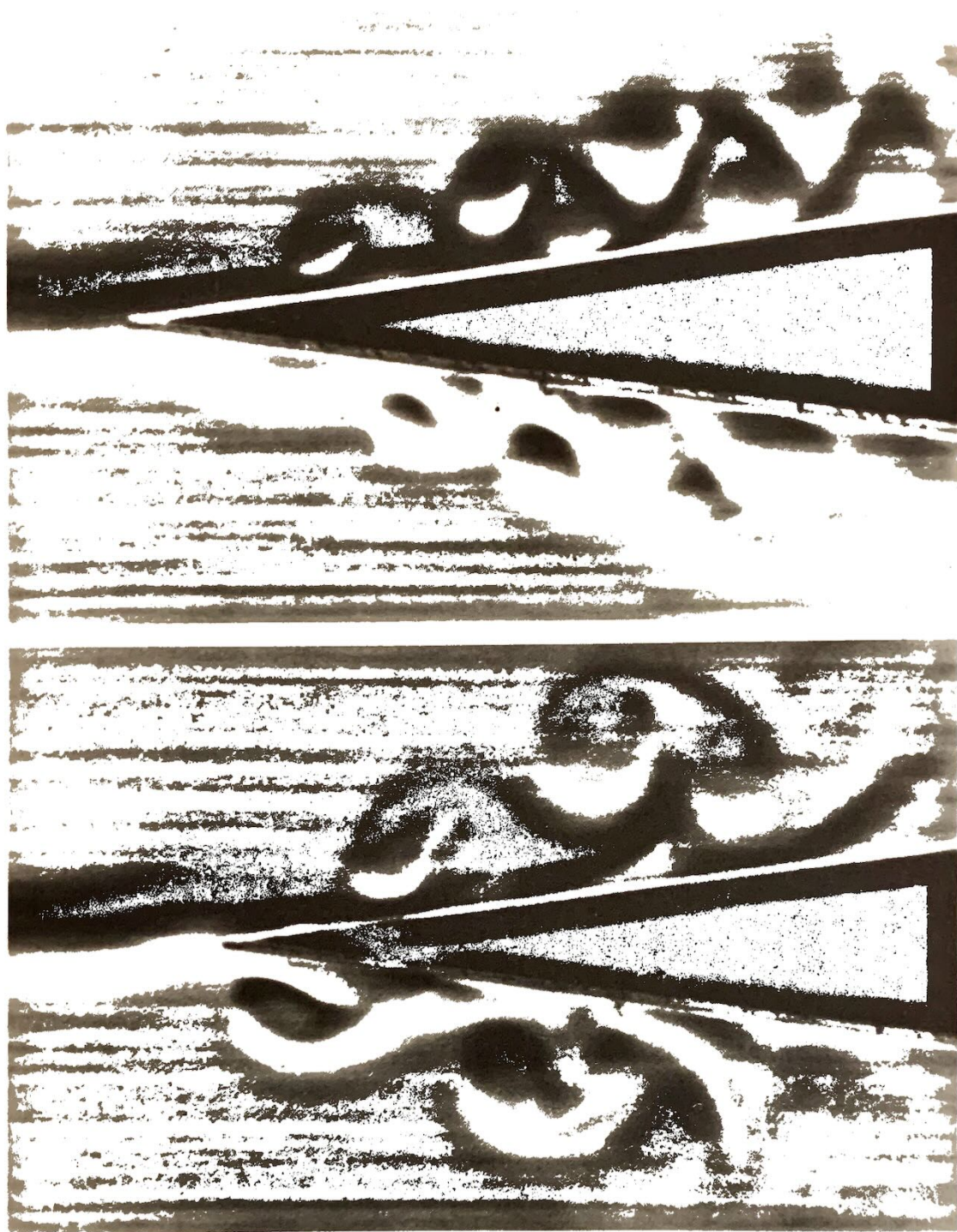


Fig. 2.26 Vortex structure in edge-tone configuration. (From Reference 48, courtesy Isaac Grebur.)

in the form of a large-scale orderly structure of the turbulence and that it may have a direct bearing on the production of noise from high-speed jets. Thus the pressure fluctuations measured outside a turbulent jet by Mollo-Christensen⁴⁶ appear to be composed of well defined, more or less identical, wave packets—with the only really random element being the relative positions of the packets.

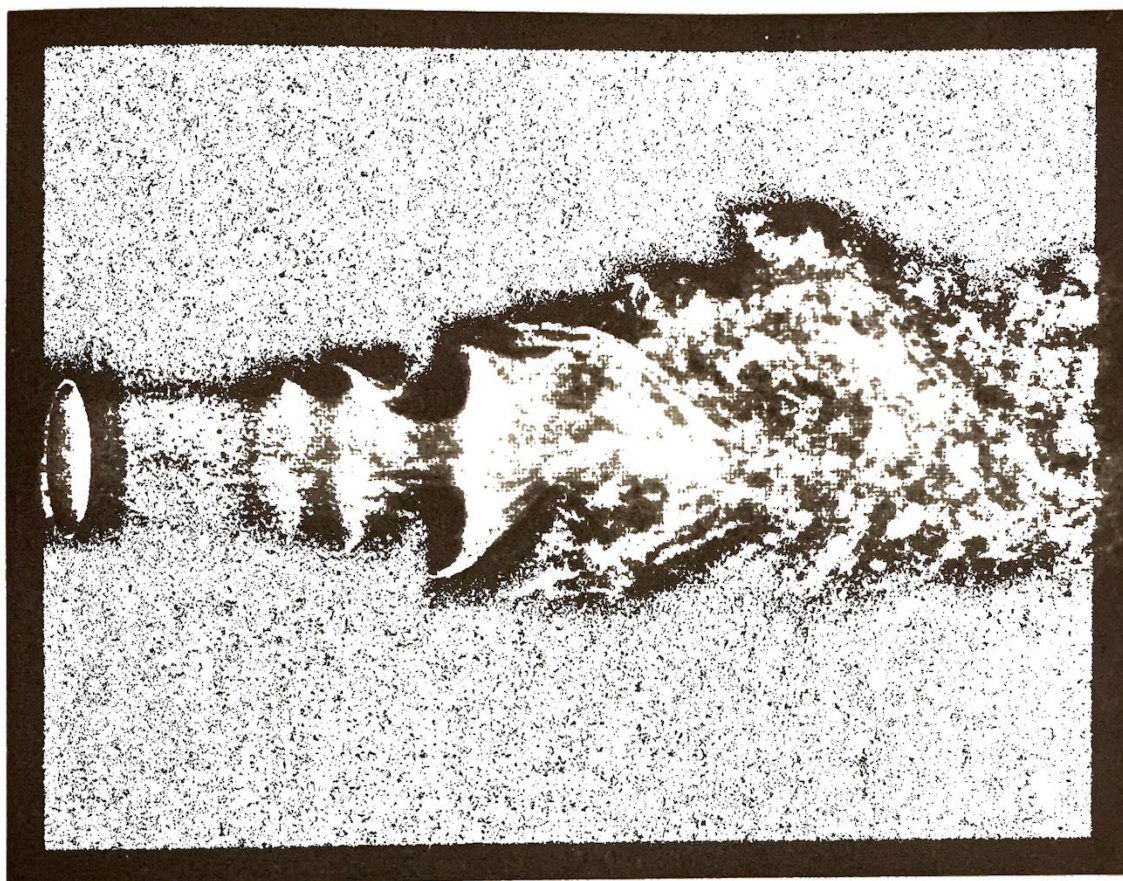


Fig. 2.27 Rollup of low-Reynolds-number jet. (From Reference 45, courtesy of Cambridge University Press.)

Sensitive jets. When a jet is on the verge of becoming turbulent, it is very sensitive to musical notes. Rayleigh⁸ attributed this behavior to the excitation of instability waves on the vortex sheath surrounding the jet column by sound waves at the exit plane of the nozzle. The “sensitive jet” phenomenon has received a great deal of study since it was first observed in 1850 in the form of a gas flame dancing in response to a violoncello. In more recent times it has been found that even turbulent jets can be unstable to certain types of disturbances. Indeed Crow and Champagne⁴⁵ have shown that a plane wave incident on a nozzle (from within the tailpipe) can produce axisymmetric dispersive waves which are amplified by the mean flow as they propagate downstream.

2.6 CONCLUDING REMARKS

We have seen that, while Lighthill’s theory is able to explain a number of the most prominent characteristics of the acoustic radiation from jets, there are other less prominent features that it is not able to account for (page 97). It will be shown in Chap. 6 that this discrepancy results from treating the

sound sources as if they are moving through a stationary medium while in reality they are embedded in flow field relative to which they are nearly stationary.

There are a number of noise sources, in addition to those discussed in this chapter, that contribute to the sound field emanating from the exhaust of real jet engines. Aside from the fan noise, which will be discussed in Chap. 4, these include combustion noise, which is generally of low frequency and relatively nondirectional and the noise generated by internal engine components, which exhibits a pronounced peak somewhere around 60° from the downstream jet axis. The latter is for the most part associated with the turbine and struts and splitters within the exhaust system. There is also the possibility that instabilities in the mean jet flow can act to amplify the sound fields produced by these internal noise sources. Finally, it should be pointed out that forward flight effects can significantly alter the characteristics of the acoustic radiation from jet engines in a way that has not as yet been adequately explained by theory.

The next two chapters show how Lighthill's analogy can be used to study many other types of aerodynamic and sound generation processes.

APPENDIX—TRANSFORMATION OF SOURCE CORRELATION FUNCTION

Since the flow is assumed to be time stationary the integrand in Eq. (2.13) can be written as

$$A \equiv \lim_{T \rightarrow \infty} \frac{1}{2T} \int_{-T}^T \frac{\partial^2 T'_{ij}}{\partial t^2} \frac{\partial^2 T''_{kl}}{\partial t^2} dt$$

where we have written T'_{ij} in place of $T_{ij}(\mathbf{y}', t')$ and T''_{kl} in place of $T_{kl}(\mathbf{y}'', t'')$. Then it follows from Eq. (2.14) that

$$A = \lim_{T \rightarrow \infty} \frac{1}{2T} \int_{-T}^T \frac{\partial^2 T'_{ij}}{\partial t^2} \frac{\partial^2 T''_{kl}}{\partial \tau^2} d\tau = \lim_{T \rightarrow \infty} \frac{1}{2T} \frac{\partial^2}{\partial \tau^2} \int_{-T}^T \frac{\partial^2 T'_{ij}}{\partial t^2} T''_{kl} dt$$

But since all stationary functions must remain bounded even at large times, integrating by parts yields

$$\begin{aligned} A &= \lim_{T \rightarrow \infty} \frac{1}{2T} \frac{\partial^2}{\partial \tau^2} \left(\frac{\partial T'_{ij}}{\partial t} T''_{kl} \Big|_{-T}^T - \int_{-T}^T \frac{\partial T'_{ij}}{\partial t} \frac{\partial T''_{kl}}{\partial t} dt \right) \\ &= - \lim_{T \rightarrow \infty} \frac{1}{2T} \frac{\partial^2}{\partial \tau^2} \int_{-T}^T \frac{\partial T'_{ij}}{\partial t} \frac{\partial T''_{kl}}{\partial t} dt \end{aligned}$$

Then using the second Eq. (2.14) again, yields

$$A = - \lim_{T \rightarrow \infty} \frac{1}{2T} \frac{\partial^3}{\partial \tau^3} \int_{-T}^T \frac{\partial T'_{ij}}{\partial t} T''_{kl} dt$$

Finally, upon integrating by parts a second time, we find that

$$\begin{aligned}
 A &= \lim_{T \rightarrow \infty} \frac{1}{2T} \frac{\partial^4}{\partial \tau^4} \int_{-T}^T T'_{ij} T''_{kl} dt \\
 &= \frac{\partial^4}{\partial \tau^4} \overline{T'_{ij}(\mathbf{y}', t') T_{kl}(\mathbf{y}'', t'')}
 \end{aligned}$$

REFERENCES

1. Gutin, L., "On the Sound Field of a Rotating Propeller," NACA TM 1195, 1948.
2. Lighthill, M. J., "On Sound Generated Aerodynamically. I. General Theory," *Proc. Roy. Soc. (London)*, **211A**, 1107, 564-587, 1952.
3. Lighthill, M. J., "On Sound Generated Aerodynamically. II. Turbulence as a Source of Sound," *Proc. Roy. Soc. (London)*, **222A**, 1148, 1-32, 1954.
4. Curle, N., "The Influence of Solid Boundaries on Aerodynamic Sound," *Proc. Roy. Soc. (London)*, **231A**, 1187, 505-514, 1955.
5. Powell, Alan, "Aerodynamic Noise and the Plane Boundary," *J. Acoust. Soc. Am.*, **32**, 8, 982-990, 1960.
6. Ffowcs Williams, J. E. and L. H. Hall, "Aerodynamic Sound Generation by Turbulent Flow in the Vicinity of a Scattering Half Plane," *J. Fluid Mech.*, **40**, pt 4, 657-670, 1970.
7. Phillips, O. M., "On the Sound Generated by Turbulent Shear Layers," *J. Fluid Mech.*, **9**, pt, 1, 1-28, 1960.
8. Rayleigh, John W., *The Theory of Sound*, Dover Publications, 1945.
9. Crow, S. C., "Aerodynamic Sound Emission as a Singular Perturbation Problem," *Stud. Appl. Math.*, **49**, 1, 21-44, 1970.
10. Ribner, H. S., "The Generation of Sound by Turbulent Jets," in *Advances in Applied Mechanics*, **8**, 104-182, Academic Press, 1964.
11. Ribner, H. S., "Quadrupole Correlations Governing the Pattern of Jet Noise," *J. Fluid Mech.*, **38**, pt. 1, 1-24, 1969.
12. Goldstein, M. and B. Rosenbaum, "Effect of Anisotropic Turbulence on Aerodynamic Noise," *J. Acoust. Soc. Am.*, **54**, 3, 630-645, 1973.
13. Davies, P. O. A. L., M. J. Fisher and M. J. Barratt, "The Characteristics of the Turbulence in the Mixing Region on a Round Jet," *J. Fluid Mech.*, **15**, pt. 3, 337-367, 1963.
14. Ffowcs Williams, J. E., "The Noise from Turbulence Convected at High Speed," *Phil. Trans. Roy. Soc.*, **A225**, 469-503, 1963.
15. Lilley, G. M., "On the Noise from Air Jets," ARC-20, 376; N. 40; FM-2724, British Aeronautical Research Council, September 1958.
16. Karchmer, A., R. Dorsch and R. Friedman, "Acoustic Tests of 15.2 Centimeters Diameter Potential Flow Nozzle," TM X-2980, NASA, 1974.
17. Laurence, James C., "Intensity, Scale, and Spectra of Turbulence in Mixing Region of Free Subsonic Jet," NACA TR 1292, 1956.
18. Bradshaw, P., D. H. Ferriss and R. F. Johnson, "Turbulence in the Noise-Producing Region of a Circular Jet," *J. Fluid Mech.*, **19**, pt. 4, 591-624, 1964.
19. Wills, J. A. B., "On Convection Velocities in Turbulent Shear Flows," *J. Fluid Mech.*, **20**, pt. 3, 417-432, 1964.
20. Fisher, M. J. and P. O. A. L. Davies, "Correlation Measurements in a Non-frozen Pattern of Turbulence," *J. Fluid Mech.*, **18**, pt. 1, 97-116, 1964.
21. Chu, Wing T., "Turbulence Measurements Relevant to Jet Noise," UTIAS-119, University of Toronto (AD-645322), 1966.
22. Olsen, W. A., O. A. Gutierrez and R. G. Dorsch, "The Effect of Nozzle Inlet Shape, Lip Thickness, and Exit Shape and Size on Subsonic Jet Noise," TM X-68182, NASA, 1973.
23. Lush, P. A., "Measurements of Subsonic Jet Noise and Comparison with Theory," *J. Fluid Mech.*, **46**, pt. 3, 477-500, 1971.
24. Powell, Alan, "A Survey of Experiments on Jet Noise," *Aircraft Engineering*, **26**, 2-9, 1954.

25. Ribner, H. S., "New Theory of Jet Noise Generation Directionality, and Spectra," *J. Acoust. Soc. Am.*, **31**, 245-246, 1959.
26. Olsen, W. and R. Friedman, "Jet Noise from Coaxial Nozzles Over a Wide Range of Geometric and Flow Parameters," AIAA paper No. 74-43, January 1974.
27. Ribner, H. S. and G. R. MacGregor, "The Elusive Doppler Shift in Jet Noise," Presented at the 6th International Congress on Acoustics, Tokyo, Japan, August 21-28, 1968.
28. Nagamatsu, H. T. and R. E. Sheer, Jr., "Supersonic Jet Noise Theory and Experiments in Basic Aerodynamic Noise Research," *Basic Aerodynamic Noise Research*, NASA SP-207, 17-51, 1969.
29. Bishop, K. A., J. E. Ffowcs Williams and W. Smith, "On the Noise Sources of the Unsuppressed High-Speed Jet," *J. Fluid Mech.*, **50**, pt. 1, 21-32, 1971.
30. Potter, R. C., "An Investigation to Locate the Acoustics Sources in a High Speed Jet Exhaust Stream," WR-68-4, Wyle Labs., (NASA CR-101105), 1968.
31. Yu, James C. and Darshan S. Dosanjh, "Noise Field of a Supersonic Mach 1.5 Cold Model Jet," *J. Acoust. Soc. Am.*, **51**, 5, (pt. 1), 1400-1410, 1972.
32. Mull, Harold R. and John C. Erickson, Jr., "Survey of the Acoustic Near Field of Three Nozzles at a Pressure Ratio of 30," NACA TN 3978, 1957.
33. Nagamatsu, H. T., R. E. Sheer, Jr. and M. S. Gill, "Flow and Acoustic Characteristics of Subsonic and Supersonic Jets from Convergent Nozzle," Research and Development Center, General Electric Co., (NASA CR-108850), 1969.
34. Lowson, M. V. and J. B. Ollerhead, "Visualization of Noise from Cold Supersonic Jets," *J. Acoust. Soc. Am.*, **44**, 2, 624-630, 1968.
35. Dosanjh, Darshan S. and James C. Yu, "Noise from Underexpanded Axisymmetric Jet Flow Using Radial Jet Flow Impingement," *Aerodynamic Noise; Proceedings of the Symposium*, University of Toronto, Toronto, Canada, May 20 and 21, 1968.
36. Eggers, J. M., "Velocity Profile and Eddy Viscosity Distributions Downstream of a Mach 2.2 Nozzle Exhausting to Quiescent Air," TN D-3601, NASA, 1966.
37. Jones, Ian S. F., "Finite Amplitude Waves from a Supersonic Jet," Paper 71-151, AIAA, January 1971.
38. Tam, Christopher K. W., "On the Noise of a Nearly Ideally Expanded Supersonic Jet," *J. Fluid Mech.*, **51**, pt. 1, 69-96, 1972.
39. Lighthill, M. J., "On the Energy Scattered from the Interaction of Turbulence with Sound or Shock Waves," *Proc. Cambridge Phil. Soc.*, **49**, 531-551, 1953.
40. Ribner, H. S., "Acoustic Energy Flux from Shock-Turbulence Interaction," *J. Fluid Mech.*, **35**, pt. 2, 299-310, 1969.
41. Kerrebrock, Jack Leo, *The Interaction of Flow Discontinuities with Small Disturbances in a Compressible Fluid*. Ph.D. thesis, Calif. Inst. Tech., 1956.
42. Powell, Alan, "The Noise of Choked Jets," *J. Acoust. Soc. Am.*, **25**, 3, 385-389, 1953.
43. Stone, J. and O. Gutierrez, "Noise Tests of a High-Aspect-Ratio Slot Nozzle with Various V-Gutter Target Thrust Reversers," TM X-71470, NASA, 1973.
44. Tanna, and Dean: An Experimental Study of Shock-Free Supersonic Jet Noise," AIAA paper No. 75-480, 1975.
45. Crow, S. C. and F. H. Champagne, "Orderly Structure in Jet Turbulence," *J. Fluid Mech.*, **48**, pt. 3, 547-592, 1971.
46. Mollo-Christensen, Erik, "Jet Noise and Shear Flow Instability Seen from an Experimenter's Viewpoint," *J. Appl. Mech.*, **34**, 1-7, 1967.
47. Howarth, Leslie, ed., *Modern Developments, Fluid Dynamics: High Speed Flow*. Vol. 1, Clarendon Press, Oxford, 1953.
48. McCartney, M. S. and Isaac Greber, *An Experimental and Theoretical Investigation of the Edgetone Phenomenon*, FTAS TR 73-87, Department of Fluid, Thermal and Aerospace Sciences, Case Western Reserve University, June 1973.
49. Harper-Bourne, M. and M. J. Fisher, "The Noise from Shock Waves in Supersonic Jets," *Proc. AGARD Conf. on Noise Mechanisms* (Brussels, Belgium), September 1973.

3

EFFECT OF SOLID BOUNDARIES

3.1 INTRODUCTION

In Chap. 2, we showed how Lighthill's equation could be used to study the sound generated by unsteady flows in which there are no solid boundaries (or more correctly, by flows where the effect of such boundaries can be neglected). On the other hand, there are many cases of technological interest where solid boundaries play a direct role in the sound generation process. In fact, they are often responsible for producing large increases in the radiated sound. Thus, solid surface interactions are directly involved in the generation of sound by helicopter rotors, by airplane propellers, and by aircraft engine fans, compressors, and turbines. They also have a significant effect on the noise generated by externally blown flap STOL aircraft, as well as by high-performance aircraft aboard aircraft carriers.

We know from classical acoustics that solid boundaries will always reflect and diffract the sound generated by the volume quadrupole sources that appear in Lighthill's theory. More importantly, however, they are able, under certain conditions, to support surface distributions of dipole or even

monopole noise sources, which arise from the forces and motions imparted to the surface by the unsteady flow.

In this chapter Lighthill's acoustic analogy is extended to include the effects of solid boundaries.

3.2 DERIVATION OF FUNDAMENTAL EQUATION

We shall suppose that the effects of initial transients can be neglected, so that the integral formula (1.65) can be used to obtain a solution to Lighthill's Eq. (2.5) in any region $v(\tau)$ bounded, wholly or partially, by a surface $S(\tau)$. But since his result is, in effect, a stationary-medium wave equation, it is appropriate to put $U = 0$ and, as a consequence, to require that the functions p and G satisfy the stationary-medium wave Eqs. (1.69) and (1.70), respectively. Indeed, comparing Eqs. (1.69) and (2.5), we find (upon identifying $c_0^2 \rho'$ with p) that

$$\begin{aligned} \rho' = & \frac{1}{c_0^2} \int_{-T}^T \int_{v(\tau)} G \frac{\partial^2 T_{ij}}{\partial y_i \partial y_j} dy d\tau \\ & + \int_{-T}^T \int_{S(\tau)} \left[G \left(\frac{\partial}{\partial n} + \frac{V_n}{c_0^2} \frac{\partial}{\partial \tau} \right) \rho' - \rho' \left(\frac{\partial}{\partial n} + \frac{V_n}{c_0^2} \frac{\partial}{\partial \tau} \right) G \right] dS(y) d\tau \end{aligned} \quad (3.1)$$

where

$$\rho' \equiv \rho - \rho_0$$

denotes the fluctuating density, V_n is (since $U = 0$) the normal component of the surface velocity \mathbf{V}_s , and

$$G \equiv G(\mathbf{y}, \tau | \mathbf{x}, t) \quad (3.2)$$

denotes any solution of the inhomogeneous wave Eq. (1.70) that satisfies the causality condition (1.63) and vanishes at infinity (if v is an exterior region).

It is easy to show by using the identity

$$\frac{\partial}{\partial y_i} G \frac{\partial T_{ij}}{\partial y_j} - \frac{\partial}{\partial y_j} T_{ij} \frac{\partial G}{\partial y_i} = G \frac{\partial^2 T_{ij}}{\partial y_i \partial y_j} - T_{ij} \frac{\partial^2 G}{\partial y_i \partial y_j}$$

to eliminate $G \partial^2 T_{ij} / \partial y_i \partial y_j$ and then applying the divergence theorem (1.B.1) to eliminate resulting volume integrals (after inserting the definition (1.67) of V_n and the definition $n_i(\partial/\partial y_i)$ of $\partial/\partial n$), that

$$\begin{aligned} \rho' = & \frac{1}{c_0^2} \int_{-T}^T \int_{v(\tau)} \frac{\partial^2 G}{\partial y_i \partial y_j} T_{ij} dy d\tau \\ & + \frac{1}{c_0^2} \int_{-T}^T \int_{S(\tau)} G n_i \left[\frac{\partial}{\partial y_j} (T_{ij} + c_0^2 \delta_{ij} \rho') + V_i^s \frac{\partial \rho'}{\partial \tau} \right] dS d\tau \end{aligned}$$

$$- \frac{1}{c_0^2} \int_{-T}^T \int_{S(\tau)} n_j \left[(T_{ij} + c_0^2 \delta_{ij} \rho') \frac{\partial G}{\partial y_i} + V_j^s \rho' \frac{\partial G}{\partial \tau} \right] dS d\tau$$

which becomes, upon changing the names of dummy indices and introducing Eqs. (2.3) and (2.4),

$$\begin{aligned} \rho' &= \frac{1}{c_0^2} \int_{-T}^T \int_{v(\tau)} \frac{\partial^2 G}{\partial y_i \partial y_j} T_{ij} dy d\tau + \frac{1}{c_0^2} \int_{-T}^T \int_{S(\tau)} \frac{\partial G}{\partial y_i} f_i dS(\mathbf{y}) d\tau \\ &\quad - \frac{1}{c_0^2} \int_{-T}^T \int_{S(\tau)} n_i h_i dS(\mathbf{y}) d\tau \end{aligned} \quad (3.3)$$

where

$$f_i \equiv -n_i(p - p_0) + n_j e_{ij} \quad (3.4)$$

is essentially the i th component of the force per unit area exerted by the boundaries on the fluid, $\rho' \equiv \rho - \rho_0$, and

$$h_i \equiv G \left(\frac{\partial \rho v_i}{\partial \tau} - V_i^s \frac{\partial \rho'}{\partial \tau} \right) + \rho v_i v_j \frac{\partial G}{\partial y_j} + \rho' V_i^s \frac{\partial G}{\partial \tau}$$

We shall consider only the case where the surfaces are impermeable to the flow† so that

$$n_i v_i = n_i V_i^s \quad \text{for } \mathbf{y} \text{ on } S$$

Then

$$n_i h_i = n_i \left(G \rho \frac{\partial v_i}{\partial \tau} + \rho v_i \frac{\partial G}{\partial \tau} + \rho v_j v_i \frac{\partial G}{\partial y_j} \right) - n_i \rho_0 v_i \frac{\partial G}{\partial \tau}$$

and as a result the continuity Eq. (2.1) implies that

$$n_i h_i = n_i \left(\frac{\partial \rho v_i G}{\partial \tau} + v_i \frac{\partial}{\partial y_j} \rho v_j G \right) - n_i \rho_0 v_i \frac{\partial G}{\partial \tau} \quad (3.5)$$

But applying Leibniz's rule (1.B.2) and the divergence theorem (1.B.1) to $\partial \rho v_i G / \partial y_i$ yields

$$\begin{aligned} \frac{d}{d\tau} \int_{v(\tau)} \frac{\partial \rho v_i G}{\partial y_i} dy &= \int_{v(\tau)} \frac{\partial^2 \rho v_i G}{\partial y_i \partial \tau} dy + \int_{S(\tau)} n_i v_i \frac{\partial \rho v_j G}{\partial y_j} dS \\ &= \int_{S(\tau)} n_i \left(\frac{\partial \rho v_i G}{\partial \tau} + v_i \frac{\partial}{\partial y_j} \rho v_j G \right) dS \end{aligned}$$

Hence, after using the argument that follows Eq. (1.B.6) to omit the integrated term

$$\int_{v(\tau)} \frac{\partial \rho v_i G}{\partial y_i} dy \Big|_{\tau=-T}^{\tau=T}$$

† Since our interest here is in the generation of sound and not its absorption by acoustically soft surfaces.

we find that *only* the last term

$$- n_i \rho_0 v_i \frac{\partial G}{\partial \tau} = - \rho_0 V_n \frac{\partial G}{\partial \tau}$$

in Eq. (3.5) contributes to the integral in Eq. (3.3) and hence that

$$\begin{aligned} \rho' = & \frac{1}{c_0^2} \int_{-T}^T \int_{v(\tau)} \frac{\partial^2 G}{\partial y_i \partial y_j} T_{ij} dy d\tau + \frac{1}{c_0^2} \int_{-T}^T \int_{S(\tau)} \frac{\partial G}{\partial y_i} f_i dS(y) d\tau \\ & + \frac{1}{c_0^2} \int_{-T}^T \int_{S(\tau)} \rho_0 V_n \frac{\partial G}{\partial \tau} dS(y) d\tau \end{aligned} \quad (3.6)$$

This is the fundamental equation governing the generation of sound in the presence of solid boundaries. It is, aside from the omission of a possible initial transient, an exact result. It applies to any region $v(\tau)$ which is bounded by impermeable surfaces $S(\tau)$ in arbitrary motion provided the source distributions T_{ij} and f_i are localized enough to ensure convergence of the integrals (see Sec. 2.3).

In the acoustic analogy approach it is assumed that the stress tensor T_{ij} and the surface force f_i can either be modeled mathematically or determined experimentally. Then we can consider the right side of the equation as known, and the density fluctuations in the sound field can be calculated. The first term represents the generation of sound by volume sources; the second represents the sound generated by unsteady forces exerted on the fluid by the solid boundaries; and the third represents the sound generated as a result of the volume displacement (thickness) effects of the surface. It might at first appear that we can use almost any fundamental solution G when applying this formula to a given aeroacoustics problem, and this would indeed be the case if we had precise knowledge of the sources f_j , T_{ij} , and $\rho_0 V_n$. But, since this almost never happens in practice and since even small errors made in approximating the sources can lead to excessive errors in the resulting predictions of the sound field unless the proper fundamental solution is used, we are, in fact, often quite limited in our choice of G .

3.3 FFWCS WILLIAMS-HAWKINGS EQUATION

When the region v is all of space, the surface integrals in Eq. (3.6) will not be present, and the only possible choice of G will be the free-space Green's function G^0 given by Eq. (1.56), in which case, Eq. (2.11) (which was the starting point for the jet noise analysis in Chap. 2) is recovered. Now even when solid boundaries are present, there is no reason why G cannot, in theory, still be taken as the free-space Green's function. In this section, we investigate the consequences of such a choice.

3.3.1 The General Equation

Since Eq. (1.56) shows that G^0 depends on \mathbf{x} and \mathbf{y} only through $R = |\mathbf{x} - \mathbf{y}|$, it follows that

$$\frac{\partial G^0}{\partial y_i} = - \frac{\partial G^0}{\partial x_i} \quad (3.7)$$

Hence, inserting Eq. (1.56) into Eq. (3.6) yields

$$\begin{aligned} \rho' = & \frac{1}{c_0^2} \frac{\partial}{\partial x_i} \frac{\partial}{\partial x_j} \int_{-T}^T \int_{v(\tau)} \frac{1}{4\pi R} \delta\left(t - \tau - \frac{R}{c_0}\right) T_{ij} dy d\tau \\ & - \frac{1}{c_0^2} \frac{\partial}{\partial x_i} \int_{-T}^T \int_{S(\tau)} \frac{1}{4\pi R} \delta\left(t - \tau - \frac{R}{c_0}\right) f_i dS(\mathbf{y}) d\tau \\ & + \frac{1}{c_0^2} \int_{-T}^T \int_{S(\tau)} \frac{\rho_0 V_n}{4\pi R} \frac{\partial}{\partial \tau} \delta\left(t - \tau - \frac{R}{c_0}\right) dS(\mathbf{y}) d\tau \end{aligned} \quad (3.8)$$

In order to carry out the integrations over τ , it is convenient to introduce a moving coordinate system, say $\zeta(\mathbf{y}, \tau)$, in which the surface $S(\tau)$ remains fixed. Then the velocity \mathbf{V} and the acceleration \mathbf{a} of any fixed point ζ in this system are given by

$$\left. \begin{aligned} \mathbf{V} &= \frac{\partial \mathbf{y}(\zeta, \tau)}{\partial \tau} \Big|_{\zeta = \text{Constant}} \\ \mathbf{a} &= \frac{\partial \mathbf{V}(\zeta, \tau)}{\partial \tau} \Big|_{\zeta = \text{Constant}} \end{aligned} \right\} \quad (3.9)$$

And since $S(\tau)$ is stationary relative to these coordinates

$$\mathbf{V}^s = \mathbf{V} \quad (3.10)$$

for each point of $S(\tau)$. (The ζ -coordinate system could be required to move with the flow, but this restriction is not really necessary for the present development.)

Let us now suppose that the region $v(\tau)$ occupies the exterior of the impermeable surface $S(\tau)$, as shown schematically in Fig. 3.1. The last term in Eq. (3.8), which is associated with sound generated by volume displacement

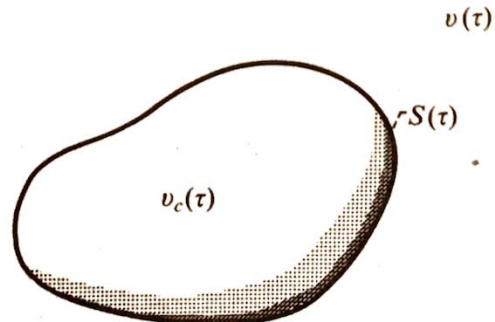


Fig. 3.1 Moving surface.

effects, appears to be a source of monopole order. And indeed if the volume of the region $v_c(\tau)$ enclosed by $S(\tau)$ were actually changing with time we should certainly expect this to be the case. If, on the other hand, the motion were such that the total volume of $v_c(\tau)$ remained constant, we would only expect to see higher order sources. Thus, it is shown in books on elementary fluid mechanics¹ that the time rate of change of an element of volume in any moving coordinate system is proportional to the divergence of the velocity \mathbf{V} of a fixed point in that system. Then if the volume of $v_c(\tau)$ is to remain constant in time, there will be at least one coordinate system ζ such that

$$\nabla \cdot \mathbf{V} = 0 \quad (3.11)$$

at all points within v_c . But when this condition is satisfied, Eq. (3.A.3) of Appendix 3.A can be used with $f(r, \tau) = \rho_0 \delta(t - \tau - (R/c_0))/4\pi R c_0^2$ to write the last integral in Eq. (3.8) as

$$\begin{aligned} & -\frac{1}{c_0^2} \frac{\partial}{\partial x_j} \int_{-T}^T \int_{v_c(\tau)} \frac{1}{4\pi R} \delta\left(t - \tau - \frac{R}{c_0}\right) \rho_0 a_j d\mathbf{y} d\tau \\ & + \frac{1}{c_0^2} \frac{\partial^2}{\partial x_i \partial x_j} \int_{-T}^T \int_{v_c(\tau)} \frac{1}{4\pi R} \delta\left(t - \tau - \frac{R}{c_0}\right) \rho_0 V_i V_j d\mathbf{y} d\tau \end{aligned} \quad (3.12)$$

Thus, in this case the effect of the surface motion can be represented by a dipole source whose strength is proportional to its acceleration plus a quadrupole source of strength $\rho_0 V_i V_j$.

Rather than evaluating the integrals in Eqs. (3.8) and (3.12) for a surface in arbitrary motion, we choose to restrict our attention to the case where the surface is rigid. We can then suppose, without loss of generality, that ζ refers to a Cartesian coordinate system (as shown in Fig. 3.2) that translates with velocity $\mathbf{V}_0(\tau)$ and rotates with angular velocity $\boldsymbol{\Omega}(\tau)$ but otherwise

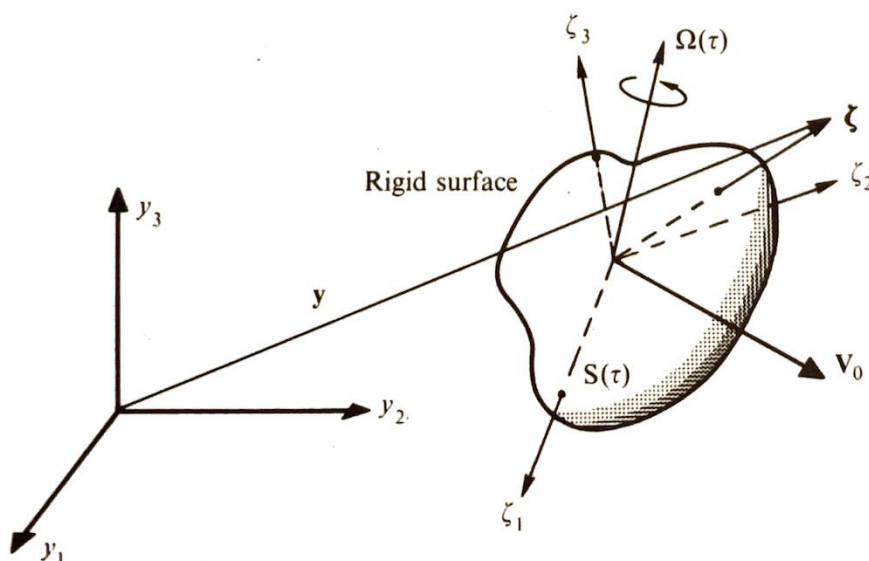


Fig. 3.2 Coordinate system fixed in a surface.

remains unchanged. Indeed, any book on classical mechanics (e.g., Ref. 2) will show that the velocity $\mathbf{V}(\zeta, \tau)$ of any fixed point ζ in this system is simply

$$\mathbf{V}(\zeta, \tau) = \mathbf{V}_0(\tau) + \boldsymbol{\Omega}(\tau) \times \zeta \quad (3.13)$$

Before introducing these coordinates into Eqs. (3.8) and (3.12) recall that the Jacobian of the length preserving transform $\mathbf{y} \rightarrow \zeta$ between two Cartesian coordinate systems is unity and that the element of surface area $dS(\zeta)$ in the ζ -coordinate system is equal to the element of surface area $dS(\mathbf{y})$ in the \mathbf{y} -coordinate system. Then since the limits of integration of the volume and surface integrals are independent of τ in the ζ -coordinate system, the order of the integrations can be interchanged and Eqs. (3.8) and (3.12) can be combined to obtain

$$\begin{aligned} \rho' = & \frac{1}{c_0^2} \frac{\partial^2}{\partial x_i \partial x_j} \int_{v(t_0)} \left[\int_{-\infty}^{\infty} \frac{1}{4\pi R} \delta\left(t - \tau - \frac{R}{c_0}\right) T_{ij} d\tau \right] d\zeta \\ & - \frac{1}{c_0^2} \frac{\partial}{\partial x_i} \int_{S(t_0)} \left[\int_{-\infty}^{\infty} \frac{1}{4\pi R} \delta\left(t - \tau - \frac{R}{c_0}\right) f_i d\tau \right] dS(\zeta) \\ & - \frac{1}{c_0^2} \frac{\partial}{\partial x_j} \int_{v_c(t_0)} \left[\int_{-\infty}^{\infty} \frac{1}{4\pi R} \delta\left(t - \tau - \frac{R}{c_0}\right) \rho_0 a_j d\tau \right] d\zeta \\ & + \frac{1}{c_0^2} \frac{\partial^2}{\partial x_i \partial x_j} \int_{v_c(t_0)} \left[\int_{-\infty}^{\infty} \frac{1}{4\pi R} \delta\left(t - \tau - \frac{R}{c_0}\right) \rho_0 V_i V_j d\tau \right] d\zeta \end{aligned}$$

where we have allowed T to approach ∞ .

We can now use the identity (1.97), with g given by $\tau - t + (R/c_0)$, to carry out the integrations with respect to τ . In fact, since it follows from Eq. (3.9) that

$$\left(\frac{\partial g}{\partial \tau}\right)_{\zeta} = 1 - \frac{\mathbf{R}}{c_0 R} \cdot \left(\frac{\partial \mathbf{y}}{\partial \tau}\right)_{\zeta} = 1 - \frac{\mathbf{R}}{R} \cdot \mathbf{M} \quad (3.14)$$

(where

$$\mathbf{M} \equiv \frac{\mathbf{V}}{c_0} \quad (3.15)$$

and $\mathbf{R} \equiv \mathbf{x} - \mathbf{y}$), this leads to the Ffowcs Williams–Hawkings equation^{†3}

$$\begin{aligned} \rho' = & \frac{1}{4\pi c_0^2} \frac{\partial^2}{\partial x_i \partial x_j} \int_{v(t_0)} \left[\frac{T_{ij}}{R |1 - (\mathbf{R}/R) \cdot \mathbf{M}|} \right]_{\tau=\tau_e} d\zeta \\ & - \frac{1}{4\pi c_0^2} \frac{\partial}{\partial x_i} \int_{S(t_0)} \left[\frac{f_i}{R |1 - (\mathbf{R}/R) \cdot \mathbf{M}|} \right]_{\tau=\tau_e} dS(\zeta) \end{aligned}$$

[†] The equation actually devised by Ffowcs Williams and Hawkings is more general in that it does not require that the surfaces be rigid.

$$\begin{aligned}
& - \frac{1}{4\pi c_0^2} \frac{\partial}{\partial x_j} \int_{v_e(t_0)} \left[\frac{\rho_0 a_j}{R |1 - (\mathbf{R}/R) \cdot \mathbf{M}|} \right]_{\tau=\tau_e} d\zeta \\
& + \frac{1}{4\pi c_0^2} \frac{\partial^2}{\partial x_i \partial x_j} \int_{v_e(t_0)} \left[\frac{\rho_0 V_i V_j}{R |1 - (\mathbf{R}/R) \cdot \mathbf{M}|} \right]_{\tau=\tau_e} d\zeta \quad (3.16)
\end{aligned}$$

where the notation $[]_{\tau=\tau_e}$ indicates that the quantity enclosed within the brackets is to be evaluated at ζ and the retarded time $\tau_e = \tau_e(\mathbf{x}, t, \zeta)$, which is obtained by solving equation

$$g(\tau_e, t, \mathbf{x}, \zeta) \equiv \tau_e - t + \frac{1}{c_0} |\mathbf{x} - \mathbf{y}(\zeta, \tau_e)| = 0 \quad (3.17)$$

And if more than one solution to this equation exists (as it does at supersonic speeds), each term in Eq. (3.16) should be interpreted as a sum over all such solutions.

The solution (1.113) for a point multipole source moving with a constant velocity shows that the sound field can be thought of as a superposition of elementary waves; with each moving volume element $d\zeta$ outside of $S(\tau)$ contributing a wave which is the same as that emitted by a moving quadrupole source of strength $T_{ij} d\zeta$ (see Fig. 3.3), each element of surface area $dS(\zeta)$ contributing a wave which is the same as that emitted by a

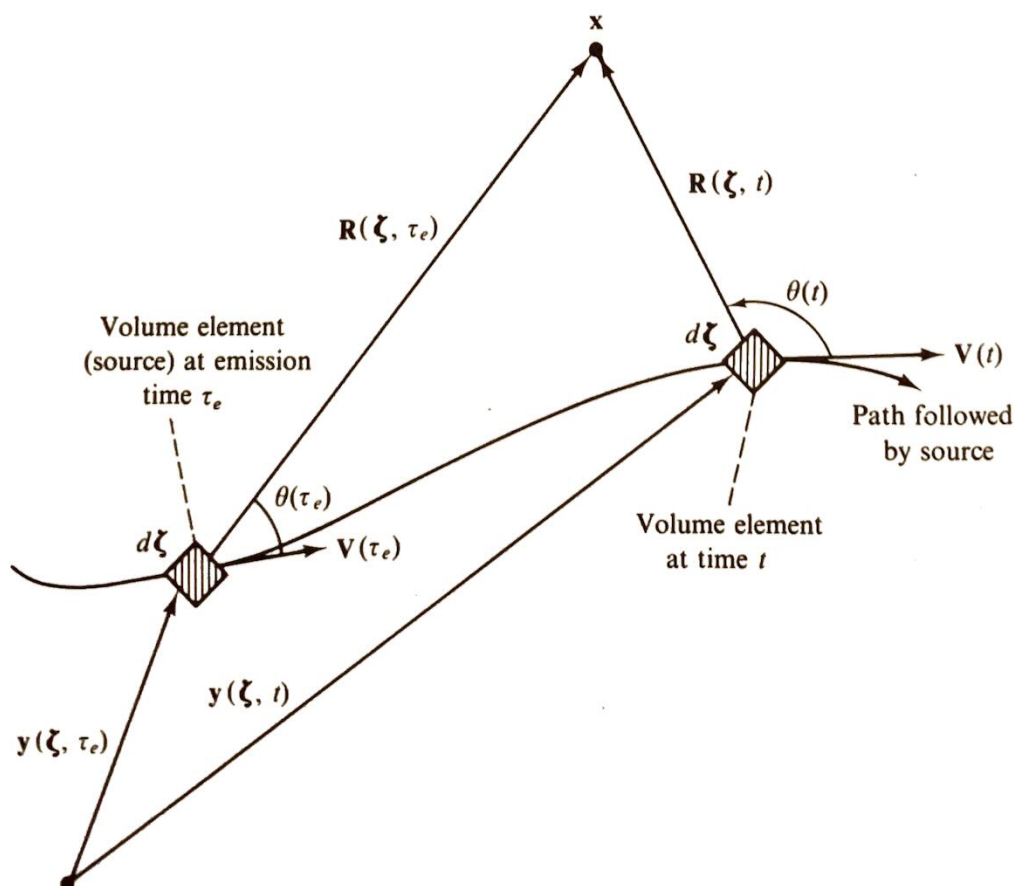


Fig. 3.3 Moving-source configuration.

moving dipole source of strength $-f_i dS(\zeta)$, and each moving volume element $d\zeta$ within S contributing waves that are the same as those emitted by a dipole source of strength $-\rho_0 a_j$ and a quadrupole of strength $\rho_0 V_i V_j$. The first term of Eq. (3.16) corresponds to the solution that arises in Lighthill's theory, while the direct effects of the solid boundaries are accounted for by the three remaining terms. The first of these represents the sound generated by the fluctuating force f_i exerted by the solid boundaries on the fluid. The remaining two represent the sound generated by the volume displacement effects—the dipole term resulting from the acceleration of the surface.

If the velocity V of any point of the source region is supersonic, the Doppler factor

$$C^\dagger \equiv 1 - \frac{\mathbf{R}}{R} \cdot \mathbf{M} = 1 - M \cos \theta \quad (3.18)$$

that occurs in the denominator of each term in Eq. (3.16) will vanish at the angle

$$\theta = \cos^{-1} \frac{1}{M} \quad (3.19)$$

The resulting singularities are, in essence, the same as those that were associated with Mach wave emission in Sec. 2.5.2. However, when supported by solid surfaces Mach waves are often able to coalesce into the intense shocks that are usually associated with supersonically moving objects. Since the propagation of these waves is basically a steady-state phenomenon, they are usually treated by methods similar to the direct calculational procedures discussed in Chap. 5.

When the surface S is stationary, $\mathbf{a} \equiv \mathbf{M} = \mathbf{V} = 0$, $\zeta = \mathbf{y}$, and Eq. (3.16) reduces to Curle's equation⁴

$$\begin{aligned} \rho' = & \frac{1}{4\pi c_0^2} \frac{\partial^2}{\partial x_i \partial x_j} \int_v \frac{T_{ij}}{R} \left(\mathbf{y}, t - \frac{R}{c_0} \right) d\mathbf{y} \\ & - \frac{1}{4\pi c_0^2} \frac{\partial}{\partial x_i} \int_S \frac{f_i}{R} \left(\mathbf{y}, t - \frac{R}{c_0} \right) dS(\mathbf{y}) \end{aligned} \quad (3.20)$$

3.3.2 Far-Field Equations

Now suppose that $S(\tau)$ is bounded and that the volume source region remains concentrated near this surface. We shall require that the velocity \mathbf{V} be subsonic at each point of this region so that the Doppler factor C^\dagger can never vanish. Then Eq. (3.16) can be put in a form that more nearly exhibits the true character of its radiation field (see remarks near the end

of Sec. 1.5.2). To this end, notice that applying the chain rule to Eq. (3.17) yields

$$\left(\frac{\partial g}{\partial x_j}\right)_{\tau_e} + \left(\frac{\partial g}{\partial \tau_e}\right)_x \frac{\partial \tau_e}{\partial x_j} = 0$$

Then using Eqs. (3.14), (3.17), and (3.18) to eliminate g from this result, we find that $\partial \tau_e / \partial x_j = -[R_j / c_0 C^\dagger R]_{\tau=\tau_e}$. Consequently, the chain rule can be applied to an arbitrary function $f(\mathbf{x}, \tau_e)$ to show that

$$\frac{\partial f}{\partial x_i} = \left(\frac{\partial f}{\partial x_i}\right)_{\tau_e} - \left(\frac{\partial f}{\partial \tau_e}\right)_x \left[\frac{R_i}{c_0 C^\dagger R}\right]_{\tau=\tau_e} \quad (3.21)$$

and therefore, in particular, that

$$\frac{\partial R}{\partial x_i} = \frac{R_i}{R} - \frac{R_i}{c_0 C^\dagger R} \frac{\partial R}{\partial y_j} \frac{\partial y_j}{\partial \tau_e} = \frac{R_i}{R C^\dagger} \quad \text{at } \tau = \tau_e \quad (3.22)$$

Now each integral in Eq. (3.16) involves a first or second derivative with respect to x_i of a term of the form $h \equiv [A(\tau)/R | C^\dagger |]_{\tau=\tau_e}$ where (in order to simplify the notation) dependence on ζ has been suppressed. But since A does not depend on \mathbf{x} explicitly, Eqs. (3.22) and (3.18) show that $(\partial h / \partial x_i)_{\tau_e} = O(R^{-2})$ as $R \rightarrow \infty$. Hence, Eq. (3.21) shows that

$$\frac{\partial h}{\partial x_i} = - \left[\frac{R_i}{c_0 R^2 C^\dagger} \frac{\partial}{\partial \tau} \frac{A}{|C^\dagger|} \right]_{\tau=\tau_e} + O(R^{-2})$$

and hence that

$$\frac{\partial^2 h}{\partial x_i \partial x_j} = \left[\frac{R_i R_j}{c_0^2 R^3 C^\dagger} \frac{\partial}{\partial \tau} \frac{1}{C^\dagger} \frac{\partial}{\partial \tau} \frac{A}{|C^\dagger|} \right]_{\tau=\tau_e} + O(R^{-2})$$

Thus, at large values of R , Eq. (3.16) can be approximated by

$$\begin{aligned} \rho' \sim & \frac{1}{4\pi c_0^4} \int_{v(t_0)} \left[\frac{R_i R_j}{R^3 C^\dagger} \frac{\partial}{\partial \tau} \frac{1}{C^\dagger} \frac{\partial}{\partial \tau} \frac{T_{ij}}{|C^\dagger|} \right]_{\tau=\tau_e} d\zeta \\ & + \frac{1}{4\pi c_0^3} \int_{S(t_0)} \left[\frac{R_i}{R^2 C^\dagger} \frac{\partial}{\partial \tau} \frac{f_i}{|C^\dagger|} \right]_{\tau=\tau_e} dS(\zeta) \\ & + \frac{1}{4\pi c_0^3} \int_{v_c(t_0)} \left[\frac{R_j}{R^2 C^\dagger} \frac{\partial}{\partial \tau} \frac{\rho_0 a_j}{|C^\dagger|} \right]_{\tau=\tau_e} d\zeta \\ & + \frac{1}{4\pi c_0^4} \int_{v_c(t_0)} \left[\frac{R_i R_j}{R^3 C^\dagger} \frac{\partial}{\partial \tau} \frac{1}{C^\dagger} \frac{\partial}{\partial \tau} \frac{\rho_0 V_i V_j}{|C^\dagger|} \right]_{\tau=\tau_e} d\zeta \end{aligned} \quad (3.23)$$

When S is stationary, this becomes

$$\rho' \sim \frac{x_i x_j}{4\pi c_0^4 x^3} \int_v \frac{\partial^2 T_{ij}}{\partial t^2} \left(\mathbf{y}, t - \frac{R}{c_0} \right) d\mathbf{y} + \frac{x_i}{4\pi c_0^3 x^2} \int_S \frac{\partial f_i}{\partial t} \left(\mathbf{y}, t - \frac{R}{c_0} \right) dS(\mathbf{y})$$

which shows that stationary surfaces will radiate no sound when the source functions T_{ij} and f_i are steady (i.e., independent of time). On the other hand, Eq. (3.23) shows that accelerative motion of a surface (for which \mathbf{V} and as a consequence, C^\dagger depend on time) will result in the emission of sound, even when the sources are steady, whereas a merely steady motion will not. Of course, this conclusion only applies for subsonic velocities (for which the convection factor C^\dagger never vanishes). Surfaces moving with a constant supersonic velocity will generate shock waves which will reach the far field and be sensed as sound (often called a sonic boom).

It was shown in Sec. 1.5.2 that the acoustic equations for a stationary compact source could be simplified by neglecting variations in retarded time. A similar simplification can be obtained for a moving source region. Thus let $\delta\mathbf{y}$ denote a distance across such a region. Then it follows from the mean-value theorem that the corresponding change in retarded time $\Delta\tau_e$ is approximately

$$\Delta\tau_e \equiv \tau_e(\mathbf{y} + \delta\mathbf{y}) - \tau_e(\mathbf{y}) \simeq \frac{\partial\tau_e}{\partial y_i} \delta y_i \quad (3.24)$$

Applying the chain rule

$$\frac{\partial g}{\partial y_i} + \frac{\partial g}{\partial \tau_e} \frac{\partial \tau_e}{\partial y_i} = 0$$

to Eq. (3.17) and using the result to eliminate $\partial\tau_e/\partial y_i$ yields

$$\Delta\tau_e \simeq \frac{1}{c_0(1 - M \cos \theta)} \frac{\mathbf{R}}{R} \cdot \delta\mathbf{y}$$

Hence, the change in retarded time across the source region is roughly

$$\Delta\tau_e \simeq \frac{1}{1 - M \cos \theta} \frac{L}{c_0}$$

where $L = |\delta\mathbf{y}|$ is a characteristic source dimension. As pointed out on page 83 (for the case of moving eddies), $\Delta\tau_e$ represents the time it takes a sound wave to cross the moving source volume. Thus it ought to be possible to neglect retarded time variations in the integrals of Eq. (3.23) whenever the characteristic time T_ζ for the source fluctuations in the moving frame is large compared with the variation in retarded time $\Delta\tau_e$ across the source region; that is, whenever

$$\frac{L}{c_0(1 - M \cos \theta)} \ll T_\zeta \quad (3.25)$$

provided, of course, that the correct multipole structure of the sources has been uncovered. (This structure may not be the same for a moving source as it is for the corresponding stationary source. See remarks near end of Sec. 1.5.2.) Now, suppose, in addition, that the Mach number is nearly

constant across the source region. Then Eq. (3.23) becomes

$$\rho' \sim \frac{(R_e)_i(R_e)_j}{4\pi c_0^4 C_0^\dagger R_e^3} \frac{\partial}{\partial \tau_e} \frac{1}{C_0^\dagger} \frac{\partial}{\partial \tau_e} \left[\frac{Q_{ij}(\tau_e) + v_c \rho_0 V_i^0(\tau_e) V_j^0(\tau_e)}{|C_0^\dagger|} \right] - \frac{(R_e)_i}{4\pi c_0^3 C_0^\dagger R_e^2} \frac{\partial}{\partial \tau_e} \left[\frac{F_i(\tau_e) - v_c \rho_0 a_i^0(\tau_e)}{|C_0^\dagger|} \right] \quad (3.26)$$

where τ_e now denotes the retarded time at the center of the source region, V_i^0 and a_i^0 are the velocity and acceleration of this point, \mathbf{R}_e denotes the vector connecting it to the observation point at the time τ_e ,

$$C_0^\dagger \equiv 1 - \frac{\mathbf{V}^0(\tau_e) \cdot \mathbf{R}_e}{c_0 R_e} \quad (3.27)$$

and $v_c = \int_{v_c(t_0)} d\zeta$ is the net volume enclosed by S , while $Q_{ij} = \int_v T_{ij} d\zeta$ and $F_i(t) = -\int_S f_i(\zeta, t) dS(\zeta)$ represent the integrated strength of the external quadrupoles and the net force exerted by the fluid on the surface, respectively.

The first term in Eq. (3.26) is clearly a quadrupole source while the second is clearly a dipole. If these two sources are of equal strength and if their spatial and temporal scales are roughly equal, their ratio will be of the order $L/[(1 - M \cos \theta) T_\zeta c_0]$. Then, Eq. (3.25) implies that the quadrupole source can be neglected in Eq. (3.26) and, as a consequence, that†

$$\rho' \sim \frac{-(R_e)_i}{4\pi c_0^3 C_0^\dagger R_e^2} \frac{\partial}{\partial \tau_e} \left[\frac{F_i(\tau_e) - v_c \rho_0 a_i^0(\tau_e)}{|C_0^\dagger|} \right] \quad (3.28)$$

This result, of course, also holds when the quadrupole strength is smaller than the dipole, which, as will be shown in Chap. 5, is often the case for aerodynamic surfaces. Consequently, the quadrupole terms can frequently be neglected in Eq. (3.23) even when the surfaces are not compact, but it is then necessary to account for variations in retarded time over the source region.

When the surface S is stationary, Eq. (3.28) reduces to

$$\rho' \sim \frac{-x_i}{4\pi c_0^3 x^2} \frac{\partial F_i}{\partial t} \left(t - \frac{x}{c_0} \right) \quad (3.29)$$

where

$$F_i(t) = - \int_S f_i(\mathbf{y}, t) dS(\mathbf{y}) \quad (3.30)$$

is the total force acting on S (compare with Eq. (1.79)). The inequality (3.25) shows that this result applies when

$$\frac{L}{c_0} \ll T_\zeta \quad (3.31)$$

† This equation was first obtained by Lowson⁶ without the acceleration term which was subsequently included by Ffowcs Williams and Hawkins.³

When the flow is time stationary Eq. (3.29) shows (in view of Eqs. (1.16) and (1.92) and the fact that time averages are invariant under translations), that

$$\bar{I} \sim \frac{1}{16\pi^2 c_0^3 \rho_0} \frac{x_i x_j}{x^4} \overline{\frac{dF_i(t)}{dt} \frac{dF_j(t)}{dt}} \quad (3.32)$$

Now suppose that the unsteady forces generating the sound are caused by a turbulent flow with mean velocity U and correlation length l . Then, as indicated on page 78, the turbulent eddies will evolve only very slowly relative to the time $T_f = l/U$ they take to pass a fixed observer (Taylor's hypothesis). The forces induced on any fixed object will therefore fluctuate on the latter time scale so that inequality (3.31) becomes

$$L \ll \frac{l}{M} \quad (3.33)$$

where $M = U/c_0$ is the mean-flow Mach number. Thus, unless M is very small (as it frequently is in water), this implies that the characteristic source dimensions must be much smaller than the turbulence correlation length. Although such conditions are almost never encountered in practice, it turns out that Eq. (3.32) can very often provide fairly accurate estimates of the sound field, even when the acoustic wavelength is comparable to the dimensions of the surface. Some assessment of the errors that occur will be given in Chap. 5.

Equation (3.32) can be used to obtain similarity relations (analogous to those obtained for jet noise) for the sound field generated by a fluctuating flow in the vicinity of a small stationary object. Thus, we anticipate that

$$\frac{\partial F_i}{\partial t} \frac{\partial F_j}{\partial t} \propto \frac{1}{T_f^2} |\mathbf{F}|^2$$

$$|\mathbf{F}| \propto \rho_0 U_c^2 L^2 \quad \text{and} \quad T_f \propto \frac{L}{U_c}$$

where T_f denotes the characteristic period of the fluctuation and U_c denotes an appropriate characteristic flow velocity. Hence, it follows from Eq. (3.32) that

$$\bar{I} \propto \frac{\rho_0 U_c^6 L^2}{c_0^3 x^2}$$

The total radiated power \mathcal{P}_D will therefore be proportional to

$$\mathcal{P}_D \propto \frac{\rho_0 U_c^6 L^2}{c_0^3}$$

It was shown on page 93 that the corresponding result for a volume quadrupole source is

$$\mathcal{P}_Q \propto \frac{\rho_0 U_c^8 D^2}{c_0^5}$$

Consequently,

$$\frac{\mathcal{P}_Q}{\mathcal{P}_D} \propto \left(\frac{U_c}{c_0} \right)^2$$

which gives at least some indication that the volume quadrupole sources in the vicinity of (even somewhat noncompact) surfaces ought to become progressively more important relative to the surface dipoles as the Mach number increases.

Equation (3.29) implies that the cross correlation

$$\overline{F_2(t)p(t+\tau)}$$

between the lift fluctuation acting on a body and the far-field sound pressure should be proportional to the time derivative

$$\frac{\partial}{\partial \tau} \overline{F_2(t)F_2(t+\tau)}$$

of the lift autocorrelation function. Clark and Ribner⁷ measured these correlations for a small airfoil in a turbulent jet. Their results are shown in Fig. 3.4. They attribute the small discrepancy (17 percent max.) to the false enhancement of lift resulting from model vibrations.

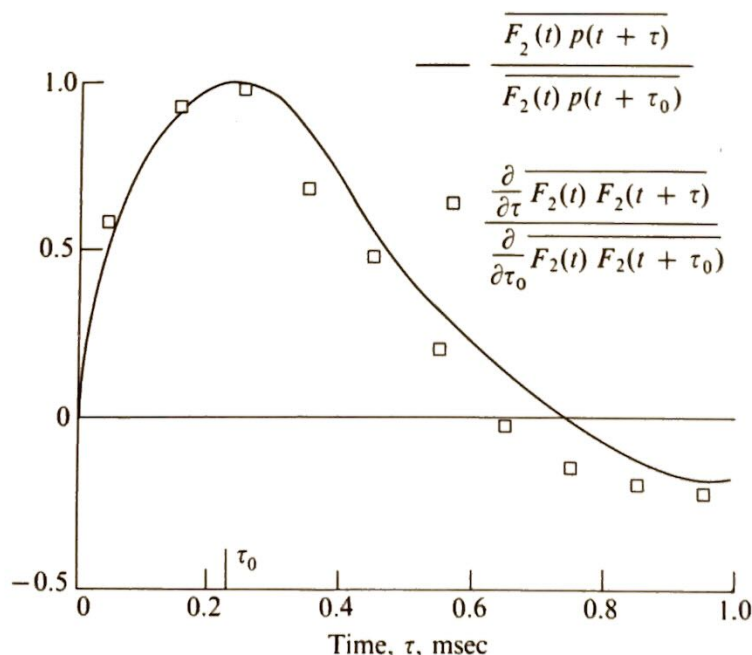


Fig. 3.4 Comparison of cross correlation of lift and sound pressure and first derivative of autocorrelation of lift — both normalized. (From Reference 7.)

3.4 CALCULATION OF AERODYNAMIC FORCES

Now, we have shown that it is often possible to calculate the sound field by using only the dipole term in Eq. (3.23). Consequently, it is important to devise some means of estimating the surface force \mathbf{f} that appears in this term. In this section we describe a number of analytical methods that have been developed for this purpose. Some additional results will be presented in Chap. 5.

The calculation of these flow induced surface forces is, in general, a very difficult task. All the purely analytical results obtained so far involve the assumption that the fluctuating velocity is small compared with the steady velocity—primarily because the problem can then be linearized.

Thus, it is assumed in this section that the unsteady flow results from the convection past a stationary body of a frozen small-amplitude disturbance pattern (often called a *gust*) by an otherwise uniform mean flow $\hat{\mathbf{i}}U_r$. Consequently, the magnitude of the disturbance velocity $\mathbf{u}_\infty = \{u_\infty, v_\infty, w_\infty\}$ will be small compared to U_r and far upstream from the body the flow velocity $\hat{\mathbf{i}}U_r + \mathbf{u}_\infty$ will be steady (but spatially nonuniform) in a reference frame moving with the mean velocity $\hat{\mathbf{i}}U_r$. This might, for example, be a good approximation for a turbulent flow which, as we have seen, changes only slowly with time in the moving frame.

3.4.1 Quasi-Steady Approximation

First, consider the case where the spatial scale of the disturbance is large compared with a typical dimension of the body and suppose that the velocity is low enough so that the flow can be considered incompressible. Then it is not unreasonable to assume that the forces acting on the body obey the same relations as they do in a steady flow. This is called the “*quasi-steady*” approximation. Thus, we suppose that the lift and drag forces acting on the body (L and D , respectively) are related to the upstream velocity V by

$$\left. \begin{aligned} L &= \frac{1}{2}\rho_0 V^2 C_L A \\ D &= \frac{1}{2}\rho_0 V^2 C_D A \end{aligned} \right\} \quad (3.34)$$

where A is some suitable cross-sectional area of the body, and the lift and drag coefficients, C_L and C_D , respectively, are functions only of the orientation of the body relative to the oncoming flow. The latter is usually characterized by specifying two angles, say α and γ , that determine the direction of the oncoming flow relative to three mutually perpendicular axes fixed to the body which we shall denote by (y_1, y_2, y_3) . These angles can be conveniently defined in the manner indicated in Fig. 3.5. Then for the

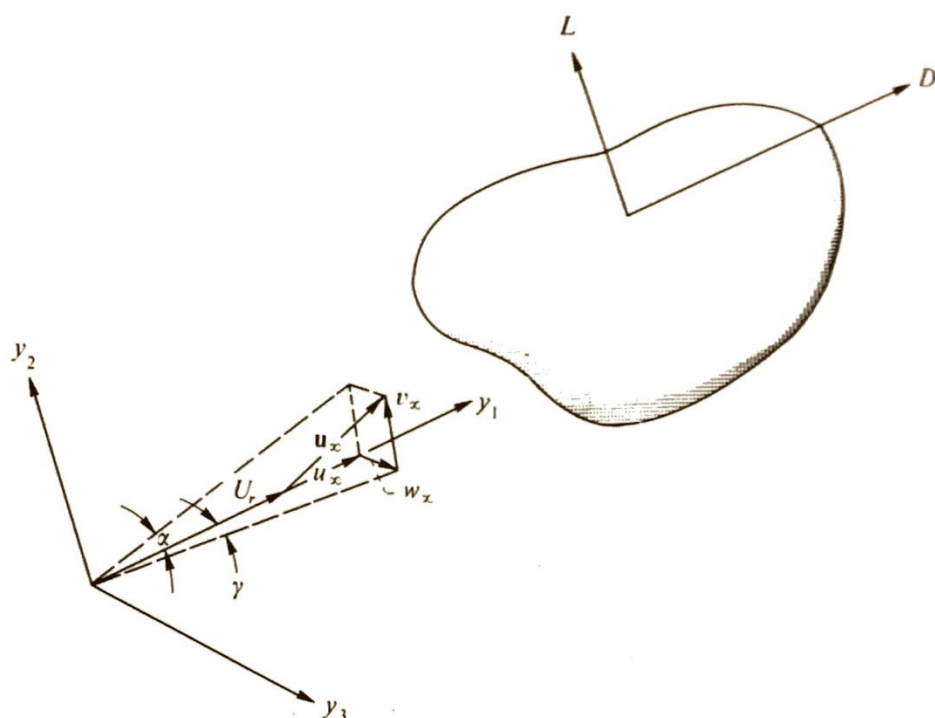


Fig. 3.5 Coordinates for orienting body relative to oncoming flow.

thin, relatively two-dimensional bodies that are most often of interest in applications (e.g., blown flaps and fan and compressor blades) α will measure changes in angle of attack and γ will correspond to the angle between the projection of the oncoming flow onto the plane of the body and the mean flow direction (see Fig. 3.6).

In any case, the total oncoming flow velocity V is given by

$$V^2 = (\hat{\mathbf{i}}U_r + \mathbf{u}_\infty) \cdot (\hat{\mathbf{i}}U_r + \mathbf{u}_\infty) \quad (3.35)$$

But since \mathbf{u}_∞ is assumed to be small relative to U_r , we find upon neglecting squares of small quantities that

$$C_L \simeq \bar{C}_L + \frac{\partial C_L}{\partial \alpha} \alpha + \frac{\partial C_L}{\partial \gamma} \gamma \simeq \bar{C}_L + \frac{\partial C_L}{\partial \alpha} \frac{v_\infty}{U_r} + \frac{\partial C_L}{\partial \gamma} \frac{w_\infty}{U_r}$$

$$C_D \simeq \bar{C}_D + \frac{\partial C_D}{\partial \alpha} \frac{v_\infty}{U_r} + \frac{\partial C_D}{\partial \gamma} \frac{w_\infty}{U_r}$$

and

$$V^2 \simeq U_r^2 + 2u_\infty U_r$$

where \bar{C}_L and \bar{C}_D denote the time-averaged lift and drag coefficients, and the lift and drag slopes are taken as constants. Hence, it follows from Eq. (3.34) that the fluctuating lift and drag forces $L' \equiv L - \bar{L}$ and $D' \equiv D - \bar{D}$ are given by

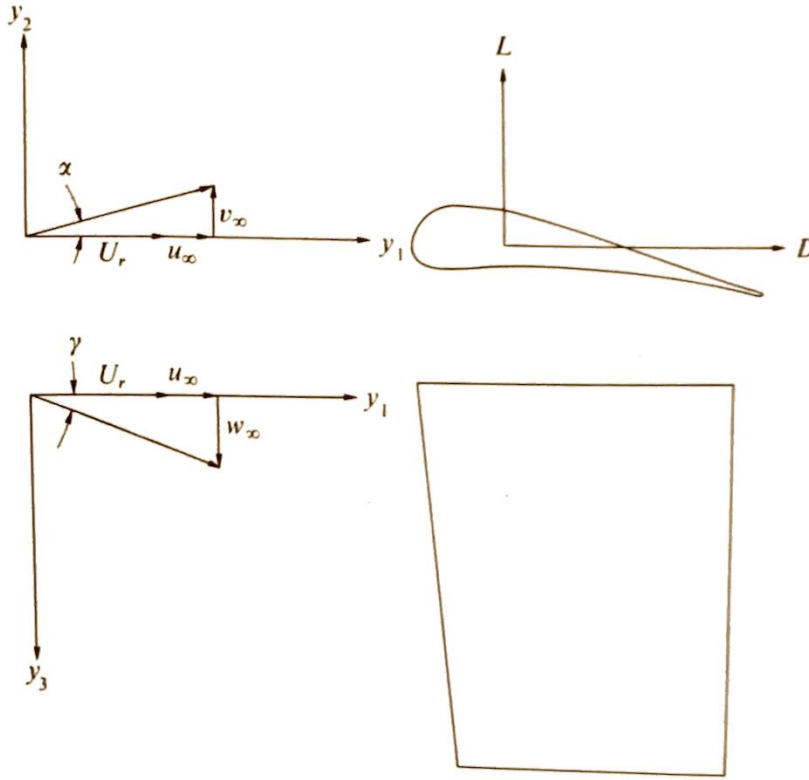


Fig. 3.6 Coordinates for orienting airfoil-shaped body relative to oncoming flow.

$$\begin{aligned}
 L' &= \frac{1}{2}\rho_0 A U_r \left(\frac{\partial C_L}{\partial \alpha} v_\infty + \frac{\partial C_L}{\partial \gamma} w_\infty + 2\bar{C}_L u_\infty \right) \\
 D' &= \frac{1}{2}\rho_0 A U_r \left(\frac{\partial C_D}{\partial \alpha} v_\infty + \frac{\partial C_D}{\partial \gamma} w_\infty + 2\bar{C}_D u_\infty \right)
 \end{aligned} \tag{3.36}$$

The first two terms in these expressions result from the transverse components of the gust velocity while the last are the result of the longitudinal component. In aeronautical applications one is usually concerned with thin bodies operating at high Reynolds numbers so that $C_D \ll C_L$. Under these conditions, it should certainly be safe to ignore D' .

The theoretical lift slope $\partial C_L / \partial \alpha$ of a two-dimensional flat plate at a small angle of attack, say α_0 , to the oncoming flow is equal to 2π . The fluctuating lift due to a two-dimensional gust, $\mathbf{u}_\infty = \{u_\infty, v_\infty, 0\}$, is therefore given by

$$\frac{L'}{A} = \rho_0 U_r \pi v_\infty + 2\pi \rho_0 U_r \alpha_0 u_\infty$$

But since α_0 is assumed to be small, the second term in this equation should be negligible compared to the first so that

$$\frac{L'}{A} = \frac{1}{2}\rho_0 U_r v_\infty \frac{dC_L}{d\alpha} = \rho_0 U_r v_\infty \pi \tag{3.37}$$

This result also applies to two-dimensional airfoil shapes with small thickness and camber. It shows that in two-dimensional flows the lift fluctuations acting on such bodies arise solely from the fluctuations in angle of attack caused by changes in the upwash velocity v_∞ . We shall see that this conclusion holds even when the quasi-steady approximation does not apply.

3.4.2 Calculations Based on Unsteady-Thin-Airfoil Theory

It turns out that, as a practical matter, the quasi-steady approximation is limited to very large-scale disturbances. Fortunately, we are usually interested in bodies that are relatively thin in the direction perpendicular to the flow, and in this case we are able to obtain results that apply to much smaller-scale disturbances. The development of the relevant theory began in the middle 1920's with the work of Wagner,⁸ who determined the growth of lift on an airfoil starting impulsively from rest. Ten years later, Theodorsen calculated the lift on a sinusoidally oscillating airfoil,⁹ and Küssner,¹⁰ introduced a unit response function (called the Küssner function) that relates the fluctuating lift on a two-dimensional airfoil to a step change in the upwash velocity. In 1938, von Kármán and Sears¹¹ devised a general approach that could be used to calculate the lift for any small-amplitude motion of a two-dimensional airfoil. And in 1941, Sears¹² used this result to obtain a simple expression, called the Sears function, for the fluctuating lift due to a frozen sinusoidal gust impinging on a fixed airfoil in an incompressible flow. The remainder of this section is concerned with Sears' problem and its subsequent generalizations.

Incompressible flows. Consider a stationary (nonmoving) thin body subject to a small-amplitude gust with velocity \mathbf{u}_∞ . Since the amplitude of the incident disturbance and the thickness of the body are now both small, we anticipate that the deviation \mathbf{u} of the velocity \mathbf{v} from the mean velocity $\hat{\mathbf{i}}U_r$ will also be small. Hence, \mathbf{u} will be determined (to the first order) by linear equations. We shall also suppose that the flow is inviscid and incompressible. Then substituting

$$\mathbf{v} = \hat{\mathbf{i}}U_r + \mathbf{u} \quad (3.38)$$

into the inviscid continuity and momentum Eqs. (1.1) and (1.2) (with $\rho = \rho_0$ and the source terms omitted) and neglecting terms involving squares of \mathbf{u} , yields

$$\frac{\partial \mathbf{u}}{\partial \tau} + U_r \frac{\partial \mathbf{u}}{\partial y_1} = -\frac{1}{\rho_0} \nabla p \quad (3.39)$$

and

$$\nabla \cdot \mathbf{u} = 0 \quad (3.40)$$

It is now convenient to put

$$\mathbf{u} = \mathbf{u}_\infty + \mathbf{w} \quad (3.41)$$

where \mathbf{u}_∞ can be thought of as the velocity fluctuation that would exist if the body were not present. Then \mathbf{u} will approach the nonuniform incident flow as $|\mathbf{y}| \rightarrow \infty$ only if we insist that

$$\mathbf{w} \rightarrow 0 \quad \text{as } |\mathbf{y}| \rightarrow \infty \quad (3.42)$$

Consequently, it is natural to require that \mathbf{u}_∞ itself satisfy the continuity equation

$$\nabla \cdot \mathbf{u}_\infty = 0 \quad (3.43)$$

And since \mathbf{u}_∞ is assumed to be steady in a coordinate system that moves with the mean flow, it must also satisfy the relation

$$\frac{\partial \mathbf{u}_\infty}{\partial \tau} + U_r \frac{\partial \mathbf{u}_\infty}{\partial y_1} = 0 \quad (3.44)$$

Hence, it follows from Eqs. (3.39) to (3.44) that \mathbf{w} satisfies the same equations as \mathbf{u} , namely,

$$\frac{\partial \mathbf{w}}{\partial \tau} + U_r \frac{\partial \mathbf{w}}{\partial y_1} = -\frac{1}{\rho_0} \nabla p \quad (3.45)$$

$$\nabla \cdot \mathbf{w} = 0 \quad (3.46)$$

The boundary condition (3.42) implies that $\nabla \times \mathbf{w} \rightarrow 0$ as $|\mathbf{y}| \rightarrow \infty$ while taking the curl of Eq. (3.45) yields

$$\left(\frac{\partial}{\partial \tau} + U_r \frac{\partial}{\partial y_1} \right) \nabla \times \mathbf{w} = 0$$

Consequently,

$$\nabla \times \mathbf{w} = 0 \quad (3.47)$$

everywhere except perhaps across a trailing vortex sheet (see p. 133 below).

In an inviscid flow it is appropriate to require that only the normal component of the velocity vanish at the surface of the body. Hence, it follows from Eqs. (3.38) and (3.41) that we must put

$$n_1 U_r + \hat{\mathbf{n}} \cdot \mathbf{u}_\infty = -\hat{\mathbf{n}} \cdot \mathbf{w} \quad \text{for } \mathbf{y} \text{ on } S \quad (3.48)$$

where S denotes the surface of the body and $\hat{\mathbf{n}} = \{n_1, n_2, n_3\}$ is its unit normal. It is evident from Eqs. (3.42), (3.45), (3.46), and (3.48) that $\hat{\mathbf{i}}U_r + \mathbf{w}$ is identical to the velocity field generated by a thin body undulating normal to itself with velocity $-\hat{\mathbf{n}} \cdot \mathbf{u}_\infty$.

Since the body is thin, with only small camber and angle of attack, we can assume that it lies very nearly in the y_1 - y_3 plane and that the boundary condition (3.48) on its surface S can be "transferred" to this plane. In fact, the equation of S can be written as $[y_2 - \varepsilon f(y_1, y_3)]^2 = \varepsilon^2 g(y_1, y_3)$ where $g(y_1, y_3) > 0$ on the projection of the body on the y_1 - y_3 plane, $g = 0$ corresponds to the edge of the body, and ε is a small parameter of the order of $|\mathbf{u}_\infty|$. The relation $y_2 = \varepsilon f(y_1, y_3)$ determines the mean position of the surface of the body, and $\varepsilon \sqrt{g}$ determines its thickness distribution. Then the right side of Eq. (3.48) can be written as $-\hat{\mathbf{n}} \cdot \mathbf{w}(y_1, \varepsilon[f + g^{1/2}], y_3)$ for $y_2 = \varepsilon[f + g^{1/2}]$. Hence, the small parameter ε will appear explicitly in the argument of a quantity which is itself assumed to be of order ε . The boundary condition (3.48) will therefore introduce higher order terms that unnecessarily complicate the results. But whenever \mathbf{w} and \mathbf{u}_∞ possess Taylor series expansions at $y_2 = 0$ the right side of Eq. (3.48) can be written as $-\hat{\mathbf{n}} \cdot \mathbf{w}(y_1, 0, y_3) - \varepsilon(f + g^{1/2})\hat{\mathbf{n}} \cdot \partial \mathbf{w} / \partial y_2 + O(\varepsilon^3)$ while the left side can be expressed in a similar form. Transferring the boundary condition (3.48) to the $y_1 - y_3$ plane therefore introduces an error that is no worse than that created by linearizing the differential equations. On the other hand the normal vector $\hat{\mathbf{n}}$ is to within first-order terms in ε

$$\left\{ -\varepsilon \left(\frac{\partial f}{\partial y_1} \pm \frac{\partial g^{1/2}}{\partial y_1} \right), 1, -\varepsilon \left(\frac{\partial f}{\partial y_3} \pm \frac{\partial g^{1/2}}{\partial y_3} \right) \right\} \quad (3.49)$$

where the upper sign refers to the upper side of the body and the lower sign to the lower side. Since \mathbf{u}_∞ is assumed to be of the same order as the thickness parameter ε , the boundary condition (3.48) is to within terms of order ε

$$-\varepsilon \left(\frac{\partial f}{\partial y_1} \pm \frac{1}{2g^{1/2}} \frac{\partial g}{\partial y_1} \right) U_r + v_\infty = -w_2 \quad \text{for } y_2 = \pm 0 \quad \text{and } g > 0 \quad (3.50)$$

which shows that \mathbf{w} , and as a result the fluctuating lift, is only affected by the upwash component v_∞ of the gust. Notice that the first term on the left side of this equation, which contains the effects of thickness, camber, and angle of attack, is independent of time while the second term, which depends on time, is uninfluenced by these geometric effects. Consequently, it follows from the linearity of the problem that its solution (and, as a result, the force acting on the body) will also consist of a time-independent term which involves the effects of thickness, camber, and angle of attack and a time-dependent term which is independent of these effects. Thus, in the linearized approximation the effects of thickness, camber, and angle of attack contribute only to the steady force acting on the body and make no contribution to the unsteady component. This means that, as long as we are only interested in calculating the unsteady forces, nothing will be lost if the body is replaced by an equivalent flat plate with the same y_1 - y_3 projection. Correspondingly,

the boundary condition (3.50) becomes

$$w_2 = -v_\infty \quad \text{for } y_2 = 0 \quad \text{and } g > 0 \quad (3.51)$$

We have assumed in this section that the flow is governed by the inviscid equations of motion. Nevertheless, the effects of viscosity cannot be entirely neglected. To understand the reason for this, consider (for definiteness) a two-dimensional sharp-edged airfoil impulsively accelerated to a uniform velocity from a state of rest. Initially, the action of viscosity will cause a thin boundary layer to form along the surface of the body while the rest of the flow remains inviscid and irrotational. The high velocity at the sharp trailing edges reduces the pressure at this point, while the pressure at the rear stagnation point remains high. The resultant adverse pressure gradient causes the boundary layer to separate and form a concentrated vortex, as shown in Fig. 3.7(b). But the velocity induced by this vortex sets up a circulatory flow about the airfoil that eliminates the pressure gradient by shifting the rear stagnation point to the trailing edge. Then, as shown in Fig. 3.7(c), the vortex separates from the trailing edge and is swept downstream to infinity. The rear stagnation point remains at the trailing edge, and no further large changes in pressure occur in this region. This behavior is known as the Kutta-Joukowski condition.

A similar process takes place in a periodic flow. However, a new trailing vortex is shed every time the lift, and hence the circulation around the airfoil, changes. Thus, there is a continuous trail of vorticity forming a vortex wake that must be accounted for in the analysis. Its strength is determined by requiring that the Kutta-Joukowski condition be instantaneously satisfied at the trailing edge. Moreover, it can be shown that the normal velocity and pressure must be continuous across this wake which, in the context of the linear theory, can be assured to lie in the plane of the airfoil. The Kutta condition is usually imposed in practice by

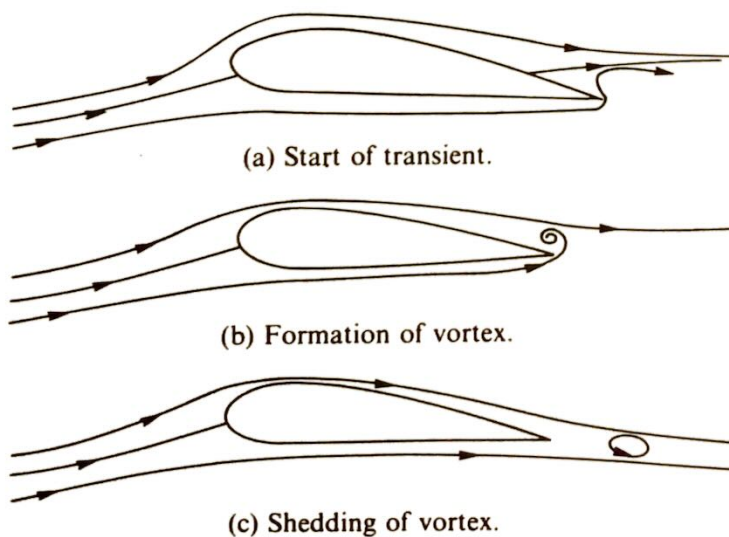


Fig. 3.7 Initiation of flow about an airfoil starting from rest.

requiring that the pressure be continuous at the trailing edge. But in view of the pressure continuity across the wake, one can alternatively require that there be no pressure jump across the airfoil at the trailing edge.

Since the incident gust velocity \mathbf{u}_∞ is independent of time when measured in a coordinate system

$$\mathbf{y}' = \mathbf{y} - \hat{\mathbf{i}} U_r \tau \quad (3.52)$$

that moves with the flow, we can write

$$\mathbf{u}_\infty = \int \mathbf{a}(\mathbf{k}) e^{i\mathbf{k} \cdot \mathbf{y}'} d\mathbf{k} = \int \mathbf{a}(\mathbf{k}) e^{i(\mathbf{k} \cdot \mathbf{y} - k_1 U_r \tau)} d\mathbf{k} \quad (3.53)$$

which shows that \mathbf{u}_∞ can be represented as a superposition of plane waves. This result will not satisfy Eq. (3.43) unless

$$\mathbf{a} \cdot \mathbf{k} = 0 \quad (3.54)$$

for all \mathbf{k} , which implies that the amplitudes of the waves must be perpendicular to their propagation directions (i.e., they are transverse waves).

Since \mathbf{w} is determined by linear equations and boundary conditions, the solution for any disturbance velocity \mathbf{u}_∞ can be found simply by superposing solutions to the problem for an incident harmonic gust

$$\mathbf{u}_\infty = \mathbf{a} e^{i(\mathbf{k} \cdot \mathbf{y} - k_1 U_r \tau)} \quad (3.55)$$

Hence, it is only necessary to consider an incident disturbance of this type. The boundary condition (3.51) then becomes

$$-w_2 = a_2 e^{i(k_1 y_1 + k_3 y_3 - k_1 U_r \tau)} \quad \text{for } y_2 = 0; g > 0 \quad (3.56)$$

The velocity \mathbf{w} can now be found by solving Eqs. (3.46) and (3.47) subject to the boundary conditions (3.42) and (3.56). But in order to satisfy the Kutta-Joukowski condition, the tangential component of \mathbf{w} will, in general, have to be discontinuous across the trailing vortex sheet. It is also necessary to allow the velocity to possess a singularity at the leading edge. However, the actual calculation of such a solution is, in general, a difficult task and the best that can usually be done is to reduce the problem to one of solving an integral equation.[†] Nevertheless, it is possible to obtain a simple closed form solution when both the airfoil and the gust are two dimensional (corresponding to $k_3 = 0$ and g independent of y_3 in Eq. (3.56)).

This was first done by Sears.¹² His solution shows that the pressure jump across the plate (which is assumed to lie between $-c/2$ and $c/2$ on the y_1 axis) is given by

$$\longrightarrow \Delta p = -2a_2 \rho_0 U_r e^{-ik_1 U_r \tau} S(\sigma_1) \sqrt{\frac{(c/2) - y_1}{(c/2) + y_1}} \quad (3.57)$$

[†] Fairly efficient collocation techniques have been developed to solve these equations.

where

$$S(\sigma_1) = \frac{1}{-i\sigma_1[K_0(-i\sigma_1) + K_1(-i\sigma_1)]} \quad (3.58)$$

is called *Sears' function*, K_0 and K_1 are modified Bessel functions, and

$$\sigma_1 \equiv \frac{k_1 c}{2} \quad (3.59)$$

is the *reduced frequency*. The latter quantity is related to the frequency $\omega = k_1 U_r$ of the fluctuating force by

$$\sigma_1 = \frac{\omega c}{2U_r} \quad (3.60)$$

The variation in pressure along the airfoil is determined by the factor

$$\sqrt{\frac{(c/2) - y_1}{(c/2) + y_1}} \quad (3.61)$$

which also describes the pressure distribution on a flat plate at a small angle of attack to a steady flow. Finally, taking moments of Eq. (3.57) we find that *the fluctuating lift always acts through the quarter-chord point* while integrating this equation over the surface of the plate yields an expression for the total fluctuating force per unit span acting on the airfoil. This force, F_2 , is perpendicular to the flow and is given by

$$F_2 = \pi a_2 \rho_0 U_r c e^{-ik_1 U_r \tau} S(\sigma_1) \quad (3.62)$$

By using the asymptotic expansions for the modified Bessel functions (Ref. 13), it can easily be shown that

$$S(\sigma_1) \sim \frac{\exp[-i(\sigma_1 - \pi/4)]}{\sqrt{2\pi\sigma_1}} \quad \text{as } \sigma_1 \rightarrow \infty \quad (3.63)$$

which implies that an airfoil should be unaffected by gusts of sufficiently high reduced frequency.

On the other hand, $S(\sigma_1) \rightarrow 1$ as $\sigma_1 \rightarrow 0$ so that Eq. (3.62) reduces to the quasi-steady approximation (3.37) at low reduced frequencies. In fact, von Kármán and Sears¹¹ showed that the difference between Eq. (3.62) and the quasi-steady approximation (3.37) is equal to the lift resulting from the "apparent mass" effects† plus the lift generated by the vorticity in the wake acting back on the body. The former effect occurs whenever a body undergoes an unsteady motion in an inviscid fluid, even when no wake is present.

† That is, the force required to accelerate the surrounding fluid.

Sears' function can be approximated to within a few percent over most of its effective range by

$$S(\sigma_1) \simeq \frac{\exp \left\{ -i\sigma_1 \left[1 - \frac{\pi^2}{2(1 + 2\pi\sigma_1)} \right] \right\}}{\sqrt{1 + 2\pi\sigma_1}} \quad \text{for } \sigma_1 \geq 0 \quad (3.64)$$

Notice that this result approaches the same high-frequency limit as the exact formula (3.58). The approximation for the amplitude was first suggested by Liepmann,¹⁴ and the approximation for the phase was suggested by Geising, Stahl, and Rodden.¹⁵

At high frequencies ($\omega c/2c_0 = U_r\sigma_1/c_0 > 1$) the time c/c_0 for an acoustic disturbance to cross the chord is no longer short compared with the period of oscillation $2\pi/\omega$. Hence we can no longer assume that c_0 is infinite and the fluid cannot be considered incompressible even when $U_r \rightarrow 0$. The Sears' function, therefore, cannot be used to calculate the lift at these frequencies. But even at low frequencies there has been surprisingly little experimental verification of the validity of Eq. (3.62). However, low-frequency ($\sigma_1 < 1$) oscillating airfoil data collected by Acum¹⁶ show discrepancies of the order of 10 to 20 percent when compared with the Theodorsen function which is the oscillating airfoil counterpart of Sears' function.

We have seen that the linearized approximation to the unsteady lift is completely unaffected by the angle of attack, camber, and thickness of the airfoil and is influenced only by the upwash component a_2 of the incident gust (and not its chordwise component a_1). To account for the effects of these quantities, it is necessary to carry the analysis to second order. Horlock¹⁷ has developed a theory that includes some of the effects of angle of attack while Neumann and Yeh¹⁸ use a similar approach to account for camber effects. However, these theories are incomplete in that they do not account for all of the coupling effects. A complete second order theory that includes all of the coupling terms has recently been developed by Goldstein and Atassi.¹⁹ One of the new effects included in this approach is the distortion of the oncoming gust by the steady-state potential flow field about the airfoil. This distortion acts to cause significant variations in the wavelength of the oncoming vorticity wave while causing variations in both the amplitude and phase of its associated velocity field.

Equation (3.62) is only valid if the gust is two dimensional. However, the problem of a two-dimensional flat-plate airfoil subject to the full three-dimensional disturbance field (3.55), called an oblique gust, has also received considerable attention.

A simple approximate solution can be obtained by dividing the plate into a number of strips (parallel to the flow) and treating each strip as if it were a two-dimensional plate subject to a fictitious two-dimensional gust whose amplitude is equal to the actual amplitude of the gust at that point. Thus, in the *strip theory* approximation, the fluctuating lift per unit

span is given by Eq. (3.62) with a_2 replaced by the local upwash velocity $a_2 e^{ik_3 y_3}$ to obtain

$$F_2 \simeq \pi a_2 \rho_0 U_r c e^{i(k_3 y_3 - k_1 U_r \tau)} S(\sigma_1) \quad (3.65)$$

It is usual to express the more exact solutions to this problem in terms of a response function $T(\sigma_1, \sigma_3)$ defined by†

$$F_2 = \pi \rho_0 U_r a_2 c e^{i(k_3 x_3 - k_1 U_r \tau)} T(\sigma_1, \sigma_3) \quad (3.66)$$

where $\sigma_i = k_i c/2$ for $i = 1, 3$.

Graham²⁰ arrived at an exact seminumerical solution for this quantity in the form of a series whose coefficients can be calculated successively. His result represents an improvement over the collocation procedures, which must be used for thin bodies of arbitrary shape. On the other hand, Filotas²¹ obtained an approximate expression for T that reduces to the approximation (3.64) to Sears' result when the gust is two dimensional and gives the correct high-frequency limit for an arbitrary gust. His result can be written as

$$T(\sigma_1, \sigma_3) \simeq \frac{\exp \left\{ -i\sigma_0 \left[\sin v - \frac{\pi v (1 + \frac{1}{2} \cos v)}{1 + 2\pi\sigma_0 (1 + \frac{1}{2} \cos v)} \right] \right\}}{[1 + \pi\sigma_0 (1 + \sin^2 v + \pi\sigma_0 \cos v)]^{1/2}} \quad (3.67)$$

where $v = \tan^{-1}(\sigma_1/\sigma_3)$ and $\sigma_0 = \sqrt{\sigma_1^2 + \sigma_3^2}$. Mugridge²² derived an approximate multiplicative correction $M(\sigma_1, \sigma_2)$ to the strip theory approximations (3.65). The amplitude of his correction factor, which is only valid for $\sigma_0 > 2$, is given by

$$|M(\sigma_1, \sigma_3)| = \frac{(\sigma_1^2 + 2/\pi^2)^{1/2}}{(\sigma_0^2 + 2/\pi^2)^{1/2}} \quad (3.68)$$

The center of lift resulting from an oblique gust does not remain fixed at the quarter-chord point as it does in the purely two-dimensional case. In fact, it approaches the leading edge when σ_0 is allowed to approach infinity with σ_1/σ_3 held fixed. This implies that the leading edge region should become progressively more important as a source of sound as the frequency increases.

Two-dimensional compressible flows. We have already indicated that compressibility effects will cause the Sears solution to become invalid whenever the product $(U_r/c_0)\sigma_1$ gets to be much above unity‡—even when the freestream Mach number U_r/c_0 is small. However, it is well known that (as in the case of an oblique gust) the fluctuating lift in a real com-

† Since the solution is coupled to the disturbance field only through the boundary condition (3.58), only the longitudinal and transverse components, k_1 and k_3 , of the wave number influence the fluctuating lift.

‡ Notice that this is also the frequency where the quadrupole terms can become equal to the dipoles and the acoustic sources can become noncompact.

pressible flow does not act through the quarter-chord point as it does in an incompressible flow, but rather moves toward the leading edge as the frequency increases. Hence, the trailing-edge region ought to be relatively unimportant at the higher reduced frequencies, and, as a result, the fluctuating lift on the airfoil should be the same as it would be on a long plate that extends downstream to infinity (i.e., a semi-infinite plate).

A detailed discussion of compressibility effects is deferred to Chap. 5 where it is shown that it is still appropriate to use the decompositions (3.38) and (3.41) for the velocity field with the gust velocity defined by Eq. (3.55). Then, it is not hard to show, by using methods similar to those described in Chap. 5, that the fluctuating pressure difference across a semi-infinite flat plate due to a gust of this type is given by

$$\Delta p(y_1) = \frac{-i2\rho_0 U_r a_2 e^{-i\sigma_1}}{[\pi i \sigma_1 (1 + M_r)(1 + 2y_1/c)]^{1/2}} e^{[iM_r \sigma_1 / (1 + M_r)](2y_1/c) + 1}$$

where

$$M_r \equiv \frac{U_r}{c_0} \quad (3.69)$$

is the free-stream Mach number and the leading edge is assumed to be at $y_1 = -c/2$. This result can be integrated over the surface of the airfoil to show that the net fluctuating force is given by†

$$F_2 = \pi a_2 \rho_0 U_r c e^{-ik_1 U_r \tau} S_c(\sigma_1, M_r)$$

where

$$S_c(\sigma_1, M_r) \equiv \frac{e^{-i\sigma_1}}{\sigma_1 \pi} \sqrt{\frac{i2}{M_r}} \mathcal{F}\left(\sqrt{\frac{4\sigma_1 M_r}{\pi(1 + M_r)}}\right) \quad (3.70)$$

is the high-frequency approximation to the compressible Sears function and

$$\mathcal{F}(x) \equiv \int_0^x e^{i(\pi/2)\xi^2} d\xi$$

is the complex Fresnel integral. This formula is accurate to within about 10 percent wherever $(M_r \sigma_1)/(1 - M_r^2)$ is greater than unity.

By using the asymptotic expansion for the Fresnel integral, it is easy to show that

$$S_c \sim \frac{1}{\pi \sigma_1} \frac{e^{-i[\sigma_1 - (\pi/2)]}}{\sqrt{M_r}} \quad \text{as } \sigma_1 \rightarrow \infty$$

Hence, we can conclude from the corresponding incompressible result (3.63) that compressibility effects increase the high-frequency decay rate of the

† This solution is given by Landahl (Ref. 23, pp. 27–29) for an arbitrary upwash velocity.

response function. However, it is shown by Goldstein and Atassi¹⁹ that the effects of thickness, angle of attack and camber become important enough at high frequencies to invalidate the linearized theory.

Amiet²⁵ extended an analysis initiated by Osborne²⁴ to obtain the following low-frequency approximation to the compressible Sears function.

$$S_c(\sigma_1, M_r) = \frac{S(\sigma_1/\beta_r^2)}{\beta_r} [J_0(M_r^2 \sigma_1/\beta_r^2) + iJ_1(M_r^2 \sigma_1/\beta_r^2)] e^{-i\sigma_1 f(M_r)/\beta_r^2} \quad (3.71)$$

where S still denotes the ordinary Sears function,

$$\beta_r \equiv \sqrt{1 - M_r^2}$$

$$f(M_r) \equiv (1 - \beta_r) \ln M_r + \beta_r \ln(1 + \beta_r) - \ln 2$$

and J_0 and J_1 are Bessel functions. This result appears to be quite accurate in the range $\sigma_1 M_r/\beta_r^2 < 1$ where Eq. (3.70) is invalid.

The General case. The compressible response function \mathcal{G} for an oblique gust incident on an airfoil of infinite span is usually defined by

$$F_2 = \pi a_2 \rho_0 U_{rc} e^{i(k_3 y_3 - k_1 U_{rc} \tau)} \mathcal{G}(k_1, k_3, M_r) \quad (3.72)$$

Then since

$$\mathcal{G}(k_1, 0, 0) = S(\sigma_1) \quad (3.73a)$$

$$\mathcal{G}(k_1, 0, M_r) = S_c(\sigma_1, M_r) \quad (3.73b)$$

$$\mathcal{G}(k_1, k_3, 0) = T(\sigma_1, \sigma_3) \quad (3.73c)$$

the response functions defined in the preceding sections can always be obtained as special cases of \mathcal{G} . Surprisingly, the converse of this statement is also true. Thus, Graham²⁶ has shown that there is a simple relation between $\mathcal{G}(k_1, k_3, M_r)$ and the three-dimensional incompressible response function $T(\sigma_1, \sigma_2)$ when the intersection of the gust and the airfoil moves subsonically relative to the fluid and that there is a simple relation between $\mathcal{G}(k_1, k_3, M_r)$ and the two-dimensional compressible response function $S_c(\sigma_1, M_r)$ when this point moves supersonically.

3.5 APPLICATIONS OF THE FFWCS WILLIAMS-HAWKINGS EQUATION

In the remainder of this chapter the general results obtained in the preceding sections will be applied to specific flows which either exemplify certain fundamental aeroacoustic phenomena or are of technological importance in their own right. This section is concerned with flows whose acoustic behavior can be analyzed by applying Eq. (3.23), while the next section is devoted to those that require the full analogy Eq. (3.6).

3.5.1 Sound Emission from a Thin Strut in a Turbulent Flow

We shall first consider a long strut or airfoil fixed in a turbulent (time stationary) flow of finite lateral extent (as it is in a jet or open acoustic wind tunnel). This problem is of technological interest because it relates to the broadband sound emission from flap segments under the wings of externally blown flap aircraft and from internal support struts and splitters in aircraft engines as well as from propellers and aircraft engine fans. The configuration is illustrated in Fig. 3.8.

Since the fluctuating lift will usually be much larger than the fluctuating drag, it is only necessary to consider the y_2 -component of the unsteady force. We would like to use the simplified Eq. (3.29) to calculate the sound field produced by this force but Eq. (3.33) shows that this result will not apply at reasonable Mach numbers unless the characteristic dimension L of the body is smaller than the eddy size. However, the span b of the airfoil will usually be too long for this to occur. On the other hand, Eq. (3.29) can be used to calculate the sound emitted per unit span of any airfoil whose chord c is sufficiently small and, since the problem is linear, the results can be summed to obtain the total sound emission. To this end we write Eq. (3.29) in the form

$$\rho'(\mathbf{x} | y_3) \sim \frac{-x_2}{4\pi c_0^3 x^2} \frac{\partial F_2(t - R/c_0 | y_3)}{\partial t}$$

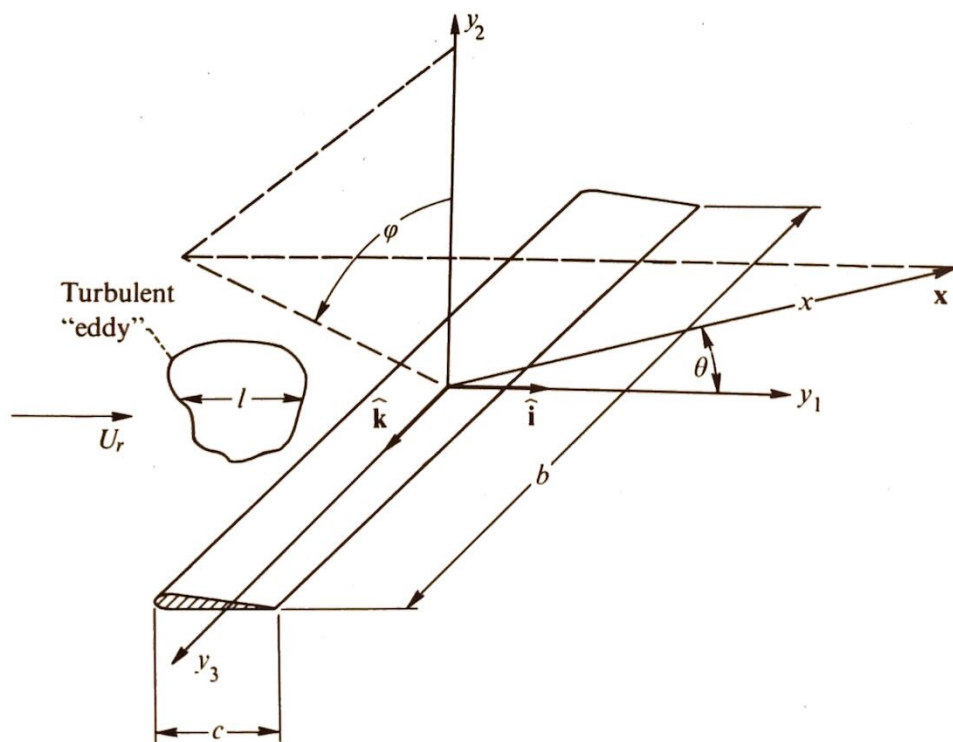


Fig. 3.8 Coordinate system for strut.

where

$$R = |\mathbf{x} - \mathbf{k}y_3| = x - \frac{x_3 y_3}{x} + O(x^{-1})$$

is the distance between the observation point and the point along the strut from which the sound is emitted and $\rho'(\mathbf{x}|y_3)$ is the density fluctuation at \mathbf{x} due to a unit length of strut at y_3 . Hence,

$$\rho'(\mathbf{x}) = \int_{-b/2}^{b/2} \rho'(\mathbf{x}|y_3) dy_3$$

The normalized pressure autocorrelation function Γ defined in Eq. (1.94) is then given by

$$\Gamma(\mathbf{x}, \tau) = \frac{x_2^2}{16\pi^2 c_0^3 \rho_0 x^4} \int_{-b/2}^{b/2} \int_{-b/2}^{b/2} \frac{\partial F_2(t'|y'_3)}{\partial t} \frac{\partial F_2(t''|y''_3)}{\partial t} dy'_3 dy''_3 \quad (3.74)$$

where

$$t' = t + \frac{x_3}{c_0 x} y'_3$$

$$t'' = t + \tau + \frac{x_3}{c_0 x} y''_3$$

This result could also have been obtained from the dipole term in Eq. (3.20) by neglecting the chordwise retarded-time variation while retaining the spanwise variation. It represents the sound that would be emitted by a spanwise line of point dipoles whose strengths are adjusted to account for the total emission over the chord.

By using the manipulations described in the appendix of Chap. 2 and the fact that the correlation is independent of translations in time (since the flow is time stationary), we can put Eq. (3.74) in the form

$$\Gamma(\mathbf{x}, \tau) = \frac{-x_2^2}{16\pi^2 c_0^3 \rho_0 x^4} \frac{\partial^2}{\partial \tau^2} \int_{-b/2}^{b/2} \int_{-b/2}^{b/2} \overline{F_2(t|y'_3) F_2(\tau_0|y''_3)} dy'_3 dy''_3 \quad (3.75)$$

where

$$\tau_0 = t + \tau + \frac{x_3}{x c_0} (y''_3 - y'_3)$$

It is convenient to use the separation vector $\eta_3 = y''_3 - y'_3$ as a new variable of integration and write the double integral as

$$\int_{-b/2}^{b/2} \int_{-(b/2)-y_3}^{(b/2)-y_3} \overline{F_2(t|y_3) F_2(\tau_0|y_3 + \eta_3)} d\eta_3 dy_3 \quad (3.76)$$

But since the correlation length of $\overline{F_2(t|y_3) F_2(\tau_0|y_3 + \eta_3)}$ is of the same order as the transverse turbulence correlation length, which we shall suppose

is much smaller than the span b , the length η_3 over which the integrand in Eq. (3.76) is nonzero should also be small compared to b . The limits of integration in the inner integral can therefore be taken as $-\infty$ and ∞ so that Eq. (3.75) becomes

$$\Gamma(\mathbf{x}, \tau) = \frac{-x_2^2}{16\pi^2 c_0^3 \rho_0 x^4} \frac{\partial^2}{\partial \tau^2} \int_{-b/2}^{b/2} \int_{-\infty}^{\infty} \overline{F_2(t|y_3) F_2(\tau_0|y_3 + \eta_3)} d\eta_3 dy_3 \quad (3.77)$$

One might at this point be tempted to neglect the retarded-time variations that appear in τ_0 by arguing, as we did in Chap. 2, that the decay time of the turbulence is large compared with its correlation length. But since the time is now measured relative to the fixed frame, its characteristic value can be much shorter than the time associated with the oscillations of the eddies.

Since the intensity spectrum \bar{I}_ω is the Fourier transform of Γ , Eq. (3.77) implies that

$$\bar{I}_\omega(\mathbf{x}) = \frac{\omega^2}{8\pi c_0^3 \rho_0} \frac{x_2^2}{x^4} \int_{-b/2}^{b/2} H_{22}\left(y_3; \frac{\omega x_3}{c_0 x}, \omega\right) dy_3 \quad (3.78)$$

where

$$H_{22}(y_3; k_3, \omega) \equiv \frac{1}{(2\pi)^2} \int_{-\infty}^{\infty} \int_{-\infty}^{\infty} e^{i(\omega\tau - k_3\eta_3)} \overline{F_2(y_3, t) F_2(y_3 + \eta_3, t + \tau)} d\tau d\eta_3$$

is the power spectral density of the fluctuating lift force on the body.

We again suppose that the turbulence is effectively frozen during the time it takes an eddy to traverse the strut. Then, as long as U_r is relatively constant, the fluctuating lift force resulting from a single Fourier component

$$a_2(\mathbf{k}) e^{i\mathbf{k} \cdot \mathbf{y}'}$$

of the turbulence upwash velocity will be given by Eq. (3.72). If, on the other hand, the turbulence is also relatively homogeneous, the moving-frame turbulence correlation

$$\mathcal{R}_{22}(\eta_0 - \hat{\mathbf{i}}U_r\tau) \equiv \overline{u_2(\mathbf{y} - \hat{\mathbf{i}}U_r t) u_2(\mathbf{y} + \eta_0 - \hat{\mathbf{i}}U_r(t + \tau))}$$

will depend only on the indicated argument, and, as shown in Appendix 1.A, will be related to the moving-axis spectral density $\Phi_{22}(\mathbf{k})$ of the upwash velocity by

$$\mathcal{R}_{22}(\eta_0 - \hat{\mathbf{i}}U_\infty\tau) = \iiint e^{i\mathbf{k} \cdot (\eta_0 - \hat{\mathbf{i}}U_r\tau)} \Phi_{22}(\mathbf{k}) d\mathbf{k} \quad (3.79)$$

These results are used in Appendix 3.B to show that the lift power spectral density is related to Φ_{22} by

$$H_{22}(y_3; k_3, \omega) = \pi^2 \rho_0^2 c^2 U_r \left| \mathcal{G}\left(\frac{\omega}{U_r}, k_3, M_r\right) \right|^2 \int_{-\infty}^{\infty} \Phi_{22}\left(\frac{\omega}{U_r}, k_2, k_3\right) dk_2$$

Hence, Eq. (3.78) becomes

$$\begin{aligned}\bar{I}_\omega(\mathbf{x}) &= \bar{I}_\omega(x, \theta, \varphi) \\ &= \frac{U_r b \omega^2 \pi \rho_0 c^2 \sin^2 \theta \cos^2 \varphi}{8 c_0^3 x^2} \left| \mathcal{G}\left(\frac{\omega}{U_r}, \frac{\omega}{c_0} \sin \theta \sin \varphi, M_r\right) \right|^2 \\ &\quad \times \int_{-\infty}^{\infty} \Phi_{22}\left(\frac{\omega}{U_r}, k_2, \frac{\omega}{c_0} \sin \theta \sin \varphi\right) dk_2\end{aligned}\quad (3.80)$$

where we have introduced the spherical coordinates θ and φ defined in Fig. 3.8.

It remains to determine the spectral density function Φ_{22} . This can be accomplished by assuming an idealized model for the turbulence. Thus, the isotropic turbulence spectral density tensor Φ_{ij} can be written as²⁷

$$\Phi_{ij} = \frac{E(k)}{4\pi k^2} \left(\delta_{ij} - \frac{k_i k_j}{k^2} \right)$$

where

$$k \equiv \sqrt{k_1^2 + k_2^2 + k_3^2}$$

Hence, the upwash spectral density becomes

$$\Phi_{22} = \frac{E(k)}{4\pi k^4} (k_1^2 + k_3^2)$$

Then if it is also assumed that the moving-frame longitudinal correlation function $\mathcal{R}_{22}(\mathbf{j}\xi_2)$ is given by

$$\mathcal{R}_{22}(\mathbf{j}\xi_2) = \overline{u_2^2} e^{-\xi_2/l}$$

it can be shown²⁷ that

$$E(k) = \frac{\overline{u_2^2} 8k^4}{\pi l (l^{-2} + k^2)^3}$$

and as a result that

$$\Phi_{22} = \frac{2\overline{u_2^2}}{\pi^2 l} \frac{k_1^2 + k_3^2}{(l^{-2} + k^2)^3}$$

Substituting this into Eq. (3.80) and performing the integration now yields

$$\begin{aligned}\bar{I}_\omega(x, \theta, \varphi) &= \frac{3b\rho_0\overline{u_2^2}}{32} \left(\frac{c}{x}\right)^2 \frac{M_r^3 \sin^2 \theta \cos^2 \varphi h^2 \sigma_1^2}{\alpha_0(\alpha_0^{-2} + h^2)^{5/2}} \\ &\quad \times \left| \mathcal{G}\left(\frac{2\sigma_1}{c}, \frac{2\sigma_1}{c} M_r \sin \theta \sin \varphi, M_r\right) \right|^2\end{aligned}$$

where the reduced frequency σ_1 and the free-stream Mach number M_r are defined by Eqs. (3.60) and (3.69), respectively, $h^2 \equiv \sigma_1^2(1 + M_r^2 \sin^2 \theta \sin^2 \varphi)$ and, $\alpha_0 \equiv 2l/c$.

It follows from Eq. (3.73b) that

$$\bar{I}_\omega(x, \theta, 0) = \frac{3b\rho_0\bar{u}_2^2}{32} \left(\frac{c}{x}\right)^2 \frac{M_r^3 \sin^2 \theta \sigma_1^4}{\alpha_0(\alpha_0^{-2} + \sigma_1^2)^{5/2}} |S_c(\sigma_1, M_r)|^2$$

which shows that the sound field in the plane perpendicular to the strut is completely determined by the two-dimensional response function. This equation holds at the point $\theta = \pi/2$ even when the frequency is too high for Eq. (3.29) to be valid (since the sound field at this angle is unaffected by variations in retarded time over the strut). When both the reduced frequency and Mach number are sufficiently small we can replace S_c by the approximation (3.64) to the incompressible Sears function to obtain†

$$\bar{I}_\omega(x, \theta, 0) = \frac{3b\rho_0\bar{u}_2^2}{32} \left(\frac{c}{x}\right)^2 \frac{M_r^3 \sin^2 \theta \sigma_1^4}{\alpha_0(\alpha_0^{-2} + \sigma_1^2)^{5/2}(1 + 2\pi\sigma_1)} \quad (3.81)$$

And, more generally, Mugridge's approximation (3.68) can be used to obtain

$$\bar{I}_\omega(\mathbf{x}) = \frac{3b\rho_0\bar{u}_2^2}{32} \left(\frac{c}{x}\right)^2 \frac{M_r^3 \sin^2 \theta \cos^2 \varphi h^2 \sigma_1^2}{\alpha_0(\alpha_0^{-2} + h^2)^{5/2}(1 + 2\pi\sigma_1)} \left(\frac{\sigma_1^2 + 2/\pi^2}{h^2 + 2/\pi^2}\right)$$

Equation (3.81) can easily be integrated over all frequencies to establish that the mean sound intensity in the plane perpendicular to the strut is given by

$$\bar{I}(x, \theta, 0) = \frac{3bc\rho_0\bar{u}_2^2 M_r^4 c_0}{16\pi x^2} A(\alpha) \sin^2 \theta \quad (3.82)$$

where

$$A(\alpha) \equiv \frac{\alpha}{(\alpha^2 + 1)^2} \left\{ \frac{1}{\sqrt{\alpha^2 + 1}} \ln \left[\frac{\alpha(\alpha + \sqrt{\alpha^2 + 1})}{\sqrt{\alpha^2 + 1} - 1} \right] + \alpha - 1 + \left(\frac{2\alpha - 1}{3} \right) (\alpha^2 + 1) \right\}$$

and

$$\alpha \equiv \frac{c\pi}{l}$$

Notice that $A(\alpha)$ becomes equal to $\frac{2}{3}$ at large values of α . In fact, $A(\alpha)$ remains within 10 percent of this value whenever α is greater than 2.

In order to verify this analysis, W. A. Olsen of the Lewis Research Center measured the sound emission for a long thin symmetrical strut in a turbulent jet. The strut was centered in the mixing region 4 diameters

† Notice that when M_r is not too large, the approximations made in replacing S_c by the incompressible Sears function S is consistent with basing the analysis on the approximate Eq. (3.29), which amounts to neglecting variations in retarded time along the chord.

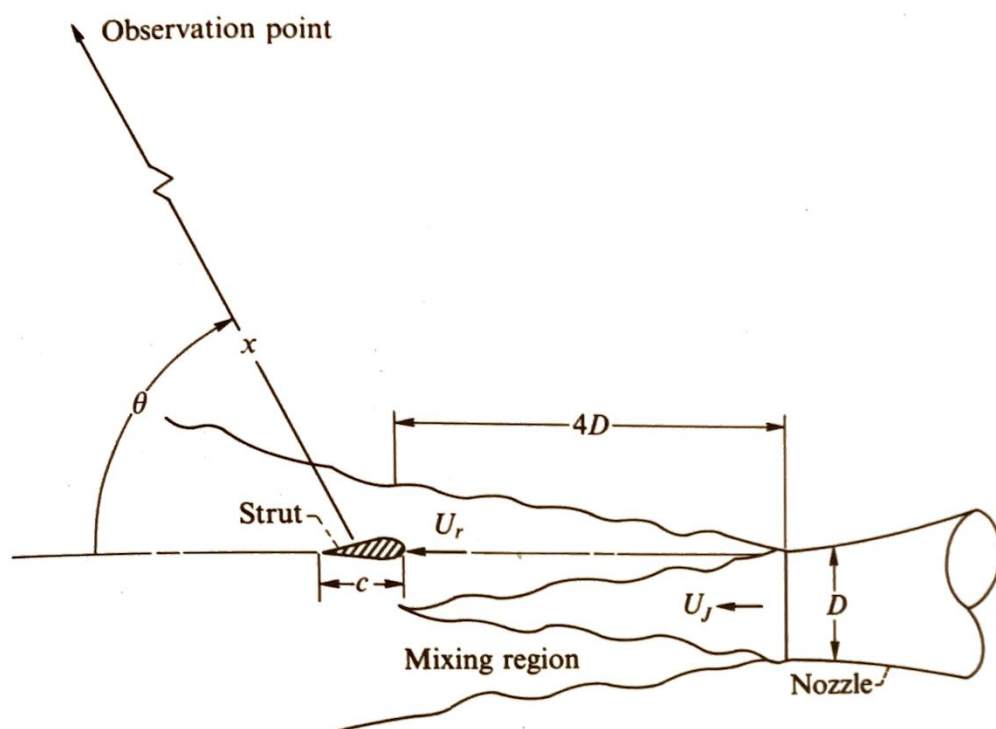


Fig. 3.9 Configuration of strut experiment. Nozzle diameter, D , 10 cm (4 in.); blade chord, $c = \frac{9}{32}D$; blade span, $b = \sqrt{3}D$; distance to observation point, x , 4.56 m (15 ft.).

downstream from the nozzle, as shown in Fig. 3.9. The geometric parameters that appear in the analysis are indicated on the figure. The aerodynamic parameters can be estimated from the measurements summarized in Sec. 2.5.1 (page 90). These results show that U_r should be related to the jet velocity U_J by $U_r = 0.62 U_J$ and that it is reasonable to take $l = (l_1 + l_2)/2$ and $(\overline{u_2^2})^{1/2} = 1.2u'_{\max}$. Then Eqs. (2.42) and (2.43) show that $l \simeq 0.3 D$ and $(\overline{u_2^2})^{1/2} \simeq 0.129 U_r$ (where D is the jet diameter). The theoretical directivity pattern, obtained by inserting these parameters into Eq. (3.82) is compared with Olsen's experiments[†] in Fig. 3.10. The agreement is seen to be quite good. (It should be noted that the actual level of these curves is determined by the analysis and not adjusted to fit the data.) Nevertheless, the restriction $c \ll l/M_r$ which we imposed on the analysis is only moderately well satisfied in the experiment. And the requirement that U_r be constant over the strut is not even approximately satisfied. Notice that the former restriction is most closely satisfied at the low velocities, where the agreement is best.

3.5.2 Aeolian Tones

The singing of the wind through telephone wires and leafless trees and the whistle of the tension rods of airplanes and the rigging of ships are but a

[†] The first combined analytical-experimental study of sound emission from solid bodies in jets was carried out by Sharland.²⁸

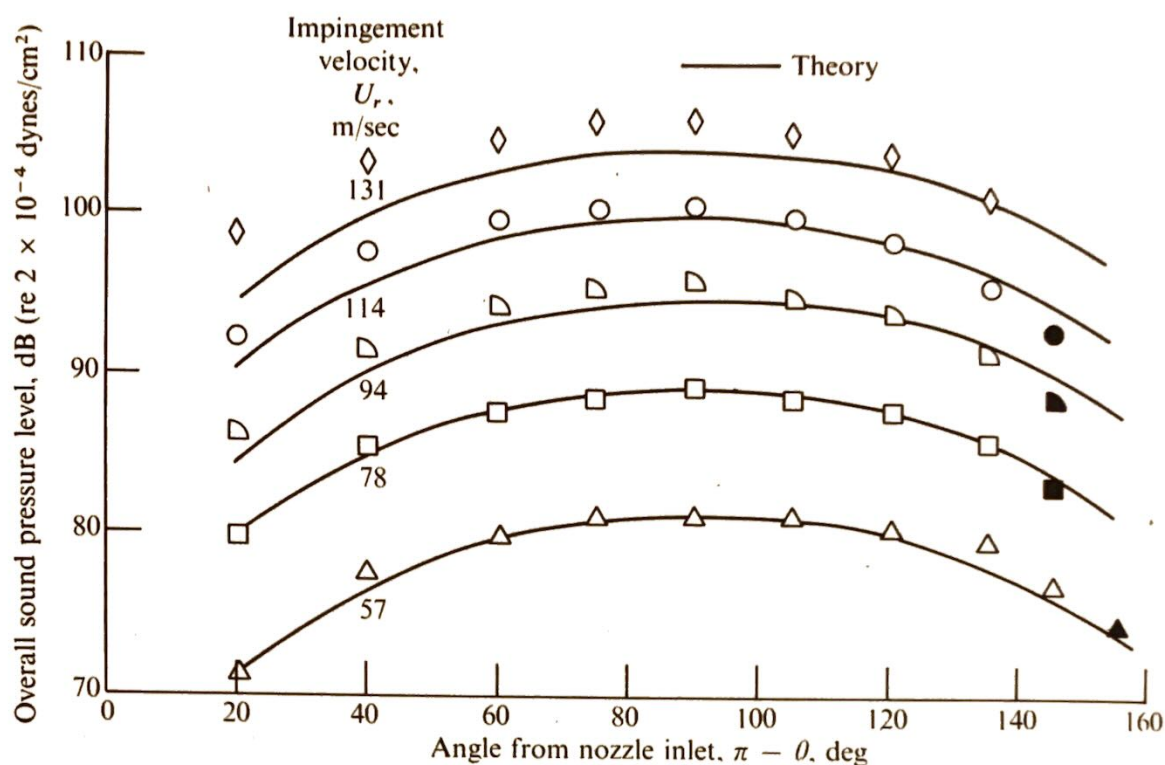


Fig. 3.10 Comparison of data and theory for strut experiment. Nozzle diameter, D , 10 cm (4 in.); ratio of distance to observation point to nozzle diameter, x/D , 4; φ , 0° .

few examples of Aeolian tones. They were first studied in 1878 by Strouhal, who was primarily concerned with their frequency.

The nature of the flow about a cylinder moving through a fluid with a subsonic velocity V^0 is largely determined by the Reynolds number $\rho_0 V^0 D / \mu$ based on the cylinder diameter D . When this quantity is sufficiently small the flow is steady and its main effect is to cause a drag force on the cylinder. However, the flow becomes unstable to small disturbances at a Reynolds number of about 50, and the wake starts to oscillate beginning at a point some distance downstream of the cylinder. Further increases in this parameter cause the oscillations in the wake to move upstream until, when the Reynolds number reaches about 60, the oscillations appear as the alternate shedding of lumps of fluid from the top and bottom of the cylinder. Most of the vorticity in the wake is now concentrated in these lumps, which move downstream in a regular array called the *Kármán vortex street*. This behavior persists up to a Reynolds number of about 10^4 . The periodic shedding of vorticity into the wake exerts a periodic lift force on the cylinder and, as was first recognized by von Kármán and Ruback, it is this oscillating force which is principally responsible for the Aeolian tones. The angular frequency Ω of the force is equal to the frequency of vortex shedding

$$\Omega = S_t \frac{2\pi V^0}{D} \quad (3.83)$$

where the Strouhal number S_t depends to some degree on the Reynolds number but remains close to 0.2. The vortex shedding also induces a periodic

drag force on the cylinder, which turns out to be quite small compared with the fluctuating lift, and will, therefore, be neglected in the following discussion.

If the cylinder is not rigidly supported, the fluctuating lift might cause it to oscillate and (see Eq. (3.28)) thereby introduce an additional sound source. However, the term Aeolian tones usually refers to the sound generated by the oscillating force itself, and we shall limit the discussion to the case where the cylinder is rigidly supported.

Thus, we consider a circular cylinder of length b and diameter D moving with a constant velocity V^0 in the x_1 -direction through a fluid at rest at infinity. The cylinder, whose long axis remains parallel to the x_3 -direction, carries along the ζ -coordinate system shown in Fig. 3.11.

As in the last section we let $F_2(t|\zeta_3)$ denote the fluctuating lift force per unit length acting on the cylinder so that its total lift $F_2(t)$ is given by

$$F_2(t) = \int_{-b/2}^{b/2} F_2(t|\zeta_3) d\zeta_3 \quad (3.84)$$

Phillips²⁹ showed that $F_2(t|\zeta_3)$ can be approximated by

$$F_2(t|\zeta_3) = \kappa \frac{\rho_0 (V^0)^2}{2} D e^{-i[\Omega t + \Phi(\zeta_3)]} \quad (3.85)$$

where κ is a numerical constant which lies somewhere between $\frac{1}{2}$ and 2. This variation is probably due to the sensitivity of the force to the amount of turbulence in the oncoming stream and the dependence of the phase Φ on the length of the cylinder and the geometry of the flow system. The

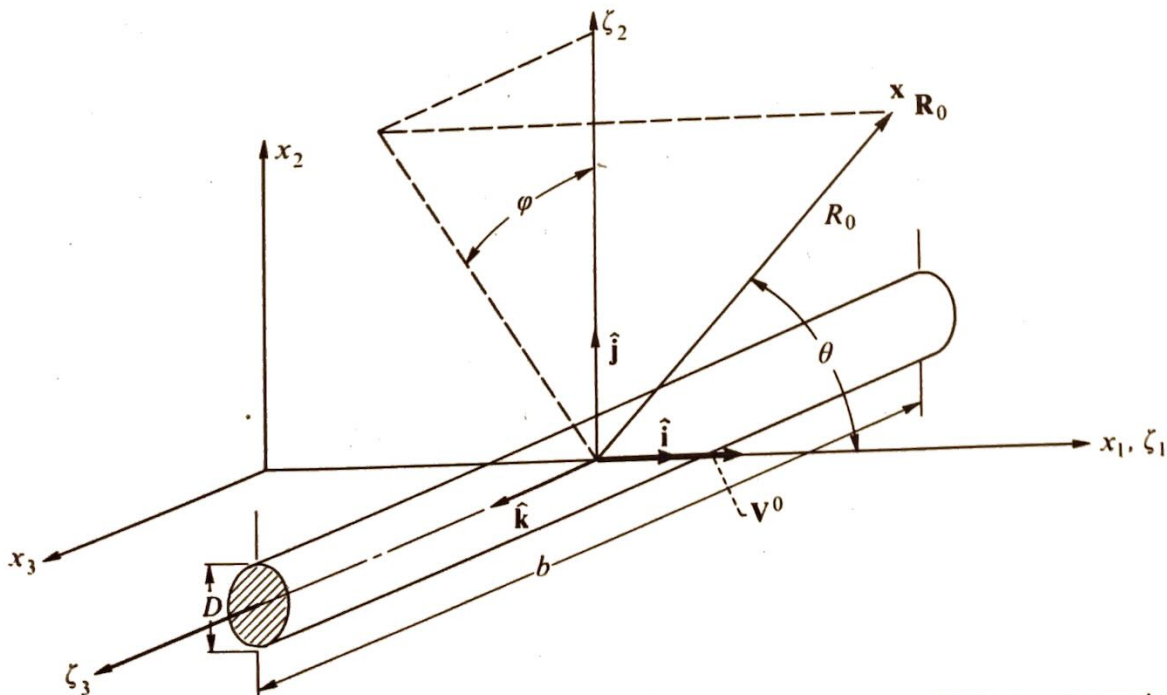


Fig. 3.11 Coordinate systems for sound emission from Aeolian tones. (Cylinder shown in its location at emission time τ_e .)

variation in Φ along the cylinder reflects the fact that the vortex shedding is only in phase over a relatively short length, perhaps on the order of 3 to 4 diameters. The frequency Ω is given by Eq. (3.83). Hence, the characteristic time T_ζ of the oscillation is

$$T_\zeta = \frac{2\pi}{\Omega} \simeq \frac{D}{0.2 V^0}$$

The inequality (3.25) therefore shows that Eq. (3.28) can be used to predict the sound from this flow only if

$$\frac{M}{1 - M \cos \theta} \ll \frac{5D}{L}$$

where L is a characteristic dimension of the cylinder

$$M = \frac{V^0}{c_0}$$

and

$$\cos \theta = \frac{\mathbf{R}_e \cdot \mathbf{M}}{R_e M}$$

Even though Aeolian tones are usually found only in very low Mach number flows, cylinder lengths are in many cases long enough so that the inequality is not satisfied. We therefore proceed as in the previous section and use Eq. (3.28) only on a unit length basis.

Since the cylinder velocity V^0 is constant, we can put \mathbf{a}^0 equal to zero and neglect the derivative of C_b^\dagger with respect to τ_e (since it yields higher order terms in R_e^{-1} when \mathbf{x} is in the radiation field). Then inserting Eq. (3.27) into (3.28) yields

$$\rho'(\mathbf{x} | \zeta_3) \sim \frac{-(R_e)_2}{4\pi c_0^3 R_e^2 [1 - (\mathbf{R}_e/R_e) \cdot \mathbf{M}]^2} \frac{\partial F_2(\tau_e | \zeta_3)}{\partial \tau_e} \quad (3.86)$$

where

$$\left. \begin{aligned} \mathbf{R}_e &= \mathbf{x} - \mathbf{k}\zeta_3 - \mathbf{i}c_0 M \tau_e \\ \tau_e &= t - \frac{R_e}{c_0} \end{aligned} \right\} \quad (3.87)$$

and $\rho'(\mathbf{x} | \zeta_3)$ is the density fluctuation at \mathbf{x} due to a unit length of cylinder so that

$$\rho'(\mathbf{x}) = \int_{-b/2}^{b/2} \rho'(\mathbf{x} | \zeta_3) d\zeta_3 \quad (3.88)$$

Since Eq. (3.87) shows $(R_e)_2 = x_2$, substituting Eq. (3.85) into (3.86) and

using Eqs. (3.83) and (3.87) yields

$$\rho'(\mathbf{x} | \zeta_3) \sim \frac{i\kappa S_t \rho_0 (V^0)^3 x_2}{4c_0^3 R_e^2 [1 - (\mathbf{R}_e/R_e) \cdot \mathbf{M}]^2} e^{-i\Omega[t - (R_e/c_0)]} e^{-i\Phi(\zeta_3)} \quad (3.89)$$

But for large \mathbf{x} ,

$$R_e = |\mathbf{x} - \hat{\mathbf{k}}\zeta_3 - c_0 \hat{\mathbf{i}} M \tau_e| = R_0 - \frac{x_3 \zeta_3}{R_0} + O(R_0^{-1})$$

where

$$\mathbf{R}_0 = \mathbf{x} - \hat{\mathbf{i}} c_0 M \tau_e$$

is the value of R_e at the center of the cylinder. Hence, replacing R_e by $R_0 - (x_3 \zeta_3 / R_0)$ in the exponent of Eq. (3.89) (and by R_0 in all other places) and substituting the result into Eq. (3.88) yields

$$\begin{aligned} \rho'(\mathbf{x}) \sim & \frac{i\kappa S_t \rho_0 (V^0)^3 \sin \theta \cos \varphi}{4c_0^3 R_0 (1 - M \cos \theta)^2} e^{-i\Omega[t - (R_0/c_0)]} \\ & \times \int_{-b/2}^{b/2} \exp \left\{ -i \left[\left(\frac{\Omega}{c_0} \right) \zeta_3 \sin \theta \sin \varphi + \Phi(\zeta_3) \right] \right\} d\zeta_3 \end{aligned} \quad (3.90)$$

where, as shown in Fig. 3.11 (wherein the cylinder is shown in its position at the emission time τ_e)

$$\begin{aligned} \cos \theta &= \frac{\mathbf{R}_0 \cdot \hat{\mathbf{i}}}{R_0} \\ \sin \theta \cos \varphi &= \frac{\mathbf{R}_0 \cdot \hat{\mathbf{j}}}{R_0} = \frac{x_2}{R_0} \\ \sin \theta \sin \varphi &= \frac{\mathbf{R}_0 \cdot \hat{\mathbf{k}}}{R_0} = \frac{x_3}{R_0} \end{aligned}$$

Since R_0 and θ depend on t , the density fluctuation is not periodic. However, as shown in Sec. 1.8.4, the observation point can be moved far enough from the source so that θ and $R_0(t)$ are nearly constant over one period of oscillation and hence equal to their values, say $R_0(t_0)$ and $\theta_0 = \theta(t_0)$, at some time t_0 during this period. In fact, it follows from the results of that section that

$$\begin{aligned} \rho' \sim & \frac{i\kappa S_t \rho_0 (V^0)^3 \sin \theta_0 \cos \varphi}{4c_0^3 R_0(t_0) (1 - M \cos \theta_0)^2} \exp \left\{ -i\Omega \left[\frac{t - t_0}{1 - M \cos \theta_0} - \frac{R_0(t_0)}{c_0} + t_0 \right] \right\} \\ & \times \int_{-b/2}^{b/2} \exp \left\{ -i \left[\left(\frac{\Omega}{c_0} \right) \zeta_3 \sin \theta_0 \sin \varphi + \Phi(\zeta_3) \right] \right\} d\zeta_3 \end{aligned} \quad (3.91)$$

for time intervals of the order of one period. Hence, we can treat the motion as periodic and use Eqs. (1.16) and (1.92) to define an average intensity

over the effective period

$$T_p = \frac{2\pi}{\Omega} (1 - M \cos \theta_0)$$

Consequently,

$$\begin{aligned} \bar{I} \sim & \frac{\kappa^2 S_t^2 \rho_0 (V^0)^6 \sin^2 \theta \cos^2 \varphi}{32 c_0^3 R_0^2 (1 - M \cos \theta)^4} \\ & \times \int_{-b/2}^{b/2} \int_{-b/2}^{b/2} \exp \left\{ i \left[\left(\frac{\Omega}{c_0} \right) \xi \sin \theta \sin \varphi + \Phi(\zeta_3 + \xi) - \Phi(\zeta_3) \right] \right\} d\zeta_3 d\zeta'_3 \end{aligned} \quad (3.92)$$

where we have put

$$\xi = \zeta'_3 - \zeta_3$$

and dropped the zero subscript on θ since, now that the intensity has been calculated, there is no need to distinguish between t_0 and t .

We shall consider two limiting cases. First, suppose that the cylinder length b is small enough so that the vortex shedding is roughly in phase over the length of the cylinder.† Then

$$e^{i[\Phi(\zeta_3 + \xi) - \Phi(\zeta_3)]} \simeq 1$$

But, since Eq. (3.83) shows that $\omega\xi/c_0$ changes by an amount

$$\frac{\Omega}{c_0} b \simeq (2\pi)(0.2)M \frac{b}{D}$$

and since the Mach number is fairly low, it follows that

$$e^{i(\Omega/c_0)\xi \sin \theta \sin \varphi} \simeq 1$$

over the range of integration. Hence, Eq. (3.92) becomes

$$\bar{I} \sim \frac{\kappa^2 S_t^2 b^2 \rho_0 (V^0)^6 \sin^2 \theta \cos^2 \varphi}{32 c_0^3 R_0^2 (1 - M \cos \theta)^4} \quad (3.93)$$

Now suppose that the cylinder is very long compared with the length l over which the shed vortices are correlated. In this case it is convenient to change the variables of integration in Eq. (3.92) to ζ_3 and ξ so that

$$\begin{aligned} \bar{I} \sim & \frac{\kappa^2 S_t^2 \rho_0 (V^0)^6 \sin^2 \theta \cos^2 \varphi}{32 c_0^3 R_0^2 (1 - M \cos \theta)^4} \\ & \times \int_{-b/2}^{b/2} e^{i(\Omega/c_0)\xi \sin \theta \sin \varphi} \int_{-(b/2)-\zeta_3}^{(b/2)-\zeta_3} e^{i[\Phi(\zeta_3 + \xi) - \Phi(\zeta_3)]} d\xi d\zeta_3 \end{aligned} \quad (3.94)$$

† The cylinder would then have to be less than 4 diameters in length, and end effects could become important.

Then since the correlation length is small compared with the length of the cylinder, we can (as in the last section) take the limits of the inner integral to be $-\infty$ and ∞ . Moreover, it is reasonable to assume that the correlation coefficient

$$\frac{1}{b} \int_{-b/2}^{b/2} e^{i[\Phi(\zeta_3 + \xi) - \Phi(\zeta_3)]} d\zeta_3$$

of the fluctuating force acting on the cylinder is Gaussian and therefore equal to $e^{-(\xi^2/2l^2)}$. Then since

$$\begin{aligned} \int_{-\infty}^{\infty} \left\{ \exp \left[i \left(\frac{\Omega}{c_0} \right) \xi \sin \theta \sin \varphi - \left(\frac{\xi^2}{2l^2} \right) \right] \right\} d\xi \\ = \sqrt{2\pi} l \exp \left[-\frac{1}{2} \left(\frac{\Omega^2}{c_0^2} \right) l^2 \sin^2 \theta \sin^2 \varphi \right] \end{aligned}$$

Eq. (3.94) becomes

$$\begin{aligned} \bar{I} \sim \frac{\sqrt{2\pi} \kappa^2 S_t^2 l b \rho_0 (V^0)^6 \sin^2 \theta \cos^2 \varphi}{32 c_0^3 R_0^2 (1 - M \cos \theta)^4} \\ \times \left\{ \exp \left[-\frac{1}{2} \left(\frac{2\pi M S_t l}{D} \right)^2 \sin^2 \theta \sin^2 \varphi \right] \right\} \quad (3.95) \end{aligned}$$

If the Mach number is so small that the exponent can be neglected, this formula differs from the short-cylinder formula (3.93) only in that b^2 is replaced by $\sqrt{2\pi} l b$.

These results (without convection effects) were obtained by O. M. Phillips²⁹ in 1956. By using a specific model for the wake flow, Phillips determined that κ should be approximately equal to 1. His measurements are compared† with Eq. (3.95) (with the convection and exponential factors neglected) in Fig. 3.12.

As the Reynolds number is increased and the wake behind the cylinder becomes turbulent, the vortex shedding mechanism appears to persist in a less organized state with randomly shed, large-scale vorticity causing broadband lift fluctuations and hence broadband noise. In fact, a surprisingly distinct large-scale eddy structure is found to exist in the wakes of cylinders even at very high Reynolds numbers—with about one-half the turbulent energy in the wake contained in these eddies.²⁹ Experiments at these higher Reynolds numbers tend to show that the sound intensity still follows the prediction of Eq. (3.95)—provided l is taken to be independent of D .

The formulas derived in this section are not restricted to circular cylinders and should apply equally well to bluff bodies with other cross sectional shapes. For streamlined bodies such as airfoils, random vortex shedding has been assumed to occur and be an important source of broad-

† Phillips took $\sqrt{2\pi} l \simeq 17D$.

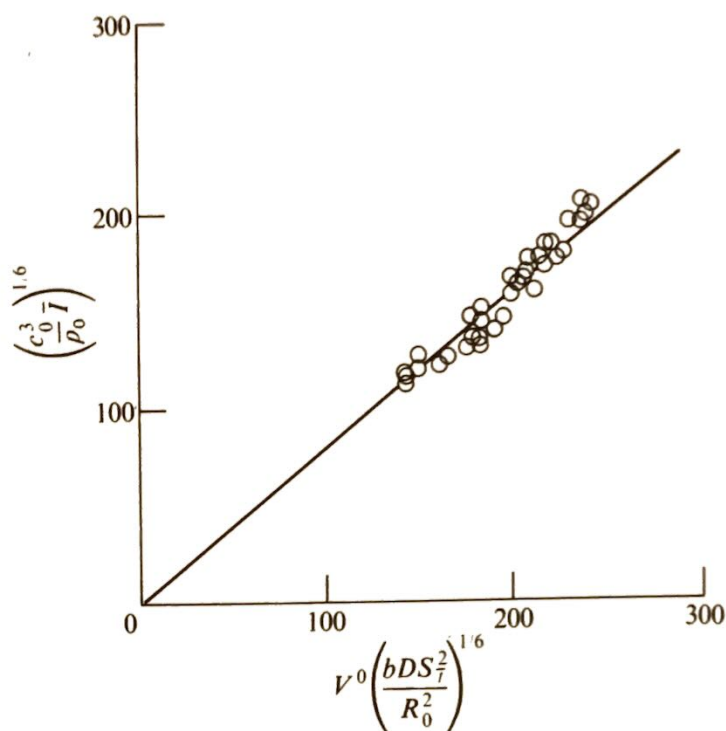


Fig. 3.12 Comparison of Aeolian tone measurements with experiment. (Data from Reference 29.) Cylinder velocity $1300 < V^0 < 2000$ cm/sec; Reynolds number, $110 < Re < 160$; nozzle diameter, D , 0.0123 cm (0.0048 in.).

band noise. However, Patterson, Vogt, and Fink³⁰ recently found that certain typical two-dimensional helicopter rotor airfoils emitted only pure tones† when their pressure-surface boundary layers were laminar and that no sound could be detected above the very low level background noise when the boundary layers were turbulent. Although the data taken by these investigators correlated well with a Strouhal number of 0.2, based on the total laminar boundary layer thickness, Tam³¹ has shown that there are a number of factors which indicate that these tones may not be produced by vortex shedding. Indeed, flow visualization studies of airfoil wakes show that the formation of discrete vortices is delayed until the flow has moved far downstream. Moreover, Aeolian tone theory cannot explain certain detailed features of the data such as the simultaneous occurrence of tones at more than one frequency and the jumps in frequency that arise when the flow velocity is increased through certain ranges. Consequently, Tam has postulated that these tones may be caused by a feedback mechanism that is very similar to those associated with edge tone production (see page 105) and jet “screech” (page 104). Thus, disturbances propagating downstream from the trailing edge are assumed to be amplified by an instability of the flow. However, in this case the sound emission is the result of a lateral motion imparted to the wake by the disturbance. The sound wave then impinges on the pressure surface boundary layer and initiates a new

† Often called “propeller singing.”

disturbance which continues the cycle. This model is capable of explaining many of the observed features of the experimental data. Patterson, et al., even suggest that much of the broadband noise produced by actual helicopter rotors may also be generated by this mechanism—with the variation in tone frequency that results from the spanwise speed variations causing the sound to be emitted over a range of frequencies.

Blade boundary layer turbulence may be another source of broadband helicopter rotor noise. A simple theoretical model for predicting the sound generated by this mechanism was developed by Mugridge,³² and his results show fair agreement with experiment at low frequencies. Moreover, the analysis in Sec. 3.5.1 demonstrates that incident atmospheric turbulence is also capable of producing broadband helicopter rotor (or propeller) noise.

3.5.3 Propeller Noise: Gutin's Theory

Up to this point the examples have been concerned with noise generated by the fluctuating forces exerted on a body. On the other hand, it was shown in Sec. 3.3.2 that a body in accelerative motion can generate sound even when these forces are steady. It is generally believed that this mechanism is responsible for the production of pure tones by airplane propellers operating at moderate tip speeds. In 1937, Gutin³³ recognized the dipole character of this noise source and was able to develop the first successful theory of propeller noise.†

The basic equation. Figure 3.13 shows a propeller rotating with angular velocity Ω in the y_1 – y_2 plane. The ζ -coordinate system is fixed to the blades with its origin at the hub and its ζ_3 axis perpendicular to the y_1 – y_2 plane.

The noise produced by this propeller can be calculated from Eq. (3.23). We shall again suppose, for reasons discussed in Chap. 5, that the quadrupole terms can be omitted. Moreover, the noise generated by the volume displacement effects will also be neglected. Then, with this understanding, Eq. (3.23) becomes

$$\rho' \sim \frac{1}{4\pi c_0^3} \int_{S(t_0)} \left[\frac{R_j}{R^2 C^\dagger} \frac{\partial}{\partial \tau} \frac{f_j}{C^\dagger} \right]_{\tau=\tau_e} dS(\zeta) \quad (3.96)$$

where we take $S(t_0)$ to be the surface of the blades, and the retarded time τ_e and the convection factor C^\dagger are defined by Eqs. (3.17) and (3.18), respectively. The Mach number which appears in Eq. (3.18) is defined in terms of the velocity V of a fixed point in the ζ -coordinate system by Eq. (3.15)

† Earlier attempts at formulating theories of propeller noise were made by Lynam and Webb³⁴ in 1919 and by Bryan³⁵ in 1920.

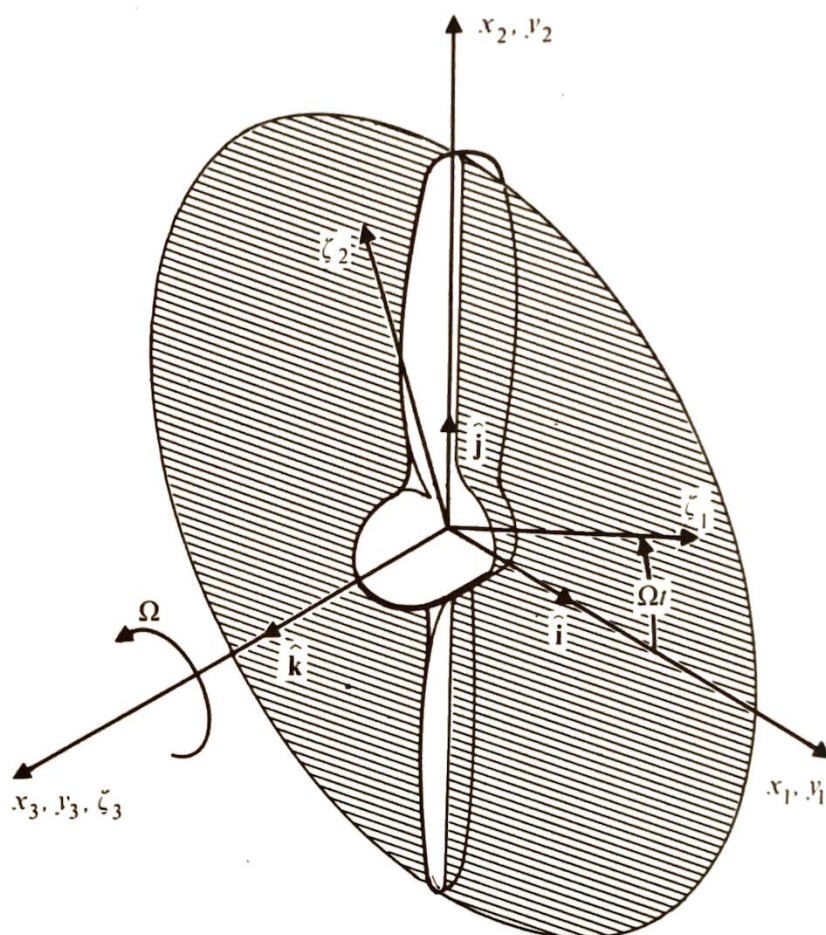


Fig. 3.13 Coordinate system for propeller.

while Eq. (3.13) and Fig. 3.13 show that

$$\mathbf{V} = \Omega \mathbf{k} \times \boldsymbol{\zeta} \quad (3.97)$$

for a stationary propeller.

We shall (for simplicity) limit the discussion to the case where the velocity V is everywhere subsonic. Then Eq. (3.17) has only a single root τ_e for each value of t , and the integrand in Eq. (3.96) need not be interpreted as a sum of terms (see remarks following Eq. (3.17)).

The analysis is also restricted to the case where the sources, and hence the sound field, is periodic with angular frequency Ω . This will occur whenever the flow entering the propeller is steady—even if it is spatially non-uniform. It, therefore, follows from Eqs. (3.96) and (1.A.2) of Appendix 1.A that the amplitude ρ_n of the n th harmonic of the density fluctuation is given by

$$\rho_n \sim \frac{\Omega}{8\pi^2 c_0^3} \int_{S(t_0)} \int_0^{2\pi/\Omega} \left[\frac{R_j}{R^2 C^\dagger} \frac{\partial}{\partial \tau} \frac{f_j}{C^\dagger} \right]_{\tau=\tau_e} e^{in\Omega t} dt dS(\boldsymbol{\zeta}) \quad (3.98)$$

Since the integrand is evaluated at $\boldsymbol{\zeta}$ and the retarded time $\tau_e(\boldsymbol{\zeta}, t)$, it is convenient to make these the variables of integration. But differentiating

Eq. (3.17) and using Eqs. (3.9), (3.15), (3.17), and (3.18) yields

$$\frac{dt}{d\tau_e} = [C^\dagger]_{\tau=\tau_e} \quad (3.99)$$

Then since τ_e is a single-valued function of t , changing the variable of integration from t to τ_e in Eq. (3.98) we get

$$\rho_n \sim \frac{\Omega}{8\pi^2 c_0^3} \int_{S(t_0)} \int_{\tau_e(\zeta, 0)}^{\tau_e(\zeta, 2\pi/\Omega)} e^{in\Omega[\tau_e + (R/c_0)]} \frac{R_j}{R^2} \frac{\partial}{\partial \tau_e} \frac{f_j}{|C^\dagger|} d\tau_e dS(\zeta) \quad (3.100)$$

where we have dropped the notation $[]_{\tau=\tau_e}$ with the understanding that all quantities in the integrand are evaluated at ζ and the retarded time τ_e .

Since R is a periodic function of τ with period $2\pi/\Omega$, $[R]_{\tau=\tau_e}$ is a periodic function of τ_e with this same period. Hence, it follows from Eq. (3.17) that increasing τ_e by $2\pi/\Omega$ increases t by the same amount. But since the velocity is subsonic, Eqs. (3.18) and (3.99) show that t is a monotonically increasing function of τ_e . Hence, increasing t by $2\pi/\Omega$ must also increase τ_e by this amount. The limits of integration of the integral with respect to τ_e in Eq. (3.100) can therefore be replaced by $[\tau_e(\zeta, 0), \tau_e(\zeta, 0) + 2\pi/\Omega]$. But since the integrand is a periodic function of τ_e , the value of the integral cannot be changed by translating both limits the same amount, and Eq. (3.100) becomes

$$\rho_n \sim \frac{\Omega}{8\pi^2 c_0^3} \frac{x_j}{x^2} \int_{S(t_0)} \int_0^{2\pi/\Omega} e^{in\Omega[\tau_e + (R/c_0)]} \frac{\partial}{\partial \tau_e} \frac{f_j}{|C^\dagger|} d\tau_e dS(\zeta) \quad (3.101)$$

where, since $\mathbf{y}(\zeta, \tau_e)$ is confined to the propeller disk and \mathbf{x} is in the radiation field, we have replaced R_j/R by its asymptotic value x_j/x .

Since $C^\dagger > 0$, integrating Eq. (3.101) by parts and using Eqs. (3.17) and (3.99) yields

$$\rho_n \sim -\frac{i n \Omega^2}{8\pi^2 c_0^3} \frac{x_j}{x^2} \int_0^{2\pi/\Omega} \int_{S(t_0)} e^{in\Omega[\tau_e + (R/c_0)]} f_j(\zeta, \tau_e) dS(\zeta) d\tau_e$$

But since

$$R = x - \frac{\mathbf{x}}{x} \cdot \mathbf{y} + O(x^{-1})$$

whenever \mathbf{x} is in the radiation field and \mathbf{y} is confined to the propeller disk, this equation becomes

$$\rho_n \sim -\frac{i n \Omega^2}{8\pi^2 c_0^3} \frac{x_j}{x^2} \int_0^{2\pi/\Omega} e^{in\Omega[\tau_e + (x/c_0)]} \int_{S(t_0)} e^{-in\Omega(\mathbf{x}/x) \cdot \mathbf{y}/c_0} f_j(\zeta, \tau_e) dS(\zeta) d\tau_e \quad (3.102)$$

It is convenient to distinguish the front surfaces of the propeller blades, say $S_1(t_0)$ with unit normal $\hat{\mathbf{n}}^{(1)}$, from the back surfaces, say $S_2(t_0)$ with

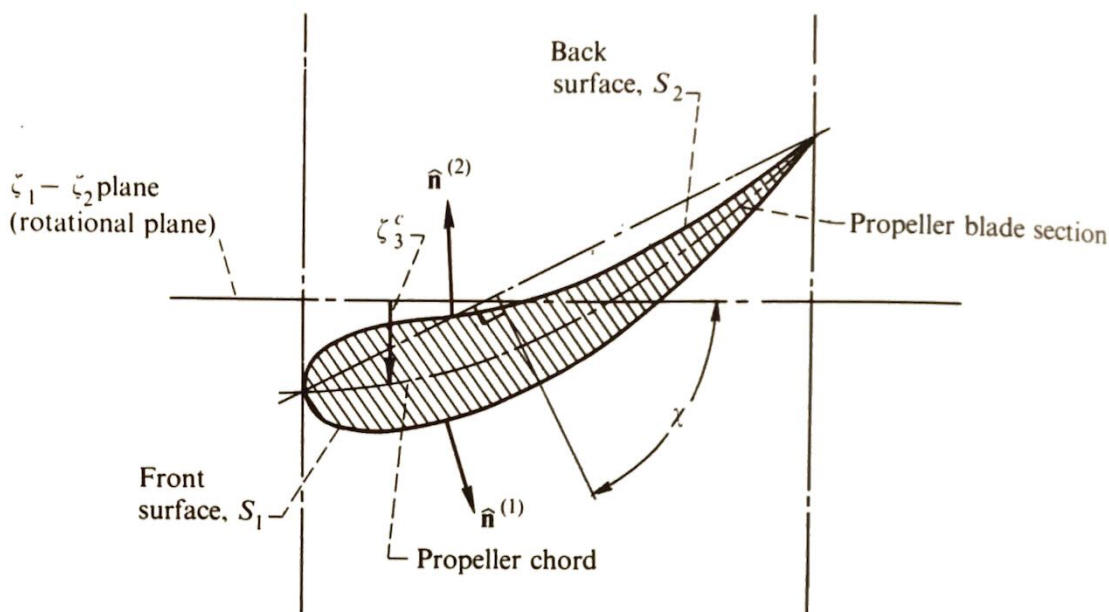


Fig. 3.14 Propeller blade surfaces.

unit normal $\hat{n}^{(2)}$. Thus, as shown in Fig. 3.14, these two sets of surfaces join along the trailing edges of the blades and along the lines that pass through the fronts of each blade section at the points where the tangents of these sections are parallel to the ζ_3 -axis. The surface integral in Eq. (3.102) can then be written as the sum of two integrals—one over each of these two sets of surfaces. The latter integrals can be evaluated in the usual way by integrating over the projection A of the blade surfaces in the ζ_1 – ζ_2 plane. Then the inner integral in Eq. (3.102) becomes

$$\begin{aligned} \frac{x_j}{x} \int_{S(t_0)} e^{-in\Omega(\mathbf{x}/x) \cdot \mathbf{y}/c_0} f_j(\zeta, \tau_e) dS(\zeta) \\ = \frac{x_j}{x} \int_A \left[\frac{f_j^{(1)}}{|\hat{n}_3^{(1)}|} e^{-(in\Omega/c_0)(\mathbf{x}/x) \cdot \mathbf{y}^{(1)}} \right. \\ \left. + \frac{f_j^{(2)}}{|\hat{n}_3^{(2)}|} e^{-(in\Omega/c_0)(\mathbf{x}/x) \cdot \mathbf{y}^{(2)}} \right] d\zeta_1 d\zeta_2 \end{aligned} \quad (3.103)$$

where $\zeta_3^{(1)}$ is the value of ζ_3 on the front blade surface and more generally the superscript (1) indicates that the quantity on which it appears is to be evaluated at ζ_1 , ζ_2 , and $\zeta_3^{(1)}$. In order to transform Eq. (3.102) into a more explicit form, we first introduce the spherical coordinates x , θ , and φ for the observation point \mathbf{x} and the cylindrical coordinates r' , φ' , and ζ_3 for the source point ζ , as shown in Fig. 3.15. Since the vector \mathbf{y} denotes the location of the source point ζ relative to the fixed \mathbf{y} -coordinate system, it follows from this figure that

$$\begin{aligned} \mathbf{y} &= \{r' \cos(\varphi' + \Omega\tau_e), r' \sin(\varphi' + \Omega\tau_e), \zeta_3\} \\ \mathbf{x} &= \{x \sin \theta \cos \varphi, x \sin \theta \sin \varphi, x \cos \theta\} \end{aligned} \quad (3.104)$$

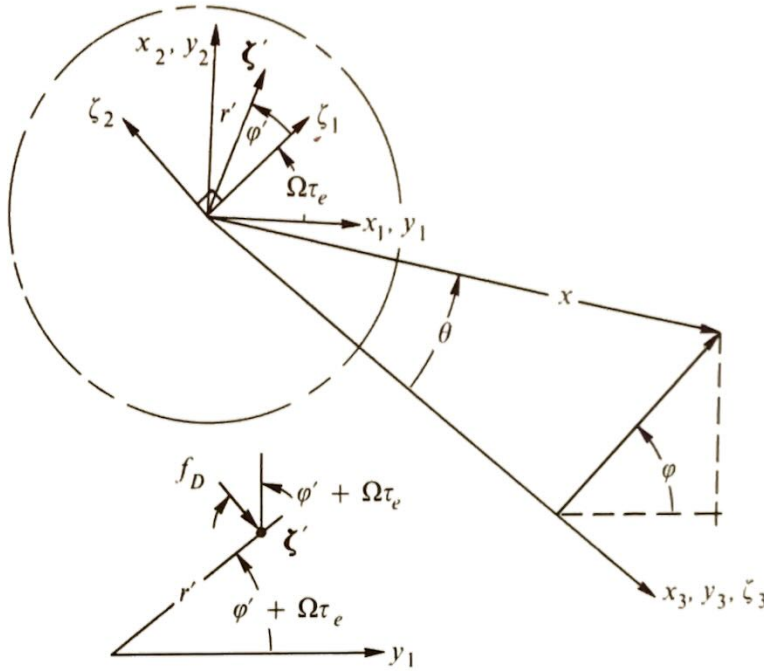


Fig. 3.15 Polar coordinates for propeller.

Moreover, when dealing with propellers it is customary to divide the force acting on the blades into a thrust component f_T in the ζ_3 -direction and a drag component (equal to minus the torque) f_D in the φ' -direction. These are related to the components f_i of \mathbf{f} in the fixed \mathbf{y} -coordinate system by

$$\mathbf{f} = \{-f_D \sin(\varphi' + \Omega\tau_e), f_D \cos(\varphi' + \Omega\tau_e), -f_T\}$$

Introducing this into Eq. (3.103), inserting the result into Eq. (3.102), and using the polar angles defined in Eqs. (3.104) now yields

$$\begin{aligned} \rho_n \sim & \frac{i n \Omega^2}{8 \pi^2 c_0^3 x} \int_0^{2\pi/\Omega} \int_A \exp \left\{ i n \Omega \left[\tau_e + \left(\frac{x}{c_0} \right) - \left(\frac{r'}{c_0} \right) \sin \theta \cos(\varphi' + \Omega\tau_e - \varphi) \right] \right\} \\ & \times [g_T \cos \theta + g_D \sin \theta \sin(\varphi' + \Omega\tau_e - \varphi)] d\tau_e r' dr' d\varphi' \quad (3.105) \end{aligned}$$

where

$$\begin{aligned} g_\alpha \equiv & \frac{f_\alpha^{(1)}}{|\hat{n}_3^{(1)}|} \left\{ \exp \left[-i \frac{n \Omega}{c_0} \zeta_3^{(1)} \cos \theta \right] \right\} \\ & + \frac{f_\alpha^{(2)}}{|\hat{n}_3^{(2)}|} \left\{ \exp \left[-i \frac{n \Omega}{c_0} \zeta_3^{(2)} \cos \theta \right] \right\} \quad \text{for } \alpha = T, D \quad (3.106) \end{aligned}$$

The factors

$$\exp \left[-i \frac{n \Omega}{c_0} \zeta_3^{(i)} \cos \theta \right] \quad , \quad i = 1, 2$$

account for the difference in retarded time between the blade surfaces and the rotational plane of the propeller. However, it is unlikely that any propeller blade will be thick enough for the difference in retarded-time between

its front and back surfaces to be important. We therefore neglect this variation and thereby obtain

$$g_\alpha \simeq \left[\exp \left(-i \frac{n\Omega}{c_0} \zeta_3^c \cos \theta \right) \right] \tilde{f}_\alpha \quad \text{for } \alpha = T, D$$

where† $\zeta_3^c(r', \varphi')$ is the ζ_3 coordinate of the blade chord and

$$\tilde{f}_\alpha \equiv \frac{f_\alpha^{(1)}}{|\hat{n}_3^{(1)}|} + \frac{f_\alpha^{(2)}}{|\hat{n}_3^{(2)}|} \quad \text{for } \alpha = T, D$$

is just the net thrust or drag force per unit projected area acting on the blades at the point (ζ_1, ζ_2) . Hence, using the well-known generating function¹³

$$e^{-iZ \cos \beta} = \sum_{m=-\infty}^{\infty} (-i)^m J_m(Z) e^{-im\beta}$$

for the Bessel function $J_m(Z)$ of the first kind together with the derivative of this result with respect to β

$$-\sin \beta e^{-iZ \cos \beta} = \frac{1}{Z} \sum_{m=-\infty}^{\infty} (-i)^m m J_m(Z) e^{-im\beta}$$

we can write Eq. (3.105) as

$$\begin{aligned} \rho_n \sim \frac{ik_n}{4\pi c_0^2 x} e^{ik_n x} \sum_{m=-\infty}^{\infty} e^{im[\varphi - (\pi/2)]} \int_A J_m(k_n r' \sin \theta) e^{-i(m\varphi' + k_n \zeta_3^c \cos \theta)} \\ \times \left(\cos \theta F_{n-m}^T - \frac{m}{k_n r'} F_{n-m}^D \right) r' dr' d\varphi' \end{aligned} \quad (3.107)$$

where

$$k_n \equiv \frac{n\Omega}{c_0} \quad (3.108)$$

is the wave number of the n th harmonic of the rotational frequency Ω and

$$F_p^\alpha \equiv \frac{\Omega}{2\pi} \int_0^{2\pi/\Omega} e^{ip\Omega\tau} \tilde{f}_\alpha(\zeta', \tau) d\tau \quad \text{for } \alpha = T, D \quad (3.109)$$

is simply the p th Fourier coefficient of the force \tilde{f}_α . Finally, by shifting the index of summation to $p = n - m$, Eq. (3.107) can be put in the slightly more familiar form

$$\begin{aligned} \rho_n \sim \frac{ik_n}{4\pi c_0^2 x} e^{ik_n x} \sum_{p=-\infty}^{\infty} e^{i(n-p)[\varphi - (\pi/2)]} \int_A J_{n-p}(k_n r' \sin \theta) \\ \times \left(\exp \left\{ i \left[p\varphi' - n \left(\varphi' + \frac{\Omega \zeta_3^c \cos \theta}{c_0} \right) \right] \right\} \right) \left(\cos \theta F_p^T - \frac{n-p}{k_n r'} F_p^D \right) r' dr' d\varphi' \end{aligned} \quad (3.110)$$

† The definition of ζ_3 in the region between the blades is irrelevant since \tilde{f}_α vanishes there.

This result is quite general and applies even if the flow approaching the propeller is spatially nonuniform and every blade is different from every other. However, we are usually interested in propellers that have B identical equally spaced blades. Consequently, let $f_\alpha^0(r', \varphi, \tau)$ denote the force per unit projected area acting on a particular blade†—individuated by setting an index s equal to 1. Then since the force distribution acting on the $s = 1$ blade at the time τ is the same as that which acted at the time $\tau - (2\pi/\Omega B)(s - 1)$ on the blade that is displaced from it by the angle $(2\pi/B)(s - 1)$, the force distribution on the latter blade must be

$$f_\alpha^0\left(r', \varphi' - \frac{2\pi}{B}(s - 1), \tau + \frac{2\pi}{\Omega B}(s - 1)\right).$$

Hence,

$$\tilde{f}_\alpha = \sum_{s=1}^B f_\alpha^0\left(r', \varphi' - \frac{2\pi}{B}(s - 1), \tau + \frac{2\pi}{\Omega B}(s - 1)\right) \quad \text{for } \alpha = T, D \quad (3.111)$$

We can now insert this into Eq. (3.109) to obtain

$$F_p^\alpha = \sum_{s=1}^B e^{-i2\pi(s-1)p/B} F_{\alpha,p}^0\left(r', \varphi' - \frac{2\pi}{B}(s - 1)\right) \quad \text{for } \alpha = T, D \quad (3.112)$$

where

$$F_{\alpha,p}^0(r', \varphi') \equiv \frac{\Omega}{2\pi} \int_0^{2\pi/\Omega} e^{ip\Omega\tau} f_\alpha^0(r', \varphi', \tau) d\tau \quad \text{for } \alpha = T, D \quad (3.113)$$

is the p th Fourier coefficient of the force per unit projected area acting on the $s = 1$ blade. Then substituting Eq. (3.112) into (3.110), shifting the variable of integration from φ' to $\varphi' - 2\pi(s - 1)/B$, using the identity

$$\sum_{s=1}^B e^{-in2\pi(s-1)/B} = \begin{cases} B & \text{for } n = mB \\ 0 & \text{for } n \neq mB \end{cases} \quad m = 0, \pm 1, \pm 2, \dots$$

and noting that

$$\zeta_3^\epsilon(\zeta', \varphi') = \zeta_3^\epsilon\left(r', \varphi' - \frac{2\pi}{B}(s - 1)\right)$$

yields

$$\begin{aligned} \rho_{nB} &\sim \frac{iBk_{nB}}{4\pi c_0^2 x} e^{ik_{nB}x} \sum_{p=-\infty}^{\infty} e^{i(nB-p)(\varphi - (\pi/2))} \int_{A_0} J_{nB-p}(k_{nB}r' \sin \theta) \\ &\times e^{ip\varphi' - inB(\varphi' + \Omega\zeta_3^\epsilon \cos \theta/c_0)} \left(\cos \theta F_{T,p}^0 - \frac{nB-p}{k_{nB}r'} F_{D,p}^0 \right) r' dr' d\varphi' \quad (3.114) \end{aligned}$$

† We can assume that f_α^0 is equal to zero when (r', φ') does not lie in the projected area of the blade.

where A_0 is the cross-sectional area of the $s = 1$ blade. In many cases ζ_3^c can be approximated fairly closely by

$$\zeta_3^c = r' \varphi' \cot \chi$$

where the *stagger angle* χ is shown in Fig. 3.18.

Steady blade forces: Gutin's theory. Now consider the case where the approaching flow is completely uniform in space and hence where the blade forces are steady in the rotating reference frame. Then Eq. (3.113) becomes

$$F_{\alpha,p}^0 = f_{\alpha}^0(\zeta') \frac{\Omega}{2\pi} \int_0^{2\pi/\Omega} e^{ip\Omega\tau} d\tau = f_{\alpha}^0(\zeta') \delta_{p,0} \quad \text{for } \alpha = T, D$$

Thus, only the $p = 0$ term contributes to the sum in Eq. (3.114), and we obtain the following generalization of Gutin's formula† for the "rotational" noise from propellers.³³

$$\begin{aligned} \rho_{nB} \sim & \frac{ik_{nB}B}{4\pi c_0^2 x} e^{i\{k_{nB}x + nB[\varphi - (\pi/2)]\}} \int_{A_0} \left\{ \exp \left[inB\varphi' \left(1 + \frac{\Omega r'}{c_0} \cos \theta \cot \chi \right) \right] \right\} \\ & \times J_{nB}(k_{nB}r' \sin \theta) \left(f_T^0 \cos \theta - \frac{c_0}{\Omega r'} f_D^0 \right) r' dr' d\varphi' \quad \text{for } n = 1, 2, \dots \end{aligned} \quad (3.115)$$

In order to gain some insight into the properties of the sound field predicted by this result, notice that the Bessel function $J_m(Z)$ can be approximated by the first term in its series expansion

$$J_m(Z) \simeq \frac{Z^m}{2^m m!} \quad (3.116)$$

over much of the range, $0 < Z < m$, where its argument is less than its order. But for r' less than the tip radius r_t of the propeller,

$$\frac{\Omega r'}{c_0} < \frac{\Omega r_t}{c_0} \equiv M_t$$

where M_t is the tip Mach number, which we have assumed to be less than unity. Consequently, Eq. (3.108) shows that the arguments of the Bessel functions in Eq. (3.115) are less than their orders and, as a result, that the approximation (3.116) can be used. Moreover, the variation over A_0 of the exponent

$$-inB\varphi' \left(1 + \frac{\Omega r'}{c_0} \cos \theta \cot \chi \right)$$

† Unlike Gutin's formula, Eq. (3.115) accounts for the variation in retarded time over the blades.

will be less than $2nB/AR$ where AR is the aspect ratio of the blades. We shall suppose that AR is large enough and that the number of blades is small enough so that the exponent is nearly zero. Then with these approximations, Eq. (3.115) becomes

$$\rho_{nB} \sim \frac{ik_{nB}B}{4\pi c_0^2 x (nB)!} \left(\frac{k_{nB}r_t \sin \theta}{2} \right)^{nB} e^{i\{k_{nB}x + nB[\varphi - (\pi/2)]\}} \times \left(\cos \theta - \frac{a_n}{M_t} \right) \int_{A_0} \left(\frac{r'}{r_t} \right)^{nB} f_T^0 r' dr' d\varphi' \quad (3.117)$$

where

$$a_n = \frac{r_t \int_{A_0} \left(\frac{r'}{r_t} \right)^{nB} f_D^0 dr' d\varphi'}{\int_{A_0} \left(\frac{r'}{r_t} \right)^{nB} f_T^0 r' dr' d\varphi'}$$

is the ratio of the nB th drag moment to the nB th thrust moment, or roughly the drag-thrust ratio.

Equation (3.117) shows that the phase of the nB th harmonic $\rho_{nB} e^{-inB\Omega t}$ of the density fluctuation is (see page 14)

$$nB(\varphi - \Omega t) + k_{nB}x + \text{Constant}$$

Hence, its phase surface rotates with the rotational speed Ω of the propeller while it propagates in the radial direction with the speed of sound. The sound waves are therefore said to be *phase locked* to the propeller.

The nB th harmonic of the intensity is

$$\bar{I}_{nB} \sim \frac{B^2 k_{nB}^2 (k_{nB}r_t \sin \theta)^{2nB} (\cos \theta - a_n/M_t)^2}{\pi^2 \rho_0 c_0^2 x^2 2^{2nB+4} [(nB)!]^2} \left| \int_{A_0} \left(\frac{r'}{r_t} \right)^{nB} f_T^0 d\zeta_1 d\zeta_2 \right|^2 \quad (3.118)$$

As we have already indicated, this formula does not account for the "thickness noise" generated by the volume displacement effects of the blades. The extension of Gutin's theory to include this effect was given by Deming^{36,37} and completed by Gutin himself³⁸ in 1942. However, this noise source is generally found to be unimportant until the tip speed approaches the speed of sound.⁶⁴

Equation (3.118) shows that the intensity is always zero along the propeller axis ($\theta = 0$ and $\theta = \pi$) and, since a_n/M_t is usually somewhat less than unity, that it has a strong peak just behind the rotational plane of the propeller. This peak rapidly becomes narrower as the number of blades increases. The intensity is also zero at the angle $\theta = \cos^{-1}(a_n/M_t)$. The corresponding directivity pattern therefore has the general shape indicated in Fig. 3.16.

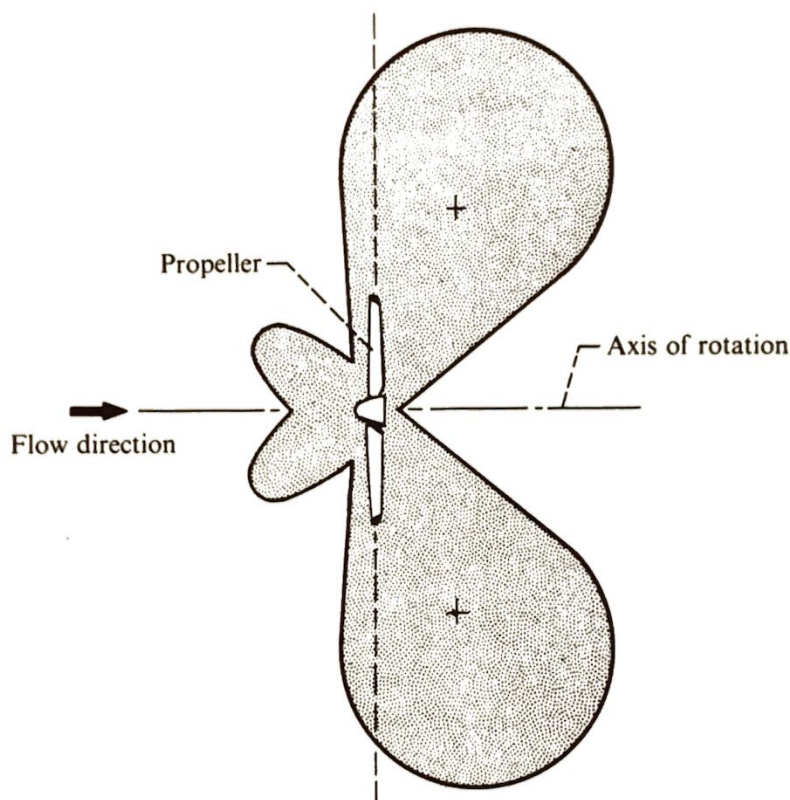


Fig. 3.16 Polar plot of intensity.

For a given tip speed the fundamental frequency $c_0 k_B = \Omega B$ increases with increasing blade number because of a phase cancellation of the lower harmonics of the rotational speed Ω . Increasing the blade number also causes the sound intensity to drop rapidly to zero. This is a consequence of the fact that the higher order Bessel functions are very nearly equal to zero whenever their argument is less than their order, which, as we have seen, is always the case for subsonic tip speeds. Thus, we expect that this type of noise will *not* be important for jet engine fans, which usually have larger numbers of blades.

The fundamental harmonic tends to be dominant at the lower tip speeds, with the higher harmonics becoming progressively more important as the tip speed is increased.

Hubbard and Lassiter³⁹ compared Eq. (3.115) with sound pressure measurements in the rotational plane of a two-bladed propeller. (See Fig. 3.17). These and other comparisons indicate that the theory developed in this section (extended if necessary to include thickness noise) is able to predict with reasonable accuracy the lower order harmonics (perhaps the first 10 or so) for tip Mach numbers ranging from $\frac{1}{2}$ to 1. On the other hand, it is found that the sound radiated by an actual propeller persists at considerably higher frequencies than those predicted by the theory. The additional sound is now believed to result from the nonuniformity of the incident flow—

an effect which is also believed to be responsible for the discrepancy between theory and experiment at Mach numbers below $\frac{1}{2}$.

Flow distortion noise. There are many cases where propellers and fans must operate in much more nonuniform flows than those encountered by airplane propellers. Thus, for example, a ship's propeller operates in the ship's inhomogeneous wake, a jet engine fan frequently operates in the wakes of inlet guide vanes, and helicopter blades must often pass through their own wakes and operate in ground effect. Moreover, the noise due to flow inhomogeneities can dominate over the rotational noise even for very small nonuniformities.

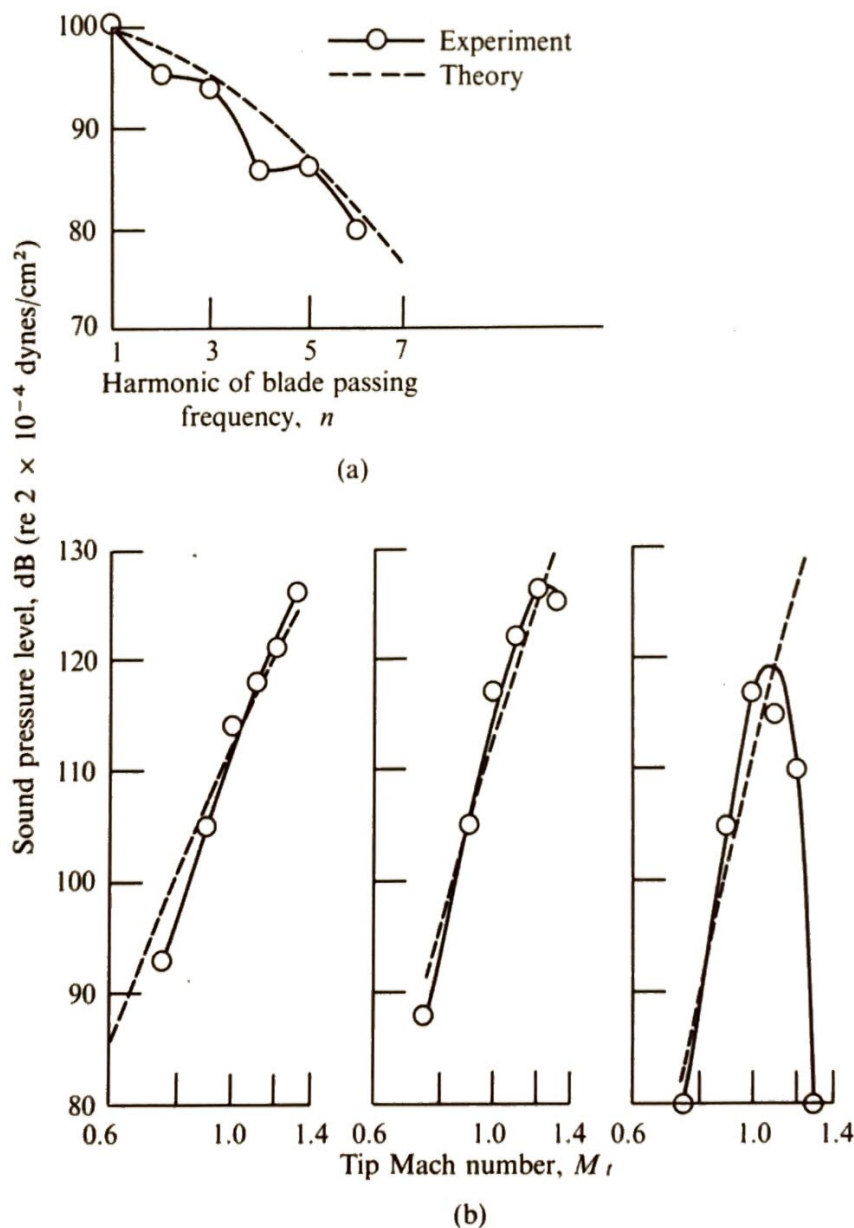


Fig. 3.17 Propeller noise measurement of Hubbard and Lassiter.³⁹ Circumferential angle, θ , 90° ; distance to observation point, x , 10 m (30 ft). (a) Sound pressure as function of order of harmonic. Number of blades, B , 2. (b) Sound pressure as function of tip Mach number for three harmonics of a two-bladed propeller.

When the oncoming flow is nonuniform, it can no longer be assumed that the forces acting on the blades are steady in a reference frame rotating with the propeller and we must use the complete Eq. (3.114) to calculate the acoustic radiation. In order to evaluate the integrals in this formula, it is generally necessary to know the force distribution over the blades. However, we can obtain a qualitative picture of the sound field by assuming that the force on each blade acts through a single point whose radius is r_M . Then, we can orient the ζ_1 -axis so that the force distribution f_α^0 acting on the first blade becomes

$$f_\alpha^0(\zeta', \tau) = \frac{1}{r'} \delta(r' - r_M) \delta(\varphi') \tilde{f}_\alpha^0(\tau) \quad \alpha = T, D$$

where \tilde{f}_α^0 denotes the total (thrust or drag) force acting on the blade. Inserting this into Eq. (3.113) and using the result in Eq. (3.114) now yields

$$\rho_{nB} \sim \frac{ik_{nB}B}{4\pi c_0^2 x} e^{ik_{nB}x} \sum_{p=-\infty}^{\infty} e^{i(nB-p)[\varphi - (\pi/2)]} J_{nB-p}(k_{nB}r_M \sin \theta) \times \left(\cos \theta T_p - \frac{nB-p}{k_{nB}r_M} D_p \right) \quad (3.119)$$

where

$$\alpha_p \equiv \frac{\Omega}{2\pi} \int_0^{2\pi/\Omega} e^{ip\Omega\tau} \tilde{f}_\alpha^0(\tau) d\tau \quad \text{for } \alpha = T, D$$

is simply the Fourier coefficient of the total (thrust or drag) force acting on the blade. This formula was obtained by Lowson⁴⁰ starting from a circular array of point sources rotating with the same angular velocity about their common center.[†]

The $p = 0$ term corresponds to the mechanism discussed in the previous section and its Fourier coefficients T_0 and D_0 are equal to the time-averaged forces. Hence, we can think of these as the steady part of the blade forces with the Fourier coefficients T_p and D_p for $p \neq 0$ corresponding to the fluctuating or unsteady forces. Each of these contributes a term, or "mode", to the nB th harmonic of the sound field, whose phase is (see page 14)

$$k_{nB}x + (nB - p)\varphi - nB\Omega t + \text{Constant}$$

The corresponding phase surface therefore rotates with the angular velocity

$$\frac{nB}{nB - p} \Omega$$

[†] The point force approximation can be justified rigorously in the limit where the wavelength is long compared with both the chord and span. Since it is more likely that the wavelength will be long compared with the chord, a better approximation might be to consider the force concentrated along a radial line.

Thus, the modes whose indices p and nB are of the same sign will rotate with greater angular velocity than the propeller rotational speed Ω —which shows that subsonically rotating propellers can actually give rise to supersonically rotating modes. On the other hand, the modes whose indices are of opposite sign will have angular velocities that are correspondingly less than Ω . This type of interaction can be most easily visualized by considering a simple optical analogue called the Moiré effect.[†] If the periodic disturbance field is represented by an array of (say 48) radial spokes drawn on a stationary background (one spoke for each cycle) and if the propeller is represented similarly (by say 46 spokes) on a sheet of clear plastic, the interference of dark and light regions will produce an interference pattern whenever the two configurations are overlaid. If now the plastic sheet is turned slowly about the common center of the two arrays, the interference pattern will be observed to spin $46/(48 - 46)$, or 23, times as fast as the plastic sheet but in the opposite direction.

When p and n are of opposite sign, the Bessel functions of order $nB - p$, which appear in the n, p th term, will be smaller than the Bessel function of order nB , which appears in the steady force term. And, since the unsteady forces are usually much smaller than the steady loads, it ought to be possible to neglect any modes whose indices are of opposite sign.

On the other hand, the Bessel functions that appear in terms whose indices are of the same sign will be larger than the one in the steady force term. In fact, for any given n the absolute magnitude of the $p = nB$ term is

$$\frac{k_{nB}}{4\pi c_0^2 x} B |J_0(k_{nB} r_M \sin \theta) \cos \theta T_{nB}|$$

whereas the absolute value of the steady force ($p = 0$) term is

$$\frac{k_{nB} B}{4\pi c_0^2 x} \left| J_{nB}(k_{nB} r_M \sin \theta) T_0 \left(\cos \theta - \frac{a}{M_t} \right) \right|$$

where a is the drag-thrust ratio. Consequently, the relative magnitude of these two terms is primarily determined by the relative magnitude of the Bessel functions and the ratio T_{nB}/T_0 of the unsteady force to the steady force. The latter quantity should roughly equal the ratio of the magnitude of the nB th harmonic of the disturbance field to the mean flow velocity. Hence, the larger B is, the greater the importance of the disturbance term—which is not all that small even when B takes on its smallest possible value of 2. Thus, when $n = 1$, for example, the argument of the Bessel functions is $2M_0 \sin \theta$, where $M_0 = \Omega r_M / c_0$ is the Mach number at the radius r_M . Consequently, $J_0 = 1$ and $J_2 = 0$ at $\theta = 0$, and (taking $M_0 = 0.7$) $J_0 \simeq 0.57$ and $J_2 \simeq 0.207$ at $\theta = \pi/2$. Hence, the unsteady force term can be half as large at $\theta = 0^\circ$ as the steady force term is at $\theta = 90^\circ$.

[†] This example is presented in Ref. 41.

even when the amplitude of the first harmonic of the disturbance is only 10 percent of the mean velocity.

Determination of blade forces. The results obtained in the last section will only be complete when the unsteady blade forces are known. We shall now show how, once certain approximations are made, the results of Sec. 3.4.2 can be used to calculate these forces. Since it is assumed in that section that linearized-thin-airfoil theory applies, we require that the propeller blades have small camber and are at a small angle of attack to the oncoming flow relative to the blade. Of course, the fluctuating velocity must likewise be small. It is also necessary to suppose that the blades are separated enough to insure that their mutual interference effects can safely be neglected. Then, each blade will act like an isolated thin airfoil. Finally, we shall suppose, for the purpose of illustration, that the flow can be considered to be two dimensional and parallel. With these approximations the blade forces can be calculated from the two-dimensional model illustrated in Fig. 3.18.

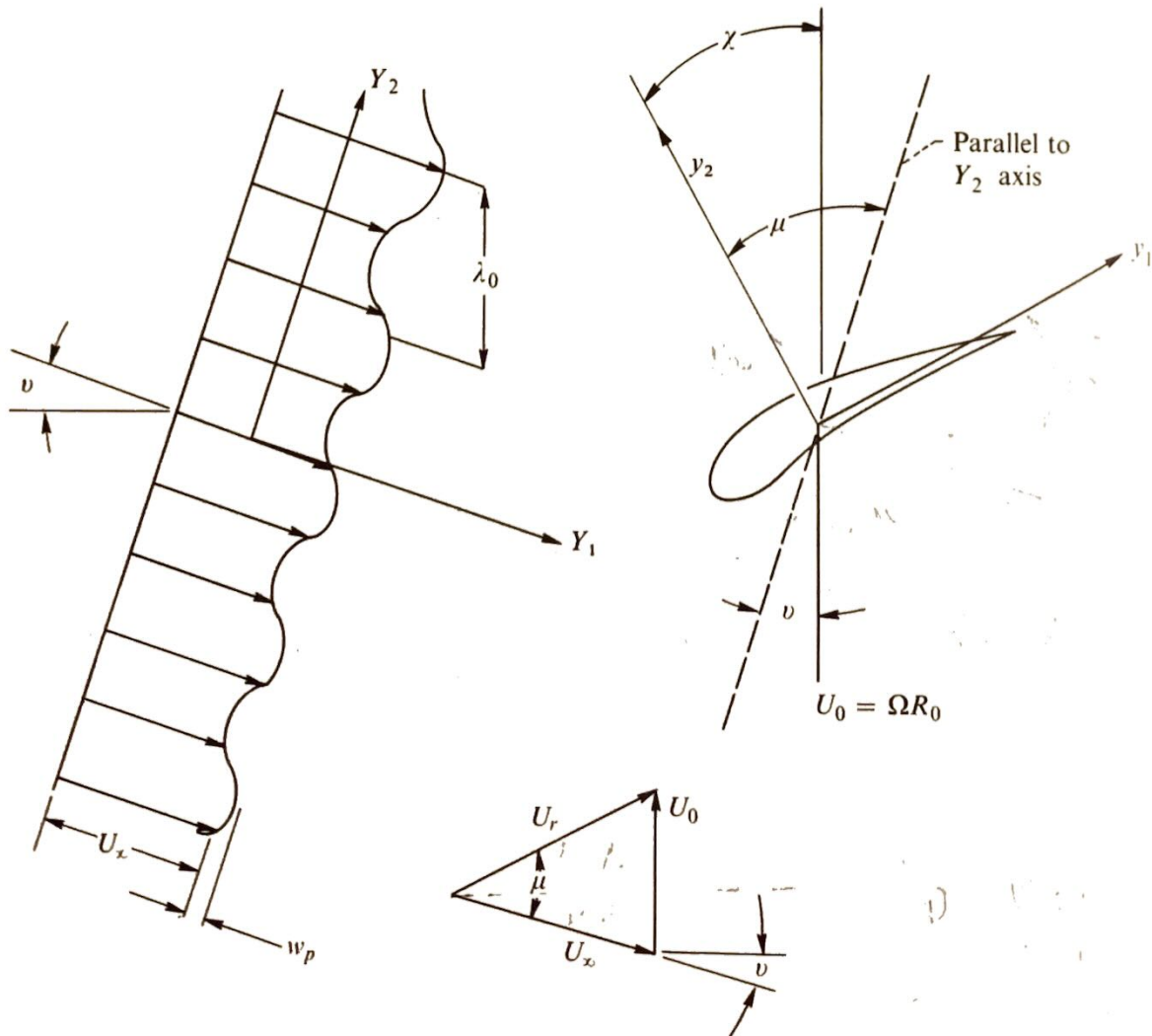


Fig. 3.18 Coordinate systems for calculating fluctuating blade forces.

The oncoming steady flow is parallel to the Y_1 axis, varies only in the Y_2 -direction,[†] and consists of a uniform part U_∞ plus a small spatially variable part. Since (as we shall see) the problem is linear, we again need only consider (as explained in Sec. 3.4.2) a single harmonic component of the nonuniform flow—whose amplitude and wavelength we shall denote by w_p and $\lambda_0 \cos v$, respectively. Then, the incident velocity will be

$$U_\infty + w_p e^{2\pi i Y_2 / (\lambda_0 \cos v)} \quad (3.120)$$

To relate this problem to the one discussed in Sec. 3.4.2, it is necessary to introduce a set of coordinates, say y_1 and y_2 , that remain fixed relative to the blades. We suppose that the y_1 -axis is aligned with the mean flow velocity relative to the blades—which we denote by U_r . (See Fig. 3.18.) Then the y_1, y_2 -coordinates will be rotated from the Y_1 - Y_2 system by the angle μ between U_r and the incident velocity U_∞ and in a time τ will be translated a distance $(U_0 \cos v)\tau$ by the component of the blade motion in the Y_2 -direction. Consequently,

$$Y_2 = y_1 \sin \mu + y_2 \cos \mu - U_0 \tau \cos v \quad (3.121)$$

Then, since $(U_0 / \sin \mu) = (U_r / \cos v)$, as can be seen from the velocity triangle in Fig. 3.18, the incident velocity field (3.120) becomes

$$U_\infty + w_p \exp \left[2\pi i \frac{U_0}{\lambda_0} \left(\frac{y_1 + y_2 \cot \mu}{U_r} - \tau \right) \right]$$

Let r_M denote the radius corresponding to the plane of Fig. 3.18. Then, since the circumference $2\pi r_M$ must equal an integral number of wavelengths, $\lambda_0 = 2\pi r_M / p$, $U_0 = \Omega r_M$, and the oncoming velocity becomes

$$U_\infty + w_p \exp \left[ip\Omega \left(\frac{y_1 + y_2 \cot \mu}{U_r} - \tau \right) \right]$$

And since this velocity is in the Y_1 -direction, the velocity relative to the blades has the components

$$U_r + w_p \cos \mu \exp \left[ip\Omega \left(\frac{y_1 + y_2 \cot \mu}{U_r} - \tau \right) \right]$$

and

$$-w_p \sin \mu \exp \left[ip\Omega \left(\frac{y_1 + y_2 \cot \mu}{U_r} - \tau \right) \right]$$

in the y_1 and y_2 directions, respectively. But these formulas clearly describe an incident gust of the type defined by Eqs. (3.54) and (3.55). The results obtained in Sec. 3.4.2, therefore, imply that the fluctuating lift force per unit

[†] The mean flow is allowed to make an angle v with the perpendicular to the rotational plane of the propeller in order to include the case where the oncoming flow is turned by guide vanes.

span is related to the compressible Sears functions by Eqs. (3.72) and (3.73b), which, in the present notation, show that the amplitude F_p/b of the fluctuating lift force per unit span, $(F_p/b) e^{-ip\Omega t}$, is given by

$$\frac{F_p}{b} = -\pi c \rho_0 U_r w_p \sin \mu S_c(\sigma_p, M_r) \quad (3.122)$$

where the reduced frequency σ_p is now

$$\sigma_p \equiv \frac{p\Omega c}{2U_r}$$

This result shows that the lift force acting on the blade is periodic in time, that its fundamental frequency is equal to the blade rotational speed, and that its p th harmonic depends only on the p th spatial harmonic of the incoming disturbance field. The Fourier components of the thrust T_p and drag D_p forces that appear in Eq. (3.119) are now given by

$$T_p = F_p \sin \chi$$

$$D_p = F_p \cos \chi$$

where χ is the stagger angle (Fig. 3.18).

Helicopter rotor noise. Helicopter noise often places severe restrictions on the way in which these vehicles can be operated. In fact, it even limits the civilian application for which they seem best suited; namely, intercity transportation. In military applications the noise can provide an unnecessary early warning of the vehicle's approach.

A typical helicopter noise spectrum is shown in Fig. 3.19. Its complex nature is a result of the large number of individual sources, both mechanical and aerodynamic, that contribute to the sound field. The principal aerodynamic sources are indicated in the figure.

Since a helicopter rotor is a special case of a propeller, its sound field should be described reasonably well by Eq. (3.115) extended, if necessary, to include a *coning force* that acts in the radial direction. In fact, Gutin's theory⁴² does fairly well in predicting the experimentally observed fundamental harmonic. But the higher harmonics fall off much more slowly with frequency than is predicted by the theory. This indicates that the fluctuating forces acting on helicopter blades should be considerably larger than those acting on propellers. It is therefore necessary to use the full Eq. (3.114) or, perhaps, the point force approximation (3.119) to calculate the sound field. This is often made difficult in practice by an almost complete lack of knowledge of the unsteady loading harmonics T_p and D_p , which, in any case, vary widely with operating conditions. Thus, the blade loading can vary from the impulsive-type force associated with "blade slap" to the nearly periodic force caused by the cyclic incidence variations of the blades in level flight (that must be used to compensate for the differences in

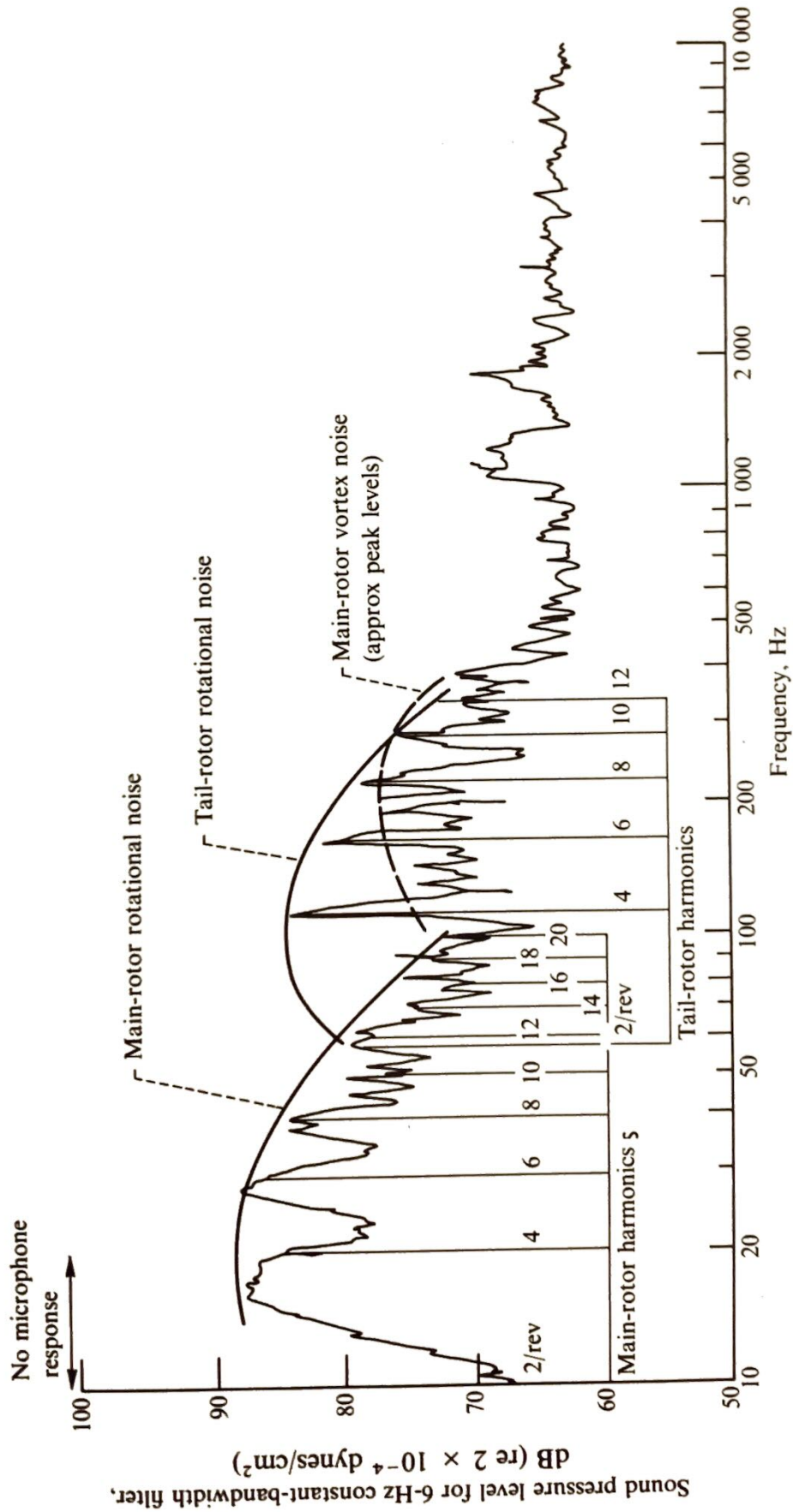


Fig. 3.19 External noise spectrum for helicopter HU-1A. Tiedown thrust, 600 lb; tip velocity, 720 ft/sec; microphone distance from source, 200 ft. (From Reference 45, originally derived from Reference 62; courtesy of University of Toronto Press.)

relative blade speed during forward and backward motion). Blade slap is the name given to the sharp banging or slapping noise heard under some operating conditions (such as low-power descent). It occurs at the blade passing frequency and, because of its impulsive nature, is very rich in higher harmonics. It is believed to be the result of a particularly severe interaction of the blades with the shed tip vortices.

By using the blade loading harmonics measured by Schieman,⁴³ Schlegel, King, and Mull⁴⁴ calculated the tones produced by a rotor during hover and compared them with experiment. Their results are shown in Fig. 3.20 which is taken from Reference 45. Also shown in this figure is a calculation based on Gutin's theory and a calculation carried out by Lowson and Ollerhead⁴⁵ using a larger number of unsteady loading harmonics.

Fan noise. It can be argued that the theory developed in the first part of this section ought to be able to predict the essential features of the high-frequency noise from axial flow fans and compressors, which after all, are little more than ducted propellers. Consequently, propeller type models have been adopted by Morfey,⁴⁶ Barry and More,⁴⁷ Lowson,⁴⁰ and many others to analyze various aspects of fan noise. The main conceptual difference appears to be due to the cutoff phenomenon, which is discussed in Chap. 4. Thus, as we shall see, the modes generated by a fan in a very long (i.e., infinite) duct will simply not propagate until the frequency is above a certain

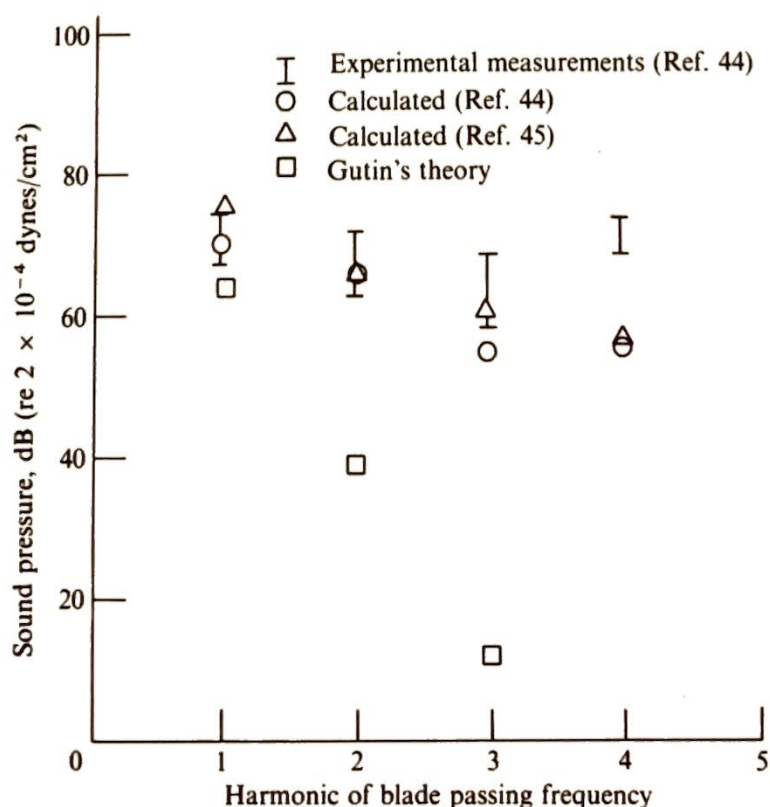


Fig. 3.20 Comparison of rotor noise theory with experiment. (From Reference 45.)

“cutoff” frequency for that mode. However, due to the incomplete cancellations of the sound waves that result from small variations in retarded time over the propeller’s disk, the corresponding modes merely have small (but nonzero) far-field amplitudes when they are emitted by a propeller. This results in a gradual cutoff with frequency as opposed to the sharp cutoff that occurs in ducts. The effect of the duct on the sound field is assessed in Sec. 4.3.5 where it is shown that the free-space theory developed in this chapter becomes more accurate with increasing frequency.

3.6 FLOWS WITH SOUND FIELD DETERMINED BY GREEN’S FUNCTION EQUATIONS TAILORED TO THE GEOMETRY

Up to now our interpretation of the role played by rigid surfaces has, in the main, been based on Eq. (3.23) which was obtained by using the free-space Green’s function in the general formula (3.6). But, this result will sometimes lead to erroneous conclusions unless the surface forces that appear in its second member are known with extreme precision. Indeed, the dipole sources from the various portions of any noncompact boundary surface have a tendency to add destructively and thereby produce a sound field of quadrupole order. In fact, there are even situations in which the opposite behavior occurs. In any case, the predicted sound field will then be in error unless we know enough about the surface forces to insure that these interference effects are properly modeled—a rather formidable task when the sound is caused by a turbulent flow. On the other hand, this difficulty can be avoided by using a Green’s function that is “tailored” to make the contribution from the surface dipole term as small as possible.

It is therefore necessary to return to Eq. (3.6) which, since only stationary boundaries† are treated in this section, can be written as

$$\rho' = \frac{1}{c_0^2} \int_{-T}^T \int_V \frac{\partial^2 G}{\partial y_i \partial y_j} T_{ij} dy d\tau + \frac{1}{c_0} \int_{-T}^T \int_S \frac{\partial G}{\partial y_i} f_i dS(y) d\tau \quad (3.123)$$

3.6.1 Sound Generated Near an Infinite Plane Surface

The effects discussed at the beginning of this section become especially apparent when the sound is generated by an unsteady flow in the vicinity of a perfectly rigid infinite plane (shown schematically in Fig. 3.21). In this case,

† The treatment of moving boundaries by this approach is taken up in Chap. 4.

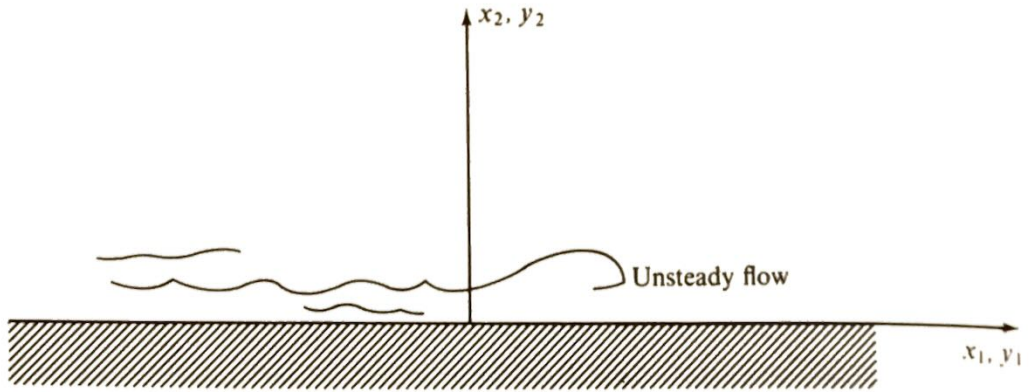


Fig. 3.21 Infinite-plane boundary.

we must use the Green's function (1.C.1) whose normal derivative vanishes on the boundary. Thus, inserting Eq. (1.C.1) into (3.123) and noting that

$R' = R$ when $y_2 = 0$ yields

$$\begin{aligned} \rho' = & \frac{1}{c_0^2} \int_{-T}^T \int_{y_2 > 0} \frac{\partial^2 G^0(R)}{\partial y_i \partial y_j} T_{ij} dy d\tau + \frac{1}{c_0^2} \int_{-T}^T \int_{y_2 > 0} \frac{\partial^2 G^0(R')}{\partial y_i \partial y_j} T_{ij} dy d\tau \\ & + \frac{2}{c_0^2} \int_{-T}^T \int_{y_2 = 0} \frac{\partial G^0(R)}{\partial y_\sigma} f_\sigma dy_1 dy_3 d\tau \end{aligned} \quad (3.124)$$

where we have used the notation (1.56), with the time dependence suppressed, and the repeated index σ can assume only the odd values 1 and 3—corresponding to the coordinates lying in the surface. The second term in this equation can be transformed into an integral over the region $y_2 < 0$ within the solid surface by changing the variable of integration from y_2 to $-y_2$ to obtain

$$\frac{1}{c_0^2} \int_{-T}^T \int_{y_2 < 0} \frac{\partial^2 G^0(R)}{\partial y_i \partial y_j} T_{ij}^\dagger dy d\tau$$

where

$$T_{ij}^\dagger = (-1)^{i+j} T_{ij}(y_1, -y_2, y_3, \tau) \quad (\text{no sum on } i, j)$$

is the “mirror image” reflection of T_{ij} in the $y_2 = 0$ plane.

It is convenient to introduce an extended quadrupole distribution \tilde{T}_{ij} that is defined on all space in such a way that it is equal to T_{ij} for $y_2 > 0$ and to its mirror image T_{ij}^\dagger for $y_2 < 0$. Then the first two integrals in Eq. (3.124) can be combined into a single integral over all space (where, as usual, the omission of the limits indicates that the integration is to be over all space) to obtain

$$\rho' = \frac{1}{c_0^2} \int_{-T}^T \int \frac{\partial^2 G^0(R)}{\partial y_i \partial y_j} \tilde{T}_{ij} dy d\tau + \frac{2}{c_0^2} \int_{-T}^T \int_{y_2 = 0} \frac{\partial^2 G^0(R)}{\partial y_\sigma} f_\sigma dy_1 dy_3 d\tau$$

Since G^0 depends on x and y only through R , the derivatives with respect to y_i can be changed to derivatives with respect to x_i and the integration over the delta function can be carried out to obtain

$$\rho' = \frac{1}{4\pi c_0^2} \frac{\partial^2}{\partial x_i \partial x_j} \int \tilde{T}_{ij} \left(\mathbf{y}, t - \frac{R}{c_0} \right) \frac{1}{R} d\mathbf{y} - \frac{1}{2\pi c_0^2} \frac{\partial}{\partial x_\sigma} \times \int_{y_2=0} \frac{1}{R} f_\sigma \left(\mathbf{y}, t - \frac{R}{c_0} \right) dy_1 dy_3$$

This equation was first derived by Powell.⁴⁸

Since the surface normal $\hat{\mathbf{n}}$ is now in the y_2 -direction, it follows from Eqs. (2.2) and (3.4) that

$$f_\sigma = e_{2\sigma} = \mu \left(\frac{\partial v_2}{\partial y_\sigma} + \frac{\partial v_\sigma}{\partial y_2} \right) = \mu \frac{\partial v_\sigma}{\partial y_2}$$

The strength of the surface dipole is therefore equal to the fluctuating viscous stress so that

$$\rho' = \frac{1}{4\pi c_0^2} \frac{\partial^2}{\partial x_i \partial x_j} \int \frac{1}{R} \tilde{T}_{ij} \left(\mathbf{y}, t - \frac{R}{c_0} \right) d\mathbf{y}$$

for an inviscid flow.[†] This shows that *the net effect of an infinite-plane rigid boundary can be accounted for by introducing an image distribution of volume quadrupole sources obtained by reflecting in the plane surface the volume quadrupole distribution T_{ij}* . Thus the solid boundary does little more than reflect the sound generated within the flow. Nevertheless, it must be kept in mind that the presence of solid boundaries always has a strong effect on the unsteady flow which generates the sound.

Of course, in any real flow the fluctuating viscous shear will produce surface dipole sources that are potentially more efficient sound generators than the volume quadrupoles. However, at the high Reynolds numbers where aerodynamic sound emission usually becomes significant the dipole term, being essentially a viscous quantity, ought to be quite small compared with the fluctuating Reynolds stress component of the quadrupole source (especially when the Mach number is sufficiently high).

An interesting experiment that tends to verify this conclusion was conducted by Olsen, Miles, and Dorsch.⁴⁹ It consisted of measuring the sound field that is produced when a turbulent jet impinges on a very large plate. The acoustic power showed a significant increase over that radiated by the jet itself—indicating that most of the noise was probably associated with the presence of the plate. However, the emitted sound intensity always varied as the eighth power of the velocity (which is characteristic of a volume quadrupole) and not as the sixth power (which is characteristic of a

[†] Compare this with Eq. (2.11), obtained for an unsteady flow with no solid boundaries present.

dipole)—indicating that the surface dipole term was indeed small. The noise emitted from boundary layers on large surfaces is usually found to be fairly small unless the velocities are extremely large (which is consistent with the relatively low efficiency of the quadrupole source). However, large surfaces inserted into jets often exhibit a ratio of turbulent pressure fluctuations to dynamic pressure that is an order of magnitude larger than what it would be in a turbulent boundary layer.

The general conclusions of this section apply to any surface whose typical dimensions and radius of curvature are both large compared to the wavelength of the sound (see Refs. 50 and 63). Thus, under these conditions, each surface element merely reflects the incident sound field that results from the nearby volume quadrupole sources. Of course, such reflection effects can significantly alter the directional pattern of the radiated sound—by producing, for example, a shadow region on the side of the surface that is shielded from the acoustic sources.

3.6.2 Sound Generated Near Finite Surfaces

Up to now we have considered the sound generated by unsteady flows near surfaces whose dimensions are either large or small compared to a typical wavelength. However, practical surfaces at practical air speeds frequently generate significant sound at wavelengths that are neither small nor large compared to their dimensions.

General equations. Fortunately (as pointed out by Doak⁵¹), the ideas developed in the last section can be extended to fixed boundaries of arbitrary size and shape simply by using (in Eq. (3.123)) the Green's function whose normal derivative vanished at the boundary. Then since

$$\frac{\partial G}{\partial n} \equiv n_j \frac{\partial G}{\partial y_j} = 0 \quad \text{on the surface } S$$

substituting Eq. (3.4) into (3.123) shows that

$$\rho' = \frac{1}{c_0^2} \int_{-T}^T \int_V \frac{\partial^2 G}{\partial y_i \partial y_j} T_{ij} dy d\tau + \frac{1}{c_0^2} \int_{-T}^T \int_S \frac{\partial G}{\partial y_j} e_{ij} n_i dS(\mathbf{y})$$

And if, as before, the sound generated by the fluctuating viscous stress is assumed to be negligible at the Reynolds numbers of interest, this becomes

$$\rho' = \frac{1}{c_0^2} \int_{-T}^T \int_V \frac{\partial^2 G}{\partial y_i \partial y_j} T_{ij} dy d\tau \quad (3.125)$$

If we were to apply this result to a bounding surface that is compact in at least one of its dimensions, we would simply confirm our conclusion

that acoustic radiation is correctly predicted by the dipole term in Eq. (3.20), provided, of course, that the sound source is within a wavelength from the surface. Indeed surfaces at large distances from the source region should play no role at all in the sound generation process.

It is frequently simpler to deal with the Fourier transform of Eq. (3.125) than with the equation itself. Thus, let Δ denote the Fourier transform of ρ' and T_{ij}^t denote the Fourier transform of T_{ij} . Then since Eq. (1.C.5) shows that G depends on t and τ only in the combination $t - \tau$, the last entry in table 1.1 (Appendix 1.A) shows that the Fourier transform of Eq. (3.125) is

$$\Delta = \frac{1}{c_0^2} \int \frac{\partial^2 G_\omega}{\partial y_i \partial y_j} T_{ij}^t dy \quad (3.126)$$

where, as indicated in Appendix (1.C.2), G_ω denotes an outgoing-wave solution of the Helmholtz equation

$$(\nabla^2 + k_0^2)G_\omega(\mathbf{y}|\mathbf{x}) = -\delta(\mathbf{x} - \mathbf{y}); \quad k_0 \equiv \frac{\omega}{c_0}$$

Edge noise. The half-plane problem: Perhaps the simplest geometry (after the infinite plane) to which Eq. (3.126) can be applied is the semi-infinite plate shown in Fig. 3.22. (Ffowcs Williams and Hall.⁵²)

The far field expansion of the outgoing-wave Green's function whose normal derivative vanishes on the half-plane $y_1 > 0, y_2 = 0$ can be written as (McDonald,⁵³)

$$G_\omega \sim \frac{1}{4\pi} \left[\frac{e^{ik_0 R}}{R} F(a) + \frac{e^{ik_0 R'}}{R'} F(a') \right] \quad (3.127)$$

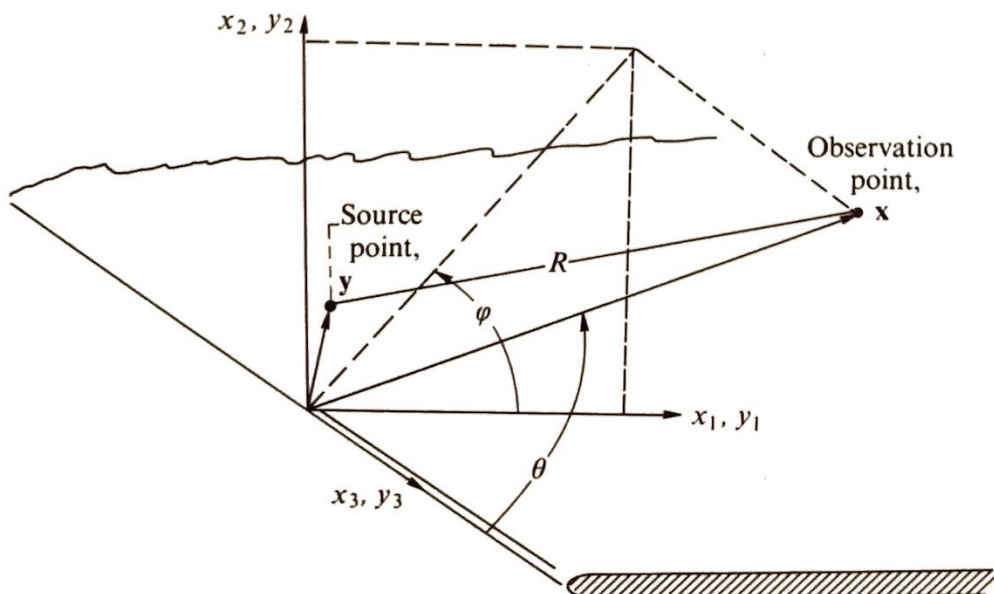


Fig. 3.22 Semi-infinite plane.

where, as usual, $R = |\mathbf{x} - \mathbf{y}|$ is the distance between the source point and the observation point and $R' = |\mathbf{x} - \mathbf{y}'|$ with $\mathbf{y}' = \{y_1, -y_2, y_3\}$ is the distance between the image point (source point reflected in y_1 - y_3 plane) and the observation point. $F(a)$ denotes what is essentially the complex Fresnel integral

$$F(a) = \frac{1}{2} + \frac{e^{-i\pi/4}}{\sqrt{\pi}} \int_0^a e^{iu^2} du \quad (3.128)$$

and

$$\begin{aligned} a &= (2k_0 r_0 \sin \theta)^{1/2} \cos \frac{1}{2}(\varphi - \varphi_0) \\ a' &= (2k_0 r_0 \sin \theta)^{1/2} \cos \frac{1}{2}(\varphi + \varphi_0) \end{aligned} \quad (3.129)$$

where

$$r_0 = \sqrt{y_1^2 + y_2^2}$$

and

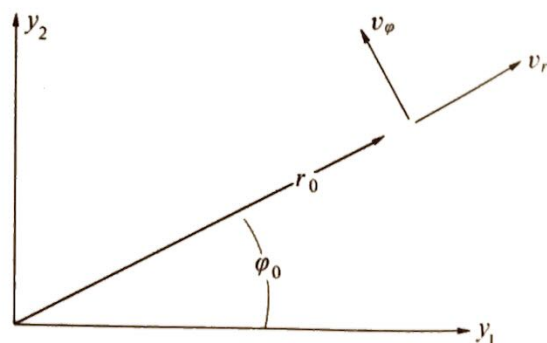
$$\varphi_0 = \tan^{-1} \frac{y_2}{y_1}$$

are the cylindrical coordinates of the source point shown in Fig. 3.23. It is important to notice that this Green's function has a "potential-field singularity" at the edge which means that the acoustic field behaves like a potential flow in this region.

Equation (3.127) closely resembles the reduced infinite-plane Green's function (see Eqs. (1.C.1) and (1.C.5))—the principal difference being that each term is now weighted by a Fresnel integral that varies (roughly) between 0 and 1. Hence, any enhancement of the sound field over that which results from an infinite flat plate must occur through derivatives of the Fresnel integral (or more specifically derivatives of a and a').

Very little sound will reach an observer if the source is far from the edge and on the opposite side of the plate. When the source and observer are on the same side and the source is far from the edge, the plate will act like an infinite plane. We therefore anticipate that any substantial amplification of the sound field that results from the presence of the plate

Fig. 3.23 Cylindrical coordinates for source.



must occur when the source is near the edge. Thus, we consider only the case where

$$2k_0r_0 \ll 1$$

that is, where the distance between the source point and the leading edge is very small compared to a wavelength. Then since

$$\int_0^a e^{-iu^2} du = a + O(a^3)$$

for small a , Eq. (3.127) becomes

$$G_\omega = \frac{e^{ik_0R}}{4\pi R} \left[\frac{1}{2} + \frac{e^{-i\pi/4}}{\sqrt{\pi}} (2k_0r_0 \sin \theta)^{1/2} \cos\left(\frac{\varphi - \varphi_0}{2}\right) \right] \\ + \frac{e^{ik_0R'}}{4\pi R'} \left[\frac{1}{2} + \frac{e^{-i\pi/4}}{\sqrt{\pi}} (2k_0r_0 \sin \theta)^{1/2} \cos\left(\frac{\varphi + \varphi_0}{2}\right) \right] + O((k_0r_0)^{3/2})$$

And, since

$$k_0R' \sim k_0R + 2k_0r_0 \sin \varphi_0 \sin \varphi \sin \theta \quad \text{as } R \rightarrow \infty$$

we can neglect the difference between k_0R and k_0R' to obtain

$$G_\omega = \frac{1}{4\pi R} e^{ik_0R} \left[1 + \frac{2e^{-i\pi/4}}{\sqrt{\pi}} (2k_0r_0 \sin \theta)^{1/2} \cos \frac{1}{2}\varphi_0 \cos \frac{1}{2}\varphi \right] + O(k_0r_0)$$

Inserting this into Eq. (3.126) shows that the contribution from the sound sources near the edge is

$$\Delta \sim \frac{2\omega^2}{4\pi c_0^4} \frac{e^{-i\pi/4}}{\sqrt{\pi}} \sin^{1/2} \theta \cos \frac{1}{2}\varphi \int_{v_0} \frac{e^{ik_0R}}{R} T_{\mu\sigma}^t \frac{\partial^2 \left[\left(\frac{2r_0}{k_0^3} \right)^{1/2} \cos \frac{1}{2}\varphi_0 \right]}{\partial y_\mu \partial y_\sigma} dy \quad (3.130)$$

where the integral is now evaluated over the cylindrical region v_0 wherein $2k_0r_0 \ll 1$, and the repeated Greek indices are used to indicate that the sum is only over 1 and 2 (since the term in square brackets is independent of y_3).

Now suppose that T_{ij} can be approximated by Eq. (2.7). Then introducing the radial and circumferential velocities shown in Fig. 3.23 and carrying out the indicated differentiations yields

$$\Delta \sim \frac{2\omega^2 \rho_0}{4\pi c_0^4} \frac{e^{-i\pi/4}}{\sqrt{\pi}} \sin^{1/2} \theta \cos \frac{1}{2}\varphi \\ \times \int_{v_0} \frac{1}{(2k_0r_0)^{3/2}} [(v_\varphi^2 - v_r^2)' \cos \frac{1}{2}\varphi_0 + 2(v_r v_\varphi)' \sin \frac{1}{2}\varphi_0] \frac{e^{ik_0R}}{R} dy \quad (3.131)$$

where the superscript t is used to denote Fourier transforms. The large factor $(2k_0r_0)^{-3/2}$ that multiplies the integrand of this result would not be present if the free space Green's function had been used in place of Eq. (3.127). It is responsible for producing a significant increase in the far-field pressure over that which would occur if the edge were not present. Thus, the edge acts to increase the acoustic efficiency of the compact quadrupole sources by destroying, as it were, some of the phase cancellation that would otherwise occur between the radiation fields of the individual monopole components of the quadrupole sources. It occurs because the near field pressure fluctuations, which would otherwise only be weakly coupled to the radiation field, are scattered by the edge into strongly propagating sound waves.

Only the Reynolds stress components $\rho_0 v_r^2$, $\rho_0 v_\phi^2$, and $\rho_0 v_r v_\phi$ produce sound fields that are augmented over the unbounded field by the factor $(2k_0r_0)^{-3/2}$. The components $\rho_0 v_r v_3$ and $\rho_0 v_\phi v_3$, which are omitted from Eq. (3.131), are increased by a factor of only $(2k_0r_0)^{-1/2}$, while the sound field produced by the component ρv_3^2 shows no increase at all.

Now, suppose the acoustic radiation is generated by a turbulent flow. To estimate the sound field, we assume (as Lighthill did in his original papers on aerodynamic noise) that the flow is divided into a number of acoustically compact regions. The turbulence within each of these regions is regarded as completely correlated, while the turbulence in any two different regions is regarded as completely uncorrelated. Then the total acoustic intensity can be found simply by calculating the sound intensity from each of these volumes and adding the results. Thus, applying Eq. (3.131) to a single correlation volume N_0 and supposing that v_ϕ and v_r do not vary over this region yields

$$\Delta \sim \frac{2\omega^2 \rho_0}{4\pi c_0^4} \frac{e^{ik_0 R}}{R} \frac{e^{-i\pi/4}}{\sqrt{\pi}} \sin^{1/2} \theta \cos \frac{1}{2}\varphi \\ \times \left[(v_\phi^2 - v_r^2)^t \int_{N_0} \frac{\cos \frac{1}{2}\varphi_0}{(2k_0 r_0)^{3/2}} dy + 2(v_r v_\phi)^t \int_{N_0} \frac{\sin \frac{1}{2}\varphi_0}{(2k_0 r_0)^{3/2}} dy \right]$$

Then approximating the integrals in this equation by

$$4 \left\{ \begin{array}{c} \cos \frac{\langle \varphi_0 \rangle}{2} \\ \sin \frac{\langle \varphi_0 \rangle}{2} \end{array} \right\} (2k_0 \langle r_0 \rangle)^{-3/2} N_0$$

where $\langle \varphi_0 \rangle$ and $\langle r_0 \rangle$ denote the polar coordinates of the center of "the eddy," we find

$$\Delta \simeq \sqrt{\frac{2}{\pi}} \frac{2\omega^2 \rho_0}{4\pi c_0^4} \frac{e^{i(k_0 R - \pi/4)}}{R(k_0 \langle r_0 \rangle)^{3/2}} \sin^{1/2} \theta \cos \frac{1}{2}\varphi A N_0 \quad (3.132)$$

where

$$A \equiv (v_\phi^2 - v_r^2)^t \cos \frac{1}{2} \langle \phi_0 \rangle + 2(v_r v_\phi)^t \sin \frac{1}{2} \langle \phi_0 \rangle$$

is roughly equal to $(v^2)^t$. Hence, the average far-field intensity from each correlation volume is

$$\bar{I}_{v_0} \simeq \frac{\omega_p \rho_0 \overline{v^4}}{2\pi^3 c_0^2 \langle r_0 \rangle^3} \frac{N_0^2}{R^2} \sin \theta \cos^2 \frac{1}{2} \phi \quad (3.133)$$

where ω_p denotes a peak or characteristic frequency.[†]

Since the total turbulence volume is equal to N_0 times the number of correlation volumes, the sound intensity per unit volume of turbulence is

$$\bar{I} \sim \frac{\omega_p \rho_0 \overline{v^4} N_0}{2\pi^3 c_0^2 \langle r_0 \rangle^3 R^2} \sin \theta \cos^2 \frac{1}{2} \phi \quad (3.134)$$

This result shows that the sound field produced in the vicinity of an edge should exhibit a distinct radiation pattern that is more or less independent of the sources and is characterized in the $\theta = \pi/2$ plane by the factor $\cos^2 (1/2)\phi$. In Fig. 3.24 this prediction is compared with the radiation pattern produced by a slot nozzle attached to one side of a large flat plate (Hayden,⁵⁴).

Equation (3.134) can also be used to obtain similarity estimates of the sound field. To this end, let l denote the correlation length and suppose that the turbulence velocity u' is related to the mean flow velocity U by $u' \simeq \alpha U$. Then, since the correlation volume is roughly l^3 and $\omega_p \simeq u'/l$, Eq. (3.134) implies that the maximum intensity behaves like

$$\bar{I}_{\max} \simeq \frac{\rho_0 U^5 \alpha^5}{2\pi^3 c_0^2 l R^2} \left(\frac{l}{\langle r_0 \rangle} \right)^3 \quad (3.135)$$

which shows that the sound intensity varies as U^5 . Hence, the acoustic field generated near an edge will be even stronger at low velocities than the dipole field produced near a compact surface and certainly much stronger than the quadrupole field produced near a very large surface.

It is instructive to compare the sound power output predicted by this equation with that which would be produced if there were no edge present. Now it was shown in Sec. 3.6.1 that sound produced in the vicinity of an infinite plate ought to be roughly the same as that produced by free turbulence (provided, of course, that the turbulence itself is the same in both cases). We can therefore use the results of Sec. 2.5.1 to estimate the power output from the turbulence far from the edge. To this end, we notice that

[†] In order to obtain Eq. (3.133), it was assumed that the frequency could be replaced by its peak value in Eq. (3.132). The results of Sec. 1.7.3 and Eq. (2.6) were then applied to calculate the intensity, and the results of Appendix 1.A (Sec. 1.A.3) were used to relate the product of the Fourier transforms of the squared velocities to their time averages.

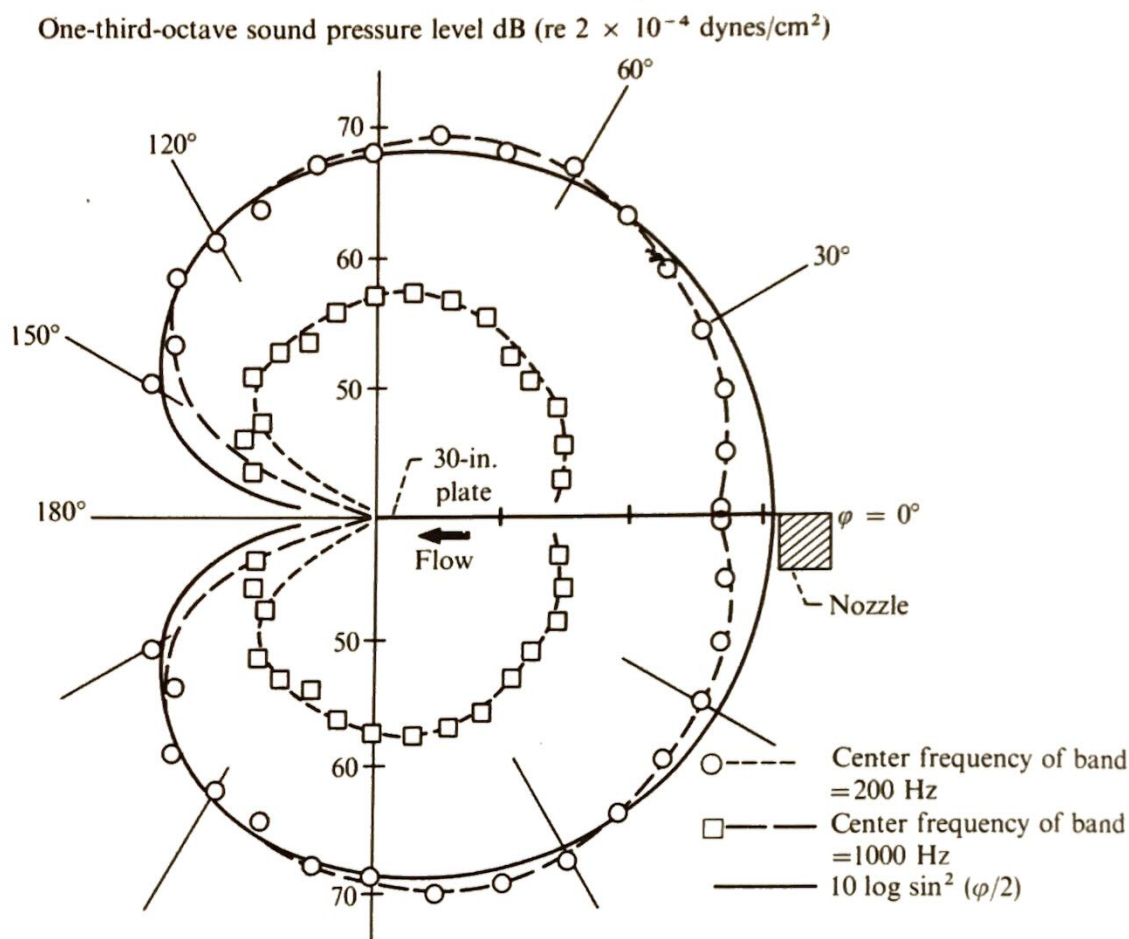


Fig. 3.24 One-third-octave sound pressure level directivity pattern in plane perpendicular to edge (from Reference 54). (All data points from $\varphi = 0^\circ$ to 180° are reflection of opposite side of plate—spot checks were made.)

Eqs. (2.44) and (2.42) show

$$\frac{u'}{\tau_\xi} \simeq \frac{\alpha^2 U^2}{l}$$

where $\alpha \simeq u'/U$ is roughly the proportionality constant between the mean velocity U and the fluctuating velocity u' . Hence, upon neglecting directional effects, Eq. (2.40) shows that the sound intensity from free turbulence is roughly

$$\bar{I}_{\text{free}} \simeq \frac{\rho_0 \alpha^8 U^8}{16\pi^2 c_0^5 R^2 l}$$

In order to get some idea about the relative importance of the edge, we use this expression together with Eq. (3.135) to estimate the plate size where the edge effects begin to play a dominant role. Thus, it follows from these two results that the edge regions will have equivalent sound-generating ability to the remainder of the plate when

$$\frac{\bar{I}_{\text{max}}(2L_{\text{edge}})}{\bar{I}_{\text{free}} L_{\text{plate}}} = \frac{16}{\pi} \left(\frac{c_0 l}{U \alpha \langle r_0 \rangle} \right)^3 \frac{\langle r_0 \rangle}{L_{\text{plate}}} = O(1)$$

where $L_{\text{edge}} \simeq \langle r_0 \rangle$ is the length of the region where the edge amplifies the sound and L_{plate} is the length of the total plate. But since the size of the edge region is determined by the inequality

$$\langle r_0 \rangle \ll \frac{c_0}{2\omega_p} \simeq \frac{lc_0}{2U\alpha}$$

this shows that the edge noise should be dominant when the plate is less than $64/(\pi\alpha M)$ correlation lengths long (where M is the mean-flow Mach number). Of course, these estimates are highly approximate and could easily be off by an order of magnitude or so. It should also be noted that they are based on the assumption that the turbulence in the vicinity of the edge is the same as it is at the center of the plate, while pressure measurements in the vicinity of a trailing edge indicate that the flow is strongly modified in this region. Crighton and Leppington⁵⁵ have shown that the general conclusions of this section apply to any plate whose thickness is small compared with the wavelength, provided that the rounding of its edge occurs on a scale that is not larger than a wavelength.

In order to actually produce the turbulence, it is generally necessary to insert the plate in a mean flow. This raises the question as to whether it is not more appropriate to employ a Kutta condition at the edge rather than allowing Green's function to have a potential flow regularity at this point. Jones⁵⁶ analyzed the sound generated in a uniform flow by acoustic sources in the vicinity of the trailing edge of a semi-infinite flat plate—both with and without a Kutta condition. (See Sec. 3.4.2.) He found that the imposition of this condition can only alter the sound radiation in a region near the plane of the plate.

Lip noise: the semi-infinite cylinder problem. An analysis similar to the one described in the previous section was used by Leppington⁵⁷ to estimate the sound generated by turbulence in the vicinity of the exit plane of an open tube (such as shown in Fig. 3.25). The appropriate Green's function was constructed by applying the reciprocity principle to the solution of a related scattering problem that had already been solved by the Wiener-Hopf technique.⁵⁸ The analysis is ultimately restricted to the case where the wavelength of the sound is long compared with the pipe radius. The conclusion is then that the sound power emitted by the turbulence now varies as the velocity to the sixth power as found by Curle rather than to the fifth power as found by Ffowcs Williams and Hall.

It is also of interest to note that the trailing vortex sheet emanating from a nozzle lip is unstable to small disturbances (Kelvin-Helmholtz instability) and that the nonradiating instability waves can be scattered by the edge into propagating sound waves (Crighton⁵⁹). The radiation field generated by this process is, in both its directivity and parametric dependence, identical to the one found by Leppington.

The analyses presented in the last two sections imply that there should be a noise source associated with the nozzle lip that contributes to the

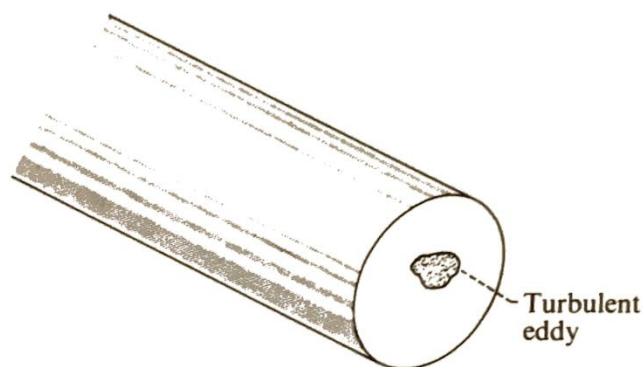


Fig. 3.25 Semi-infinite cylinder.

sound field of a jet. Its strength should increase with the velocity to the fifth or sixth power—so that it should be more important relative to the mixing noise when the jet velocity is low—and it should be detectable in the upstream direction where the jet noise is lowest. However, recent careful cold-jet experiments (e.g., Olsen and Friedman⁶⁰) show no indication of this noise source even at the lowest velocities. In fact, the sound radiated at the upstream angles always increased as the eighth power of the jet velocity and not the fifth or sixth. On the other hand, data taken by Olsen on an extended-core coaxial nozzle (shown schematically in Fig. 3.26) reveals the existence of tones that seem to exhibit the $\cos^2(\varphi/2)$ directional dependence found by Ffowcs Williams and Hall—but not the directional dependence found by Leppington for the edge of a circular duct. These tones, which can be detected whenever the ratio of the inner to outer stream velocities is less than 0.5, have peak frequencies that correspond to a Strouhal number of about 0.2, based on the nozzle lip thickness. On the other hand, flow visualization studies made on a similar configuration show that large, well defined vortices form at the nozzle lip whenever the inner to outer stream velocity ratio is less than 0.5 and disappear when it is greater than this value. Moreover, the strengths of these vortices appear to correlate with the intensity of the tone.⁶¹

3.7 CONCLUDING REMARKS

We have shown how Lighthill's theory can be extended to include the effects of moving surfaces. The development was based on a general integral formula (Eq. (3.6)) that relates the sound field to its sources by means of an outgoing wave Green's function. The more or less classical theories were recovered by choosing this to be the free-space Green's function. However, it was shown that this choice may lead to erroneous results when the surfaces are non-compact so that it often becomes necessary to use a specific Green's function that has been chosen to eliminate extraneous surface sources.

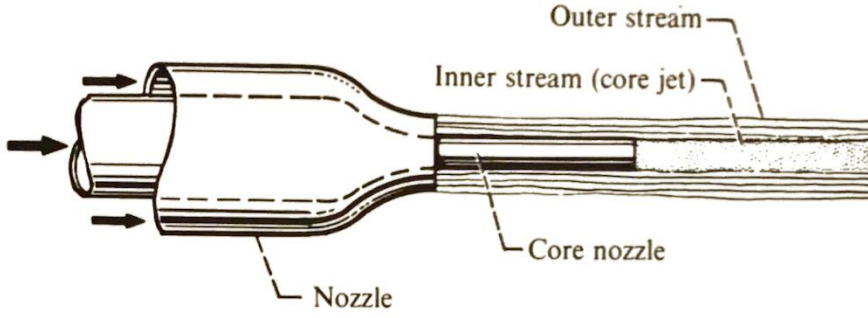


Fig. 3.26 Extended core coaxial nozzle

Nevertheless, a number of examples were worked out by using the free-space Green's function and neglecting the resultant volume quadrupole source—a procedure that we justified only for compact surfaces. However, it will be shown in Chap. 5 that such an approximation is also justified for non-compact bounding surfaces that are suitably streamlined (as they were in these examples).

APPENDIX 3.A

REDUCTION OF VOLUME DISPLACEMENT TERM TO DIPOLE AND QUADRUPOLE TERMS

We shall show that the apparent multipole order of the last integral in Eq. (3.8) can be increased whenever

$$\frac{\partial V_i}{\partial y_i} = 0 \quad (3.A.1)$$

To this end, let $f(R, \tau)$ denote an arbitrary function of R and τ that vanishes outside the interval $-T < \tau < T$. Then, Eqs. (3.A.1) and (3.7) imply

$$\begin{aligned} \frac{\partial}{\partial y_j} V_j \left[\frac{\partial f(R, \tau)}{\partial \tau} + V_i \frac{\partial f(R, \tau)}{\partial x_i} \right] + \frac{\partial}{\partial \tau} V_i \frac{\partial f(R, \tau)}{\partial x_i} \\ = \frac{\partial}{\partial x_j} a_j f(R, \tau) - \frac{\partial}{\partial x_i \partial x_j} V_i V_j f(R, \tau) \end{aligned} \quad (3.A.2)$$

where, in view of the chain rule and Eq. (3.9),

$$a_j \equiv \left(\frac{\partial V_j}{\partial \tau} \right)_y + V_i \frac{\partial V_j}{\partial y_i} = \left(\frac{\partial V_j}{\partial \tau} \right)_y + \frac{\partial V_j}{\partial y_i} \left(\frac{\partial y_i}{\partial \tau} \right)_\zeta = \left(\frac{\partial V_j}{\partial \tau} \right)_\zeta$$

is the acceleration of a fixed point in the ζ -coordinate system. But applying Leibniz's rule (Eq. (1.B.2)) to the region v_c interior to S and using Eq. (3.10)

yields (upon noting that the direction of the outward-drawn normal changes sign)

$$\begin{aligned} 0 &= \int_{-T}^T \frac{d}{d\tau} \int_{v_c(\tau)} V_i \frac{\partial}{\partial x_i} f \, dy \, d\tau \\ &= \int_{-T}^T \int_{v_c(\tau)} \frac{\partial}{\partial \tau} V_i \frac{\partial}{\partial x_i} f \, dy \, d\tau - \int_{-T}^T \int_{S(\tau)} V_j n_j V_i \frac{\partial f}{\partial x_i} \, dS \, d\tau \end{aligned}$$

Hence, the divergence theorem implies that

$$\begin{aligned} \int_{-T}^T \int_{S(\tau)} n_i V_i \frac{\partial f}{\partial \tau} \, dS \, d\tau \\ = - \int_{-T}^T \int_{v_c(\tau)} \left[\frac{\partial}{\partial y_j} V_j \left(\frac{\partial f}{\partial \tau} + V_i \frac{\partial}{\partial x_i} f \right) + \frac{\partial}{\partial \tau} V_i \frac{\partial f}{\partial x_i} \right] \, dy \, d\tau \end{aligned}$$

And as a result it follows from Eqs. (3.A.2) and (3.10) that

$$\begin{aligned} \int_{-T}^T \int_{S(\tau)} n_i V_i \frac{\partial f}{\partial \tau} \, dS \, d\tau &= - \frac{\partial}{\partial x_j} \int_{-T}^T \int_{v_c(\tau)} a_j f(R, \tau) \, dy \, d\tau \\ &\quad + \frac{\partial}{\partial x_i \partial x_j} \int_{-T}^T \int_{v_c(\tau)} V_i V_j f(R, \tau) \, dy \, d\tau \quad (3.A.3) \end{aligned}$$

APPENDIX 3.B

LIFT SPECTRA

Suppose the frozen upwash velocity $u_2(\mathbf{y} - \hat{\mathbf{i}}U_r t)$ is cut off outside some large volume element ΔV in the manner described in Appendix 1.A (Sec. 1.A.3). Then the Fourier-transform

$$a_2(\mathbf{k}) = \frac{1}{(2\pi)^3} \iiint u_2(\mathbf{y} - \hat{\mathbf{i}}U_r t) e^{-i\mathbf{k} \cdot (\mathbf{y} - \hat{\mathbf{i}}U_r t)} \, dy$$

exists and the lift force $F_2(y_3, t)$ produced by u_2 can be found by superposing the elementary lift forces given by Eq. (3.72) to obtain

$$\begin{aligned} F_2(y_3, t) &= \pi \rho_0 U_r c \iiint a_2(\mathbf{k}) \mathcal{G}(k_1, k_3, M_r) e^{i(k_3 y_3 - k_1 U_r t)} \, d\mathbf{k} \\ &= \iiint K(\mathbf{y}') u_2(\mathbf{y}' + \hat{\mathbf{k}} y_3 - \hat{\mathbf{i}}U_r t) \, dy' \end{aligned}$$

where we have put

$$K(\mathbf{y}') \equiv \frac{1}{(2\pi)^3} \pi \rho_0 U_r c \iiint \mathcal{G}(k_1, k_3, M_r) e^{-i\mathbf{k} \cdot \mathbf{y}'} \, d\mathbf{k}$$

Hence, the cross correlation of the fluctuating lift is given by

$$\overline{F_2(y_3, t) F_2(y_3 + \eta_3, t + \tau)} = \iiint \iiint K^*(\mathbf{y}') K(\mathbf{y}'') \mathcal{R}_{22}(\mathbf{y}'' - \mathbf{y}' + \mathbf{k}\eta_3 - \mathbf{i}U_r\tau) d\mathbf{y}' d\mathbf{y}'' \quad (3.B.1)$$

where we have used the fact that the turbulence is assumed to be homogeneous so that

$$\mathcal{R}_{22} \equiv \overline{u_2(\mathbf{y}' + \mathbf{k}y_3 - iU_r t) u_2(\mathbf{y}'' + \mathbf{k}(y_3 + \eta_3) - \mathbf{i}U_r(t + \tau))}$$

depends only on the indicated argument. Introducing the turbulence spectral density Φ_{22} via Eq. (3.79) therefore yields

$$\overline{F_2(y_3, t) F_2(y_3 + \eta_3, t + \tau)} = \pi^2 \rho_0^2 U_r^2 c^2 \iint e^{i(k_3 \eta_3 - \omega \tau)} \left| \mathcal{G}(k_1, k_3, M_r) \right|^2 \int_{-\infty}^{\infty} \Phi_{22}(\mathbf{k}) dk_2 dk_1 dk_3$$

We assume that this equation exists in the limit as ΔV grows to fill all space. Then taking its inverse transform with respect to k_3 and $\omega \equiv k_1 U_r$ shows that the function H_{22} (defined immediately below Eq. (3.78)) is related to Φ_{22} by

$$H_{22}(y_3; k_3, \omega) = \pi^2 \rho_0^2 U_r c^2 \left| \mathcal{G}\left(\frac{\omega}{U_r}, k_3, M_r\right) \right|^2 \int_{-\infty}^{\infty} \Phi_{22}\left(\frac{\omega}{U_r}, k_2, k_3\right) dk_2$$

REFERENCES

1. Prandtl, Ludwig and Oskar G. Tietjens, *Fundamentals of Hydro- and Aeromechanics*. Translated by L. Rosenhead, 1st ed., McGraw-Hill, Inc., 1934.
2. Shames, Irving, *Engineering Mechanics, Dynamics*, Prentice Hall, Inc., 1958.
3. Ffowcs Williams, J. E. and D. L. Hawkings, "Sound Generation by Turbulence and Surfaces in Arbitrary Motion," *Phil. Trans. Roy. Soc. (London)*, Ser. A, **264**, 321-342, 1969.
4. Curle, N., "The Influence of Solid Boundaries on Aerodynamic Sound," *Proc. Roy. Soc. (London)*, Ser. A, **231**, 1187, 505-514, 1955.
5. Uberoi, Mahinder S., "Correlations Involving Pressure Fluctuations in Homogeneous Turbulence," NACA TN 3116, 1954.
6. Lowson, M. V., "The Sound Field for Singularities in Motion," *Proc. Roy. Soc. (London)*, Ser. A, **286**, 559-572, 1965.
7. Clark, P. J. F. and H. S. Ribner, "Direct Correlation of Fluctuating Lift and Radiated Sound for an Airfoil in Turbulent Flow," *J. Acoust. Soc. Am.*, **46**, pt. 2, no. 3, 802-805, 1969.
8. Wagner, H., "Über die Entstehung des Dynamischen Auftriebes von Tragflügeln," *ZAMM*, **5**, 1, 17-35, 1925.
9. Theodorsen, Theodore, "General Theory of Aerodynamic Instability and the Mechanism of Flutter," NACA TR 496, 1935.
10. Küssner, H. G., "Summarized Report on the Unstable Lift of Wings," *Luftfahrtforschung*, **13**, 410-424, 1936.
11. von Kármán, Th. and W. R. Sears, "Airfoil Theory for Non-Uniform Motion," *J. Aeron. Sci.*, **5**, 10, 379-390, 1938.

12. Sears, William R., "Some Aspects of Non-Stationary Airfoil Theory and its Practical Applications," *J. Aeron. Sci.*, **8**, 3, 104-188, 1941.
13. Abramowitz, Milton and Irene A. Stegun, *Handbook of Mathematical Functions With Formulas, Graphs and Mathematical Tables*. National Bureau of Standards Applied Mathematics Series 55, 1964.
14. Liepmann, H. W., "On the Application of Statistical Concepts to the Buffeting Problem," *J. Aeron. Sci.*, **19**, 12, 793-800, 1952.
15. Giesing, Joseph P., William P. Rodden and Bernhard Stahl, "Sears Function and Lifting Surface Theory for Harmonic Gusts," *J. Aircraft*, **7**, 252-255, 1970.
16. Acum, W. E. A., *The Comparison of Theory with Experiment for Oscillating Wings*. ARC-CP-681, British Aeronautical Research Council, 1962.
17. Horlock, J. H., "Fluctuating Lift Forces on Airfoils Moving Through Transverse and Chordwise Gusts," *J. Basic Eng.*, Ser. D, **90**, 4, 494-500, 1968.
18. Neumann, H. and H. Yeh, "Lift and Pressure Fluctuations of a Cambered Airfoil Under Periodic Gusts and Applications in Turbomachinery," Paper 72-GT-30, ASME, Mar. 1972.
19. Goldstein, M. E. and H. Atassi, "A Complete Second-Order Theory for the Unsteady Flow About an Airfoil Due to a Periodic Gust," *J. Fluid Mech.*, **74**, 741-765, 1976.
20. Graham, J. M. R., "Lifting Surface Theory for the Problem of an Arbitrarily Yawed Sinusoidal Gust Incident on a Thin Aerofoil in Incompressible Flow," *Aeron. Quart.*, **21**, 182-198, 1970.
21. Filotas, L. T., *Theory of Airfoil Response in a Gusty Atmosphere. Part I—Aerodynamic Transfer Function*. UTIAS-139, Toronto University, 1969.
22. Mugridge, B. D., "Gust Loading on a Thin Airfoil," *Aeron. Quart.*, **22**, pt. 3, 301-310, 1971.
23. Landahl, M., *Unsteady Transonic Flow*, Pergamon Press, 1961.
24. Osborne, C., "Unsteady Thin-Airfoil Theory for Subsonic Flow," *AIAA J.*, **11**, 2, 205-209, 1973.
25. Amiet, R., "Compressibility Effects in Unsteady Thin-Airfoil Theory," *AIAA J.*, **12**, 2, 252-255, 1974.
26. Graham, J. M. R., "Similarity Rules for Thin Airfoils in Non-Stationary Flows," *J. Fluid Mech.*, **43**, 753-766, 1970.
27. Batchelor, George Keith, *The Theory of Homogeneous Turbulence*, Cambridge University Press, 1953.
28. Sharland, I. J., "Sources of Noise in Axial Flow Fans," *J. Sound Vibr.*, **1**, 3, 302-322, 1964.
29. Phillips, O. M., "The Intensity of Aeolian Tones," *J. Fluid Mech.*, **1**, pt. 6, 607-624, 1956.
30. Paterson, R. W., P. G. Vogt and M. R. Fink, "Vortex Noise of Isolated Airfoils." Paper 72-656, AIAA, June 1972.
31. Tam, C. K. W., "Discrete Tones of Isolated Airfoils," *J. Acoust. Soc. Am.*, **55**, 6, 1173-1177, 1974.
32. Mugridge, B. D., "Acoustic Radiation from Airfoils with Turbulent Boundary Layers," *J. Sound Vibr.*, **16**, 4, 593-614, 1971.
33. Gutin, L., "On the Sound Field of a Rotating Propeller," NACA TM 1195, 1948.
34. Lynam, E. J. H. and H. A. Webb, *The Emission of Sound by Airscrews*. ARC R&M 624, British Advisory Committee for Aeronautics, 1919.
35. Bryan, G. H., *The Acoustics of Moving Sources with Application to Airscrews*. ARC R&M 684, British Aeronautical Research Committee, 1920.
36. Deming, A. F., "Noise from Propellers with Symmetrical Sections at Zero Blade Angle," NACA TN 605, 1937.
37. Deming, A. F., "Noise from Propellers with Symmetrical Sections at Zero Blade Angle, II," NACA TN 679, 1938.
38. Gutin, L., "On the 'Rotational Sound' of an Airscrew," *Zhurnal Tekhnicheskoi Fiziki*, **12**, 76-83. (In Russian.) Translated as British National Lending Library for Science and Technology RTS 7543, 1942.
39. Hubbard, Harvey, H. and Leslie W. Lassiter, "Sound from a Two-Blade Propeller at Supersonic Tip Speeds," NACA TR 1079, 1952.
40. Lowson, M. V., "Theoretical Analysis of Compressor Noise," *J. Acoust. Soc. Am.*, **47**, 1 (part 2), 371-385, 1970.

41. Kramer, J. J., M. J. Hartman, B. R. Leonard, J. F. Klapproth and T. G. Sofrin, "Fan Noise and Performance. Aircraft Engine Noise Reduction," pp. 7-61, NASA SP-311, 1972.
42. Stuckey, T. J. and J. O. Goddard, "Investigation and Prediction of Helicopter Rotor Noise. Part I. Wessex Whirl Tower Results," *J. Sound Vibr.*, **5**, 1, 50-80, 1967.
43. Scheiman, James, "A Tabulation of Helicopter Rotor-Blade Differential Pressures, Stresses and Motions, as Measured in Flight," NASA TM X-952, 1964.
44. Schlegel, Ronald G., Robert J. King and Harold R. Mull, *Helicopter Rotor Noise Generation and Propagation*. United Aircraft Corp. (USAAVLABS-TR-66-4; AD-645884), 1966.
45. Lowson, M. V. and J. B. Ollerhead, "A Theoretical Study of Helicopter Rotor Noise," *Aerodynamic Noise*, 351-369, H. S. Ribner, ed., University of Toronto Press, 1969. (See also *J. Sound Vibr.*, **9**, 2, 197-222, 1969.)
46. Morfey, C. L., "Sound Generated in Subsonic Turbomachinery," *J. Basic Eng.*, Ser. D, **92**, 450-458, 1970.
47. Barry, B. and C. J. Moore, "Subsonic Fan Noise," *J. Sound Vibr.*, **17**, 2, 207-220, 1971.
48. Powell, Alan, "Aerodynamic Noise and the Plane Boundary," *J. Acoust. Soc. Am.*, **32**, 8, 982-990, 1960.
49. Olsen, William A., Jeffrey H. Miles and Robert G. Dorsch, "Noise Generated by Impingement of a Jet Upon a Large Flat Plate," NASA TN D-7075, 1972.
50. Davies, H. G., "The Radiated Fields of Multipole Point Sources Near a Solid Spherical Surface," *J. Fluid Mech.*, **43**, 597-606, 1970.
51. Doak, P. E., "Acoustic Radiation from a Turbulent Fluid Containing Foreign Bodies," *Proc. Roy. Soc. (London)*, Ser. A, **254**, 129-145, 1960.
52. Ffowcs Williams, J. E. and L. H. Hall, "Aerodynamic Sound Generation by Turbulent Flow in the Vicinity of a Scattering Half Plane," *J. Fluid Mech.*, **40**, part 4, 657-670, 1970.
53. McDonald, H. M., "A Class of Diffraction Problems," *Proc. London Math. Soc.*, **2**, 14, 410-427, 1915.
54. Hayden, R. E., *Sound Generation by Turbulent Wall Jet Flow Over a Trailing Edge*. M.S. Thesis, Mech. Eng. Dept., Purdue Univ., 1969.
55. Crighton, D. G. and F. G. Leppington, "On the Scattering of Aerodynamic Noise," *J. Fluid Mech.*, **46**, 577-597, 1971.
56. Jones, D. S., "Aerodynamic Sound Due to a Source Near a Half-Plane," *J. Inst. Math. Applics.*, **9**, 114-122, 1972.
57. Leppington, F. G., "Scattering of Quadrupole Sources Near the End of a Rigid Semi-Infinite Circular Pipe," *Aeronautical Research Council Papers on Novel Aerodynamic Noise Source Mechanisms at Low Jet Speeds*, ARC-CP-1195, British Aeronautical Research Council, 1972.
58. Noble, Benjamin, *Methods Based on the Wiener-Hopf Technique*, Pergamon Press, 1958.
59. Crighton, D. G., "The Excess Noise Field of Subsonic Jets," *J. Fluid Mech.*, **56**, 683-694, 1972.
60. Olsen, W. and R. Friedman, "Jet Noise from Coaxial Nozzles over a Wide Range of Geometric and Flow Parameters," Paper 74-43, AIAA, Jan. 1974.
61. Boldman, D., P. Brinich and M. Goldstein, "Vortex Shedding as Related to Lip Noise," Presented at 27th Annual Meeting of the American Physical Society Division of Fluid Dynamics. Pasadena, Calif., Nov. 1974.
62. Cox, C. R. and R. A. Lynn, *A study of the Origin and Means of Reducing Helicopter Noise*. Bell Helicopter Company TCREC Tech. Rep. 62-73, U.S. Army Transportation Research Command, Fort Eustis, Virginia, November 1962.
63. Meecham, W. C., *Surface and Volume Sound from Boundary Layers*, *J. Acoust. Soc. Am.*, **37**, 3, 516-522, 1965.
64. Metzger, F. B., B. Magliozzi, G. Towle and L. Gray, "A Study of Propeller Noise Research," *Aerodynamic Noise*, 371-386, H. S. Ribner, ed., University of Toronto Press, 1969.

4 EFFECT OF UNIFORM FLOW

4.1 INTRODUCTION

The formulation of the aerodynamic sound problem developed in the last two chapters is only useful when the acoustic waves propagate through a medium that is largely at rest relative to the observer. There are numerous situations, however, where the surrounding medium is more nearly in a state of uniform motion. For example, aircraft engine fans and compressors can often be modeled, in so far as their acoustics is concerned, as if they were embedded in an infinite straight duct containing a nearly uniform flow (as indicated in Fig. 4.1).

4.2 DERIVATION OF BASIC EQUATION

On page 16 we showed that it is often possible to transform problems involving sound propagation in a uniformly moving medium into equivalent stationary-medium problems. Thus, when the mean flow velocity U is

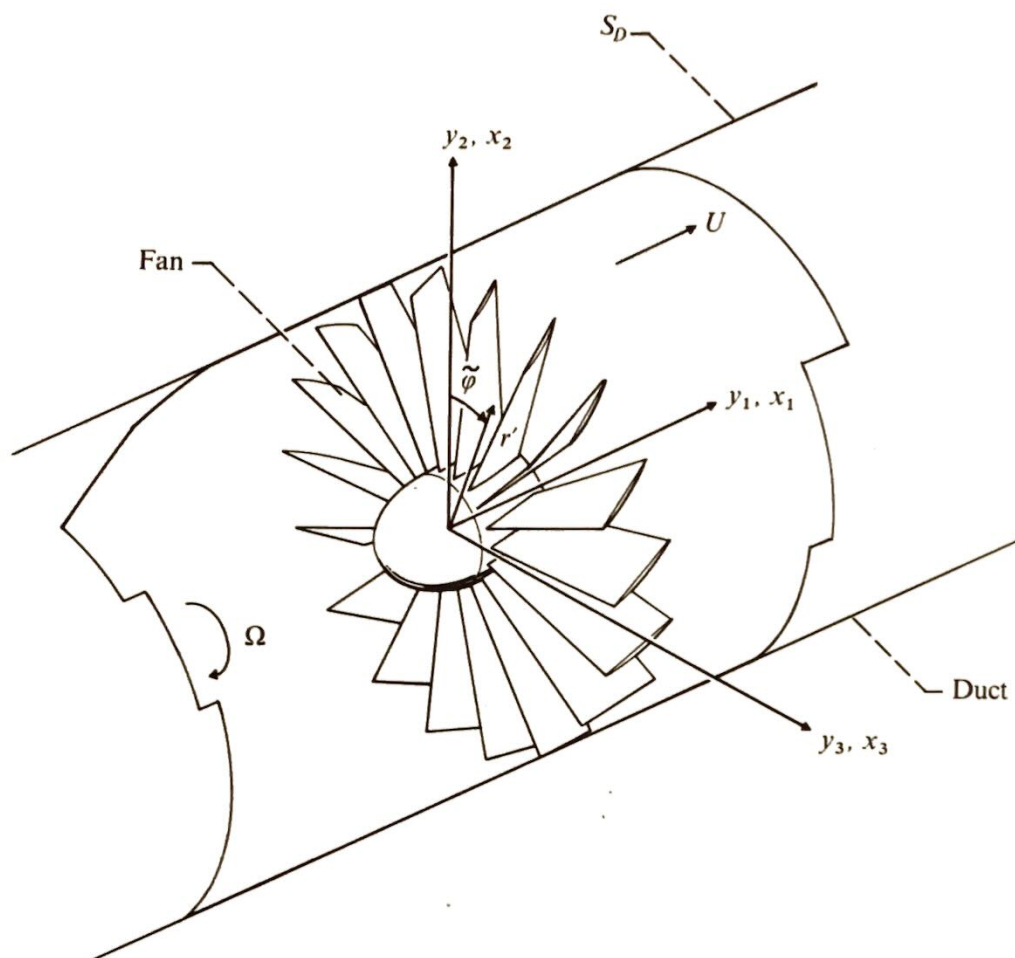


Fig. 4.1 Fan in an infinite duct.

effectively constant and parallel to the y_1 direction, it is appropriate to introduce the transformation

$$y'_i = y_i - \delta_{1i} U \tau \quad (4.1)$$

Then since the acoustic propagation is governed by a stationary-medium wave equation in the y' frame, it ought to be possible to describe the sound emission from a localized source region embedded in a uniform flow by applying Lighthill's equation in these coordinates. In fact, since Lighthill's equation is an exact consequence of the continuity and momentum equations and since the latter equations are invariant under the Galilean transform (4.1), Eqs. (2.4) and (2.5) show that

$$\frac{\partial^2 \rho'}{\partial \tau^2} - c_0^2 \frac{\partial^2 \rho'}{\partial y'_i \partial y'_i} = \frac{\partial^2 T'_{ij}}{\partial y'_i \partial y'_j} \quad (4.2)$$

where

$$T'_{ij} = \rho v'_i v'_j + \delta_{ij} [(p - p_0) - c_0^2 (\rho - \rho_0)] - e_{ij} \quad (4.3)$$

is Lighthill's stress tensor expressed in terms of the velocity

$$v'_i = v_i - \delta_{1i} U \quad (4.4)$$

measured in the moving frame and as before $\rho' \equiv \rho - \rho_0$. But, since it is usually more convenient to work in a stationary coordinate system, we reintroduce the fixed-frame coordinates y_i into Eq. (4.2) (but retain the moving-frame velocities) to obtain

$$\frac{D_0^2}{D\tau^2} \rho' - c_0^2 \frac{\partial^2 \rho'}{\partial y_i \partial y_i} = \frac{\partial^2 T'_{ij}}{\partial y_i \partial y_j} \quad (4.5)$$

where

$$\frac{D_0}{D\tau} \equiv \frac{\partial}{\partial \tau} + U \frac{\partial}{\partial y_1} \quad (4.6)$$

The density fluctuations will therefore satisfy an inhomogeneous *convected* wave equation which, like Lighthill's result, is an exact consequence of the continuity and momentum equations. Hence, the unsteady flow outside the source region should exhibit the characteristics of acoustic waves in a uniformly moving medium.

A procedure similar to the one described above can be used to show that the momentum Eq. (2.3) can be put in the form

$$\frac{D_0}{D\tau} \rho v'_i + c_0^2 \frac{\partial \rho}{\partial y_i} = - \frac{\partial T'_{ij}}{\partial y_j} \quad (4.7)$$

Since Eq. (4.5) has the same form as Eq. (1.61), the integral formula (1.65) can be applied to this result in the same way it was applied to Lighthill's equation in Sec. 3.2 to obtain, upon using essentially the same manipulations (but with Eq. (4.7) used in place of Eq. (2.3)),

$$\begin{aligned} \rho' = & \frac{1}{c_0^2} \int_{-T}^T \int_{v(\tau)} \frac{\partial^2 G}{\partial y_i \partial y_j} T'_{ij} dy d\tau + \frac{1}{c_0^2} \int_{-T}^T \int_{S(\tau)} \frac{\partial G}{\partial y_i} f_i dS(y) d\tau \\ & - \frac{1}{c_0^2} \int_{-T}^T \int_{S(\tau)} n_i h'_i dS(y) d\tau \end{aligned} \quad (4.8)$$

where G now denotes a fundamental solution of the uniformly moving-medium wave equation (i.e., it satisfies Eq. (1.62)) and h'_i is given by

$$n_i h'_i = n_i \left(\frac{D_0}{D\tau} \rho v'_i G + v'_i \frac{\partial}{\partial y_j} \rho v'_j G \right) - n_i \rho_0 v'_i \frac{D_0 G}{D\tau} \quad (4.9)$$

rather than by Eq. (3.5).

Instead of using Leibniz's rule (Eq. (1.B.2)) to transform the last integral in Eq. (4.8) (as is done in Sec. 3.2), it is convenient to first add on the divergence theorem to obtain

$$\frac{d}{d\tau} \int_{v(\tau)} \varphi dy = \int_{v(\tau)} \frac{D_0 \varphi}{D\tau} dy + \int_{S(\tau)} V'_n \varphi dS(y)$$

where V'_n is defined by Eq. (1.64). Then upon applying this formula to $\partial \rho v'_i G / \partial y_i$ in the same way as Leibniz's rule was applied to $\partial \rho v_i G / \partial y_i$ in Sec. 3.2 we find that the first term in Eq. (4.9) will not contribute to the last integral in Eq. (4.8), and as a consequence that

$$\begin{aligned} \rho'(\mathbf{x}, t) = & \frac{1}{c_0^2} \int_{-T}^T \int_{v(\tau)} \frac{\partial^2 G}{\partial y_i \partial y_j} T'_{ij} dy d\tau + \frac{1}{c_0^2} \int_{-T}^T \int_{S(\tau)} \frac{\partial G}{\partial y_i} f_i dS(\mathbf{y}) d\tau \\ & + \frac{1}{c_0^2} \int_{-T}^T \int_{S(\tau)} \rho_0 V'_n \frac{D_0 G}{D\tau} dS(\mathbf{y}) d\tau \end{aligned} \quad (4.10)$$

where

$$V'_n = V_n - n_1 U \quad (4.11)$$

This equation differs from Eq. (3.6) in several respects. First, it involves a fundamental solution for the moving-medium wave equation (determined by Eq. (1.62)) instead of a fundamental solution for the stationary-medium wave equation. Second, Lighthill's stress tensor is expressed in terms of the relative velocity $v'_i = v_i - \delta_{1i} U$ instead of the total velocity v_i . And finally, the volume displacement term is expressed in terms of $V'_n = V_n - n_1 U$ and $D_0/D\tau$ rather than V_n and $\partial/\partial\tau$.

4.3 APPLICATION TO FAN AND COMPRESSOR NOISE

4.3.1 Derivation of Basic Equation

Equation (4.10) is especially suitable for predicting *axial flow* fan and compressor noise. We shall use it to calculate the sound emitted by a single fan (or compressor) in an infinite circular duct (see Fig. 4.1) containing a uniform flow with velocity U . In this case it is natural to use the Green's function (1.C.14) whose normal derivative vanishes on the surface S_D of the duct. Then since the pressure component of the surface force f_i (given by Eq. (3.4)) is in the normal direction, the contribution of S_D to the first surface integral in Eq. (4.10) is

$$\frac{1}{c_0^2} \int_{-T}^T \int_{S_D} \frac{\partial G}{\partial y_i} e_{ij} n_j dS(\mathbf{y}) d\tau$$

Since this term represents the generation of sound by the fluctuating viscous stresses acting on the duct boundary, its contribution to the sound field is almost certainly negligible (see Sec. 3.6.1) at the high Reynolds numbers that are of interest in practical engineering devices. Moreover, since $n_1 = V_n = 0$ on S_D , this boundary will also not contribute to the third integral in

Eq. (4.10). Hence the surface integrals in this equation need only be carried out over the periphery $S_F(\tau)$ of the rotor blades so that

$$\begin{aligned} \rho'(\mathbf{x}, t) = & \frac{1}{c_0^2} \int_{-T}^T \int_{v(\tau)} \frac{\partial^2 G}{\partial y_i \partial y_j} T'_{ij} dy d\tau + \frac{1}{c_0^2} \int_{-T}^T \int_{S_F(\tau)} \frac{\partial G}{\partial y_i} f_i dS(\mathbf{y}) d\tau \\ & + \frac{1}{c_0^2} \int_{-T}^T \int_{S_F(\tau)} \rho_0 V'_n \frac{D_0 G}{D\tau} dS(\mathbf{y}) d\tau \end{aligned} \quad (4.12)$$

where $v(\tau)$ now denotes the region inside the duct, excluding the space occupied by the rotor blades. The first term in this equation can be interpreted as a volume quadrupole sound source while the second term can be interpreted as a dipole source arising from the fluctuating forces exerted on the flow by the rotor. The last term represents the sound generated by the volume displacement effects of the blades.

We shall follow the procedure used for propeller noise in Sec. 3.5.3. Thus, we again neglect the contributions of the volume quadrupole term and the volume displacement effects† to obtain

$$\rho'(\mathbf{x}, t) = \frac{1}{c_0^2} \int_{-T}^T \int_{S_F(\tau)} \frac{\partial G}{\partial y_i} f_i dS(\mathbf{y}) d\tau \quad (4.13)$$

As in the case of a propeller, it is usual to express the force \mathbf{f} exerted by the blades on the flow in terms of an axial thrust component f_T and a circumferential drag component f_D so that $\mathbf{f} = \{f_T, -f_D \sin \tilde{\varphi}, f_D \cos \tilde{\varphi}\}$ and

$$f_j \frac{\partial}{\partial y_j} = \frac{f_D}{r'} \frac{\partial}{\partial \tilde{\varphi}} + f_T \frac{\partial}{\partial y_1} \quad (4.14)$$

where $r' = \sqrt{y_2^2 + y_3^2}$, $\tilde{\varphi} = \tan^{-1}(y_3/y_2)$ and y_1 are cylindrical coordinates of the source point (see Fig. 4.1). It is also convenient to introduce the cylindrical coordinates $r = \sqrt{x_2^2 + x_3^2}$, $\varphi = \tan^{-1}(x_3/x_2)$ and x_1 of the observation point. Then inserting Eq. (4.14) and the Green's function (1.C.14) with the circular-duct eigen-functions (1.C.15) into Eq. (4.13), and carrying out the differentiations yields

$$\begin{aligned} \rho' = & \frac{1}{4\pi c_0^2} \sum_{m=-\infty}^{\infty} \sum_{n=1}^{\infty} \frac{J_m(\kappa_{m,n} r)}{\Gamma_{m,n}} \int_{-\infty}^{\infty} \frac{e^{-i(\gamma_{n,m}^{\pm} x_1 + \omega t)}}{k_{n,m}} \\ & \times \int_{-T}^T \int_{S_F(\tau)} J_m(\kappa_{m,n} r') e^{-i(m\tilde{\varphi} - \gamma_{n,m}^{\pm} y_1)} \left(\frac{m}{r'} f_D - \gamma_{n,m}^{\pm} f_T \right) e^{i\omega\tau} d\tau dS(\mathbf{y}) d\omega \end{aligned} \quad (4.15)$$

† It can be shown that the sound produced by the volume displacement effects will not propagate in an infinite duct at subsonic tip speeds (see page 198 below), while, as indicated in Chap. 3, the justification for neglecting the quadrupole source will be given in Chap. 5.

where

$$\left. \begin{aligned} \beta &= \sqrt{1 - M^2} = \sqrt{1 - \left(\frac{U}{c_0}\right)^2} \\ k_{n,m}(k_0) &\equiv \sqrt{k_0^2 - \beta^2 \kappa_{m,n}^2} \end{aligned} \right\} \quad (4.16)$$

$$\gamma_{n,m}^{\pm}(k_0) \equiv \frac{Mk_0}{\beta^2} \pm \frac{k_{n,m}(k_0)}{\beta^2} \quad (4.17)$$

$k_0 \equiv \omega/c_0$ and the plus (upper) sign holds when the observer is upstream of the rotor ($x_1 < y_1$), while the minus sign holds when the observer is downstream of the rotor ($x_1 > y_1$). The remaining quantities are defined in Appendix 1.C where the duct radius is denoted by r_d .

It is again convenient to express the source integrals in terms of a coordinate system ζ that rotates with the blades. The cylindrical coordinates corresponding to this frame are r' , y_1 , and

$$\varphi' \equiv \tilde{\varphi} - \Omega\tau \quad (4.18)$$

where Ω is the angular velocity of the fan. Then the limits of integration in the surface integral over the rotor blades become independent of τ , and we can interchange the order of this integration with the one over time to obtain

$$\begin{aligned} \rho' &= \frac{1}{4\pi c_0^2} \sum_{m=-\infty}^{\infty} \sum_{n=1}^{\infty} \frac{J_m(\kappa_{m,n}r)}{\Gamma_{m,n}} \int_{-\infty}^{\infty} \frac{e^{-i(\gamma_{n,m}^{\pm}x_1 + \omega t)}}{k_{n,m}} \\ &\quad \times \int_{S_F} J_m(\kappa_{m,n}r') e^{-i(m\varphi' - \gamma_{n,m}^{\pm}y_1)} \int_{-T}^T \left(\frac{m}{r'} f_D - \gamma_{n,m}^{\pm} f_T \right) e^{i(\omega - m\Omega)\tau} d\tau dS(\zeta) d\omega \end{aligned}$$

The procedure developed for propellers in Sec. 3.5.3 can now be used to transform the integration over the front surfaces of the rotor blades (Fig. 3.14), denoted by superscript (1), and the back surface, denoted by a superscript (2), to an integration over the projected area A of the blades on the rotational plane of the fan (or compressor). Then the preceding equation becomes

$$\begin{aligned} \rho' &= \frac{1}{4\pi c_0^2} \sum_{m=-\infty}^{\infty} \sum_{n=1}^{\infty} \frac{J_m(\kappa_{m,n}r)}{\Gamma_{m,n}} \int_{-\infty}^{\infty} \frac{e^{-i(\gamma_{n,m}^{\pm}x_1 + \omega t)}}{k_{n,m}} \\ &\quad \times \int_A J_m(\kappa_{m,n}r') e^{-im\varphi'} \int_{-T}^T \left(\frac{m}{r'} g_D^{\pm} - \gamma_{n,m}^{\pm} g_T^{\pm} \right) e^{i(\omega - m\Omega)\tau} d\tau \\ &\quad \times r' dr' d\varphi' d\omega \end{aligned} \quad (4.19)$$

where

$$g_{\alpha}^{\pm} \equiv \frac{f_{\alpha}^{(1)}}{|\hat{n}_1^{(1)}|} e^{i\gamma_{n,m}^{\pm}y_1^{(1)}} + \frac{f_{\alpha}^{(2)}}{|\hat{n}_1^{(2)}|} e^{i\gamma_{n,m}^{\pm}y_1^{(1)}} \quad \text{for } \alpha = T, D$$

and, as in Chap. 3, $\hat{n}_1^{(1)}$ denotes the y_1 -component as the unit normal $\hat{\mathbf{n}}^{(1)}$ to the front surfaces of the fan blades. We again assume that the variation

in retarded time between the front and back surfaces of the rotor blades can be neglected so that $g_\alpha^\pm \simeq \tilde{f}_\alpha \exp(i\gamma_{n,m}^\pm y_1^c)$ where $y_1^c(r', \varphi')$ is the axial (y_1) coordinate of the blade chord (measured in the rotating reference frame) and

$$\tilde{f}_\alpha \equiv \frac{f_\alpha^{(1)}}{|\hat{n}_1^{(1)}|} + \frac{f_\alpha^{(2)}}{|\hat{n}_1^{(2)}|} \quad \text{for } \alpha = T, D \quad (4.20)$$

is the net thrust or drag force per unit projected area acting on the blades at the point r', φ' . With this approximation, Eq. (4.19) becomes

$$\begin{aligned} \rho' = & \frac{1}{4\pi c_0^2} \sum_{m=-\infty}^{\infty} \sum_{n=1}^{\infty} \frac{J_m(\kappa_{m,n} r)}{\Gamma_{m,n}} \int_{-\infty}^{\infty} \frac{e^{-i(\gamma_{n,m}^\pm x_1 + \omega t)}}{k_{n,m}} \\ & \times \int_A J_m(\kappa_{m,n} r') e^{i(\gamma_{n,m}^\pm y_1^c - m\varphi')} \int_{-T}^T \left(\frac{m}{r'} \tilde{f}_D - \gamma_{n,m}^\pm \tilde{f}_T \right) e^{i(\omega - m\Omega)\tau} d\tau \\ & \times r' dr' d\varphi' d\omega \end{aligned} \quad (4.21)$$

4.3.2 Application to Pure Tones

A typical subsonic aircraft engine fan noise spectrum is shown in Fig. 4.2. Figure 4.2(a) corresponds to the frequency range above 1 kilohertz (1000 cycles/sec), while Fig. 4.2(b) corresponds to the range from 0.1 to 1 kilohertz (100 to 1000 cycles/sec) measured with a narrower bandwidth filter. As in the case of propeller noise, the spectrum consists of a broadband component on which pure tones (corresponding to fan whine) are imposed at various multiples of the shaft rotational speed Ω .

Now Eq. (4.21) is quite general and can be used equally well to predict both pure tone and broadband noise. The latter is the result of essentially random blade forces, while the former results from periodic forces. In this section, Eq. (4.21) will be used to predict the sound generated by blade forces that are periodic at the shaft rotational frequency Ω . Such forces are usually caused by steady but nonuniform flows that enter the fan or compressor as a result of upstream obstructions such as inlet guide vanes (stator) or the inlet flow distortions that arise from crossflows, streamwise vorticity sucked into the duct from nearby obstacles and very large scale inlet turbulence.†

Derivation of equations. Since the blade forces are now assumed to be periodic they can now be represented by a Fourier series

$$\tilde{f}_\alpha(\tau) = \sum_{p=-\infty}^{\infty} F_p^\alpha e^{-ip\Omega\tau} \quad \text{for } \alpha = T, D \quad (4.22)$$

† The first estimates of the pure tone fan noise resulting from inlet guide vanes were made by Hetherington¹ in 1963, who combined the unsteady-lift theories of Sears and Kemp with a free-space radiation model in which each blade was regarded as a line force. The effect of the duct on the radiated sound field was first discussed by Tyler and Sofrin.²

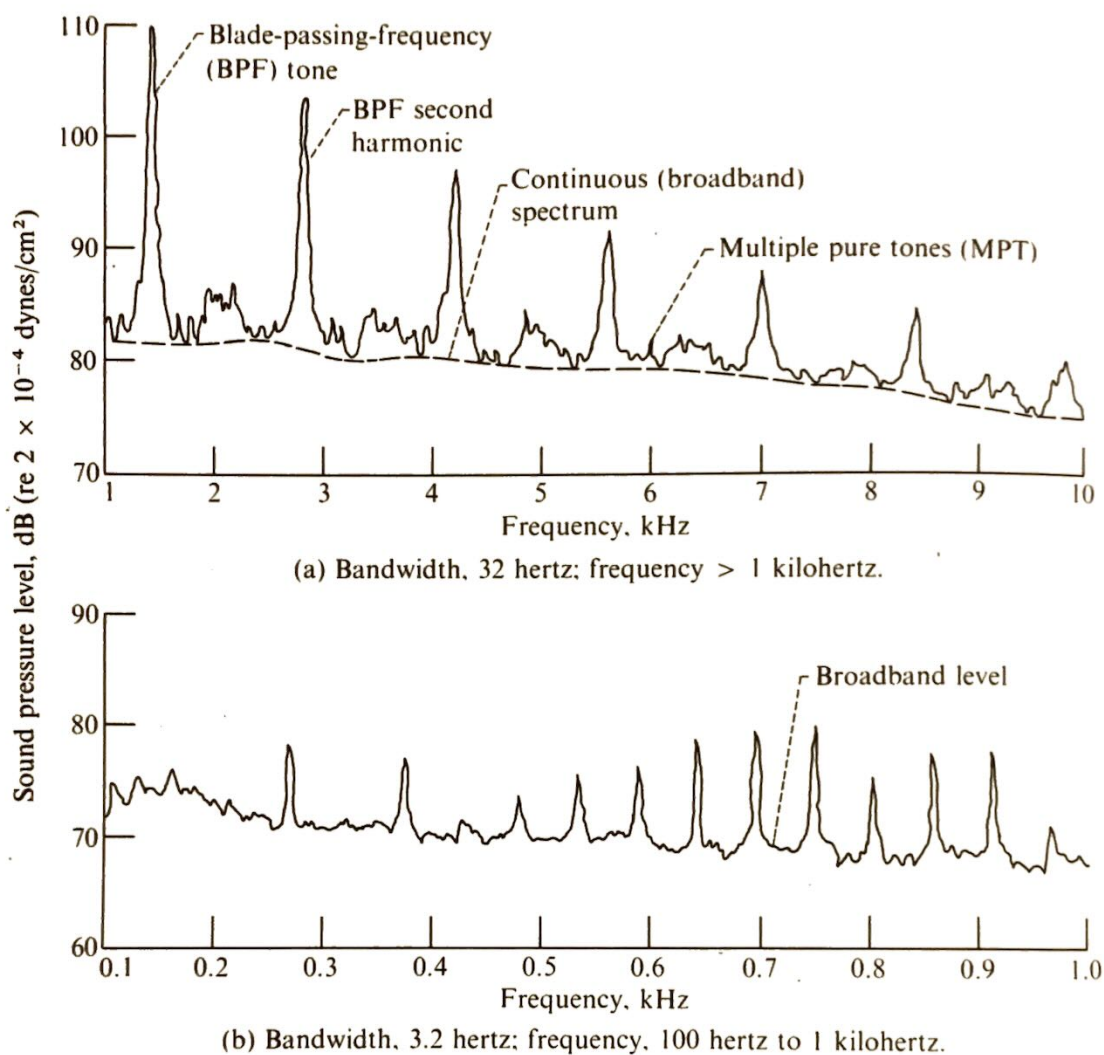


Fig. 4.2 Typical sound pressure level spectrum. Azimuth angle, 40° from fan inlet. (Measurements taken at NASA Lewis Research Center.)

whose Fourier coefficients are determined by (Appendix 1.A.1)

$$F_p^\alpha = \frac{\Omega}{2\pi} \int_0^{2\pi/\Omega} \tilde{f}_\alpha e^{ip\Omega\tau} d\tau \quad (4.23)$$

Then inserting Eq. (4.22) into (4.21), using the fact that

$$\lim_{T \rightarrow \infty} \int_{-T}^T e^{i(\omega - s\Omega)\tau} d\tau = 2\pi\delta(\omega - s\Omega)$$

and putting

$$s = m + p \quad (4.24)$$

we find after summing over s and p instead of m and p that the sound field can itself be expressed as a Fourier series

$$\rho' = \sum_{s=-\infty}^{\infty} \rho_s(\mathbf{x}) e^{-is\Omega t} \quad (4.25)$$

whose s th harmonic ρ_s is given by

$$\rho_s(\mathbf{x}) = \frac{1}{2c_0^2} \sum_{p=-\infty}^{\infty} \sum_{n=1}^{\infty} \frac{J_m(\kappa_{m,n}r)}{\Gamma_{m,n}k_{n,m,s}} e^{i(m\varphi - \gamma_{n,m,s}^{\pm}x_1)} \times (m\tilde{D}_{n,m,p}^{\pm} - \gamma_{n,m,s}^{\pm}\tilde{T}_{n,m,p}^{\pm}) \quad (4.26)$$

where

$$k_{n,m,s} \equiv k_{n,m} \left(\frac{\Omega s}{c_0} \right) = \sqrt{\frac{\Omega^2 s^2}{c_0^2} - \beta^2 \kappa_{m,n}^2} \quad (4.27)$$

$$\gamma_{n,m,s}^{\pm} \equiv \gamma_{n,m}^{\pm} \left(\frac{\Omega s}{c_0} \right) = \frac{M\Omega s}{\beta^2 c_0} \pm \frac{k_{n,m,s}}{\beta^2} \quad (4.28)$$

and the thrust and drag coupling coefficient to $\tilde{T}_{n,m,p}^{\pm}$ and $\tilde{D}_{n,m,p}^{\pm}$ are defined by

$$\left. \begin{aligned} \tilde{T}_{n,m,p}^{\pm} &\equiv \int_A J_m(\kappa_{m,n}r') e^{i(\gamma_{n,m,s}^{\pm}x_1' - m\varphi')} F_p^T r' dr' d\varphi' \\ \tilde{D}_{n,m,p}^{\pm} &\equiv \int_A J_m(\kappa_{m,n}r') e^{i(\gamma_{n,m,s}^{\pm}x_1' - m\varphi')} F_p^D dr' d\varphi' \end{aligned} \right\} \quad (4.29)$$

Equation (4.25) shows that the density fluctuation is the sum of an infinite number of tones at multiples of the shaft rotational frequency Ω . The amplitudes of these tones are expressed via Eq. (4.26) as a sum of terms called *modes*. When the tones result from a nonuniform flow entering a fan with B identical blades, the blade force distribution must satisfy Eq. (3.111). Hence, its Fourier coefficients (4.23) are related to the Fourier coefficients (3.113) of individual blade forces by Eq. (3.112). Upon inserting this into Eq. (4.26) and transforming the result in the manner described in Sec. 3.5.3 we find that only harmonics of the blade passing frequency ΩB actually contribute to the sum (4.25) and, consequently, that

$$\rho_{sB}(\mathbf{x}) = \frac{B}{2c_0^2} \sum_{p=-\infty}^{\infty} \sum_{n=1}^{\infty} \frac{J_m(\kappa_{m,n}r)}{\Gamma_{m,n}k_{n,m,sB}} e^{i(m\varphi - \gamma_{n,m,sB}^{\pm}x_1)} \times (mD_{n,m,p}^{\pm} - \gamma_{n,m,sB}^{\pm}T_{n,m,p}^{\pm}) \quad (4.30)$$

where

$$m = sB - p \quad (4.31)$$

the single blade force coupling coefficients, $D_{n,m,p}^{\pm}$ and $T_{n,m,p}^{\pm}$, are given by

$$\left. \begin{aligned} T_{n,m,p}^{\pm} &\equiv \int_{A_0} J_m(\kappa_{m,n}r') e^{i(\gamma_{n,m,sB}^{\pm}x_1' - m\varphi')} F_{T,p}^0 r' dr' d\varphi' \\ D_{n,m,p}^{\pm} &\equiv \int_{A_0} J_m(\kappa_{m,n}r') e^{i(\gamma_{n,m,sB}^{\pm}x_1' - m\varphi')} F_{D,p}^0 dr' d\varphi' \end{aligned} \right\} \quad (4.32)$$

and A_0 is the projected area on the rotational plane of a single fan (or compressor) blade. In many cases, y_1^c can be approximated quite closely by $y_1^c \simeq r'\varphi' \cot \chi$ where χ is the stagger angle of the blade (defined in Chap. 3).

Equation (4.30) is based on the assumption that all blades are identical, and as a result it only predicts tones at harmonics of the blade passing frequency. However, nonuniformities in either blade geometry or spacing can cause tones to be generated at multiples of the disk or shaft rotational frequency. It can be seen from the fan spectrum in Fig. 4.2 that these tones, which presumably result from small nonuniformities in the fan geometry, are indeed much weaker than those at the blade passing frequency.

Effect of duct on propagation. Equations (4.27) and (4.28) and the remarks following Eq. (1.C.11) show that $\mathcal{I}m \gamma_{n,m,sB}^+ > 0$ and $\mathcal{I}m \gamma_{n,m,sB}^- < 0$ whenever

$$\beta^2 \kappa_{m,n}^2 > \frac{s^2 \Omega^2 B^2}{c_0^2} \quad (4.33)$$

Hence, any mode in Eq. (4.30) that satisfies condition (4.33) will decay exponentially fast at large values of $|x_1|$. Such modes are said to be *cut off* since they do not propagate along the duct and therefore do not contribute to the sound field at large distances. Moreover, since $\kappa_{m,n}^2 \rightarrow \infty$ whenever m or n becomes infinite,³ only a finite number of modes contribute to the sound radiated in any given tone.

The index p in Eq. (4.30) individuates the harmonic of the unsteady force that generates the mode. The $p = 0$ modes are generated by the steady, or time-averaged, force. They correspond to the Gutin mechanism for propellers and, since the unsteady blade forces are caused by nonuniform inflow (page 164), they will be the only modes that occur when the inflow is spatially uniform. But since Eq. (4.31) shows that $m = sB$ when p is zero, Eq. (1.C.16) shows that the corresponding eigenvalues $\kappa_{sB,n}$ are determined by $J'_{sB}(\kappa_{sB,n} r_d) = 0$. Then since³ the smallest root $\kappa_{sB,1}$ of this equation is always larger than† sB/r_d , the cutoff condition (4.33) shows that this mode will not propagate if

$$\beta^2 \frac{s^2 B^2}{r_d^2} > \frac{\Omega^2 s^2 B^2}{c_0^2}$$

or equivalently if $M_r^2 \equiv M_t^2 + M^2 < 1$ where $M_t = r_d \Omega / c_0$ is the Mach number based on tip speed of the blade and hence $M_r \equiv \sqrt{M_t^2 + M^2}$ is the Mach number of the flow relative to the blade tip. Thus, the $p = 0$ modes will not propagate unless the flow is supersonic relative to the blade tip.‡

† For large values of sB , $\kappa_{sB,1} \simeq sB/r_d$.

‡ The precise value of M_r at which cutoff occurs approaches unity as blade number is increased.

When the blade number B is large, the decay rates of these modes (which are determined by the magnitudes of $k_{n,m,sB}$) are enormous. This is clearly evident in Fig. 4.3 (taken from Ref. 2) which corresponds to the case where $n = 1$ and $M = 0$. (The figure also serves to show the precise value of the tip Mach number at which cutoff occurs.) Thus, a fan (or compressor) operating at subsonic relative tip speeds (as many fans are designed to do) could not generate any sound if the inflow were completely uniform. However, any high-speed fan operating subsonically in a duct certainly does produce a large amount of noise. It is generally believed that this sound results from a nonuniform flow entering the rotor. Thus, in the more general case where p is not necessarily zero, the smallest root $\kappa_{sB-p,1}$ of Eq. (1.C.16) is $\kappa_{sB-p,1} \simeq (sB - p)/r_d$. Hence, the cutoff condition (4.33) becomes approximately

$$\left| \frac{sB - p}{sB} \right| > \frac{M_t}{\sqrt{1 - M^2}} \quad (4.34)$$

Suppose that the mean-flow Mach number is negligibly small (i.e., $M \simeq 0$). Then Eq. (4.34) shows there are modes (which can be generated by nonuniform inflow) that will propagate even at subsonic tip speeds. The index p of these modes must, of course, have the same sign as s .

It can be seen from Eqs. (4.25), (4.30), and (4.31) that the phase surfaces of the propagating modes rotate with angular velocity (see Sec. 1.3.2).

$$\frac{sB}{sB - p} \Omega$$

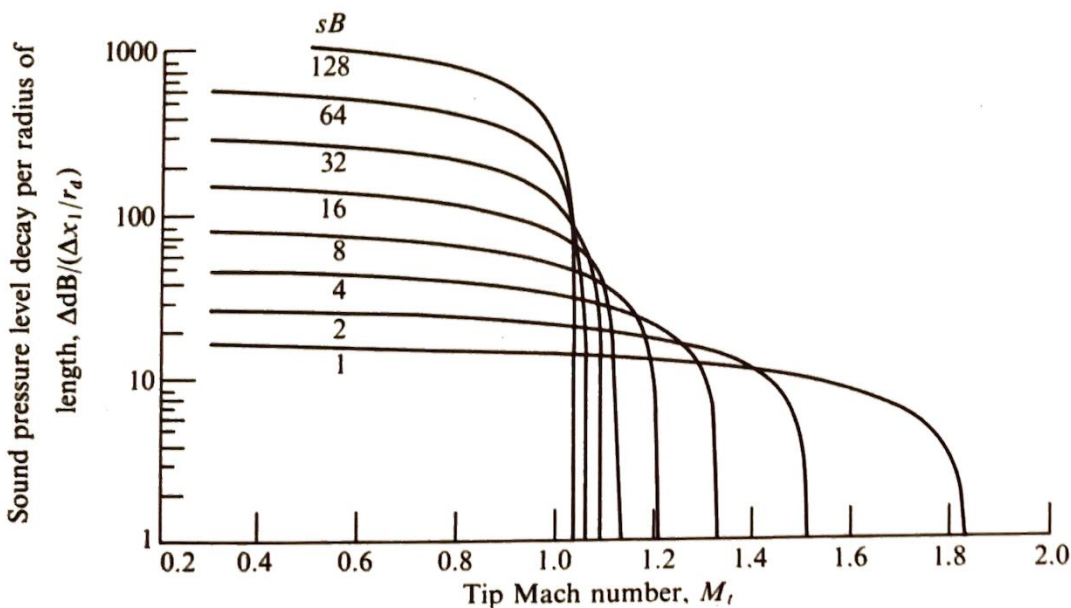


Fig. 4.3 Cylindrical duct decay rates. Mach number, M , 0; radial mode, n , 1. (From Reference 2.)

Hence, the circumferential velocity at the duct wall is

$$\frac{sB}{sB - p} M_t c_0$$

Thus, the cutoff condition (4.34) shows that *only modes that achieve supersonic rotational speeds will propagate through the duct when $M \simeq 0$.*

Radiated power. The quantity that is perhaps of most interest is the total acoustic power \mathcal{P}_{sB} radiated in a given harmonic of the blade passing frequency. This can be calculated by integrating the axial component \bar{I}_{sB} of the sB th harmonic of the intensity over the cross-sectional area of the duct. Thus,†

$$\mathcal{P}_{sB} = \mp \lim_{x_1 \rightarrow \mp \infty} 2 \int_0^{2\pi} \int_0^{r_d} \bar{I}_{sB} r dr d\varphi \quad (4.35)$$

while Eq. (1.89) and Eq. (1.A.5) of Appendix 1.A show that

$$\bar{I}_{sB} = (1 + M^2) P_{sB} U_{sB}^* + \frac{M}{\rho_0 c_0} |P_{sB}|^2 + \rho_0 c_0 M |U_{sB}|^2 \quad (4.36)$$

where

$$P_{sB} = c_0^2 \rho_{sB} \quad (4.37)$$

is the amplitude of the sB th harmonic of the pressure fluctuation and U_{sB} is the amplitude of the sB th harmonic of the acoustic (fluctuating) velocity. Since the axial component of the first Eq. (1.15) implies that U_{sB} and P_{sB} are related by

$$\frac{\partial P_{sB}}{\partial x_1} = \rho_0 c_0 \left(\frac{isB\Omega}{c_0} - M \frac{\partial}{\partial x_1} \right) U_{sB}$$

we can use Eqs. (4.30) and (4.37) to eliminate P_{sB} and thereby obtain

$$U_{sB} = \frac{1}{\rho_0 c_0} \frac{B}{2} \sum_{p=-\infty}^{\infty} \sum_{n=1}^{\infty} \frac{J_m(\kappa_{m,n} r)}{\Gamma_{m,n} k_{n,m,sB}} e^{i(m\varphi - \gamma_{n,m,sB}^{\pm} x_1)} \times \lambda_{n,m,sB}^{\pm} (m D_{n,m,p}^{\pm} - \gamma_{n,m,sB}^{\pm} T_{n,m,p}^{\pm}) \quad (4.38)$$

where

$$\lambda_{n,m,sB}^{\pm} \equiv - \frac{\gamma_{n,m,sB}^{\pm} \beta^2}{(\Omega sB/c_0) \pm M k_{n,m,sB}}$$

Then substituting Eqs. (4.30) and (4.38) into Eq. (4.36), inserting the result

† The factor 2 arises because both \bar{I}_{sB} and $\bar{I}_{-sB} = \bar{I}_{sB}$ contribute to the power in the sB th harmonic.

in Eq. (4.35) and recalling that the duct modes (1.C.15) satisfy the orthogonality condition (1.C.9) we obtain

$$\mathcal{P}_{sB} = \frac{B^2 \beta^4}{2\rho_0 c_0} \left(\frac{\Omega s B}{c_0} \right) \sum_{\substack{\text{all } p, n \text{ with} \\ \beta^2 \kappa_{m,n}^2 < \left(\frac{sB\Omega}{c_0} \right)^2}} \frac{|mD_{n,m,p}^\pm - \gamma_{n,m,p}^\pm T_{n,m,p}^\pm|^2}{\Gamma_{m,n} k_{n,m,sB} \left(\frac{\Omega s B}{c_0} \pm M k_{n,m,sB} \right)^2} \quad (4.39)$$

where

$$m = sB - p$$

And since the cutoff modes do not contribute to Eq. (4.35), the sum in Eq. (4.39) is only carried out over propagating modes. This result shows that the radiated power is just the sum of the powers radiated in each mode. Its properties are discussed further in Sec. 4.3.5.

Calculation of blade forces from flow distortion. In order to use Eq. (4.30) to predict the sound emitted from a fan, it is necessary to determine the unsteady force harmonics $F_{\alpha,p}^0$ (for $\alpha = T, D$) that appear in the single blade coupling coefficients (4.32). They can be related to the distortion velocity entering the fan by using the results already obtained in connection with propeller theory. In fact, if we suppose (for purposes of illustration) that the forces are concentrated along radial lines passing through the center of the blades (which for the $s = 1$ blade we can take without loss of generality to be the line $\varphi' = 0$), the results of the two-dimensional analysis developed on pages 166–168 can be used directly. Thus we assume that this analysis can be applied to predict the force per unit length at each radial position r' in terms of the Fourier amplitudes

$$w_p(r') = \frac{1}{2\pi} \int_0^{2\pi} e^{ip\tilde{\varphi}} w(r', \tilde{\varphi}) d\tilde{\varphi}$$

of the circumferential harmonics of the distortion velocity $w(r', \tilde{\varphi})$ which, as in the analysis just mentioned, is assumed to be in the direction of the oncoming flow. In fact, we suppose that all the assumptions on page 166 are valid. (The consequences of using such rough approximations will be discussed in Chap. 5.) Then it follows from Eq. (3.122) that the Fourier coefficients $F_{T,p}^0$ and $F_{D,p}^0$ of the torque and drag forces are given by

$$F_{T,p}^0 = - \frac{\delta(\varphi')}{r'} \pi c \rho_0 U_r w_p(r') S_c(\sigma_p, M_r) \sin \chi \sin \mu$$

$$F_{D,p}^0 = - \frac{\delta(\varphi')}{r'} \pi c \rho_0 U_r w_p(r') S_c(\sigma_p, M_r) \cos \chi \sin \mu$$

where the various quantities appearing in these equations are defined on page 168 (Fig. 3.18). These results can now be substituted into Eq. (4.32) to calculate the coupling coefficients. When radial variations in the stagger

angle χ , angle of attack μ , relative velocity U_r , and chord length c can be neglected, the resulting formulas become

$$\left. \begin{aligned} T_{n,m,p}^{\pm} \equiv T_{n,m,p} &= -\frac{c}{2} \rho_0 U_r \sin \chi \sin \mu S_c(\sigma_p, M_r) W_{n,m,p}^0 \\ D_{n,m,p}^{\pm} \equiv D_{n,m,p} &= -\frac{c}{2} \rho_0 U_r \cos \chi \sin \mu S_c(\sigma_p, M_r) W_{n,m,p}^1 \end{aligned} \right\} \quad (4.40)$$

where

$$W_{n,m,p}^j \equiv \int_0^{r_d} \int_0^{2\pi} e^{ip\tilde{\varphi}} J_m(\kappa_{m,n} r') w(r', \tilde{\varphi}) (r')^{-j} dr' d\tilde{\varphi} \quad (4.41)$$

are the distortion harmonics and c , U_r , χ , μ , and σ_p are to be interpreted as suitable average values over the duct radius. The coupling coefficients, and hence the sound field, can be calculated from these formulas once the distribution of the distortion velocity $w(r', \tilde{\varphi})$ over the fan face is known.

It is easy to show from the orthogonality property (1.C.9) of the duct eigenfunctions that the distortion harmonics $W_{n,m,p}^j$ (with p given by Eq. (4.31)) are just the coefficients of the Fourier-Bessel expansion

$$w(r', \tilde{\varphi}) = (r')^{1+j} \sum_{m=-\infty}^{\infty} \sum_{n=1}^{\infty} \frac{W_{n,m,p}^j}{\Gamma_{m,n}} J_m(\kappa_{m,n} r') e^{i(m-sB)\tilde{\varphi}} \quad (4.42)$$

of the distortion velocity in terms of the circular-duct eigenfunctions. This equation, together with Eqs. (4.30), (4.40), and (4.41), shows that the various radial modes in the acoustic field are each determined by the corresponding "modes" in the distortion field. Hence, the more radially nonuniform the distortion, the more higher order radial modes will appear in the sound field. An improved treatment of the radial velocity variation (over this simple strip theory result) can be obtained by using Eq. (3.72) to calculate the blade forces. However, this formula requires that the velocity be decomposed in an exponential Fourier series in r' which is somewhat incompatible with the natural Fourier-Bessel expansion (4.42).

Sound generated by rotor-stator interactions. In the last section we showed how the sound field can be calculated once the distortion velocity distribution entering the fan is known. But it is frequently difficult to determine this quantity, since it can vary from fan to fan in a rather unpredictable manner and in any given fan it can vary widely with operating conditions. However, it is relatively predictable, when the rotor operates behind inlet guide vanes (IGV's) or stators (as shown in Fig. 4.4). The stator-rotor interaction was first studied by Kemp and Sears.^{4,5} They pointed out that the IGV's can affect the rotors as a result of both their potential flow fields and their viscous wakes. (Of course, the same is true for a rotor

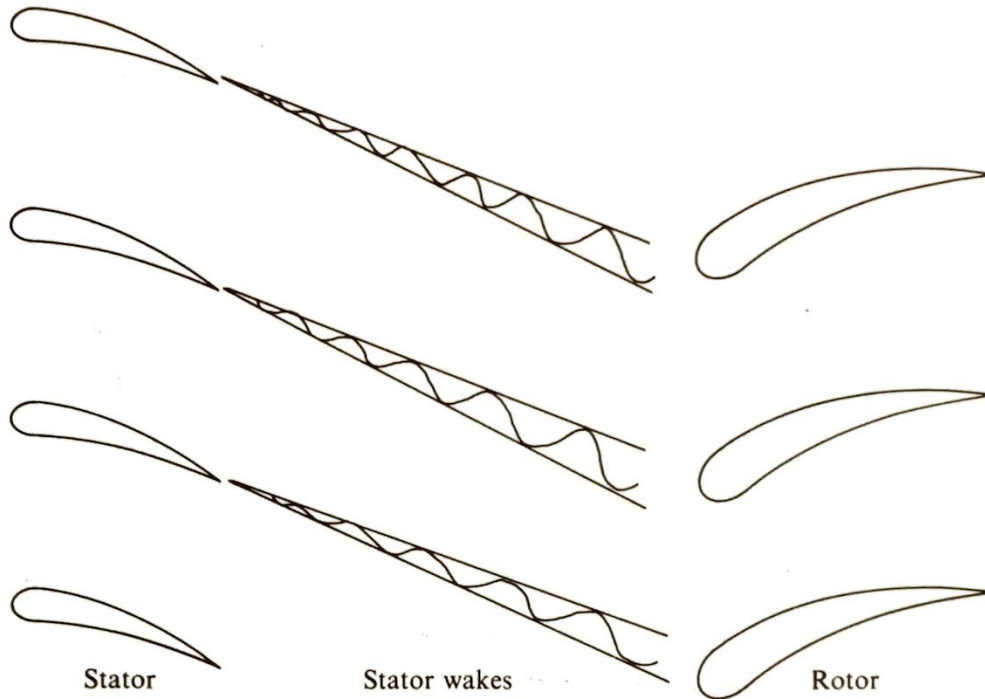


Fig. 4.4 Stator-rotor interaction.

operating in front of a stator.) Since the incompressible potential-flow field due to a two-dimensional object decays inversely with distance, while the velocity decrement in its wake decreases approximately as the square root of distance, Kemp and Sears concluded that viscous-wake interference effects will probably be important at large rotor-stator separations while potential-flow interactions will tend to dominate at small spacing. This is especially true for the high solidity stators used in current aircraft engines, since their potential flow fields actually decay exponentially fast at large distances. On the other hand, it should be kept in mind that the decay rate of a real *compressible* flow can be quite slow when its Mach number is in the high subsonic or transonic range—as it often is in fans and compressors. In any case, it appears that, in most instances, the wake effect will be of about the same order as the potential flow effects only when the rotor-stator separation is equal to a small fraction of the stator chord length. Thus since rotor-stator separations in modern aircraft engines are usually greater than a chord length, it is unlikely that the stator potential flow field will contribute significantly to the disturbance field felt by the rotor in such a device.

Suppose the viscous effects in the wake can be neglected and that the two-dimensional model developed in Sec. 3.5.3 applies (Fig. 3.17). Then the coupling coefficients are related to the wake velocity profiles (roughly) by Eqs. (4.40) and (4.41). However, a rotor operating behind a stator with V blades will see a distortion pattern that is periodic with period $2\pi/V$. Hence, the distortion harmonics (4.41) will be nonzero only when the azimuthal index p is an integral multiple of V . It therefore follows from Eq. (4.40) that

Eqs. (4.30) and (4.31) become

$$\rho_{sB} = \frac{B}{2c_0^2} \sum_{p=-\infty}^{\infty} \sum_{n=1}^{\infty} \frac{J_m(\kappa_{m,n}r)}{\Gamma_{m,n}k_{n,m,sB}} e^{i(m\varphi - \gamma_{n,m,sB}^{\pm}x_1)} \times (mD_{n,m,pV}^{\pm} - \gamma_{n,m,sB}^{\pm}T_{n,m,pV}^{\pm}) \quad (4.43)$$

and

$$m = sB - pV \quad (4.44)$$

A very similar analysis can be used to predict the sound field resulting from the passage of the rotor wakes over outlet guide vanes (OGV's). However, in this case, there is no need to transform the variables of integration into a moving-coordinate system and the OGV blade forces will be periodic in time, with period $2\pi/\Omega B$. The result

$$\rho_{sB} = \frac{V}{2c_0^2} \sum_{p=-\infty}^{\infty} \sum_{n=1}^{\infty} \frac{J_m(\kappa_{m,n}r)}{\Gamma_{m,n}k_{n,m,sB}} e^{i(m\varphi - \gamma_{n,m,sB}^{\pm}x_1)} \times (mD_{n,m,sB}^{\pm} - \gamma_{n,m,sB}^{\pm}T_{n,m,sB}^{\pm}) \quad (4.45)$$

where m is still given by Eq. (4.44), is remarkably similar to Eq. (4.43)—which is indicative of the essential similarity of the two sound-generation processes. In fact, the principal difference between these equations is that the last argument of the coupling coefficients is changed from pV to the harmonic number sB of the radiated sound frequency. It can therefore be seen from Eqs. (4.40) that the sound radiated at any given frequency by a stator is only affected by the angular harmonic of the wake velocity field with the same frequency. On the other hand, the sound radiated at a given frequency by a rotor depends upon all angular harmonics of the wake velocity field, and any given harmonic of the wake contributes to all harmonics of the sound field.

Increasing the rotor-stator separation decreases the wake velocity decrement at the downstream blade row. Hence, Eqs. (4.40) and (4.41) show that the wake interaction noise from both rotors and stators decreases with increasing separation from the upstream blade row. This effect is indeed observed in practice.

Since (as shown in Sec. 3.4.2) the Sears function, or for that matter any other response function, approaches zero at high reduced frequencies, Eqs. (4.40) imply that the noise generated by a fan stage can be reduced by increasing the reduced frequency $\sigma_p \equiv p\Omega c/2U_r$, while holding c fixed. This can always be accomplished for a fixed relative velocity by increasing the frequency $p\Omega$ of the gust. Then since Eqs. (4.40) and (4.45) imply that $p \propto B$ for rotor wake-stator interactions, it may sometimes be possible to reduce the stator noise by increasing the number of fan blades.

The wake velocity profiles tend to be sharp in the region immediately behind an upstream blade row, with many circumferential harmonics

contributing to the wake disturbance velocity. However, they tend to smooth out further downstream, and the first few harmonics probably make the dominant contributions to the velocity in this region. Hence, we expect that the sound field radiated by a stator will contain many harmonics of the blade passing frequency at small rotor-stator separations and that increasing the separation will preferentially tend to reduce the higher harmonics of the sound field. On the other hand, increasing the separation between a rotor and an upstream blade row should tend to decrease the sound in all harmonics.†

A wake that is highly nonuniform in the radial direction should contain a larger number of radial harmonics than one which is uniform. Hence, Eqs. (4.40) show that as the wake becomes more nonuniform there is a tendency to increase the higher order radial modes in the sound field. On the other hand, these modes are more likely to be cut off by the duct.

In order to calculate the acoustic radiation, it is necessary to determine the wake velocity profiles that enter the coupling coefficients (4.40) through Eq. (4.41). Kemp and Sears⁵ used the Silverstein, Katzoff, and Bullivant⁷ single-airfoil wake model in an analysis of the type described in Sec. 3.5.3 to calculate the fluctuating blade forces in a cascade. Since then this model has been used by a number of investigators to study fan noise. However, it is currently recognized that, due to such effects as the thickening caused by strong axial pressure gradients, an isolated-airfoil wake model is wholly inadequate to describe the wakes that occur in modern turbomachines. In fact, it turns out that the wakes of real fans and compressors are highly skewed.⁸ This introduces large streamwise vorticity components that are not accounted for by Silverstein's two-dimensional model and causes large radial variations in the phases of the lift fluctuations acting on the stator. An improved wake model, based on data taken behind a low speed fan rotor, was developed by Raj and Lakshminarayana.⁹

For high-solidity (i.e., high ratio of blade chord to interblade spacing) cascades the mutual interference effects between the blades could have an important influence on the fluctuating lift forces. This effect was analyzed by Henderson and Daneshyar¹¹ for two-dimensional cascade in an incompressible flow (still using linearized theory). There have been a large number of studies (which we have not mentioned) of the fluctuating blade forces in cascades. Virtually all of these (except for some recent purely numerical studies) use linearized-thin-airfoil theory. This approximation implies (since the angle of attack and camber must be small) that the blades are lightly loaded. The effects of variations in retarded time over the blade chord, which can also be important at the high Mach numbers where jet engine fans and compressors operate, are discussed in Chap. 5.

† These conclusions appear to have been first obtained by Lowson⁶ who used a free-space rotor model.

The dominant source of noise in modern high bypass ratio fan jet engines is the fan stage itself. However, most engine designs do not utilize inlet guide vanes for the fan. Therefore, the wake interaction mechanism of primary technological interest is the rotor wake–stator (OGV) interaction governed by Eq. (4.45). On the other hand, since this equation is composed of the same modes as Eq. (4.43), the cutoff condition (4.34) also applies to the rotor wake–stator interaction. But since p is now an integral multiple of V , this condition becomes

$$\left| \frac{sB - pV}{sB} \right| > \frac{M_t}{\sqrt{1 - M^2}}$$

Hence, the sound generated at the fundamental harmonic ($s = 1$) of the blade passing frequency will not propagate if

$$\left| 1 - p \frac{V}{B} \right| > \frac{M_t}{\sqrt{1 - M^2}}$$

for every integer p . This implies that a subsonic fan stage (i.e., $M_r^2 \equiv M_t^2 + M^2 < 1$), should produce no fundamental blade-passing-frequency tones if its vane-blade ratio V/B is greater than 2. Nevertheless, many fan stages designed to take advantage of this cutoff phenomenon do exhibit spectra containing strong fundamental blade-passing-frequency (BPF) tones when tested on the ground. It is generally believed that these tones are caused by steady inlet flow distortions and large scale inlet turbulence entering the fan.

Sound generated by inlet flow distortions. When aircraft engine fans are tested without being attached to aircraft the primary source of tones is often the flow distortion caused by the test rig.¹² On the other hand, Filluel¹³ and Sofrin and McCann¹⁴ have observed tones that under certain conditions, appear to be caused by inlet turbulence. Thus, inlet turbulence will always produce broadband sound by the mechanism described in Sec. 3.5.1. But a rotating fan is able to cut an effectively stationary turbulence pattern several times before the turbulent eddies decay—provided, of course, that its blade passing frequency is large compared with the frequency associated with the convection of the eddies past the fan. The radiated energy will then become concentrated around the blade passing frequency and its harmonics, and the acoustic spectrum will appear to contain tones of finite bandwidth (such as those in the experimental spectrum shown in Fig. 4.2).

Thus, inlet turbulence can be a source of both pure-tone and broadband noise. Since the frequency at which the eddies pass the fan face is U_c/l , where U_c is the convection speed and l is a typical turbulence correlation length, we expect the tones to become narrower and more pronounced as l is increased. In fact, the inlet turbulence interaction was analyzed by Mani¹⁵ (who used a model similar to the one described in Sec. 3.5.1 but applied it

to a moving cascade rather than to a single stationary strut). His results indicate that these tones will be much broader than those observed experimentally unless the turbulent eddies are extremely long (typically of the order of a couple of feet). However, there is now considerable evidence that large-scale eddies in the atmosphere become very elongated when drawn into a stationary fan and as a result are the dominant source of pure tones from engines operating on the ground. (In fact, recent measurements carried out by Hansen at Hamilton Standard¹⁰ indicate that these eddies may be over a hundred engine diameters long.) Conversely, the eddies are not stretched when the aircraft is in forward flight and as a result are so large in the direction transverse to the flow that they simply pass over the engine without generating any noise. Supporting this conjecture are recent measurements by Cumpsty and Lowrie³⁰ which indicate that the tones produced by the RB.211 engine are considerably reduced in amplitude and frequently much less fluttery in forward flight.

Of course, the most intense eddies entering the fan are confined to the casing boundary layer. But since the characteristic scale of the turbulence in this region is usually quite small, it is probably not responsible for producing blade passing frequency tones.

Inlet turbulence can also produce sound in an isolated rotor through a quadrupole interaction that was first proposed by Ffowcs Williams and Hawkings.¹⁶ Thus, a loaded rotor induces a spinning "rotor-locked" asymmetric pressure field in the fan duct which, as we have seen, cannot propagate at subsonic tip speeds. But when this pattern interacts with inlet turbulence, it produces a fluctuating Reynolds stress that can act as a quadrupole sound source.

This process has been studied in some detail by Chandrashekhara¹⁷ for low-speed (tip Mach number less than 0.3) fans. A free-space rotor model of the type described in Sec. 3.5.3 was used. He found that the dipole noise always exceeded the quadrupole noise and, that Mani's dipole theory¹⁵ actually agreed fairly well with his measurements of the sound field. However, the ratio of the strength of the quadrupole to that of a dipole varies as a typical Mach number squared, while the intensity of the quadrupole increases in direct proportion to the blade loading. Hence, it is quite possible that the quadrupole source will dominate at the higher Mach numbers and high blade loadings where real aircraft engine fans operate. In fact, the amplitudes of the blade passage frequency tones produced by actual aircraft fans do not always increase with tip Mach number as the dipole model seems to predict. Thus, as pointed out by Mani,¹⁹ recent experiments by Gelder and Soltis¹⁸ on very clean inlet fans show that the inlet BPF power levels often increase with increasing blade loading even when the relative tip Mach number decreases—a behavior that is not uncharacteristic of the quadrupole source.

On the other hand, it is shown in the next chapter that the quadrupole source will not be significant, even at very high subsonic Mach numbers,

unless the turning of the flow produced by the fan is a significant fraction of the flow velocity relative to the blades—a condition that does not usually occur at the blade tips where most of the sound is generated.

The possibility that the quadrupole term in Eq. (4.10) dominates the dipole term at higher Mach numbers also exists for other rotor noise sources. Thus, Goldstein, Dittmar, and Gelder²⁰ developed a combined dipole-quadrupole model for predicting the noise caused by a steady inlet flow distortion interacting with a fan rotor. Their analysis indicates that the quadrupole term may begin to dominate the dipole at a tip Mach number of about 0.9 or so.

4.3.3 Broadband Noise Sources

Aside from inlet turbulence, there are a large number of other possible sources of broadband fan noise. For example, the noise produced by the turbulence generated in the blade boundary layers (discussed at the end of Sec. 3.5.2) may make a significant contribution to the broadband spectrum. Another source could arise from nonuniform wake profiles. Thus, measurements of the “mean” velocity profiles of wakes show that they are not the same from blade to blade but vary in a random manner about some mean value. This random component of the nonuniform flow impinging on the downstream blade row could certainly generate broadband sound.

There are, in addition to the fan and compressor stages, a number of other broadband noise sources that can occur in the interior of an aircraft engine. These include the turbulent wakes from struts and splitters as well as the turbulence in casing wall boundary layers. However, such sources are usually relatively weak compared with those associated with the fan. Davies and Ffowcs Williams²¹ analyzed the sound radiation from a finite volume of turbulence that is carried along by a uniform flow in an infinite straight duct. Their results show that the radiated sound increases as the sixth power of the flow velocity at low frequencies; while at higher frequencies (above the cut-off frequency of the second mode) this changes to nearly an eighth power dependence on the flow velocity (at least when the scale of the turbulence is sufficiently small).

4.3.4 Multiple Pure Tones

Most of the noise mechanisms discussed up to now can occur at both subsonic and supersonic speeds. However, at supersonic relative tip Mach numbers the phase-locked rotating steady pressure field (associated with the $p = 0$ modes in Eq. (4.30)) can propagate out of the duct. Since the strength of this field is proportional to the steady blade forces, which are considerably larger than the unsteady forces, we would expect it to dominate at supersonic

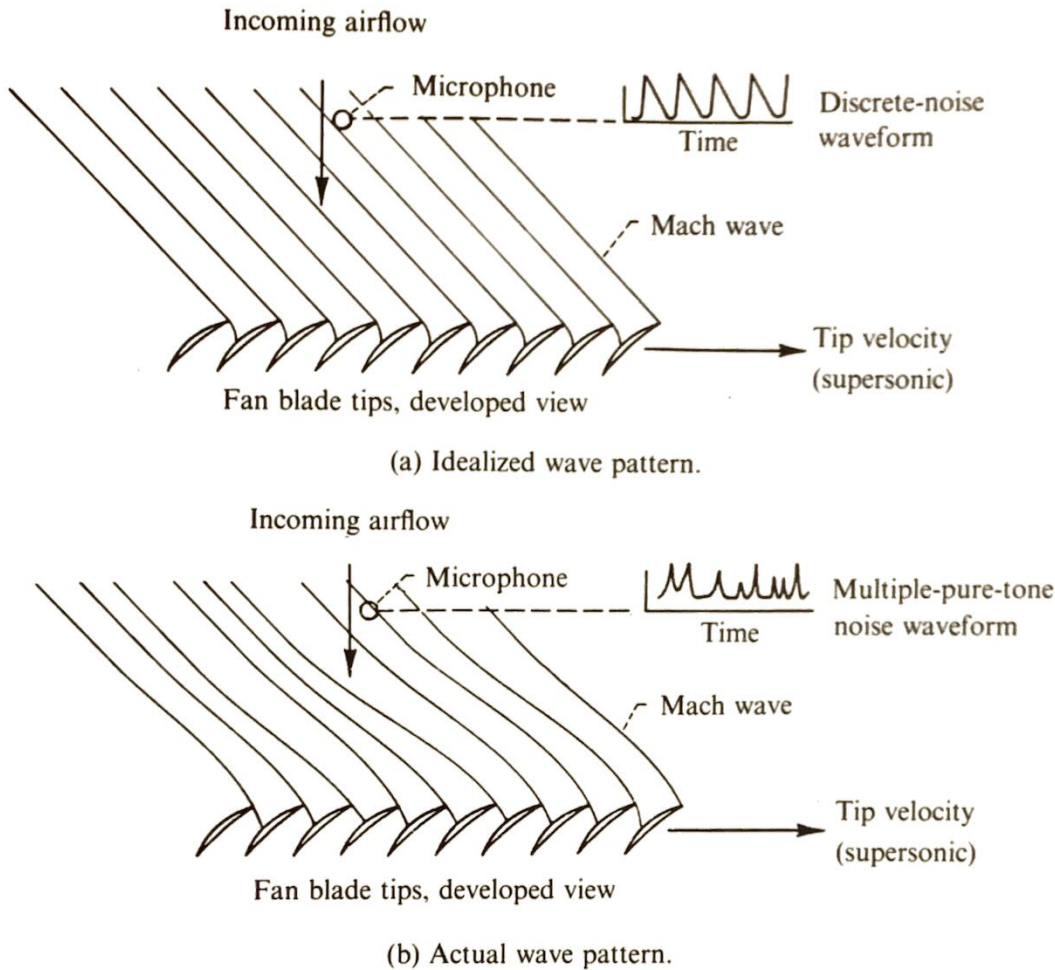


Fig. 4.5 Multiple-pure-tone noise at supersonic tip speeds.

speeds. But, due to nonlinear effects associated with the formation of shock waves, Eq. (4.30) does not actually hold at supersonic speeds—though there is some reason to believe that it will be adequate at slightly supersonic relative tip Mach numbers. Thus, the shock wave structure attached to the leading edges of the blades of a perfectly periodic rotor would appear as shown in Fig. 4.5(a). To the right of the figure is a schematic of the pressure-time history that would be observed by a probe microphone. However, the small nonuniformities in blade geometry and spacing that occur in any real rotor cause perturbations in the shock pattern. And, as shown in Fig. 4.5(b), the dynamics of the propagating shock train tends to emphasize these imperfections through the mechanisms of shock overtaking and coalescence.[†] The pressure-time history observed by a probe microphone will therefore appear as shown at the right of Fig. 4.5(b). In this case there is no longer any evidence of blade-passing-frequency periodicity, but the pattern does repeat itself with every turn of the rotor. Thus, the sound is produced at the shaft rotational speed. A typical supersonic fan spectrum is shown in Fig. 4.6. It is evident that this spectrum (unlike the subsonic

[†] Recall, for example, that higher amplitude shocks propagate faster than lower amplitude ones.

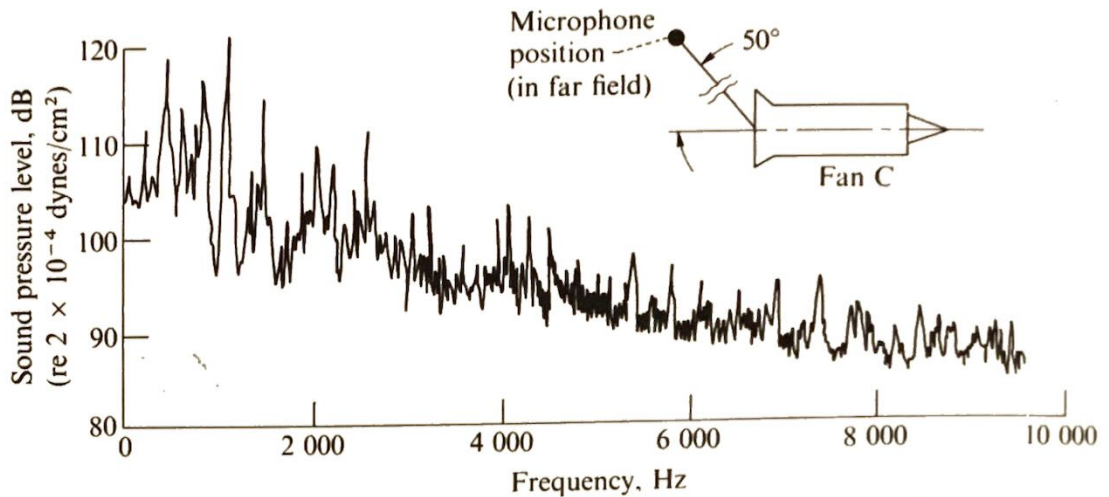


Fig. 4.6 Typical narrow-band spectrum from a supersonic fan.

fan spectrum shown in Fig. 4.2) is dominated by tones at the shaft rotational speed. They are called multiple pure tones (or combination tones) and produce a sound described as “raspy” or “buzz saw.”

Morfey and Fisher²² and Hawkings²³ have analyzed the shock wave coalescence by using one-dimensional saw-toothed shock models. Their analyses describe how an initially nonuniform wave train evolves to become increasingly irregular with distance. They show that the shock strength eventually becomes independent of the initial conditions and decays as the inverse power of distance. They also show that the axial-flow Mach number has a strong influence on this decay rate. Hence, changes in cross-sectional area of the flow duct (that result in changes of axial Mach number) can be very significant. However, analyses of this type cannot be directly related to the irregularities in fan geometry. The drawback was overcome by Kurosaka,²⁴ who used the method of characteristics and oblique shock relations to carry out a two-dimensional analysis. He showed that errors in blade stagger (and contour) are much more important for producing multiple pure tones than errors in blade spacing. Indeed spacing errors only cause changes in upstream shock spacing, while stagger errors cause changes in both position and strength.

At supersonic speeds there is the possibility of an additional broadband noise source associated with the passage of turbulence through the shocks.

4.3.5 Effects of Finite Duct Length

The analyses developed in the previous sections do not directly predict the sound in the far field, where it is of principal interest. However, this limitation can be removed by using the semi-infinite-duct Green's function† (Fig. 3.25) in Eq. (4.13) instead of the infinite-duct Green's function.

† This Green's function can easily be obtained from the results given in Ref. 25.

In addition to being able to calculate the sound in the far field, this approach has the advantage of including the effects of reflection from the end of the duct and diffraction by the duct lip. An analysis of this type was carried out by Lansing.²⁶⁻²⁸

A more approximate analysis which uses the infinite-duct solutions was given by Tyler and Sofrin² for the case of zero mean flow. Thus, if the reflections from the end of the duct are neglected, the sound field at this point can be calculated from the infinite-duct model. Tyler and Sofrin replace the duct opening by a flexible diaphragm in an infinite rigid baffle (as indicated in Fig. 4.7). They then assume that the diaphragm vibrates with the acoustic velocity predicted by the infinite-duct solution (4.30). Thus, inserting the half-space Green's function (1.C.1) into the Green's formula (1.68) shows, upon recalling that $\partial p/\partial n$ is zero on the rigid boundary, that the far-field pressure fluctuation is given by

$$p \sim \frac{1}{2\pi R} \int_0^{r_d} \int_0^{2\pi} \frac{\partial p}{\partial y_1} \left(\mathbf{y}, t - \frac{R}{c_0} + r \frac{\sin \theta \cos(\varphi - \varphi_1)}{c_0} \right) r dr d\varphi_1$$

where

$$\mathbf{y} = \{-l, r \cos \varphi_1, r \sin \varphi_1\}$$

with the polar coordinates defined in Fig. 4.8. For a single harmonic component $p = P_{sB} e^{-isB\Omega t}$ of the blade passing frequency, this becomes (upon using Eq. (4.37))

$$\rho_{sB} \sim \frac{e^{ik_{sB}R}}{2\pi R} \int_0^{r_d} \int_0^{2\pi} \frac{\partial \rho_{sB}(\mathbf{y})}{\partial y_1} e^{-irk_{sB} \sin \theta \cos(\varphi - \varphi_1)} r dr d\varphi_1 \quad (4.46)$$

where

$$k_{sB} \equiv \frac{sB\Omega}{c_0}$$

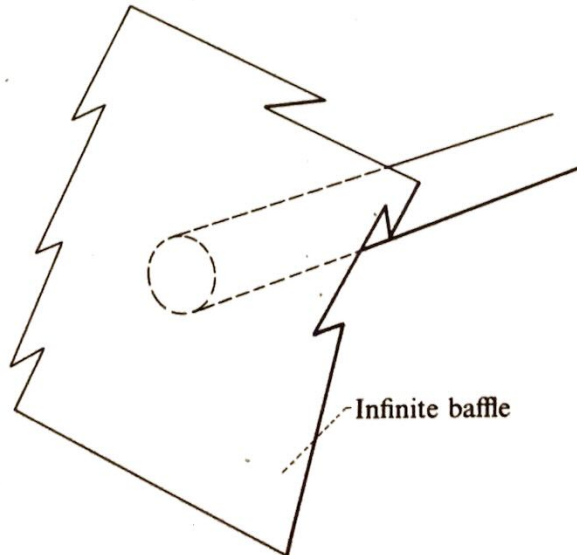


Fig. 4.7 Flanged duct.

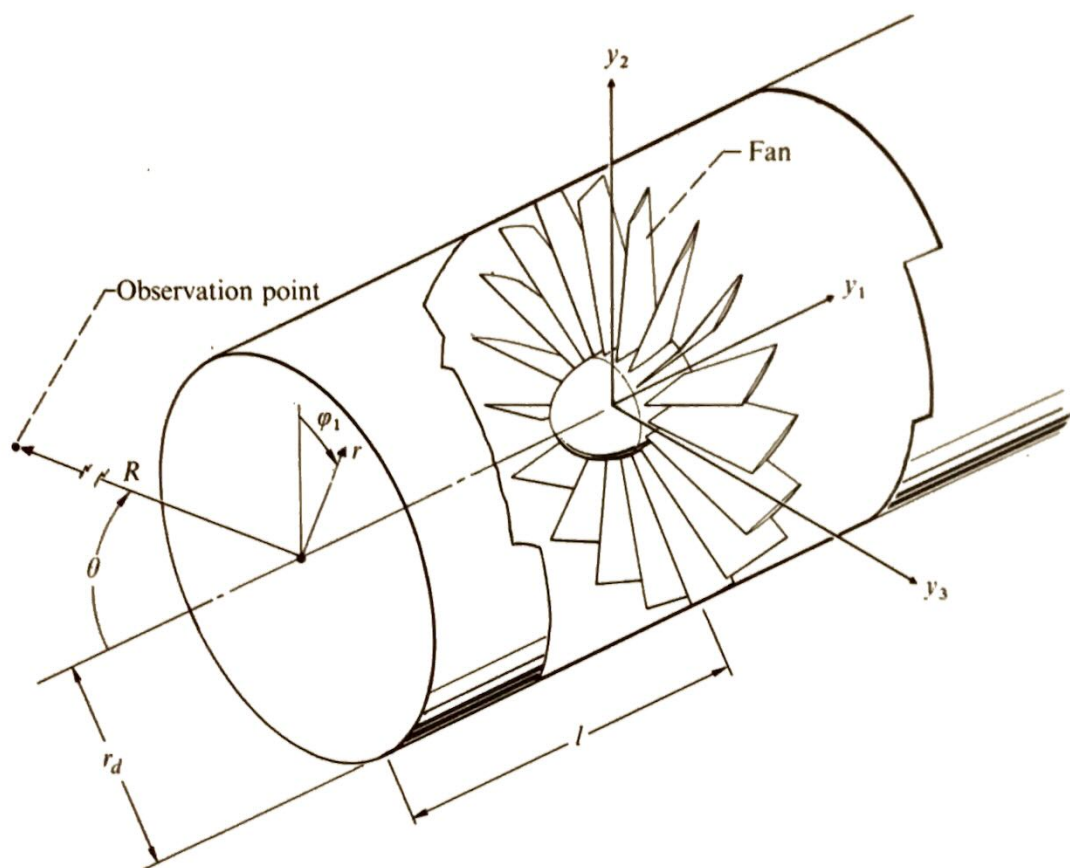


Fig. 4.8 Fan in a semi-infinite duct.

Then setting $M = 0$ in Eq. (4.30) (so that $\gamma_{n,m,sB}^{\pm} = \pm k_{n,m,sB}$) and inserting the result in Eq. (4.46) yields†

$$\rho_{sB} \sim \frac{B}{2c_0^2} \frac{r_d}{R} e^{ik_{sB}R} \sum_{p=-\infty}^{\infty} \sum_{n=1}^{\infty} \frac{J_m(\kappa_{m,n}r_d)}{\Gamma_{m,n}k_{n,m,sB}} e^{i(m\varphi + k_{n,m,sB}l)} \times H_{n,m}(k_{sB}, \theta)(mD_{n,m,p}^+ - k_{n,m,sB}T_{n,m,p}^+) \quad (4.47)$$

where the directivity factor $H_{n,m}(k_{sB}, \theta)$ is defined by

$$H_{n,m}(k_{sB}, \theta) = -i \frac{k_{n,m,sB}k_{sB} \sin \theta e^{-(im\pi/2)}}{\kappa_{m,n}^2 - k_{sB}^2 \sin^2 \theta} J'_m(k_{sB}r_d \sin \theta) \quad (4.48)$$

and the prime on the Bessel function J_m denotes differentiation with respect to its argument.

The sum in Eq. (4.47) must now be carried out over all modes, whether or not they correspond to propagating waves in an infinite duct. But, due to the exponential factor $\exp(ilk_{n,m,sB})$, the nonpropagating modes contribute only weakly to the sound field whenever the duct length l is larger than its radius.

† Of course, this result cannot be used to calculate the sound field in the region behind the duct opening ($\theta > 90^\circ$).

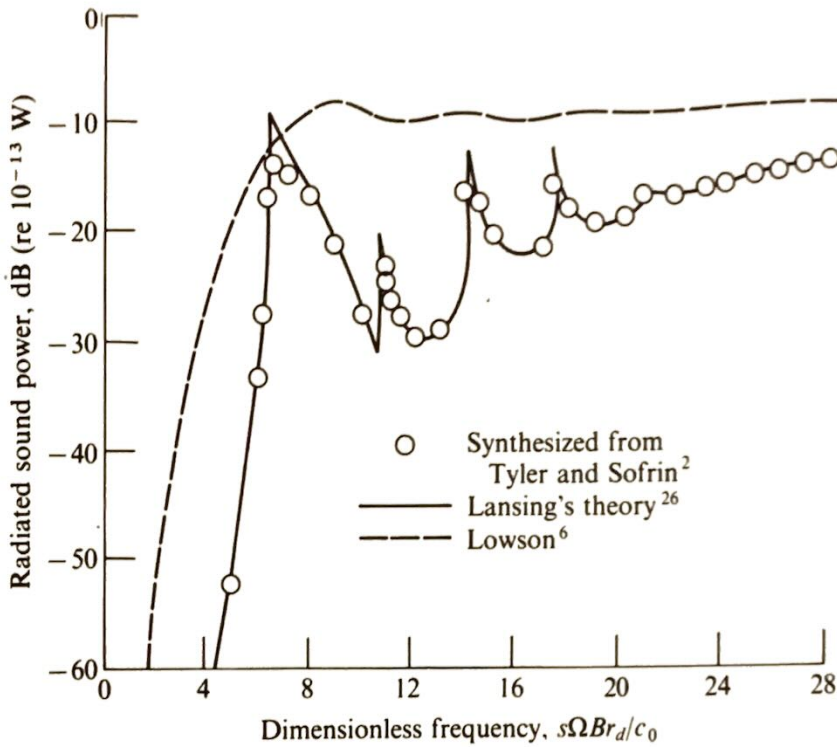


Fig. 4.9 Radiated sound power due to torque and thrust. Ratio of torque to thrust, 0.75; $sB - pV = 5$; $l/R = 1$.

When Lansing's more exact solution is used, Eq. (4.47) remains the same but the directivity factor (4.48) becomes²⁷

$$H_{n,m}(k_{sB}, \theta) = -i \tan \frac{\theta}{2} e^{-(im\pi/2)} J'_m(r_d k_{sB} \sin \theta) \times \frac{(k_{sB} + k_{n,m,sB})(k_{sB} \cos \theta + k_{n,m,sB}) K_+^{(m)}(k_{n,m,sB})}{2(\kappa_{m,n}^2 - k_{sB}^2 \sin^2 \theta) K_+^{(m)}(k_{sB} \cos \theta)}$$

where the term $K_+^{(m)}(\sigma)$ is defined to be the limiting value $\lim_{\varepsilon \rightarrow 0} K^{(m)}(\sigma + i\varepsilon)$;

$\varepsilon \geq 0$ of the Cauchy integral.[†]

$$\ln K^{(m)}(\lambda) = \frac{1}{2\pi i} \int_{-\infty}^{\infty} \frac{\ln [-2K'_m(\gamma)I'_m(\gamma)]}{\sigma - \lambda} d\sigma$$

$$\gamma \equiv r_d \sqrt{\sigma^2 - k_{sB}^2}$$

and the primes on the Bessel functions J_m , K_m , and I_m denote differentiation with respect to their arguments.

Lansing²⁶ compared the Tyler and Sofrin result with his exact semi-infinite-duct solution. He also compared these equations with solutions obtained by Lowson⁶ from a free-space rotor model. The total radiated power calculated by these three methods is plotted as a function of frequency

[†] In taking this limit, it is necessary to use the Plemelj formulas (see Ref. 29, page 42).

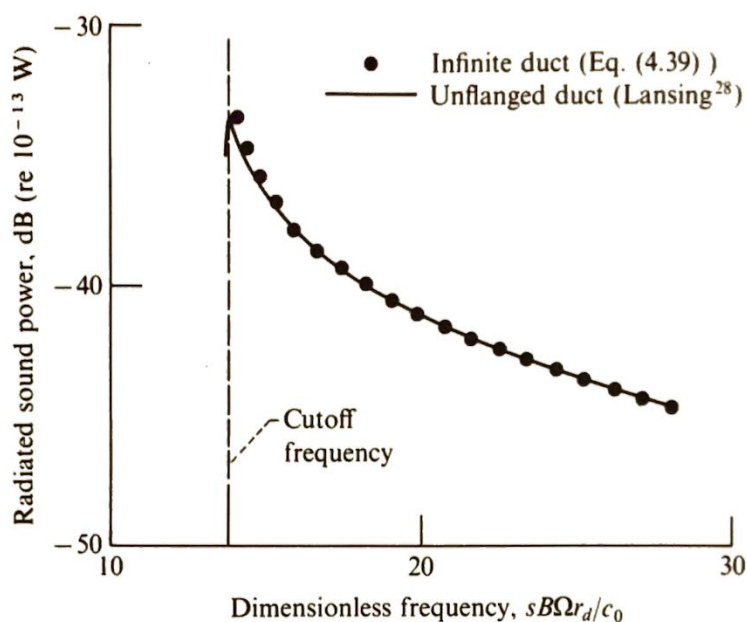


Fig. 4.10 Radiated sound power for circumferential mode $m = 5$; third radial mode, $n = 3$. (From Reference 28.)

in Fig. 4.9. Notice that at all frequencies shown, Tyler and Sofrin's solution is in close agreement with Lansing's result.

Due to the factor $k_{n,m,sB}$ (which vanishes at resonance) in the denominator of Eq. (4.39), the infinite-duct model predicts infinite acoustic power as the cutoff frequencies of the various modes are approached from

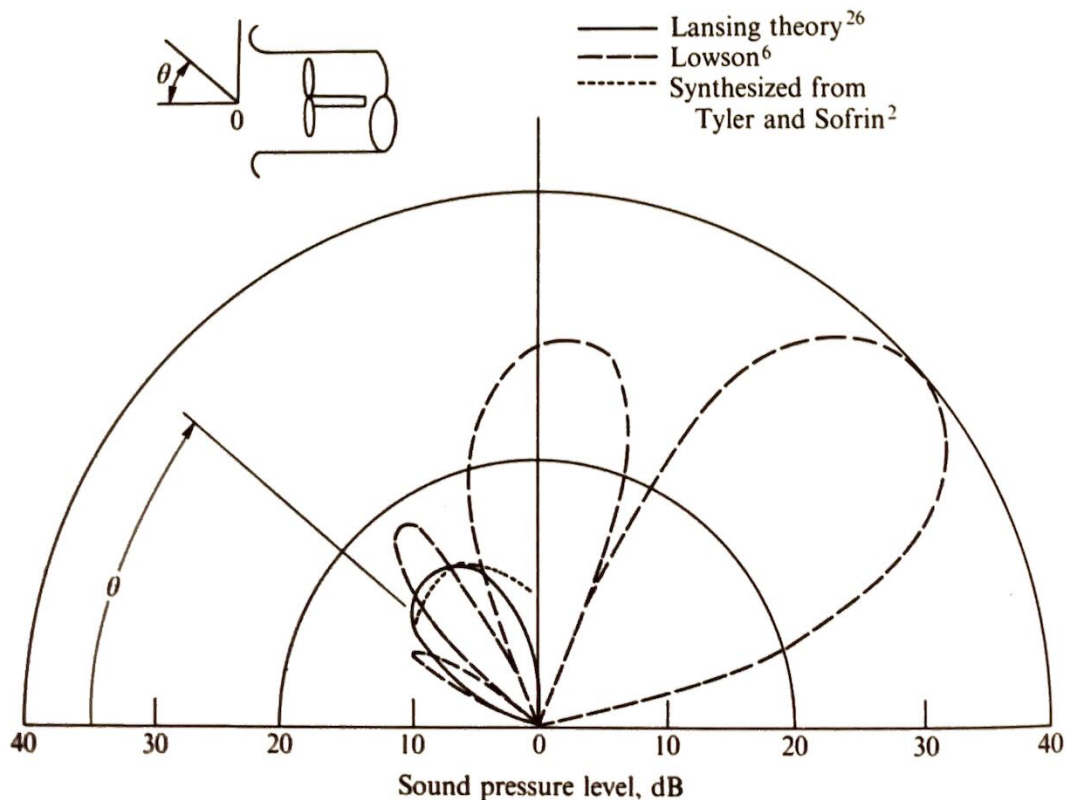


Fig. 4.11 Directivity patterns due to thrust and torque. Ratio of torque to thrust, 0.75; $sB - pV = 5$; $s\Omega BR/c_0 = 12$. (From Reference 26)

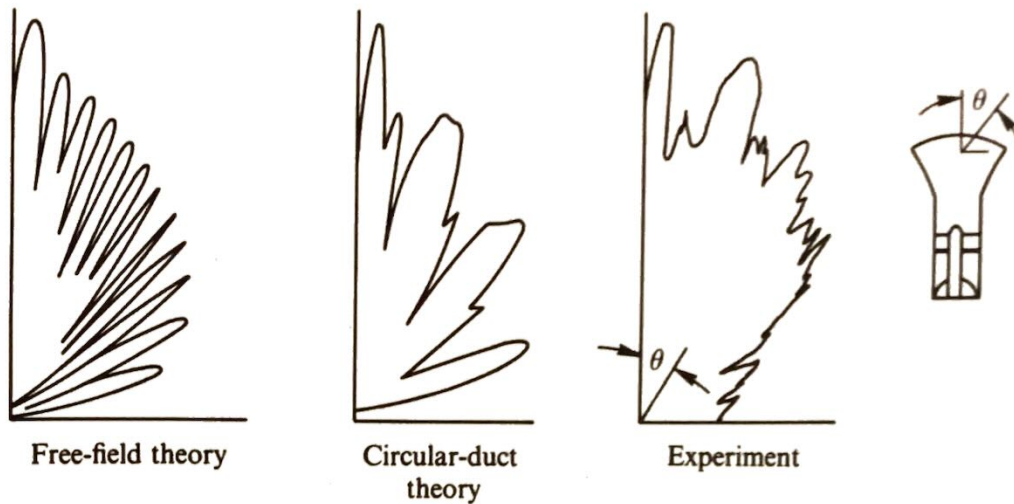


Fig. 4.12 Radiation patterns for a research compressor. (From Reference 27.)

above.[†] The sharp peaks exhibited by Lansing's solution (see Fig. 4.9) also occur at these cutoff frequencies. But, these peaks remain finite. The Tyler-Sofrin solution also tends to increase[‡] abruptly as these frequencies are approached but does not seem to exhibit the sharp peaks found by Lansing.

A comparison between the infinite-duct solution (Eq. (4.39)) and Lansing's result is shown in Fig. 4.10. In this figure (taken from Ref. 28) the normalized sound power radiated in the $n = 5$, $m = 3$ mode is plotted against the dimensionless frequency $sBr_d\Omega/c_0$. It shows that the infinite-duct model provides an excellent method for calculating the total radiated power as long as the frequency is even slightly above cutoff.

Lansing also compared the directivity patterns predicted by these three solutions at the dimensionless frequency $s\Omega Br_d/c_0 = 12$. This comparison is shown in Fig. 4.11. In Ref. 27, directivity patterns calculated from Lowson's and Lansing's solutions are compared with data from a research compressor. These results are shown in Fig. 4.12.

4.4 CONCLUDING REMARKS

The material of this chapter is for the most part developed from the general integral acoustic analogy Eq. (4.10). Moreover, Eqs. (3.6) and (2.9), which serve as a basis for the material in Chaps. 2 and 3, are themselves special cases of this equation. Hence, Eq. (4.10) serves as a unifying base for most of the material developed up to this point.

In the remainder of the book the Lighthill analogy is abandoned, and alternative approaches are evolved.

[†] It is shown in Chap. 5, however, that cascade interference effects will change the blade forces in a way that keeps the power finite.

[‡] The radiated power predicted by Eq. (4.39) can differ from that predicted by the Tyler-Sofrin method since the latter procedure does not require that continuity be satisfied across the duct exit plane.

REFERENCES

1. Hetherington, R., "Compressor Noise Generated by Fluctuating Lift Resulting from Rotor-Stator Interaction," *AIAA J.*, **1**, 2, 473-474, 1963.
2. Tyler, J. M. and T. G. Sofrin, "Axial Flow Compressor Noise Studies," *Trans. SAE*, **70**, 309-332, 1962.
3. Abramowitz, Milton and Irene A. Stegun, *Handbook of Mathematical Functions with Formulas, Graphs, and Mathematical Tables*. National Bureau of Standards Applied Mathematics Series 55, 1964.
4. Kemp, N. H. and W. R. Sears, "Aerodynamic Interference Between Moving Blade Rows," *J. Aeron. Sci.*, **20**, 9, 585-597, 1953.
5. Kemp, Nelson H. and W. R. Sears, "The Unsteady Forces Due to Viscous Wakes in Turbomachines," *J. Aeron. Sci.*, **22**, 7, 478-483, 1955.
6. Lowson, M. V., "Theoretical Analysis of Compressor Noise," *J. Acoust. Soc. Am.*, **47**, 1 (pt 2), 371-385, 1970.
7. Silverstein, Abe, S. Katzoff and Kenneth W. Bullivant, "Downwash and Wake Behind Plain and Flapped Aerofoils," NACA TR 651, 1939.
8. Johnsen, Irving A. and Robert O. Bullock, eds., *Aerodynamic Design of Axial Flow Compressors*, NASA SP-36, 1965.
9. Raj, R. and B. Lakshminarayana, "Three-Dimensional Characteristics of Turbulent Wakes Behind Rotors of Axial Flow Turbomachinery," ASME Paper No. 75-GT-1 presented at the Gas Turbine Conference, Houston, Texas, March 1975.
10. Hanson, D. B., *The Spectrum of Turbomachine Rotor Noise Caused by Inlet Guide Vane Wakes and Atmospheric Turbulence*. Ph.D. Thesis, Connecticut Univ., 1973.
11. Henderson, R. E. and H. Daneshyar, *Theoretical Analysis of Fluctuating Lift on the Rotor of an Axial Turbomachine*. R&M 3684, British Aeronautical Research Council, 1972.
12. Povinelli, Frederick P., James H. Dittmar and Richard P. Woodward, "Effects of Installation Caused Flow Distribution on Noise from a Fan Designed for Turbofan Engines," NASA TN D-7076, 1972.
13. Filleul, N. LeS, "An Investigation of Axial Flow Fan Noise," *J. Sound Vibr.*, **3**, 2, 147-165, 1966.
14. Sofrin, Thomas G. and John C. McCann, "Pratt & Whitney Experience in Compressor-Noise Reduction," *J. Acoust. Soc. Am.*, **40**, 5, 1248-1249, 1966.
15. Mani, R., "Noise Due to the Interaction of Inlet Turbulence with Isolated Stators and Rotors," *J. Sound Vibr.*, **17**, 2, 251-260, 1971.
16. Ffowcs Williams, J. E. and D. L. Hawkings, "Theory Relating to the Noise of Rotating Machinery," *J. Sound Vibr.*, **10**, 1, 10-21, 1969.
17. Chandrashekhara, N., "Sound Radiation from Inflow Turbulence in Axial Flow Fans," *J. Sound Vibr.*, **19**, 2, 133-146, 1971.
18. Gelder, Thomas F. and Richard F. Soltis, "Inlet Plenum Chamber Noise Measurement Comparison of 20-Inch Diameter Fan Rotors with Aspect Ratios 3.6 and 6.6," NASA TM X-2191, 1971.
19. Mani, R., "Inlet Turbulence Rotor Noise," Presented at 87th Meeting of Acoustical Soc. of America, New York, April 1974.
20. Goldstein, M. E., J. Dittmar and T. Gelder, *Combined Quadrupole-Dipole Model for Inlet Flow Distortion Noise from a Subsonic Fan*. NASA TN D-7676, May 1974.
21. Davies, H. G. and J. E. Ffowcs Williams, "Aerodynamic Sound Generation in Pipes," *J. Fluid Mech.*, **32**, 4, 765-778, 1968.
22. Morfey, C. L. and M. J. Fisher, "Shock-Wave Radiation from a Supersonic Ducted Rotor," *J. Roy. Aeron. Soc.*, **74**, 579-585, 1971.
23. Hawkings, D. L., "Multiple Tone Generation by Transonic Compressors," *J. Sound Vibr.*, **17**, 2, 241-250, 1971.
24. Kurosaka, M., "A Note on Multiple Pure Tone Noise," *J. Sound Vibr.*, **19**, 4, 453-462, 1971.
25. Noble, Benjamin, *Methods Based on the Wiener-Hopf Technique for the Solution of Partial Differential Equations*. Pergamon Press, 1958.
26. Lansing, Donald L., "Exact Solution for Radiation of Sound from a Semi-Infinite Circular Duct with Application to Fan and Compressor Noise," *Analytic Methods in Aircraft Aerodynamics*, pp. 323-332. NASA SP-228, 1970.

-
27. Hubbard, H. H., D. L. Lansing and H. L. Runyan, "A Review of Rotating Blade Noise Technology," *J. Sound Vibr.*, **19**, 3, 227-249, 1971.
 28. Lansing, D. L., J. A. Drischler and C. G. Pusey, "Radiation of Sound from an Unflanged Circular Duct with Flow," *J. Acoust. Soc. Am.*, **48**, 1, pt. 1, 75, 1970.
 29. Muskhelishvili, M. I., *Singular Integral Equations*, P. Noordhoff, Holland, 1958.
 30. Cumpsty, N. A. and D. W. Lowrie, "The Cause of Tone Generation by Aeroengine Fans at High Subsonic Tip Speeds and the Effect of Forward Speed," Paper No. 73-WA/GT-4, ASME, 1973.

5 THEORIES BASED ON SOLUTION OF LINEARIZED VORTICITY- ACOUSTIC FIELD EQUATIONS

5.1 INTRODUCTION

The last three chapters were in the main based on the acoustic analogy approach, wherein the sound field is calculated by constructing a model for an equivalent acoustic source term. Because of the inherent limitations of this procedure (which are discussed in detail in Chap. 2), we would like to calculate the sound emission by solving the differential equations governing the flow. Unfortunately, this is nearly impossible for most real flows. But recall that the sound field produced by the dipole term is linearly related to the surface forces, which in most cases were calculated from the oncoming flows by using linearized equations. It, therefore, ought to be possible to obtain solutions to certain aeroacoustic problems by directly solving the linearized momentum and continuity equations. In this chapter we shall, by considering a specific example, show how this approach can be carried out. Before proceeding with this, however, we shall first establish certain general properties of these linearized solutions.

5.2 DECOMPOSITION OF LINEARIZED SOLUTIONS INTO ACOUSTICAL AND VORTICAL MODES: SPLITTING THEOREM

When the mean velocity U is constant, the linearized continuity and momentum Eqs. (1.15) become (in the absence of volume sources)

$$\rho_0 \frac{D_0 \mathbf{u}}{D\tau} = -\nabla p \quad (5.1)$$

$$\frac{1}{\rho_0 c_0^2} \frac{D_0 p}{D\tau} = -\nabla \cdot \mathbf{u} \quad (5.2)$$

where, as usual

$$\frac{D_0}{D\tau} = \frac{\partial}{\partial \tau} + U \frac{\partial}{\partial y_1} \quad (5.3)$$

We shall now show that the velocity \mathbf{u} can be decomposed into solenoidal (zero divergence) and irrotational (zero curl) parts in such a way that the pressure fluctuations are determined solely by the irrotational part. Thus, we shall show that there exist vectors \mathbf{u}_1 and \mathbf{u}_2 such that†

$$\mathbf{u} = \mathbf{u}_1 + \mathbf{u}_2 \quad (5.4)$$

$$\nabla \times \mathbf{u}_1 = \nabla \cdot \mathbf{u}_2 = 0 \quad (5.5)$$

$$\left. \begin{aligned} \rho_0 \frac{D_0 \mathbf{u}_1}{D\tau} &= -\nabla p \\ \frac{1}{\rho_0 c_0^2} \frac{D_0 p}{D\tau} &= -\nabla \cdot \mathbf{u}_1 \end{aligned} \right\} \quad (5.6)$$

$$\frac{D_0 \mathbf{u}_2}{D\tau} = 0 \quad (5.7)$$

To this end, notice that since every vector field can be decomposed into solenoidal and irrotational parts there must certainly exist vectors \mathbf{u}'_1 and \mathbf{u}'_2 such that

$$\mathbf{u} = \mathbf{u}'_1 + \mathbf{u}'_2 \quad (5.8)$$

$$\nabla \times \mathbf{u}'_1 = \nabla \cdot \mathbf{u}'_2 = 0 \quad (5.9)$$

Hence, Eq. (5.1) can be written as

$$\mathbf{A} \equiv \rho_0 \frac{D_0 \mathbf{u}'_1}{D\tau} + \nabla p = -\rho_0 \frac{D_0 \mathbf{u}'_2}{D\tau} \quad (5.10)$$

† This result is called the *splitting theorem*.

Then since the second member of this equation has zero curl and the last member has zero divergence, the vector \mathbf{A} must be both solenoidal and irrotational. It follows that the vector \mathbf{u}_0 defined by

$$\mathbf{u}_0(\mathbf{y}, \tau) \equiv \frac{1}{\rho_0} \int_0^\tau \mathbf{A}[\mathbf{y} + \hat{\mathbf{i}}(t - \tau)U, t] dt \quad (5.11)$$

has the property that

$$\nabla \times \mathbf{u}_0 = \nabla \cdot \mathbf{u}_0 = 0 \quad (5.12)$$

and satisfies the relation

$$\rho_0 \frac{D_0 \mathbf{u}_0}{D\tau} = \mathbf{A} \quad (5.13)$$

Hence, inserting Eq. (5.13) into Eq. (5.10) shows that the vectors

$$\left. \begin{aligned} \mathbf{u}_1 &= \mathbf{u}'_1 - \mathbf{u}_0 \\ \mathbf{u}_2 &= \mathbf{u}'_2 + \mathbf{u}_0 \end{aligned} \right\} \quad (5.14)$$

satisfy the first Eq. (5.6) and Eq. (5.7), respectively. Moreover, it follows from Eqs. (5.9) and (5.12) that Eq. (5.5) holds, while the last Eq. (5.6) is a direct consequence of Eqs. (5.5) and (5.2).

Since (as can be seen from Eq. (5.6)) the irrotational vector \mathbf{u}_1 is the part of the velocity associated with the pressure fluctuations, it is called the *acoustical particle velocity*. And since the vorticity

$$\boldsymbol{\omega} \equiv \nabla \times \mathbf{u} = \nabla \times \mathbf{u}_2$$

is determined solely by the velocity \mathbf{u}_2 , the latter quantity is called the *vortical velocity*. Thus, within the flow the interactions between the acoustic and vortical motions must occur through second (or higher) order nonlinear terms.

We have seen that the sound source in Lighthill's theory can be modeled by the fluctuating Reynolds stress $\rho_0 u_i u_j$, with u_i and u_j effectively taken as the vortical part of the velocity field. Thus (at least for sufficiently small motions) the generation of sound by Lighthill's quadrupole mechanism is just such a second-order interaction process.† Equation (5.7) shows that the vortical modes, aside from being convected by the mean flow, remain unchanged. This is consistent with the results described on pages 87–90 (Taylor's hypothesis), which show that jet flow turbulence‡ decays only slowly in the moving frame.

Although the acoustic and vortical modes each behave, in the linear approximation, as if the other were not present, they can easily be coupled

† The sound field can generate vorticity through a second-order interaction. In fact, this problem was studied by Rayleigh nearly 100 years ago. The second-order interactions were later studied in detail by Chu and Kovasznay.¹

‡ Which is essentially pure vortical motion if the Mach number is not too high.

by any rigid surface that bounds the flow. Thus, since the normal component of the total velocity \mathbf{u} must vanish on any such surface, it follows that \mathbf{u}_1 and \mathbf{u}_2 must be related by

$$\mathbf{u}_1 \cdot \hat{\mathbf{n}} = -\mathbf{u}_2 \cdot \hat{\mathbf{n}}$$

where $\hat{\mathbf{n}}$ is normal to the surface. In fact, it is this coupling between the acoustic and vortical modes that is responsible for the dipole-type sound sources that often occur at solid boundaries. And since these sources are linear in the perturbation quantities, it is not surprising that they dominate over the nonlinear quadrupole volume sources wherever the fluctuating velocities are small.

5.3 SOUND GENERATED BY A BLADE ROW

5.3.1 Formulation

We shall now show how the sound generated by the mechanism described above can be calculated by solving the linearized acoustic-vorticity Eqs. (5.4) to (5.7). To this end, we shall reconsider the problem of a fan rotating with angular velocity Ω through a stationary convected disturbance.

The problem is formulated in this section and is reduced to solving an integral equation in the next section. After discussing the various methods that have been used to solve this equation, we show how the results can be used to predict the sound field, and in the last section the connection with the acoustic analogy approach is made. This allows us to assess the importance of including the cascade effects as well as chordwise retarded time variations in the source model.

In order to simplify the problem, suppose that the hub-tip ratio of the fan is close enough to unity so that curvature effects can be neglected and the blades can be "unrolled" to form a linear cascade. Thus, we consider an infinite row of blades moving transversely between two infinite parallel plates as shown in Fig. 5.1. The linear velocity of the cascade is

$$U_0 = \Omega r_M \quad (5.15)$$

where r_M denotes some mean radius of the fan and the spacing b between the plates is equal to the blade span.

We suppose that the vortical velocity field \mathbf{u}_∞ is specified upstream of the blade row. Moreover, it will be assumed that the blades are thin and at a small angle to the oncoming mean relative velocity U_r , which in turn is assumed to be large compared to \mathbf{u}_∞ . Then the flow will be governed by the linearized Eqs. (5.1) and (5.2). On the other hand, it was shown in Sec. 3.4.2 that the unsteady part of a linearized incompressible flow past an airfoil is independent of the camber and angle of attack. It can be shown

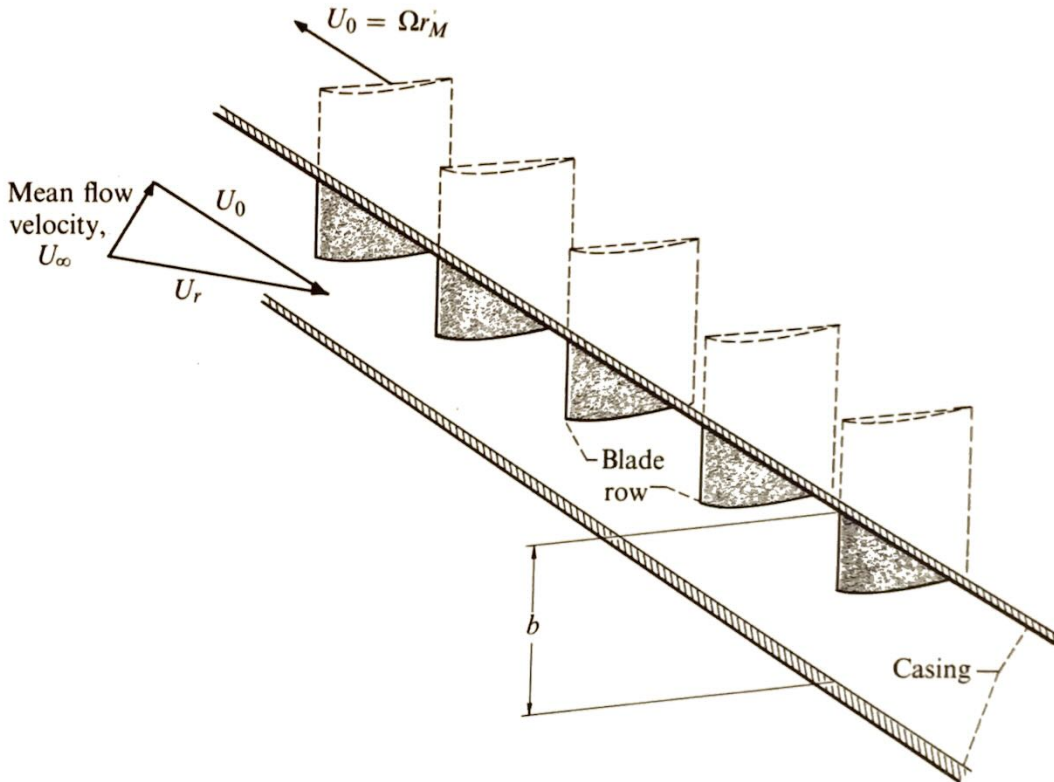


Fig. 5.1 Infinite cascade.

that this decoupling between the steady and unsteady flows also occurs in the compressible flow problem being considered in this section. Hence, we can replace the blades of the cascade by flat plates at zero angle to the relative flow U_r .

Now let the Y -coordinate system be aligned with the oncoming mean flow velocity U_∞ as shown in Fig. 5.2. Upstream of the blade row the nonuniform velocity consists of a vortical part \mathbf{u}_∞ and an acoustic part. We shall require that the latter represent an outgoing wave far from the blades but it will otherwise be left unspecified. On the other hand, the vortical flow is steady (relative to a fixed observer) and can therefore depend only† on Y_2 and Y_3 . Moreover, if the problem is to correspond to an unrolled annulus, \mathbf{u}_∞ must be periodic in the direction of motion of the blade row with the circumferential distance $2\pi r_M$ being equal to an integral multiple of its wavelength. Then since the dimension in the Y_3 -direction is finite, \mathbf{u}_∞ can be represented by the double Fourier series

$$\mathbf{u}_\infty = \sum_{p,q} \left[(\hat{\mathbf{I}}A_{p,q} + \hat{\mathbf{J}}B_{p,q}) \cos\left(\frac{\pi q Y_3}{b}\right) + \hat{\mathbf{K}}C_{p,q} \sin\left(\frac{\pi q Y_3}{b}\right) \right] e^{(2\pi i p Y_2)/(L_0 \cos \nu)} \quad (5.16)$$

† Equation (5.7) shows that the vortical motion depends on Y_1 and τ only in the combination $Y_1 - U\tau$.

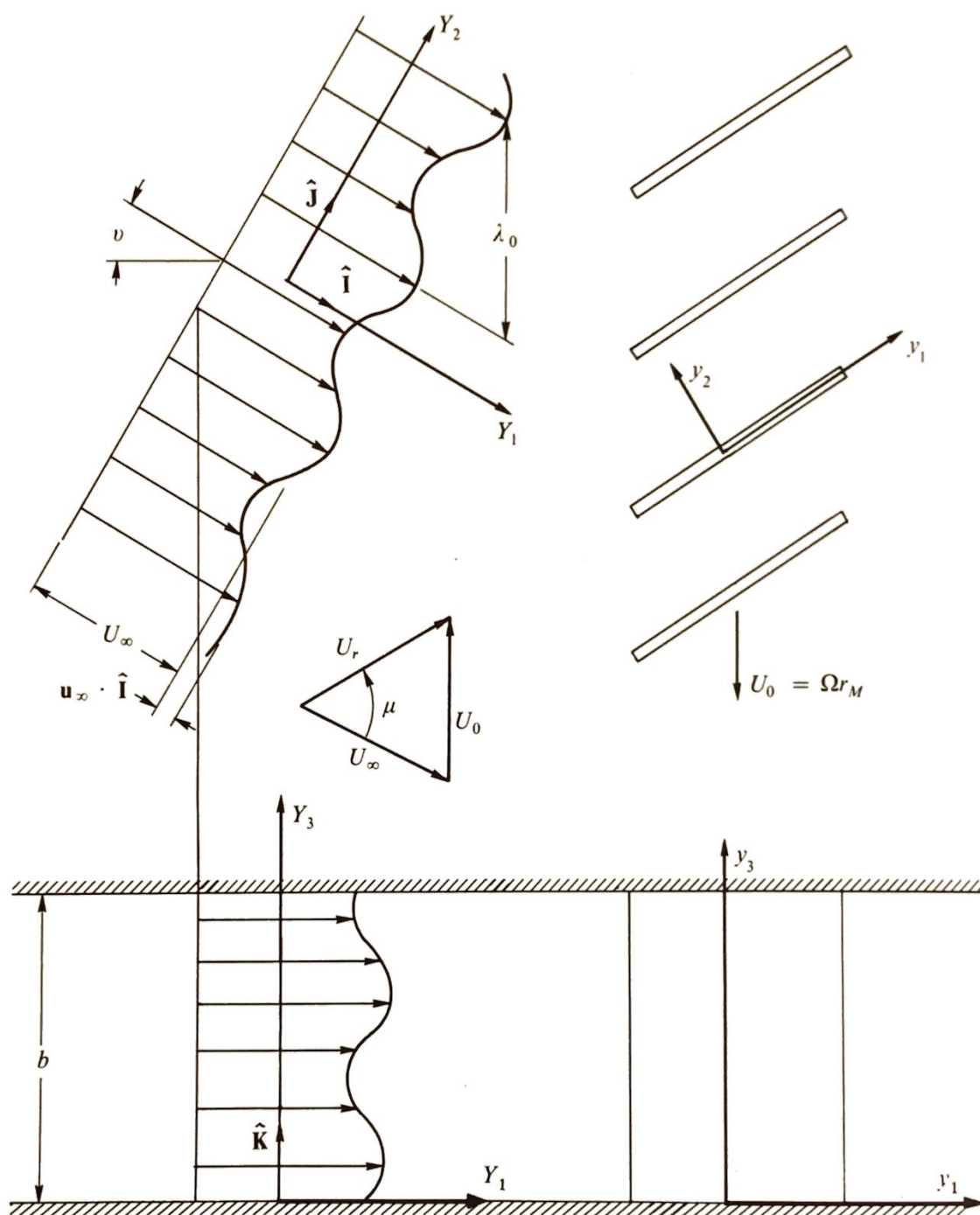


Fig. 5.2 Flow into cascade.

where

$$L_0 = 2\pi r_M \quad (5.17)$$

is the circumference at the mean radius r_M ; $A_{p,q}$, $B_{p,q}$, and $C_{p,q}$ are complex constants; $\hat{\mathbf{I}}$, $\hat{\mathbf{J}}$, and $\hat{\mathbf{K}}$ are unit vectors in the Y_1 -, Y_2 -, and Y_3 -directions, respectively; and v is the angle between the oncoming flow direction and the perpendicular to the blade row. Notice that the Y_3 -component (normal component) of each term in this series vanishes at the end walls, $Y_3 = 0, b$.

Since \mathbf{u}_∞ represents a purely vortical velocity, it must certainly satisfy

the solenoidal condition $\nabla_Y \cdot \mathbf{u}_\infty = 0$ (where ∇_Y denotes the divergence operator in the \mathbf{Y} -coordinate system). But this will occur only if the coefficients $B_{p,q}$ and $C_{p,q}$ in Eq. (5.16) satisfy the condition

$$\frac{2ip}{L_0 \cos v} B_{p,q} + \frac{q}{b} C_{p,q} = 0$$

Moreover, due to the linearity of the problem, it is only necessary, as explained in Sec. 3.4.2, to calculate the flow field generated by a single harmonic component

$$\mathbf{u}_\infty = \left[(\hat{\mathbf{I}} A_{p,q} + \hat{\mathbf{J}} B_{p,q}) \cos \left(\frac{\pi q Y_3}{b} \right) - \hat{\mathbf{K}} \frac{2ipb}{L_0 q \cos v} B_{p,q} \sin \left(\frac{\pi q Y_3}{b} \right) \right] \times e^{(2\pi i p Y_2)/(L_0 \cos v)} \quad (5.18)$$

of the sum. This disturbance pattern is a generalization of the one considered in Sec. 3.5.3 and, as in that section, it is again convenient to express the disturbance velocity in terms of a coordinate system \mathbf{y} fixed to the blades. We choose a typical blade, individuated by means of a subscript 0, and suppose that the origin of the coordinate system is centered at its root (as shown in Fig. 5.2). Then the coordinate transformation $\mathbf{Y} \rightarrow \mathbf{y}$ is the same as in Sec. 3.5.3, and hence Y_2 is related to the \mathbf{y} -coordinates by Eq. (3.121). Inserting this equation into Eq. (5.18) and using Eqs. (5.15) and (5.17) to simplify the result now yields

$$\mathbf{u}_\infty = \left[(\hat{\mathbf{I}} A_{p,q} + \hat{\mathbf{J}} B_{p,q}) \cos \left(\frac{\pi q y_3}{b} \right) - \hat{\mathbf{K}} \frac{2ipb}{L_0 q \cos v} B_{p,q} \sin \left(\frac{\pi q y_3}{b} \right) \right] \times e^{ip\Omega[(y_1 + y_2 \cot \mu)/U_r - \tau]} \quad (5.19)$$

(where the unit vectors $\hat{\mathbf{I}}$, $\hat{\mathbf{J}}$, and $\hat{\mathbf{K}}$ are still oriented in the \mathbf{Y} -coordinate directions). The orientation of the blade row in the \mathbf{y} -coordinate system is shown in Fig. 5.3. In these coordinates the blades are stationary and parallel to the mean relative velocity U_r . Hence, the unsteady flow, which is caused by the small amplitude gust (5.19), must satisfy the linearized Eqs. (5.1) and (5.2) (with U replaced by U_r in $D_0/D\tau$).

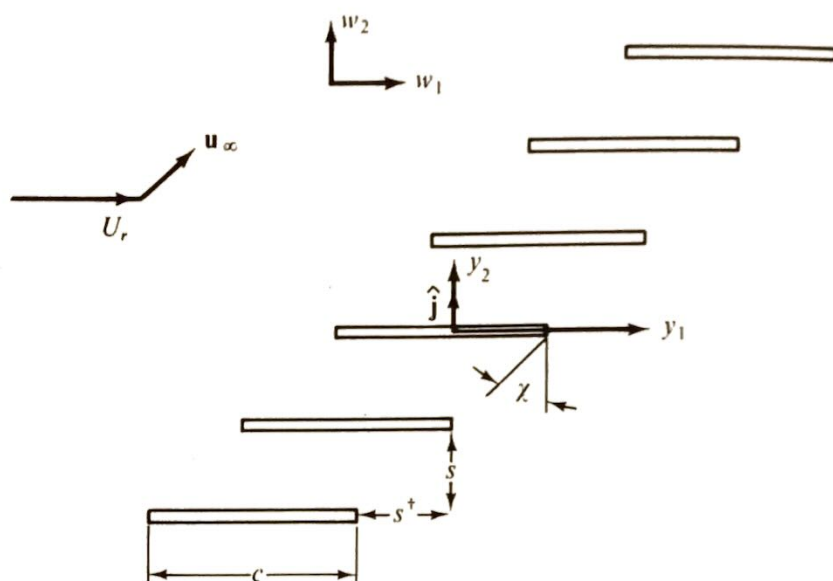
As in Sec. 3.4.2, it is again convenient to explicitly separate out the disturbance velocity by putting

$$\mathbf{u} = \mathbf{u}_\infty + \mathbf{w} \quad (5.20)$$

where \mathbf{w} is sometimes called the "scattered" velocity. Then since \mathbf{u}_∞ is solenoidal and satisfies Eq. (5.7), the scattered velocity \mathbf{w} must itself satisfy Eqs. (5.1) and (5.2). Thus,[†]

$$\rho_0 \frac{D_0 \mathbf{w}}{D\tau} = -\nabla p \quad (5.21)$$

[†] We can associate \mathbf{w} with the acoustic velocity defined in Sec. 5.2 if we ignore its discontinuity across the trailing vortex sheets.

Fig. 5.3 Cascade in y -coordinate system.

$$\frac{1}{\rho_0 c_0^2} \frac{D_0 p}{D\tau} = -\nabla \cdot \mathbf{w} \quad (5.22)$$

Since the flow is assumed to be inviscid, we impose the boundary condition that the normal velocity $\mathbf{u} \cdot \hat{\mathbf{j}} = (\mathbf{u}_\infty + \mathbf{w}) \cdot \hat{\mathbf{j}}$ (where $\hat{\mathbf{j}}$ is the unit vector in the y_2 -direction) vanish at the surface of the blades. Then inserting Eq. (5.19) shows that \mathbf{w} must satisfy the boundary condition (Figs. 5.2 and 5.3)

$$w_2 = -a \left(\cos \frac{\pi q y_3}{b} \right) e^{i p \Omega [(y_1 + m s \cot \mu)/U_r - \tau]} \quad (5.23)$$

$$\text{for } \begin{cases} y_2 = m s \\ -\frac{c}{2} < y_1 - m s^+ < \frac{c}{2} \\ 0 < y_3 < b \end{cases} \quad m = 0, \pm 1, \pm 2, \dots$$

where $a \equiv -A_{p,q} \sin \mu + B_{p,q} \cos \mu$ and, as indicated in Fig. 5.3, s is the *gap distance* measured normal to the chord, s^+ is the *stagger distance* measured parallel to the chord, and c is the chord length.

We must also require that the normal velocity vanish on the walls at $y_3 = 0, b$. But since (by construction) \mathbf{u}_∞ already satisfies this requirement, \mathbf{w} must satisfy the boundary condition

$$w_3 = 0 \quad \text{at } y_3 = 0, b \quad (5.24)$$

Thus, the problem has been reduced to finding an outgoing-wave solution to Eqs. (5.21) and (5.22) that satisfies the boundary conditions† (5.23) and (5.24). However, as explained in Sec. 3.4.2 it is also necessary to require that this solution satisfy the Kutta–Joukowski condition at the trailing edges of the blades, and as a consequence, allowance must be made for a trailing vortex wake. The continuity of pressure across these wakes therefore suggests the adoption of this quantity as a dependent variable. Then, since Eqs. (5.21) and (5.22) are special cases of the first two Eqs. (1.15), we can follow the procedure used in Chap. 1 to eliminate the velocity and thereby obtain the wave equation

$$\frac{1}{c_0^2} \frac{D_0^2 p}{D\tau^2} - \nabla^2 p = 0 \quad (5.25)$$

It follows from the y_3 -component of Eq. (5.21) that the boundary condition (5.24) can be replaced by the condition

$$\frac{\partial p}{\partial y_3} = 0 \quad \text{at } y_3 = 0, b \quad (5.26)$$

And since the pressure is entirely associated with acoustic motion, we require that

$$p \rightarrow \text{Outgoing-wave solution} \quad \text{as } y_1 \rightarrow \infty$$

The w_2 -component of the velocity, which enters through the boundary condition (5.23), is related to the pressure by the y_2 -component of Eq. (5.21).

5.3.2 Reduction to Integral Equations

It can be seen by inspection that the solutions to Eq. (5.25) and the y_2 -component of Eq. (5.21) that satisfy the boundary conditions (5.23) and (5.26) must be of the form

$$p = -\rho_0 U_r a P(y_1, y_2) e^{-i\omega t} \cos\left(\frac{\pi q y_3}{b}\right) \quad (5.27)$$

$$w_2 = -a V(y_1, y_2) e^{-i\omega \tau} \cos\left(\frac{\pi q y_3}{b}\right) \quad (5.28)$$

where we have put

$$\omega \equiv p\Omega = p \frac{U_0}{r_M} \quad (5.29)$$

† The effects of the vorticity generated by leakage at the blade tips is being neglected. The inclusion of this effect would introduce unsteady crossflows (in the Y_3 -direction) with a considerable increase in complication. There is some experimental evidence to indicate that the elimination of tip leakage has little effect on the sound produced by fans.

and P and V are determined by the equations

$$(1 - M_r^2) \frac{\partial^2 P}{\partial y_1^2} + \frac{\partial^2 P}{\partial y_2^2} + 2i \left(\frac{\omega}{c_0} \right) M_r \frac{\partial P}{\partial y_1} + \left[\left(\frac{\omega}{c_0} \right)^2 - \left(\frac{\pi q}{b} \right)^2 \right] P = 0 \quad (5.30)$$

$$M_r \frac{\partial P}{\partial y_2} = \left(\frac{i\omega}{c_0} - M_r \frac{\partial}{\partial y_1} \right) V \quad (5.31)$$

with the relative Mach number M_r defined by

$$M_r \equiv \frac{U_r}{c_0} \quad (5.32)$$

The boundary condition (5.26) is automatically satisfied, and the boundary condition (5.23) becomes

$$V = e^{i\omega(y_1 + ms \cot \mu)/U_r} \quad \text{for} \quad \left\{ \begin{array}{l} y_2 = ms \\ -\frac{c}{2} < y_1 - ms^\dagger < \frac{c}{2} \end{array} \right\} m = 0, \pm 1, \pm 2, \dots \quad (5.33)$$

At this point, it is convenient to assume that ω has a small positive imaginary part that will be set to zero at the end of the analysis. The net effect of this is to replace the usual outgoing-wave boundary condition at infinity by a boundedness requirement. Physically it amounts to introducing a small amount of damping into the system.¹³

It is shown in Appendix 5.A that the outgoing-wave solution of Eqs. (5.30) and (5.31) that satisfies the boundary condition (5.33) is given in terms of the dimensionless Prandtl-Glauert coordinates $\xi = y_1/c$, $\eta = \beta_r(y_2/c)$ by

$$V(\xi, \eta) = \frac{i\beta_r}{4} \int_{-\infty}^{\infty} \frac{M_r f_0(\alpha) \gamma e^{-i(\alpha + M_r K)\xi}}{K + M_r \alpha} \left[\frac{e^{-\eta\gamma + (1/2)\Delta_+}}{\sinh \frac{1}{2}\Delta_+} - \frac{e^{\eta\gamma + (1/2)\Delta_-}}{\sinh \frac{1}{2}\Delta_-} \right] d\alpha$$

for $0 \leq \eta < \frac{s\beta_r}{c}$ (5.34)

where the function $f_0(\alpha)$ is the solution of the simultaneous integral equations

$$1 = e^{-i(K/M_r)\beta_r^2\xi} \lim_{\eta \rightarrow 0} V(\xi, \eta)$$

$$= \frac{i\beta_r}{2} \int_{-\infty}^{\infty} \frac{f_0(\alpha)}{\frac{K}{M_r} + \alpha} e^{-i[\alpha + (K/M_r)]\xi} \frac{\gamma \sinh \frac{s\beta_r\gamma}{c}}{\cosh \frac{s\beta_r\gamma}{c} - \cos \left(\Gamma + \frac{\alpha s^\dagger}{c} \right)} d\alpha$$

for $-\frac{1}{2} < \xi < \frac{1}{2}$ (5.35)

$$f_0(\alpha) = \frac{1}{2\pi} \int_{-1/2}^{1/2} [P] e^{i(\alpha + M_r K)\xi} d\xi \quad (5.36)$$

that causes the pressure jump $[P] \equiv \lim_{\varepsilon \rightarrow 0} [P(\xi, \varepsilon) - P(\xi, -\varepsilon)]$ to vanish at the trailing edge ($\xi = \frac{1}{2}$) of the $m = 0$ airfoil.[†] The functions $\Delta_{\pm}(\alpha)$ and $\gamma(\alpha)$ are defined by

$$\Delta_{\pm}(\alpha) = i \left(\Gamma + \frac{\alpha s^{\dagger}}{c} \right) \pm \frac{s \beta_r \gamma}{c} \quad (5.37)$$

$$\gamma(\alpha) = \sqrt{\alpha^2 - K^2 + K_q^2} \quad (5.38)$$

where the branch of the square root is chosen so that its real part is always positive. Furthermore, the parameters β_r , K , K_q , and Γ that appear in these equations are defined by

$$\beta_r \equiv \sqrt{1 - M_r^2} \quad (5.39)$$

$$K \equiv \frac{\omega c}{c_0 \beta_r^2} = \frac{p \Omega c}{c_0 \beta_r^2} = \frac{p U_0 c}{\beta_r^2 r_M c_0} \quad (5.40)$$

$$K_q \equiv \frac{\pi q c}{\beta_r b} \quad (5.41)$$

and

$$\Gamma \equiv \sigma + M_r K \frac{s^{\dagger}}{c} = \frac{K}{M_r} \left(\frac{s^{\dagger}}{c} + \frac{\beta_r^2 s}{c} \cot \mu \right) \quad (5.42)$$

where

$$\sigma = \frac{K}{M_r} \beta_r^2 \left(\frac{s^{\dagger} + s \cot \mu}{c} \right) = \frac{\omega}{U_r} (s^{\dagger} + s \cot \mu) \quad (5.43)$$

is called the *interblade phase angle*. Finally, outside of the range of η for which Eq. (5.34) is defined, the solution can be determined from the periodicity condition

$$V \left(\xi + \frac{m s^{\dagger}}{c}, \eta + \frac{m s}{c} \beta_r \right) = e^{i m \sigma} V(\xi, \eta) \quad (5.44)$$

5.3.3 Solution of Integral Equations

In order to complete the solution, it is necessary to solve the coupled integral Eqs. (5.35) and (5.36) for f_0 and $[P]$ subject to the Kutta condition

$$[P] = 0 \quad \text{at } \xi = \frac{1}{2} \quad (5.45)$$

[†] Notice that these equations simultaneously determine the two unknowns $f_0(\alpha)$ and $[P(\xi)]$.

This has been done for the two-dimensional case (corresponding to $K_q = 0$) by Lane and Friedman³ and more recently by Whitehead.⁴ The method used by these authors consists of expanding the pressure jump $[P]$ across the blades in the trigonometric series (commonly used in both steady- and unsteady-thin-airfoil theory)

$$[P] = \frac{1}{2} A_0 \cot\left(\frac{\theta}{2}\right) + \sum_{m=1}^{\infty} A_m \sin m\theta$$

where $\cos \theta \equiv -2\xi$. This expansion ensures that the Kutta condition (5.45) will always be satisfied at the trailing edge. When it is substituted into Eq. (5.36), the various integrations can be carried out to obtain an expansion of $f_0(\alpha)$ in terms of Bessel functions. Then this series can in turn be substituted into Eq. (5.35), to obtain an equation for the expansion coefficients A_n (which can be solved by collocation methods, i.e., by requiring that the equation be satisfied only at a finite number of points along the airfoil chord). This approach entails the use of relatively large amounts of computation time. However, the problem can also be solved by combining Eqs. (5.35) and (5.36) into a single integral equation for the weighed pressure jump

$$g(\xi) = [P] e^{-i(K\beta_r^2/M_r)\xi} \quad (5.46)$$

Thus, substituting Eq. (5.36) into Eq. (5.35) yields (assuming the order of integration can be interchanged)

$$1 = \int_{-1/2}^{1/2} \mathcal{K}(\xi - \xi') g(\xi') d\xi' \quad (5.47)$$

where the kernel function $\mathcal{K}(\xi - \xi')$ is given by

$$\mathcal{K}(\xi - \xi') \equiv \frac{i\beta_r}{4\pi} \int_{-\infty}^{\infty} \frac{e^{-i[\alpha + (K/M_r)](\xi - \xi')}}{(K/M_r) + \alpha} \frac{\gamma \sinh s\beta_r\gamma/c}{\cosh \frac{s\beta_r\gamma}{c} - \cos\left(\Gamma + \frac{\alpha s^\dagger}{c}\right)} d\alpha \quad (5.48)$$

Since the integrand in Eq. (5.48) goes to ± 1 for large values of α , the integral does not exist in the usual sense and must be treated as the Fourier transform of a distribution.[†]

The effect of the various airfoils in the cascade on the $m = 0$ airfoil (which passes through the line $\eta = 0$) is accounted for by the term

$$\frac{\sinh s\beta_r\gamma/c}{\cosh s\beta_r\gamma/c - \cos(\Gamma + \alpha s^\dagger/c)}$$

Hence, if this term were put equal to unity in Eq. (5.48), Eq. (5.47) would become the integral equation for the force on an isolated airfoil. On the

[†] A very clear and concise discussion of the ideas involved can be found in Lighthill.⁵

other hand, we can express Eq. (5.48) in terms of convergent integrals by first subtracting out the single airfoil contribution to obtain

$$\begin{aligned} \mathcal{H}(\xi - \xi') &= \frac{i\beta_r}{4\pi} \int_{-\infty}^{\infty} \frac{e^{-i[\alpha(K/M_r)](\xi - \xi')}}{K/M_r + \alpha} \gamma d\alpha \\ &+ \frac{i\beta_r}{4\pi} \int_{-\infty}^{\infty} \frac{e^{-i[\alpha + (K/M_r)](\xi - \xi')}}{K/M_r + \alpha} \gamma \left[\frac{\sinh s\beta_r\gamma/c}{\cosh s\beta_r\gamma/c - \cos(\Gamma + \alpha s^\dagger/c)} - 1 \right] d\alpha \end{aligned}$$

Then the first integral can be computed from Eq. (5.B.1) in Appendix 5.B. And since the integrand of the second integral goes to zero exponentially fast as $\alpha \rightarrow \pm\infty$, this integral is absolutely convergent and therefore represents a bounded function of $\xi - \xi'$. However, the results of Appendix 5.B show that the first integral is singular at $\xi - \xi' = 0$. In fact, it follows from Eq. (5.B.2) that \mathcal{H} can be expressed in the form

$$\mathcal{H}(\xi - \xi') = \frac{\beta_r}{2\pi} \left(\frac{1}{\xi - \xi'} + \frac{iK}{M_r} \ln |\xi - \xi'| \right) + \mathcal{H}(\xi - \xi') \quad (5.49)$$

where \mathcal{H} denotes a nonsingular function. Thus, as is usual in thin-airfoil theory, the kernel of the integral Eq. (5.47) has a nonintegrable singularity of the type $(\xi - \xi')^{-1}$. This equation is, therefore, said to be singular and it can be shown that the integral must be interpreted as a Cauchy principal value.

Equation (5.47) is known to possess a single eigensolution. Since the complete solution to this equation consists of a particular solution added to an arbitrary multiple of this eigensolution, there is enough arbitrariness in the result to accommodate the imposition of the Kutta condition (5.45). However, we must then allow $g(\xi)$ to have a square-root singularity at the leading edge $\xi = -\frac{1}{2}$.

Although these results reveal the general structure of the kernel function, they do not provide convenient formulas for computing this quantity. However, notice that the integrand of Eq. (5.48), being an even function of γ , will have only simple poles in the complex α -plane. But since it does not vanish at infinity, the residue theorem cannot be used to evaluate the integral. If, on the other hand, we delay taking the limit $\eta \rightarrow 0$ in Eq. (5.47), we find that the kernel function can be written as

$$\begin{aligned} \mathcal{H}(\xi - \xi') &= \frac{i\beta_r}{8\pi} \lim_{\eta \rightarrow 0} \frac{\partial^2}{\partial \eta^2} \int_{-\infty}^{\infty} \frac{e^{-i[\alpha + (K/M_r)](\xi - \xi')}}{(K/M_r + \alpha)\gamma} \\ &\times \left[\frac{e^{-\eta\gamma} e^{(1/2)\Delta_+}}{\sinh \frac{1}{2}\Delta_+} - \frac{e^{\eta\gamma} e^{(1/2)\Delta_-}}{\sinh \frac{1}{2}\Delta_-} \right] d\alpha \end{aligned}$$

Then since, as can be seen by replacing γ by $-\gamma$, the integrand is still an even function of γ , it again possesses no branch points even when η is

finite. However, it now behaves either like

$$\frac{1}{\alpha^2} e^{-i\alpha(\xi - \xi')}$$

or like

$$\frac{1}{\alpha^2} e^{-i\alpha(\xi - \xi' - \eta s^\dagger / s\beta_r)}$$

as $|\alpha| \rightarrow \infty$. Consequently Jordan's lemma¹⁴ insures that the integration contour can be closed on a large semicircle and therefore that the residue theorem can be applied. (The location of the relevant poles is discussed in the next section.) The contour must be closed in the upper half-plane when

$$\xi < \xi' \quad (5.50)$$

and in the lower half-plane when

$$\xi > \xi' + \frac{\eta s^\dagger}{s\beta_r} \quad (5.51)$$

Two different expressions are obtained depending on whether condition (5.50) or condition (5.51) holds. And since there are infinitely many poles in both the upper and lower half-planes, these expressions are infinite series. The resulting expansion of the kernel function turns out to be identical to the one obtained by Kaji and Okazaki,^{7,8} who used an entirely different approach based on an ingenious application of the Poisson summation formula. The Kaji-Okazaki series is rapidly convergent whenever $\xi - \xi'$ is bounded away from zero and provides a convenient method for calculating the kernel function.

5.3.4 Acoustic Radiation

From the point of view of acoustics, our main interest is in the pressure field at large distances from the blade row. We shall show that the solution in this region is determined by the poles of the integrand in Eq. (5.34). One of these occurs at the point

$$\alpha = -\frac{K}{M_r}$$

and the remainder occur at the points where

$$\Delta_\pm = i2n\pi \quad \text{for } n = 0, \pm 1, \pm 2, \dots$$

It follows from Eqs. (5.37) and (5.38) that the latter points are given by

$$\alpha_n^\pm = -\Gamma_n \frac{cs^\dagger}{(d^\dagger)^2} \pm i \frac{s\beta_r}{d^\dagger} \sqrt{\left(\frac{c\Gamma_n}{d^\dagger}\right)^2 - K^2 + K_q^2} \quad \text{for } n = 0, \pm 1, \pm 2, \dots \quad (5.52)$$

where we have put

$$d^\dagger = \sqrt{(s^\dagger)^2 + \beta_r^2 s^2} \quad (5.53)$$

and

$$\Gamma_n = \Gamma - 2n\pi \quad (5.54)$$

The plus sign in Eq. (5.52) refers to the poles lying in the upper half-plane and the minus sign refers to those in the lower half-plane (provided we adhere to our convention about the branch of the square root).

These poles will approach the real axis when $\mathcal{I}m K \rightarrow 0$ only if

$$\left(\frac{c\Gamma_n}{d^\dagger}\right)^2 + K_q^2 < K^2 \quad (5.55)$$

in which case, Eq. (5.52) can be written as

$$\alpha_n^\pm = -\Gamma_n \frac{cs^\dagger}{(d^\dagger)^2} \pm \frac{s\beta_r}{d^\dagger} \sqrt{K^2 - K_q^2 - \left(\frac{c\Gamma_n}{d^\dagger}\right)^2} \equiv \kappa \sin \Theta_n^\pm \quad (5.56)$$

where in this expression $\sqrt{\quad}$ denotes the positive square root,

$$\kappa \equiv \sqrt{K^2 - K_q^2} \quad (5.57)$$

and Θ_n^\pm are always real. Then it follows from Eq. (5.37) that

$$\gamma(\alpha_n^\pm) = \mp i\kappa \left(\frac{\cos \delta_n + \sin \chi^\dagger \sin \Theta_n^\pm}{\cos \chi^\dagger} \right) = \mp i\kappa \cos \Theta_n^\pm \quad (5.58)$$

We can simplify the notation somewhat by introducing the angle

$$\delta_n \equiv \cos^{-1} \frac{c\Gamma_n}{\kappa d^\dagger} \quad (5.59)$$

and the stagger angle

$$\chi^\dagger = \tan^{-1} \frac{s^\dagger}{s\beta_r}$$

in the Prandtl–Glauert plane. Then Eq. (5.56) becomes

$$\sin \Theta_n^\pm = -\cos \delta_n \sin \chi^\dagger \pm \cos \chi^\dagger \sin \delta_n = \sin(-\chi^\dagger \pm \delta_n)$$

so that with no loss of generality we can put

$$\Theta_n^\pm = -\chi^\dagger \pm \delta_n \quad (5.60)$$

Upon separating out the singularities that occur in its integrand when $\mathcal{I}m K \rightarrow 0$, Eq. (5.34) becomes

$$V(\xi, \eta) = \int_{-\infty}^{\infty} \left\{ \frac{A(\xi, \eta)}{K/M_r + \alpha} + \sum_{n=m_1}^{m_2} \left[\frac{B_n^+(\xi, \eta)}{\alpha - \alpha_n^+} + \frac{B_n^-(\xi, \eta)}{\alpha - \alpha_n^-} \right] + D(\xi, \eta, \alpha) \right\} d\alpha$$

where $D(\xi, \eta, \alpha)$ possesses no real poles as $\mathcal{I}m K \rightarrow 0$; A and B_n^\pm are the residues at the poles at $-K/M_r$ and α_n^\pm , respectively; and m_1 and m_2 are the minimum and maximum values of n for which the inequality (5.55) holds. Then, evaluating the residues and using Eqs. (5.56) through (5.60) to simplify the results yields

$$B_n^\pm(\xi, \eta) = \frac{i\beta_r M_r c \kappa \cos^2 \Theta_n^\pm e^{-i[(\kappa \sin \Theta_n^\pm + M_r K)\xi - \kappa(\cos \Theta_n^\pm)\eta]} f_0(\kappa \sin \Theta_n^\pm)}{\mp 2d^\dagger(K + M_r \kappa \sin \Theta_n^\pm) \sin \delta_n} \quad (5.61)$$

and

$$A(\xi, \eta) = h(\eta) e^{(iK\beta_r^2 \xi)/M_r} \quad (5.62)$$

Now it follows from the theory of Fourier transforms that $D(\xi, \eta, \alpha)$ does not contribute to the integral in the limit as $|\xi| \rightarrow \infty$. The remaining terms can be evaluated by closing the contour in the appropriate half-plane and using Cauchy's theorem to set the integrals equal to $2\pi i$ times the sum of their residues. Hence if $\xi \ll 0$ (corresponding to a position far upstream),

$$V \sim 2\pi i \sum_{n=m_1}^{m_2} B_n^+(\xi, \eta) \quad (5.63)$$

and if $\xi \gg 0$ (corresponding to a position far downstream),

$$V \sim -2\pi i A(\xi, \eta) - 2\pi i \sum_{n=m_1}^{m_2} B_n^-(\xi, \eta) \quad (5.64)$$

The term $A(\xi, \eta)$ represents a convected (but non-vortical) disturbance and therefore does not contribute to the pressure. In fact, it can be seen from Eqs. (5.62) and (5.A.6) that this term makes no contribution to Ψ and therefore (in view of Eq. (5.A.2)) no contribution to the pressure P . Equation (5.61) shows that the remaining terms in Eqs. (5.63) and (5.64) satisfy the periodicity condition (5.44). Hence, these solutions apply for all values of η and not just those in the range $0 < \eta < s\beta_r/c$ where Eq. (5.34) holds. Finally, these results can be inserted into Eqs. (5.A.6), (5.A.2), and (5.27) to show that the asymptotic pressure field is given by

$$\left. \begin{aligned} p &\sim \sum_{n=m_1}^{m_2} p_n^+ & \text{as } \xi \rightarrow -\infty \\ p &\sim \sum_{n=m_1}^{m_2} p_n^- & \text{as } \xi \rightarrow +\infty \end{aligned} \right\} \quad (5.65)$$

where

$$\begin{aligned} \frac{p_n^\pm}{\rho_0 a U_r} &= -\frac{\pi c \cos \Theta_n^\pm}{d^\dagger \sin \delta_n} f_0(\kappa \sin \Theta_n^\pm) \\ &\times e^{-i[\omega\tau + (\kappa \sin \Theta_n^\pm + M_r K)\xi - \kappa(\cos \Theta_n^\pm)\eta]} \cos\left(\frac{\pi q y_3}{b}\right) \end{aligned} \quad (5.66)$$

Thus, at large distances from the blade row, the pressure can be expressed as a finite sum which contains only those p_n^\pm that satisfy the cutoff condition (5.55). In fact, if we let

$$\chi \equiv \tan^{-1} \frac{s^\dagger}{s} \quad (5.67)$$

denote the stagger angle and introduce the stationary coordinate system (see Fig. 5.4)

$$\left. \begin{aligned} x_1 &= y_1 \cos \chi - y_2 \sin \chi \\ x_2 &= y_1 \sin \chi + y_2 \cos \chi - U_0 \tau \\ x_3 &= y_3 \end{aligned} \right\} \quad (5.68)$$

into Eq. (5.66) we can show, by using the results of Appendix 5.C, that

$$\begin{aligned} \frac{p_n^\pm}{\rho_0 a U_r} &= \frac{1}{2} e^{-i[nB\Omega\tau + (nB-p)(x_2/r_M) + x_1\gamma_{q,p,nB}^\pm]} \\ &\times \cos\left(\frac{\pi q x_3}{b}\right) \frac{c}{k_{q,p,nB} d} \left(\frac{nB-p}{r_M} \cos \chi - \gamma_{q,p,nB}^\pm \sin \chi \right) 2\pi f_0(\kappa \sin \Theta_n^\pm) \end{aligned} \quad (5.69)$$

where

$$\begin{aligned} \gamma_{q,p,nB}^\pm &= \frac{Mk_0}{\beta^2} \pm \frac{k_{q,p,nB}}{\beta^2} \\ k_{q,p,nB} &= \sqrt{k_0^2 - \beta^2 \left[\left(\frac{nB-p}{r_M} \right)^2 + \left(\frac{\pi q}{b} \right)^2 \right]} \end{aligned}$$

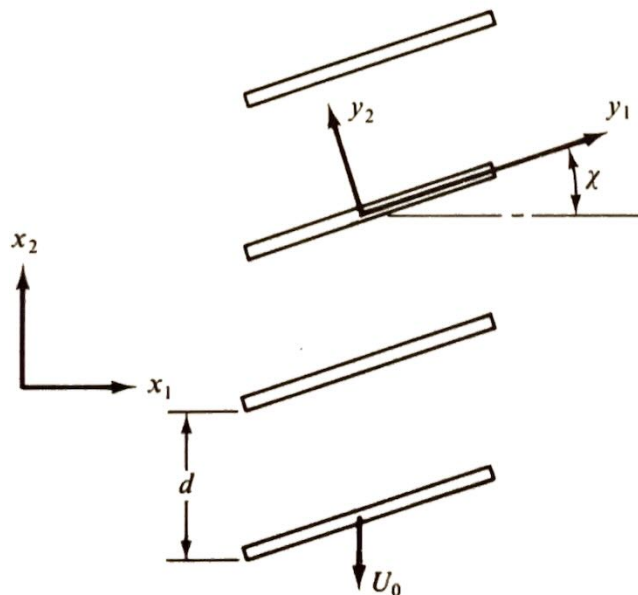


Fig. 5.4 Duct-oriented coordinates.

$k_0 \equiv (nB\Omega/c_0) + M(p - nB) \tan v/r_M$, $\beta = \sqrt{1 - M^2}$, $M \equiv (U_\infty/c_0) \cos v$ is the Mach number of the oncoming flow in the axial direction (perpendicular to the blade row) and $d = \sqrt{(s^\dagger)^2 + s^2}$ is the interblade distance. Thus, p_n^\pm is simply a wave which propagates down the duct in the x_1 -direction (with propagation constant $\gamma_{q,p,nB}^\pm$) while it moves in the transverse direction (x_2 -direction) with the phase velocity $r_M(nB\Omega)/(nB - p)$. Moreover, it is easy to see from the results of Appendix 5.C that the condition (5.55) does indeed correspond to the cutoff condition

$$k_0^2 > \beta^2 \left[\left(\frac{nB - p}{r_M} \right)^2 + \left(\frac{\pi q}{b} \right)^2 \right]$$

for this wave. Thus, for any given spatial harmonic of the disturbance field (characterized by the indices p and q), the sound field consists of all those blade-passing-frequency harmonics whose frequency is above the cutoff frequency for the p, q th mode. These results are qualitatively the same as those given in Sec. 4.3.2 for a circular duct. The principal difference is that there is now a mean crossflow $c_0 M \tan v$ in the transverse direction in addition to the axial velocity $c_0 M$. In fact, since Eq. (5.36) shows that†

$$2\pi f_0(\kappa \sin \Theta_n^\pm) = \int_{-1/2}^{1/2} e^{i(\kappa \sin \Theta_n^\pm + M, K)\xi} [P] d\xi \quad (5.70)$$

and since $a[P]\rho_0 U_r \sin \chi$ is the amplitude of the thrust force per unit area acting on the blade while $a[P]\rho_0 U_r \cos \chi$ is the amplitude of the drag force per unit area, we see that Eqs. (5.65) and (5.69) are indeed similar to Eq. (4.30).

5.3.5 Implications of Solution

The resemblance of Eqs. (5.69) and (5.70) to the terms in Eq. (4.30) is not coincidental since the former are precisely the results that would be obtained if the acoustic analogy approach of Chap. 4 were applied to the infinite cascade configuration analyzed in this chapter. The new feature introduced in the present approach is the integral Eq. (5.47) for calculating the blade forces, which were determined from a single-airfoil two-dimensional flow

† For real compressors the flow at large distances from the blade row will be oriented mostly in the x_1 -direction. A possible way of compensating for this is to set $v = 0$ in k_0 while leaving it unchanged in the integral (5.70). This can be justified by arguing that the terms in the integral, being associated with the local unsteady lift, are relatively uninfluenced by the turning of the flow in the axial direction. The net effect of this turning is to eliminate the crossflow in the propagation terms of Eq. (5.69).

model in the last chapter. Consequently, we are now able to account for the mutual interference between the airfoils of the cascade. Such effects are particularly important near cutoff, where they cause the blade forces to vanish⁴ and thereby keep the radiated power from becoming infinite at this condition as predicted by the isolated airfoil model used in Chap. 4 (see discussion near end of Sec. 4.3.5).

The exponent in the integrand of Eq. (5.70) is associated with changes in retarded time. If we neglect its variation along the blade (as is done in Chap. 4), the integral reduces to the response function (see Sec. 3.4.2)

$$\frac{F}{c\rho_0 U_r a \pi} = \frac{1}{\pi} \int_{-1/2}^{1/2} [P] d\xi \quad (5.71)$$

It can be seen from Eqs. (5.C.3), (5.C.4), (5.40), and (5.41), that both this quantity and the radiated sound field can be completely characterized by the following parameters: The transverse wave number $\pi q/b$, the relative Mach number M_r , the interblade phase angle $\sigma = 2\pi p/B$, the stagger angle χ , the solidity c/d , and the reduced frequency $\beta_r^2 K/2M_r = \omega c/2U_r$. But since the wavelength λ_0 of the incident gust (see Fig. 5.2) is equal to $2\pi r_M/p$ and since $2\pi r_M = Bd$, the ratio of the gust wavelength to the interblade spacing d is related to σ by $\lambda_0/d = 2\pi/\sigma$; while Eq. (5.29) shows that the reduced frequency is related to the ratio of the transverse to relative velocity U_0/U_r by (see Fig. 5.2) $\omega c/2U_r = (c/d)(\sigma/2)(U_0/U_r)$. Hence the parameters λ_0/d and U_0/U_r can be used in place of the reduced frequency and interblade phase angle.

The response function (5.71) was calculated by Fleeter⁶ for various values of these parameters in the range of interest for compressors. Typical results taken from his paper are shown in Fig. 5.5. Also included is the corresponding incompressible flow solution. The figure shows that compressibility effects can change the response function by more than a factor of 2. We anticipate that they will cause similar changes in the magnitude of the acoustic pressure fluctuations.

Notice that, as the Mach number M_r increases, the magnitude of the fluctuating lift force increases toward a maximum and then decreases rapidly to zero. It becomes equal to zero at the Mach number where the blade passing frequency becomes equal to the cutoff frequency for the lowest-order mode. But, as we indicated in Sec. 4.3.5, the expression for the radiated power has a zero in its denominator at precisely this frequency. The corresponding zero in its numerator caused by the vanishing of the blade forces therefore serves to keep the radiated acoustic power finite—an effect which would not occur if an isolated airfoil analysis were used to predict the blade forces. This behavior is an example of how a sound field can exert a powerful back reaction on its source (the fluctuating blade forces).

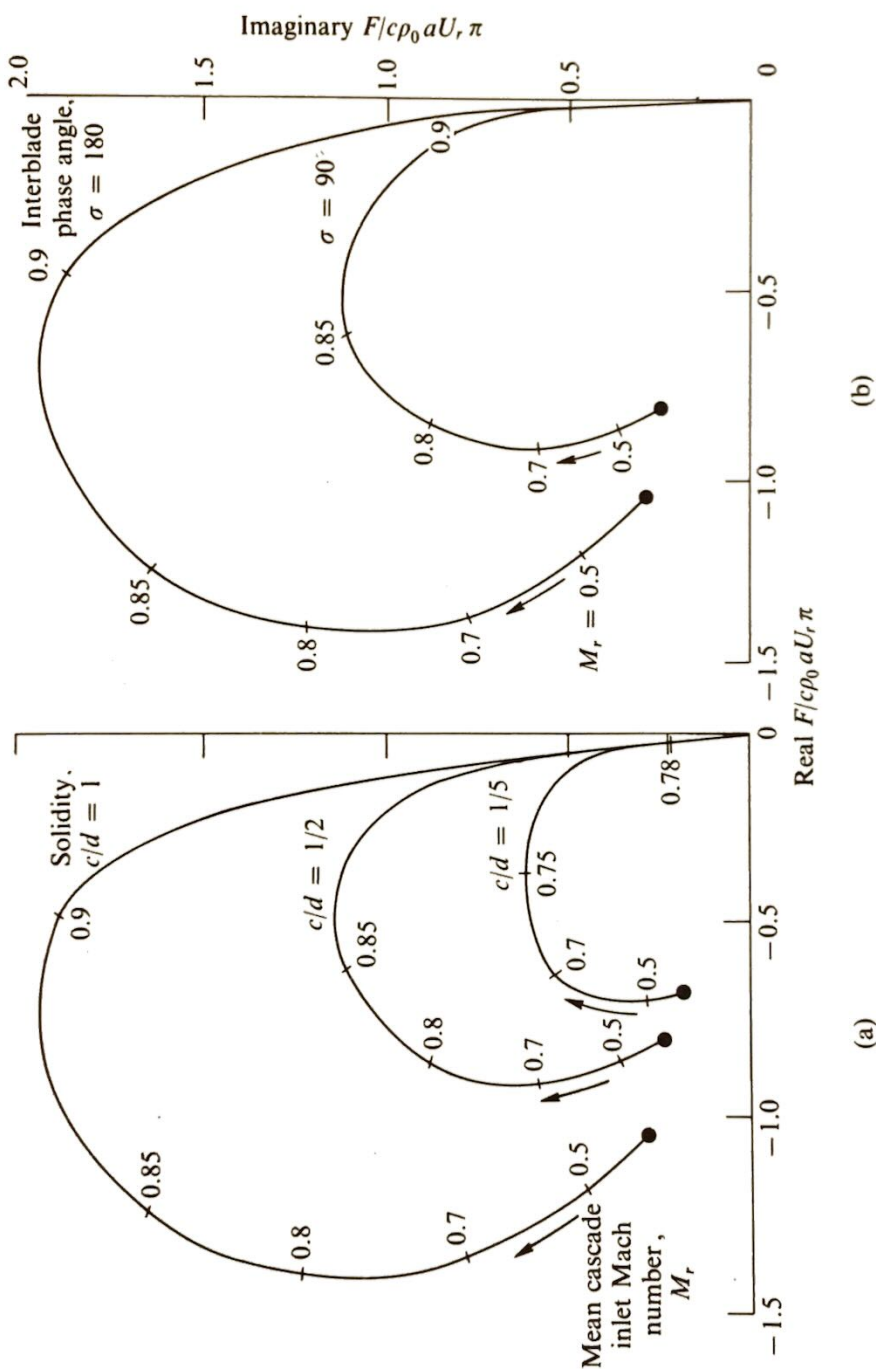


Fig. 5.5 Effect of compressibility on response function. Stagger angle, χ , 0° ; reduced frequency, $\omega c/2U_r$, 0.25; transverse Mach number, $\pi q/b$, 0. (a) Solidity effect on response function with mean cascade inlet Mach number M_r as a parameter. Interblade phase angle, σ , 180° . (b) Interblade-phase-angle effect on response function with mean cascade inlet Mach number as parameter. Solidity, c/d , 1.

Kaji¹² used an analysis of the type given in this chapter to calculate the intensity of the fundamental blade passing frequency tones radiated both upstream of and downstream from a rotor. His results are plotted against λ_0/d in Fig. 5.6. However, in this case, the velocity ratio U_0/U_r , rather than the reduced frequency, is held constant. The dashed curves are obtained by neglecting the retarded time variations in Eqs. (5.69) and (5.70). They show that such an approximation can overestimate the upstream radiation by as much as 5 to 10 dB. After carrying out a number of similar calculations, Kaji concluded that reasonable predictions of the downstream radiation can

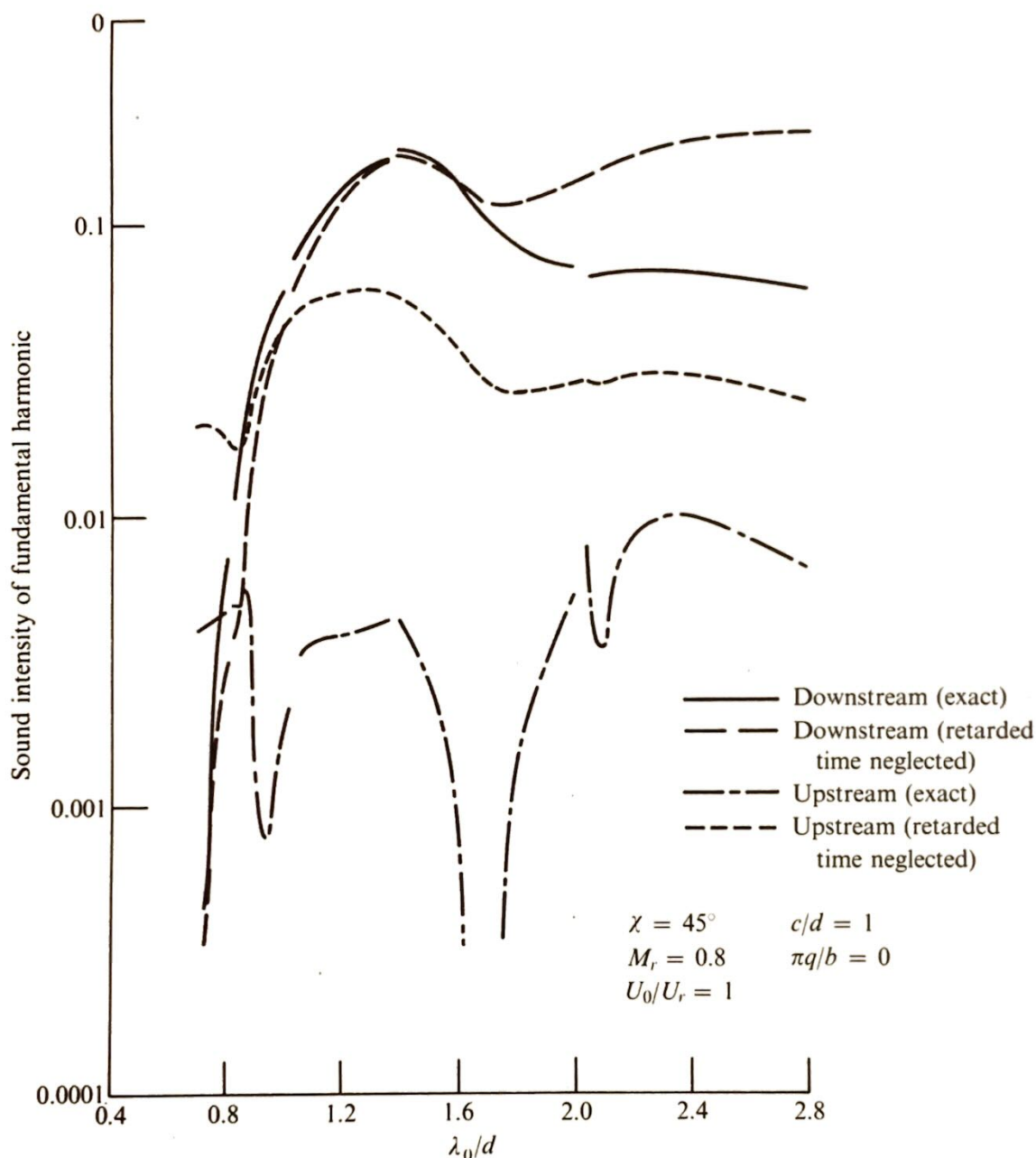


Fig. 5.6 Variation of sound intensity with wavelength of incident gust. (From Reference 12.)

be obtained when the retarded time is neglected but that the use of this approximation to calculate the upstream radiated sound will generally result in overestimates of from 3 to 10 dB. On the other hand, Fig. 5.5(a) shows that the response function for a cascade with unit solidity can be considerably greater than the isolated airfoil response function (which should be fairly well approximated by the curve for the lowest solidity cascade) so that, due to two compensating errors, the results given in Chap. 4 could be reasonably accurate even at high Mach numbers.

The curves in Fig. 5.6 are cut at the values $\lambda_0/d = 2, 1.4, 1.0$, and 0.8 where higher order modes begin to contribute to the sound field.

5.4 CONCLUDING REMARKS

We have shown that exact aeroacoustic calculations can be carried out for flows that can be treated as small perturbations about a uniform motion. The results indicate that the volume quadrupole sources can always be neglected for such flows even if the source region is not compact. This may explain why the dipole model can often be used to obtain good predictions of the sound emissions from fans and compressors even at high subsonic Mach numbers.

APPENDIX 5.A SOLUTION TO CASCADE PROBLEM

In this appendix we shall obtain an outgoing-wave solution to Eqs. (5.30) and (5.31) that satisfies the boundary condition (5.33).

In order to transform this problem into an equivalent (and somewhat more familiar) stationary-medium problem, we introduce the dimensionless Prandtl–Glauert coordinates

$$\left. \begin{aligned} \xi &= \frac{y_1}{c} \\ \eta &= \frac{y_2}{c} \beta_r \end{aligned} \right\} \quad (5.A.1)$$

and the new dependent variable

$$\Psi = P e^{iM_r K \xi} \quad (5.A.2)$$

where

$$K \equiv \frac{\omega c}{c_0 \beta_r^2} = \frac{p \Omega c}{c_0 \beta_r^2} = \frac{p U_0 c}{\beta_r^2 r_M c_0} \quad (5.A.3)$$

and

$$\beta_r \equiv \sqrt{1 - M_r^2} \quad (5.A.4)$$

Then Eqs. (5.30), (5.31), and the boundary condition (5.33) become

$$\frac{\partial^2 \Psi}{\partial \xi^2} + \frac{\partial^2 \Psi}{\partial \eta^2} + (K^2 - K_q^2) \Psi = 0 \quad (5.A.5)$$

$$e^{(i\beta_r^2 K/M_r) \xi} \frac{\partial}{\partial \xi} e^{-(i\beta_r^2 K/M_r) \xi} V = -\beta_r e^{-iM_r K \xi} \frac{d\Psi}{d\eta} \quad (5.A.6)$$

$$V = e^{(iK/M_r)\beta_r^2[\xi + (ms/c) \cot \mu]} \quad \text{for} \quad \left\{ \begin{array}{l} \eta = \frac{ms}{c} \beta_r \\ -\frac{1}{2} < \xi - \frac{ms^\dagger}{c} < \frac{1}{2} \end{array} \right\} m = 0, \pm 1, \dots \quad (5.A.7)$$

where

$$K_q \equiv \frac{\pi qc}{\beta_r b} \quad (5.A.8)$$

Notice that Eq. (5.A.5) possesses a separation-of-variables solution of the form

$$e^{-i\alpha\xi - \gamma\eta} \quad (5.A.9)$$

where the branch of the square root

$$\gamma = \sqrt{\alpha^2 - K^2 + K_q^2}$$

is chosen so that its real part is always positive (in the complex α -plane).¹³ In order to apply this solution to the present problem, it is convenient to introduce for each integer $m = 0, \pm 1, +2, \dots$, a coordinate system

$$\left. \begin{array}{l} \eta_m = \eta - \frac{ms}{c} \beta_r \\ \xi_m = \xi - \frac{ms^\dagger}{c} \end{array} \right\} \quad (5.A.10)$$

that has its origin on the m th blade. Then, superposing the solutions (5.A.9) with respect to the separation parameter α yields the following outgoing-wave solution to Eq. (5.A.5):

$$\Psi_m(\xi, \eta) = \frac{\text{sgn}(\eta_m)}{2} \int_{-\infty}^{\infty} f_m(\alpha) e^{-i\alpha\xi_m - |\eta_m|\gamma} d\alpha \quad (5.A.11)$$

where $f_m(\alpha)$ is an, as yet, undetermined function and

$$\text{sgn } x = \begin{cases} 1 & \text{for } x > 0 \\ -1 & \text{for } x < 0 \end{cases}$$

This solution possesses a jump discontinuity

$$[\Psi_m(\xi)] = \int_{-\infty}^{\infty} f_m(\alpha) e^{-i\alpha\xi_m} d\alpha \quad (5.A.12)$$

across the line $\eta = (ms/c)\beta_r$ passing through the m th blade. Since the boundary conditions can only be satisfied if the pressure function P is

discontinued across the blades, we seek a solution in the form

$$\Psi = \sum_{m=-\infty}^{\infty} \Psi_m \quad (5.A.13)$$

of a superposition of the solutions (5.A.11). Then the jump $[\Psi]$ in Ψ across the m th blade is given by $[\Psi_m]$ alone. Hence, it follows from Eq. (5.A.2) that the jump $[P]$ in the pressure function along the line $\eta = (ms/c)\beta_r$ is

$$[P] = e^{-iM_r K \xi} \int_{-\infty}^{\infty} f_m(\alpha) e^{-i\alpha \xi_m} d\alpha \quad (5.A.14)$$

We shall subsequently eliminate the portion of the discontinuity that lies outside the interval $|\xi - (ms^\dagger/c)| < \frac{1}{2}$.

Since the upwash velocity w_2 vanishes at $\xi = -\infty$, Eq. (5.A.6) can be integrated to obtain

$$V = -\beta_r e^{(i\beta_r^2 K/M_r)\xi} \int_{-\infty}^{\xi} e^{-(iK/M_r)\xi'} \frac{\partial \Psi}{\partial \eta}(\xi', \eta) d\xi' \quad (5.A.15)$$

Then substituting Eq. (5.A.11) into Eq. (5.A.13), inserting the result into Eq. (5.A.15), interchanging the order of integration, and integrating with respect to ξ yields†

$$V = \frac{\beta_r i}{2} e^{-iM_r K \xi} \int_{-\infty}^{\infty} \frac{M_r \gamma}{K + M_r \alpha} \sum_{m=-\infty}^{\infty} f_m(\alpha) e^{-(i\alpha \xi_m + |\eta_m| \gamma)} d\alpha \quad (5.A.16)$$

And, since the boundary condition (5.A.7) can be written as

$$V\left(\xi_m + \frac{ms^\dagger}{c}, \frac{ms}{c} \beta_r\right) = e^{(iK/M_r)\beta_r^2 \xi_m} e^{i m \sigma} \quad (5.A.17)$$

for $m = 0, \pm 1, \pm 2, \dots; -\frac{1}{2} < \xi_m < \frac{1}{2}$

where

$$\sigma \equiv \frac{K}{M_r} \beta_r^2 \left(\frac{s^\dagger + s \cot \mu}{c} \right) = \frac{\omega}{U_r} (s^\dagger + s \cot \mu) \quad (5.A.18)$$

is called the *interblade phase angle*, we can ensure that satisfying this condition on the $m = 0$ blade will also cause it to be satisfied on the remaining blades if the functions f_m can be related to f_0 in such a way that

$$V\left(\xi + \frac{ms^\dagger}{c}, \eta + \frac{ms}{c} \beta_r\right) = e^{i m \sigma} V(\xi, \eta) \quad (5.A.19)$$

We shall now show that this occurs when

$$f_m(\alpha) = e^{i m \Gamma} f_0(\alpha) \quad (5.A.20)$$

† Where we use the fact that the imaginary part of ω , and hence of K , is slightly positive to show that the integrated term vanishes at minus infinity.

where

$$\Gamma \equiv \sigma + M_r K \frac{s^\dagger}{c} = \frac{K}{M_r} \left(\frac{s^\dagger}{c} + \frac{\beta_r^2 s}{c} \cot \mu \right) \quad (5.A.21)$$

To this end, insert Eq. (5.A.20) into Eq. (5.A.16) to obtain

$$\begin{aligned} V(\xi, \eta) &= \frac{i\beta_r}{2} \int_{-\infty}^{\infty} \frac{M_r \gamma f_0(\alpha)}{K + M_r \alpha} e^{-i(\alpha + M_r K)\xi} \sum_{m=-\infty}^{\infty} e^{im[\Gamma + (\alpha s^\dagger/c)] - |\eta_m| \gamma} d\alpha \\ &= \frac{i\beta_r}{2} \int_{-\infty}^{\infty} \frac{M_r \gamma f_0(\alpha)}{K + M_r \alpha} \sum_{m=-\infty}^{\infty} e^{im\sigma - i(\alpha + M_r K)\xi_m - |\eta_m| \gamma} d\alpha \end{aligned} \quad (5.A.22)$$

Then the fact that

$$\begin{aligned} V\left(\xi + \frac{ms^\dagger}{c}, \eta + \frac{ms}{c} \beta_r\right) &= \frac{i\beta_r}{2} \int_{-\infty}^{\infty} \frac{M_r \gamma f_0(\alpha)}{K + M_r \alpha} \sum_{n=-\infty}^{\infty} e^{in\sigma - i(\alpha + M_r K)[\xi - (n-m)(s^\dagger/c)] - |\eta - (n-m)(s/c)\beta_r| \gamma} d\alpha \\ &= \frac{i\beta_r}{2} \int_{-\infty}^{\infty} \frac{M_r \gamma f_0(\alpha)}{K + M_r \alpha} e^{im\sigma} \sum_{p=-\infty}^{\infty} e^{ip\sigma - i(\alpha + M_r K)\xi_p - |\eta_p| \gamma} d\alpha \\ &= e^{im\sigma} V(\xi, \eta) \end{aligned}$$

proves the assertion.

The remaining condition that must be imposed on the solution is that the pressure jump (5.A.14) vanish outside the interval $|\xi - (ms^\dagger/c)| < \frac{1}{2}$. But it follows from Eqs. (5.A.20) and (5.A.14) that this condition will hold for every m if it holds for $m = 0$. Hence, the problem will be solved if the function $f_0(\alpha)$ in Eq. (5.A.22) can be chosen in such a way that condition (5.A.17) is satisfied on the $m = 0$ blade while $[P] = 0$ along the remainder of the line $\eta = 0$. Before showing that this can be done, it is convenient to simplify Eq. (5.A.22). Thus, it follows from the geometric expansion

$$\sum_{m=0}^{\infty} z^m = \frac{1}{1-z} \quad \text{for } |z| < 1$$

that for $0 \leq \eta < s\beta_r/c$

$$\begin{aligned} \sum_{m=-\infty}^{\infty} e^{im(\Gamma + \alpha s^\dagger/c) - |\eta_m| \gamma} &= \frac{e^{-\eta\gamma}}{1 - e^{-i[\Gamma + (\alpha s^\dagger/c)] - s\beta_r\gamma/c}} + \frac{e^{\eta\gamma} e^{i[\Gamma + (\alpha s^\dagger/c)] - s\beta_r\gamma/c}}{1 - e^{i[\Gamma + (\alpha s^\dagger/c)] - s\beta_r\gamma/c}} \\ &= \frac{1}{2} \left[\frac{e^{-\eta\gamma + (1/2)\Delta_+}}{\sinh \frac{1}{2}\Delta_+} - \frac{e^{\eta\gamma + (1/2)\Delta_-}}{\sinh \frac{1}{2}\Delta_-} \right] \end{aligned}$$

where

$$\Delta_{\pm} \equiv i \left(\Gamma + \frac{\alpha s^\dagger}{c} \right) \pm \frac{s\beta_r\gamma}{c} \quad (5.A.23)$$

Inserting this result into Eq. (5.A.22) shows that the upwash velocity is now determined by

$$V(\xi, \eta) = \frac{i\beta_r}{4} \int_{-\infty}^{\infty} \frac{M_r f_0(\alpha) \gamma e^{-i(\alpha + M_r K)\xi}}{K + M_r \alpha} \left[\frac{e^{-\eta\gamma + (1/2)\Delta_+}}{\sinh \frac{1}{2}\Delta_+} - \frac{e^{\eta\gamma + (1/2)\Delta_-}}{\sinh \frac{1}{2}\Delta_-} \right] d\alpha$$

for $0 \leq \eta < \frac{s\beta_r}{c}$ (5.A.24)

While for the remaining values of η , $V(\xi, \eta)$ can be determined from the periodicity condition (5.A.19).

Inserting Eq. (5.A.24) into the boundary condition (5.A.17) with $m = 0$ yields (after using the addition formulas for the hyperbolic functions to simplify the results)

$$1 = e^{-i(K/M_r)\beta_r^2\xi} \lim_{\eta \rightarrow 0} V(\xi, \eta)$$

$$= \frac{i\beta_r}{2} \int_{-\infty}^{\infty} \frac{f_0(\alpha)}{K/M_r + \alpha} e^{-i[\alpha + (K/M_r)]\xi} \frac{\gamma \sinh(s\beta_r\gamma/c)}{\cosh(s\beta_r\gamma/c) - \cos(\Gamma + \alpha s^\dagger/c)} d\alpha$$

for $-\frac{1}{2} < \xi < \frac{1}{2}$ (5.A.25)

On the other hand, Eq. (5.A.14) (with $m = 0$) shows that

$$[P] = \int_{-\infty}^{\infty} f_0(\alpha) e^{-i(\alpha + M_r K)\xi} d\alpha$$

But since $[P] = 0$ for $|\xi| > \frac{1}{2}$, we can invert this Fourier transform to obtain

$$f_0(\alpha) = \frac{1}{2\pi} \int_{-1/2}^{1/2} [P] e^{i(\alpha + M_r K)\xi} d\xi \quad (5.A.26)$$

Thus, the boundary conditions on the blades can be satisfied by requiring that $f_0(\alpha)$ be a solution of the coupled integral Eqs. (5.A.25) and (5.A.26) wherein, in order to ensure that the Kutta condition holds at the trailing edge (see Sec. 3.4.2), we must also require that $[P] = 0$ at $\xi = \frac{1}{2}$.

APPENDIX 5.B EVALUATION OF SINGLE-AIRFOIL INTEGRAL

It is shown in tables of Fourier transform⁹ that

$$H_0^{(1)}(\kappa \sqrt{x^2 + y^2}) = \frac{1}{\pi i} \int_{-\infty}^{\infty} \frac{e^{-ix\alpha - y\sqrt{\alpha^2 - \kappa^2}}}{\sqrt{\alpha^2 - \kappa^2}} d\alpha$$

where $H_0^{(1)}$ denotes the Hankel function of the first kind. Hence,†

$$\begin{aligned} \frac{i\beta_r}{4\pi} \int_{-\infty}^{\infty} \frac{e^{-i[\alpha + (K/M_r)](\xi - \xi')}}{K/M_r + \alpha} \gamma d\alpha \\ = \frac{i\beta_r}{4} \lim_{y \rightarrow 0} \int_{-\infty}^{(\xi - \xi')} e^{-(iK/M_r)x} \frac{\partial^2}{\partial y^2} H_0^{(1)}(\kappa \sqrt{x^2 + y^2}) dx \end{aligned}$$

But by using the identity¹⁰

$$\frac{\partial^2}{\partial y^2} H_0^{(1)}(\kappa \sqrt{x^2 + y^2}) = -\frac{\partial^2}{\partial x^2} H_0^{(1)}(\kappa \sqrt{x^2 + y^2}) - \kappa^2 H_0^{(1)}(\kappa \sqrt{x^2 + y^2})$$

and integrating twice by parts we can put this result in the form

$$\begin{aligned} \frac{i\beta_r}{4\pi} \int_{-\infty}^{\infty} \frac{e^{-i[\alpha + (K/M_r)](\xi - \xi')}}{K/M_r + \alpha} \gamma d\alpha \\ = -\frac{i\beta_r}{4} \left\{ e^{-i(K/M_r)(\xi - \xi')} \left[-\kappa \operatorname{sgn}(\xi - \xi') H_1^{(1)}(\kappa |\xi - \xi'|) \right. \right. \\ \left. \left. + i \frac{K}{M_r} H_0^{(1)}(\kappa |\xi - \xi'|) \right] + \left(\kappa^2 - \frac{K^2}{M_r^2} \right) \lim_{y \rightarrow 0} \int_{-\infty}^{(\xi - \xi')} \right. \\ \left. \times e^{-i(K/M_r)x} H_0^{(1)}(\kappa \sqrt{x^2 + y^2}) dx \right\} \quad (5.B.1) \end{aligned}$$

Since the integral on the right side of this expression remains bounded as $\xi - \xi' \rightarrow 0$, it is easy to show from the small-argument asymptotic representation for the Hankel functions¹¹ that

$$\begin{aligned} \frac{i\beta_r}{4\pi} \int_{-\infty}^{\infty} \frac{e^{-i[\alpha + (K/M_r)](\xi - \xi')}}{K/M_r + \alpha} \gamma d\alpha \\ = \frac{\beta_r}{2\pi} \left(\frac{1}{\xi - \xi'} + \frac{iK}{M_r} \ln |\xi - \xi'| \right) + O(1) \quad \text{as } \xi - \xi' \rightarrow 0 \quad (5.B.2) \end{aligned}$$

APPENDIX 5.C EVALUATION OF TERMS IN DUCT COORDINATES

Since (Figs. 5.2 and 5.3)

$$\frac{U_0}{\sin \mu} = \frac{U_r}{\cos \nu} = \frac{c_0 M_r}{\cos(\chi - \mu)} \quad (5.C.1)$$

† κ is defined by Eq. (5.57).

and since the number of blades is related to the interblade distance d by (Fig. 5.4)

$$B = \frac{2\pi r_M}{d} \quad (5.C.2)$$

it follows from using Eqs. (5.29) and (5.67) in the definition (5.43) of the interblade phase angle that

$$\sigma = \frac{pd}{r_M} = \frac{2\pi p}{B} \quad (5.C.3)$$

while inserting this into Eq. (5.42) implies

$$\Gamma = \frac{2\pi p}{B} + M_r K \frac{d}{c} \sin \chi \quad (5.C.4)$$

Then Eq. (5.54) becomes

$$\Gamma_n = \frac{d}{r_M} (p - nB) + M_r K \frac{d}{c} \sin \chi \quad (5.C.5)$$

and Eq. (5.59) implies that

$$\kappa \cos \delta_n = \frac{d}{d^\dagger} \left[\frac{c}{r_M} (p - nB) + M_r K \sin \chi \right] \quad (5.C.6)$$

and, consequently, that

$$\kappa \sin \delta_n = \frac{d}{d^\dagger} \sqrt{\left(\frac{d^\dagger}{d}\right)^2 \kappa^2 - \left[\frac{c}{r_M} (p - nB) + M_r K \sin \chi \right]^2} \quad (5.C.7)$$

It follows from Eq. (5.53) that

$$\left(\frac{d^\dagger}{d}\right)^2 = 1 - M_r^2 \cos^2 \chi \quad (5.C.8)$$

and it can be seen from Fig. 5.2 that

$$c_0 M_r \cos \chi = U_\infty \cos \nu \quad (5.C.9)$$

$$c_0 M_r \sin \chi + U_\infty \sin \nu = U_0 \quad (5.C.10)$$

Hence, it follows from Eqs. (5.40), (5.41), and (5.57) that

$$\frac{d}{d^\dagger} \beta_r \kappa \sin \delta_n = \frac{c}{\beta^2} k_{q,p,nB} \quad (5.C.11)$$

where we have put

$$k_{q,p,nB} \equiv \sqrt{k_0^2 - \beta^2 \left[\left(\frac{nB - p}{r_M}\right)^2 + \left(\frac{\pi q}{b}\right)^2 \right]} \quad (5.C.12)$$

$$k_0 = \frac{nB\Omega}{c_0} + \frac{M(p - nB)}{r_M} \tan v \quad (5.C.13)$$

$$\beta = \sqrt{1 - M^2} \quad (5.C.14)$$

and

$$M = M_r \cos \chi = \frac{U_\infty}{c_0} \cos v \quad (5.C.15)$$

is the axial-flow Mach number.

Upon using Eq. (5.60) and the addition formulas for the sines and cosines, the exponent

$$E \equiv \omega\tau + (\kappa \sin \Theta_n^\pm + M_r K)\xi - \kappa(\cos \Theta_n^\pm)\eta$$

that appears in Eq. (5.66) can be written as

$$E = -\kappa(\xi \sin \chi^\dagger + \eta \cos \chi^\dagger) \cos \delta_n \\ \pm \kappa(\xi \cos \chi^\dagger - \eta \sin \chi^\dagger) \sin \delta_n + KM_r \xi + \omega\tau$$

But since the blade spacing d and the stagger angle χ are related to the Prandtl–Glauert plane blade spacing d^\dagger and stagger angle χ^\dagger by

$$\left. \begin{aligned} d \sin \chi &= d^\dagger \sin \chi^\dagger \\ \beta_r d \cos \chi &= d^\dagger \cos \chi^\dagger \end{aligned} \right\} \quad (5.C.16)$$

we can use Eq. (5.68) to eliminate the dimensionless variables ξ, η to obtain

$$E = \frac{x_2}{c} \left[M_r K \sin \chi - \frac{\kappa d}{d^\dagger} (1 - M_r^2 \cos^2 \chi) \cos \delta_n \right] \\ + \frac{x_1}{c} \left[M_r K \cos \chi - \frac{\kappa d}{d^\dagger} (M_r^2 \sin \chi \cos \chi \cos \delta_n \mp \beta_r \sin \delta_n) \right] \\ + \frac{\tau c_0}{c} \left[K \left(\beta_r^2 + \frac{U_0}{c_0} M_r \sin \chi \right) - \frac{\kappa d}{d^\dagger} \frac{U_0}{c_0} (1 - M_r^2 \cos^2 \chi) \cos \delta_n \right]$$

Finally, it follows from Eq. (5.40) and Eqs. (5.C.6) and (5.C.8) to (5.C.12) that

$$\omega\tau + (\kappa \sin \Theta_n^\pm + M_r K)\xi - \kappa(\cos \Theta_n^\pm)\eta = nB\Omega\tau + \frac{x_2}{M_r} (nB - p) + x_1 \gamma_{q,p,nB}^\pm$$

where

$$\gamma_{q,p,nB}^\pm \equiv \frac{1}{\beta^2} (Mk_0 \pm k_{p,q,nB}) \quad (5.C.17)$$

Equations (5.60) and (5.C.16) and the addition formulas for trigonometric functions imply that

$$\frac{c}{d^\dagger} \frac{\cos \Theta_n^\pm}{\sin \delta_n} = \frac{cd}{(d^\dagger)^2 \sin \delta_n} (\beta_r \cos \chi \cos \delta_n \pm \sin \chi \sin \delta_n)$$

which, in view of Eqs. (5.C.6), (5.C.8), (5.C.11), (5.C.14), and (5.C.15), becomes

$$\frac{c \cos \Theta_n^\pm}{d^\dagger \sin \delta_n} = \frac{1}{\beta^2 k_{q,p,nB} d} \left\{ \beta_r^2 \left[\frac{c}{r_M} (p - nB) + M_r K \sin \chi \right] \cos \chi \pm c k_{q,p,nB} \sin \chi \right\}$$

Then, inserting Eqs. (5.40), (5.C.1), (5.C.9), (5.C.10), (5.C.14), (5.C.15), and (5.C.17) yields

$$\frac{c \cos \Theta_n^\pm}{d^\dagger \sin \delta_n} = \frac{c}{k_{q,p,nB} d} \left[\gamma_{q,p,nB}^\pm \sin \chi - \left(\frac{nB - p}{r_M} \right) \cos \chi \right] \quad (5.C.18)$$

REFERENCES

1. Chu, Boa-Teh and Leslie S. G. Kovasznay, "Non-Linear Interactions in a Viscous Heat-Conducting Gas," *J. Fluid Mech.*, **3**, 494-515, Oct. 1957-Mar. 1958.
2. McCune, James E., *The Three-Dimensional Flow Field of an Axial Compressor Blade Row—Subsonic, Transonic and Supersonic*, AFOSR TN 58-72, Cornell University, Feb. 1958.
3. Lane, Frank and Manfred Friedman, "Theoretical Investigation of Subsonic Oscillatory Blade-Row Aerodynamics," NACA TN 4136, 1958.
4. Whitehead, D. S., *Vibration and Sound Generation in a Cascade of Flat Plates in Subsonic Flow*, R&M 3685, British Aeronautical Research Council, 1972.
5. Lighthill, M. J., *Introduction to Fourier Analysis and Generalized Functions*, Cambridge University Press, 1964.
6. Fleeter, Sanford, "Fluctuating Lift and Moment Coefficients for Cascaded Airfoils in a Nonuniform Compressible Flow," *J. Aircraft*, **10**, 2, 93-98, 1973.
7. Kaji, S. and T. Okazaki, "Propagation of Sound Waves Through a Blade Row. II. Analysis Based on the Acceleration Potential Method," *J. Sound Vibr.*, **11**, 3, 355-375, 1970.
8. Kaji, S. and T. Okazaki, "Generation of Sound by Rotor-Stator Interaction," *J. Sound Vibr.*, **13**, 3, 281-307, 1970.
9. Campbell, George A. and Ronald M. Foster, *Fourier Integrals for Practical Applications*, Bell Telephone Laboratories, 1942.
10. Runyan, Harry L. and Charles E. Watkins, "Considerations on the Effect of Wind-Tunnel Walls on Oscillating Air Forces for Two-Dimensional Subsonic Compressible Flow," NACA TN 2552, 1951.
11. Abramowitz, Milton and Irene A. Stegun, eds., *Handbook of Mathematical Functions*, National Bureau of Standards Applied Mathematics Series 55, 1954.
12. Kaji, S., "Noncompact Source Effect on the Prediction of Tone Noise from a Fan Rotor," AIAA Paper 75-446, 1975.
13. Noble, Benjamin, *Methods Based on the Wiener-Hopf Technique for the Solution of Partial Differential Equations*, Pergamon Press, 27-31, 1958.
14. Carrier, G., M. Krook and C. Pearson, *Functions of a Complex Variable*, McGraw-Hill, 80-81, 1966.

6

EFFECTS OF NONUNIFORM MEAN FLOW ON GENERATION OF SOUND

6.1 INTRODUCTION

The last two chapters were, for the most part, concerned with the generation of sound in the presence of a uniform mean flow. However, real flows usually have velocity gradients in the vicinity of the source region that can affect the acoustic impedance acting on the sources enough to significantly influence the radiated sound. For example, Lighthill's theory of jet noise treats the sound sources as if they were moving through a stationary medium. In fact, the entire directivity pattern of the radiated sound is accounted for by the convective amplification that results from this aspect of the theory. However, it is the motion of the sound sources relative to the mean flow in their immediate vicinity (i.e., within about a wavelength or so) rather than their motion relative to the medium at infinity which should have the dominant influence on the sound emission process. Indeed, there should be no convective amplification of the overall power when the wavelength of the sound is small relative to the dimensions of the jet—since the sources will then, in essence, be stationary relative to their surroundings.

In order to include these effects in Lighthill's theory it is necessary to adjust the source term in some manner. But since this can not be done without prior knowledge of the sound field a better approach might be to develop an appropriate moving-medium wave equation to describe the sound emission process.

One possible way of obtaining such a result is by extending the linearized acoustic analysis developed in Sec. 1.2. Thus, it is shown in Sec. 5.2 that, while the generation of sound through surface interactions is accounted for by the linear terms, the generation of sound by the volume quadrupoles depends upon the second-order nonlinear coupling of the acoustic and vortical modes. Hence, if the first-order perturbation equations developed in Sec. 1.2 were extended to next higher order, all the interactions involved in the sound generation processes would be included. This approach was developed by Chu and Kovasznay.¹ Rather than pursuing these ideas further, however, we shall attempt to extend Lighthill's approach by putting the full nonlinear equations into the form of a moving-medium wave equation. Equations of this type were derived by Phillips² and Lilley,[†] and much of the material in this chapter is based on their results. In developing such formulae—wherein more of the real fluid effects are included in the wave operator part of the equation and less in the source term—we are, to some extent, moving away from the acoustic analogy approach and toward a direct calculational approach similar to the one developed in Chap. 5.

6.2 DERIVATION OF PHILLIPS' EQUATION

The continuity and momentum equations given in Sec. 2.2.1 can be put in the form

$$\frac{1}{\rho} \frac{D\rho}{D\tau} + \frac{\partial v_j}{\partial y_j} = 0 \quad (6.1)$$

$$\frac{Dv_i}{D\tau} = -\frac{1}{\rho} \frac{\partial p}{\partial y_i} + \frac{1}{\rho} \frac{\partial e_{ij}}{\partial y_j} \quad (6.2)$$

where

$$\frac{D}{D\tau} \equiv \frac{\partial}{\partial \tau} + v_j \frac{\partial}{\partial y_j} \quad (6.3)$$

[†] Fourth Monthly Progress Report on contract F-33615-71-C-1663. Appendix: Generation of Sound in a Mixing Region. Lockheed Aircraft Company, Marietta, Ga., 1971.

denotes the substantive derivative. We shall, for simplicity, limit the discussion to the case of an ideal gas. Then

$$p = \rho \mathcal{R} \Theta \quad (6.4)$$

$$de = c_v d\Theta \quad (6.5)$$

and

$$c_p = c_v + \mathcal{R}$$

where as before \mathcal{R} denotes the gas constant; e denotes the internal energy; Θ the absolute temperature; and c_p and c_v the specific heats at constant pressure and volume, respectively. Hence, the second law of thermodynamics $\Theta dS = de + pd(1/\rho)$ can be written as

$$\frac{d\rho}{\rho} = \frac{1}{\kappa} \frac{dp}{p} - \frac{dS}{c_p} \quad (6.6)$$

where

$$\kappa \equiv \frac{c_p}{c_v} \quad (6.7)$$

is the specific-heat ratio.

In order to obtain an expression that resembles the moving-medium wave equation, we generalize the approach used in Sec. 1.2 to derive the wave Eq. (1.17) from the linearized continuity and momentum equations. Thus, substituting Eq. (6.6) into Eq. (6.1) yields

$$\frac{D\Pi}{D\tau} + \frac{\partial v_i}{\partial y_i} = \frac{1}{c_p} \frac{DS}{D\tau} \quad (6.8)$$

where

$$\Pi \equiv \frac{1}{\kappa} \ln \frac{p}{p_0} \quad (6.9)$$

and p_0 is some convenient (constant) reference pressure. Then it follows from Eq. (1.25) that the momentum Eq. (6.2) can be written as

$$\frac{Dv_i}{D\tau} = -c^2 \frac{\partial \Pi}{\partial y_i} + \frac{1}{\rho} \frac{\partial e_{ij}}{\partial y_j} \quad (6.10)$$

The close resemblance between Eqs. (6.8) and (6.10) and the first two Eqs. (1.15) suggests that a moving-medium wave equation can be obtained (as was done in Sec. 1.2) by differentiating these equations and subtracting the results. To this end we take the divergence of Eq. (6.10) and use the identity

$$\frac{\partial}{\partial y_i} \frac{D}{D\tau} \equiv \frac{D}{D\tau} \frac{\partial}{\partial y_i} + \frac{\partial v_j}{\partial y_i} \frac{\partial}{\partial y_j} \quad (6.11)$$

to obtain

$$\frac{D}{D\tau} \frac{\partial v_i}{\partial y_i} + \frac{\partial}{\partial y_i} c^2 \frac{\partial \Pi}{\partial y_i} = -\frac{\partial v_j}{\partial y_i} \frac{\partial v_i}{\partial y_j} + \frac{\partial}{\partial y_i} \frac{1}{\rho} \frac{\partial e_{ij}}{\partial y_j} \quad (6.12)$$

But applying the operator $D/D\tau$ to Eq. (6.8) shows that

$$\frac{D^2 \Pi}{D\tau^2} + \frac{D}{D\tau} \frac{\partial v_i}{\partial y_i} = \frac{D}{D\tau} \frac{1}{c_p} \frac{DS}{D\tau}$$

We can now subtract Eq. (6.12) from this result to obtain *Phillips' equation*²

$$\frac{D^2 \Pi}{D\tau^2} - \frac{\partial}{\partial y_i} c^2 \frac{\partial \Pi}{\partial y_i} = \frac{\partial v_j}{\partial y_i} \frac{\partial v_i}{\partial y_j} - \frac{\partial}{\partial y_i} \frac{1}{\rho} \frac{\partial e_{ij}}{\partial y_j} + \frac{D}{D\tau} \frac{1}{c_p} \frac{DS}{D\tau} \quad (6.13)$$

The left side of this result is seen to correspond closely to that of the linearized moving-medium wave Eq. (1.17), the principal difference being that the left side of Eq. (1.17) contains an additional term which accounts for certain mean flow acoustic interaction effects. On the other hand, the left side of this equation differs from that of Lighthill's Eq. (2.5) mainly in that the time derivative $\partial/\partial\tau$ in Lighthill's result is replaced by the substantive derivative $D/D\tau$. Thus, Phillips' equation ought, at least partially, to account for the interaction of the mean flow with the sound. As in Lighthill's theory the quantities on the right side are to be interpreted as source terms.

In fact, Phillips concluded that since "the terms on the left hand side of [his] equation are those of a wave equation in a moving medium with variable speed of sound," the first term on the right side represents the generation of pressure fluctuations by velocity fluctuations in the fluid, while the remaining terms describe the effects of entropy fluctuations and fluid viscosity. However, as pointed out by Lilley and Doak³ this interpretation is not strictly correct since the left side of this result does not contain all the terms that appear in a moving-medium wave equation—even for a unidirectional transversely sheared mean flow. As a consequence, the remaining terms must be contained in the first member on the right side which therefore cannot be treated as a pure source term. Thus, suppose that the mean flow can be characterized by Eq. (1.12). Then upon neglecting squares of small quantities we can write the left side of Eq. (6.13) as

$$\frac{1}{c_0^2 \rho_0} \left(\frac{D_0^2 p}{D\tau^2} - c_0^2 \nabla^2 p \right)$$

while the right side can be written as

$$2 \frac{\partial u_r}{\partial y_1} \frac{dU}{dx} g$$

Comparing this with Eq. (1.17) shows that (in this limit) the "source term" in Phillips' equation actually contains a term associated with the propagation of sound waves.

6.3 DERIVATION OF LILLEY'S EQUATION

In order to obtain an equation in which all the "propagation effects" occurring in a transversely sheared mean flow are accounted for in the wave operator part of the equation, Lilley† derived a third-order equation analogous to Eq. (1.22). Thus, applying the operator $D/D\tau$ to both sides of Eq. (6.13) yields

$$\frac{D}{D\tau} \left(\frac{D^2\Pi}{D\tau^2} - \frac{\partial}{\partial y_i} c^2 \frac{\partial \Pi}{\partial y_i} \right) = 2 \frac{\partial v_j}{\partial y_i} \frac{D}{D\tau} \frac{\partial v_i}{\partial y_j} - \frac{D}{D\tau} \frac{\partial}{\partial y_i} \frac{1}{\rho} \frac{\partial e_{ij}}{\partial y_j} + \frac{D^2}{D\tau^2} \frac{1}{c_p} \frac{DS}{D\tau}$$

which, with the aid of Eqs. (6.10) and (6.11) can be transformed into *Lilley's equation*

$$\frac{D}{D\tau} \left(\frac{D^2\Pi}{D\tau^2} - \frac{\partial}{\partial y_i} c^2 \frac{\partial \Pi}{\partial y_i} \right) + 2 \frac{\partial v_j}{\partial y_i} \frac{\partial}{\partial y_j} c^2 \frac{\partial \Pi}{\partial y_i} = -2 \frac{\partial v_j}{\partial y_i} \frac{\partial v_k}{\partial y_j} \frac{\partial v_i}{\partial y_k} + \Psi \quad (6.14)$$

where

$$\Psi = 2 \frac{\partial v_j}{\partial y_i} \frac{\partial}{\partial y_j} \frac{1}{\rho} \frac{\partial e_{ik}}{\partial y_k} - \frac{D}{D\tau} \frac{\partial}{\partial y_i} \frac{1}{\rho} \frac{\partial e_{ij}}{\partial y_j} + \frac{D^2}{D\tau^2} \frac{1}{c_p} \frac{DS}{D\tau}$$

represents the effects of entropy fluctuations and fluid viscosity.

Notice that when this result is linearized about the unidirectional transversely sheared mean flow Eq. (1.12), its left side reduces to that of the moving-medium wave Eq. (1.22). Thus, at least in the case of parallel or nearly parallel mean flows (such as those which occur in jets and axial-flow fans), no inconsistency is obtained when we interpret the right side as a source term.

6.4 INTERPRETATION OF EQUATIONS

Lilley's, Phillips', and Lighthill's equations, being exact consequences of the momentum and continuity equations, are all equivalent to one another. The associated jet noise theories differ primarily because of the interpretation that is ultimately given to the various terms in these equations. Thus, in Lighthill's theory the interaction between the sound field and the mean flow (which includes such effects as convection and refraction of the sound by the flow) must be accounted for by adjusting the source term—which, as we have already indicated, cannot be done until after the equation is actually solved. In the theories of Phillips and Lilley these effects have, to some extent, been moved from the source term to the wave-operator part of the equation and can therefore be calculated as part of the solution. On the other hand, the mean velocity variations normally occur in the vicinity of the source

† Fourth Monthly Progress Report on contract F-33615-71-C-1663. Appendix: Generation of Sound in a Mixing Region. Lockheed Aircraft Company, Marietta, Ga., 1971.

region where the unsteady flow is usually governed by nonlinear equations. Hence, we cannot be sure that it is physically realistic to separate the mean flow-acoustic field interaction effects from the sound generation process itself. Indeed, it is not even possible to unambiguously determine what part of the unsteady flow in this region is actually associated with the acoustic field. Nevertheless, the equations of Phillips and Lilley do seem to predict certain aspects of the sound field surrounding a jet that are not accounted for in Lighthill's theory.

The price which must be paid for including the convection and refraction effects in the wave-operator part of the equation is a great increase in the complexity of the solutions. In practice, this turns out to be a serious drawback, and to date only limited solutions of Lilley's and Phillips' equations have been found.

6.5 SIMPLIFICATION OF PHILLIPS' AND LILLEY'S EQUATION

Another disadvantage of Eqs. (6.13) and (6.14) is that their left sides involve the total velocity \mathbf{v} and not (as in the case of the linearized equations in Sec. 1.2) just the mean velocity. Thus, these equations are, in general, nonlinear even when the source terms and the mean flow are assumed to be known. However, in many cases of interest (e.g., sound generation in jets and aircraft engine fans and compressors), it is reasonable to replace the velocity and the square of the speed of sound by their mean values $V_i = \bar{v}_i$ and \bar{c}^2 , respectively. In Phillips' equation the former approximation amounts to replacing the operator $D/D\tau$ by the operator

$$\frac{\bar{D}}{D\tau} \equiv \frac{\partial}{\partial \tau} + V_i \frac{\partial}{\partial y_i} \quad (6.15)$$

Thus, the sound which is generated by the unsteady flow in the vicinity of a fan or compressor frequently propagates through a relatively long duct containing a steady shear flow. Hence, it can be argued that the propagation terms appearing on the left sides of Eqs. (6.13) and (6.14) will be determined mainly by this large region of steady flow and not by the usually much smaller region of unsteady flow in the vicinity of the fan.

On the other hand, the turbulence velocities in a jet are fairly small (usually less than 20 percent) compared to the mean velocity while the acoustic quantities are almost certainly even smaller. Hence, it is reasonable to neglect any terms on the left sides of Eqs. (6.13) and (6.14) that involve only products of fluctuating quantities compared to the terms that involve products of fluctuating quantities with mean quantities. But this again amounts to replacing v_i by V_i and c^2 by \bar{c}^2 since the time averaged pressure in a turbulent jet is so nearly constant that Π can be treated as a fluctuating quantity, provided, of course, that p_0 is suitably chosen. Physically, this

has the effect of suppressing such phenomena as the scattering of sound by turbulence. However, due to the mismatch between the turbulence scales and the acoustic wavelengths—the acoustic wavelength being for the most part much larger†^{6,7}—turbulent scattering is generally considered to be relatively unimportant in jets.⁵ In fact, it has been found⁸ that the introduction of a series of vortex generators into the nozzle of a subsonic jet failed to influence the directivity pattern even though a noticeable increase in the volume of strong turbulence is presumed to have resulted. But since the dominant effect of scattering should be to change the directivity, we tend to conclude that scattering is not important over most of the spectrum.‡

We now consider the terms on the right sides of Eqs. (6.13) and (6.14). In the absence of chemical reaction or other heat sources the energy equation can be written as

$$\rho\Theta \frac{DS}{D\tau} = \frac{\partial}{\partial y_i} K \frac{\partial \Theta}{\partial y_i} + \Upsilon$$

where K is the thermal conductivity and Υ denotes the volume rate of energy dissipation due to viscous effects. Thus, the second two terms on the right sides of Eq. (6.13) and the last term on the right side of Eq. (6.14) represent the effects of heat conduction and viscous dissipation. Hence (assuming that the Mach number is not too large) the arguments used in connection with Lighthill's equation in Sec. 2.2.3 show that these terms should be negligible at the Reynolds numbers which are usually of interest in aerodynamic sound problems.

Upon making these approximations in Eqs. (6.13) and (6.14) (i.e., replacing v_i by V_i and c^2 by \bar{c}^2 on the left sides and neglecting viscous and heat conduction effects on the right sides) we obtain

$$\frac{\bar{D}^2 \Pi}{D\tau^2} - \frac{\partial}{\partial y_i} \bar{c}^2 \frac{\partial \Pi}{\partial y_i} = \frac{\partial v_j}{\partial y_i} \frac{\partial v_i}{\partial y_j} \quad (6.16)$$

$$\frac{\bar{D}}{D\tau} \left(\frac{\bar{D}^2 \Pi}{D\tau^2} - \frac{\partial}{\partial y_i} \bar{c}^2 \frac{\partial \Pi}{\partial y_i} \right) + 2 \frac{\partial V_j}{\partial y_i} \frac{\partial}{\partial y_j} \bar{c}^2 \frac{\partial \Pi}{\partial y_i} = -2 \frac{\partial v_j}{\partial y_i} \frac{\partial v_k}{\partial y_j} \frac{\partial v_i}{\partial y_k} \quad (6.17)$$

where $\bar{D}/D\tau$ is defined by Eq. (6.15).

6.6 EQUATIONS FOR TRANSVERSELY SHEARED MEAN FLOWS

Since we are, for the most part, interested in sound generation by flows whose mean velocity field can be approximated fairly well by Eq. (1.12) (or

† Except, of course, at high acoustic frequencies.

‡ This may not be true for multitube nozzles containing large numbers of tubes or for the noise generated within the nozzle itself.

perhaps by its generalization (1.23)) it is reasonable to suppose that

$$v_i = \delta_{1i} U(\mathbf{r}) + u_i \quad (6.18)$$

where the transverse coordinate variable $\mathbf{r}(y_2, y_3)$ is discussed in Sec. 1.2 and u_i represents the fluctuating part (i.e., the part with zero time average) of the velocity v_i . Then since

$$\frac{\bar{D}}{D\tau} = \frac{D_0}{D\tau} \equiv \frac{\partial}{\partial \tau} + U \frac{\partial}{\partial y_1} \quad (6.19)$$

substituting Eq. (6.18) into Eq. (6.16) yields

$$\frac{D_0^2}{D\tau^2} \Pi - c_0^2 \nabla^2 \Pi - 2g \frac{dU}{d\mathbf{r}} \frac{\partial u_r}{\partial y_1} = \frac{\partial u_j}{\partial y_i} \frac{\partial u_i}{\partial y_j} \quad (6.20)$$

where \bar{c}^2 is replaced by $c_0^2 = \text{Constant}$ and as in Sec. 1.2 $g \equiv |\nabla \mathbf{r}|$, while $u_r \equiv (\nabla \mathbf{r} / |\nabla \mathbf{r}|) \cdot \mathbf{u}$ represents the transverse velocity in the \mathbf{r} -direction. Notice that the quantity $2g(dU/d\mathbf{r})(\partial u_r / \partial y_1)$ has been removed from the source term in Phillips' equation and that, as a consequence, the left side of this result now closely corresponds to the linearized Eq. (1.17). Then since taking the dot product of Eq. (6.10) with $\nabla \mathbf{r} / |\nabla \mathbf{r}|$ yields

$$\frac{D_0}{D\tau} u_r = -c_0^2 g \frac{\partial \Pi}{\partial \mathbf{r}} - \frac{\nabla \mathbf{r}}{|\nabla \mathbf{r}|} \cdot \left(u_i \frac{\partial}{\partial y_i} \mathbf{u} \right) \quad (6.21)$$

we can proceed as in Sec. 1.2 and eliminate u_r between Eqs. (6.20) and (6.21) to obtain the third-order wave equation

$$\begin{aligned} \frac{D_0}{D\tau} \left(c_0^2 \nabla^2 \Pi - \frac{D_0^2}{D\tau^2} \Pi \right) - 2c_0^2 g^2 \frac{dU}{d\mathbf{r}} \frac{\partial^2 \Pi}{\partial y_1 \partial \mathbf{r}} = & - \frac{D_0}{D\tau} \left(\frac{\partial u_j}{\partial y_i} \frac{\partial u_i}{\partial y_j} \right) \\ & + 2g \frac{dU}{d\mathbf{r}} \frac{\partial}{\partial y_1} \left[\frac{\nabla \mathbf{r}}{|\nabla \mathbf{r}|} \cdot \left(u_i \frac{\partial}{\partial y_i} \mathbf{u} \right) \right] \end{aligned} \quad (6.22)$$

Although the left side of this result is the same as in Lilley's Eq. (6.17) the right side is somewhat different.

Since the velocity \mathbf{u} only appears in the terms on the right side of Eq. (6.22) and since these terms are to be interpreted as sources, it is reasonable to suppose that this quantity satisfies the solenoidal condition

$$\nabla \cdot \mathbf{u} = 0 \quad (6.23)$$

Thus if Eq. (6.22) were applied to a turbulent jet \mathbf{u} could be associated with the fluctuating turbulence velocity which is at most 20 percent of the mean flow velocity. Hence, it would certainly be reasonable to impose the incompressibility condition (6.23) in this case. Then since it follows from this condition that $u_i(\partial/\partial y_i)\mathbf{u} = (\partial/\partial y_i)u_i\mathbf{u}$ and $(\partial u_i/\partial y_j)(\partial u_j/\partial y_i) = \partial^2 u_i u_j / \partial y_i \partial y_j$,

Eq. (6.22) can be written as

$$\frac{D_0}{D\tau} \left(c_0^2 \nabla^2 \Pi - \frac{D_0^2}{D\tau^2} \Pi \right) - 2c_0^2 \frac{dU}{d\tau} g^2 \frac{\partial^2 \Pi}{\partial y_1 \partial \tau} = c_0^2 \left(\frac{D_0}{D\tau} \nabla \cdot \mathcal{f} - 2 \frac{dU}{d\tau} g \frac{\partial}{\partial y_1} \mathcal{f}_\tau \right) \quad (6.24)$$

where we have put

$$\mathcal{f}_i \equiv - \frac{1}{c_0^2} \frac{\partial u_i u_j}{\partial y_j} \quad (6.25)$$

This result is identical to Eq. (1.22) with the mass source q put equal to zero and the external force \mathcal{f} determined by Eq. (6.25). We have seen (in Sec. 1.5.2) that an external volume force \mathcal{f} acts like a volume dipole source (of strength \mathcal{f}) in flows with no mean velocity. But in such flows a dipole source of strength \mathcal{f}_i will act like a quadrupole source (of strength ψ_{ij}) if there exist nine functions ψ_{ij} such that

$$\mathcal{f}_i = \frac{\partial \psi_{ij}}{\partial y_j}$$

We can therefore use these relations to extend the definition of a quadrupole source, which was given only for a stationary medium, to a transversely sheared mean flow. Then the right side of Eq. (6.24) can be interpreted as an acoustic quadrupole source of strength $-u_i u_j / c_0^2$. But since this quantity depends only on the fluctuating velocities and not on the mean velocity U , there is now no shear noise term—at least not in the same sense that there is in Lighthill's theory.

On the other hand, it is well known that a stress acting on a fluid can be represented by a tensor, say ψ_{ij} and that the net force per unit volume, say \mathcal{f}_i , that results from this stress is given by $\mathcal{f}_i = \partial \psi_{ij} / \partial y_j$. Consequently, Eqs. (6.24) and (6.25) imply that there is an approximate analogy between the variation in Π that occurs in certain real flows and the acoustic pressure fluctuation imposed on a transversely sheared mean flow by an unsteady externally applied stress equal to $-u_i u_j / c_0^2$.

Equation (6.24) can be generalized to account for variations in c_0^2 with \mathbf{r} simply by replacing the first term in parentheses on the left side by $\nabla \cdot (c_0^2 \nabla \Pi)$.

It is shown in Appendix 6.A that, when restricted to the parallel shear flow (1.14), Eq. (6.24) can be further transformed to obtain

$$\frac{D_0^2}{D\tau^2} \Gamma - c_0^2 \nabla^2 \Gamma = \gamma \quad (6.26)$$

where

$$\Gamma \equiv \frac{D_0}{D\tau} \Pi \quad (6.27)$$

and

$$\gamma \equiv \left[\frac{\partial^2}{\partial y_i \partial y_j} \left(\frac{\partial}{\partial \tau} + U \frac{\partial}{\partial y_1} \right) (u_i u_j) \right] - 4 \frac{\partial}{\partial y_1} \left[\frac{dU}{dy_2} \frac{\partial}{\partial y_i} (u_2 u_i + c_0^2 \delta_{2i} \Pi) \right] - \frac{\partial}{\partial y_1} \left[\frac{d^2 U}{dy_2^2} (u_2^2 + c_0^2 \Pi) \right] \quad (6.28)$$

Although the left side of this result formally resembles Phillip's equation, both the dependent variable and the source term are quite different. The latter quantity has been adjusted to account for a portion of the acoustic field-mean flow interaction effect that originally appeared on the left side of Eq. (6.24). As a result it now contains the pressure Π . But for jet-like flows where the mean velocity gradients only occur in the source region, the most important part of this dependence can be eliminated. Thus since we have already assumed that \mathbf{u} satisfies the condition (6.23) in this region, Eq. (6.21) can be written as

$$-\frac{\partial}{\partial y_i} (u_2 u_i + \delta_{2i} c_0^2 \Pi) = \left(\frac{\partial}{\partial \tau} + U \frac{\partial}{\partial y_1} \right) u_2 \quad (6.29)$$

And since the second term on the right side of Eq. (6.28) contains a factor, dU/dy_2 , that vanishes outside the mixing region, we can use the approximation (6.29) in this term to obtain

$$\gamma = \left[\frac{\partial^2}{\partial y_i \partial y_j} \frac{D_0}{D\tau} (u_i u_j) \right] + 4 \frac{\partial}{\partial y_1} \left(\frac{dU}{dy_2} \frac{D_0}{D\tau} u_2 \right) - \frac{\partial}{\partial y_1} \left[\frac{d^2 U}{dy_2^2} (u_2^2 + c_0^2 \Pi) \right] \quad (6.30)$$

The solenoidal condition (6.23) implies that (e.g., Sec. 5.3 of Ref. 10) the vector potential

$$\mathbf{A}(\mathbf{x}, t) = \frac{1}{4\pi} \nabla \times \int \frac{\mathbf{u}(\mathbf{y}, t)}{|\mathbf{x} - \mathbf{y}|} d\mathbf{y}$$

satisfies the relations

$$\mathbf{u} = \nabla \times \mathbf{A} \quad (6.31)$$

and

$$\nabla \cdot \mathbf{A} = 0$$

Hence, introducing the permutation tensor† ε_{ijk} and using Eq. (6.31) to eliminate u_2 in the second term on the right side of Eq. (6.30) we find that

† $\varepsilon_{ijk} = 0$ if i, j , and k are not all different;
 $\varepsilon_{ijk} = 1$ if i, j, k is a cyclic permutation of 1, 2, 3;
 $\varepsilon_{ijk} = -1$ if i, j, k is an anticyclic permutation of 1, 2, 3.

Eq. (6.26) can be written in the form

$$\left(\frac{D_0^2}{D\tau^2} - c_0^2 \nabla^2 \right) \Gamma = \frac{\partial^2}{\partial y_i \partial y_j} \left(\frac{D_0}{D\tau} T_{ij}^0 \right) - \frac{\partial}{\partial y_1} \left[\frac{d^2 U}{dy_2^2} (u_2^2 + c_0^2 \Pi) \right] \quad (6.32)$$

where

$$T_{ij}^0 = u_i u_j + 4\delta_{1i} \varepsilon_{2jk} \frac{dU}{dy_2} A_k \quad (6.33)$$

6.7 APPLICATIONS OF ACOUSTIC EQUATIONS TO ROUND JETS

We have now derived a number of equations (Eqs. (6.16), (6.17), (6.24), and (6.32)) which are designed to account, in some sense, for the effect of the mean flow velocity on the sound generation process. In a circular jet this velocity field can be fairly well approximated by a transversely sheared flow with its transverse coordinate variable given by Eq. (1.13)—in which case Eqs. (6.16), (6.17), (6.24), and (6.32) can be written as†

$$L_y^{(l)} \Pi = -2 \frac{\partial v_j}{\partial y_i} \frac{\partial v_k}{\partial y_j} \frac{\partial v_i}{\partial y_k} ; \quad L_y^{(l)} \Pi = \frac{D_0}{D\tau} \frac{\partial^2 u_i u_j}{\partial y_i \partial y_j} - 2 \frac{dU}{dr_0} \nabla r_0 \cdot \frac{\partial^2 \mathbf{u} \mathbf{u}_i}{\partial y_1 \partial y_i} \quad (6.34a, b)$$

$$L_y^{(p)} \Pi = \frac{\partial v_j}{\partial y_i} \frac{\partial v_i}{\partial y_j} ; \quad L_y^{(p)} \Gamma = \frac{\partial^2}{\partial y_i \partial y_j} \frac{D_0}{D\tau} T_{ij}^0 - \frac{\partial}{\partial y_1} \left[\frac{d^2 U}{dy_2^2} (u_2^2 + c_0^2 \Pi) \right] \quad (6.35a, b)$$

where r_0 is defined by Eq. (1.13),

$$L_y^{(l)} \equiv \frac{D_0}{D\tau} \left(\frac{D_0^2}{D\tau^2} - \nabla \cdot c_0^2 \nabla \right) + 2c_0^2 \frac{dU}{dr_0} \frac{\partial^2}{\partial y_1 \partial r_0}$$

and

$$L_y^{(p)} \equiv \frac{D_0^2}{D\tau^2} - \nabla \cdot c_0^2 \nabla$$

We have therefore arrived at several wave equations that presumably describe the same sound generation process. Although they all have wave operators which exhibit the correct behavior outside the source region, their source terms are radically different from one another. If this seems somewhat surprising, it should be recalled that Kirchhoff's theorem (derived in Sec. 1.5.1) shows that there is always more than one source distribution that can produce any given sound field.

† In Eq. (6.35b) we have reinserted the geometric factors for the cylindrical coordinate system in the wave operator part of the equation, even though this equation was originally derived for a parallel mean flow in which these factors are unity.

But even if these equations are all correct, we are still left with the problem of not knowing the source terms very well. In fact, since only a small fraction of the flow energy gets radiated as sound, it could happen that even relatively small errors made in accounting for phase cancellation in the source term could cause some of the nonpropagating energy to appear in the theory as sound—resulting in large errors in the predicted sound field. Ultimately, of course, we must rely on experiment to test the validity of the theory.

The final difficulty involves finding the solutions to these equations.

6.7.1 Formal Solutions to Acoustic Equations

In Sec. 2.3, a solution to Lighthill's equation was obtained by using the free-space, stationary-medium Green's function in the integral formula (1.66). A similar approach can be used to solve Eqs. (6.34) and (6.35). Thus, let $g_l(\mathbf{x}, t | \mathbf{y}, \tau)$ and $g_p(\mathbf{x}, t | \mathbf{y}, \tau)$ denote outgoing-wave (in the variables \mathbf{x}, t) solutions to the inhomogeneous equations

$$L_x^{(l)} g_l = c_\infty^2 \delta(\mathbf{x} - \mathbf{y}) \delta(t - \tau) \quad (6.36)$$

$$L_x^{(p)} g_p = c_\infty^2 \delta(\mathbf{x} - \mathbf{y}) \delta(t - \tau) \quad (6.37)$$

where c_∞ is the ambient speed of sound,

$$L_x^{(l)} \equiv \frac{D_0}{Dt} \left(\frac{D_0^2}{Dt^2} - \frac{\partial}{\partial x_i} c_0^2 \frac{\partial}{\partial x_i} \right) + 2c_0^2 \frac{dU}{dr} \frac{\partial^2}{\partial x_1 \partial r} \quad (6.38)$$

$$L_x^{(p)} \equiv \frac{D_0^2}{Dt^2} - \frac{\partial}{\partial x_i} c_0^2 \frac{\partial}{\partial x_i} \quad (6.39)$$

$$\frac{D_0}{Dt} \equiv \frac{\partial}{\partial t} + U(r) \frac{\partial}{\partial x_1} \quad \text{and} \quad r = \sqrt{x_3^2 + x_2^2}$$

Then it is easy to see upon reinserting Eq. (6.27) that the outgoing-wave solutions to Eqs. (6.34) and (6.35) are given by

$$\Pi(\mathbf{x}, t) = -\frac{2}{c_\infty^2} \int_{-T}^T \int g_l \frac{\partial v_j}{\partial y_i} \frac{\partial v_k}{\partial y_j} \frac{\partial v_i}{\partial y_k} dy d\tau ;$$

$$\Pi(\mathbf{x}, t) = \frac{1}{c_\infty^2} \int_{-T}^T \int g_l \left(\frac{D_0}{D\tau} \frac{\partial^2 u_i u_j}{\partial y_i \partial y_j} - 2 \frac{dU}{dr_0} \nabla r_0 \cdot \frac{\partial^2 \mathbf{u} \mathbf{u}_i}{\partial y_1 \partial y_i} \right) dy d\tau \quad (6.40a, b)$$

$$\Pi(\mathbf{x}, t) = \frac{1}{c_\infty^2} \int_{-T}^T \int g_p \frac{\partial v_j}{\partial y_i} \frac{\partial v_i}{\partial y_j} dy d\tau ;$$

$$\left(\frac{\partial}{\partial t} + U \frac{\partial}{\partial x_1} \right) \Pi(\mathbf{x}, t) = \frac{1}{c_\infty^2} \int_{-T}^T \int g_p \left\{ \frac{\partial^2}{\partial y_i \partial y_j} \frac{D_0}{D\tau} T_{ij}^0 - \frac{\partial}{\partial y_1} \right.$$

$$\times \left[\frac{d^2 U}{dy_2^2} (u_2^2 + c_0^2 \Pi) \right] \} dy d\tau \quad (6.41a, b)$$

When the observation point \mathbf{x} is outside the jet the mean velocity U is zero and the operator on the left side of Eq. (6.41b) can be replaced by $\partial/\partial t$.

It is frequently assumed (e.g., in Reference 24) that the first term on the right side of Eq. (6.34b) can itself provide a good approximation to the source term. Equation (6.40b) can then be integrated by parts to obtain

$$\Pi(\mathbf{x}, t) = \frac{1}{c_\infty^2} \int_{-T}^T \int \frac{\partial^2 g_L}{\partial y_i \partial y_j} u_i u_j dy d\tau \quad (6.42)$$

where it follows from Eq. (6.36) that

$$g_L \equiv -\frac{D_0}{D\tau} g_l$$

must satisfy the equation

$$L_x^{(l)} g_L = -c_\infty^2 \frac{D_0}{D\tau} \delta(\mathbf{x} - \mathbf{y}) \delta(t - \tau) = c_\infty^2 \frac{D_0}{Dt} \delta(\mathbf{x} - \mathbf{y}) \delta(t - \tau) \quad (6.43)$$

Rather than imposing the strict causality condition

$$\frac{D_0}{Dt} g_\alpha = g_\alpha = 0 \quad \text{for} \quad t < \tau, \alpha = p, L$$

we only require that g_α behave like an outgoing wave at infinity and remain bounded. These two sets of conditions are equivalent for g_p . But the expression for g_L resulting from the former conditions may differ from that resulting from the latter by a linear combination of unstable "eigensolutions" of the operator (6.38). These solutions, which grow with time, are associated with the hydrodynamic instabilities that occur whenever the mean velocity profile of the jet has an inflection point. However, there are a number of real fluid effects that have either been omitted from Eq. (6.34) (or are included only in the source term) which could act to damp these instabilities. These include such things as non-linear dispersive phenomena, jet spreading, viscous effects, and the interaction of the instability waves with the turbulent flow. In fact, it has frequently been conjectured that the principal effect of the small scale turbulence is to cause an apparent large increase in viscosity and thereby inhibit the large scale motion of the flow. If such effects were retained in the wave operator part of the equation, they would presumably either limit the growth of the unstable solutions or else eliminate them almost completely. If only the former is true the unstable solutions could (as indicated in Secs. 2.5.2 and 2.5.3) play a role in the sound generation process. However, our interest here is in the direct jet mixing noise and we shall therefore eliminate any unstable solutions that might otherwise occur by requiring that g_L remain bounded.

Because of the relative coarseness of the theory developed in Chap. 2, quantitative comparisons with experiment were, for the most part, attempted only for overall sound pressure levels. But the presumably more detailed

theories developed in this section ought to be capable of predicting spectral characteristics of the sound field. Rather than calculating such characteristics from Π and Γ at the end of the analysis, it is simpler to take the Fourier transforms of Eqs. (6.36) to (6.43) and thereby deal with spectral quantities at the outset. To this end, notice that since Eqs. (6.36), (6.37), and (6.43) do not introduce a characteristic scale for the time variable, their solutions g_l , g_p , and g_L can depend on this quantity only in the combination $t - \tau$. Hence, as long as the observation point \mathbf{x} is outside jet, the last and first entries in Table 1.1 of Appendix 1.A show that the Fourier transforms of Eqs. (6.41b) and (6.42) are

$$P(\mathbf{x}) = \frac{i}{c_\infty^2 \omega} \int G_\omega^p(\mathbf{x}|\mathbf{y}) \left\{ \frac{\partial^2}{\partial y_i \partial y_j} \frac{D_0}{D\tau} T_{ij}^0 - \frac{\partial}{\partial y_1} \left[\frac{d^2 U}{dy_2^2} (u_2^2 + c_0^2 \Pi) \right] \right\}^t dy \quad (6.44)$$

$$P(\mathbf{x}) = \frac{1}{c_\infty^2} \int \frac{\partial^2 G_\omega^L(\mathbf{x}|\mathbf{y})}{\partial y_i \partial y_j} (u_i u_j)^t dy \quad (6.45)$$

where the superscript t is used to denote the Fourier transforms of the source terms while

$$P = \frac{1}{2\pi} \int_{-\infty}^{\infty} e^{i\omega t} \Pi(\mathbf{x}, t) dt$$

is the Fourier transform of the pressure variable and

$$G_\omega^p(\mathbf{x}|\mathbf{y}) = \int_{-\infty}^{\infty} e^{i\omega(t-\tau)} g_p dt \quad (6.46)$$

$$G_\omega^L(\mathbf{x}|\mathbf{y}) = \int_{-\infty}^{\infty} e^{i\omega(t-\tau)} g_L dt \quad (6.47)$$

are effectively the Fourier transforms of the Green's functions—sometimes called the “reduced” Green's functions.

The characteristic frequency ω_c of the jet turbulence is inversely proportional to the turbulent decay time τ_ξ introduced in Sec. 2.4.2. Hence, Eqs. (2.43) and (2.44) show that ω_c varies inversely with distance from the nozzle lip for at least four diameters. Then since ω_c is a measure of the frequency of the acoustic field produced by the turbulence, the high frequency sound should, in the main, be generated in the jet mixing region. But, as indicated in Sec. 2.5.1 the mean velocity gradient dU/dy_2 is very nearly constant over the relatively narrow strip in the center of this region where most of the sound is actually produced. Hence, it should be possible to neglect the second term in the integrand of Eq. (6.44) when ω is sufficiently large. The result can then be integrated by parts to obtain

$$P(\mathbf{x}) = \frac{i}{c_\infty^2 \omega} \int \frac{\partial^2 G_\omega^p(\mathbf{x}|\mathbf{y})}{\partial y_i \partial y_j} \left(\frac{D_0}{D\tau} T_{ij}^0 \right)^t dy \quad (6.48)$$

The problem of calculating the sound field has now been reduced to that of finding the Fourier transforms G_ω^L and G_ω^p of the solutions to Eqs. (6.37) and (6.43). But since the coefficients of these equations depend only on the radial coordinate $r = \sqrt{x_2^2 + x_3^2}$, G_ω^L and G_ω^p must be of the form

$$G_\omega^\alpha(\mathbf{x}|\mathbf{y}) = \frac{1}{(2\pi)^2} \sum_{n=-\infty}^{\infty} e^{in\Delta\varphi} \int_{-\infty}^{\infty} G_n^\alpha(r|r_0; \omega, k_1) e^{-ik_1(x_1-y_1)} dk_1$$

for $\alpha = L, p$ (6.49)

where $\Delta\varphi \equiv \tan^{-1}(x_3/x_2) - \tan^{-1}(y_3/y_2)$ is the difference in azimuthal angles of the observation and source point coordinates and r_0 is defined by Eq. (1.13). Upon inserting this into Eqs. (6.37) and (6.43) and using the fact that the cylindrical coordinate representation of the delta function is

$$\delta(\mathbf{x} - \mathbf{y}) = \frac{1}{r} \delta(r - r_0) \delta(\Delta\varphi) \delta(x_1 - y_1)$$

we find that the Fourier coefficients G_n^α are determined by the ordinary differential equations

$$a^2 \frac{\Phi^2}{r} \left\{ \frac{d}{dr} \left(\frac{r}{\Phi^2} \frac{dG_n^L}{dr} \right) + \left[k_0^2 \left(1 - \frac{\kappa^2}{\Phi^2} \right) r - \frac{n^2}{r\Phi^2} \right] G_n^L \right\} = - \frac{\delta(r - r_0)}{r} \quad (6.50)$$

and

$$\frac{1}{r} \left\{ \frac{d}{dr} \left(r a^2 \frac{dG_n^p}{dr} \right) + a^2 \left[k_0^2 (\Phi^2 - \kappa^2) r - \frac{n^2}{r} \right] G_n^p \right\} = - \frac{\delta(r - r_0)}{r} \quad (6.51)$$

where

$$\Phi \equiv \frac{1 + \kappa M(r)}{a(r)} \quad (6.52)$$

$k_0 \equiv \omega/c_\infty$, $\kappa \equiv k_1/k_0$ is the wave number ratio, $a(r) \equiv c_0(r)/c_\infty$ is the speed of sound normalized by the ambient speed of sound c_∞ , and $M(r) = U(r)/c_\infty$ is the local Mach number based on the ambient sound speed.

We are only interested in the region $r > r_J > r_0$ where the observation point is outside the jet and the source point is inside. Then the results given in Appendix 6.B show that the solutions to these equations can be expressed in terms of any two linearly independent homogeneous solutions, say $w_1(r)$ and $w_2(r)$, by using the relation

$$G_n^\alpha(r|r_0) = \frac{w_1(r)w_2(r_0)}{a^2(r_0)r_0 W(r_0)} \quad \text{for } \alpha = L, p \quad (6.53)$$

where

$$W(r) = w_1(r)w_2'(r) - w_2(r)w_1'(r) \quad (6.54)$$

is the *Wronskian* and the primes denote differentiation with respect to r .

The Green's function will satisfy the same boundary condition at infinity as w_1 and the same boundary condition at $r = 0$ as w_2 . Hence, it is necessary to require that w_2 remain unbounded at $r = 0$, and it is not hard to show that g_z will behave like an outgoing wave only if we require that

$$w_1 \sim r^{-1/2} \exp(ik_0 \sqrt{1 - \kappa^2} r) \quad \text{as } r \rightarrow \infty \quad (6.55)$$

There are three procedures that have been used to solve Eqs. (6.50) and (6.51). The first of these amounts to solving the equations numerically, as was done for example by Tester and Burrin.²⁴ The second approach is to replace the actual jet velocity and speed of sound profiles by idealized shapes which are uniform inside the jet and zero outside. When this is done, it is necessary to obtain separate solutions for the interior and exterior regions and to match the results by using appropriate "jump" conditions across the velocity discontinuity at the edge of the jet. Conditions appropriate for the "acoustic limit" were deduced in Sec. 1.3.2 (Eqs. (1.45) and (1.46)). It is usually assumed that these requirements should also be imposed on g_{11} . The corresponding jump conditions for G_n^L can then be found by taking Fourier transforms. Perhaps the earliest work along these lines was done by Gottlieb.¹⁶ But he only used his results to calculate the sound emission from a single monopole source embedded in the mean flow and his analysis was subsequently extended by Slutsky, Tamagno, and Moretti¹⁷⁻¹⁹ to include quadrupole sources and distributions of sources. Finally, the effects of source convection were included by Mani²⁰ who showed that this model is able to qualitatively explain a number of the discrepancies pointed out in Sec. 2.5.1. The corresponding two-dimensional problem, including source convection effects, was treated by Phillips,² Pao,²³ and Graham and Graham.^{21,22}

The third approach is to consider only the limiting cases of high and low frequency. In these limits the equations become simple enough to be solved analytically. Since the relevant physical facts emerge most easily and directly from this approach, it is the only one which will be worked out in detail. Thus, suppose that the radial variable r in Eqs. (6.50) and (6.51) is nondimensionalized by the jet radius r_j . Then the wave number k_0 will appear only in the dimensionless combination $r_j k_0 = r_j \omega / c_\infty$, which is the ratio of the jet radius to the wavelength of the sound divided by 2π . We shall consider the two limiting cases wherein this parameter becomes very large and very small while the remaining dimensionless quantities M , a , κ , and $n/r_j k_0$ remain finite. We first deal with the high-frequency limit.

High-frequency solution. For simplicity, only Eq. (6.50) will be treated in detail. It is convenient to first express the homogeneous solutions w_1 and w_2 to this equation in terms of a new set of variables, say v_1 and v_2 , by

$$w_j(r) = \frac{\Phi(r)}{\sqrt{r}} v_j(r) \quad \text{for } j = 1, 2 \quad (6.56)$$

Then inserting this into Eq. (6.50) shows that v_1 and v_2 must satisfy the equation

$$v'' + [k_0^2 q_n(r) + s(r)]v = 0 \quad (6.57)$$

where

$$q_n \equiv \Phi^2 - \kappa^2 - \left(\frac{n}{k_0 r}\right)^2 \quad (6.58)$$

and

$$s(r) \equiv \frac{\Phi''}{\Phi} + \frac{\Phi'}{\Phi r} - 2\left(\frac{\Phi'}{\Phi}\right)^2 + \left(\frac{1}{2r}\right)^2$$

In this section our interest is in obtaining solutions to this equation that are valid in the limit where $r_J k_0 \rightarrow \infty$ while κ and $n/k_0 r_J$ remain finite. This can be accomplished by using the methods outlined in Appendix 6.C. However, it is first necessary to locate the turning points. For simplicity, we restrict our attention to the case of a simple isothermal subsonic jet so that $a = 1$, $M(r) < 1$, and $dM(r)/dr < 0$. However, the principal conclusions that we reach will also apply to simple subsonic heated jets. Finally, we require that $r_0 \neq 0$.

It follows from Eqs. (6.52) and (6.58) that the turning points of Eqs. (6.57) are the solutions to the equations

$$M(r) = \pm \left[1 + \left(\frac{n}{\kappa k_0 r} \right)^2 \right]^{1/2} - \frac{1}{\kappa} \quad (6.59)$$

First consider the case where $\kappa < 0$. Then since $1 + (n/\kappa k_0 r)^2 \geq 1$ and $M(r) < 1$, Eq. (6.59) can only hold if the sign of the first term is negative. But then the right side will be a monotonically increasing function of r while the left side will be a monotonically decreasing function. Hence, there can only be a single turning point, say r_δ , which satisfies this equation. Moreover since q'_n is equal to

$$\frac{2\kappa^2}{r} \left\{ -rM' \left[1 + \left(\frac{n}{\kappa r k_0} \right)^2 \right]^{1/2} + \left(\frac{n}{k_0 \kappa r} \right)^2 \right\}$$

at this point, the condition $M' \leq 0$ ensures that $q'_n \neq 0$ and as a result that q_n has a simple zero at r_δ . The situation is considerably more complicated when $\kappa > 0$. In this case the number of turning points and the order of the zeros of q_n will depend on the detailed shape of the velocity profiles. However, it appears that the important features of the sound field are more or less independent of these characteristics and we shall suppose, for simplicity, that the conclusions reached for $\kappa < 0$ will apply for all values of κ that influence the sound field. The situation is then covered by case (b) in Appendix 6.C, and it follows from Eq. (6.C.6) that Eq. (6.57) possesses the two linearly independent asymptotic solutions

$$\left. \begin{aligned} v_+ &= \sqrt{\frac{k_0 \pi}{3}} \frac{\xi^{3/4}}{q_n^{1/4}} H_{1/3}^{(1)} \left(\frac{2}{3} k_0 \xi^{3/2} \right) e^{i5\pi/12} \\ v_- &= \sqrt{\frac{k_0 \pi}{3}} \frac{\xi^{3/4}}{q_n^{1/4}} H_{1/3}^{(2)} \left(\frac{2}{3} k_0 \xi^{3/2} \right) e^{-i5\pi/12} \end{aligned} \right\} \quad \text{as } k_0 \rightarrow \infty$$

where

$$\xi = \begin{cases} \left(\frac{3}{2} \int_{r_\delta}^r \sqrt{q_n(r)} dr \right)^{2/3} & \text{for } r > r_\delta \\ - \left(\frac{3}{2} \int_r^{r_\delta} \sqrt{-q_n(r)} dr \right)^{2/3} & \text{for } r < r_\delta \end{cases}$$

and the H 's denote Hankel functions. When r is not in the immediate vicinity of the turning point, $k_0 \xi^{3/2}$ will be large and we can replace these functions by their large-argument asymptotic expansions (Reference 25, p. 364) to show that

$$v_\pm = \frac{\exp\left(\pm i k_0 \int_{r_\delta}^r \sqrt{q_n(r)} dr\right)}{[q_n(r)]^{1/4}} \quad r \neq r_\delta; k_0 \rightarrow \infty \quad (6.60)$$

provided we choose the branch of the square root so that $\sqrt{q_n} = i|\sqrt{q_n}|$ when $q_n < 0$. Then it follows from Eqs. (6.52) and (6.58) that $\sqrt{q_n} \sim i|n/k_0 r|$ as $r \rightarrow 0$ and $\sqrt{q_n} \sim \sqrt{1 - \kappa^2}$ as $r \rightarrow \infty$ so that $v_\pm \sim \text{constant} \times r^{(1/2) \mp |n|}$ as $r \rightarrow 0$ and $v_\pm \sim \text{constant} \times \exp(\pm i k_0 \sqrt{1 - \kappa^2} r)$ as $r \rightarrow \infty$. Equations (6.55) and (6.56) therefore show that we must choose†

$$w_1 = v_+ \frac{\Phi}{r^{1/2}}, \quad w_2 = v_- \frac{\Phi}{r^{1/2}} \quad (6.61)$$

Then Eq. (6.60) can be inserted into these results to show that

$$w_j \sim \frac{\exp\left(-(-1)^j i k_0 \int_{r_\delta}^r \sqrt{q_n(r)} dr\right)}{\sqrt{r}(1 - \kappa^2)^{1/4}} \quad \text{as } r \rightarrow \infty; \text{ for } j = 1, 2 \quad (6.62)$$

But inserting this into Eq. (6.54) and using Eqs. (6.52) and (6.58) yields

$$-\frac{r}{\Phi^2} W(r) \sim 2ik_0 \quad \text{as } r \rightarrow \infty$$

Hence comparing Eq. (6.50) with Eq. (6.B.1) and using Abel's formula (Appendix 6.B) we find that the left side of this result is independent of r

† Actually, we have only established the necessity of this choice for the case where $n \neq 0$. When $n = 0$ the argument is more complicated but the conclusion is the same.

and, consequently, that

$$W(r) = -\frac{2ik_0\Phi^2(r)}{r}$$

for all r . Inserting this together with Eqs. (6.60) to (6.62) into Eq. (6.53) now yields

$$G_n^L(r|r_0) \sim \frac{i \left[\exp \left(ik_0 \int_{r_0}^r \sqrt{q_n(r)} dr \right) \right]}{2k_0 \sqrt{rr_0} a^2(r_0) \Phi(r_0) [(1 - \kappa^2) q_n(r_0)]^{1/4}} \quad \text{as } r \rightarrow \infty$$

and finally inserting this into Eq. (6.49) yields

$$G_\omega^L \sim \frac{1}{(2\pi)^2} \sum_{n=-\infty}^{\infty} \frac{e^{in\Delta\varphi}}{k_0} \Lambda_n(r|r_0, k_0) \quad \text{as } r \rightarrow \infty$$

where

$$\Lambda_n(r|r_0, k_0) \equiv \frac{i}{2\sqrt{rr_0}} \int_{-\infty}^{\infty} \frac{\exp \left[ik_0 \int_{r_0}^r \sqrt{q_n(r)} dr - ik_1(x_1 - y_1) \right]}{a^2(r_0) \Phi(r_0) [(1 - \kappa^2) q_n(r_0)]^{1/4}} dk_1 \quad (6.63)$$

Although we have already expanded this result for large r the expressions for the phases of the various terms have not as yet been altered and therefore apply at all values of r . But since q_n will be positive when $r > r_\delta$, G_ω^L will then be a linear combination of modes whose phases are to within a constant

$$k_0 S \equiv k_0 \left[\left(\frac{n}{k_0} \right) \Delta\varphi + \int_{r_\delta}^r \sqrt{q_n(r)} dr - \kappa(x_1 - y_1) \right]$$

where $S(x_1, r, \varphi)$ denotes the eikonal introduced in Sec. 1.3.2. Hence, it follows from Eqs. (6.52) and (6.58) that $|\nabla S| = |\Phi| = [1 + \kappa M(r)]/a(r)$. And since ∇S is normal to the phase surfaces of the modes, the angle Θ that this normal makes with the x_1 -axis is given by

$$\cos \Theta \equiv \frac{\partial S / \partial x_1}{|\nabla S|} = -\frac{\kappa a(r)}{1 + \kappa M(r)}$$

Consequently, $\kappa = -\cos \Theta / [a(r) + M(r) \cos \Theta]$ and the phase velocity V_p of the modes is

$$V_p = \frac{c_\infty}{|\nabla S|} = c_0(r) + U(r) \cos \Theta$$

This result is identical to the expression given in Sec. 1.3.2 for the phase velocity of a wave traversing a uniformly moving medium and its interpretation is the same. However, the nonuniformity of the mean velocity profile will now cause the wave to alter its direction. Thus, when the wave front

has a component of its motion in the downstream direction, the higher mean flow velocity on the part of the wave near the center of the jet will cause it to be bent away from the jet axis. This refraction effect is completely analogous to the behavior that was shown (in Sec. 1.3.2) to occur when a wave impinges on a region of velocity adjustment.

On the other hand, waves originating at $r_0 < r$ do not actually propagate when $r < r_\delta$ but rather suffer a progressive decay with distance due to the factor

$$\exp\left(-k_0 \int_{r_0}^r |q_n^{1/2}(r)| dr\right).$$

Once the signal reaches the turning point, however, this decay will cease and the wave will propagate in the manner described above.

The radius r_0 of the source point will be greater than r_δ only if $q_n(r_0) > 0$, i.e., only if

$$[\omega + k_1 U(r_0)]^2 > c_0^2(r_0)(k_1^2 + n^2/r_0^2) \quad (6.64)$$

However, the n, k_1 th-component of the Green's function will be weighted by the n, k_1 th-spectral component of the turbulence in the actual formula for jet noise. Consequently, only the spectral components of the turbulence that satisfy the inequality (6.64) will be able to generate a sound field that does not initially suffer a strong exponential decay. Moreover, it is easy to show—by applying the procedure used in Sec. 1.3.2—that the left side of this inequality represents the frequency ω' of the k_1, n th-spectral component of the turbulence as seen by an observer moving with the mean flow. But since, as shown in Sec. 2.5.1, $\omega'/c_0 k_1$ is typically an order of magnitude less than the mean flow Mach number, these results imply that only a small fraction of the available turbulent energy should actually be radiated as sound.

It is convenient to introduce the usual polar coordinates

$$\left. \begin{aligned} R &= \sqrt{(r - r_0)^2 + (x_1 - y_1)^2} \\ \theta &= \cos^{-1} \left(\frac{x_1 - y_1}{R} \right) \end{aligned} \right\} \quad (6.65)$$

with origin at the source point. Then the integral in Eq. (6.63) can be expanded for large values of R by standard methods (e.g., Reference 26, p. 51) to obtain

$$\Lambda_n \sim -\sqrt{\frac{i\pi k_0}{2r_0}} \frac{\exp\left\{ik_0\left[\int_{r_0}^r Q_n(r) dr + (x_1 - y_1) \cos \theta\right]\right\}}{a(r_0)R[1 - M(r_0) \cos \theta] \sqrt{Q_n(r_0)}} \quad \text{as } R \rightarrow \infty$$

where

$$Q_n(r) \equiv Q_n(r, \cos \theta) \equiv \sqrt{\left[\frac{1 - M(r) \cos \theta}{a(r)}\right]^2 - \cos^2 \theta - \left(\frac{n}{k_0 r}\right)^2} \quad (6.66)$$

the square root has a positive imaginary part for negative arguments and since R is large, θ is independent of r . Hence, we find that at large distances from the jet (i.e., in the radiation field) the reduced Green's function for Lilley's wave operator behaves like

$$G_{\omega}^L(\mathbf{x}|\mathbf{y}) \sim \frac{G_{\omega}^0(\mathbf{x}|\mathbf{y})\mathcal{R}_{\omega}(\mathbf{x}|\mathbf{y})}{a(r_0)[1 - M(r_0) \cos \theta]} \quad \text{as } \begin{cases} k_0 r_J \rightarrow \infty \\ R \rightarrow \infty \end{cases} \quad (6.67)$$

where G_{ω}^0 is the reduced free-space Green's function defined by Eq. (1.57) and

$$\mathcal{R}_{\omega}(\mathbf{x}|\mathbf{y}) \equiv -\sqrt{\frac{i}{2r_0 k_0 \pi}} \sum_{n=-\infty}^{\infty} \frac{\exp \left\{ in\Delta\varphi + ik_0 \int_{r_0}^r [Q_n(r) - Q_n(\infty)] dr \right\}}{\sqrt{Q_n(r_0)}} \quad (6.68)$$

An almost identical procedure beginning with the reduced Phillips' Eq. (6.51) yields

$$G_{\omega}^P(\mathbf{x}|\mathbf{y}) \sim \frac{G_{\omega}^0(\mathbf{x}|\mathbf{y})\mathcal{R}_{\omega}(\mathbf{x}|\mathbf{y})}{a(r_0)} \quad \text{as } \begin{cases} kr_J \rightarrow \infty \\ R \rightarrow \infty \end{cases} \quad (6.69)$$

The reduced Green's function $G_{\omega}^l(\mathbf{x}|\mathbf{y})$ associated with g_l is given by $i\{k_0 c_{\infty}[1 - M(r_0) \cos \theta]\}^{-1} G_{\omega}^L(\mathbf{x}|\mathbf{y})$.

Recall that the reduced free-space Green's function is the correct solution to the present problem when the mean flow is zero and the sound speed is constant. The factors multiplying this quantity in Eqs. (6.67) and (6.69) can therefore be thought of as correction factors which, in the high-frequency limit, account for embedding the sound sources in a mean flow containing density gradients. Since the Lighthill theory developed in Chap. 2 is based on the free-space Green's function and since the source terms in both Phillips' equation and Eq. (6.24) are not radically different from the one in Lighthill's equation, there is hope that these factors can, in some sense, also be thought of as corrections to the acoustic spectra predicted by Lighthill's theory.

In order to interpret the effect of the factor \mathcal{R}_{ω} , notice that (since the imaginary part of the square root in Eq. (6.66) is positive when its argument is negative the n th term in Eq. (6.68) will contain the factor

$$\exp \left[-k_0 \int_{r_0}^{r_{\delta}} |Q_n(r)| dr + ik_0 \int_{r_{\delta}}^r |Q_n(r)| dr \right]$$

whenever r_{δ} (the point where the argument of Q_n goes through zero and changes sign) is greater than the source radius r_0 . Moreover Eq. (6.66) shows that this occurs whenever

$$[1 - M(r_0) \cos \theta]^2 < a^2(r_0) \left[\cos^2 \theta + \left(\frac{n}{k_0 r_0} \right)^2 \right]$$

that is, whenever θ is outside the range $\theta_+^{(n)} < \theta < \theta_-^{(n)}$ where

$$\theta_{\pm}^{(n)} \equiv \cos^{-1} \left\{ \frac{\pm a(r_0) \sqrt{1 - \left(\frac{n}{k_0 r_0}\right)^2 [a^2(r_0) - M^2(r_0)]} - M(r_0)}{a^2(r_0) - M^2(r_0)} \right\}$$

when the argument of the \cos^{-1} is greater than -1 , and $\theta_{\pm}^{(n)} \equiv \pi$ when the argument is < -1 . (When $M(r_0)$ is reasonably large $\theta_-^{(n)}$ will always be close to π where the sound field is small and difficult to measure.) Thus, for angles outside the range $\theta_+^{(n)} < \theta < \theta_-^{(n)}$, the n th term in \mathcal{R}_ω will contain the exponential damping factor

$$\exp \left(-k_0 \int_{r_0}^{r_s} |Q_n(r)| dr \right) \quad (6.70)$$

which, since k_0 is assumed to be large, will strongly diminish the contribution of this term. And since $\theta_+^{(n)}$ increases with increasing n , all of the terms in Eq. (6.68) will be subjected to this damping when $\theta < \theta_c \equiv \theta_+^{(0)}$ where

$$\theta_c = \cos^{-1} \left[\frac{1}{M(r_0) + a(r_0)} \right]$$

Notice that when $a = 1$ (i.e., for an isothermal jet) this becomes equal to the critical angle (1.41), which was shown in Sec. 1.3.2 to determine the boundary of the "zone of silence" that occurs when a plane wave propagates from a moving medium into a stationary medium across a two-dimensional velocity-adjustment interface. Thus, there exists a cone centered on the downstream jet axis, wherein the far field sound intensity is greatly reduced, but unlike the situation that was discussed in Sec. 1.3.2, not equal to zero.

For $\theta_+^{(n)} < \theta < \theta_-^{(n)}$ the exponent of the n th term in \mathcal{R}_ω is purely imaginary and therefore only affects the relative phasing between the various modes comprising the sum (6.68). Moreover, the factors $\sqrt{Q_n(r_0)}$ which appear in the denominators of these terms do not appreciably alter the directional character of \mathcal{R}_ω except in the vicinity of the points at which $Q_n(r_0) = 0$ —where they cause \mathcal{R}_ω to become infinite. However, this behavior is spurious since it occurs at the turning points where, as a result of the invalidity of the approximation (6.60), the expression (6.68) is also invalid. In order to obtain a uniformly valid solution which remains finite at these points it is merely necessary to replace the factor $e^{-i\chi}$

$$\left(\text{where } \chi \equiv -k_0 \int_{r_0}^{r_s} Q_n(r) dr \right)$$

by its original value

$$(\pi\chi/2)^{1/2} H_{1/3}^{(2)}(\chi) \exp \left(-\frac{i5\pi}{12} \right).$$

Thus, the dominant effect of \mathcal{R}_ω is to drastically reduce the high-frequency sound in the zone of silence.

Since the exponential damping factor (6.70) increases with n , the modes with smaller values of n will dominate the sound field within the zone of silence. In the actual formula for jet noise, each of these modes will be weighted by the amplitude of the corresponding circumferential wave number component of the turbulence spectrum so that at angles near 90° to the axis the model content of the sound field should more nearly reflect that of the turbulence. On the other hand the radical in $\theta_\pm^{(n)}$ will become imaginary when n becomes larger in absolute magnitude than some critical value, say n_0 . But before this occurs the range $\theta_+^{(n)} < \theta < \theta_-^{(n)}$ will have shrunk to zero and all terms of \mathcal{R}_ω with indices greater than n_0 will be exponentially damped. Thus \mathcal{R}_ω (and, as a consequence, the sound field itself) will contain only a finite number of undamped modes.

The remaining factor in the Phillips' Green's function G_ω^p is the sound speed ratio $a(r_0) = c_0(r_0)/c_\infty$ which appears in the denominator. Since c_0 increases as the square root of the absolute temperature, this factor will act to decrease the high-frequency sound radiated by hot jets, but only very slightly.

Finally, the Lilley's Green's function G_ω^L contains an additional Doppler factor $[1 - M(r_0) \cos \theta]$ which will combine with the Doppler factors $(1 - M_c \cos \theta)$ that were shown in Chap. 2 to arise from source convection effects. (At the center of the mixing region the convection Mach number M_c was shown (in Sec. 2.5.1) to be equal to the local jet Mach number $M(r_0)$.) Thus, at angles well outside of the zone of silence, the third octave intensity should vary like $(1 - M_c \cos \theta)^{-5}(1 - M \cos \theta)^{-2}$ rather than like $(1 - M_c \cos \theta)^{-5}$ as the theory of Chap. 2 would indicate.

It is worth recalling that the results obtained thus far are only valid for subsonic jets with monotonic velocity profiles. When these conditions are not satisfied Eq. (6.57) can have several turning points whose relative locations can strongly effect the behavior of the solutions. Thus, supersonic jets with monotonic velocity profiles will have two turning points whenever the Mach number is sufficiently high. These points can be treated more or less independently (by the method described above) when their separation is large compared with the wavelength. Otherwise they must be treated simultaneously. The solution can then be expressed in terms of parabolic cylinder functions (or Weber functions) by methods similar to those developed in Appendix 6.C. However, the results can be simplified when the distance between the points is much less than a wavelength; the solution can then be expressed in terms of 1/4th order Bessel functions. In fact, this is the problem that was originally considered by Phillips.² The distance between the transition points is a function of the angle θ and the maximum Mach number M_0 , decreasing with increasing M_0 .

As indicated in Chap. 2, the sound field produced by a moving point source is of considerable relevance to the issue of jet noise. The acoustic

pressure produced by a moving harmonic source can be found by solving $L_x^{(l)} p = c_\infty^2 e^{-i\omega t} \delta(\mathbf{x} - \mathbf{y} - \hat{\mathbf{i}} U_c t)$, where U_c is the source convection velocity. The far field solution of this equation can be written as (page 269) $e^{-i\omega t} G_\omega^l(\mathbf{x}|\mathbf{y})$, provided we (1) interpret the distance $R = |\mathbf{x} - \mathbf{y}|$ that appears in G_ω^0 to be the distance $|\mathbf{R}_e|$ (where as usual \mathbf{R}_e is the vector connecting the observation and source points at the time of emission of the sound wave; see Sec. 1.8) and (2) replace $Q_n(r, \cos \theta)$ by $Q_n(r, \cos \theta_e)/(1 - M_c \cos \theta_e)$, where θ_e is the angle that \mathbf{R}_e makes with the jet axis.

In a real jet the high-frequency sound is strongly scattered by the turbulence and can be significantly influenced by the radial divergence of the flow field. There is therefore an upper limit to the range of frequencies where these results apply. In fact, there may be no frequencies where they are actually valid. Nevertheless, it will be shown in Sec. 6.7.3 that they do seem to predict certain experimentally observed trends. Before making such comparisons we must deal with the low-frequency solutions.

Low-frequency solution. Equations (6.50) and (6.51) also possess analytical solutions that are valid in the limit $k_0 r_J \rightarrow 0$; κ, n finite. We shall restrict our attention to the $n = 0$ mode. Indeed it can be shown^{38,39} that this mode, if present, will always dominate the radiation field.

Again, only the solution to Eq. (6.50) will be worked in detail. When $n = 0$, the left side of this equation contains two terms and it might appear that the one multiplied by k_0^2 can simply be neglected. But when r becomes as large as k_0^{-1} , the first term will be just as small as the one multiplied by k_0^2 , so that neither can be neglected. However, the mean velocity U is effectively zero (and $a \simeq 1$) at these values of r . Thus, $\Phi = 1$ and Eq. (6.50) (with $n = 0$) possesses a homogeneous solution

$$w_1 \sim H_0^{(1)}(k_0 \sqrt{1 - \kappa^2} r) \quad \text{as } r \rightarrow \infty \quad (6.71)$$

which also satisfies the outgoing-wave condition (6.55).

On the other hand the second term can certainly be neglected when r is of the order of r_J and Eq. (6.50) then possesses the two homogeneous solutions

$$w_1 = c_1 \int \Phi^2(r) \frac{dr}{r}; \quad w_2 = 1 \quad (6.72a, b)$$

where c_1 is an arbitrary constant. The solution w_2 obviously satisfies the requirement that it remain bounded at $r = 0$. But, as anticipated, w_1 cannot be made to satisfy the radiation condition (6.55) since it behaves like

$$w_1 \sim c_1 \ln r \quad \text{for } r \gg r_J \quad (6.73)$$

The correct solution in this region is given by Eq. (6.71). However, suppose that there exists some "overlap region" between the domain of validity of the "outer solution" (6.71) and the domain where the "inner solution" (6.72a) is valid. In such a region, r will be much larger than the jet radius

r_J , which is the scale on which the inner solution changes, and much smaller than the length k_0^{-1} which is the scale on which the outer solution changes. This is possible because $k_0 r_J \ll 1$. Thus, in the overlap region $r_J \ll r \ll (1/k_0)$. But for $r \gg r_J$ the behavior of the inner solution is given by Eq. (6.73), while for small values of $k_0 r$ the Hankel function in Eq. (6.71) will behave like $(2i/\pi) \ln r$. Hence, these two solutions will be identical in the overlap region if we take the arbitrary constant c_1 in Eq. (6.72a) to be $(2i/\pi)$. Then inserting Eqs. (6.72) into Eq. (6.54) yields

$$rW(r) = -\frac{2i}{\pi} \Phi^2(r)$$

while inserting this together with Eqs. (6.71) and (6.72b) into Eq. (6.53) yields

$$\begin{aligned} G_0^L(r|r_0) &\sim \frac{i\pi H_0^{(1)}(k_0\sqrt{1-\kappa^2}r)}{2a^2(r_0)\Phi^2(r_0)} \\ &\sim \sqrt{\frac{\pi i}{2k_0 r}} \frac{\exp(ik_0\sqrt{1-\kappa^2}r)}{\Phi^2(r_0)a^2(r_0)(1-\kappa^2)^{1/4}} \quad \text{as } k_0 r \rightarrow \infty \end{aligned}$$

where the large-argument expansion for the Hankel function (Reference 25, p. 364) was used to obtain the last member. We can now insert this result into Eq. (6.49), introduce the polar coordinates (6.65), and (as we did in the high frequency case) asymptotically expand the integral over k_1 for large $k_0 r$ to show that

$$G_\omega^L(\mathbf{x}|\mathbf{y}) = \frac{G_\omega^0(\mathbf{x}|\mathbf{y})}{[1 - M(r_0) \cos \theta]^2} \quad (6.74)$$

Moreover, applying a nearly identical procedure to Eq. (6.51) yields

$$G_\omega^p(\mathbf{x}|\mathbf{y}) = G_\omega^0(\mathbf{x}|\mathbf{y})$$

Thus, for sufficiently low frequencies, the Green's function for Phillips' equation becomes equal to the free-space Green's function, while the Green's function for Lilley's equation differs from it only as a result of the Doppler factor $[1 - M(r_0) \cos \theta]^{-2}$. This should have the effect of causing the low-frequency sound to be much more concentrated around the downstream jet axis than Lighthill's theory would indicate.

6.7.2 Approximate Theory for Intermediate Frequencies

We have seen that the Green's function for Phillips' equation G_ω^p is the same as the free-space Green's function G_ω^0 at low frequencies, while at high frequencies they differ only as a result of the refraction factor \mathcal{R}_ω —which is mainly important in the zone of silence. Hence, there is some hope that these two Green's functions will not be too different even at intermediate

frequencies—at least for angles outside the zone of silence. We might therefore attempt to calculate the sound field by inserting the free-space Green's function into Eq. (6.48). But since this equation is only valid when the frequency is high enough so that the sound can be attributed to the turbulence in the mixing region and since the frequency must also be low enough so that refractive effects, turbulent scattering, and even jet spreading are not too important, there may be no range of frequencies where this result actually applies. The validity of these approximations must therefore ultimately be decided by comparing the predictions with experimental data.

When G_ω^p is replaced by G_ω^0 , Eq. (6.48) will differ from the Fourier transform of Eq. (2.8) only in the details of its source term so that the methods developed in Chap. 2 to deal with Lighthill's equation can also be applied to this result. Thus after introducing the moving-frame correlation tensor (2.26) and neglecting variations in retarded time and mean velocity across an "eddy," we can¹³ show that the intensity spectrum $\bar{I}_\omega(\mathbf{x}|\mathbf{y})$ of the sound emitted by the unit volume of turbulence located at the point \mathbf{y} is given by

$$\bar{I}_\omega(\mathbf{x}|\mathbf{y}) = \frac{\Omega^4 \rho_0}{32\pi^3 c_0^5 (1 - M_c \cos \theta)^2} \frac{x_i x_j x_k x_l}{x^6} \Re \int \int e^{i\Omega\tau} R_{ijkl}^+ d\xi d\tau$$

where

$$\Omega = \omega(1 - M_c \cos \theta)$$

is the source frequency

$$R_{ijkl}^+(\mathbf{y}, \xi, \tau) = R_{ijkl}(\mathbf{y}, \xi, \tau) + 16\delta_{1i}\delta_{1k}\varepsilon_{2jm}\varepsilon_{2ln} \left(\frac{dU}{dy_2} \right)^2 Q_{mn}(\mathbf{y}, \xi, \tau) \\ + 8\delta_{1i}\varepsilon_{2jm} \frac{dU}{dy_2} Q_{m,kl}(\mathbf{y}, \xi, \tau)$$

$$R_{ijkl}(\mathbf{y}, \xi, \tau) \equiv \overline{u_i u_j u'_k u'_l} - \overline{u_i u_j} \overline{u'_k u'_l}$$

$$Q_{m,kl}(\mathbf{y}, \xi, \tau) \equiv \overline{A_m u'_k u'_l}$$

$$Q_{m,n}(\mathbf{y}, \xi, \tau) \equiv \overline{A_m A'_n}$$

A_m is defined by Eq. (6.31), and the remaining quantities are defined in Chap. 2. It can also be shown¹³ that the correlations $Q_{m,n}$ and $Q_{m,kl}$ can be expressed in terms of second and third order velocity correlations to obtain

$$\int R_{ijkl}^+ d\xi = \int R_{ijkl} d\xi - \frac{8}{15} \delta_{1i} \delta_{1k} (\delta_{2p} \delta_{jq} - \delta_{2q} \delta_{jp}) (\delta_{2r} \delta_{ls} - \delta_{2s} \delta_{lr}) \left(\frac{dU}{dy_2} \right)^2 \\ \times \int (2\xi_p \xi_r + \delta_{pr} \xi^2) R_{qs} d\xi + \frac{8}{3} \delta_{1i} \frac{dU}{dy_2} \int (\xi_2 R_{j,kl} - \xi_j R_{2,kl}) d\xi$$

provided it can be assumed (as is done in Sec. 2.5.1) that the turbulence is locally homogeneous and incompressible. Finally, after introducing the

joint normality hypothesis and assuming that the turbulence is isotropic (Sec. 2.5.1), we can show that the azimuthally averaged intensity spectrum $\bar{I}_\omega(\mathbf{x}|\mathbf{y})_{av}$ (Fig. 2.6) defined in Sec. 2.5.1 now becomes

$$I_\omega(\mathbf{x}|\mathbf{y})_{av} = \frac{\Omega^4 \rho_0}{32\pi^3 c_0^5 (1 - M_c \cos \theta)^2 X^2} \int_{-\infty}^{\infty} e^{i\Omega\tau} \int R_{1111}^0 d\xi d\tau \times \left[1 + \frac{\cos^4 \theta + \cos^2 \theta}{2} A^\dagger(\Omega) \right] \quad (6.75)$$

where

$$A^\dagger(\Omega) = \frac{-\frac{16}{3} \left(\frac{dU}{dy_2} \right)^2 \int_{-\infty}^{\infty} e^{i\Omega\tau} \int \xi_2^2 R_{11}^0 d\xi d\tau}{\int_{-\infty}^{\infty} e^{i\Omega\tau} \int R_{1111}^0 d\xi d\tau}$$

in the ratio of the maximum shear noise to the self-noise. Thus when the source frequency Ω is held constant and the shear noise is neglected (i.e., when A^\dagger is put equal to zero) the power in a one-third octave band, which is proportional to $I_\omega(\mathbf{x}|\mathbf{y})_{av} \omega$, will vary with angle like $(1 - M_c \cos \theta)^{-3}$. In fact the principal difference between this result and the corresponding equation (i.e., Eq. (2.38)) obtained from Lighthill's theory is that the convection factor is (for the power in a one-third octave band) changed from $(1 - M_c \cos \theta)^{-5}$ to $(1 - M_c \cos \theta)^{-3}$. Notice that Eq. (6.75) is at most valid over some (probably narrow) range of frequencies.

By means of a totally different analysis, Jones¹⁵ obtained a convection factor $(1 - M_c \cos \theta)^{-3}$ for the shear-noise term while still retaining the convection factor $(1 - M_c \cos \theta)^{-5}$ for the self-noise. But since the shear noise is always zero at 90° to the jet axis, his results do not agree particularly well with experiment.

6.7.3 Comparison with Experiment

The validity of the formulas developed in the previous section depends on the existence of a range of frequencies in which it is possible to satisfy both the condition which restricts their validity at high frequencies and the one which restricts it at low frequencies. The existence of such a range of frequencies can only be established by comparing the results with experimental data. Thus, Eq. (6.75) implies that the power in a one-third-octave band, which is proportional to $\bar{I}_\omega \omega$, should vary with angle like $(1 - M_c \cos \theta)^{-3}$ when the source frequency $\Omega \equiv \omega(1 - M_c \cos \theta)$ is held constant—provided we are willing to neglect any small angular variations due to the source structure itself. This result is compared in Fig. 6.1 with measurements taken by Olsen on a 4-inch-diameter jet at Lewis Research Center. Comparisons are presented for three subsonic jet Mach numbers. In

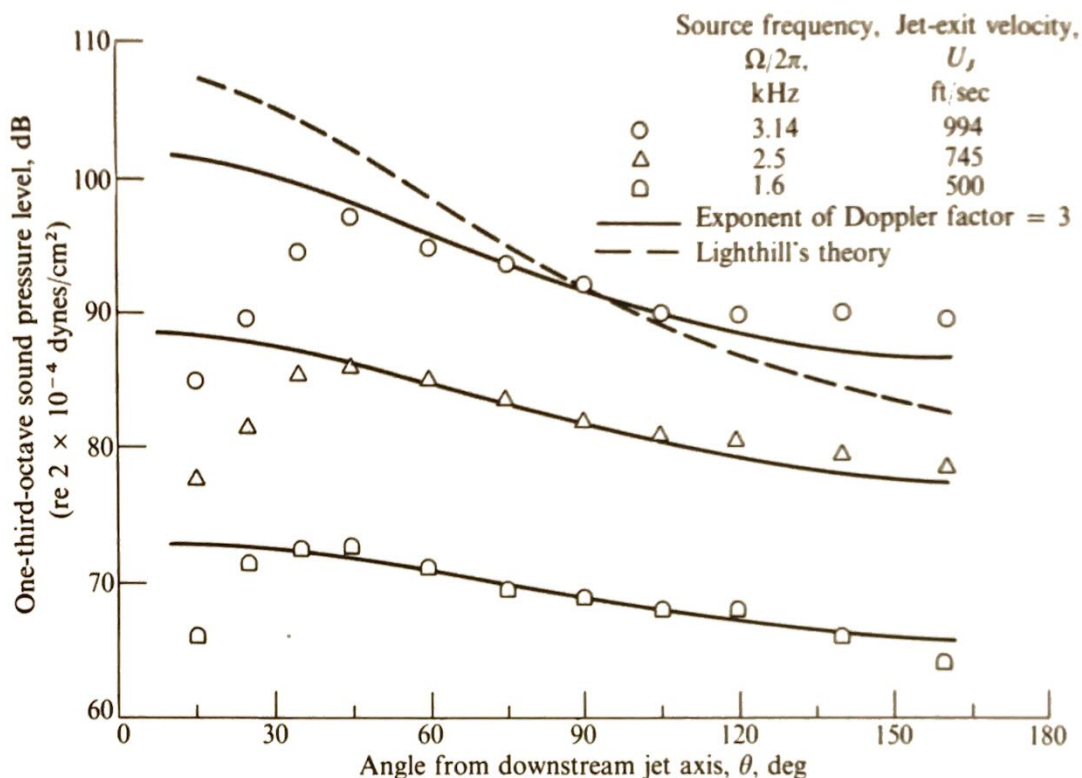


Fig. 6.1 Experimental one-third-octave directivity data of Olsen²⁷ plotted at constant source frequency $\Omega = \omega(1 - M_c \cos \theta)$ where $\Omega/2\pi$ is equal to the peak frequency of the spectrum at 90° from the jet axis. Jet nozzle diameter, D , 10.16 cm (4 in.). Figure prepared by experimenter.

each case, Ω is set equal to the peak frequency of the spectrum at 90° from the jet axis (where $\Omega = \omega$). The level of the curves is adjusted to go through the data point at 90° and, as in Chap. 2, M_c is put equal to $0.62 U_j/c_0$. It can be seen that excellent agreement is obtained for all angles greater than about 30° from the jet axis, where the experimental intensity begins to exhibit the rapid dropoff predicted by the high-frequency solutions developed in Sec. 6.7.1. In fact, the measurements show that, in accordance with these solutions, increasing the Mach number causes the dropoff in intensity to become more pronounced and to occur at progressively larger angles to the jet axis.

One-third-octave intensities are plotted (at the highest jet velocity) for several source frequencies in Fig. 6.2. It can be seen that the depth of the zone of silence increases with increasing source frequency. Thus, at high frequencies, the acoustic behavior in this region is, at least qualitatively, predicted by the refraction factor \mathcal{R}_ω that multiplies and high-frequency Green's functions (6.67) and (6.69).

One-third-octave data for a low-source frequency are also plotted in this figure. Rather than dropping off at small angles to the jet axis, these results exhibit a hump in this region. This behavior can probably be explained by the additional Doppler factors that appear in the denominator of the low-frequency Lilley's equation Green's function (6.74).

If Eq. (6.75) were integrated over all frequencies, the resulting expres-

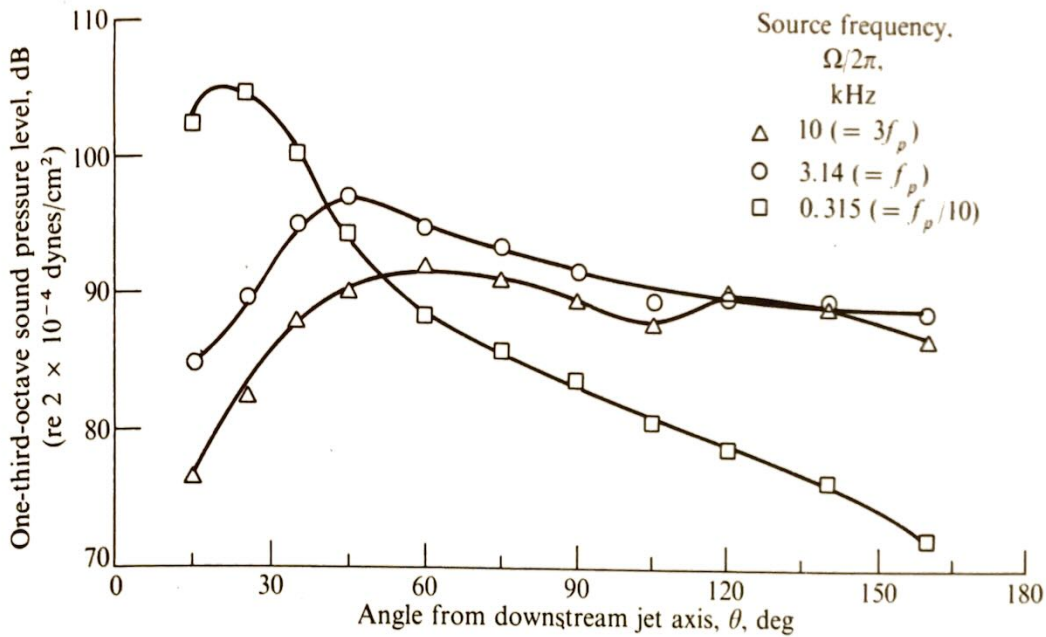


Fig. 6.2 Experimental one-third-octave directivity data of Olsen²⁷ plotted at constant source frequency $\Omega = \omega(1 - M_c \cos \theta)$ where f_p is the peak frequency of the spectrum at 90° from the jet axis. Jet nozzle diameter, D , 10.16 cm (4 in.); jet-exit velocity, U_j , 994 ft/sec. Figure prepared by experimenter.

sion for the average intensity would again vary with angle as $(1 - M_c \cos \theta)^{-3}$. This result is compared with experimental measurements in Figs. 6.3 and 6.4. These plots are the same as Figs. 2.14 and 2.15 with additional curves corresponding to the new convection factor $(1 - M_c \cos \theta)^{-3}$ included. The value of M_c remains unchanged. It can be seen that the results obtained in this section are in somewhat better agreement with the data. Further successful comparisons† with cold jets from coaxial, plug, and slot nozzles are given in Reference 14.

The agreement at angles outside the zone of silence is probably due to the fact that the frequencies of the curves shown in Fig. 6.1 are not too different from those of the spectral peaks in this region (see Sec. 2.5.1).‡ Since most of the acoustic energy is concentrated in a few octave bands near its peak frequency, the agreement between experiment and theory exhibited in Fig. 6.1 insures that similar agreement will be obtained for overall sound pressure levels. The correspondence at angles within the zone of silence is probably the result of a fortuitous balance between the increase in level of low-frequency sound and the decrease in level of the high-frequency sound that occurs in this region.

The theory implies that most of the sound outside the zone of silence originates from the mixing region of the jet while the low-frequency sound

† In making these comparisons, A^\dagger was set to zero.

‡ The total acoustic power spectrum has a peak frequency which is somewhat lower than this because of the strong weighting of its low-frequency end by the energy in the zone of silence.

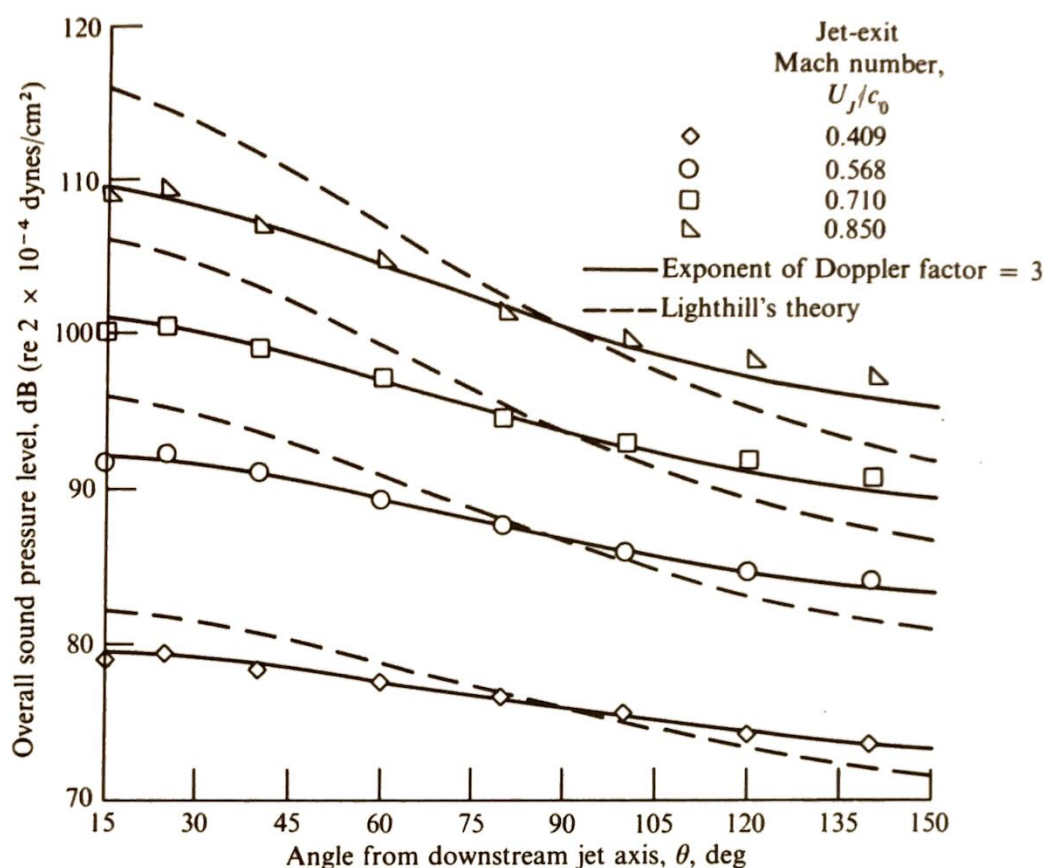


Fig. 6.3 Experimental directivity data of Reference 22 of Chap. 2. Jet nozzle diameter, 5.08 cm (2 in.).

within the zone of silence (which makes a substantial contribution to the total acoustic power radiated by the jet) probably originates downstream of this region.

6.8 FLOWS OF FINITE EXTENT

All the solutions of the convected wave equations discussed up to now have been for transversely sheared unidirectional mean flows, which must extend from $-\infty$ to $+\infty$. However, the relatively slow spreading and attendant decay in mean velocity with axial distance that occurs in real jets could certainly influence the radiated sound. In order to assess the effects of a mean flow on the acoustic field, a number of experimental^{8,30-32} and analytical^{28,29,33} studies have been carried out by Ribner and his co-workers at the University of Toronto.

The experiments consisted of measuring the far-field directivity pattern of a harmonic point source placed within the potential core† of an air jet.

† In some experiments the source was moved to the side of the core to determine the effect of this displacement.

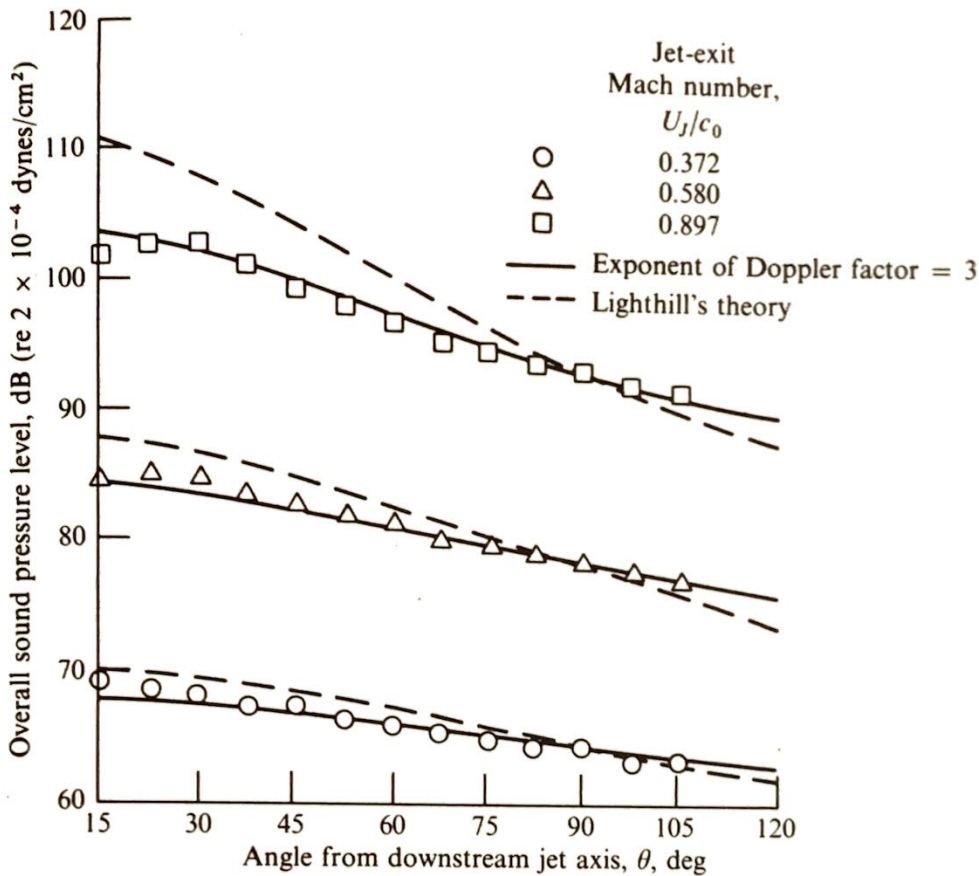


Fig. 6.4 Experimental directivity data of Reference 23 of Chap. 2. Jet nozzle diameter, 2.54 cm (1 in.).

The source was the orifice of a tube ($\sim \frac{1}{16}$ in. inside diam) driven through a conical coupling by a horn-type loudspeaker driver. With the jet turned off the source radiated essentially omnidirectionally—so that any non-uniformity of the directivity patterns observed with the jet turned on can presumably be attributed to the mean flow.[†] Typical results obtained with the source frequency set equal to the peak frequency of the jet noise are shown in Fig. 6.5. These investigations tend to confirm that the observed dropoff, or cleft, in the directivity pattern is indeed due to the mean flow.

The analytical studies were carried out²⁸ “to verify the refraction interpretation analytically and at the same time extend the available data.” Since these studies were purely numerical, they were able to use mean velocity profiles that correspond closely to those observed in an actual jet. Nevertheless, there have been some objections raised³ concerning the fact that the wave equation used by Schubert was based on Obukhov’s quasi-potential,³⁴ which applies only when the mean-flow Mach number is very small. This difficulty has been overcome by Mungar, Plumlee, and Doak³⁶ who obtained detailed numerical solutions to the complete linearized gas dynamic equations. Their results are compared with Grande’s measurements³² in

[†] The effects of the turbulence on the emitted sound can probably be neglected for the reasons given in Sec. 6.5.

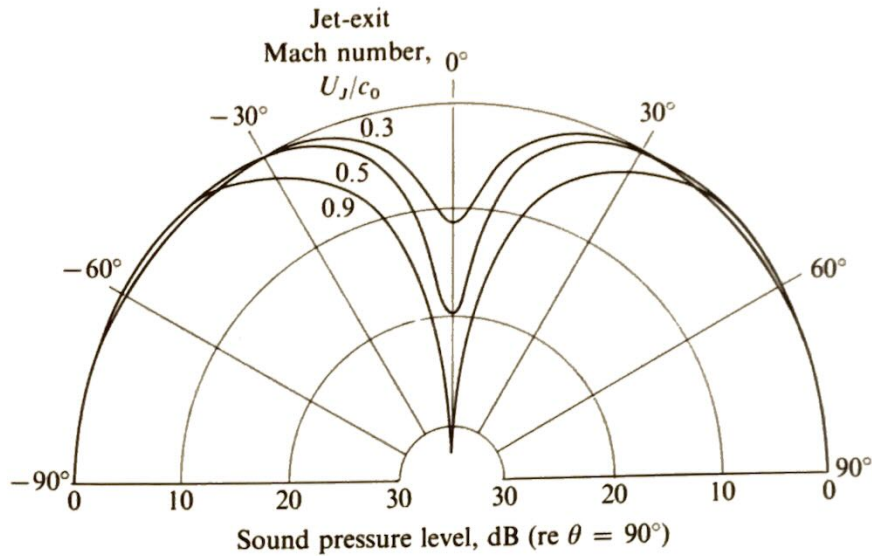


Fig. 6.5 Effect of jet velocity on directivity. Jet temperature, ambient; average effective source frequency, 3000 hertz ($fD/c_0 = 0.168$); source position, on jet axis 2 nozzle diameters downstream of nozzle. (From Reference 32.)

Fig. 6.6. It can be seen that the agreement is excellent. Also shown in the figure is a calculation by Tester and Burrin²⁴ based on the Lilley's equation Green's function discussed in Sec. 6.7.1. It can be seen that this solution has a tendency to greatly overpredict the dropoff in intensity within the zone of silence.

6.9 CONCLUDING REMARKS

We have now developed a number of acoustic analogue theories which were designed to account for the effects of mean velocity gradients on the

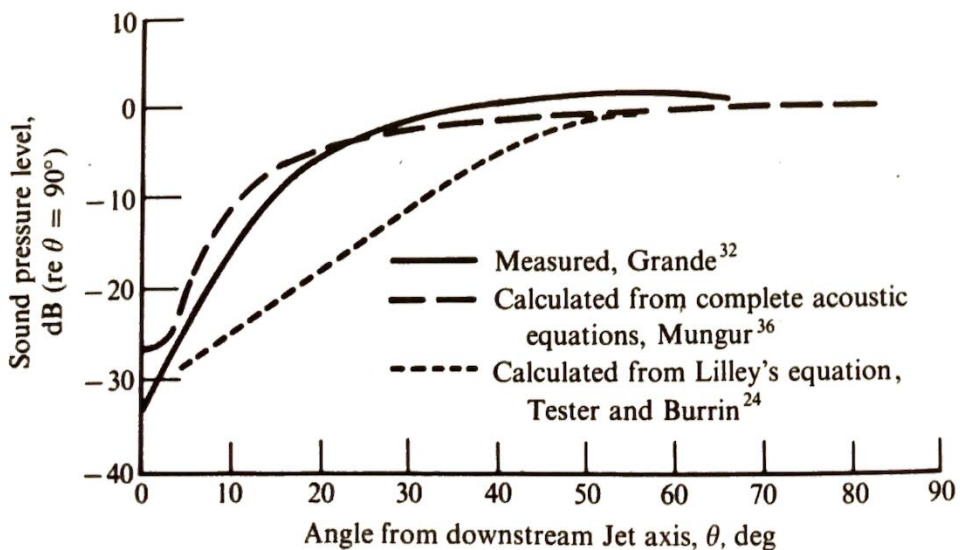


Fig. 6.6 Variation of sound pressure level with angle. Dimensionless frequency, $\omega r_j/c_0$, 0.53; Jet exit Mach number, U_j/c_0 , 0.9; source location, on Jet axis 2 diameters downstream of nozzle.

generation of aerodynamic sound. But unlike Lighthill's theory, they lead to equations which are quite difficult to solve analytically. Nevertheless, low- and high-frequency asymptotic solutions were obtained and it was shown how these results explain, at least qualitatively, many of the observed features of subsonic jet noise not explained by Lighthill's theory. An approximate theory which gives good quantitative agreement at angles which are not too close to the jet axis was also presented. Finally, it was shown that there are real flow effects that limit the validity of even these more general theories.

APPENDIX 6.A

DERIVATION OF EQUATION (6.26)

For a parallel shear flow wherein U is given by Eq. (1.14),

$$\begin{aligned} \frac{\partial}{\partial y_1} U \frac{\partial^2(u_i u_j)}{\partial y_i \partial y_j} &= \frac{\partial}{\partial y_1} \left\{ \frac{\partial}{\partial y_i} \left[U \frac{\partial(u_i u_j)}{\partial y_j} \right] - \frac{dU}{dy_2} \frac{\partial(u_i u_j)}{\partial y_i} \right\} \\ &= \frac{\partial}{\partial y_1} \left[\frac{\partial^2}{\partial y_i \partial y_j} (U u_i u_j) - 2 \frac{dU}{dy_2} \frac{\partial}{\partial y_i} (u_i u_j) - u_j^2 \frac{d^2 U}{dy_2^2} \right] \end{aligned}$$

and

$$\frac{\partial}{\partial y_1} U \nabla^2 \Pi = \frac{\partial}{\partial y_1} \left(\nabla^2 U \Pi - 2 \frac{dU}{dy_2} \frac{\partial \Pi}{\partial y_2} - \frac{d^2 U}{dy_2^2} \Pi \right)$$

which show that Eqs. (6.24) and (6.25) can be put in form

$$\begin{aligned} \frac{D_0^2}{D\tau} \Gamma - c_0^2 \nabla^2 \Gamma &= \left[\frac{\partial^2}{\partial y_i \partial y_j} \left(\frac{\partial}{\partial \tau} + U \frac{\partial}{\partial y_1} \right) (u_i u_j) \right] \\ &\quad - 4 \frac{\partial}{\partial y_1} \left[\frac{dU}{dy_2} \frac{\partial}{\partial y_i} (u_i u_j + c_0^2 \delta_{2i} \Pi) \right] - \frac{\partial}{\partial y_1} \left[\frac{d^2 U}{dy_2^2} (u_j^2 + c_0^2 \Pi) \right] \end{aligned}$$

where $\Gamma \equiv D_0 \Pi / D\tau$.

APPENDIX 6.B

CONSTRUCTION OF ONE-DIMENSIONAL GREEN'S FUNCTION

Any function $G(r|r_0)$ satisfying the inhomogeneous equation

$$\left[\frac{d}{dr} p(r) \frac{d}{dr} + q(r) \right] G = \delta(r - r_0) \quad (6.B.1)$$

on the interval $a \leq r \leq b$ can be expressed in terms of two linearly independent homogeneous solutions, say w_1 and w_2 , by

$$G(r|r_0) = \begin{cases} \frac{w_1(r)w_2(r_0)}{A} & \text{if } r > r_0 \\ \frac{w_2(r)w_1(r_0)}{A} & \text{if } r < r_0 \end{cases} \quad (6.B.2)$$

where

$$A \equiv -p(r)W(r)$$

and

$$W(r) \equiv w_1(r)w_2'(r) - w_2(r)w_1'(r)$$

is the Wronskian of w_1 and w_2 . G will then satisfy the same homogeneous boundary conditions as w_1 and w_2 at $r = b$ and $r = a$, respectively. Moreover, *Abel's theorem* states that $A = \text{Constant}$.

These results can easily be verified by integrating both sides of Eq. (6.B.1) over a small interval about r_0 , noting that the dominant contribution to the left side comes from the first term, and inserting Eq. (6.B.2) into the result.

APPENDIX 6.C

ASYMPTOTIC SOLUTIONS TO STURM-LIOUVILLE EQUATION

In this appendix we discuss the asymptotic expansions as $k \rightarrow \infty$ of the solutions to the general Sturm-Liouville equation

$$v'' + [k^2q(r) + s(r)]v = 0 \quad (6.C.1)$$

where q and s are arbitrary functions of r .

Case 1: $q(r) > 0$

First, consider the case where $q(r)$ is strictly positive. Liouville obtained the asymptotic solutions for this case by introducing the new variables

$$\xi = \int \sqrt{q(r)} dr$$

$$\chi = [q(r)]^{1/4} v$$

which transform Eq. (6.C.1) into the equation

$$\frac{d^2\chi}{d\xi^2} + k^2\chi = B(\xi)\chi \quad (6.C.2)$$

where

$$B = \frac{1}{4} \frac{q''}{q^2} - \frac{5}{16} \frac{q'^2}{q^3} - \frac{s}{q}$$

and the primes denote differentiation with respect to r . By treating the terms on the right side as known, we can solve the remaining linear inhomogeneous equation with constant coefficients in the usual way to obtain the Volterra integral equation

$$\chi = c_1 \cos k\xi + c_2 \sin k\xi + \frac{1}{k} \int_a^\xi [\sin k(\xi - t)] B(t) \chi(t) dt$$

where c_1, c_2 , and a are arbitrary constants. The method of successive approximations yields a solution to this equation of the form³⁷

$$\chi = \sum_{n=0}^{\infty} \chi_n$$

where

$$\chi_0 = c_1 \cos k\xi + c_2 \sin k\xi$$

and

$$\chi_{n+1} = \frac{1}{k} \int_a^\xi [\sin k(\xi - t)] B(t) \chi_n(t) dt$$

This series converges and also represents an asymptotic expansion of the solution in the limit as $k \rightarrow \infty$. However, the iterated solution becomes extremely complicated if one attempts to carry it much beyond the first iteration. Still, the first approximation to the solution of Eq. (6.C.1) is simply

$$v = c_1 [q(r)]^{-1/4} \cos \left[k \int \sqrt{q(r)} dr \right] + c_2 [q(r)]^{-1/4} \sin \left[k \int \sqrt{q(r)} dr \right] \quad (6.C.3)$$

Case 2: $q(r_\delta) = 0$ for some point r_δ

The asymptotic solution (6.C.3) will have a singularity at any point $r = r_\delta$ where $q(r_\delta) = 0$. But since r_δ is not a singular point of Eq. (6.C.1), its solution must be non-singular there. Hence, Eq. (6.C.3) cannot be an asymptotic representation of the solution to Eq. (6.C.1) in the neighborhood of any point where $q(r) = 0$. r_δ is called a *turning point*.

We consider only the case where $q(r)$ has a simple zero at r_δ . Thus,

$$q(r) \sim a(r - r_\delta) \quad \text{as } r \rightarrow r_\delta$$

Then for r near r_δ Eq. (6.C.1) can be approximated by the equation

$$v'' + k^2 a(r - r_\delta) v = 0 \quad (6.C.4)$$

whose solution can be expressed in terms of either Bessel functions of order $1/3$ or Airy functions.

Since the solution for case 1 was obtained by transforming Eq. (6.C.1) into an equation with approximately constant coefficients, it is natural, in the present case, to attempt to find a solution in the neighborhood of r_δ by transforming (6.C.1) approximately into the form (6.C.4). Thus, assume for definiteness, that

$$\frac{dq}{dr}(r_\delta) > 0$$

Then upon introducing the new variables

$$\xi = \begin{cases} \left(\frac{3}{2} \int_{r_\delta}^r \sqrt{q(t)} dt \right)^{2/3} & \text{for } r > r_\delta \\ - \left(\frac{3}{2} \int_r^{r_\delta} \sqrt{-q(t)} dt \right)^{2/3} & \text{for } r < r_\delta \end{cases}$$

and

$$\chi = \sqrt{\frac{d\xi}{dr}} v$$

Eq. (6.C.1) becomes

$$\frac{d^2 \chi}{d\xi^2} + k^2 \xi \chi = B(\xi) \chi \quad (6.C.5)$$

where

$$B(\xi) = \frac{1}{2} \frac{d^3 \xi / dr^3}{(d\xi/dr)^3} - \frac{3}{4} \frac{(d^2 \xi / dr^2)^2}{(d\xi/dr)^4} - \frac{s}{(d\xi/dr)^2}$$

The procedure used to obtain the asymptotic solutions of Eq. (6.C.2) can also be applied to Eq. (6.C.5) and, if $q(r)$ has no other zeros, the resulting expansions will represent the solution over all space. This approach is referred to as the WKBJ approximation. The lowest-order iterated solution to Eq. (6.C.5) is

$$\chi_0 = c_1 \xi^{1/2} H_{1/3}^{(1)}(\frac{2}{3} k \xi^{3/2}) + c_2 \xi^{1/2} H_{1/3}^{(2)}(\frac{2}{3} k \xi^{3/2})$$

where $H_{1/3}^{(j)}$ denote $1/3$ -order Hankel functions. Hence, the first approximation to the solution to Eq. (6.C.1) is

$$v = c_1 \frac{\xi^{3/4}}{q^{1/4}} H_{1/3}^{(1)}(\frac{2}{3} k \xi^{3/2}) + c_2 \frac{\xi^{3/4}}{q^{1/4}} H_{1/3}^{(2)}(\frac{2}{3} k \xi^{3/2}) \quad (6.C.6)$$

REFERENCES

1. Chu, Boa-Teh and Leslie S. G. Kovasznay, "Non-Linear Interactions in a Viscous Heat-Conducting Compressible Gas," *J. Fluid Mech.*, **3**, pt. 5, 494-514, 1958.
2. Phillips, O. M., "On the Generation of Sound by Supersonic Turbulent Shear Layers," *J. Fluid Mech.*, **9**, pt. 1, 1-28, 1960.
3. Doak, P. E., "Analysis of Internally Generated Sound in Continuous Materials: 2. A Critical Review of the Conceptual Adequacy and Physical Scope of Existing Theories of Aerodynamic Noise, With Special Reference to Supersonic Jet Noise," *J. Sound Vibr.*, **25**, 2, 263-335, 1972.
4. Lighthill, M. J., "On Sound Generated Aerodynamically. I. General Theory," *Proc. Roy. Soc. (London)*, ser. A, **211**, 564-587, 1952.
5. Kraichnan, Robert H., "The Scattering of Sound in a Turbulent Medium," *J. Acoust. Soc. Am.*, **25**, 6, 1096-1104, 1953.
6. Müller, Ernst-August and Klaus R. Matschat, *The Scattering of Sound by a Single Vortex and by Turbulence*, AFOSR-TN-59-337, U.S. Air Force Office of Scientific Research, 1959.
7. Schmidt, D. W., *Experiments Relating to the Interaction of Sound and Turbulence*, AFOSR-TN-60-347, U.S. Air Force Office of Scientific Research, 1959.
8. Atvars, J., L. K. Schubert and H. S. Ribner, "Refraction of Sound From a Point Source Placed in an Air Jet," *J. Acoust. Soc. Am.*, **37**, 1, 168-170, 1965.
9. Lush, P. A., "Measurements of Subsonic Jet Noise and Comparison with Theory," *J. Fluid Mech.*, **46**, pt. 3, 477-500, 1971.
10. Jackson, John D., *Classical Electrodynamics*, John Wiley & Sons, Inc., 1962.
11. Bradshaw, P., D. H. Ferriss and R. F. Johnson, "Turbulence in the Noise-Producing Region of a Circular Jet," *J. Fluid Mech.*, **19**, pt. 4, 591-624, 1964.
12. Davies, P. O. A. L., M. J. Fisher and M. J. Barratt, "The Characteristics of the Turbulence in the Mixing Region of a Round Jet," *J. Fluid Mech.*, **15**, pt. 3, 337-367, 1963.
13. Goldstein, Marvin E. and Walton L. Howes, "New Aspects of Subsonic Aerodynamic Noise Theory," NASA TN D-7158, 1973.
14. Olsen, W. A., O. A. Gutierrez and R. G. Dorsch, "The Effect of Nozzle Inlet Shape, Lip Thickness and Exit Shape and Size on Subsonic Jet Noise," Paper 73-187, AIAA, Jan. 1973.
15. Jones, Ian S. F., "Aerodynamic Noise Dependent on Mean Shear," *J. Fluid Mech.*, **33**, pt. 1, 65-72, 1968.
16. Gottlieb, Peter, *Acoustics in Moving Media*, Ph.D. Thesis, Mass. Inst. of Tech., June 1959.
17. Slutsky, Simon and J. Tamagno, *Sound Field Distribution About a Jet*, Tech. Rept. 259, General Applied Science Lab. (AFOSR TN-1935), 1961.
18. Moretti, Gino and Simon Slutsky, *The Noise Field of a Subsonic Jet*, Tech. Rept. 150, General Applied Science Lab. (AFOSR TN-59-1310), 1959.
19. Slutsky, S., *Acoustic Field of a Cylindrical Jet due to a Distribution of Random Sources of Quadrupoles*, Tech. Rept. 281, General Applied Science Lab. (AFOSR TN-2455), 1962.
20. Mani, R., A Moving Source Problem Relevant to Jet Noise, *J. Sound Vibr.*, **25**, 2, 337-347, 1972.
21. Graham, E. W. and B. B. Graham, *The Acoustical Source in a Two-Dimensional Jet*, DI-82-0909, Boeing Scientific Research Laboratories, 1969.
22. Graham, E. W., *A Sequence of Transient Acoustical Sources in an Idealized Jet*, DI-82-1002, Boeing Scientific Research Laboratories, 1970.
23. Pao, S. P., "A Generalized Theory on the Noise Generation From Supersonic Shear Layers," *J. Sound Vibr.*, **19**, 4, 401-410, 1971.
24. Tester, Brian J. and Robert H. Burrin, "On Sound Radiation from Sources in Parallel Sheared Jet Flows," AIAA Paper 74-57 presented at 12th Aerospace Sciences Meeting, Washington, D.C.
25. Abramowitz, Milton and Irene A. Stegun, *Handbook of Mathematical Functions with Formulas, Graphs, and Mathematical Tables*, National Bureau of Standards Applied Mathematics Series 55, 1964.

26. Erdélyi, Arthur, *Asymptotic Expansions*, Dover Publications, 1956.
27. Olsen, W. and R. Friedman, "Jet Noise from Co-axial Nozzles Over a Wide Range of Geometric and Flow Parameters," AIAA Paper 74-43 presented at 12th Aerospace Sciences Meeting, Washington, D.C.
28. Schubert, L. K., "Numerical Study of Sound Refraction by a Jet Flow. I. Ray Acoustics," *J. Acoust. Soc. Am.*, **51**, 2, pt. 1, 439-446, 1972.
29. Schubert, L. K., "Numerical Study of Sound Refraction by a Jet Flow. II. Wave Acoustics," *J. Acoust. Soc. Am.*, **51**, 2, pt. 1, 447-463, 1972.
30. Atvars, J., L. K. Schubert and H. S. Ribner, "Refraction of Sound by Jet Flow or Jet Temperature," NASA CR-494, May 1966.
31. Atvars, J., L. K. Schubert and H. S. Ribner, "Refraction of Sound From a Point Source Placed in an Air Jet," pp. 25-27. Paper 65-82, AIAA, Jan. 1965.
32. Grande, E., "Refraction of Sound by Jet Flow and Jet Temperature," NASA CR-840, 1967.
33. Schubert, L., "Refraction of Sound by a Jet: A Numerical Study," *UTIAS-144-Rev.*, University of Toronto (AFOSR-69-3039TR; AD-701370), 1969.
34. Blokhintsev, D. I., "Acoustics of a Nonhomogeneous Moving Medium," NACA TM 1399, 1956.
35. Tester, Brian J. and Christopher L. Morfey, "Developments in Jet Noise Modeling—Theoretical Predictions and Comparisons with Measured Motor," AIAA Paper 75-477 presented at 2nd Aero-Acoustics Conference, Hampton, Va.
36. Mungar, P., H. E. Plumblee and P. E. Doak, "Analysis of Acoustic Radiation in a Jet Flow Environment," *J. Sound Vibr.*, **36**, 1, 21-52, 1974.
37. Morse, Phillip and Herman Feshbach, *Methods of Theoretical Physics*, Part II. McGraw-Hill, Inc., 1953.
38. Goldstein, M. E., "The Low Frequency Sound from Multipole Sources in Axisymmetric Shear Flows, With Applications to Jet Noise," *J. Fluid Mech.*, **70**, pt. 3, 595-604, 1975.
39. Goldstein, M. E., "The Low Frequency Sound from Multipole Sources in Axisymmetric Shear Flows—Part II," *J. Fluid Mech.*, **75** pt. 1, 17-29, 1976.

INDEX

- Abel's theorem, 266, 282
- Acoustic analogy, 68–71
 - approximate form in transversely sheared mean flows, 257
 - extended to include surface effects, 116, 192
 - extended to sheared mean flows, 250–254
 - (*See also* Generalized acoustic analogy equation)
- Acoustic energy flux:
 - definition of, 39–40
 - in isentropic-irrotational flows, 41–42
 - in stationary medium, 42
- Acoustic field, 68
- Acoustic impedance, 249
 - of free space, 39
- Acoustic intensity (*see* Intensity)
- Acoustic particle velocity, 3, 221
- Acoustic power, 41
 - from axial flow turbomachines, 200–201
 - definition, 41
 - from jets, 93–94
- Acoustic sources:
 - compact, 36–37, 70–71, 123
 - dipole, 35, 36, 37, 113, 118, 120, 124–126, 140, 148, 153, 183, 193, 222, 240, 257
 - in jets, 84–85, 91–92, 102, 103–104
 - location of, 102
 - monopole, 36, 53, 113–114, 118
 - moving, 45–53, 84, 120–121, 271–272
 - multipole, 34, 35, 53
 - quadrupole, 36, 37, 53, 70–71, 72, 84, 118, 120, 126, 173–174, 207–208, 240, 257
 - superposition of, 28–34, 120–121, 140–141, 147
 - in transversely sheared mean flows, 257
 - volume displacement, 25, 117–118
 - volume flow, 2, 25, 45
- Acoustic spectrum:
 - produced by helicopter, 169
 - produced by supersonic fan, 210
 - from subsonic turbomachinery, 196
- Aeolian tones, 145–153
- Aerodynamic forces (*see* Surface force)
- Air jets, turbulent subsonic, 87–97
- Airfoils, 126, 130, 133, 134, 138, 151–152, 156
- Airy functions, 284

- Amplitude:
 - of harmonic, 54
 - of plane wave, 12, 14
- Angle of attack, 132, 136, 202
- Appent mass effects, 135
- Aspect ratio, 161
- Asymptotic expansion, 39_n, 135, 138, 139, 264–273
- Auto-correlation function:
 - for function vanishing at infinity, 56
 - normalized pressure, 44, 75, 80, 82, 89
 - periodic, 44, 55
 - stationary, 44, 58
- Average:
 - spatial, 2, 59, 85, 178–179
 - temporal, 1, 39, 40–41, 43–44, 75, 141, 142, 149–150, 179
- Average value of stationary function, 44, 57, 58
- Axial flow turbomachinery noise:
 - based on linearized theory, 222–239
 - basic equation for, 193
 - broad band, 208
 - due to inlet flow distortion, 206–208
 - due to inlet turbulence, 206–207
 - due to rotor-stator interaction, 202–206
 - effects of steady loading on, 207
 - pure tones, 195–208
 - at supersonic tip speeds, 208–210
- Axisymmetric mean flow, 6, 259–260
(*See also* Transversely sheared mean flow)
- Bessel functions, 66, 135, 139, 158, 160, 165, 193–194, 198, 202, 213, 230
generating function for, 158
- Bird tone, 107
- Blade forces (*see* Surface forces)
- Blade passing frequency tones, 197–198, 206–207
- Blade row, 223
- Blade slap, 168, 170
- Boundary conditions:
 - for Green's function, 30–32
 - in inviscid uniform mean flows, 131, 132, 222, 226
- Boundary layer noise, 174, 153, 208
- BPF, 197–198, 206–207
- Branch of square root, 65, 232–233, 241, 266
- Branch point, 231
- Camber, 132, 136
- Cascade, 222
- Cauchy integral, 213
- Cauchy principal value, 231
- Causality, 27, 28, 31, 261
- Clebsch potentials, 44–45
- Coaxial nozzle, 182, 183
- Collocation methods, 134_n, 230
- Combustion noise, 72_n, 110
- Compact source, 36–37, 70–71, 123
- Complex conjugate, 1, 54, 56, 58, 62, 64, 200
- Compressor (*see* Axial flow turbomachinery noise)
- Condensation, 8
- Coning force, 168
- Continuity equation, 2, 69, 118, 250
for incompressible flow, 118, 131, 256
linearized, 5, 7, 220
for steady flow, 3
- Convection factor, 51, 53, 84, 98, 121, 151, 153, 271, 275, 277
- Convection Mach number of turbulence, 79, 276
- Convection velocity, 79, 81, 91, 272
(*See also* Velocity)
- Convective derivative, 250–254
- Convolution theorem, 57, 174–175, 262
- Correlation length of turbulence, 125, 143–145, 179–181, 206
definition of, 77, 90_n
in fully developed region, 92
measurements of, 90
- Correlation tensor of turbulence, 78, 84, 143, 274
- Critical angle, 18, 270
- Cross-correlation function, 126
of function vanishing at infinity, 56
periodic, 54, 55
stationary, 58, 59
- Cross-power spectral density function
(*see* Cross-power spectrum)
- Cross-power spectrum:
 - of function vanishing at infinity, 56
 - stationary, 57, 58
- Curle's equation, 121
- Cut off:
 - of blade passing frequency tone, 206
 - of modes, 171, 198–200, 208, 236
- Cylinder, flow about, 146
- Decay time of turbulent eddy:
 - in fixed frame, 78
 - in moving frame, 79, 90, 180
- Decibel, xvii
- Delta function, 27, 28, 117, 281
in cylindrical coordinates, 263
Fourier transform, 57, 196
integration over, 26, 46, 119
in three dimensions, 26, 27, 28
- Density, 2
fluctuation, 2, 3, 9, 69–70, 74, 114, 190, 191
- Dipole (*see* Acoustic source)
- Diffraction of sound, 211
- Dirac delta function (*see* Delta function)
- Directivity pattern:
 - for edge noise, 179, 180
 - for jet noise, 95–96, 275–279
 - for lip noise, 182
 - for point source in jet, 278–280
 - for propeller noise, 162
 - for turbomachinery noise, 214–215

- Dispersion, 261
- Distortion harmonics (*see* Harmonics)
- Distortion velocity (*see* Flow distortion)
- Divergence theorem, 25, 59, 73, 115, 191
- Doppler effect, 52, 81, 95, 97, 150
- Doppler factor, 52, 81, 275
(*See also* Convection factor)
- Doppler shift, 52, 81, 95, 97, 150
- Drag (*see* Surface force)
- Drag coefficient, 127–129
- Ducts:
 - Green's function for, 65, 192–194
 - sound propagation in, 198–201, 235–236
- Ear, 2, 43
- Eddy, 78, 83, 99, 206, 207
- Edge tones, 106, 107
- Eigenfunctions, 14, 64
- Eigenvalues, 64, 198
- Eikonal, 14, 267
- Energy:
 - acoustic: definition of, 39–40
 - in far field, 43–44
 - formula for, 41
 - in isentropic irrotation flow, 41, 42
 - of flow, 39
 - internal, 251
- Energy equation, 255
 - acoustic, 40, 41
 - for inviscid non-heat conducting flow, 2, 3, 5, 7
 - linearized, 5, 7
 - steady, 3
- Energy flux (*see* Acoustic energy flux)
- Entropy, 2, 42, 72*n*, 251–253, 255
 - fluctuation, 3, 72
- Euler's equation (*see* Momentum equation)
- Fan (*see* Axial flow turbomachinery noise)
- Far field (*see* Radiation field)
- Flowcs Williams-Hawking's equation, 119–120
 - applications of, 139–171
 - derivation of, 116–119
 - interpretation of, 120–126
- Flat plate (*see* Infinite plane surface)
- Flow distortion, 154, 163–168, 199, 201–202, 206–208, 223–225
- Flow instability:
 - behind a cylinder, 146
 - amplification of internal noise, 110
 - effects on jet noise, 103–104, 109, 261
 - in production of edge tones, 106, 107
 - relation to "vortex shedding noise", 152, 153
- Force on unit volume, 2, 10, 35, 257
- Forward flight effects, 110
- Fourier amplitude (*see* Harmonic)
- Fourier coefficients (*see* Harmonic)
- Fourier components, 11
- Fourier integral (*see* Fourier transform)
- Fourier transform, 44, 175, 262
 - definition of, 55
 - of distribution, 230
 - properties of, 56, 57
 - of stationary functions, 44, 57, 58, 76, 80, 81, 86
- Fourier series, 154, 195–196, 223
 - properties of, 54, 55
 - definition of, 54
- Fourier-Bessel series, 202
- Frequency, 3, 12, 95
 - angular, 12, 146, 264
 - Doppler shift in (*see* Doppler shift)
 - source, 52, 86, 95, 149–151, 275–276
- Fresnel integral, 138, 176
- Fully developed region, 88, 90
 - sound emission from, 92
- Fundamental solution, 28, 114, 191
- Gas constant, 10, 251
- Generalized acoustic analogy equation, 192
 - application to fan and compressor noise, 192–193
 - derivation of, 189–191
 - with zero mean flow, 116
 - derivation of, 114–116
- Geometric expansion, 243
- Green's formula, 29
 - generalized, 29, 59–61, 114, 191
- Green's function, 30–32, 174
 - for axisymmetric mean flow, 261–273, 276
 - calculation of, 61–66
 - for classical wave equation, 30, 31
 - in free space, 27, 116, 117, 178, 269, 273, 274
 - for half space, 62, 172, 211
 - for infinite cylinder, 65, 192–194
 - in one dimension, 64, 281–282
 - reduced, 27, 63, 175, 262, 269, 273
 - for semi-infinite cylinder, 181, 211–213
 - for semi-infinite plate, 175
 - tailored to geometry, 171–175
- Green's theorem, 60
- Gust:
 - definition of, 127
 - harmonic, 134, 225
- Gutin's mechanism:
 - for axial flow fans and compressors, 198, 208
 - for helicopters, 168, 170
 - for propellers, 160–163
- Hankel functions, 244, 245, 266, 272, 284
- Harmonic analysis (*see* Fourier series)
- Harmonic time dependence, 11, 12, 14, 147, 154, 195–196
- Harmonics:
 - of blade forces, 164, 168, 196–197, 201
 - of BPF tone, 170, 196, 204, 205, 211

- of distortion, 167, 170, 201, 202, 205, 225
- of Fourier series, 54, 154, 196, 197, 201, 211
- of shaft rotational frequency, 198, 208–210
- Heat conduction, 2, 255, 271
- Helicopter noise:
 - broad band, 153
 - pure tones, 168–170
 - spectrum, 169
- Helmholtz equation, 11, 175, 240
- Homentropic flow, 8, 42, 72
- Ideal gas, 10, 251
 - speed of sound in, 10
- IGV, 202, 203
- Infinite cascade, 222
- Infinite plane surface:
 - Green's function for, 61–62, 172, 211
 - sound generation in vicinity of, 171–174
- Inlet flow distortion (*see* Flow distortion)
- Inlet guide vanes, 202, 203
- Inner solution, 272
- Instability (*see* Flow instability)
- Integral equation, 134
 - singular, 230, 231
 - Volterra, 283
- Intensity:
 - and acoustic power, 41
 - of Aerolean tones, 150, 151
 - definition of, 39
 - in far field, 43–44
 - of sound from jets, 86–87
 - of sound from turbulence in ducts, 208
 - in stationary medium, 43, 44
 - definition of, 44
 - of propeller noise, 161
 - of sound from axial flow turbomachines, 200
 - of sound from jets, 86, 94–96, 274–275
 - of sound from strut in turbulent stream, 143, 144
 - of sound from turbulence, 80–81
 - in third octave bands, 95, 275
- Interblade phase angle, 229, 237, 242, 246
- Intermittency, 88
- Irrotational flow, 41
- Isentropic flow, 8, 42, 72
- Jets:
 - low velocity, 105–109
 - plane, 105–107
 - subsonic turbulent, 87–97
 - supersonic, 98–105, 271
- Jet engine, 110, 206, 207, 208
- Jet noise:
 - directivity pattern of, 95, 96, 275–279
 - effects of mean flow, 249, 250, 275–278
 - from large scale structure, 103, 104
 - Lighthill's theory of, 68, 83–87, 269, 271, 275, 276
 - at low Reynold's numbers, 107–109
 - scaling laws, 91–93, 100
 - spectrum, 94–97, 261–262, 275–277
 - supersonic, 98–100, 103–105, 271
- Jet screech, 104, 152
- Jet spreading, 88, 261, 278
- Joint normality hypothesis, 85, 275
- Jordan's lemma, 232
- Karman vortex street, 146
- Kelvin-Helmholtz instability, 181
 - (*See also* Instability)
- Kernal function, 230–231
- Kirchhoff's theorem, 34, 259
- Kutta-Joukowski condition, 133, 181, 227, 229, 230, 231
- Leibniz's rule, 59, 115, 191, 192
- Lift coefficient, 127–129
- Lighthill parameter, 93
- Lighthill's equation, 70
 - application to turbulent flows, 74–83
 - derivation of, 69–70
 - interpretation of, 70–71
 - for moving medium, 191
 - solution of: in free space, 72–74
 - in presence of solid boundaries, 114–116
- Lighthill's stress tensor, 69, 116, 177
 - mirror image reflection of, 172
 - in moving frame, 190
- Lilley's equation, 253, 259
 - Green's function for, 260–262, 269, 273, 276
 - solution of, 260–273
- Linearized gas dynamic equations, 5, 279
- Lip noise, 181–182
- Loudspeaker driver, 279
- Mach angle, 48
- Mach cone, 48
- Mach number, 16, 18, 46, 125, 138, 206, 208
 - effect on cascade blade forces, 237
 - relative, 198, 206, 228, 237
 - (*See also* Convection Mach number of turbulence)
- Mach waves from jets, 98–99, 102, 103
- Matched asymptotic expansions, 68*n*, 73*n*, 272
 - (*See also* Asymptotic expansions)
- Mean square value, of periodic function, 44, 55
- Method of Eigenfunctions, 32, 62–66
 - (*See also* Green's function)
- Method of images, 32, 61–62
 - (*See also* Green's function)
- Microphone, 43, 209
- Mixing layer, 88, 90, 262, 277
 - sound emission from, 91
- Mixing region (*see* Mixing layer)
- Modes, 14, 164–165, 197–200, 202, 267, 271, 272
 - in ducts, 197–199, 201, 215, 234–236

- Moiré effect, 165
Momentum equation, 69, 191, 250, 251, 256
 for inviscid flow, 2
 linearized, 5, 7, 130, 200, 220, 225
 steady, 3
Monopole source, 36, 53, 113–114, 118
Moving axis correlation tensor, 79, 274
Moving coordinate system, 16, 117–119, 154, 190, 194
Moving source (*see* Acoustic source)
Multiple pure tones, 198, 208–210
 (*See also* Shock waves)
Multipole expansion, 34, 35
Multipole moment, 34
Multipole sources, 34, 35, 53

Near field, 36, 178
Nonuniform mean flow, effects on jet noise, 249–250, 275–278
Nozzle, 88, 104, 182

Obukhov's quasi-potential, 279
OGV, 204, 206
Outer solution, 272
Outlet guide vanes, 204, 206
Overlap region, 68*n*, 272

Parabolic cylinder functions, 271
Parallel mean flow, 6, 8, 17–20, 76–77, 257, 281
 (*See also* Transversely sheared mean flow)
Particle velocity, 3*n*, 221
Period, 3, 12, 125, 150
Permutation tensor, 258
Phase:
 of acoustic signal, 12, 14, 161, 164
 of vortex shedding, 147–148, 150–151
 (*See also* Phase surface)
Phase speed, 15, 161, 164, 199–200, 236, 267
Phase surface, 12–13, 15, 161, 164, 199–200, 267
Phase velocity, 15, 161, 164, 199–200, 236, 267
 of plane wave, 13, 16
Phillips equation, 252
 derivation of, 250–251
 Green's function for, 269, 271, 273
 solution of, 260–273
Plane wave:
 propagation of, 12–13
 refraction of, 17–19
 in stationary medium, 12–14
 in uniformly moving medium, 16, 17
Plemelj formulas, 213*n*
Point source, 9, 10, 25, 26
 (*See also* Acoustic source)
Poisson's equation, 67
Poisson summation formula, 232
Pole, 231
Potential core, 88, 278
Power spectral density function (*see* Power spectrum)
Power spectral density of fluctuating lift, 142, 184–185
Power spectral density tensor for turbulent flow, 81–82, 143
Power spectrum:
 of function vanishing at infinity, 56
 stationary, 58, 44
Prandtl number, 71
Prandtl-Glauert coordinates, 228, 240
Pressure, 2, 251
 dynamic, 174
 fluctuation, 2, 3, 67, 68, 174, 220–222, 227, 234
 jump, 134, 138, 229–230, 242, 244
 surface, 134, 138, 174
 (*See also* Surface force)
Pressure auto-correlation function, 44
 for sound from turbulent flows, 76
Pressure spectrum of sound from turbulence, 95, 96
Propeller noise, 153–168
 basic equation for, 159
 due to flow distortion, 163–166
 Gutin's theory, 160–163
Pulsating sphere, 23–26

Quadrupole noise source:
 in jets (*see* Acoustic source)
 in turbomachinery, 207–208

Radiation condition, 24, 27, 227, 261, 264, 272
Radiation field:
 definition of, 38
 of moving sources, 52, 53
 of multipole sources, 35–36, 53
 properties of acoustic intensity in, 43–44
Reciprocity of Green's function, 27, 30, 31, 181
Reduced frequency, 135, 136, 204
Reduced wave equation, 11, 263
 (*See also* Helmholtz equation)
Reflection, 173, 174, 211
Refraction, 18, 97, 267–268
Refraction factor, 269, 271, 273–274, 276
Residue theorem, 231–232
Response function:
 compressible Sears function, 137–139, 144, 168, 201
 generalized, 139
 for oblique gust, 136, 137, 144
 Sears function, 135–136
Retarded time:
 for aerodynamic sources, 77–81, 82
 definition of, 26
 for moving sources, 47, 119–120, 123
 variation over blade surfaces, 157, 237
Reynolds number, 71, 105–106, 107, 146, 151
Reynolds stress, 71–72, 77, 177, 178, 221
Rotor-stator interactions, 202–206

- Scattering:
- of nonpropagating disturbances, 178, 222, 225
 - of sound by turbulence, 255, 272
- Sears' function, 135–136
- Second law of thermodynamics, 251
- Self-noise, 85, 275
- Semi-infinite duct, 181, 211–215
- Semi-infinite plate, 138
- Green's function for, 175
 - sound generation in vicinity of, 175–181
- Sensitive jets, 109
- Shadow region, 174
- Shear noise, 85, 257, 275
- Shock associated noise, 104
- Shock noise, 104
- Shock waves, 2
- coalescence of, 209
 - in ducts, 208–210
 - in jets, 101, 104–105
 - from projectiles, 123
- Simple source, 36, 53, 113–114, 118
- Slug flow model of jet, 264
- Solid surface effects:
- with uniform mean flow, 189–240
 - with zero mean flow, 113–183
- Solidity, 205, 237
- Sonic boom, 123
- Source, 2, 10, 25–26
- (*See also* Acoustic source)
- Source frequency, 52, 86, 95, 268, 274, 275–276
- Source region, 33–34
- Source strength:
- of aerodynamics sources, 70, 116, 120–121, 257
 - of multipole source, 36
- Specific heats, 251
- ratio of, 10, 251
- Spectrum (*see* Power spectrum; Pressure spectrum)
- Speed of sound (*see* Velocity)
- Spherical wave, 23–24
- Splitting theorem, 220–222
- Stagger, of blades, 210
- Stagger angle, 160, 168, 198, 201–202, 235
- in Prandtl-Glauert plane, 233, 247
- Stagger distance, 226
- Stationary functions:
- definition of, 57
 - in space, 59
 - in time, 43–44, 57–58, 74–76
- Stationary flows, 74–76
- STOL aircraft, 113
- Stokesian gas, 69
- Stress acting on fluid, 37, 257
- Strip theory, 136–137
- Strouhal number, 95, 105, 146, 152, 182
- Strut in a turbulent flow, sound emission from, 140–145, 208
- Sturm-Liouville equation, 282
- Substantive derivative, 250–254
- Summation convention, 69, 250–253, 254
- Supersonic, core, 101–102
- Surface force, 115, 116, 124–125
- acting on fan or compressor, 193, 201–202, 236–237
 - drag component, 193, 201, 236
 - thrust component, 193, 201, 236
 - acting on propeller, 157, 166–168
 - drag component, 157, 158, 168
 - thrust component, 157, 158, 168
 - based on linearized theory, 130–139, 237
 - calculation of, 127–139
 - due to vortex shedding, 146–147
 - influence of cascade effects, 215*n*, 236–238
 - influence of steady loading, 136
 - quasi-steady approximation, 127–130
 - viscous, 173, 174, 192
- Surface velocity, 28–29, 59–60, 117, 192
- Surfaces, influence on sound generation, 113–183, 189–240
- Taylor's hypothesis, 78, 221
- Temperature, 10, 71, 251
- Thermal conductivity, 255
- Third octave band sound spectra, 95, 275–277
- Thrust (*see* Surface force)
- Transition region, 88
- sound emission from, 92
- Transversely sheared mean flow, 6, 10, 252, 255–259
- acoustic equations for, 7–10
 - aerodynamic sound generation in, 255–259
- Turbomachinery noise (*see* Axial flow turbomachinery noise)
- Turbulence:
- axisymmetric, 87
 - entering a fan or compressor, 206–207
 - fourth order correlation tensor, 84, 274
 - incompressible, 83, 85, 274
 - interaction with shock waves, 104, 210
 - isotropic, 85, 143, 275
 - in jets, 88–91, 174
 - large scale orderly structure of, 103–104, 107–108
 - locally homogeneous, 83, 274
 - near an edge, 178–181
 - scattering from, 255, 272
 - second order correlation tensor, 78, 84, 143, 274
 - third order correlation tensor, 274
- Turbulent eddy, 78, 83, 99, 206–207
- Turning point, 265, 271, 283–284
- Uniformly moving medium wave equation, 8, 9, 199, 227
- Vector:
- irrotational, 220–221
 - selnoidal, 220–221, 256, 258

Vector potential, 258–259, 274

Velocity:

angular, 118–119, 153, 194, 195, 222
of boundary, 28–29, 59–60, 117, 192
fluctuation, 3, 76–77, 130–134, 220–222,
225–226

of fluid, 2, 69, 128

interface, 21–22, 264

particle, 3*n*, 221

of phase surface, 15, 161, 164, 199–200,
236, 267

relative to blades, 167, 201–202, 225, 237–
238

rotational, 166–167, 222, 237–238

scattered, 225

of sound, 3, 13, 24, 47, 70, 254, 257, 260,
263, 271

of source, 45, 124, 147

turbulent, 84, 90, 179, 254, 256

vortical, 221

(See also Convection velocity)

Velocity correlation tensor:

in moving frame, 84, 142–143, 274

for parallel mean flow, 77

Velocity gradients, of mean flow, 249, 262

Velocity potential, 45

Viscosity, 2, 69, 71

Viscous effects, 2, 69, 71, 173, 174, 192, 255,
261

Viscous shear stress, 69, 71, 173

Viscous stress tensor, 69

Volume flow source, 2, 25, 45

Volume displacement effects, 116, 117–118,
153, 161, 183–184, 193

Vortex ring, 107, 109

Vortex shedding:

behind airfoil, 133–134

behind cylinder, 146

from nozzle lip, 182

from wedge, 106, 108

Vortex sheet, 22, 131, 133, 134, 225*n*

analogy for shear layer, 21–22, 264

instability of, 181

Vortex wakes:

behind airfoil, 133, 152, 227

behind cylinder, 146

from nozzle lip, 182

Vortical velocity, 221, 223

Vorticity, 41, 221

Wakes:

behind airfoils, 133, 152, 227

behind cylinders, 146, 151

from rotor, 202–203, 205, 208

from stator, 203–205

Wave equation, 9, 69

for transversely sheared mean flow, 7–10

for uniformly moving medium, 8, 9, 199,
227

Wave front, 14, 161, 164, 199–200, 267

Wave length:

acoustic, 12, 17, 20, 36, 38, 74, 177, 181

of incident gust, 167, 223, 237

Wave number, 12, 81–82

Wave number vector, 12

Wave packets, 108

Wave propagation in ducts, 198–201, 235–236

Weber functions, 271

Wedge, 106–107

Wiener-Hopf technique, 181

WKB method, 265–266, 282–284

Wronskian, 263, 266–267, 282

Zone of silence, 18, 270, 276, 277, 280